SPACE RESEARCH IN POLAND

Report to

COMMITTEE ON SPACE RESEARCH

(COSPAR)

2020

Space Research Centre Polish Academy of Sciences

and The Committee on Space and Satellite Research PAS

Report to COMMITTEE ON SPACE RESEARCH (COSPAR)

ISBN 978-83-89439-04-8 First edition

Warsaw, 2020

Editor: Iwona Stanisławska, Aneta Popowska

1

SATELLITE GEODESY

1. SATELLITE GEODESY

Compiled by Mariusz Figurski, Grzegorz Nykiel, **Paweł Wielgosz**, and Anna Krypiak-Gregorczyk

Introduction

This part of the Polish National Report concerns research on Satellite Geodesy performed in Poland from 2018 to 2020. The activity of the Polish institutions in the field of satellite geodesy and navigation are focused on the several main fields:

- global and regional GPS and SLR measurements in the frame of International GNSS Service (IGS), International Laser Ranging Service (ILRS), International Earth Rotation and Reference Systems Service (IERS), European Reference Frame Permanent Network (EPN),
- Polish geodetic permanent network – ASG-EUPOS,
- modeling of ionosphere and troposphere,
- practical utilization of satellite methods in local geodetic applications,
- geodynamic study,
- metrological control of Global Navigation Satellite System (GNSS) equipment,
- use of gravimetric satellite missions,
- application of GNSS in overland, maritime and air navigation,
- multi-GNSS application in geodetic studies.

These activities were conducted mainly at the following research centers:

- Faculty of Civil and Environmental Engineering, Gdansk University of Technology (GUT)
- Faculty of Mining Surveying and Environmental Engineering, Department of Integrated Geodesy and Cartography, AGH University of Science and Technology
- Department of Geodesy, University of Warmia and Mazury in Olsztyn (UWM)
- Institute of Geodesy and Geoinformatics (IGG), Wrocław University of Environmental and Life Sciences (UPWr)
- Department of Geodesy and Geodetic Astronomy Warsaw University of Technology
- Faculty of Civil Engineering and Geodesy, Military University of Technology (MUT)
- Department of Planetary Geodesy, The Space Research Centre
- The Space Research Centre's Astrogeodynamical Observatory in Borowiec
- Central Office of Measures (GUM)
- Institute of Meteorology and Water Management – National Research Institute (IMGW).

This Report was compiled from information reported in a period from 2018 to 2020 by the correspondents from Polish institutions involved in the use of satellite navigation systems.

1.1 Faculty of Civil and Environmental Engineering, Gdansk University of Technology (GUT) Nykiel G., Figurski M., Baldysz Z.

GNSS meteorology

GUT have continued work related to the using of GNSS technique for meteorological application. This time, the special focus was put on the investigation of rapid and heavy weather event (derecho) occurred in Poland on 11th August 2017 (Nykiel et al. 2019). Observations from 278 GNSS permanent stations evenly distributed throughout Poland were used for this purpose. The zenith total delays (ZTD) with a 5-minute interval were estimated using Bernese GNSS Software (ver. 5.2) using PPP mode, and converted to the precipitable water vapour (PWV) parameters. Based on such prepared data two-dimensional maps of PWV distribution were created and compared with the composite reflectivity maps derived from EIG EUMETNET. Analysis of the obtained results has shown that changes of the PWV over Poland between 19:30 and 20:30 (UTC) clearly match changes of the refractivity at the same time (Fig. 1.1). The maximum PWV was observed at 20:30 and its value exceed 51 mm, which was twice as high as average PWV value in Poland. Generally, the precipitation zone was identified for the area with PWV exceeding 40 mm. Thanks to the dense network of GNSS receivers, PWV maps for the time between 16:30 and 22:00 have shown movement of the storm along with information about its intensity. It was state out that denser network of GNSS stations would improve these results, which is especially important since GNSS can provide data in real-time.

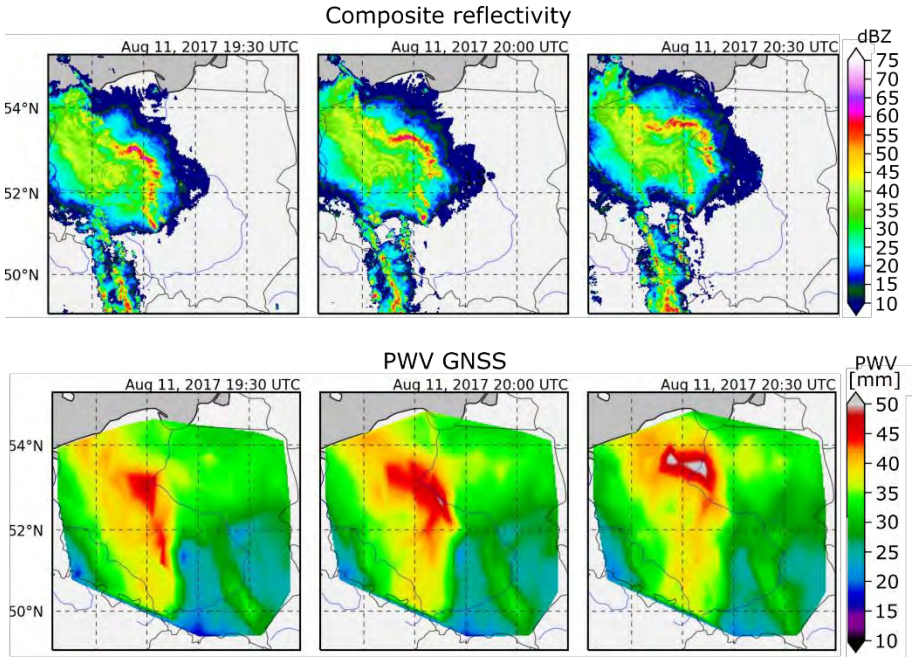

Fig. 1.1. Composite reflectivity data maps with 2-km spatial resolution (top) and GNSS PWV maps interpolated from observations from the dense network of the GNSS receivers (bottom) over the study area on 11th August 2017 (19:30 to 20:30 UTC) in 30-minute steps.

Next to the PWV, also 15-minute tropospheric gradients were analysed in this study. Since tropospheric gradients indicate anisotropy in the atmosphere, they should reflect changes in the troposphere caused by the weather events. Results have shown, that having a dense network of GNSS permanent stations, it is possible to indicate area characterized by the highest reflectivity (Fig. 1.2). Gradients estimated at 19:30 and 20:00 clearly pointed storm front, which was evidenced by both their size and direction. Although GNSS tropospheric gradients have limited range due to the number of stations and observed satellites, presented maps have shown that they can constitute for a valuable source of data for tasks related to the analysis of location and propagation of heavy weather events.

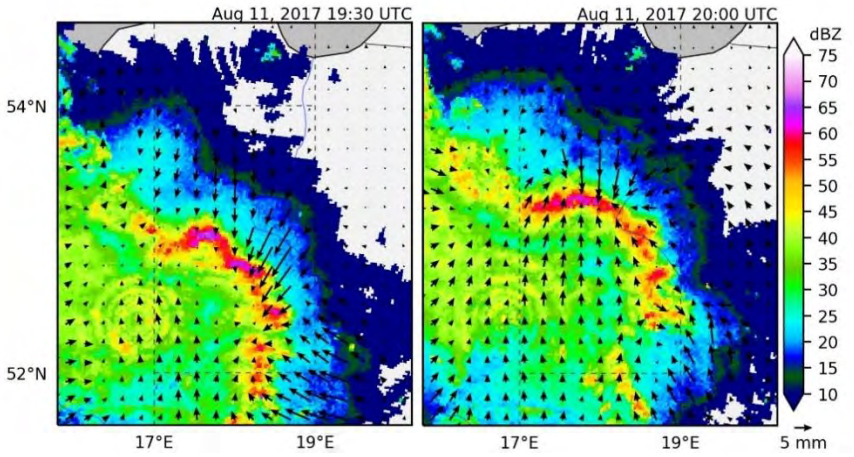

Fig. 1.2. Gridded gradients estimated from the GNSS observations (left: 19:30 UTC; right: 20:00 UTC) on the background of the composite reflectivity derived from the meteorological radars.

A detailed analysis of the case study (PIWN station) confirmed high agreement between estimated GNSS PWV and PWV obtained from microwave radiometer (MWR), as well as with precipitation from meteorological radars and reflectivity data (Fig. 1.3). As it can be noticed, through all day GNSS and microwave radiometer gave similar results. A dash line in MWR during the main phase of the storm means that there was no possibility to conduct reliable MWR measurements. In contrast to this GNSS, as a weather independent technique, provided PWV data continuously with high accuracy. The maximum value of GNSS PWV, precipitation and reflectivity occurred at a similar time. A small shift between these three values results most probably from the temporal resolution of the analysed data. Both Precipitation and reflectivity were available every 30 minutes, while GNSS PWV was estimated every 5 minutes.

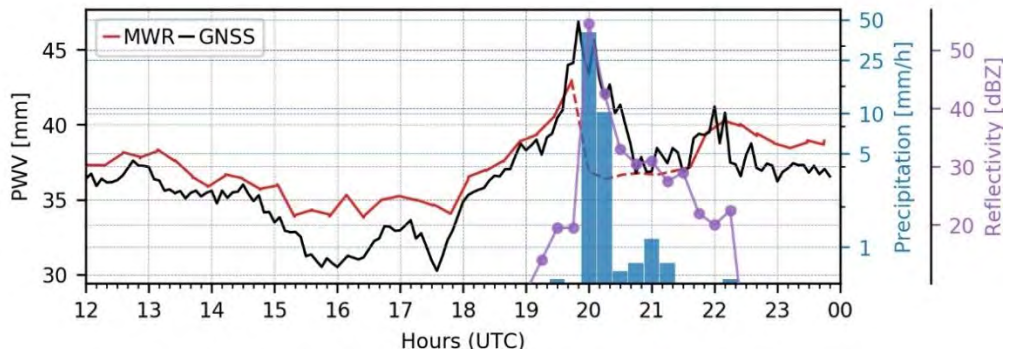

Fig. 1.3. GNSS PWV (the black line), microwave radiometer PWV (MWR) (the red line), precipitation derived from the meteorological radars (blue bars) and the reflectivity measurements (purple) at PIWN station on 11th August 2017.

GNSS ionospheric soundings

The GUT team continue research related to the ionospheric inhomogeneities based on GNSS measurements. Nykiel et al. (2019) describe the method of estimating the height of the ionospheric disturbances based on a dense network of GNSS receivers and near zenith satellites. The presented method was originally used to detect ionospheric disturbances, its modelling and determination of its parameters (Nykiel et al., 2017). However, two separately created maps derived from observations from two GNSS satellites allow determination of the height of ionospheric inhomogeneities (HII) by the cross-correlation computation (Fig. 1.4). The presented method describes the characteristics of the ionospheric disturbances in the 4D space: latitude, longitude, time, and altitude.

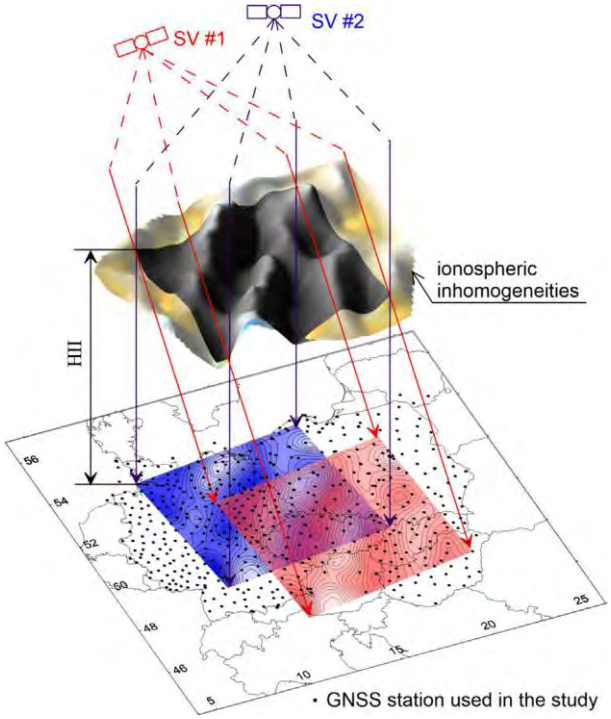

Fig. 1.4. Scheme of the idea of the height of ionospheric inhomogeneities (HII) estimation.

Signals from two GNSS satellites (SV1 and SV2) are received by the dense network of GNSS stations (black dots). Based on the acquired observations, two independently ionospheric inhomogeneities maps are created (blue and red area). The correlation coefficients are calculated for the common area. The whole process is repeated for several heights of the ionospheric layer. The highest correlation coefficient correspond to the actual HII.

In Nykiel et al. (2019) results of the HII estimation during a geomagnetic storm in March 2013 were presented. It was state that during quiet geomagnetic conditions, estimated HII are similar to the height of F2 layer (hmF2) derived from the ionosondes. However, during the active phase of the storm, the HII increased significantly. This proved to be convergent with the changes of the slab ionospheric thickness and protons flux at the POES satellites orbit over Europe (Fig. 1.5).

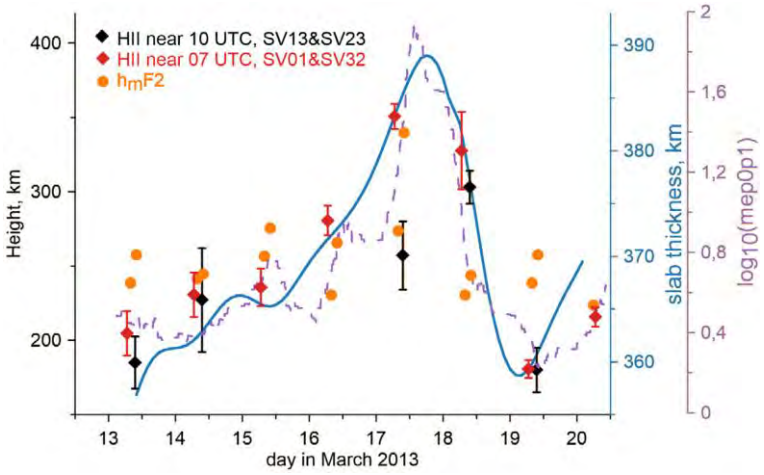

Fig. 1.5. Changes of the estimated height of the ionospheric inhomogeneities (HII) for the analysed period of time (March 13–20, 2013). Red diamonds: the HII obtained near 07 UTC from the maps derived from SV01 and SV32. Black diamonds: the HII obtained near 10 UTC from the maps derived from SV13 and SV23. As a comparison the slab thickness of ionosphere (blue solid line), the logarithm of the intensity of protons flux (mep0p1) at the POES satellites orbit over Europe (magenta dashed line), and hmF2 for corresponding epochs (orange circles) are shown.

$T_m - T_s$ empirical coefficients for the GNSS meteorology

Another work undertaken at GUT was focus on improvement of water vapour weighted mean temperature (T_m) estimation based on surface temperature (T_s). The T_m is a necessary factor for conversion ZTD to PWV/IWV. However, since its in-situ measurements do not provide as high temporal and spatial resolution as in case of GNSS measurements, there is necessity of using an empirical models to obtain T_m value using a much more accessible T_s. The most commonly used models were established years ago (e.g. by Bevis et al. (1992)) or could not be applicable for the whole Europe area. Therefore, a new analysis of radiosonde profiles from 109 stations was carried out to estimate new empirical coefficients that relate the T_m and T_s for Europe territory. This was done through fitting various linear and non-linear dependency to the T_m and T_s time series.

In total, four models were developed, namely:

- ETm - linear regression to the all available data;
- ETm2 - linear regression independently for 00:00 and 12 00 UTC data;
- ETm4 - linear regression independently for 00:00, 06:00, 12:00 and 18:00 UTC data;
- ETmPoly - obtained by fitting 5th degree polynomial function to the data.

The highest agreement between T_m obtained from developed models and T_m sourced directly from the radiosonde measurements was obtained using the ETmPoly model (RMSE 2.8 ± 0.3 K). Compared to the commonly used Bevis model (RMSE 3.1 ± 0.4 K for the analysed stations) it provide more reliable T_m values for the ZTD-IWV conversion formula, which can be noticed on Figure 1.6.

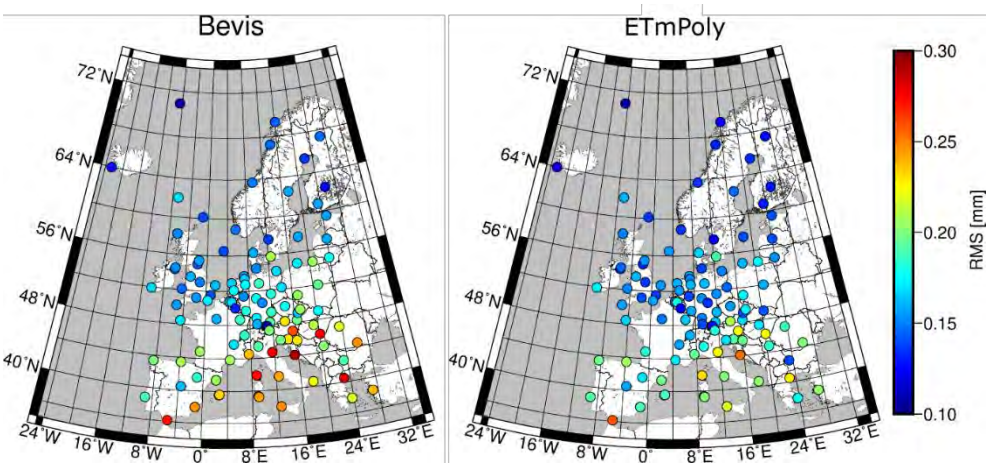

Fig. 1.6. RMS values of the precipitable water vapor (PWV) estimated using Bevis (left) and ETmPoly (right) coefficients. The PWV derived from RS profiles were adopted as a reference.

A detailed analysis has shown, that the highest differences between ETmPoly and Bevis model occurred during JJA season (June, July, August) where troposphere is characterized by much higher humidity fluctuations. More precisely, in DJF season (December January, February) standard deviations of the discrepancies between PWV estimated using ETmPoly and Bevis coefficients were in the range of 0.02 mm – 0.08 mm, while during JJA season they were in the range of 0.08 mm – 0.22 mm (Fig. 1.7).

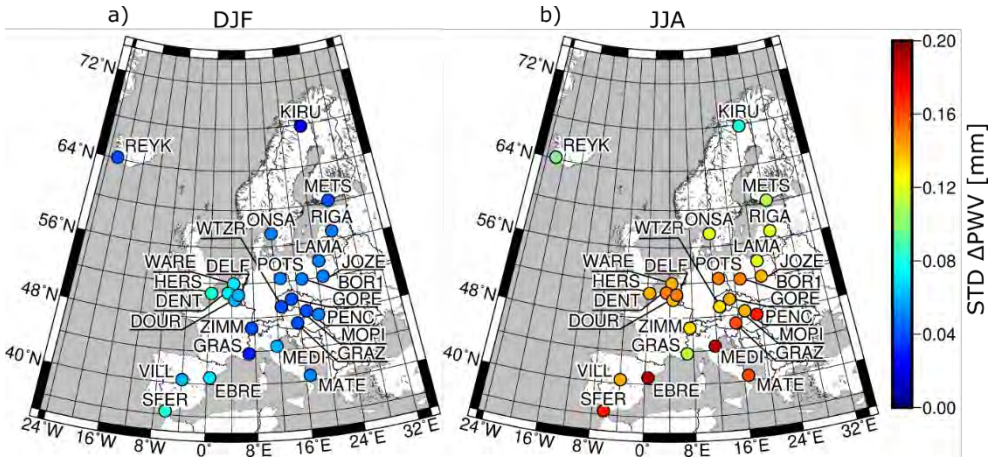

Fig. 1.7. Standard deviations of differences between GNSS PWV estimated using Bevis and ETmPoly coefficients for the seasons: (a) December/January/February (DJF) and (b) June/July/August (JJA).

GNSS velocity fields

GUT takes an active part in international works related to the velocity fields for Europe determined based on GNSS analyses. Among others, GUT is a part of the European Dense Velocities Working Group (http://pnac.swisstopo.admin.ch/divers/dens_vel/) within the EUREF Permanent GNSS Network (EPN). They delivered the velocities estimated for 319 GNSS reference stations containing data from commercial networks located on the territory of Poland (VRSNet.pl, TPI NETpro, Leica SmartNet) and selected stations of EPN network. The obtained solution is characterized by high consistency in relation to the combined one. Average biases of 0.00 ±0.14, -0.01±0.18, -0.25 ±0.41 mm/year were obtained for the velocities in the north-south, east-west, and height direction respectively. Figure 1.8 presents a comparison of different solutions available within the Working Group. The GUT solution is marked with number 019 (gut14x). In addition, GUT participates in the work of The Central European GNSS Research Network (CEGRN) where it also provides solutions in SINEX files (Zurutuza et al. 2019).

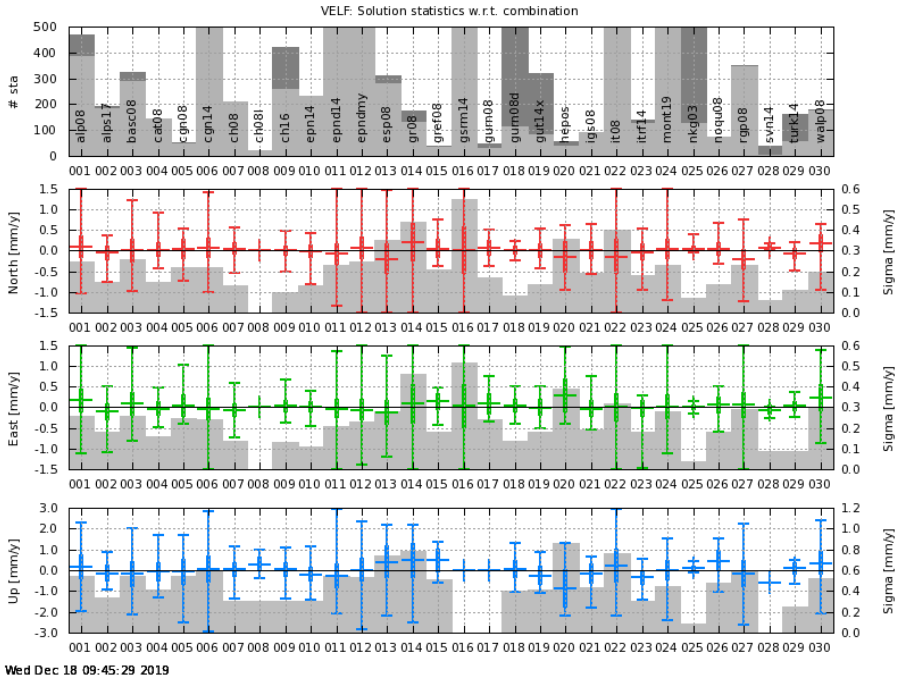

Fig. 1.8. Statistics of single solution w.r.t. combination. From the top: number of stations in each solution, sigma of north, east, and up velocities. GUT solution is identified by the number 019 (http://pnac.swisstopo.admin.ch/divers/dens_vel).

1.2 Academic Computer Centre in Gdansk (CI TASK)

All computations related to the GNSS are performed using supercomputer systems in Academic Computer Centre in Gdansk (CI TASK) (http://task.gda.pl), which is part of Gdansk University of Technology. The calculation are performed on cluster "Tryton" consisting of 3214 processors (Intel® Xeon® Processor E5 v3 @ 2,3 GHz, 12-core), 218 TB total system memory, and Mellanox InfiniBand interconnect with FDR 56 Gb/s bandwidth. Total theoretical peak performance: 1.48 PFLOPS.

References

1. Baldysz, Z., & Nykiel, G. (2019). Improved empirical coefficients for estimating water vapor weighted mean temperature over Europe for GNSS applications. Remote Sensing, 11(17). doi: 10.3390/rs11171995
2. Bevis, M., Businger, S., Herring, T. A., Rocken, C., Anthes, R. A., & Ware, R. H. (1992). GPS meteorology: remote sensing of atmospheric water vapor using the global positioning system. Journal of Geophysical Research, 97(D14). doi: 10.1029/92jd01517
3. Dach, R., Lutz, S., Walser, P., Fridez, P. (2015). Bernese GNSS Software Version 5.2. User manual. In P. Fridez (Ed.), Astronomical Institute, University of Bern. doi: 10.7892/boris.72297
4. Nykiel, G., Zanimonskiy, Y., Yampolski, Y., Figurski, M. (2017). Efficient Usage of Dense GNSS Networks in Central Europe for the Visualization and Investigation of Ionospheric TEC Variations. Sensors, 17(10), 2298. doi: 10.3390/s17102298
5. Nykiel, G., Figurski, M., Baldysz, Z. (2019). Analysis of GNSS sensed precipitable water vapour and tropospheric gradients during the derecho event in Poland of 11th August 2017. Journal of Atmospheric and Solar-Terrestrial Physics, 193. doi: 10.1016/j.jastp.2019.105082
6. Nykiel, G., Zanimonskiy, Y., Koloskov, A., Figurski, M. (2019). The possibility of estimating the height of the ionospheric inhomogeneities based on TEC variations maps obtained from dense GPS network. Advances in Space Research. doi: 10.1016/j.asr.2019.06.008
7. Zurutuza, J., Caporali, A., Bertocco, M., Ishchenko, M., Khoda, O., Steffen, H., ... Nykiel, G. (2019). The Central European GNSS Research Network (CEGRN) dataset. Data in Brief, 27. doi: 10.1016/j.dib.2019.104762

1.3 Faculty of Mining Surveying and Environmental Engineering, Department of Integrated Geodesy and Cartography, AGH University of Science and Technology Kudrys J.

Modelling of the local quasi-geoid

A new model of a local quasi-geoid has been developed at AGH. The local model QuasigeoidKR2019 is based on GNSS observations made at 66 points distributed throughout the Krakow area and normal heights obtained by reference to the detailed vertical control network. The achieved repeatability of the height anomalies from two independent determinations at 22 points is within the interval (-8.3 mm; 8.7 m), with a standard deviation of 5 mm. Such verification is the basis for evaluating the quality of GNSS and levelling measurements. Height anomalies derived from observations' processing were then used to develop an approximation function that models the residual course of a quasi-geoid within the area of Krakow with reference to the global geopotential model EGM2008; planar coordinates in the PL-2000 coordinate system are the input arguments to the approximation function. Based on comparisons and accuracy characteristics, it can be estimated that the accuracy of the local model QuasigeoidKR2019 in the area of Krakow is higher than that of the national model PL-geoid2011. This is supported by the lower value of the extreme difference equal to 14 mm for the local model and 44 for the national model. The mean absolute difference is equal to 5 mm for the local model and 16 mm for the national model.

Stability and noise of GNSS station and satellite on-board clocks

A method for the type of noise representation utilizing Allan variance has been developed in AGH-UST. Allan variances and its related methods are

commonly used to analyze a sequence of data in the time domain to measure frequency stability of oscillators. It allows for a determination of noise type as a function of the averaging time. This method is one of the most popular for identifying different noise types in the sensors data, and it is usually used for a wide range of studies on the stability of oscillators or atomic clocks. At AGH-UST, we developed own algorithm for a qualitative and quantitative expression of noise type using Allan and related variation. The methods currently used allow for the determination of the noise type graphically only, without quantifying the type and percentages for each of the integration steps. Our study allows for a numerical interpretation of the Allan (and related) variances data. A numerical verification of the described method based on GPS satellite clock corrections for 1825–2086 GPS Week (5 years) based on daily 30-s sampling interval products has been performed.

The AGH-UST also conducted research on the clock bias of GNSS receivers and short-term stability of the clock. Due to the same geometry of the satellite segment of each GNSS system, the receiver clock error may be determined with significantly smaller accuracy than the satellite clock error. The above analysis shows that maximum satellite radial velocity regarding the receiver is near the horizon plane, while velocity at the closest approach in zenith is zero; these values are directly correlated with receiver clock error. While in the case of satellite clock biases, 30 cm geometrical error corresponds to 1 ns. In the case of a receiver clock in the worst possible scenarios (horizontally close satellite position and near tropic latitudes), the receiver clock bias must be known only at the 1 μs level, which leads to only 1 mm geometrical error considerations. As such, this kind of level receiver clock error may be determined in a simple combination of code and phase observation equations. In this paper author show and principles for determination, theoretical and practical verification of the distance error generated by the

1 μs receiver clock error. A novelty related to this work is the first calculations of this type. Practical verification based on the adopted permanent reference station (QUI3, Ecuador) and satellite positions from precise MGEX orbit confirmed theoretically.

The International GNSS Service (IGS) provides high-accuracy clock products for both GNSS satellites and stations. At the board of each GNSS satellite are located 3–4 atomic oscillators. In the case of CORS oscillators, the majority of them are equipped with internal oscillators and a part uses external, high-rate clocks. In the IGS network, there are four types of external oscillators: quartz, rubidium, cesium and H-maser. These CORS are often reference stations for precise GNSS measurements or for time transfer. In the conducted research the author provides analyses of the internal and external stability of the reference stations oscillators via the usage of Allan variations. The results show a strong advantage of the external clocks over internal ones by about five orders of magnitude.

References

1. Banasik P., Bujakowski K., Kudrys J., Ligas M. (2020) Development of a precise local quasigeoid model for the city of Krakow – QuasigeoidKR2019; Reports on Geodesy and Geoinformatics, ISSN 2391-8152. — 2020 vol. 109 iss. 1, s. 25–31.
2. Ligas M., & Kulczycki M. (2018) Kriging and moving window kriging on a sphere in geometric (GNSS/levelling) geoid modelling. Survey Review, 50(359), 155–162. https://doi.org/10.1080/00396265.2016.1247131
3. Ligas M., & Szombara S. (2018). Geostatistical prediction of a local geometric geoid - kriging and cokriging with the use of EGM2008 geopotential model. Studia Geophysica et Geodaetica, 62(2), 187–205. doi: 10.1007/s11200-017-0713-7
4. Maciuk K. (2019). Monitoring of Galileo on-board oscillators variations, disturbances & noises. Measurement: Journal of the International Measurement Confederation, 147. doi: 10.1016/j.measurement.2019.07.071

5. Maciuk & Lewińska. (2019). High-Rate Monitoring of Satellite Clocks Using Two Methods of Averaging Time. Remote Sensing, 11(23), 2754. doi: 10.3390/rs11232754
6. Maciuk K., Kudrys J., Bagherbandi M., Bezmenov I. V. (2020) A new method for quantitative and qualitative representation of the noises type in Allan (and related) variances; Earth Planets and Space; ISSN 1343-8832. — 2020 vol. 72 art. no. 186, s. 1–4.
7. Maciuk K. (2020) Determination of GNSS receiver elevation-dependent clock bias accuracy; Measurement; ISSN 0263-2241. — 2020 vol. 168 art. no. 108336, s. 1–3.
8. Maciuk K. (2020) Short-term analysis of internal and external CORS clocks; Journal of Applied Geodesy; ISSN 1862-9016. — 2020 vol. 14 iss. 3, s. 355–359.
9. Skorupa B. (2019). The problem of GNSS positioning with measurements recorded using Android mobile devices. Budownictwo i Architektura 18(3) 2019, 51-62 doi: 10.35784/bud-arch.738

1.4 Department of Geodesy, University of Warmia and Mazury in Olsztyn (UWM)

Wielgosz P., Paziewski J., Cellmer S., Dawidowicz K., Jarmołowski W., Krypiak-Gregorczyk A., Sieradzki R., Stępniak K.

Research on Multi-GNSS positioning

This section summarizes researches conducted over the period 2018-2019 at the University of Warmia and Mazury in Olsztyn and devoted to GNSS positioning algorithm development. The discussed results concern the application of smartphone GNSS signals to precise positioning, the advances in the application of high-rate GNSS observations to structural health monitoring and geohazard studies and novel ambiguity resolution methods. In the initial studies the authors have proposed a novel method suited for the detection of dynamic small-scale displacements on the basis of high-rate GNSS signals processing (Paziewski et al 2018b). The signal processing method (SPM) provides the information on position changes in time domain, hence may be considered as a relative approach. These preliminary studies were followed by more advanced researches in the field of enhancement of the algorithms of PPP to meet the requirements of structural health monitoring. In the paper by Paziewski et al (2019b) the authors have proved high applicability of enhanced PPP and showed that it is possible to detect dynamic displacements of GNSS antenna at the level of a few millimeters.

The contribution to multi-GNSS signals integration studies were given in the paper by Paziewski et al (2018a). The authors investigated potential benefit from the application of the Galileo FOC satellites (E14 and E18) injected to highly eccentric orbits to precise positioning. The research presented the analysis of the stochastic properties of such GNSS signals and evaluated the positioning performance. The detailed analyses allow drawing the conclusions that the power of these satellites signal is much more diversified with respect to

other Galileo satellites, what is triggered by the satellites' changing altitude. The positioning performance experiment based on instantaneous medium range positioning revealed that E14 and E18 satellites signals are fully applicable and usable when providing precise ephemeris of satellites in a post processed mode.

The results of the continuous studies on mitigation of the ionospheric refraction in precise positioning was given in Paziewski and Sieradzki (2018). In the paper the performance of the original method suited for the elimination of the impact of the ionospheric disturbances was examined during disturbed ionosphere periods at the area of Southern High Latitudes.

The paper by Paziewski et al (2019a) aimed at a comprehensive characterization of smartphone signal quality, including carrier-to-noise density ratio, measurement noise and anomalies present in observables with the focus on the impact of duty-cycling mode which constrain the application of smartphone phase measurement to high-precision techniques such as RTK or PPP. Addressing the limitations of low-power consumption smartphones, the authors assessed the smartphone medium to long-range code-based relative positioning. The results showed that it is feasible to use a sparse countrywide GNSS network as reference stations for code-based relative positioning and revealed a discernible benefit from the C/N0-dependent weighting scheme, which is superior to the satellite-elevation one in smartphone positioning.

In addition, research on the MAFA method has been carried out. This method of precise satellite positioning is based on the Ambiguity Function Method. However, meaningful improvements were provided in comparison to the classical form of AFM. In the proposed method, the search procedure is conducted in the coordinate domain. The main advantage of searching for a fixed solution in the coordinate domain is a constant dimension of a search space. It amounts to three since the point position has three coordinates. Thus, in this method, the computational complexity is independent of the number of

satellites. The crucial problem in the search procedure conducted in the coordinate domain is setting the correct search region and a grid of candidates inside it. It was proposed in (Cellmer et al., 2018) to assume the error ellipsoid of the approximate position as the search region. In the same article, the length of the search step (density of the grid of candidates) was set empirically based on simulated data for different configurations of satellites. The detailed discussion on the new method as a non-conventional mixed integer-real least squares (MIRLS) estimation was presented in (Nowel et al, 2018). The equivalency of the criteria of the proposed method and the LAMBDA method was demonstrated. Simple numerical pretests have shown that the reliability and precision of results from the presented approach and the conventional MIRLS estimation are identical.

GNSS antenna calibrations and their influence on positioning

Some analyses were done concerning influence of GNSS antenna phase center correction model type on positioning. In Dawidowicz (2018a) the differences between position estimates obtained using individual and type mean absolute antenna calibrations were investigated to better understand how receiver antenna calibration models contribute to the Global Positioning System (GPS) positioning error budget. The station positions estimated with two absolute calibration models: the igs08.atx model which contains type-mean calibration results and individual antenna calibration models were compared. The results show that the differences in the calibrations models propagate directly into the position domain, affecting daily as well sub-daily results. The position offsets resulting from the use of individual calibrations instead of type mean igs08.atx calibrations, in daily solutions can reach up to 5 mm in the up component, while in the horizontal, the offsets generally stay below 1 mm. It was found that increasing the frequency of coordinates (sub-daily solution)

amplifies the effects of type mean vs individual PCC dependent differences as well as gives visible periodic variations in time series of GPS position differences. Similar analyses are presented in Dawidowicz (2018b). In this paper, the results of GNSS observation processing using the models included in the igs08.atx and igs14.atx files for 12 EPN and ASG-EUPOS stations were analyzed, both for daily and sub-daily time series of PPP solutions. The obtained results show that switching from the igs08.atx to igs14.atx (for the selected stations) induces differences in the vertical component, reaching up to ± 3 mm.

In Krzan et al. (2020) the authors analyzed the diferences in the antenna calibration models and their impact on the accuracy of position derived using various GNSS. Two types of antenna calibration models were analyzed: (1) the absolute robot feld calibration and (2) the anechoic chamber calibration. The PPP position time series of 19 EPN stations equipped with LEICA AR25 antennas were analyzed for GPS, GLONASS, Galileo and combined GPS+ GLONASS+Galileo GNSS signals. Satellite observations were post-processed using the NAPEOS software. The results show that the calibration method has a noticeable impact on PCC models. PCC diferences determined for the ionosphere-free combination may reach up over 20 mm and can be transferred to the position domain. Further tests concerning the positioning accuracy showed that for horizontal coordinates diferences between solutions were mostly below 1 mm, exceeding 2 mm only at two stations for the GLONASS solution. However, the height component diferences exceeded 5 mm for four, six and six stations out of 19 for the GPS, GLONASS and Galileo solutions, respectively. These diferences are strongly dependent on large L2 calibration diferences.

As is well known so far absolute field calibration models were created for GPS and GLONASS L1 and L2 frequencies. Beside GPS and GLONASS, two additional systems are approaching full operational capability. The European

Union (EU) with European Space Agency (ESA) introduce the Galileo positioning system. China has been developing the Beidou system. Additionally, the current satellite navigation systems evolve into new modernized forms. Modernized GPS and GLONASS bring new signals. The modern GNSS satellites will broadcast at least three civil signals in a multiplicity of frequency bands.

The new GNSS systems together with GPS and GLONASS modernization cause the necessity to perform calibrations of receiver antennas designed for the new signals. Therefore, at Department of Geodesy, University of Warmia and Mazury in Olsztyn in cooperation with ASTRI Polska started in 2019 the GRAVEr project founded by the European Space Agency (ESA). The purpose of the project is the development and implementation of field calibration procedure for multi-frequency and multi-system GNSS antennas. The work on the project is in progress.

Some analysis concerning the determination of the PPP accuracy were also performed. In Dawidowicz (2019), time series of position components derived from sub-hourly (30 minutes) PPP solutions were analyzed. The analysis was based on 30 days of observations performed at 8 ASG-EUPOS system stations. For processing the collected GNSS observations (in different variants) the NAvigation Package for Earth Orbiting Satellites (NAPEOS) software was chosen. The conducted analyzes prove that the sub-hourly PPP technique can provide accuracy in the order of 0.5 cm (SD below 0.5 cm) for the horizontal position components and 1 cm (SD below 1 cm) for the vertical position component. The above accuracy was obtained in the multi-station PPP approach (fixed ambiguity solution). In float ambiguity solution scenarios, the standard deviation increases up to 1 cm for horizontal components and up to 2 cm for the vertical component. The periodicity, in the obtained position components time series, were analyzed using the Lomb-Scargle periodogram.

Spectral analysis showed clear periodicity in the obtained results (especially for GPS-only fixed and float solutions). For GPS or GPS/GLONASS processing strategies 73% of detected periodic signals correspond to a multiple of the orbital periods of the satellites.

Modeling and monitoring of the ionosphere with GNSS data

The application of different stochastic, parametric modeling methods to the interpolation of TEC data has been studied with a particular focus on local ionosphere models. The enhancement and densification of global ionosphere models is also studied, and the work on new global ionosphere model is ongoing. The theoretical background related with the parametrization of Least-Squares Collocation (LSC) is still under studying (Jarmołowski, 2019). However, along with LSC parametrization, the other techniques from the kriging family are studied in parallel to LSC, i.e. Ordinary Kriging (OKR) and Universal Kriging (UKR) (Jarmolowski et al. 2019b). The studies prove similar accuracy derived from different parametric modeling techniques. However, a special attention should be put on the parametrization and detrending problems related with kriging and LSC.

The application of TEC derived from dual-frequency altimetry missions (Jason-1, Jason-2, Jason-3, Sentinel 3A and 3B) was also studied for the validation of ionospheric TEC maps based on GNSS data. Local and global GNSS-based TEC models were validated along the footprints of altimetric orbits. Dual-frequency altimeters provide direct, unbiased TEC signal, and this external validation helps to proof the advantage of stochastic methods in the application to GNSS-based TEC data, which are still sparse in many regions (Jarmołowski et al. 2018a, Jarmołowski et al. 2019). This advantage of stochastic techniques is noticeable especially in comparison to the widely used spherical harmonic modeling of the global TEC.

Along with TEC determination from ionospheric corrections based on dual-frequency altimetry, the application of different global ionospheric models in determination of ionospheric correction for the altimetry ranging was studied. The studies refer to the coastal regions, which is a zone of merging of altimetry-derived TEC and GNSS-derived TEC. The connection of the data in these regions is required, as the dual-frequency altimeters normally determining TEC signal over the oceans cannot measure it over the land, and reversely, GNSS stations dense on the continents are sparse in the ocean zone. The different corrections determined for the altimetric ranges from the variety of global models can differ up to centimeters and therefore new, more accurate TEC model are important for altimetry and other satellite observing techniques (Jarmołowski et al. 2018a).

The group started the investigations on the detection of seismic ionospheric disturbances related with the earthquakes (EQ) and tsunami, observed from low-Earth-orbit (LEO) satellites, with a special focus on Swarm mission. This research is based on two Swarm data types: in-situ electron density (ED) measured by Langmuir Probes (LP) and total electron content (TEC) from precise orbit determination (POD) GNSS receivers (Jarmołowski et al. 2020). The mathematical tools applied in this kind of research are FFT-based high-pass and band-pass filters and short-term Fourier transform (STFT) analysis of seismic ionospheric disturbances (SID) in along-track satellite data (Fig. 1.9). The classification of the spectral characteristics of disturbing along-track signals is supported by their simultaneous search in ground GNSS observations, which gives an opportunity for the validation of the spectral recognition. The analyses of Swarm data provide interesting observations of ionospheric disturbances not only directly related with the largest EQ events and tsunami, but also occurring during the entire periods of enhanced seismic activity and at larger distances

from EQ epicenter. The studies on seismic responses in the ionosphere are conducted in the frame of ESA project, in cooperation with Polytechnic University of Catalonia (UPC), Technical University of Munich (TUM) and National Observatory of Athens (NOA).

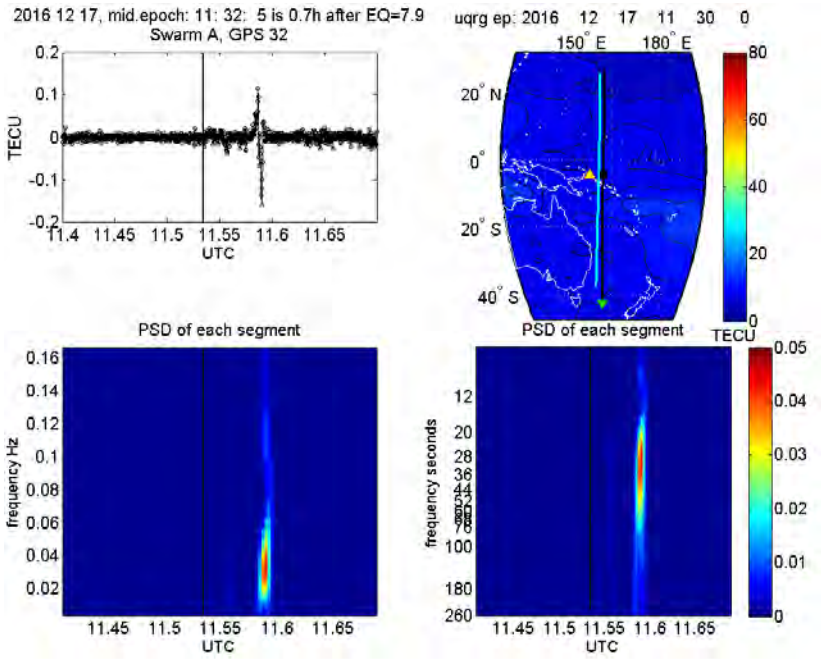

Fig. 1.9. Short-term Fourier analysis of residual POD GNSS TEC signal disturbance measured between Swarm A and 32nd GPS satellite over Papua New-Guinea, just after Mw=7.9 earthquake.

The investigations conducted at UWM were also aimed at monitoring high-latitude ionosphere (Sieradzki and Paziewski 2018, 2019). The main purpose of these studies was the proposal of methodology, which would allow the efficient detection of large-scale structures as well as determination of plasma enhancement observed for them. In order to extend the current algorithms, the authors suggest to use the relative STEC values as an indicator. In contrast to GNSS-based VTEC maps, this parameter provides the epoch-wise information on enhancement/depletion of plasma density with regard to a specified level, representing quiet ionospheric conditions. According to the

conducted tests, this background level can be approximated with 4-order polynomial, fitted to time series of geometry-free combination for particular arc of GNSS data. Finally, the relative STEC values are defined as a difference between geometry-free data and polynomial. The results in Sieradzki and Paziewski (2019), showing the comparison of the proposed methodology with maps of ROTI parameter, demonstrated that the relative STEC values provide more comprehensive view of high-latitude ionosphere. This is particularly true for large-scale structures such as polar patches or storm enhanced density (SED) and proves that the proposed methodology represents an alternative for other GNSS-based methods of ionospheric research. The results on patch occurrence presented in this work were also consistent with previous investigations and knowledge on their origin. Furthermore, the given analysis involved also the validation of the relative STEC values with SWARM measurements, which confirmed the efficiency of GNSS-based parameter. It also indicated that the integration of both datasets should allow deeper investigations of ionospheric conditions. The main goal of the second work (Sieradzki and Paziewski 2018) was evaluation of GNSS data for continuous detection of polar patches on both hemispheres as well as the comparison of these structures. The study confirmed that the distribution of stations near the south pole is less favorable, however it can be still useful for identification of patch propagation. The structures occurred simultaneously for both polar regions, but they varied in size and the stronger were observed on the southern hemisphere. According to the presented results, the reason of this disproportion is much denser stream of mid-latitude plasma for southwardly oriented IMF.

In (Paziewski and Sieradzki 2020) we present and assess the methodology that aims at reliable and accurate wide-area RTK and rapid static positioning in the presence of severe ionospheric conditions. The approach takes advantage of multi-constellation network ionospheric corrections and an algorithm which allows the elimination of the temporal variations of the

ionospheric delay. The experimental evaluation was performed on the basis of multi-station RTK and static positioning using GPS, BDS and Galileo data collected at high latitudes during the ionospheric storm on August 25–26, 2018. The results confirmed the deterioration of the accuracy of the network ionospheric corrections and consequently a decline in the positioning performance with routine models such as ionosphere-float and ionosphere-weighted. On the other hand, the results obtained with the application of the developed methodology demonstrated a very distinctive improvement in the ambiguity resolution domain and thus proved the advantage over benchmark models. In this case the developed methodology allowed up to 20% enhancement of the ambiguity success rate with respect to benchmark strategies.

Quality control of GNSS data processing

The quality control of GNSS data processing can be divided into two parts. The former is the validation of so-called underlying functional model and the latter is the quality description of final model parameter estimates. The underlying functional models are validated using statistical hypothesis testing – usually by so-called DIA testing procedure – to detect, identify and model possible faults. Since the DIA procedure is not mathematically rigorous and optimal under multiple faults in underlying model, the paper Nowel, Cellmer and Fischer (2020) adapted and discussed the information criterion (IC) approach for the validation of baseline GNSS functional models. Three IC methods were compared with the conventional DIA procedure. To verify the reliability of the two considered approaches, several scenarios differing in: the magnitude and number of faults, and the interval between measurement epochs were investigated. Generally, the DIA procedure achieved the highest rates of correct model specification when no fault existed. However, as the

number of faults was increasing one of the IC methods was starting to achieve the highest rates.

Improving tropospheric ZTD estimation with GNSS

The accuracy and homogeneity of Zenith Total Delay (ZTD) series estimated from ground-based GNSS data is strongly dependent on the data processing procedure (e.g. cut-off angle, elevation-dependent data weighting, mapping function and other details of the tropospheric model). The study conducted at the University of Warmia and Mazury in Olsztyn (UWM) in collaboration with the French National Geographic Institute (IGN LAREG) and ENSTA Bretagne, France, was intended to assess the impact of some GNSS data processing aspects on the quality the derived ZTD series for climate applications (Stępniak et al., 2018a, Stępniak et al., 2019). Results from more than 100 permanent stations using different strategies, options and software were analyzed in this study. Absolute PPP and relative solutions were processed with Bernese GNSS Software v.5.2 using different orbit and clock products, as well as PPP solutions using GIPSY-OASIS II with integer and float ambiguities. Estimated ZTD and integrated water vapor (IWV) were inter-compared and compared to ERA-Interim and ERA5 reanalysis (Stępniak et al., 2018b).

The aim of other study was to investigate the impact of different GNSS antenna calibrations models on the quality of the tropospheric estimate series for climate applications. Two years of GNSS data collected at 19 European Reference Frame (EUREF) Permanent GNSS Network (EPN) stations were processed with NAPEOS software using PPP technique. Three different antenna models were used: International GNSS Service (IGS) type-mean Phase Center Correction (PCC) models; PCC models from individual field robot calibration and calibration in anechoic chamber. All three solutions were processed several times – using GPS only, Galileo only, GPS+GLONASS, GPS+Galileo and

multi-GNSS (GPS+GLONASS+Galileo) observations. In order to validate and assess the quality of the GNSS solutions, tropospheric parameters obtained from ERA-Interim reanalysis were compared to GNSS estimates (Krzan & Stępniak, 2019).

The cooperation of UWM with the Shanghai Astronomical Observatory (SHAO) of the Chinese Academy of Sciences (CAS) and Federal University of Pará, Brazil, resulted in research on the assessment of GNSS IWV over central and northeastern Amazonia. This study assessed the suitability and evaluation of the spatiotemporal distribution of GNSS IWV, IWV products from Moderate Resolution Imaging Spectroradiometer (MODIS) and radiosonde, jointly with surface meteorological data, in two sectors of the state of Rio de Janeiro from February 2015 to August 2018 (Mota et al., 2019).

Application of high-rate GNSS signals to geohazard monitoring

The continuous progress in GNSS has led to considering this measurement technique as a powerful tool for the detection of the displacement response on seismic events and a source of comprehensive information on seismic wave propagation. At present, the relative positioning mode is considered as the most accurate method for coordinate displacement determination with GNSS measurements. This holds true providing that all errors are carefully modelled or significantly reduced, which is not a trivial task in a wide area scenario. In (Paziewski et al 2020) we validate the algorithms and the system developed for an automatic Galileo and GPS high-rate signals processing over medium-length baselines. The system aims at the characterisation of the displacement response to seismic events, which are induced by mining exploitation. Addressing the requirements of the monitoring network, the system takes advantage of a ionosphere-weighted positioning model and a multi-baseline solution, which may be considered as superior with respect to the commonly

employed single-baseline mode. The validation of the system feasibility was performed in two manners: by processing the data collected during actual M_W 3.8 seismic event and with the use of single-axis shake table. The results of the former experiment showed a high agreement between the GNSS and accelerometer-derived results in a frequency domain. The latter proved that the system is capable of detecting the dynamic displacements with a millimetre-level precision at distances of over 30 km from the reference stations.

Smartphone and low-cost positioning and applications

A number of location-based services and mass-market applications which run on smart-devices take advantage of the position derived from embedded GNSS chipsets. Since May 2016 the GNSS scientific community has paid special attention to GNSS observations derived from Android smartphones. Thereafter raw observations retrieved from GNSS chipsets in smart-devices have been available to the developers. Hence, not only code pseudorange but also carrier phase and Doppler GNSS measurements have been accessible through Application Programming Interface 24 on devices running on the Android Nougat 7 operating system. Following the availability of smartphone-derived GNSS measurements, a number of studies on signal quality and algorithm development aiming at enhancing the positioning accuracy of mass-market devices and applications have been carried out. The paper by Paziewski (2020) offers a review of the most recent advances in smartphone GNSS positioning and applications as well as an outline of possible future developments. In the light of the recent advances, continuous progress in hardware, algorithms and applications is thought to be maintained in the future. With this development, the presumption of low-performance commonly related to low-cost receivers and smartphones may not hold true, since in the near future such receivers may potentially reach the performance level close to high-grade receivers and thus open the door to novel applications.

References

1. Cellmer S., Nowel K., Kwasniak D. (2018). The New Search Method in Precise GNSS Positioning, IEEE Transactions on Aerospace and Electronic Systems, vol. 54 (1), pp. 404-415, doi:10.1109/TAES.2017.2760578
2. Dawidowicz K. (2018a) Differences in GPS coordinate time series caused by changing type-mean to individual antenna phase center calibration model, Studia Geophysica et Geodaetica, Stud. Geophys. Geod., 62 (2018), 38-56, doi:10.1007/s11200-016-0630-1 (15 pkt)
3. Dawidowicz K. (2018b), Igs08.atx to igs14.atx change dependent differences in a GNSS- derived position time series. Acta Geodyn. Geomater., 15, No. 4 (192), 363–378, 2018. doi:10.13168/AGG.2018.0027
4. Dawidowicz K. (2019). Sub-hourly precise point positioning accuracy analysis – case study for selected ASG-EUPOS stations. Survey Review, 0039-6265 (Print) 1752-2706 (Online); doi: 10.1080/00396265.2019.1579988
5. Jarmołowski W., Ren X., Wielgosz P. and Krypiak-Gregorczyk A. (2019a). On the advantage of stochastic methods in the modeling of ionospheric total electron content: Southeast Asia case study. Measurement Science and Technology 30 (4): 44008
6. Jarmołowski W. (2019). On the relations between signal spectral range and noise variance in least squares collocation and simple kriging: example of gravity reduced by EGM2008 signal. Bollettino di Geofisica Teorica et Applicata 60 (3): 457-474
7. Krzan G., Dawidowicz K., Wielgosz P. (2020). Antenna phase center correction differences from robot and chamber calibrations: the case study LEIAR25, GPS Solutions, 24:2, Article Number: 44, DOI: 10.1007/s10291-020-0957-5
8. Nowel K., Cellmer S., Kwaśniak D. (2018). Mixed integer–real least squares estimation for precise GNSS positioning using a modified ambiguity function approach, GPS Solutions, 22:31, doi:10.1007/s10291-017-0694-6
9. Nowel K., Cellmer S., Fischer A., 2020, Validation of GNSS baseline observation models using information criteria, Survey Review
10. Paziewski J., Sieradzki R., Baryła R. (2019a). Signal characterization and assessment of code GNSS positioning with low-power consumption smartphones, GPS Solutions, 23, 98. doi:10.1007/s10291-019-0892-5
11. Paziewski J., Sieradzki R., Baryła R. (2019b). Detection of Structural Vibration with High-Rate Precise Point Positioning: Case Study Results

Based on 100 Hz Multi-GNSS Observables and Shake-Table Simulation, Sensors, Volume:19 Issue:22, doi:10.3390/s19224832
12. Paziewski J., Sieradzki R., Wielgosz P. (2018a). On the Applicability of Galileo FOC Satellites with Incorrect Highly Eccentric Orbits: An Evaluation of Instantaneous Medium-Range Positioning. Remote Sensing 10(2) 208, doi:10.3390/rs10020208
13. Paziewski J., Sieradzki R., Baryła R. (2018b). Multi-GNSS high-rate RTK, PPP and novel direct phase observation processing method: application to precise dynamic displacements detection, Measurement Science and Technology, 29 035002(15pp), doi:10.1088/1361-6501/aa9ec2
14. Paziewski J., Sieradzki R. (2018). Mitigation of the Ionospheric Disturbances in GNSS Relative Positioning: A Case Study in Southern High Latitudes. 2018 Baltic Geodetic Congress (BGC Geomatics) doi:10.1109/BGC-Geomatics.2018.00058
15. Paziewski J, Sieradzki R, 2020, Enhanced wide-area multi-GNSS RTK and rapid static positioning in the presence of ionospheric disturbances. Earth Planets and Space 72, 110 (2020). https://doi.org/10.1186/s40623-020-01238-7
16. Paziewski J, Kurpinski G, Wielgosz P, Stolecki L, Sieradzki R, Seta M, Oszczak S, Castillo M, Martin-Porqueras F, 2020, Towards Galileo + GPS seismology: Validation of high-rate GNSS-based system for seismic events characterisation, Measurement, vol. 166 108236, https://doi.org/10.1016/j.measurement.2020.108236.
17. Paziewski J, 2020, Recent advances and perspectives for positioning and applications with smartphone GNSS observations. Measurement Science and Technology 31(9) 091001 https://doi.org/10.1088/1361-6501/ab8a7d
18. Sieradzki R., Paziewski J. (2018). On the Feasibility of Interhemispheric Patch Detection Using Ground-Based GNSS Measurements, Remote Sensing, Vol. 20(3), 2044, DOI: 10.3390/rs10122044
19. Sieradzki R., Paziewski J. (2019). GNSS-based analysis of high latitude ionospheric response on a sequence of geomagnetic storms performed with ROTI and a new relative STEC indicator, Journal of Space Weather and Space Climate, Vol. 9, DOI 10.1051/swsc/2019001
20. Stępniak K., Bock O., Wielgosz P., (2018). Reduction of ZTD outliers through improved GNSS data processing and screening strategies, Atmospheric Measurement Techniques, 11, 1347-1361, https://doi.org/10.5194/amt-11-1347-2018

Conference Presentations

1. Jarmołowski W., Ren X, Wielgosz P, Krypiak-Gregorczyk A., (2018a) Regional ionosphere model for China from precise point positioning interpolated by least-squares collocation. European Geosciences Union General Assembly 2018, Vienna, Austria, 8-13 April 2018
2. Jarmołowski W., Ren X., Wielgosz P., Krypiak-Gregorczyk A., (2018b). Assessment of Ionosphere TEC Determination From Dual-Frequency Altimetry Missions With Reference to Local and Global GNSS-TEC Models in Coastal Regions, 25 Years of Progress in Radar Altimetry" Symposium, Ponta Delgada, Portugal 24-29 September 2018
3. Jarmołowski W., Wielgosz P., Krypiak-Gregorczyk A., Ren X., (2019b) Comparison of stochastic methods in interpolation and extrapolation of sparse GNSS TEC observations. European Geosciences Union General Assembly 2019, Vienna, Austria, 7-12 April 2019
4. Krzan G., Stępniak K., Impact of indyvidual antenna phase center models on GNSS tropospheric estimates, (2019), Scientific and Fundamental Aspects of GNSS, 4-6.09.2019, Zurich Szwajcaria
5. Mota G.V.; Song S.; Stępniak K., (2019), Assessment of Integrated Water Vapor Estimates from the iGMAS and the Brazilian Network GNSS Ground-Based Receivers in Rio de Janeiro. Remote Sensing, 11 (22), 2652, https://doi.org/10.3390/rs11222652
6. Stępniak K., Bock O., Bosser P., (2018b), Comparison of GNSS ZTD estimates from relative and absolute processing techniques for climate applications, AGU Fall Meeting, 10-14.12.2018, Washington, USA
7. Stępniak K., Bock O., Bosser P., Wielgosz P., (2019), Impact of GNSS Data Processing Options on ZTD Time Series in Precise Point Positioning Mode, 27th IUGG General Assembly, 8-18.08.2019, Montreal, Canada
8. Jarmołowski W., Ren X, Wielgosz P, Krypiak-Gregorczyk A., Milanowska B. (2020) Analysis of Swarm Electric Field Data in View of Tsunami Events and related Earthquakes, EGU General Assembly 2020 - online 4–8 May 2020, EGU2020-18876.

1.5 **Institute of Geodesy and Geoinformatics (IGG), Wrocław University of Environmental and Life Sciences (UPWr)** Sośnica K.

ILRS Associated Analysis Center

A new service was established at IGiG, UPWr in 2017 which became an Associated Analysis Center of the International Laser Ranging Service (ILRS, Pearlman et al., 2019; Otsubo et al., 2019). The Center provides products for validating orbits of Galileo, GLONASS, BeiDou, and QZSS satellites generated by the Center for Orbit Determination in Europe with respect to laser observations collected by SLR stations distributed worldwide, and information about satellites of new GNSS systems and the characteristics of laser stations. The Center generates daily reports with the features of the quality of the orbits of GNSS satellites and the quality of laser observations provided by stations and enables performing online analyzes and data visualization (Zajdel et al., 2017). The high quality of GNSS orbits is important for the high-quality positioning and navigation based on new GNSS systems (Hadas et al., 2019; Katsigianni et al., 2019) as well as for the realization of the geodetic reference frames and determination of global geodetic parameters (Zajdel et al., 2019a; 2019b). The service is available through a dedicated website: www.govus.pl (see Fig. 1.10).

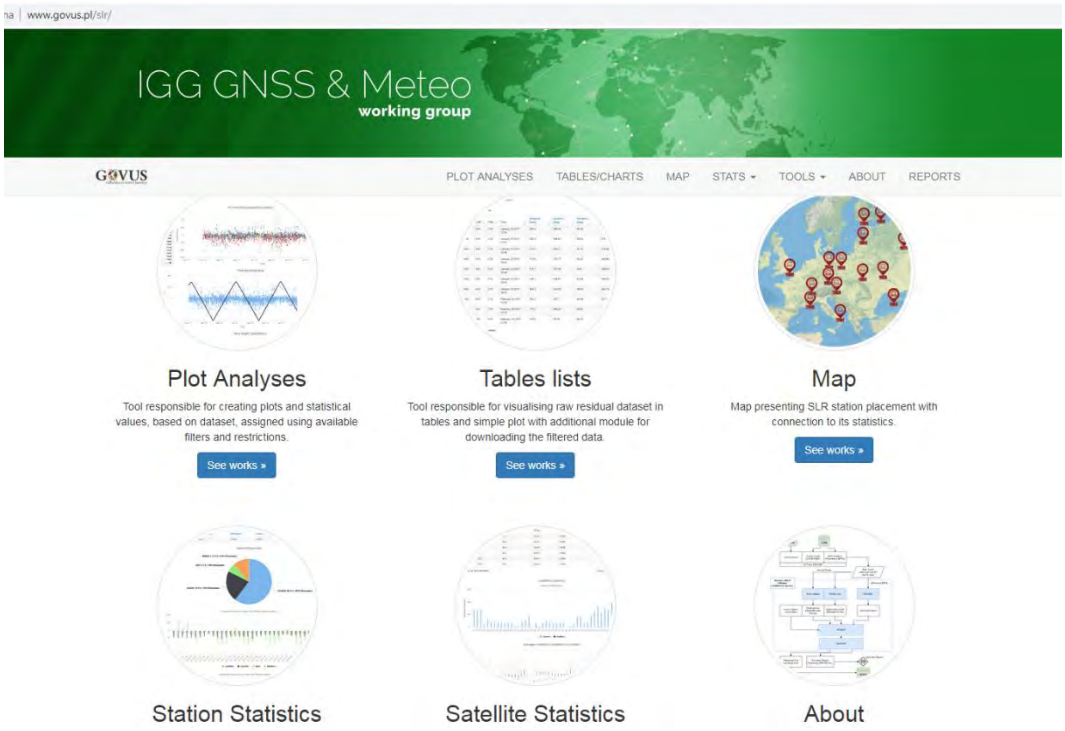

Fig. 1.10. The home page of the www.govus.pl website constituting the ILRS Analysis Center website at IGG UPWr.

Tropospheric delay model in laser observations, taking into account the heterogeneity of the Earth's atmosphere

The differences tropospheric delay modeling in the microwave and optical techniques of space geodesy constitute a limiting factor for the consistency between the Satellite Laser Ranging (SLR) and Global Navigation Satellite System (GNSS) solutions. The vulnerability of SLR measurements to tropospheric delay is different from the sensitivity of microwave observations (GNSS, Very Long Baseline Interferometry, VLBI) to the tropospheric delay. The hydrostatic delay is similar in magnitude, as it is associated with the distribution of atmospheric pressure in both optical and microwave wavelengths. In contrast, the wet delay associated with the distribution of water vapor content in the atmosphere is about 70 smaller in laser observations in relation to microwaves.

Models of the tropospheric delay dedicated to laser observations do not currently take into account horizontal gradients, which means that they assume that the atmospheric zenith (i.e. the direction of the minimal tropospheric delay) coincides with the geometric zenith (normal to the ellipsoid at a given point). The tropospheric delay function recommended by the Conventions of the International Earth Rotation and Reference Systems Service (IERS 2010 Conventions) is as follows:

$$d_{atm}(e) = d^{z}{}_{atm} \cdot m_f(e)$$

where $d^{z}{}_{atm}$ is the zenith delay caused by hydrostatic and wet part, and $m_f(e)$ means a common mapping function for the hydrostatic part and the wet delay at the zenith. In SLR measurements, both the zenith delay and the parameters of the mapping function are calculated on the basis of meteorological observations conducted simultaneously with laser measurements.

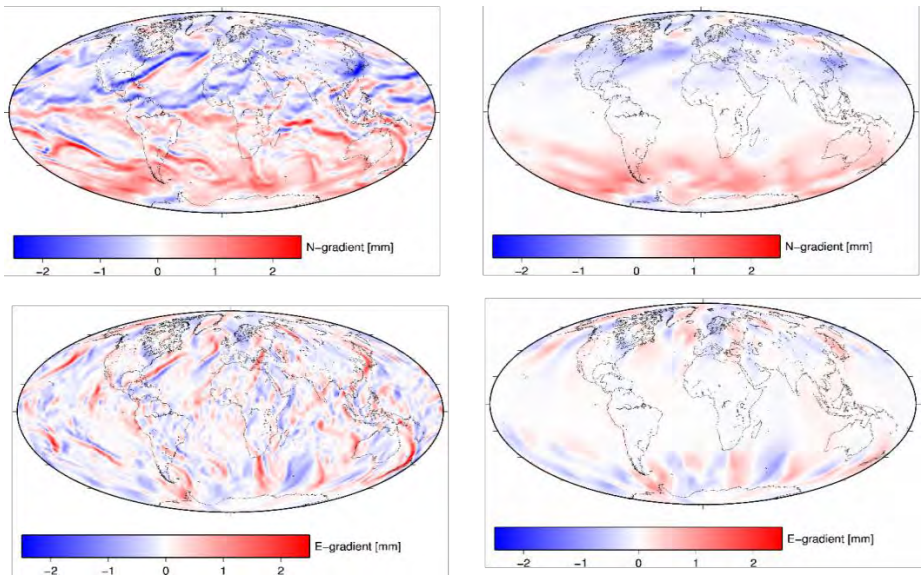

Fig. 1.11. Horizontal horizontals of tropospheric delay in GNSS microwave observations (left) and SLR laser observations (right) for the northern (top) and eastern (bottom) gradients for a chosen epoch - January 1, 2016, 0:00 based on numerical weather models, after Drożdżewski et al., (2019).

In order to improve modeling of the tropospheric delay in laser observations and to improve the consistency between SLR and GNSS, we proposed extending the currently used model with horizontal gradients that account for the asymmetry of the tropospheric state above laser stations (see Drożdżewski et al., 2019):

$$d_{atm}(e) = d^{z}{}_{atm} \cdot m_f(e) + (G_N \cos A + G_E \sin A) \cdot m_g(e).$$

Hence, the tropospheric delay in the SLR technique will be modeled in a similar way to that in the GNSS technique, taking into account the specificity of laser observations (Fig. 1.11). The susceptibility of laser observations to tropospheric asymmetry has been verified in the publication by Drożdżewski and Sośnica (2017), in which the horizontal gradients were calculated on the basis of long-term measurements to LAGEOS satellites, which are the basis for the determination of the fundamental geodetic parameters (Zajdel et al., 2019b).

Atmospheric pressure loading and the blue-sky effect

We measured the so-called the Blue-Sky effect which limits the consistency between laser techniques in satellite geodesy (SLR) and microwave techniques (GNSS, VLBI) due to the fact that SLR observations are conducted during good weather conditions (clear sky) when the surface of the Earth is deformed by high atmospheric pressure (Atmospheric Pressure Loading, Fig. 1.12). The geophysical Blue-Sky effect was first estimated for all SLR laser stations conducting observations to LAGEOS geodetic satellites, and more recently also for laser stations performing measurements to GNSS satellites. The use of SLR observation to GNSS satellites was possible thanks to intense ILRS tracking campaigns and a significant increase in laser observations to the new GNSS satellites. The method of determining the size of the Blue-Sky effect with the determination of the effect in observations for geodetic satellites and GNSS is described in the article by Bury et al., (2019a) whereas the

methodology of GNSS orbit determination using SLR was described by Bury et al. (2019b).

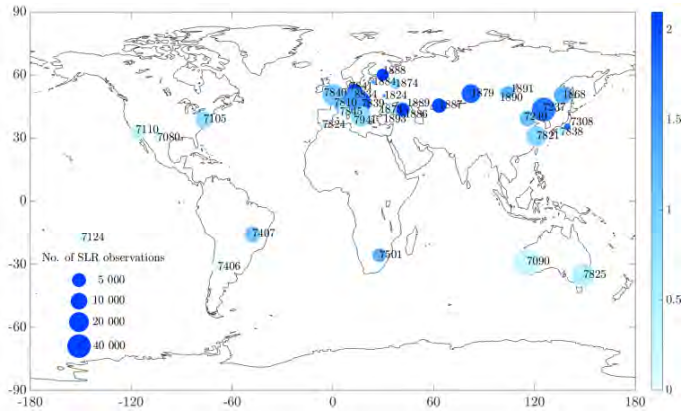

Fig. 1.12. The Blue-Sky effect determined for laser stations tracking GNSS satellites. The size of the effect is denoted in color. The surface area of the symbols used is proportional to the number of collected SLR observations, after Bury et al., (2019a).

Systematic errors in SLR and LEO solutions and SLR-PPP solutions

One of the further elements limiting the accuracy of laser measurements are hardware biases (range biases), which depend on the type of detector at the SLR stations, power and length of the laser pulse, delays in the recording circuits, laser wavelength, type of retroreflector and the number of prisms in the retroreflector array onboard the satellite (Sośnica et al., 2018a, 2018b). Neglecting hardware delays leads to significant systematic errors, especially when laser measurements are used to validate low or high satellite orbits (Strugarek et al., 2019a; 2019b, Arnold et al., 2019).

We proposed an empirical method to reduce the impact of range biases by estimating corrections to station coordinates and estimating biases for long time series (minimum 1 year) and re-substitution of estimated biases, alternatively also station coordinates in epoch solutions (e.g. 1-day). The method works both for stations affected by biases and stations that have incorrect coordinates in the a priori reference frame. For example, as a result

of applying corrections of standard deviations of laser observations to the orbit of the Sentinel-3A satellite determined using GPS observations, the corrections decreased residuals from 12.4 to 8.6 mm, or 30% (Fig. 1.13). The method improves the quality of SLR solutions using observations of LEO satellites (Strugarek et al., 2019a; 2019b) as well as SLR observations to GNSS satellites (Sośnica et al., 2018b, 2019).

Precise Point Positioning (PPP) is a technique used in GNSS solutions to derive station coordinates using precise orbit and clock products. In PPP the station coordinates of each station are determined independently. We propose a an analog technique for positioning in SLR. The SLR-PPP technique employs the high-quality orbits, especially the orbits of LEO satellites to determine the SLR station coordinates independently with no need of network constraining. In SLR-PPP, no troposphere delays have to be estimated (as opposed to GNSS), nor clock corrections have to be considered, because the same clock is used for the transmitter and receiver. The SLR-PPP has been described, for the first time in (Strugarek et al., 2019b).

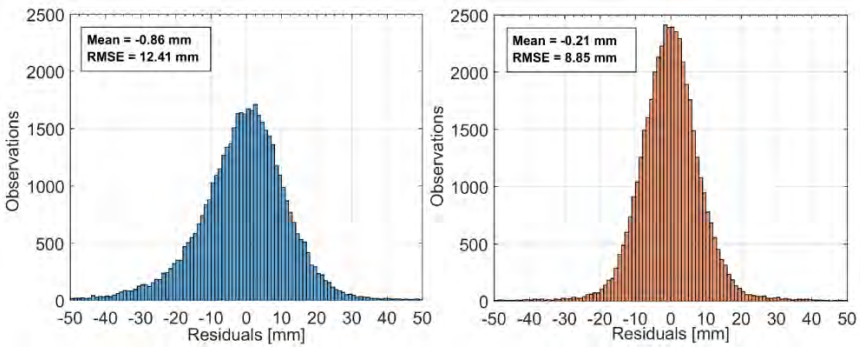

Fig. 1.13. Distribution of laser observation residuals to the microwave orbits of the Sentinel-3A satellite without taking into account the reduction of range biases and corrections to the station coordinates (left) and after taking into account corrections (right) for all SLR stations in 2016.

Experimental IGS combined orbits for GPS, GLONASS, Galileo, BeiDou, and QZSS

In 2019, the International GNSS Service (IGS) an experimental multi-GNSS orbit combination service. The combination is conducted by adapting the legacy combination used for many years for the combination of GPS and GLONASS orbits. The combined orbits are based on products generated by multi-GNSS experiment (MGEX) and IGS analysis centers. We assessed the quality the experimental IGS multi-GNSS combined orbits based on SLR observations and the mean combination position errors (Sośnica et al., 2020). The BeiDou-3 CAST and SECM are characterized by opposite SLR residual dependencies with respect to the Sun elongation angles. GLONASS-M+ has the mean bias of +29 mm. The smallest SLR residuals are obtained for Galileo, GLONASS-K1, and GLONASS-M+. The mean RMS of SLR residuals is 23, 29, 40, 50, 87 and 72 mm for Galileo, GLONASS, BeiDou MEO, BeiDou IGSO, BeiDou GEO, and QZSS, respectively (see Fig. 1.14). From the combination, the orbit errors for MEO satellites are four times lower than SLR for GEO and IGSO.

The IGS combinations are available at: https://www.igs.org/acc/experimental-multi-gnss-combinations/

Precise orbit determination of GNSS satellites and deriving global geodetic parameters

Precise GNSS orbits need a proper modeling of the impact of non-gravitational forces, especially the solar radiation pressure. Three types of orbit models are typically employed: empirical, physical, and hybrid. We propose a hybrid model that employs the a priori bow-wing model for GNSS and the estimation of a small number of empirical parameters to absorb these forces that cannot be well captured by the a priori box-wing model. The model was described by Bury et al. (2020; 2019c) for Galileo satellites, because the precise

metadata with satellite surface properties have been released by GSA and thus allow for the establishment of precise a priori box-wing models for Galileo.

High-quality GNSS orbits are also needed for deriving high-quality geodetic parameters, such as station coordinates, realization of geodetic terrestrial reference frames, Earth rotation parameters, including the pole coordinates and length-of-day excess, geocenter coordinates and many other parameters that have a fundamental meaning in space geodesy. Zajdel (2019a, 2021b) studied the impact of the Galileo system on the common realization of the terrestrial reference frames using different network constraining approaches; including and excluding the no-net-translation minimum constraint and including and excluding the co-estimation of the geocenter motion. Zajdel et al. (2021a) derived the Earth rotation parameters: pole coordinates and the length-of-day excess using three GNSS constellations: GPS, GLONASS, and Galileo. The GPS-derived length-of-day turned out to be affected by a deep resonance 1:2 between the Earth rotation and the satellite revolution period, which caused a large secular drift of the accumulated length-of-day values (which correspond to UT1-UTC). Much smaller secular variations are for the GLONASS and Galileo solutions and the multi-GNSS combinations. Three types of systematic errors were identified in GNSS-based series: related to the common periods of constellation repeatability and Earth rotation (individual for each constellation), harmonics of the draconitic year, and aliasing errors with sub-daily Earth rotation parameter models (Zajdel et al., 2020, 2021a).

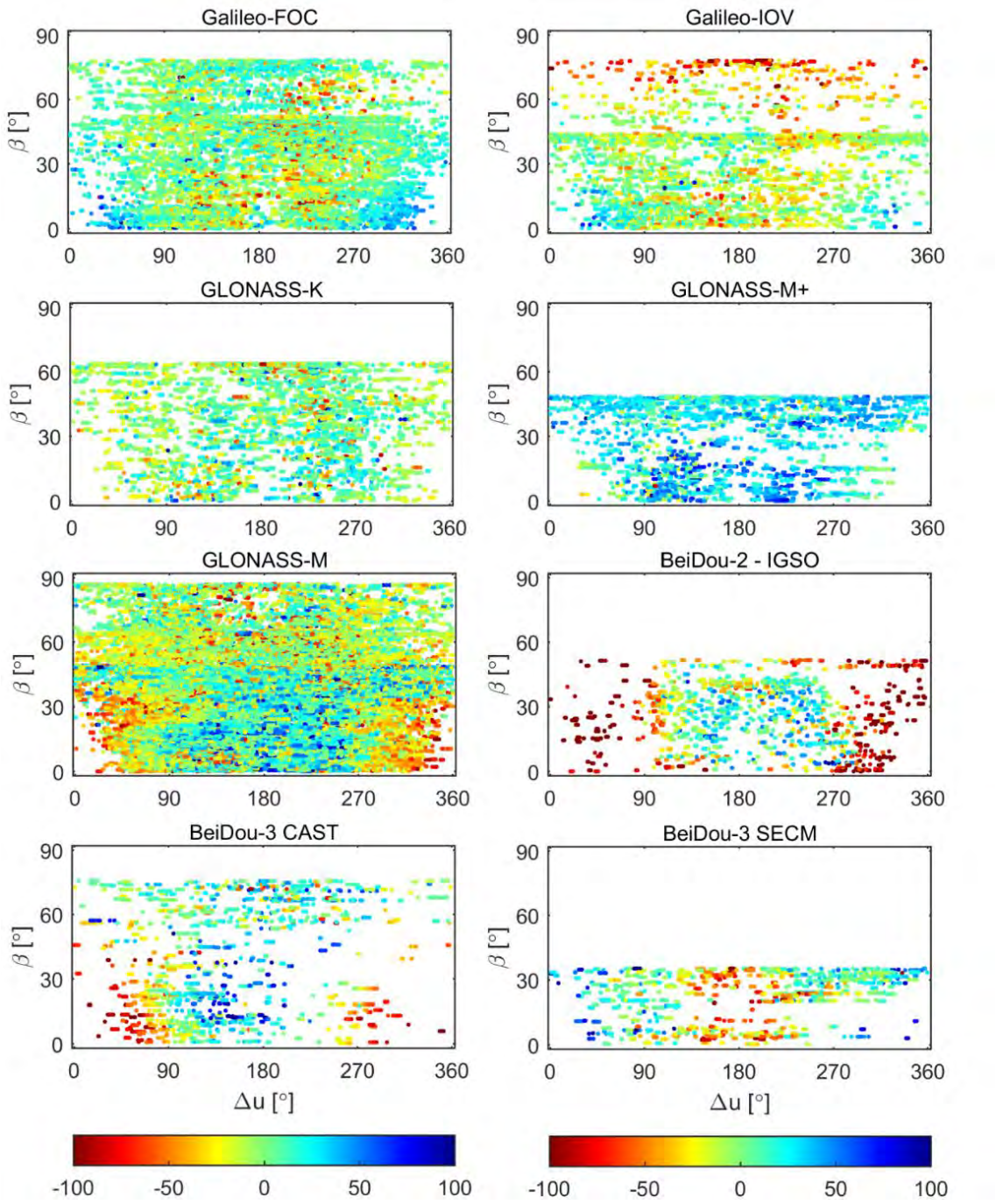

Fig. 1.14. SLR residuals in mm as a function of Sun elevation angle above the orbital plane (β) and the satellite argument of latitude with respect to the latitude of the Sun (Δu).

References

1. Arnold D., Montenbruck O., Hackel S., Sośnica K. (2019). Satellite laser ranging to low Earth orbiters: orbit and network validation. Journal of Geodesy, Vol. 93 No. 11, doi:10.1007/s00190-018-1140-4
2. Bury G., Sośnica K., Zajdel R. (2019a). Impact of the Atmospheric Non-tidal Pressure Loading on Global Geodetic Parameters Based on Satellite Laser Ranging to GNSS. IEEE Transactions on Geoscience and Remote Sensing, Vol. 57 No. 6, pp. 3574-3590. doi:10.1109/TGRS.2018.2885845
3. Bury G., Sośnica K., Zajdel R. (2019b). Multi-GNSS orbit determination using satellite laser ranging. Journal of Geodesy, Vol. 93 No. 12, Germany 2019, pp. 2447-2463. doi:10.1007/s00190-018-1143-1
4. Bury G., Zajdel R., Sośnica K. (2019c) Accounting for perturbing forces acting on Galileo using a box-wing model. GPS Solutions, Vol. 23 No. 74, Berlin - Heidelberg 2019, pp. 1-12. doi: 10.1007/s10291-019-0860-0
5. Bury G., Sośnica K., Zajdel R., Strugarek D. (2020) Toward the 1-cm Galileo orbits: challenges in modeling of perturbing forces. Journal of Geodesy, Vol. 94 No. 16, Berlin Heidelberg, Germany 2020, pp. 1-19. doi: 10.1007/s00190-020-01342-2
6. Drożdżewski M., Sośnica K. (2017). Satellite laser ranging as a tool for the recovery of tropospheric gradients. Atmospheric Research, Vol. 212, pp. 33-42. doi:10.1016/j.atmosres.2018.04.028
7. Drożdżewski M., Sośnica K., Zus F., Balidakis K. (2019). Troposphere delay modeling with horizontal gradients for satellite laser ranging. Journal of Geodesy, Vol. 93 No. 10, Berlin- Heidelberg, Germany 2019, pp. 1853-1866. doi:10.1007/s00190-019-01287-1
8. Hadaś T., Kaźmierski K., Sośnica K. (2019). Performance of Galileo-only dual-frequency absolute positioning using the fully serviceable Galileo constellation. GPS Solutions, Vol. 23 No. 108, Berlin - Heidelberg 2019, pp. 1-12. doi:10.1007/s10291-019-0900-9
9. Katsigianni G., Loyer S., Perosanz F., Mercier F., Zajdel R., Sośnica K. (2019). Improving Galileo orbit determination using zero-difference ambiguity fixing in a Multi-GNSS processing. Advances in Space Research, Vol. 63 No. 9, 2019, pp. 2952-2963. doi:10.1016/j.asr.2018.08.035
10. Otsubo T., Müller H., Pavlis E. C., Torrence M. H., Thaller D., Glotov V. D., Wang X., Sośnica K., Meyer U, Wilkinson M. J. (2019). Rapid response quality control service for the laser ranging tracking network. Journal of Geodesy, Vol. 93 No. 11, pp. 2335-2344. doi:10.1007/s00190-018-1197-0

11. Pearlman M., Arnold D., Davis M., Barlier F., Biancale R., Vasiliev V., Ciufolini I., Paolozzi A., Pavlis E. C., Sośnica K., Bloßfeld M. (2019). Laser geodetic satellites: a high-accuracy scientific tool. Journal of Geodesy, Vol. 93 No. 11, pp. 2181-2194. doi:10.1007/s00190-019-01228-y
12. Sośnica K., Bury G., Zajdel R. (2018a). Contribution of multi-GNSS constellation to SLR-derived terrestrial reference frame. Geophysical Research Letters, Vol. 45 No. 5, Washington, DC, USA 2018, pp. 2339-2348. doi:10.1002/2017GL076850
13. Sośnica K., Bury G., Zajdel R., Strugarek D., Drożdżewski M., Kaźmierski K. (2019). Estimating global geodetic parameters using SLR observations to Galileo, GLONASS, BeiDou, GPS, and QZSS. Earth Planets and Space, Vol. 71 No. 20, pp. 1-11. doi:10.1186/s40623-019-1000-3
14. Sośnica K., Prange L., Kaźmierski K., Bury G., Drożdżewski M., Zajdel R., Hadaś T. (2018b). Validation of Galileo orbits using SLR with a focus on satellites launched into incorrect orbital planes. Journal of Geodesy, Vol. 92 No. 2, Berlin Heidelberg 2018, pp. 131-148. doi:10.1007/s00190-017-1050-x
15. Sośnica K., Zajdel R., Bury G., Bosy J., Moore M., Masoumi S. (2020) Quality assessment of experimental IGS multi-GNSS combined orbits. GPS Solutions, Vol. 24 No. 54, Berlin - Heidelberg 2020, pp. 1-14. doi: 10.1007/s10291-020-0965-5
16. Strugarek D., Sośnica K., Arnold D., Jäggi A., Zajdel R., Bury G., Drożdżewski M. (2019a). Determination of Global Geodetic Parameters Using Satellite Laser Ranging Measurements to Sentinel-3 Satellites. Remote Sensing, Vol. 11 (19) No. 2282, Basel, Switzerland 2019, pp. 1-21. doi:10.3390/rs11192282
17. Strugarek D., Sośnica K., Jäggi A. (2019b). Characteristics of GOCE orbits based on Satellite Laser Ranging. Advances in Space Research, Vol. 63 No. 1, 2019, pp. 417-431. doi:10.1016/j.asr.2018.08.033
18. Zajdel R., Sośnica K., Bury G. (2017). A New Online Service for the Validation of Multi-GNSS Orbits Using SLR. Remote Sensing, Vol. 9 (10) No. 1049, Basel, Switzerland 2017, pp. 1-22. doi:10.3390/rs9101049
19. Zajdel R., Sośnica K., Dach R., Bury G., Prange L., Jäggi A. (2019a). Network effects and handling of the geocenter motion in multi-GNSS processing. Journal of Geophysical Research-Solid Earth, Vol. 124 No. 6, Washington, DC, USA 2019, pp. 5970-5989. doi:10.1029/2019JB017443
20. Zajdel R., Sośnica K., Drożdżewski M., Bury G., Strugarek D. (2019b). Impact of network constraining on the terrestrial reference frame realization

based on SLR observations to LAGEOS. Journal of Geodesy, Vol. 93 No. 11, pp. 2293-2313. doi:10.1007/s00190-019-01307-0
21. Zajdel R., Sośnica K., Bury G., Dach R., Prange L. (2020) System-specific systematic errors in earth rotation parameters derived from GPS, GLONASS, and Galileo. GPS Solutions, Vol. 24 No. 74, Berlin - Heidelberg 2020, pp. 1-15. doi: 10.1007/s10291-020-00989-w
22. Zajdel R., Sośnica K., Bury G., Dach R., Prange L., Kazmierski K. (2020a) Sub-daily polar motion from GPS, GLONASS, and Galileo. Journal of Geodesy Vol. 95, No. 3, Berlin - Heidelberg 202, doi: 10.1007/s00190-020-01453-w
23. Zajdel R., Sośnica K., Bury G. (2021b) Geocenter coordinates derived from multi-GNSS: a look into the role of solar radiation pressure modeling. GPS Solutions, Vol. 25 No. 1, Berlin - Heidelberg 2021, pp. 1-15. doi: 10.1007/s10291-020-01037-3

1.6 Department of Geodesy and Geodetic Astronomy Warsaw University of Technology Liwosz T., Próchniewicz D., Olszak T., Rajner M.

In years 2018-2020 Department of Geodesy and Geodetic Astronomy, Faculty of Geodesy and Cartography, Warsaw University of Technology (WUT) continued investigations in the field of satellite geodesy, geodynamics, and gravimetry. In 2019 WUT also contributed to the Polish National Report on Geodesy in years 2015-2019 on reference frames and reference networks (Krynski et al., 2019a), gravity field modelling and gravimetry (Krynski et al. 2019b), and Earth rotation and geodynamics (Bogusz et al., 2019).

GNSS analysis within EUREF

Warsaw University of Technology (WUT) has been operating as an EUREF Permanent Network (EPN) Analysis Centre (AC) since 1996. WUT AC regularly processes Global Navigation Satellite Systems (GNSS) data from a subnetwork of 138 EPN stations (as of December 2020) and provides to EUREF final (daily and weekly) and rapid daily coordinate solutions. WUT AC uses Bernese GNSS Software version 5.2 for GNSS data processing. Since March 10, 2019 a two-system solution (GPS, GLONASS) was extended to a three-system solution (GPS, GLONASS, Galileo). In 2018, WUT AC started creating new solutions, in which the WUT regional subnetwork was augmented by global IGS (International GNSS Service) reference stations. The purpose of creating this work is to analyze the impact of adding global stations on station coordinates of the regional network. These works were continued in 2020.

Since year 2014, WUT together with the Military University of Technology, Poland, have been operating as the EPN Analysis Combination Centre (ACC). Since year 2016 WUT is responsible for the creation and analysis of the official EPN combined coordinate solutions (final, rapid and ultra-rapid). The final EUREF combined coordinate solutions are based on GNSS solutions generated by the 16 EPN ACs.

In 2018 and 2019 the impact of Galileo observations on EPN combined station positions was analysed in EPN (Bruyninx et al., 2020). The comparison of combined test solutions based on GPS, GLONASS and Galileo observations with the EPN operational combined solutions based on only GPS and GLONASS observations done by EPN ACC at WUT showed that mean position differences (over 44 weeks of daily solutions) for the majority of stations did not exceed 1 mm in the horizontal components, and 3 mm in the vertical component (Fig. 1.15). Larger differences were noticed for stations with type mean calibrated antennas than for stations with individually calibrated antennas, especially for the vertical component. Since March 10, 2019, Galileo observations have been included officially in EPN operational products.

The impact of adding global stations to the EPN regional network on EPN station positions was also analysed by the EPN ACC at WUT (Bruyninx et al., 2020). Good position agreement between the combined solution with global stations and the operational EPN solution (regional) was obtained, and the differences between them mostly came from the alignment of both solutions to the terrestrial reference frame. These differences in the reference frame alignment are caused mainly by the non-tidal loading effects (due to atmosphere, continental water, ocean).

Detection of ice mass ice variation using GNSS

Rajner (2018) processed 11 years of GNSS data from Polish Polar Station at Hornsund (Svalbard) using GIPSY software. This new results, and data from Ny-Alesund, were used to study contemporary ice mass balance over Svalbard. The height time series from both sites indirectly revealed recent increase of mass loss of 6 Gt per year, and the total ice loss of 14.7 Gt per year was estimated. For the first time it was demonstrated that distance change between both GNSS sites is a consequence of ice loading phenomena. This

work confirmed the feasibility of using elastic deformations in order to estimate ice masses change.

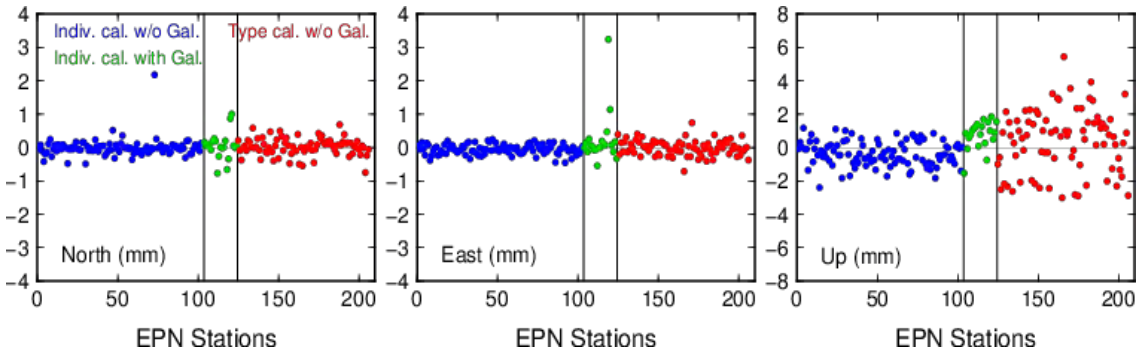

Fig. 1.15. Differences of station positions between combined three-system (GPS, GLONASS, and Galileo) test solutions and EPN combined two-system (GPS and GLONASS) operational solutions. Blue dots denote stations equipped with antennas with individual calibrations without corrections for Galileo (corrections available only for GPS and GLONASS), green dots denote stations with individual antenna calibrations with Galileo corrections, and red dots denote stations with type mean calibrations without Galileo corrections. Results presented only for stations observing Galileo satellites.

Assessment of the Network-based GNSS Positioning Services Performance in Poland

The Continuously Operating Reference Station (CORS) networks, as one of the fundamental segments of the precise GNSS positioning techniques, have been undergoing rapid development and growth in the last two decades. The existing and newly created CORS networks coincide with both the services provided and the covered area. This is the situation in Poland, where there are five nation-wide and local networks: ASG-EUPOS, SmartNet, TPI NetPro, VRSNet and NadowskiNet. Four of them are operating country-wide and one (NadowskiNet) is a local network functioning in the south of the country. In total, they include over 500 stations and provide access to similar GNSS data, Real Time Kinematic (RTK) and Network Real Time Kinematic (NRTK) services.

The research carried out at WUT was focused on comprehensive tests conducted to evaluate the quality of network-based GNSS positioning services performance provided by all CORS networks available in Poland (Prochniewicz et al., 2020). The test was performed in November 2017 and included the analysis of accuracy and reliability of positioning performance, time to first fix (TTFF), an average age of correction as well as the compliance of the reference frame realization. The test data were obtained from the field measurements of consecutive RTK/NRTK services and simultaneous continuous measurements carried out at 20 reference points of the first-order geodetic network, evenly distributed throughout Poland. Obtained results allowed to estimate the positioning performance accuracy and reliability for all tested streams and their mutual comparison of quality along with the analysis of the reference frame realization compliance implemented by all networks. Figures 1.16 and 1.17 show statistical summaries of RMS for horizontal and vertical components for tested NRTK (Fig. 1.16) and RTK (Fig. 1.17) streams. This statistics are shown in the form of a box plot for all measurement series at 20 reference points. In most cases, the results confirm the nominal accuracy of positioning based on tested streams of 1 cm for horizontal and 2 cm for vertical components. However, it was also found that for some networks and streams the obtained accuracy was twice lower (reaching up to 4 cm for the height component), and compliance with the vertical reference frame is lower.

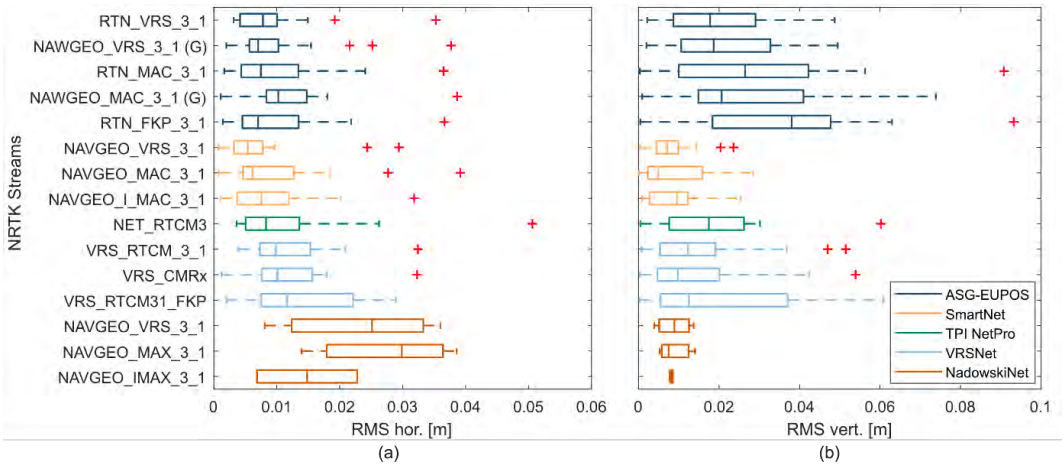

Fig. 1.16. Statistics of positioning accuracy (RMS) for NRTK services: horizontal component (a), vertical component (b).

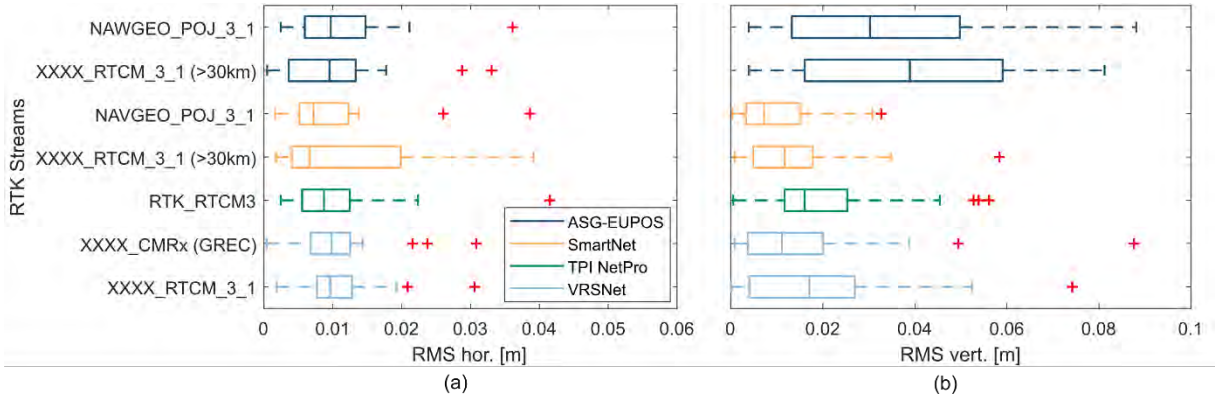

Fig. 1.17. Statistics of positioning accuracy (RMS) for RTK services: horizontal component (a), vertical component (b)

Gravimetry and gravity field modelling

Activities of the WUT research group concerning gravimetry and gravity field modelling focused on observing gravity in the Polish gravimetric network and the new Polish Geodynamical Network of Polish Geological Institute. In 2016 the works connected with the new definition of the gravity values of the Polish Fundamental Gravimetric Base were finished on 30 stations integrated with EPN and Polish GNSS permanent network. Also, the works of monitoring of long term gravity variations in gravimetric laboratory at Jozefoslaw Observatory

(permanently since 2006) were continued which give a possibility of the investigation of non-tidal gravity changes due to e.g. atmosphere and hydrology and local environmental effect connected with water table effect. The Jozefosław station is one of the two stations of planned International Gravimetric Reference Frame on the Poland's territory (Krynski et al., 2019; Olszak et al., 2017; Kuczynska-Siehien et al., 2019).

Different aspect connected with gravity field modelling focalised on the utilisation of the GOCE Gravity Gradient Grids to the determination lithosphere parameters for the Central Europe. Results presented by Lenczuk et al., (2019) suggests that forward modeling may be used for recognizing geological structures or mapping in previously undiscovered areas. Because of the sensitivity of the GOCE data to the geological structures with significant depth and/or density contrasts, these gradients can be used to improve e.g. the Moho model in not so well surveyed regions or for each of the models, where small amount of data is available.

Interesting works have been presented for GRACE temporal solutions of three main centers and comparison products of filtration parameters for monthly gravity field solutions in RL06 and RL05 releases and then to compare them to a time series of absolute gravimetric data conducted in quasi-monthly measurements in Astro-Geodetic Observatory in Józefosław (Poland). The other purpose of this study was to estimate the accuracy of GRACE temporal solutions in comparison with absolute terrestrial gravimetry data and making an attempt to indicate the significance of differences between solutions using various types of filtration (DDK, Gaussian) from selected research centres. Considering the latest GRACE reprocessed dataset, DDK3–DDK6 filters published by the CSR and the JPL are characterised by a high cross-correlation coefficient at the level of 0.8 and a satisfactory RMSE in the range of 3.7–4.0 μGal, i.e. lower than twice the measurement made by the

FG5 gravimeter. For the same filters in the RL05a data version, all three computing centres present good results for both cross-correlation coefficient and RMSE, with values of 0.7–0.8 and 4.1–4.7 μGal, respectively. (Szabo, Marjanska, 2020)

Four seismometer-gravimeter pairs were tested at three locations: Borowa Gora Geodetic-Geophysical Observatory, Jozefoslaw Astro-Geodetic Observatory and Lamkowko Satellite Observatory, in the framework of cooperation between the Institute of Geodesy and Cartography (Centre of Geodesy and Geodynamics), University of Warsaw (Faculty of Physics), Warsaw University of Technology (Faculty of Geodesy and Cartography), University of Warmia and Mazury (Space Radio-Diagnostics Research Centre). During the test period from December 2016 to May 2017 several large teleseismic events were observed with well-formed surface waves (Wilde-Piórko et al., 2017).

The new PL-EVRF2007-NH vertical reference system, introduced in the spatial reference system of Poland in 2012, will be the only binding vertical system from 2020. Elevations in the new system differ by ca. +175 mm from the respective ones in the outgoing PL-KRON86-NH system connected with the tidal gauge in Kronstadt. The introduction of the new vertical reference system makes a necessity to apply a new quasi-geoid model in geodetic surveying related to satellite levelling and defined with a common European vertical reference system. Several European Gravimetric Geoid models (EGG2008, EGG2015) has been validated and prepared fitted version of the raw EGG quasi-geoid to incorporate to the engineering practice. Final precision of the raw gravimetric geoid for Poland's territory is 23 mm, after fitting by trigonometric polynomial of the 4th degree the mean residuals value decreased to 13 mm (Marjańska et al., 2019).

References

1. Bogusz, J., Brzezinski A., Nastula J. (2019). Research on Earth rotation and geodynamics in Poland in 2015–2018, Geodesy and Cartography, vol. 68, No 1, pp. 65-86, doi:10.24425/gac.2019.126094
2. Bruyninx, C., E. Brockmann, A. Kenyeres, J. Legrand, T. Liwosz, R. Pacione, W. Söhne, C. Völksen (2020). EUREF Permanent Network, IGS Technical Report 2019, eds. A. Villiger and R. Dach, pp. 111–124, University of Bern, Bern Open Publishing, doi:10.7892/boris.144003.
3. Bruyninx, C., E. Brockmann, A. Kenyeres, J. Legrand, T. Liwosz, R. Pacione, W. Söhne, C. Völksen (2021). EUREF Permanent Network, IGS Technical Report 2020, eds. A. Villiger and R. Dach, University of Bern, Bern Open Publishing (to be published in 2021), .
4. Krynski, J., J. B. Rogowski, T. Liwosz (2019a). Research on reference frames and reference networks in Poland in 2015–2018, Geodesy and Cartography, vol. 68, No 1, pp. 5-29, doi:10.24425/gac.2019.126093
5. Krynski, J., P. Dykowski, T. Olszak (2019b). Research on gravity field modelling and gravimetry in Poland in 2015–2018, Geodesy and Cartography, vol. 68, No 1, pp. 31-63, doi:10.24425/gac.2019.126096
6. Prochniewicz, D., R. Szpunar, J. Kozuchowska, V. Szabo, D. Staniszewska & J. Walo. (2020). Performance of Network-Based GNSS Positioning Services in Poland: A Case Study. Journal of Surveying Engineering, 2020:146(3), pp.05020006, doi:10.1061/(ASCE)SU.1943-5428.0000316
7. Rajner M. (2018). Detection of ice mass variation using GNSS measurements at Svalbard. Journal of Geodynamics 121: 20–25, doi:10.1016/j.jog.2018.06.001
8. Kuczyńska-Siehień J., D. Piretzidis, M. G. Sideris, T. Olszak, V. Szabo (2019). Monitoring of extreme land hydrology events in central Poland using GRACE, land surface models and absolute gravity data, Journal of Applied Geodesy, vol. 13, nr 3, pp. 1-15, doi:10.1515/jag-2019-0003
9. Lenczuk A., J. Bogusz, T. Olszak, M. Barlik (2019). Studying the sensitivity of GOCE gravity gradients to the crustal structure: case study of Central Europe, Acta Geodaetica et Geophysica, vol. published online 05.02.2019, 2019, pp. 1-16, doi:10.1007/s40328-019-00250-y
10. Marjańska, D., T. Olszak, D. Piętka (2019). Validation of European Gravimetric Geoid models in context of realization of EVRS system in Poland, Geodesy and Cartography, vol. 68, nr 2, 2019, pp. 329-347, doi:10.24425/gac.2019.128461

11. Szabó, V., & Marjańska, D. (2020). Accuracy Analysis of Gravity Field Changes from Grace RL06 and RL05 Data Compared to in Situ Gravimetric Measurements in the Context of Choosing Optimal Filtering Type, *Artificial Satellites*, *55*(3), 100-117. doi: https://doi.org/10.2478/arsa-2020-0008
12. Olszak T., M. Barlik, A. Pachuta (2017). Hydrogeologiczne przyczyny zmian przyspieszenia siły ciężkości na stanowisku w Obserwatorium Astronomiczno-Geodezyjnym w Józefosławiu, Przegląd Geologiczny, vol. 65, nr 11/1, pp. 1139-1143 (in Polish)
13. Wilde-Piórko M., P. Dykowski, M. Polkowski et al. (2017). Expanding seismic surface waves measurements towards low periods with gravity measurements, Geoinformation Issues, vol. 9, nr 1, pp. 5-13

1.7 Faculty of Civil Engineering and Geodesy, Military University of Technology (MUT) Araszkiewicz A., Szołucha M., Kiliszek D.

GNSS analysis within EUREF and EPOS

The core of the Faculty's research activity in the field of satellite geodesy is the EPN (EUREF Permanent Network) Analysis Center, which works for the implementation and maintenance of the reference system in Europe. MUT AC (MUT AC - Military University of Technology Analysis Center) is one of two EPN centers located in Poland and one of sixteen in Europe. The solutions provided, among others by MUT AC constitute the basis of the temporary reference frame, and on the basis of the conducted analyzes of archival observations, subsequent redefinitions of the ETRF (European Terrestrial Reference Frame) system are created.

As part of the EPN Densification project (http://www.epncb.oma.be/_densification/) in cooperation with the Head Office of Geodesy and Cartography, MUT provides also solutions for ASG-

EUPOS network. It is a Polish contribution to the continental-scale (European), homogeneous position and velocity for a dense network of GNSS stations. This solutions is used by both EUREF working group on "Deformation models" and EUREF Working Group on "European Dense Velocities" (http://pnac.swisstopo.admin.ch/divers/dens_vel/index.html).

In the last years, research has focused on the influence of antenna phase center modeling on the determined positions. The goal was to check which set of the calibration tables (individual or type mean) gave better results in the case of height estimation. The paper (Araszkiewicz et. el, 2019) presents the differences between models and their impact on resulting height. Analyses showed that, in terms of the stability of the determined height, as well as its variability caused by increasing the facade mask, both models gave very similar results. Another work (Araszkiewicz and Kiliszek, 2020) concerns research on the impact of applying corrections dedicated to GPS frequencies to Galileo frequencies in the absence of the correct ones. The results for both the absolute and relative positioning methods are clear: the use of GPS L2 corrections for the Galileo E5a frequencies results in a deviation of the estimated height of almost 8 mm.

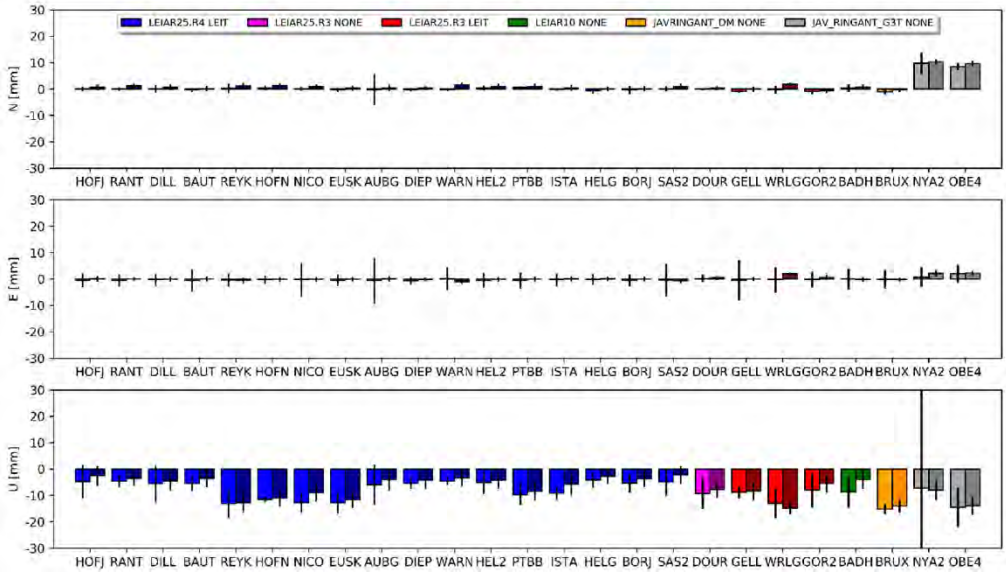

Fig. 1.18. Impact of using G2 (GPS) corrections for E5a frequencies (Galileo). Darker columns refer to the DD approach

MUT AC is also the base for the GNSS Data Research Infrastructure Center (CIBDG) under construction, which creates the GNSS data repository in Poland. This project is co-financed by EU in the frame of European Regional Development Fund (contract no. POIR.04.02.00-14-A003/16-00) within it, CIBDG will become the national node for the EPOS (European Plate Observing System) project. The repository archives observation data from all GNSS stations located in the country and belonging to domestic institutions.

As part of the EPOS project, homogenization of solutions for the Polish region is carried out in order to determine homogeneous solutions from all GNSS stations in Poland. It is crucial from the point of view of the stability of the reference system in the territory of the country and the possibility of using GNSS data to study the age-old deformations of the territory of Poland. Launched in 2019 new coordinate monitoring service RefMON (Fig. 1.19) presents the quality of observations, current coordinates of the stations, their deviations from the ones published in the RT services and tropospheric delay over Poland (previous day).

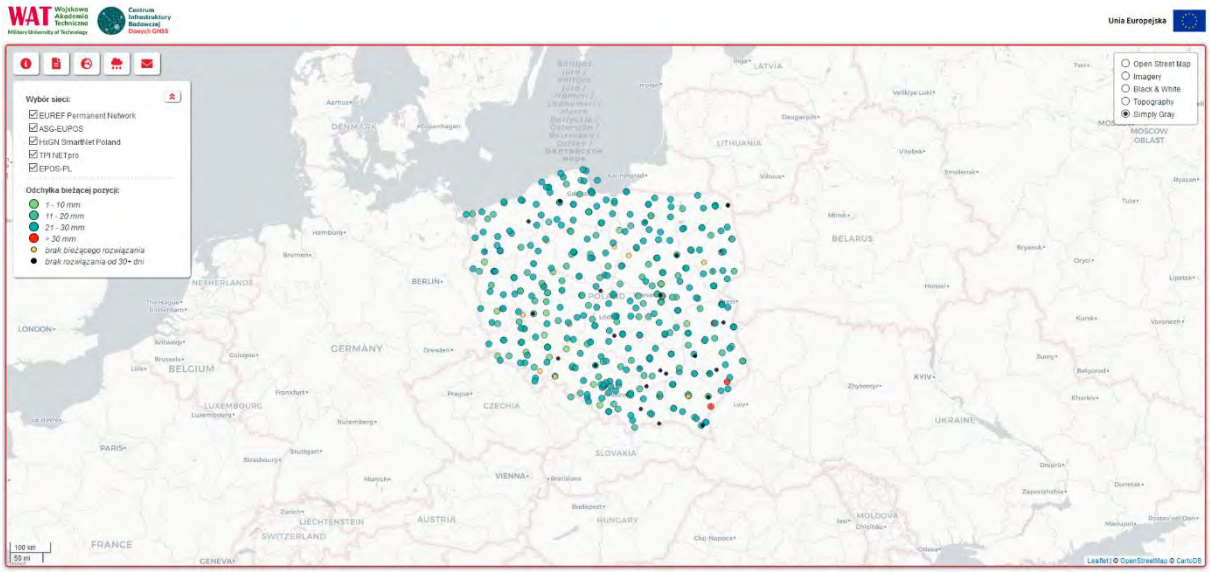

Fig. 1.19. Webpage of the coordinate monitoring service RefMON that is one of the service of CIBDG (http://www.gnss.wat.edu.pl/gnsswat/, in polish).

The infrastructure of the MUT AC is also used to analyze land deformation in areas covered by mining operations (Mutke et. al, 2019) in order to assess the impact of humans on the environment. Prepared mobile GNSS sets based on low-cost multi-GNSS cards continuously record position changes of selected points over active coal mines (Fig. 1.20).

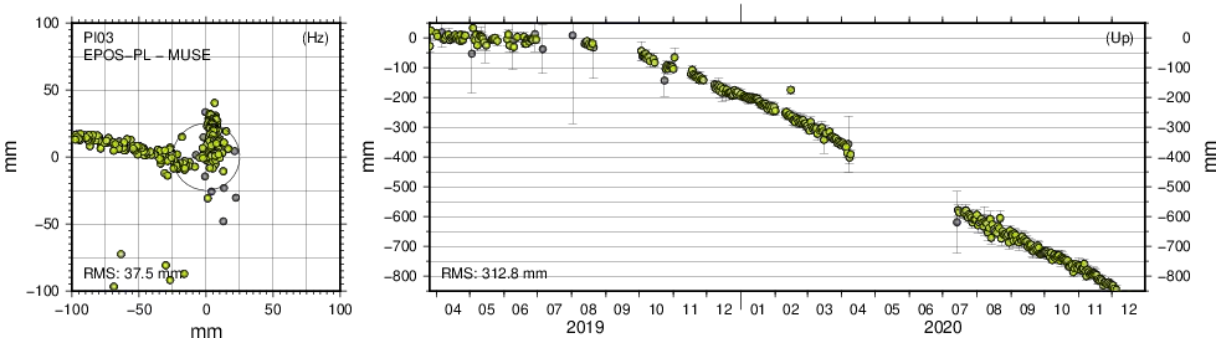

Fig. 1.20. Displacement of the point located in the mining area.

Multi-GNSS analysis

MUT team focus on the field on the study of development of the Global Navigation Satellite System-s (GNSS) and Precise Point Positioning (PPP) method. Research has been conducted on the impact of the development of GNSS systems on the accuracy of PPP positioning (Kiliszek and Kroszczyński, 2020). The research was conducted using the same software, model and products for three different periods in 2017-2019 for different combinations of GPS, GLONASS and Galileo systems for different elevation angles from 0° to 40° (simulating different observation conditions). The obtained results showed that the development of GNSS systems allowed the highest accuracy and the shortest convergence time which were obtained in 2019 using all three systems together. The development of the Galileo system, where a larger number of satellites were available each year, had the greatest impact on the results obtained. Using all three systems together enables to observe on average 22 satellites with the accuracy of 1 cm and the convergence time of 13 min. In 2019, an average of 6 Galileo satellites were observed with a positioning accuracy of about 2 cm and a convergence time of less than 1 h, which showed that the Galileo PPP was available over the globe. In addition this results is better by about 50% than in 2017. We showed that GPS and GLONASS positioning still provide high accuracy achieved the best accuracy for GPS-based solutions. We have also shown that the used multi-GNSS positioning caused greater stability by removing individual discrepancies as well as it enabled to position with high accuracy in difficult conditions, needed high cut-off elevation angles. Especially it is visible for using GLONASS + Galileo together in the second analysis period, for which for GLONASS achieved much worse accuracy, which was significantly improved when added Galileo satellites. However, for the GLONASS + Galileo achieved worse accuracy than for GPS but with a small standard deviation which may be due to a constant error (the problem of inter-frequency bias (IFB) and inter-system bias (ISB) modeling) and

also not available the PCO/PCV receiver models for Galileo observations. In multi-GNSS solutions in 2017, using the Galileo satellites did not affect accuracy but allowed to reduce the convergence time. In 2018 and 2019, it improved both accuracy and convergence, resulting in the greatest improvement in 2019. Also using all three systems together for the cut–off elevation angle of 40°, enabled to achieve about 90% availability of solutions with position estimation accuracy of cm. Based on this we showed that the Galileo had improved more with years but it was still worse than GPS and GLONASS. We can expected in the following years that the Galileo positioning will be of the same accuracy as others GNSS or even better.

Currently, the work is related to the development of own software and carrying out research related to weighting observations using GPS and Galileo systems. The conducted research will concern the already existing observation weighting functions and a new weighting function will be developed.

References

1. Araszkiewicz, A.; Kiliszek, D. Impact of Using GPS L2 Receiver Antenna Corrections for the Galileo E5a Frequency on Position Estimates. Sensors 2020, 20, 5536; DOI: 10.3390/s20195536.
2. Araszkiewicz A., Podkowa A., Kiliszek D., Height variation depending on the source of antenna phase centre corrections: LEIAR25.R3 case study, Sensors 2019, 19(18), 4010; DOI: 10.3390/s19184010.
3. Kiliszek, D.; Kroszczynski, K. Performance of the Precise Point Positioning method along with the development of GPS, GLONASS and Galileo systems. Measurement 2020, 164, 108009. DOI: 10.1016/j.measurement.2020.108009.
4. Mutke G., Kotyrba A., Lurka A., Olszewska D., Dykowski P., Borkowski A., Araszkiewicz A., Barański A.,Upper Silesian Geophysical Observation System A unit of the EPOS project, Journal of Sustainable Mining, Volume 18, Issue 4; DOI: 10.1016/j.jsm.2019.07.005.

1.8 Department of Planetary Geodesy, Space Research Centre Polish Academy of Sciences Nastula J., Śliwińska J.

Geophysical interpretation of polar motion excitation

The polar motion (PM) excitation series, namely atmospheric angular momentum (AAM), oceanic angular momentum (OAM), hydrological angular momentum (HAM) and cryospheric angular momentum (CAM) describe the impact of variations in mass redistribution of Earth surficial fluids on PM. In PM studies, the HAM and CAM are usually treated together and denoted as HAM/CAM to reflect the total effect of continental water, snow and ice. The role of AAM and OAM variability in PM excitation is well established, but the impact of HAM/CAM is the main source of uncertainties in PM budget. The HAM/CAM series can be obtained from observations of temporal variations in the gravity field, provided by the Gravity Recovery and Climate Experiment (GRACE) and GRACE Follow-On (GRACE-FO) missions. A common method to validate HAM/CAM series is to compare them with hydrological plus cryospheric signal in observed PM excitation, obtained after removing atmospheric and oceanic signals from geodetic excitation. Such reference series are denoted as geodetic residuals and abbreviated as GAO.

In 2020, we continued our research into: 1) evaluation of HAM/CAM from different GRACE solutions for various spectral bands, and 2) first determination of HAM/CAM from observations of the new GRACE Follow-On mission

In the first task, we computed HAM/CAM from various temporal GRACE solutions processed by different data centres, namely GeoForschungsZentrum (GFZ), Center for Space Research (CSR), Jet Propulsion Laboratory (JPL), Institute of Theoretical Geodesy and Satellite Geodesy (ITSG) of the Graz University of Technology, and the Centre National d'Etudes Spatiales (CNES). We also considered HAM/CAM obtained from a combination of GRACE with

Satellite Laser Ranging (SLR) data, and HAM based on hydrological model LSDM (Land Surface Discharge Model) corrected with sea-level angular momentum (SLAM). The series were then validated using GAO. The analyses were performed for trends, seasonal and non-seasonal changes, with a particular focus on the spectral bands with periods of 1000–3000, 450–1000, 100–450, and 60–100 days (Fig. 1.21). The oscillations in HAM/CAM were also analysed for different time periods characterized by different accuracy of the GRACE measurements. We noted that the level of agreement between HAM/CAM and GAO depended on the oscillation considered and was highest for interannual changes with periods of 1000–3000 days. Moreover, the consistency between HAM/CAM and GAO varied between periods and was the highest in 2006–2014. We also showed that HAM/CAM based on CSR RL06, ITSG 2018 and CNES RL04 GRACE solutions were in best agreement with GAO for most of the oscillations investigated.

In the second study, HAM/CAM series were determined for the first time from the observations of the new GRACE-FO mission (Fig. 1.22). The calculations used data from the first two years of the satellites operation. Those determinations were then compared with the HAM/CAM series obtained from the GRACE data from several selected two-year periods of its activity. Both GRACE- and GRACE-FO-based HAM/CAM were computed using two kinds of gravimetric data, namely C_{21}, S_{21} coefficients of geopotential called GSM, and terrestrial water storage (TWS) maps. HAM/CAM time series obtained from the GRACE and GRACE-FO were validated by comparison with GAO. Analysis of data from the first 19 months of GRACE-FO showed that the consistency between GRACE-FO-based HAM/CAM and GAO is similar to the consistency obtained for the initial period of the GRACE mission, worse than the consistency received for the best GRACE period, and higher than the consistency obtained for the terminal phase of the GRACE mission. However, this accuracy is expected to increase in the following months.

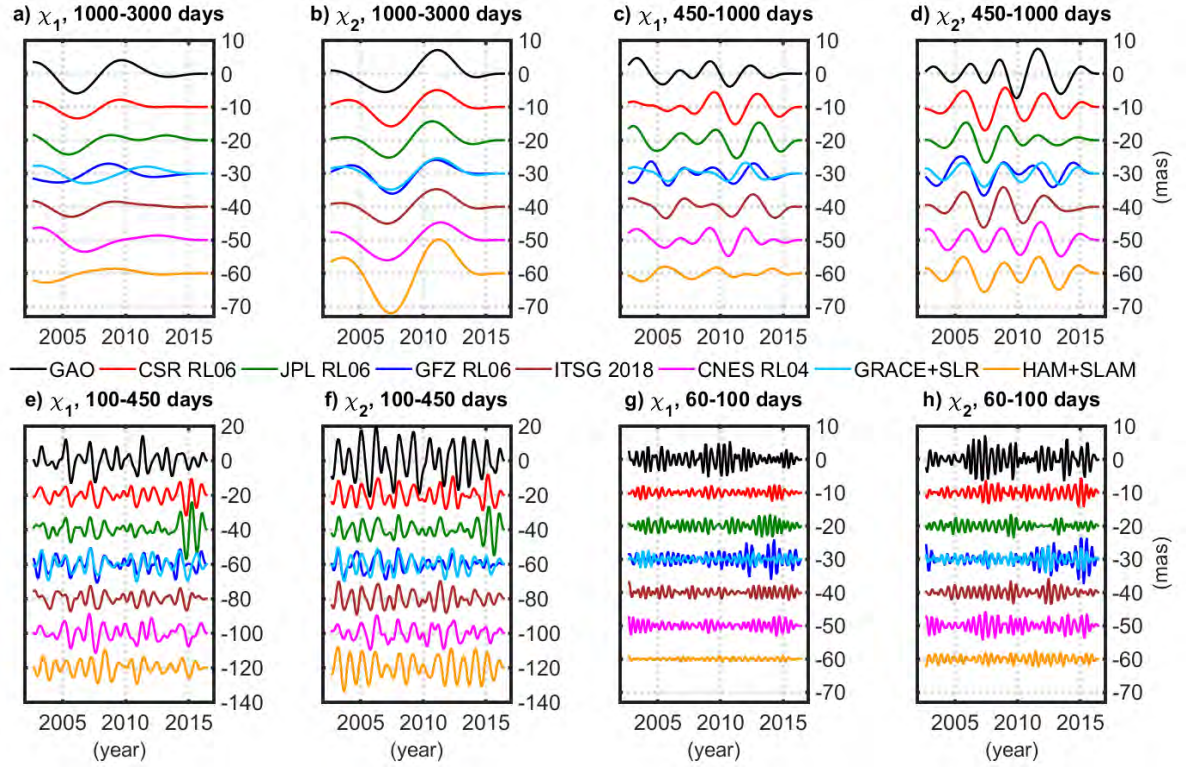

Fig. 1.21. Changes with the periods of 1000–4000 (a, b), 450–1000 (c, d), 100–450 (e, f), and 60–100 (g, h) days in χ_1 and χ_2 components of GAO, GRACE-based HAM/CAM (CSR RL06, JPL RL06, GFZ RL06, ITSG 2018, CNES RL04), GRACE+SLR combination, and HAM corrected with SLAM (HAM+SLAM) (Śliwińska et al. 2020a)

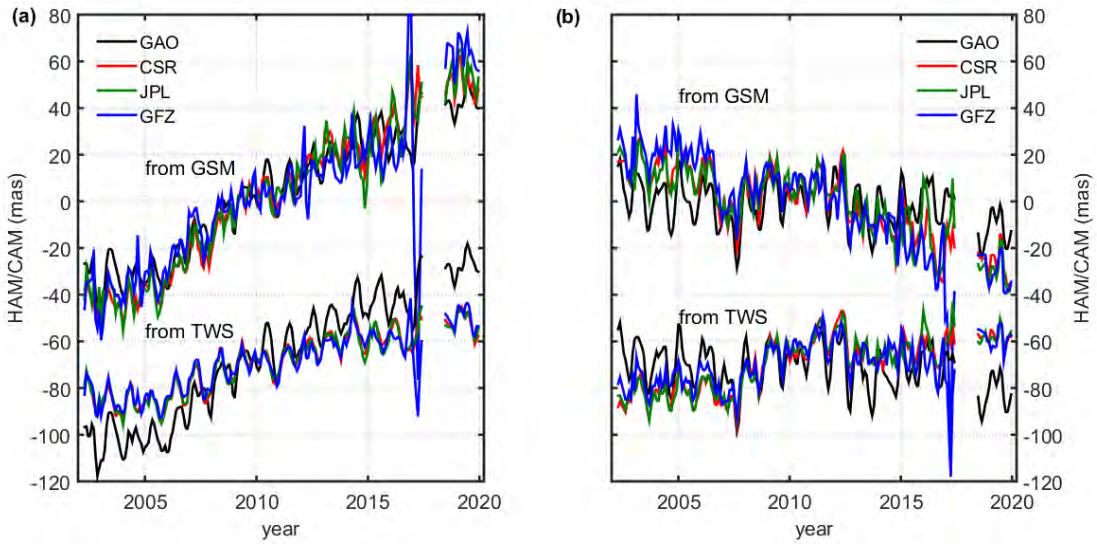

Fig. 1.22. Time series of χ_1 (a) and χ_2 (b) components of HAM/CAM) computed from the GRACE and GRACE-FO monthly solutions provided by CSR, JPL and GFZ. HAM/CAM are computed from GSM and TWS data. Time series for GAO are added for comparison. The offset value between GSM-based HAM/CAM and TWS-based HAM/CAM time series, used for better data visibility, is 70 mas (Śliwińska et al. 2020b)

Predicting celestial pole offsets (CPOs)

The Earth Orientation Parameters (EOP), which are pole coordinates, length-of-day variations and coordinates of the celestial pole (celestial pole offsets, CPO), are essential in precise positioning and navigation. To obtain the highest possible accuracy of objects position, variations in the EOP should be delivered in real time. However, due to delays caused by data processing and complex computations, EOPs are available with some delays. Consequently, accurate predictions of the EOPs are needed.

With the cooperation with scientists from the Jet Propulsion Laboratory (JPL), we used a Kalman filter and smoother to perform CPOs predictions. The prognoses were then compared with the predictions provided by the International Earth Rotation and Reference Systems Service (IERS). We also conducted an evaluation of predictions determined, which was carried out based on a comparison with geodetic observations. The results showed that our approach can be used for the successful CPO prediction. In particular, we show that after 90 days of prediction, the estimated errors are 43% lower for dX and 33% lower for dY than in the case of the official IERS products, and an average improvement is 19% and 22% for dX and dY, respectively (Fig. 1.23).

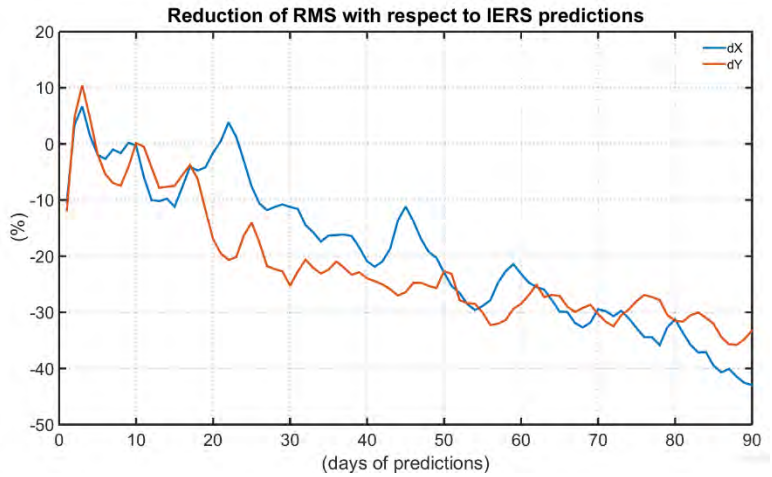

Fig. 1.23. Reduction of the RMS errors of JPL predictions, expressed in percentage with respect to the RMS of IERS predictions for dX and dY. A negative value for the percent RMS reduction means that the JPL predictions are more accurate than the IERS predictions (Nastula et al. 2020)

Geodetic SAR for Height System Unification and Sea Level Research

Traditionally, sea level is observed at tide gauge stations, which usually also serve as height reference stations for national leveling networks and therefore define a height system of a country. One of the main deficiencies to use tide gauge data for geodetic sea level research and height systems unification is that only a few stations are connected to the geometric network of a country by operating permanent GNSS receivers next to the tide gauge. As a new observation technique, absolute positioning by SAR using active transponders on ground can fill this gap by systematically observing time series of geometric heights at tide gauge stations (Fig. 1.24). By additionally knowing the tide gauge geoid heights in a global height reference frame, one can finally obtain absolute sea level heights at each tide gauge. With this information the impact of climate change on the sea level can be quantified in an absolute manner and height systems can be connected across the oceans. We applied the geodetic SAR technique at selected tide gauges at the Baltic coasts. The first results are promising, but also exhibit some problems related to the new technique.

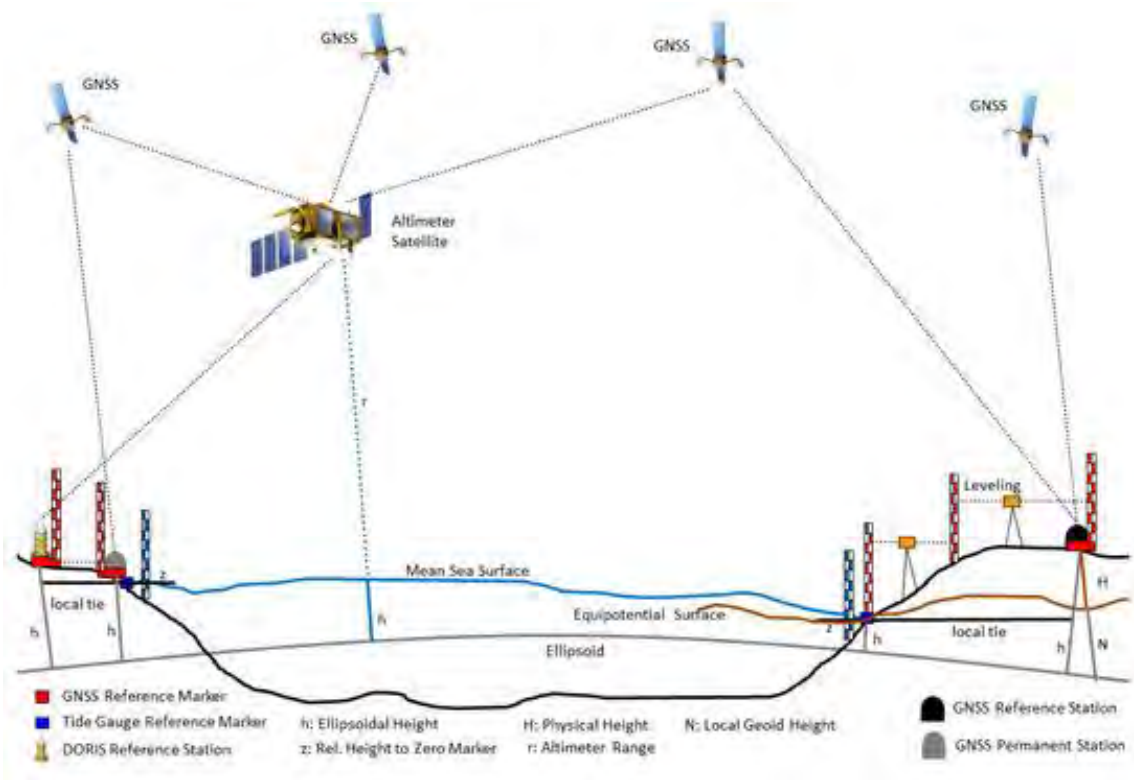

Fig. 1.24. Concept of Geodetic SAR for ellipsoidal height determination (Gruber et al. 2020) (Gruber, T., Ågren, J., Angermann, D., Ellmann, A., Engfeldt, A., Gisinger, C., Jaworski, L., Marila, S., Nastula, J., Nilfouroushan, F., Oikonomidou, X., Poutanen, M., Saari, T., Schlaak, M., Świątek, A., Varbla, S., & Zdunek, R…)

References

1. Gruber, T., Ågren, J., Angermann, D., Ellmann, A., Engfeldt, A., Gisinger, C., Jaworski, L., Marila, S., Nastula, J., Nilfouroushan, F., Oikonomidou, X., Poutanen, M., Saari, T., Schlaak, M., Świątek, A., Varbla, S., & Zdunek, R. (2020). Geodetic sar for height system unification and sea level research—observation concept and preliminary results in the Baltic sea. Remote Sensing, 12(22), 1–29. https://doi.org/10.3390/rs12223747
2. Nastula, J., Chin, T. M., Gross, R., Śliwińska, J., & Wińska, M. (2020). Smoothing and predicting celestial pole offsets using a Kalman filter and smoother. Journal of Geodesy, 94(3). https://doi.org/10.1007/s00190-020-01349-9
3. Śliwińska, J., Nastula, J., Dobslaw, H., & Dill, R. (2020a). Evaluating gravimetric polar motion excitation estimates from the RL06 GRACE

monthly-mean gravity field models. Remote Sensing, 12(6), 1–29. https://doi.org/10.3390/rs12060930

4. Śliwińska, J., Wińska, M., & Nastula, J. (2020b). Preliminary estimation and validation of polar motion excitation from different types of the grace and grace follow-on missions data. Remote Sensing, 12(21), 1–28. https://doi.org/10.3390/rs12213490

Geophysical excitation of the Chandler wobble – research using the GRACE data Brzeziński A., Nastula J.

Chandler wobble (CW) is a free motion of the Earth's pole which is the largest component of polar motion. It has been observed on regular basis since the end of XIX century. The observations show that its amplitude is changing but there is no clear decaying tendency. Therefore it must exist a process or a combination of processes which excite this oscillation against the energy dissipation. A search for the physical mechanism which excites this free polar motion to the observed level has been for decades one of the most intriguing questions regarding global dynamics of the Earth.

In this study we took an advantage of the fact that the mass term of polar motion excitation components (χ_1, χ_2) is proportional to time variable gravity coefficients ($C_{2,1}$, $S_{2,1}$) which are estimated from Gravity Recovery and Climate Experiment (GRACE) and the Satellite Laser Ranging (SLR) observations. Our purpose was 1) to estimate the Chandler wobble excitation by the mass redistributions of the external geophysical fluids using GRACE and SLR gravity data, and 2) to consider also the role of the motion term in the Chandler wobble excitation balance by using the data from geophysical models.

Analysis has been done over the 11-year period 2003.0 to 2014.0 with the highest quality GRACE data. From this analysis we could conclude what follows:

cross-correlation analysis of the de-seasoned and de-trended geodetic and geophysical excitations:

- better agreement was found for - χ2, corresponding to S2,1, than for - χ1 corresponding to C2,1;
- the best result found – correlations 0.7, 0.8 and variance reduction 50%,65%, for χ1, χ-2, respectively – was for the GRACE-derived series Center for Space Research, Austin, U.S.A,Tongji University, P.R. China ; and GNSS Research Center of Wuhan University, P.R. China,
- adding the motion term of excitation, estimated from geophysical models, improves the agreement with geodetic series to the considerably high level – correlations 0.8, 0.9 and variance re-duction about 60%,80% for χ1, χ-2;

narrow-band correlation analysis at the Chandler frequency:

- we found a high coherence and a good agreement of power at the Chandler frequency bet-ween the geodetic excitation and the three selected GRACE-based functions representing the mass term of excitation;
- adding the motion term of excitation improves slightly the coherence and the excitation power becomes higher than expected from the geodetic observations of polar motion.

Study of radon 222Rn activity changes in context of the tectonic activity of the **Świebo**dzice Depression orogen Kaczorowski M., Wronowski R., Zdunek R.

So far a lot of research has been devoted to using radon (222Rn nuclide in particular) as a natural radioactive indicator of the various geodynamic processes happening in the lithosphere (Fig. 1.25).

Due to its gaseous state and relatively low chemical reactivity with the environment, radon is widely used to characterize phenomena of gas exchange between the lithosphere and the atmosphere media. There have been attempts to apply variations in 222Rn activity concentration in soil air, groundwater or other geofluids (e.g. crude oil, natural gas or CO2 stream) to characterize and predict earthquakes phenomena, volcanic eruptions or to recognizing active fault zones.

The Geodynamic Laboratory of SRC PAS is the only Polish and one of the few European laboratories suitable for investigation of the subtle geodynamic and geochemical phenomena in tectonic areas. Our laboratory was established in underground tunnels built in the Świebodzice Depression Unit. The Świebodzice Unit is specially intersected on account of dense network of faults, which separate single blocks as well as the neighboring geological units such as Intra-Sudetic Basin (the Struga Fault in the south), Sowie Range Gneissic Block (the Szczawienko Fault in the west), Fore-Sudetic Block (the Sudetic Marginal Fault in the east) and Kaczawa Metamorphic Complex in the north with complex system of faults.

Fig. 1.25. AlphaGUARD instrument measuring 222Rn activity concentration in the LG fault zone at Ksiaz. The right photo shows the hole drilled in the fault zone, from which the atmosphere is pumped into the ionization chamber of the AlphaGUARD device.

The Świebodzice Depression is filled with Lower Carboniferous and Upper Devonian deposits. Great part of the Świebodzice Depression is filled with sedimentary rocks including conglomerates composed of gneisses, migmatites and granites. These kinds of rocks are rich with iron hydroxides (magnetite and hematite) and uranium oxides. These minerals specially densely occurring in a nearby fault zone. Decay of radionuclides uranium and tor are the source of radon in atmosphere of underground corridors of laboratory. Because density of monatomic radon gas is 9.73 [kg/m3] (about 8 times heavier than density of Earth's atmosphere), the mobility of radon molecules is much more difficult than mobility of molecules of the atmosphere.

Specially this problem appear in explanation of the mechanism of transportation of the heavy radon molecules from the rock crevice and faults. Because of short time (3.8224 days) of the half-life of the most stable isotopes 222Rn of radon the process of transportation ought to be enough fast.

As was empirically proofed that carbon dioxide CO2 plays important role in radon transportation from the crust into the atmosphere. Several hours before earthquakes on the Earth surface is observed increasing of carbon dioxide CO2 concentration simultaneously with increasing of radon activity. These phenomena are well known and reflected earthquake precursors. In the case of the Świebodzice Depression mechanism of carbon dioxide CO2 radon transportation is combined with states of the orogen kinematic activity i.e. variations of the phases of compression to the phases extension.

Permanent process of these transformations from compression to extension state as well as opposite produces effects of pump out gases from pore spaces and rock fissures to the fault zone and next to the atmosphere of underground tunnels.

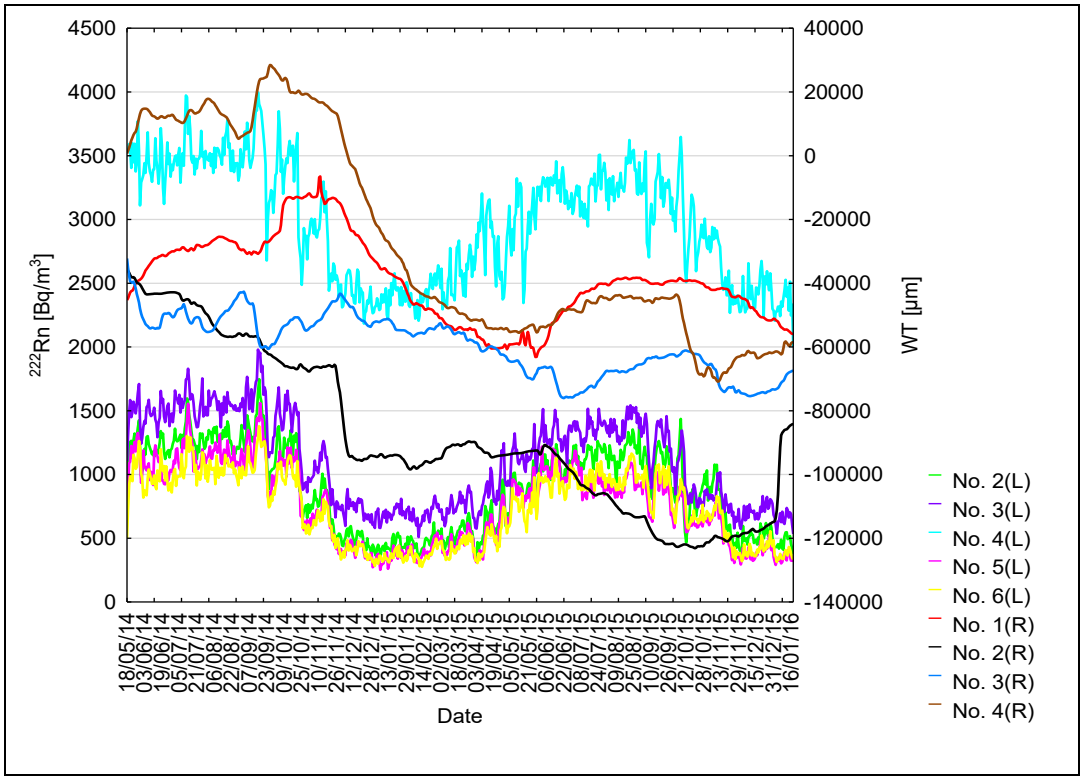

Fig. 1.26. Two years long series (18 May 2014 to 18 January 2016) of multi plots of four tectonic activity functions from WT tiltmeters and changes of 222Rn concentration registered this time by five SRDN-3 probes. Bq [one decay/sec] unit reflected number of decays in cubic meter per second.

Compression – extension sequences are determined on the basis of observations of kinematic activity of orogen. These observations are provided by two long water-tube tiltmeters working in Ksiaz laboratory. Plots of two years long series (18 May 2014 to 18 January 2016) of four tectonic activity functions from WT tiltmeters and changes of 222Rn concentration registered this time by five SRDN-3 probes were shown on the Fig. 1.26. We observed relationship between 222Rn activity concentration and variations of tectonic activity of the orogen registered by the water-tube tiltmeters.

The performed analyses of variations have demonstrated spatial character of changes in 222Rn activity concentration (Fig. 1.27). For all measure channels time-course of variations are very comparable in all parts of

the underground laboratory. This interesting result provides us two important conclusions. It means that gas migration between the lithosphere and the atmosphere occurs not only through fault zones but also through the all surfaces of the underground: the floors, the sidewalls and the roofs. High accordance between radon channels confirm the thesis of existence of the large scale homogeneous field of stresses which stimulate in the same manner kinematic activity of the whole Świebodzice Depression massif.

Problem of existence of a large-scale, well-approximated homogeneous field of tectonic forces was presented in the Report 2017 of SRC (pp. 102) and Report 2018 of SRC (pp. 92) in the context of the seismicity of the Fore-Sudetic Monocline, Upper Silesian and Czech Massif.

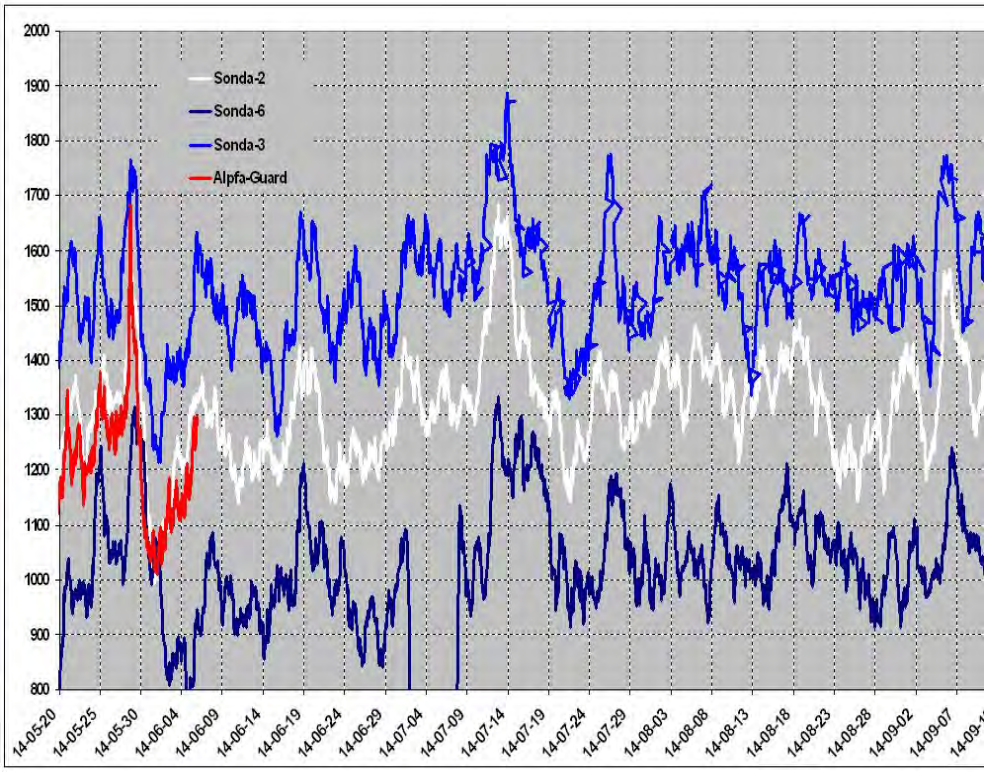

Fig. 1.27. Comparison of plots of variations of radon concentration registered by four gauges in the Ksiaz Laboratory from 17 May to 30 Jun 2014.

Accelerometers and Inter-Satellite Links in orbit determination Kalarus M., Kur T.

The Space Research Centre, PAS, after successful finalizing the GalAc project which aimed to analyse the feasibility and usefulness of equipping second-generation Galileo spacecraft with accelerometers to improve the accuracy of the Precise Orbit Determination, continue investigations on using new type of measurements in orbit determination (Fig. 1.28). Accelerometer data can be used to directly measure the unmodelled effects of nongravitational perturbations (NGP) and spacecraft acceleration due to on-board activity, as well as there is possibility to correct already existing empirical models. In parallel, analysis of the Inter-Satellite Link (ISL) was performed which can significantly enhance the orbital solution. The ISL provides precise range and range rate measurements (not affected by atmosphere) between satellites in specific constellation which is one of the key requirements for improving reliability of positioning and time transfer. It can also be a great contribution to on-board data processing and step towards autonomous GNSS constellations.

Special attention was paid to the analysis of the behaviour of the different constellation geometry (Galileo and GPS) aided with links between satellites in various conditions. Investigations included reduced number of ground stations, changeable accuracy of the Inter-Satellite Links and the total number of ISL measurements. Research indicates high improvement in accuracy of determined orbits as well as in estimated clocks. Final issue in case of combining GNSS and ISL measurements considers weighting methods is in the frame of the least squares approach. Variance Component Estimation was analysed in case of reducing influence of systematic errors on the orbit and clocks.

This research perfectly follows the Galileo evolution scheme proposed and realised by European Space Agency. It resulted in the development of the

original software package which combines recent theory, models and data to perform realistic simulations of GNSS satellites in orbit. It is also expected to update the core features of this software to pave the way for more advanced GNSS data processing especially near real-time analyses of the observation data and verification of the modern techniques that can potentially be used in the next generation positioning and navigation systems.

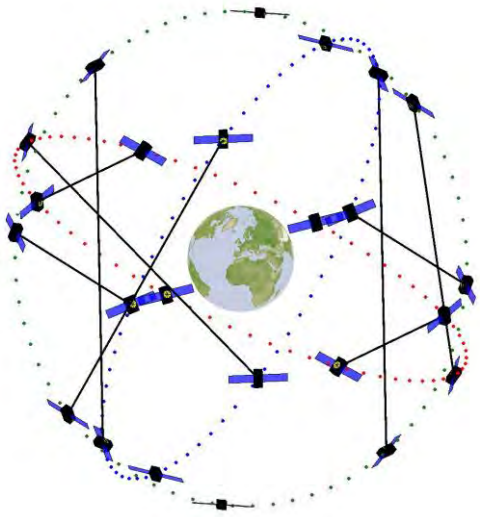

Fig. 1.28. Simulated Galileo constellation with Inter-Satellite Links.

References

1. Kur, T., Liwosz, T. & Kalarus, M. The application of inter-satellite links connectivity schemes in various satellite navigation systems for orbit and clock corrections determination: simulation study. Acta Geod Geophys (2020). https://doi.org/10.1007/s40328-020-00322-4

The Global Navigation Satellite System (GNSS) Observatory in Warsaw Jaworski L., Świątek A., Tomasik Ł., Pożoga M.

The observatory is involved in the following projects:

- the GALILEO global navigation system,
- positioning measurements and defining the national reference frame with GNSS technology,
- monitoring the quality of EGNOS corrections under the European GNSS Agency (GSA) grant - EGNOS Service Performance Monitoring Support (SPMS),
- Galileo Reference Centre – Member States.

Gallileo

In 2009, a new GESS+ (Galileo Experimental Sensor Station) was installed at the Space Research Centre. After few months of testing observed data quality, the station was included in the global monitoring network of GIOVE satellites.

Each week, ESA-ESTEC generates reports of the status of stations and observation data quality for GPS and Galileo signals. In the context of monitoring the Galileo system, the SRC is participating in the GSA project Galileo Reference Centre – Member States.

GNSS Permanent Station

Since February 2003, a permanent GPS station has operated in Warsaw, as part of the pilot project Active Geodetic Network for Poland (ASG-PL). From December 2007, that station has been included in the ASG–EUPOS project. In 2015 at the station a new GNSS Trimble NetR9 receiver was installed. Currently, the CBKA station also provides observational data for two projects awarded

by GSA and concerning quality and availability of EGNOS corrections monitoring and monitoring of the Galileo system.

The European Geostationary Navigation Overlay Service (EGNOS)

Space Research Centre in Warsaw is the location for a Ranging and Integrity Monitoring Station - the RIMS WRS station. This station is part of the EGNOS System, which is designed to broadcast correction signals in Europe for improving GPS In addition to the RIMS station, the Space Research Centre is cooperating with European institutions on research based on the EGNOS System. Specifically, it is participating in the EGNOS Service Monitoring Support project.

Monitoring of the quality of the GALILEO System

Space Research Centre since autumn 2018 is participating in GSA project Galileo Reference Centre-Member States. This project is designed to enable monitoring of the Galileo system by research institutes from EU countries, independent of the system manager. The main tasks are:

- computation of independent rapid and precise orbits for Galileo satellites,
- computation of independent ionospheric models for different world regions,
- computation and monitoring of Key Performance Indicators,
- computation and analysis of the NeQuick-G model, which is broadcasted as an ionosphere model in the Galileo navigation message.

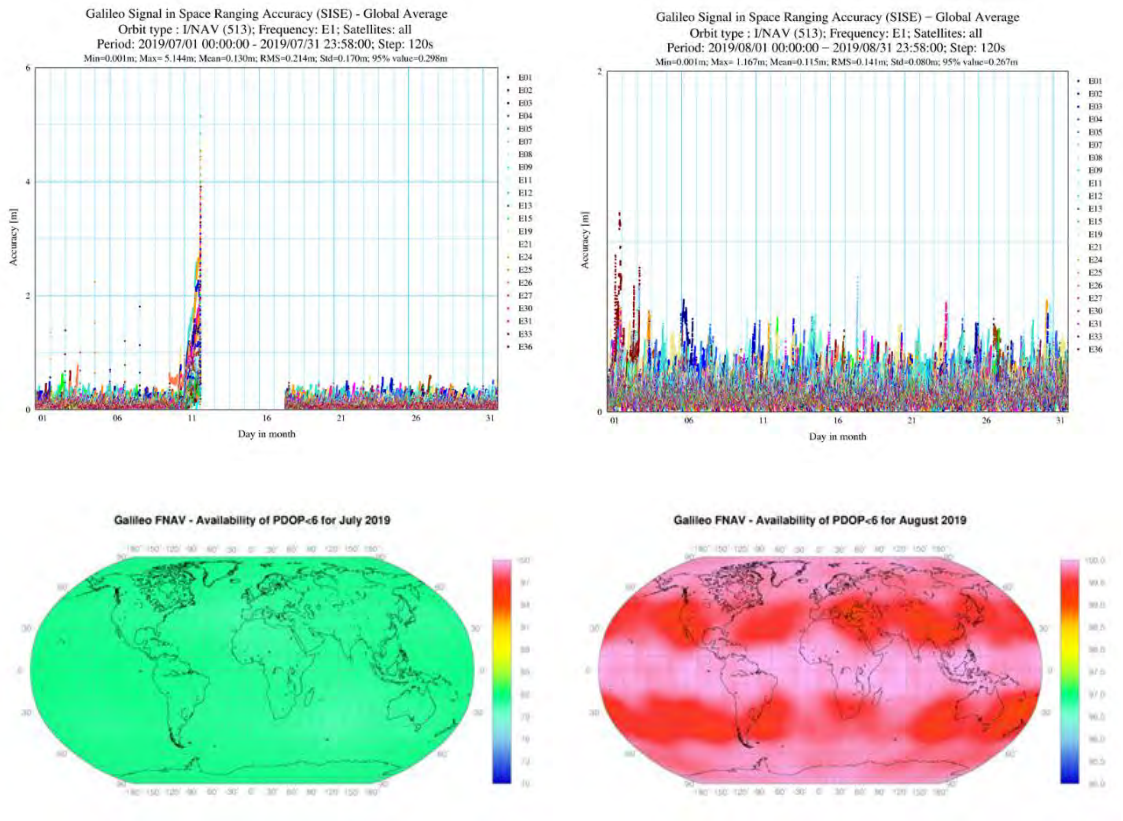

Fig. 1.29. Example of results from the analysis of the Galileo SISE and PDOP<6 for July and August 2019.

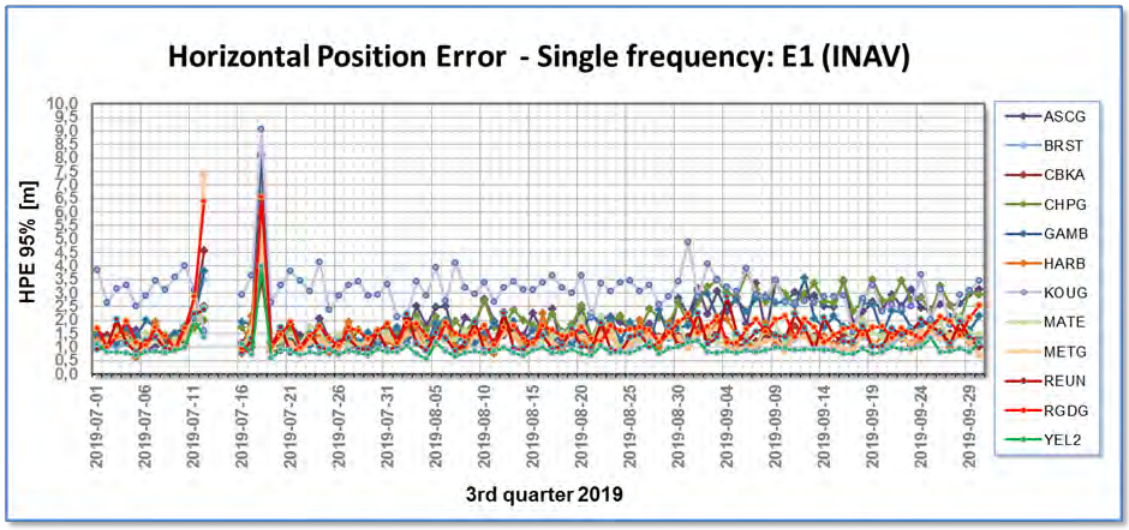

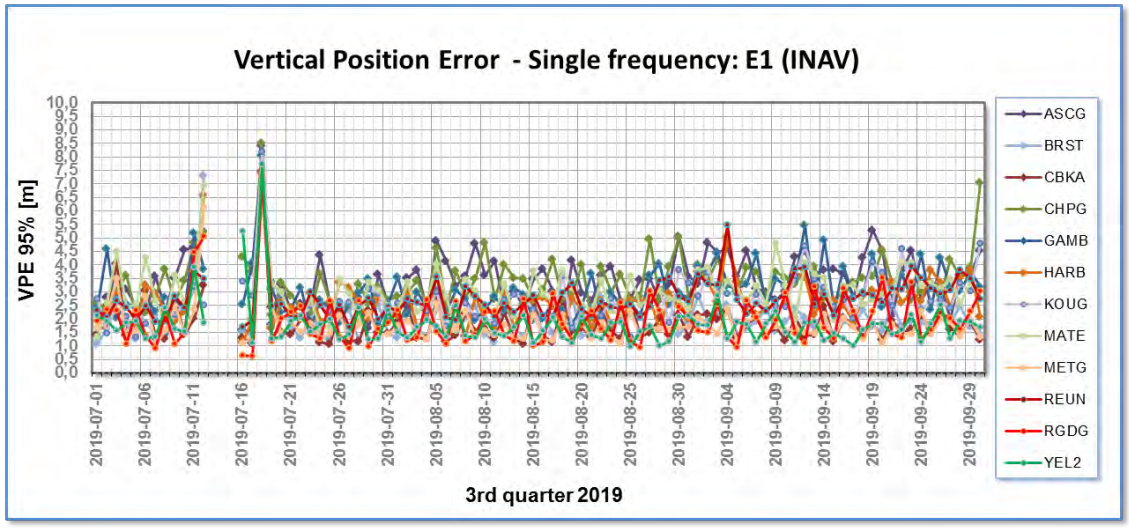

Fig. 1.30. Example of analysis results: a Horizontal and Vertical position error performed for E1 Galileo frequency over the third quarter of 2019.

Monitoring the quality of the EGNOS corrections

Space Research Centre is one of the partners in the consortium in GSA EGNOS Service Monitoring Support scheme. This project performs continuous monitoring of the availability, correctness, continuity and accuracy of the EGNOS-SIS (Signal in Space) and EGNOS-EDAS corrections. The project includes analysis and visualization of Key Performance Indicators (KPI) of the EGNOS system and a comparative analysis of EGNOS corrections transmitted directly by satellite and via the internet.

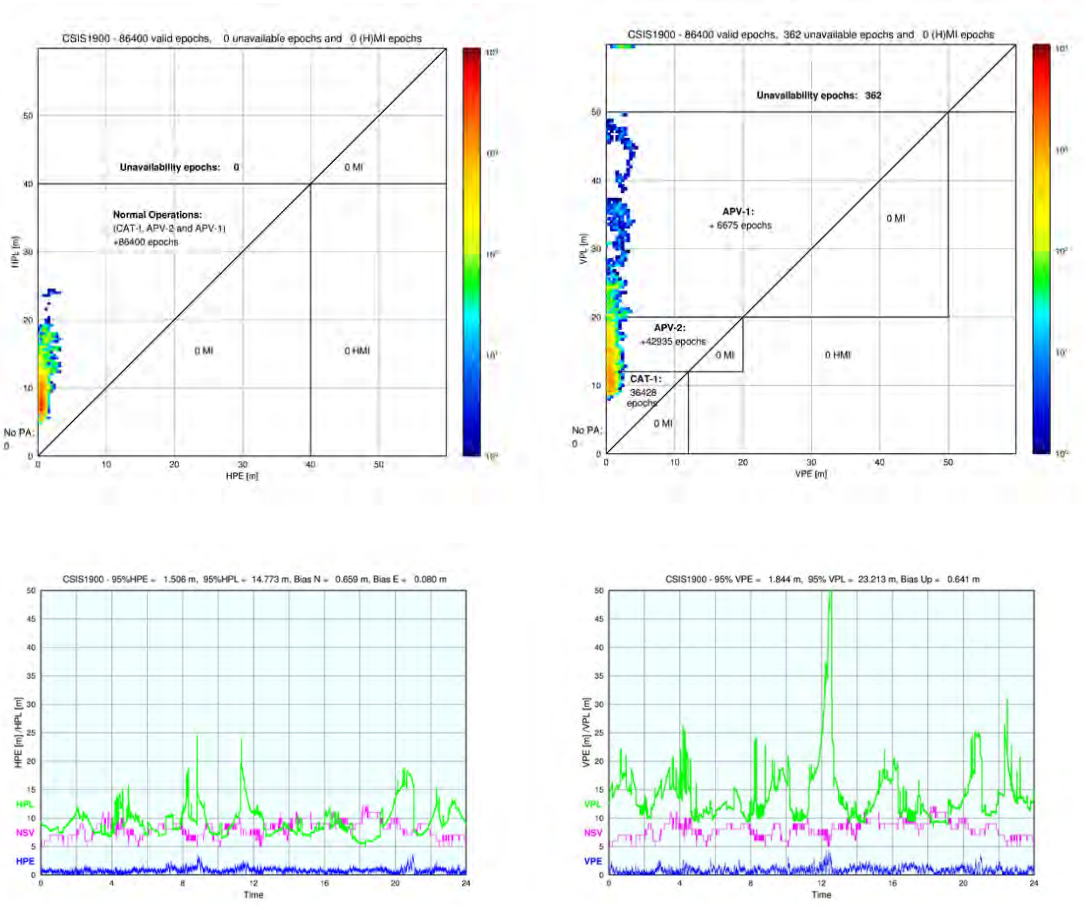

Fig. 1.31. Example of a visual analysis of the EGNOS Signal in Space corrections at the Warsaw site.

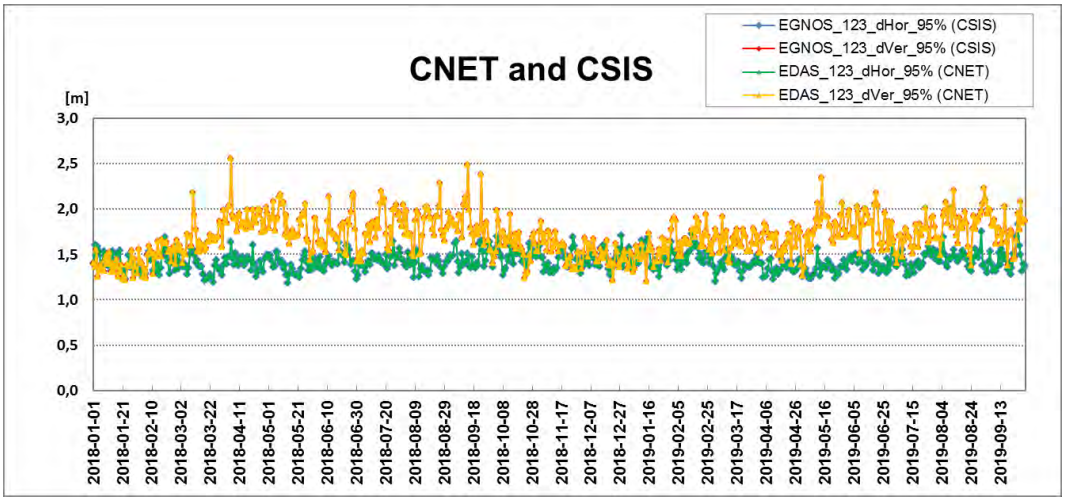

Fig. 1.32. Horizontal and Vertical Position Error in SIS and EDAS data over the last seven quarters.

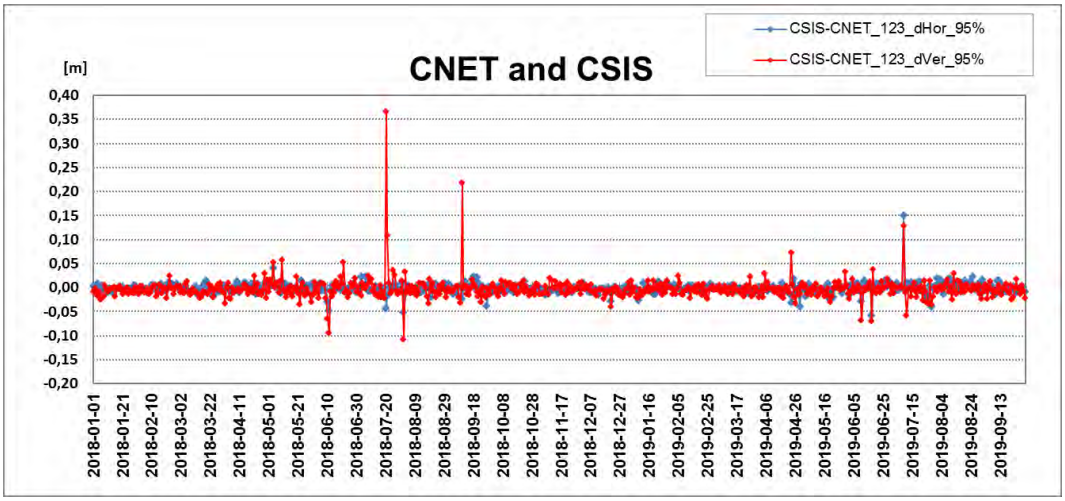

Fig. 1.33. Horizontal and Vertical position differences for SIS and EDAS data over the last seven quarters.

1.9 The Space Research Centre's Astrogeodynamical Observatory in Borowiec Michalek P. , Lejba P.

BOR1 GNSS station

In years 2018-2020, the long-term provision of Global Navigation Satellite System (GNSS) data from the BOR1 station, for national and worldwide scientific surveying was secured. This permanent GNSS station is located at the Centrum Badan Kosmicznych PAN Borowiec Observatory and, since 1996, it has been integrated into the International GNSS Service (IGS) and EUREF networks.

Data streams from the BOR1 station have been made available through IGS-IP and EUREF-IPprojects. High-quality data files make a valuable contribution to global geodesy and related research within the IGS framework. Data provided by BOR1 are used for precise orbit calculations by many international institutions, such as CODE (Central Orbit Determination Europe) at Bern, Switzerland, the GFZ-IGS Processing Centre in Germany, the JPL-IGS/ FLYNN Processing Centre at Pasadena, USA, the Massachusetts Institute of

Technology in the USA, the Scripts Institution of Oceanography in the USA, and the National Geodetic Survey in Canada. The BOR1 station is one of the reference stations within the multifunctional, precise satellite positioning system established by the Head Office of Geodesy and Cartography in Poland. All of the station's data are provided in two formats: RINEX 2.11 and RINEX 3.02. All data are gathered by a Trimble Dorne Margolin with choke ring antenna, which collects signals from GPS, GLONASS, GALILEO, BEIDOU, QZSS and SBAS systems.

Since 5 February 2015 the BOR1 station has been equipped with a multisystem Trimble NetR9 receiver. This multichannel (440 channel) receiver is capable of gathering signals simultaneously from GPS, GLONASS, GALILEO, BEIDOU, QZSS and SBAS constellations.

In 2020 the BOR1 stations worked without any failures. The number of lost epochs is 0 (Fig. 1.34).

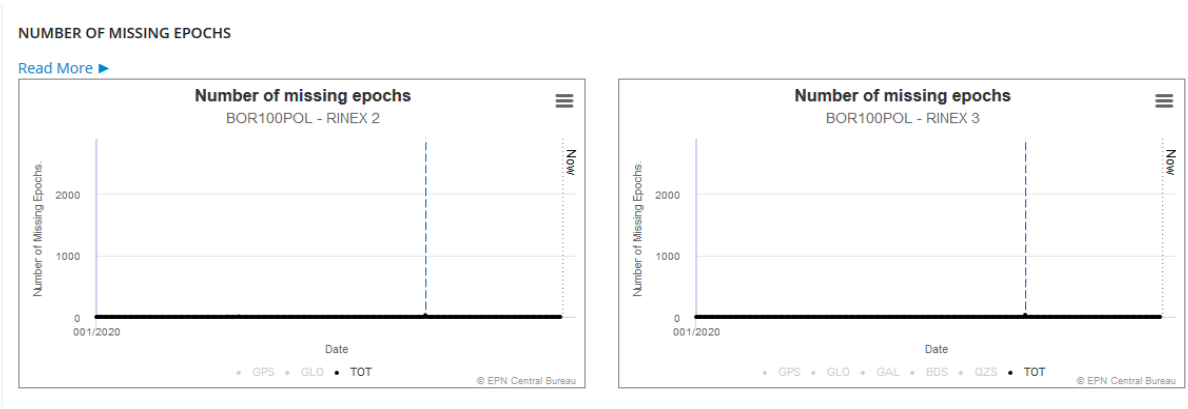

Fig. 1.34. The lost epochs in 2020. The dotted line points the update of the receiver's firmware.

After the update of the receiver's firmware, station has back to the tracking of Japanese QZSS constellation (Fig. 1.33).

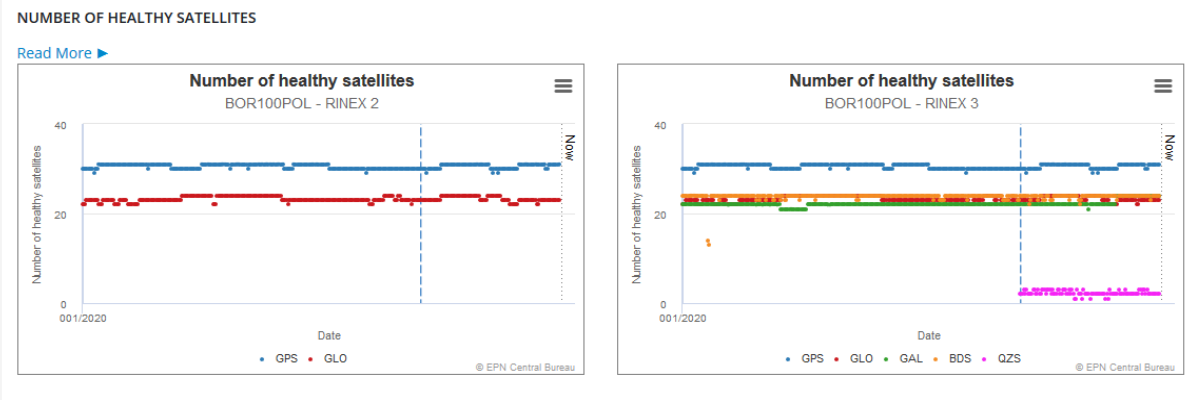

Fig. 1.35. The number of tracked satellites: GPS, GLONASS, GALILEO, BEIDOU and QZSS. The dotted line points the update of the receiver's firmware.

The BORL satellite laser ranging station in years 2018-2020

Because of pandemic situation related to the SARS-CoV-2 the 2020 was very difficult and very challenging. However, it was a successful year for the Space Research Centre's laser ranging station BORL7811. It tracked successfuly 97 different objects, satellites and space debris, with a total of 2050 full passes (Fig. 1.36). Forty were satellites, 27 were Low Earth Orbit (LEO), and 13 were Medium Earth Orbit objects giving 1352 passes, 18644 normal points and pass RMS from 1.49cm to 4.11cm. Fifty-seven objects were typical space debris, such as inactive (defunct) satellites and rocket bodies (boosters) from the LEO regime giving 698 passes, 7396 normal points and pass RMS from 1.42cm to 187.58cm. These targets were observed within the framework of the Space Debris Study Group, run by the International Laser Ranging Service (ILRS) under internal contracts signed with the European Space Agency (ESA) and the European Consortium EUSST (https://www.eusst.eu/).

A total of 698 space debris passes were performed. Information about the position and behaviour of space debris, such as defunct satellites, is very important from the point of view of future debris removal missions (e.g., ENVISAT) as the amount of space junk is increasing rapidly. Currently there are

more than 20000 objects in orbit with a diameter ≥ 10 cm. We need to know not only where all these objects are, but also precise information about their rotation/ tumbling and orientation in space. Laser measurements recorded by the BORL station support global research on the determination of space debris spin dynamics (ENVISAT, ERS-1, ERS-2, OICETS, SEASAT-1, TOPEX/ Poseidon and others), which is essential to improve theories of the movement of artificial satellites, including space debris. All of the station's results were sent to the Crustal Dynamics Data Information System (CDDIS), the EUROLAS Data Center (EDC) and Space Debris databanks.

Fig.1.36. Observational statistics of the passes recorded by the BORL station in 2020, including active satellites and space debris (green column – the highest number of passes).

Among the tracked satellites 12 were geodetic missions (AJISAI, ETALON-1, ETALON-2, Geo-IK-2, GRACE-FO-1, GRACE-FO-2, LAGEOS-1, LAGEOS-2, LARES, LARETS, STARLETTE and STELLA), which gave a total of 552 passes and 5745 normal points. Table 1.1 presents a summary of observational statistics of these satellites.

Table 1.1 Observational statistics for geodetic missions.

SATELLITE NAME	PASSES	RETURNS	NORMAL POINTS	AVG RMS [cm]
AJISAI	111	189595	1387	3.41
ETALON-1	0	0	0	0
ETALON-2	3	364	14	3.61
GEOIK-2	6	4705	38	2.22
GRACE-FO-1	21	10077	432	3.45
GRACE-FO-2	15	7731	350	3.19
LAGEOS-1	46	45220	423	1.73
LAGEOS-2	50	30870	388	1.78
LARES	104	36486	1004	1.51
LARETS	92	37412	713	1.98
STARLETTE	97	70903	931	2.02
STELLA	7	5109	65	2.02

From the typical geodynamic satellites, the highest number of passes (111), returns (189595) and normal points (1387) were obtained for AJISAI. Mean RMS from this group of objects ranged from 1.51cm (for LARES) to 3.61 (for ETALON-2).

The quality of the BORL laser sensor is regularly evaluated, based on tracking results for LAGEOS-1 and LAGEOS-2 satellites, in the form of a station performance report. As the results given in Figures 1.37 and 1.38 show, the BORL station has significantly improved the quality and effectiveness of its measurements compared to previous years.

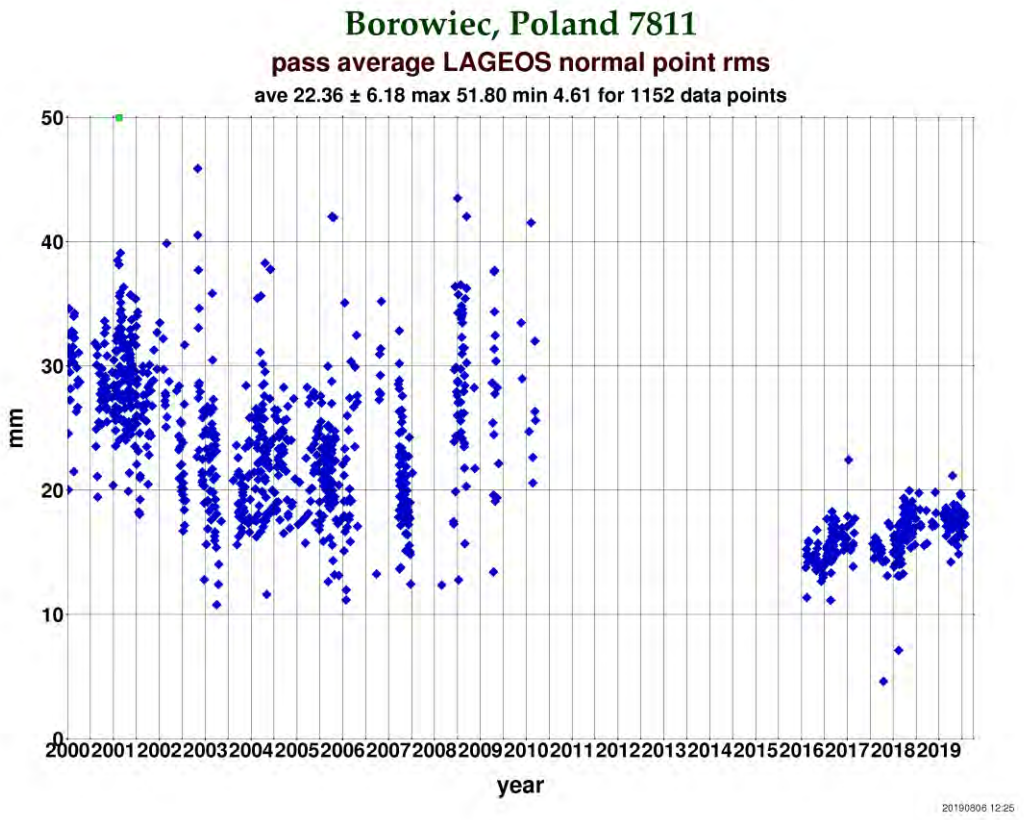

Fig. 1.37. LAGEOS normal point RMS from 2000 to 2020 for the BORL station (https://ilrs.cddis.eosdis.nasa.gov/network/stations/charts/BORL_LAG_NPT_RMS.png).

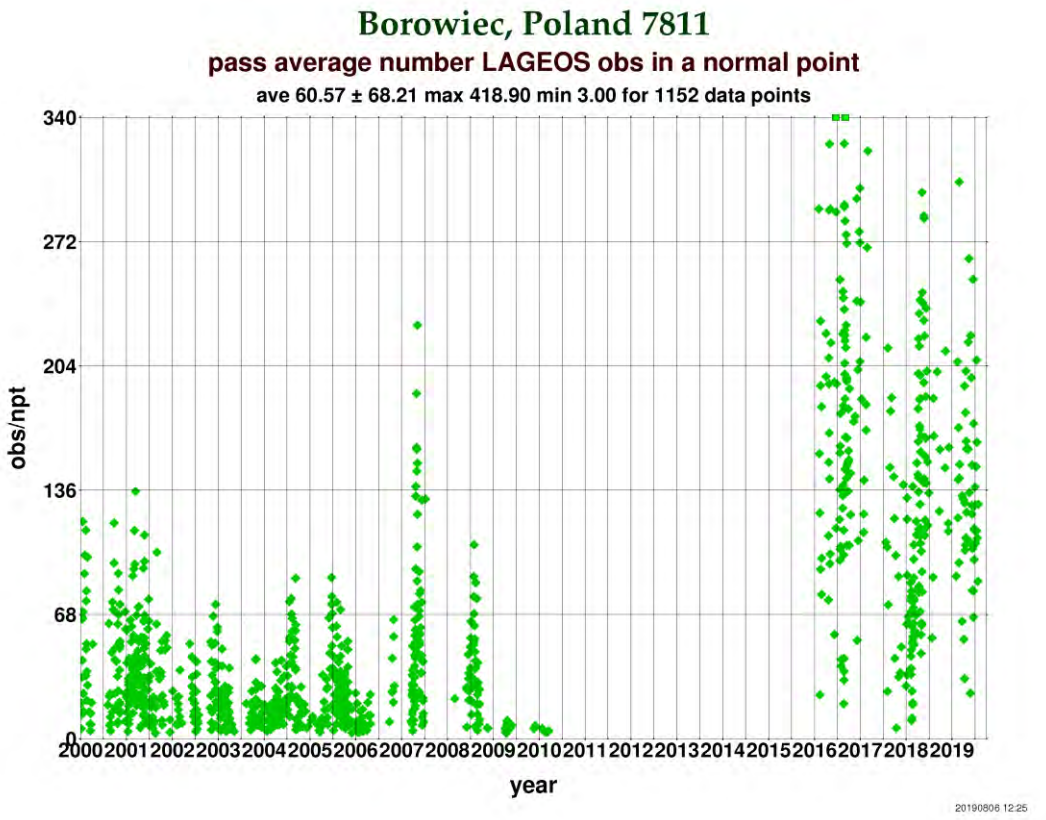

Fig. 1.38. LAGEOS normal point measurements from 2000 to 2020 for the BORL station (https://ilrs.cddis.eosdis.nasa.gov/network/stations/charts/BORL_LAGEOS_NPT_OBS.png).

One of the most important scientific achievement in 2020 was computation of the coordinates of BORL station based on LAGEOS measurements performed by ILRS network in years 2016-2019. The results are presented in the Table nr 1.2 below.

Table 1.2 Determination of the BORL's coordinates based on LAGEOS measurements (2016-2019).

PARAMETER	NP (L1+L2)	RMS (L1)	RMS (L2)	3D RMS	Distance from the ITRF2014 (3D)	Distance from the ITRF2014 (horizontal component)	Distance from the ITRF2014 (vertical component)
BORL 7811	5273	18.8mm	16.9mm	11.3 ± 4.7mm	15.9mm	6.4mm	14.5mm

Several parameters were computed: range biases (RB), orbital RMS, 3D-deviation, differences in reference to the ITRF2014. The gained results confirm high quality of the BORL station.

Another scientific work was to determine the station coordinates based on laser ranging measurements to LARES satellite for the period from February 29, 2012 to December 31, 2015 and to assess the quality of their determination by comparison with the results from the LAGEOS satellites. The average RMS (15.1 mm) of the determined orbits is the same as for LAGEOS satellites (15.2 mm). The station's 3DRMS coordinates range from 9 mm to 46 mm and are dependent on the position of the station (for LAGEOS satellites from 5 mm to 15 mm) with position uncertainty of 3-11 mm (LAGEOS 2-7 mm). The full results of this work will be available in Sensors journal (published by MDPI). The paper was submitted to Sensors on December 23, 2020 and is already (beginning of January 2021) after positive reviews.

Another important paper published in 2020, in which the BORL team was involved was a work of M. Jagoda, M. Rutkowska, P. Lejba, J. Katzer, R. Obuchovski, D. Šlikas, Satellite Laser Ranging for Retrieval of the Local Values of the Love h2 and Shida l2 Numbers for the Australian ILRS Stations, Sensors 2020, 20(23):6851, doi: 10.3390/s20236851, which presents the results of the analysis of local Love and Shida numbers (parameters h2 and l2) values of the

Australian Yarragadee and Mount Stromlo SLR stations. The research was conducted based on data from the STELLA, STARLETTE, LAGEOS-1 and LAGEOS-2 satellites. The data were taken for the period from January 1, 2014 to January 1, 2019. For the Yarragadee station, local h2=0.5756±0.0005 and l2=0.0751±0.0002 values were obtained from LAGEOS-1+LAGEOS-2 and h2=0.5742±0.0015 were obtained from STELLA+STARLETTE data. For the Mount Stromlo station, we obtained the local h2=0.5601±0.0006 and l2=0.0637±0.0003 values from LAGEOS-1+LAGEOS-2 and h2=0.5618±0.0017 from STELLA+STARLETTE.

The differences for all analyzed targets are given in RSW frame between used TLE (initial orbital elements) and performed observations of BORL station (corrected elements/positions). One short observations of rocket bodies from LEO regime from a dozen to several dozen seconds improve the covariance matrix by 20-40%.

In years 2018-2019, staff at the BORL station were involved in the following projects:

- The International Laser Ranging Service (ILRS) project, Special Mission Support, which is an observational campaign dedicated to SENTINEL-3A and SENTINEL-3B satellites. The CBK was an approved subcontractor and the project is ongoing. In 2018-2019, the BORL station collected 123 passes of SENTINEL-3A with 1930 normal points and 100 passes of SENTINEL-3B with 1550 normal points.
- The ESA project "WebPlan", within the framework of the Polish Industry Intensive Scheme. The CBK is an approved subcontractor. The project will be continued in 2020. The lider of the project is a polish company Sybilla Technologies.
- The ESA project "SST Sensor Data Acquisition". The CBK is an approved subcontractor. The BORL station is responsible for laser measurements of

cooperative and uncooperative targets. The project will be continued in 2020. The lider of the project is Airbus Defence and Space.

- The ESA project "LASER RANGING SYSTEMS EVOLUTION STUDY - LARAMOTIONS". The CBK is an approved subcontractor. The project will be continued in 2020. The lider of the project is a German Space Agency DLR.
- The observational contract within the EUSST coordinated by the Polish Space Agency. The contract is continued in 2020.

In years 2018-2019, the BORL station focused on the SST programme, which constitutes one of the pillars of the Space Situational Awareness (SSA) programme implemented by the ESA (Space Safety in the next years) and the EC (EUSST Consortium). The SST programme is dedicated to monitoring (observation, detection, identification) of active and inactive satellites, discarded launch stages and fragmentation debris orbiting Earth. The BORL station is responsible for research and development in satellite laser ranging. Poland is an official member of the EUSST Consortium, and the CBK is one of the members of the Polish SST consortium. In 2018, several events took place on the subject of laser/timing techniques, and the SSA/ SST programme, which BORL staff participated in. The most important were:

- February 23, 2018 – Users' workshop on SSA, at the Albert Borschette Conference Centre, Brussels, Belgium.
- July 3-4, 2018 – bilateral meeting at Borowiec with representatives of the DLR Institute of Technical Physics. The main topic of the meeting was related to Space Surveillance and Tracking activity.
- 5–9 November, 2018 – 21st International Workshop on Laser Ranging (International Workshop on Space Debris Management and Mitigation), Canberra, Australia, where a poster (Laser activity of the Borowiec laser station in years 2017-2018) was presented, and a presentation (Mission characterisation of LEO targets) was given by Dr Pawel Lejba, manager

of the Borowiec Observatory, and Head of the BORL station. The papers are available at http://www.iwlr2018.serc.org.au/#program.

In 2019, the BORL staff participated in ILRS Technical Workshop in Stuttgart (Germany), 21–25 October, where a talk "*CBK PAS Borowiec Second Satellite Tracking System*" has been presented. The presentation was given by Dr. Eng. Tomasz Suchodolski, a main engineer at BORL station, responsible for development of second independent optical-laser setup dedicated for SST/Space Safety (ESA) and SST (EUSST) programmes. The conference proceedings are available at

https://cddis.nasa.gov/2019_Technical_Workshop/Program/index.html.

In 2018, the results of the laser tracking of space debris carried out by the BORL station were published in the journal *Advances in Space Research*: Lejba P., Suchodolski T., Michałek P., Bartoszak J., Zapaśnik S., Schillak S., First laser measurements to space debris in Poland, Advances in Space Research, Vol. 61, Issue 10, pp. 2609–2616, DOI: doi:10.1016/j.asr.2018.02.033.

In 2019 another paper was published, titled: *Optical, Laser and Processing Capabilities of the New Polish Space Situational Awareness Centre*. The paper was published in the conference Proceedings of the Advanced Maui Optical and Space Surveillance Technologies Conference (AMOS) Conference, September 17-20, 2019 (https://amostech.com/2019-technical-papers/). In this paper, among others, the current situation of the BORL station was presented in the context of SST activity.

In 2020, staff at the BORL station were involved in the following projects:

- The International Laser Ranging Service (ILRS) project, Special Mission Support. This is an observational campaign dedicated to SENTINEL-3A and SENTINEL-3B satellites. The CBK was an approved subcontractor and the project is ongoing. In 2020, the BORL station collected 91 passes of

SENTINEL-3A with 1491 normal points, and 98 passes of SENTINEL-3B with 1486 normal points.

- Observational campaign of SENTINEL-6A with 11 passes and 175 normal points provided by BORL station. The satellite was launched on November 21, 2020.
- The European Space Agency's WebPlan project as a part of the framework of the Polish Industry Intensive Scheme. The CBK was an approved subcontractor. The project was closed in September 2020 and was led by the Polish company, Sybilla Technologies.
- The European Space Agency's project SST Sensor Data Acquisition. The CBK was an approved subcontractor. The BORL station was responsible for laser measurements of cooperative and uncooperative targets. The project has been finished in August 2020 and was led by Airbus Defence and Space.
- The European Space Agency project Laser Ranging Systems Evolution Study – Laramotions. The CBK is an approved subcontractor. The project is continuing in 2021 and it is led by the German Space Agency DLR.
- An observational contract (space debris tracking), within the EUSST, coordinated by the Polish Space Agency. The contract will continue into 2021.

Because of pandemic situation any conferences and meetings were cancelled, postponed, or limited to the online activity. The biggest SLR conference, 22nd International Workshop on Laser Ranging in Kunming (China) planed on November 6, 2020 was postponed to 2021.

BORL stuff participated in two online events:

- The Advanced Maui Optical and Space Surveillance Technologies Conference (AMOS), September 15-18, 2020, during which the poster Laser Ranging to Space Debris in Poland: Tracking and Orbit

Determination has been presented. This topic was published in the Proceedings of the conference available at https://amostech.com/2020-technical-papers/.

- ILRS Virtual World Tour 2020, November 2 -6, 2020, during which five ILRS stations could be seen.

References

1. Jagoda M., Rutkowska M., Lejba P., Katzer J., Obuchovski R., Šlikas D., Satellite Laser Ranging for Retrieval of the Local Values of the Love h2 and Shida l2 Numbers for the Australian ILRS Stations, Sensors 2020, 20(23):6851, doi: 10.3390/s20236851
2. Kaczorowski, M., Kasza, R. Zdunek, R., Wronowski, R. (2018). Application of observations of recent tectonic activity in the Świebodzice Depression (the Sudetes, SW Poland) in assessing seismic hazard in the Fore-Sudetic Monocline; E3S Web of Conferences Volume 55, Article number 00001, 23rd Autumn School of Geodesy, doi:10.1051/ e3sconf/20175500001.
3. Kasza, D., Kowalski, A., Wojewoda, J., Kaczorowski, M. (2018). Indicators of recent geodynamic activity in the Książ Castle area (Świebodzice Unit, Sudetes) in the light of structural analysis and geodetic measurements; E3S Web of Conferences Volume 29, Article number 00021, doi:10.1051/ e3sconf/20182900021
4. Lejba P., Suchodolski T., Michałek P., Laser Ranging to Space Debris in Poland: Tracking and Orbit Determination, the Proceedings of the Advanced Maui Optical and Space Surveillance Technologies Conference (AMOS), September 15-18, 2020, https://amostech.com/2020-technical-papers/
5. Nastula, J., Śliwińska, J. (2020). Prograde and Retrograde Terms of Gravimetric Polar Motion Excitation Estimates from the GRACE Monthly Gravity Field Models. Remote Sensing, 12(1), 1–29. doi:10.3390/rs12010138
6. Nastula, J., Wińska, M., Śliwińska, J., Salstein, D. (2019). Hydrological signals in polar motion excitation – Evidence after fifteen years of the GRACE mission. Journal of Geodynamics, 124, 119–132. doi:10.1016/j.jog.2019.01.014
7. Przylibski, T.A, Kaczorowski, M., Fijałkowska-Licha, L., Kasza, D., Zdunek, R., Wronowski, R. (2019). Testing of 222Rn application for recognizing

tectonic events observed on water-tube tiltmeters in underground Geodynamic Laboratory of Space Research Centre at Książ (the Sudetes, SW Poland), Applied Radtion and Isotopes, doi:10.1016/j.apradiso.2019.108967
8. Śliwińska, J., Nastula, J. (2019). Determining and Evaluating the Hydrological Signal in Polar Motion Excitation from Gravity Field Models Obtained from Kinematic Orbits of LEO Satellites. Remote Sensing, 11(15), 1–19. doi:10.3390/rs11151784
9. Śliwińska, J., Birylo, M., Rzepecka, Z., Nastula, J. (2019). Analysis of Groundwater and Total Water Storage Changes in Poland Using GRACE Observations, In-situ Data , and Various Assimilation and Climate Models. Remote Sensing, 11(24), 1–42. doi:10.3390/rs11242949
10. Śliwińska, J., Wińska, M., Nastula, J. (2019). Terrestrial water storage variations and their effect on polar motion. Acta Geophysica, 67(1), 17–39. doi:10.1007/s11600-018-0227-x
11. Schillak S., Lejba P., Michałek P., Analysis of quality of SLR station coordinates determined from laser ranging to the LARES satellite, Sensors 2020 (under review).
12. Wińska, M., Śliwińska, J. (2019). Assessing hydrological signal in polar motion from observations and geophysical models. Studia Geophysica et Geodaetica, 63(1), 95–117. doi:10.1007/s11200-018-1028-z
13. Zdunek, R., Kaczorowski, M., R. Wronowski, R., Kasza, D.; (2018). Relations Between Distribution of Extension and Compressions Phases of Świebodzice Depression Massif Registered by Water-Tube Tiltmeters With Southern Fault Wings Movements Observed On GPS Vector; Abstracts of the 19th Chech-Polish Workshop "On Recent Geodynamics Of Central Europe", 27-28, 2018

1.10 Central Office of Measures (GUM) Gruszczyński M., Czubla A., Wiśniewski M.

Central Office of Measures (GUM), as a National Metrology Institute (NMI) of Poland, acts in metrology domain by carrying out many activities for ensuring the conformity and accuracy of the national measurements standards and their traceability to the International System of Units (SI),

dissemination of the values of the legal units of measurement from the national measurement standards to measuring instruments and development of measurement technologies – in order to support the contemporary needs of science, innovation technology and trade as well as health care and natural environment. Standards, maintained by GUM, are the reference for measurements performed at each stage of production and in-use of products. Development of advanced measurement technologies and instruments, as well as ubiquitous innovation in the field of modern metrology are the reason for the implementation scientific and research projects in GUM. Some of these works relate to satellite geodesy and space technologies.

GUM is responsible, among others, for generation of the official Polish timescale UTC(PL). Active areas of research in these field include precise time and frequency transfer via satellite and optical fibre links. Research in the field of on high-accuracy GNSS-based distance metrology contribute to a better understanding of critical points within what is a complex traceability chain in geodetic reference frames realizations.

GeoMetre - Large-scale dimensional measurements for geodesy

GeoMetre is a project started in June 2019, carried out by GUM acting as a member of European NMI's consortium under the European Metrology Programme for Innovation and Research (EMPIR). GeoMetre project is developing transfer standards to disseminate to the SI metre reference baseline distances of at least 5 m to 1 mm uncertainty and develop novel devices capable of 3-D measurements over a 200 m range with 200 micron uncertainty. The primary impact target of this project is a substantial contribution to an improved ITRF solution.

Fig. 1.39. Measurement at geodetic reference baseline [photo: M Wiśniewski, GUM].

GUM established a new dedicated 200 m reference baseline in collaboration with Warsaw University of Technology. Baseline calibrated and verified (using GNSS techniques) within the upcoming actions in the project, will be an optimum reference for the calibration and verification of novel instrumentation in this project and other commercial distance meters of medium range.

Time and frequency optical fiber network related activities

GUM is actively involved in studies on precise time and frequency transfer over satellite and optical fiber links in Poland. Time and Frequency Laboratory of GUM is connected via optical fibers links (OPTIME network) with two Polish cesium fountains located in Poznań (PSNC – Poznań Supercomputing and Networking Center) and Borowiec (AOS – Astrogeodynamical Observatory of Space Research Center PAS) and with two independently operating Sr^{88} lattice clocks in Toruń (UMK – Nicolaus Copernicus University).

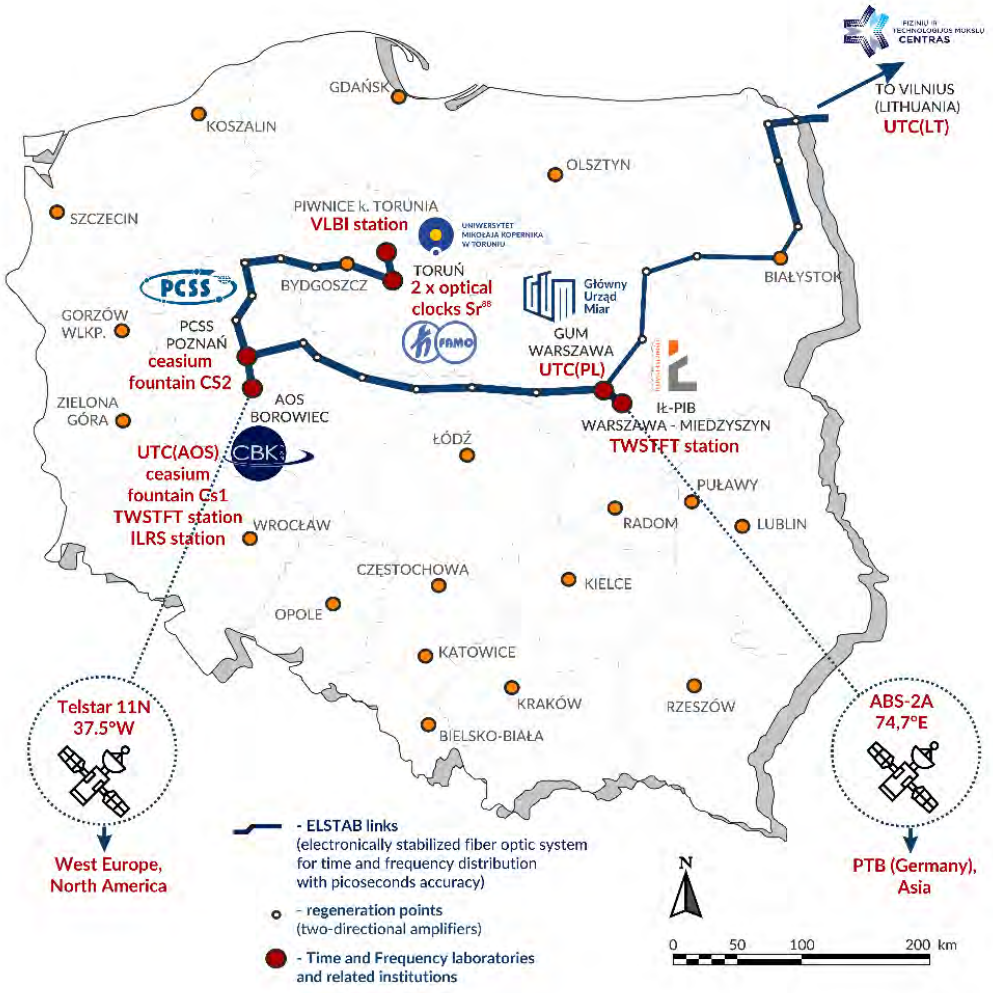

Fig. 1.40. Precise time and frequency signals generation and distribution infrastructure and its scientific use in Poland -OPTIME network [curtesy of PSNC - figure modified by GUM].

Since 2012, constantly operating over 420 km optical link with stabilization of propagation delay for T&F transfer between two UTC(k) laboratories: GUM and AOS, equipped with high performance atomic clocks, is a unique physical testbed for verification of short- and long-term stability of GNSS time transfer methods like GNSS All-in-View, GPS PPP, integer-PPP. These infrastructure supports development and investigation of satellite time transfer methods within the sub-nanosecond range. In 2018, there was proved experimentally (between GUM and AOS) that it is possible to use the remote active hydrogen

maser over the fiber link as a fly-wheel of cesium fountains. In 2019, GUM together with two Polish institutes: AOS and UMK launched the ROCIT project (Robust Optical Clocks for International Timescales) within EMPIR, where GUM investigates algorithms of steering local UTC(k) timescale to optical clocks accessed directly and remotely.

The polish T&F infrastructure includes also two, connected by a stabilized optical fiber link, Two-Way Satellite Time and Frequency Transfer (TWSTFT) stations: first one operated in Warszawa-Miedzeszyn by National Institute of Telecommunication (NIT) with cooperation of GUM for Europe-Asia comparisons (the ABS-2A geostationary satellite), while the second one operated in Borowiec near Poznań by AOS for West Europe and North America comparisons (the Telstar satellite). There are performed investigation to use this infrastructure as a bridge for international comparisons of timescales between Asia, West Europe and North America.

GNSS receiver performance monitoring is an EURAMET project of Technical Committee for Time and Frequency initiated and coordinated by GUM. The project is ongoing from 2012 and includes tests of GNSS receivers designed for T&F laboratories for the precise time transfer. A differential verification of short-term and seasonal changes of calibration constants of GNSS receivers are performed, including variation due to changes of delays of different parts of equipment. The applied method is based on collection and analysis of measurement data taken from pairs of GPS receivers working with the same local reference timescale.

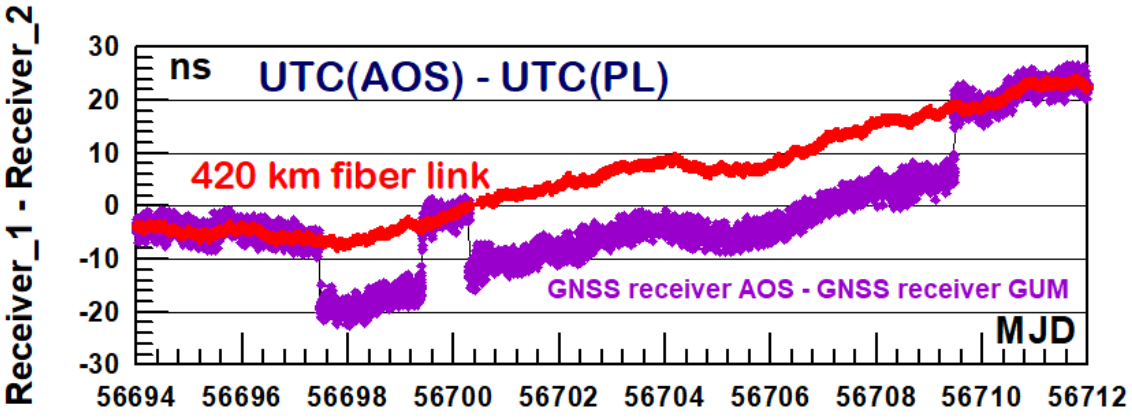

Fig. 1.41. Differences between two time transfer GNSS receivers during air-conditioning break in one-site laboratory.

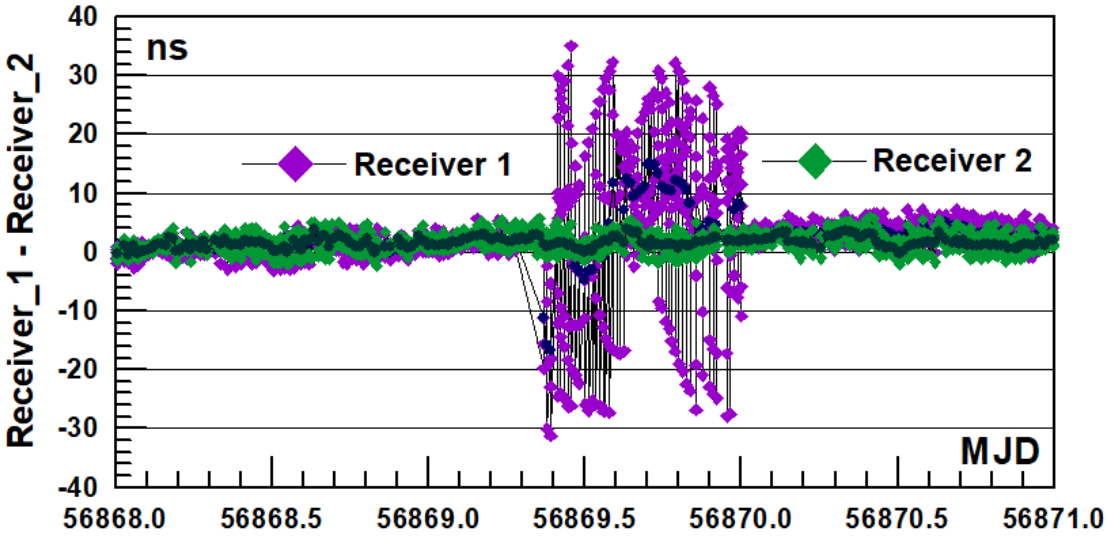

Fig. 1.42. Differences between two time transfer GNSS receivers directly after upgrading software of the receiver 1.

Analysis of the current and historical data obtained from GNSS receivers used for precise time transfer result in recognizing some special cases of abnormal behavior of the receivers. Some of them can be readily explained (e.g. as an effect of unexpected temperature influence, frequency phase shifting inside bad working frequency source, additional effect of upgrade firmware/ software, ..), as well as some more complex cases are still

investigated, e.g. the observed reverse temperature dependence of the receiver delay.

References

1. Szymaniec, K., Hendricks, R., Turza, K., Nagórny, B., Dunst, P., Nawrocki, J., Krehlik, P., Śliwczynski, Ł., Czubla, A. (2018). Operation of caesium fountain frequency standards with remote hydrogen maser references, Metrologia, vol. 55 (6). pp. 782-788, doi:10.1088/1681-7575/aae40d
2. Gruszczynski, M., Klos, A., Bogusz, J. (2018). A filtering of incomplete GNSS position time series with probabilistic Principal Component Analysis. Pure and Applied Geophysics, doi: 10.1007/s00024-018-1856-3
3. Gruszczynska, M., Rosat S., Klos, A., Gruszczynski, M., Bogusz, J. (2018). Multichannel Singular Spectrum Analysis in the estimates of common environmental effects affecting GPS observations. Pure and Applied Geophysics, doi:10.1007/s00024-018-1814-0
4. Czubla, A. et. al. (2018). Use of software-defined radio receivers in two-way satellite time and frequency transfers for UTC computation. Metrologia, vol. 55 (5). pp. 685-698. doi: 10.1088/1681-7575/aacbe6

1.11 Institute of Meteorology and Water Management – National Research Institute Łapeta B., Adalbert A.

Department of Satellite Remote Sensing (SRSD) at IMGW-PIB

The IMGW-PIB Department of Satellite Remote Sensing (SRSD) located in Cracow is responsible for the civilian satellite data ground receiving station and plays key role in the processes of gathering, processing, and analysis of satellite data for meteorological, hydrological, and civil aviation protection. IMGW-PIB

provides access to satellite data and products of the European Organization for the Exploitation of Meteorological Satellites (EUMETSAT) for internal and statutory users in Poland, as well as to level-1 Sentinel constellation and Copernicus collaborative missions provided by the European Space Agency (ESA) under the Cooperative Ground Segment Initiative (CGS) to all registered and verified users. In 2020 data from 17 meteorological and environmental satellites (METEOSAT 8, 9, 10, 11, NOAA 18,19, Metop-A, -B, and -C, Terra, Aqua, Suomi NPP, NOAA-20 Sentinel-1, Sentinel-2, Sentinel-3 and Sentinel-5P) received and processed in (near) real time were used by the SRSD to generate and distribute over 100 products and analyses, ranging from 5-minute data from meteorological satellites to maps of anomalies based on multi-year averages.

Activities in ESA Collaborative Ground Segment

With Poland's accession to ESA CGS and the role of the National Copernicus Operator attributed to IMGW-PIB, SRSD gained access to the Copernicus collaborative data hub and launched the operational provision of Copernicus data via a dedicated website (copernicus.imgw.pl) and Application Programming Interface (API). Participation in the ESA CGS allows access to data sent directly by Sentinel-1 satellites, which will significantly reduce the time after which this data can be made available to users. The expansion of the ground station with the infrastructure necessary to receive Sentinel-1 data (Figure 1.43) was carried out as part of the "Operating system for gathering, sharing and promotion of digital information about the environment (Sat4Envi)", co-funded by European Union in the frame of the Operational Programme Digital Poland, whose main purpose is to provide access to Copernicus satellite data and data from other meteorological and environmental satellites. This goal will be achieved through the construction of a comprehensive system allowing universal and user-friendly access to digital

satellite information and based on the resources of the institutions involved and modernized under the project. The system under development will enable continuous gathering and processing of satellite data for environmental monitoring, as well as data sharing for scientific, strategic and security purposes.

Fig. 1.43. Installation of the 3.8 m antenna at SRSD in Cracow (photo by B.Łapeta)

The key stage of this project was the commissioning of a new station able to receive data from the Sentinel-1 satellite in November 2020. In December 2020, the long-term testing phase of the entire system began, which will last until mid-January 2021. This system enables the reception of data from the Sentinel-1, NOAA-18, 19, 20, S-NPP, Metop-A, B, C, Terra, Aqua, FengYun 3D satellites, and in the future from Metop-SG satellites.

Activities in EUMETSAT H-SAF project

Operational EUMETSAT H-SAF precipitation, soil moisture and snow products derived from Earth observation satellites are the result of a collaboration of 23 institutions from 11 different countries. They respond to the growing demand for operational data from authorities, agencies, services, and other initiatives which need information at the ground to monitor hazards and natural disasters such as flash floods, landslides, and drought conditions, as well as to improve water management.

Monitoring and coordination of works in the framework of the H-SAF Hydrologic validation Program is led by the IMGW-PIB. This activity comes down to collecting and analyzing results delivered by the participant, providing Operational Reports to the Review Board, performing validation works at several levels including standard validation of H SAF products and case studies and various training and dissemination activities such as co-organization of Products Quality Assessment and Hydrological Validation Workshop.

Moreover, IMGW-PIB is involved in validation of H-SAF precipitation and snow products with the use of ground data. SRSD uses data from rain gauges and radar networks operated by IMGW-PIB to provide statistics, validate and asses H-SAF precipitation (Figure 1.44) and snow products. Validation with the use of operational hydrological models for selected river catchments (mountainous, highland, foothills, lowland) is undertaken by Hydrological Forecasting Office in Cracow, which also performs the analysis of techniques used to improve H-SAF satellite products.

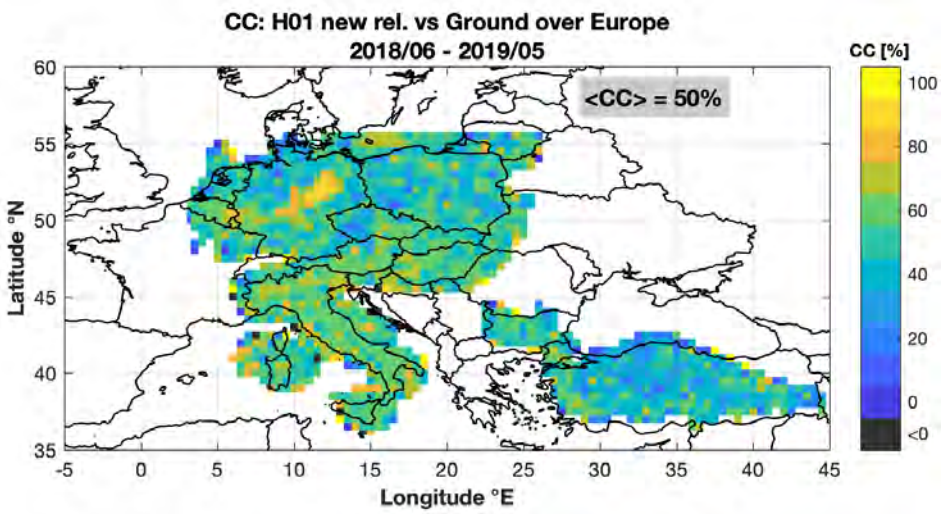

Fig. 1.44. Spatial distribution of correlation coefficient (CC) obtained after H-SAF precipitation product (H01 new rel.) validation. (Source: S.Puca, "Precipitation H SAF Precipitation Products VALIDATION preliminary RESULTS Operations Report 9)

Operational satellite monitoring of total ozone content

Satellite monitoring of the total ozone content in 2020, as in previous years, was carried out by IMGW-PIB / SRSD using satellite data from the Ozone Mapping and Profiler Suite (OMPS) sensor from the Suomi NPP (SNPP) and NOAA-20 meteorological satellites. The main operational product were daily maps of the total ozone content distribution over Central Europe as well as monthly averages and monthly multi-year averages (Figure 1.45).

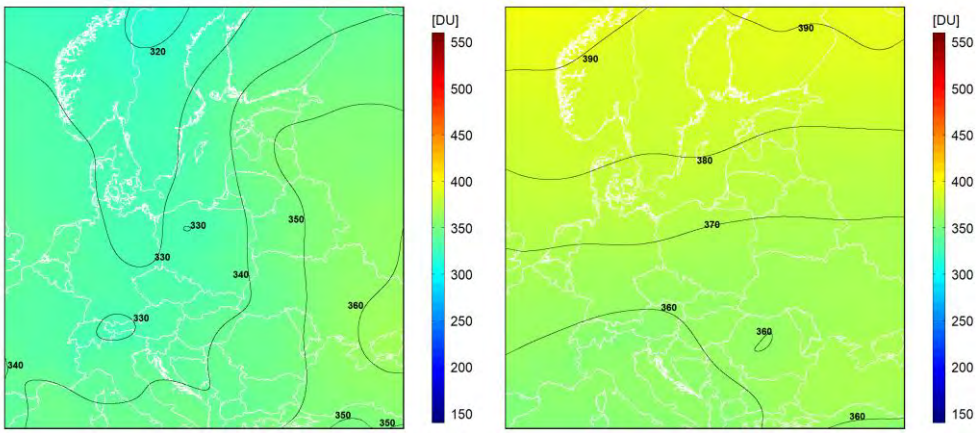

Fig. 1.45. Suomi-NPP/OMPS - total ozone content over Europe in Dobson Units (DU).

April 2020 monthly average (left) and April's multi-year (2013-2019) average (right).

The accuracy of this product is continuously monitored by comparing the total ozone content calculated from OMPS data with ground measurements from four spectrophotometric stations in Central Europe. The ground stations within the range of each SNPP transmission received directly by SRSD are: Belsk (21°E, 52°N), Hohenpeissenberg (11.0°E, 47.8°N), Hradec-Kralove (15.8°E, 50.2°N) and Poprad Ganovce (20.3°E, 49.0°N). The accuracy of the satellite ozone monitoring is determined for each station by calculating mean difference, absolute mean difference, correlation and the Root-Mean-Squared Error (RMSE) of the method expressed in percentage. Based on the values shown in Table 1.3, we can conclude that the OMPS derived total ozone content values agree well with ground measurements - the average percentage error varying from 2.09% to 3.82% and all correlation coefficients greater than 0.9.

Table 1.3 2019 annual accuracy assessment of the operational satellite monitoring of total ozone content. DU - Dobson Units

Station	Correlation	Mean difference [DU]	Absolute mean difference [DU]	RMSE %
Belsk	0.97	-0.71	8.38	3.74
Hohenpeissenberg	0.98	-1.43	5.79	2.64
Hradec-Kralove	0.96	-4.46	9.22	3.82
Poprad	0.99	-0.89	4.94	2.09

Local climate monitoring using satellite and terrestrial data

As a part of its statutory activities, SRSD performs analyzes and develops new products, the source of which are both satellite data and ground observations. They implement the guidelines of the strategic program of the European Environment Agency and the European Union on climate change monitoring. The developed products are used to assess the condition of the natural environment and climate, taking into account the administrative division of Poland. This allows for an ongoing analysis of the state of the natural environment, taking into account potential threats having a negative social or economic impact by units responsible for the protection of the economy (crisis management centers, state administration, etc.). During 2018-2020 period, an operational system for the provision of satellite products and climatological analyzes was implemented for:

- Solar insolation
- Soil moisture

Solar insolation

The analysis of the spatial distribution of solar radiation is carried out using DSSF (Down-welling Surface Shortwave Flux) product generated by EUMETSAT Land Satellite Application Facilities (SAF). This product provides 15-minute data from Meteosat satellites with a resolution of 5-6 km. Based on this data and the modelled atmosphere for cloudless and cloudy conditions, the values of radiation reaching the earth's surface in the shortwave range (0.3-4 μm) are reproduced. SRSD generates and distribute daily, 10-days, monthly, annual and long-term averages (Figure 1.46) and anomalies .

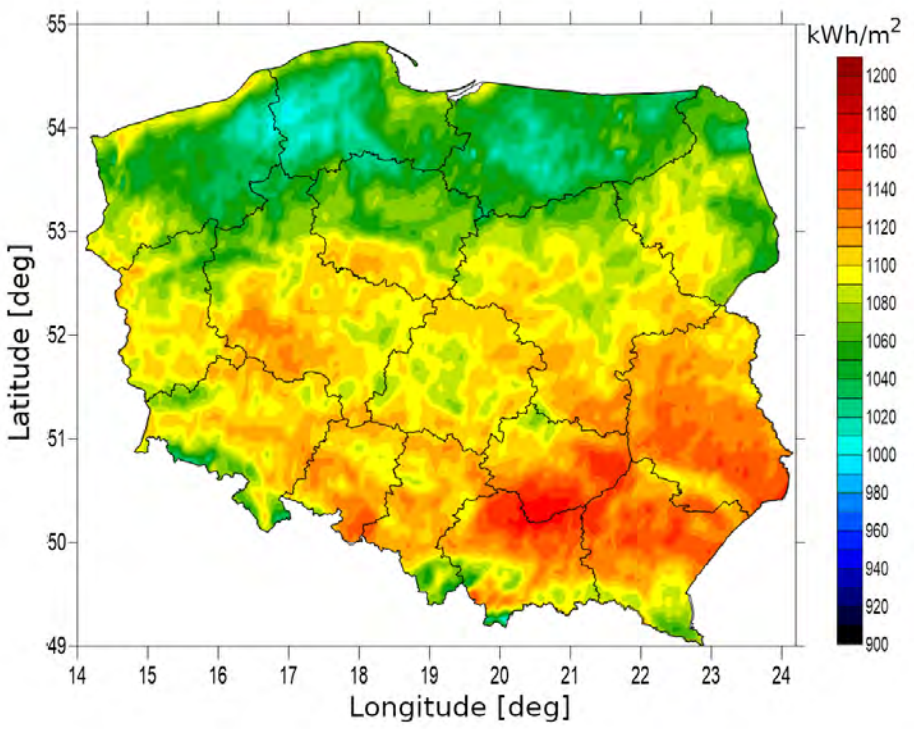

Fig. 1.46. Average total annual solar insolation in kWh/m² in 2020.

Soil moisture

The analysis of spatial distribution of soil moisture is carried out using the H-14 product generated by EUMETSAT H-SAF. This product provides 25 km resolution data from the ASCAT sensor of Metop constellation. These data, together with information on soil type, land cover, vegetation class and meteorological data are used in the ECMWF H-TESSEL Land Surface Model to estimate the current state of soil saturation for four layers at depths of 0-7cm, 7-28cm, 28-100cm and 100-289cm with a time resolution of 30 minutes. For layers 7-28 and 28-100 cm, which best reflect the root zone conditions of the plants, SRSD distribute soil moisture observations for the last 24 hours and generates daily, 10-day, monthly, annual and multiannual averages (Figure 1.47) and anomalies.

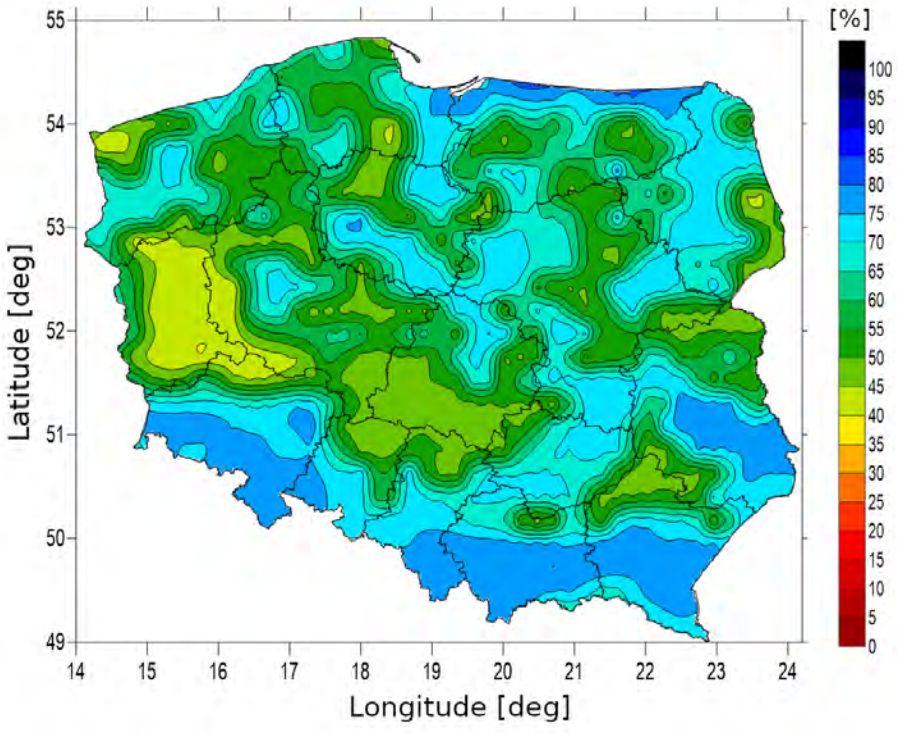

Fig. 1.47. Average annual soil moisture indicator for 7-28 cm layer in 2020.

References

1. M. Kepinska-Kasprzak, P. Struzik, 2019, "Agrometeorological service provided by Institute of Meteorology and Water Management – National Research Institute", Biological Rhythm Research, 50:2, 327-334, DOI: 10.1080/09291016.2018.1518874

2

REMOTE SENSING

2. REMOTE SENSING

2.1 EARTH OBSERVATIONS CBK PAN (Space Research Centre of the Polish Academy of Sciences)

Earth Observation Department (ZOZ) at Space Research Centre (CBK PAN) specializes in remote sensing and geographic information systems (GIS). The Group has been active in the European Commission projects, e.g. 7th Framework Programme, H2020 and ESA programs as well as in domestic research programs. Earth Observation Department handles with developing innovative applications, software and algorithms as well.

S2GLC – Sentinel-2 Global Land Cover classification

Duration: 1 February 2016 – 31 January 2018
Continuation: 1 May 2018 – 30 April 2019

The ESA founded Sentinel-2 Global Land Cover (S2GLC) project was implemented in the years 2016-2019. The project was divided into two parts:
Part 1: Development of LC classification on a global scale, 2016-2018.
Part 2: LC classification of Europe (extension of the project), 2018-2019.

The goal of Part 1 was to develop the classification methodology ready to use for the global LC mapping based on Sentinel-2 images. The developed classification procedure was tested on five study areas located in different geographical regions of the world. Two of them located in Europe included the whole territory of Germany and Italy, and the other three represented similar areas in China, Columbia and Namibia. Satellite images and auxiliary data were processed using a dedicated software developed by CBK PAN.

The main objective of Part 2 of the project (extension of the S2GLC), was to verify operability of the methodology developed during Part 1. This was done by performing LC classification over a major portion of the European continent in the CREODIAS infrastructure. For this purpose, the developed methodology was adjusted to the European landscape and undergone full automation of all processes.

Adaptation of the S2GLC classification method, including modification of the classification legend, was based on tests conducted within selected Sentile-2 tiles representing various bio-geographical regions of Europe. According to the rules established in the initial part of the S2GLC project, training samples were derived from existing LC databases – CORINE LC and High Resolution Layers. The process of selection of training samples was enhanced by introducing additional mutual filtration between the selected databases and the use of spectral indices (NDWI and NDVI). Additionally, rules of selection of images from a time series to be classified in the workflow have been established, which in assume usage of approx. 20 images per Sentinel-2 tile representing all seasons. The post-processing approach was also modified and adjusted so that it fits the European landscape.

All the classifications were carried out on the CREODIAS platform. This required adaptation of all the previously created S2GLC algorithms to the CREODIAS computing environment. Over fifteen thousands of Sentinel-2 images representing 815 Sentinel-2 tiles have been processed to map the

selected area of Europe. Validation of the final map was performed based on a large set of 52 000 randomly distributed samples representing 55 Sentile-2 tiles spread across Europe. Distribution of these tiles allowed to perform validation on both European and a country level. The overall accuracy (OA) of the complete map with 13 LC classes was estimated to be over 86%. Due to lower accuracy achieved for recognition of some of the classes (e.g. grasslands and moors), an additional merging of selected vegetation classes was proposed. It resulted in a reduction of the number of LC classes to 10 but assured an increase of OA up to 89%.The accuracy assessment on a country level revealed very good quality of the LC map with majority of countries exceeding 80% of OA. The S2GLC classification map of Europe produced for the year 2017 is presented in Figure 2.1.

Fig. 2.1. The S2GLC LC classification of Europe 2017.

In general, the LC classification performed on a continental scale confirmed the eligibility of the S2GLC approach as a tool dedicated to global/regional mapping. The developed methodology may be applied to automatically generate new editions of European Land Cover map with 10 m resolution every year. S2GLC LC map Europe 2017 was presented at ESA and EC stand during GEO summit in Canberra (November 2019)
More information can be found at the S2GLC project website: http://s2glc.cbk.waw.pl

(St. Lewinski, R. Malinowski, M. Rybicki, E. Gromny, M. Jenerowicz, M. Krupiński, C. Wojtkowski, E. Bilska)

Land Cover classification of Poland 2020, S2GLC PL 2020

At the end of the year 2020, at the request of the Polish Space Agency (POLSA) the Earth Observation Department carried out land cover classification of Poland. Sentinel-2 images collected in 2020 were processed using the algorithm developed at the CBK PAN within the S2GLC project. Automatically, without manual interpretation work, ten land cover classes were separated. Classification accuracy has been checked with nearly 12,000 validation samples, and overall accuracy of 80% was obtained. The multi-temporal satellite images (Poland is covered by 49 Sentinel-2 tiles) were processed in the CREODIAS environment using CBK PAN software, all the work including validation was done in three weeks!

Fig. 2.2. Land Cover classification of Poland 2020, S2GLC PL 2020

Stanisław Lewiński, Radek Malinowski, Małgorzata Jenerowicz, Ewa Gromny, Marcin Rybicki, Cezary Wojtkowski, Michał Krupiński, Sebastian Aleksandrowicz, Marek Ruciński

BAMS-Mazovia – Build-up Areas Monitoring Service for Mazovia

Duration: 18 September 2018 – 17 September 2020

The BAMS-Mazovia project aims at initialisation of operation of a service platform providing continuously information on newly detected changes in a settlement network. The regional authorities, which are responsible, inter alia, for the process of maintaining and updating of topographic maps, were identified as the main end-user of the service. The project consortium consists

of GEOSYSTEMS Polska Sp. z o.o. (project leader) and the Earth Observation Department of the Centrum Badań Kosmicznych PAN (research partner).

The service being currently under development utilizes multitemporal Sentinel-2 satellite imagery for detecting buildings using highly automated classification algorithms. The classification workflow developed by CBK PAN is in a tasting phase. Its outcomes will be subject to detailed assessment by comparison with up-to-date orthophotomaps and field surveys. Positive verification of the building classification results will enable implementation of the workflow into the service.

In the next step, the service platform will be used for performing spatial analysis that will compare building classification results with existing databases, e.g. Database of Topographic Objects (Baza Danych Obiektów Topograficznych). The mentioned comparison will enable automated identification of changed areas. The goal is to accelerate the process of updating existing databases and reducing maintaining costs. The project case study is based on the area of the Mazovia Province. Ultimately, the service platform shall be applicable to areas of other provinces in Poland.

Fig. 2.3. Examples of new buildings detection – Warsaw, Poland

R. Malinowski, S. Aleksandrowicz, M. Jenerowicz, M. Rybicki, St. Lewinski, C. Wojtkowski, M. Krupiński

Image classification features definition and evaluation, ACCESS4FI - Automated Crop
Classification and yield Estimation online ServiceS for Food Industry.
Duration: 15 January 2019 – 14 January 2021

This project addresses the challenge of quantification and annual monitoring of the agricultural production, as seen from the perspective of different individual actors in the agriculture sector.
The main objective is to develop a set of user-dedicated EO-based tools:
- An automated crop recognition and classification tool;
- An automated, per crop field, yield estimation tool.

For this purpose, in 2019, a series of systematic and comprehensive analysis of characteristics of both SAR and optical remote sensing data (Sentinel-1 and Sentinel-2) has been performed. The activities include the definition and the extraction of features for development of the fully automatic method for selected crop types classification. Features which potentially can be used in the classification of a specific crop are evaluated in a multi-temporal series for year 2018. The tests were performed for the Wielkopolskie Voivodeship part and they were focused on the spectral values and band combination (pixel-based approach in case of optical data) and on the coherence matrix elements, band combination and entropy and a parameters (pixel-based approach in case of SAR data). The intermediate objective of the analysis is to find the optimization of the classification algorithm and reduction of number of inputs without accuracy losses by the best possible feature selection.

M. Jenerowicz

Developing support for monitoring and reporting of GHG emissions and removals from land use, land use change and forestry

In the frame of FPCUP – Caroline Herschel Framework Partnership Agreement, CBK PAN is involved in DG CLIMA project. The goal of the project is to support monitoring and reporting greenhouse gas emissions and removals from land use, land use change and forestry (LULUCF) in selected Member States (MS). The legal basis is the new EU Regulation on (EU) 2018/841 on greenhouse gas emissions and removals from land use, land use change and forestry (LULUCF) which requires MS to improve their systems for reporting.

The role of CBK is to prepare annul Land Cover/Land Use maps with high spatial resolution using Copernicus data. In the next step change detection will be performed and carbon stock and emissions will be estimated for various LC/LU classes. During 2020 CBK PAN has prepared the LC/LU maps for Polish test site (Podlaskie) for selected years (2017, 2018, 2019, 2020). Spatial resolution of maps is 10 m. Classification was performed on multi-temporal Sentinel-2 images by application of algorithm developed within S2GLC project. Within the test site 9 LC/LU classes have been identified. 2.2 presents example of two years (2017 and 2019) and how the area of specific classes has changed during two years.

Michał Krupiński, Stanisław Lewiński

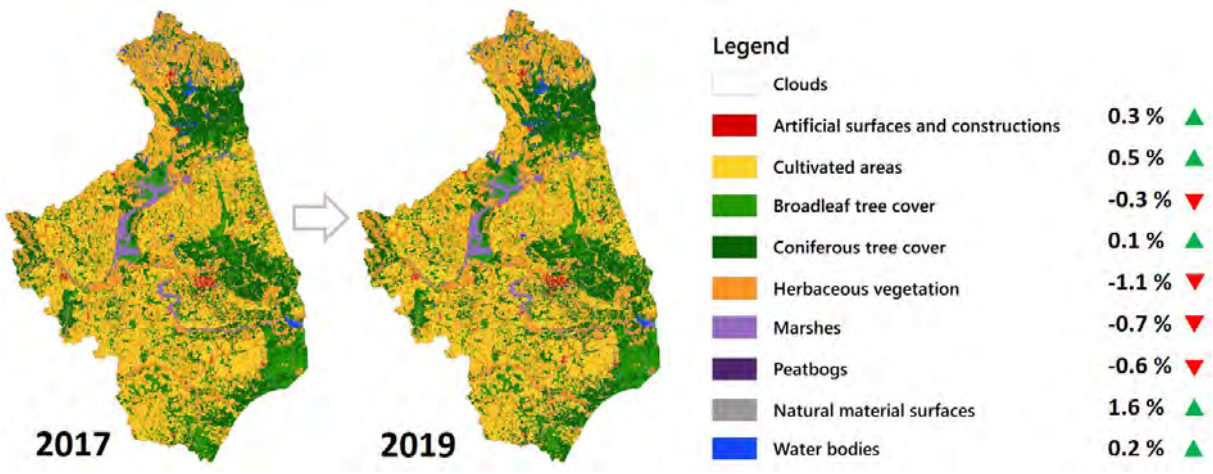

Fig. 2.4. LC/LU maps of Polish test site for year 2017 and 2019. On the right the percentage changes in area of specific classes is presented.

Evaluation of the usefulness of multifractal formalism in the processing and analysis of optical remote sensing images

Duration: 20 July 2017 – 19 December 2020

In years 2018-2020 scientists from the Space Research Centre PAS were involved in the development of multifractal description of remote sensing images, as well as in the evaluation of its applicability in the selected aspects of processing and analyzing of satellite and aerial optical data. In particular, they performed a series of systematic and comprehensive research based on different strategies for multifractal parameters estimation. The main studies can be summarized as follow:

- the complex terrain situation description with the utility of multifractal features (Jenerowicz et al., 2019a, 2019b). The study was done for the Internally Displaced Person (IDP)/refugee camps in Kenya and Sudan. The preliminary results of camps' samples analysis showed the increase of multifractality for the compact settlement area (Jenerowicz et al., 2019a). In next studies Jenerowicz et al. (2019b) developed a multifractal approach for information extraction

automation, in particular to provide a rough, but rapid estimation of IDP/refugee camps extent;

- the local multifractal description as a tool for the change detection on Very High Resolution (VHR) satellite images. In the frame of this topic Aleksandrowicz et al. (2019) examined the performance of multifractal change detection workflow on various bands of multispectral images. The main goal was to investigate usefulness of different bands in the context of urban change detection;

- verification of the usefulness of multifractal parameters as global features describing the content of VHR satellite images. It was done in a research experiment aiming at prediction of basic land-use classes shares within the image tiles cut from satellite EROS-A images (Drzewiecki et al., 2019).

Obtained results confirmed that multifractal parameters should be considered as a useful descriptors of high-resolution satellite image content;

- the application of multifractal features to the analysis of aerial hyperspectral dataset. Here, the variability of spectral profiles acquired by the Compact Airborne Spectrographic Imager (CASI) has been described by multifractal characteristics (Krupiński et al., 2019). Next, the usability of this description in the context of hyperspectral image classification has been verified, confirming multifractal parameters may improve classification accuracy. Moreover, the influence of data preprocessing methods has been analyzed. The second part of analysis stated the consideration of the multifractality as the global description of homogeneous (in the sense of landscape types) subsets of Airborne Visible/Infrared Imaging Spectrometer (AVIRIS) data (Krupiński et al., 2020). Results showed that multifractality reveals in all spectral bands, both for data before and after atmospheric correction, applied parameters could be used for evaluation of atmospheric correction quality or identification of specific landscape types;

- the application of local multifractal parameters determined by scientist from CBK (A. Wawrzaszek) for the identification and delineation of single tree crowns from very high-resolution (VHR) imagery captured by unmanned aerial vehicles (UAV) (Belcore et al., 2020).

Results obtained by Belcore et al. (2020) showed that the segmentation based on the selected multifractal parameters outclasses those based on spectral, textural, and elevation information. Despite the good results of the segmentation, it was shown that method tends to under-segment rather than over-segment, especially in areas with sloping.

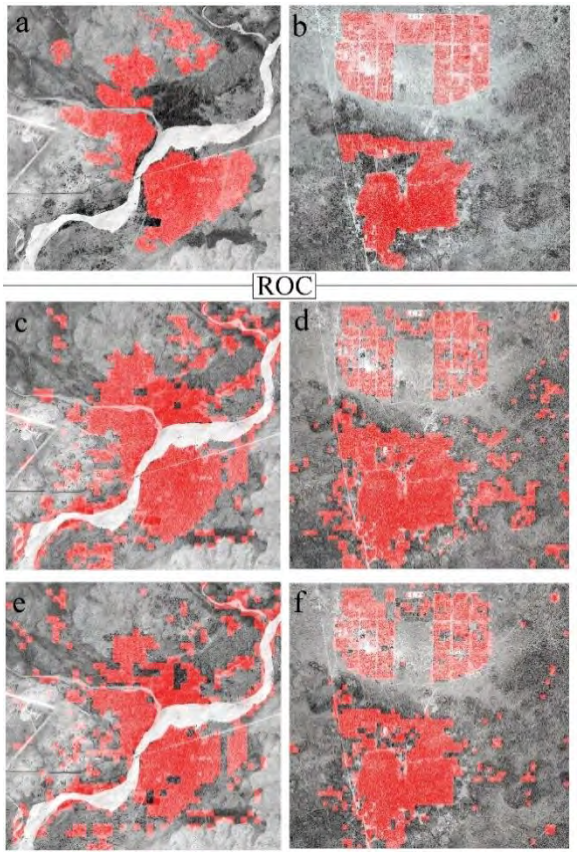

Fig. 2.5. Al Geneina (left panel) and Ifo (right panel) camps masks derived: manually by visual interpretation (a) and (b), via the multifractality methodology (c), (d), (e), and (f). Classification thresholds are determined based on a ROC analysis. (taken from Jenerowicz et al. 2019a).

It is worth to underline that described research experiments were conducted in cooperation with scientists from AGH University (W. Drzewiecki) and Polytechnic of Turin (E. Belcore), and in general, proved usability of multifractal analysis for various applications within the Earth Observation domain.

The research supported by the National Science Centre, Poland, under Grant 2016/23/B/ST10/01151.

Anna Wawrzaszek

Articles:

1. Jenerowicz M., Wawrzaszek A., Krupiński M., Drzewiecki W., Aleksandrowicz S. (2019a), "Applicability of Multifractal Features as Descriptors of the Complex Terrain Situation in IDP/Refugee Camps", IGARSS 2019 – 2019 IEEE International Geoscience and Remote Sensing Symposium, Yokohama, Japan, 2019, pp. 2662-2665, doi: 10.1109/IGARSS.2019.8898588.
2. Jenerowicz M., Wawrzaszek A., W. Drzewiecki, M. Krupiński and S. Aleksandrowicz (2019b), "Multifractality in Humanitarian Applications: A Case Study of Internally Displaced Persons/Refugee Camps", in IEEE Journal of Selected Topics in Applied Earth Observations and Remote Sensing, vol. 12, no. 11, pp. 4438-4445, doi: 10.1109/JSTARS.2019.2950970.
3. Drzewiecki W., Wawrzaszek A., Krupiński M., Aleksandrowicz S. Jenerowicz M., "Multifractal Parameters in Prediction of Land-use Components on Satellite Images", 2019 Signal Processing: Algorithms, Architectures, Arrangements, and Applications (SPA), Poznan, Poland, 2019, pp. 296-301, doi: 10.23919/SPA.2019.893668.
4. Aleksandrowicz S., Wawrzaszek A., Jenerowicz M., Drzewiecki W. and Krupiński M. (2019), "Local Multifractal Description of Bi-Temporal VHR Images", 2019 10th International Workshop on the Analysis of Multitemporal Remote Sensing Images (MultiTemp), Shanghai, China, 2019, pp. 1-3, doi:10.1109/Multi-Temp.2019.8866963.
5. Krupiński M., Wawrzaszek A., Drzewiecki W., Aleksandrowicz S., Jenerowicz M. (2019), "Multifractal Parameters for Spectral Profile Description", IGARSS 2019 – 2019 IEEE International Geoscience and Remote Sensing Symposium, Yokohama, Japan, 2019, pp. 1256-1259, doi: 10.1109/IGARSS.2019.8900247.
6. Jenerowicz M., Wawrzaszek A., Krupiński M., Aleksandrowicz S., and Drzewiecki W. (2019c), "Comparison of mathematical morphology with the

local multifractal description applied to the image samples processing", Proc. SPIE 11176, Photonics Applications in Astronomy, Communications, Industry, and High-Energy Physics Experiments 2019, 1117638, doi:10.1117/12.2536408.
7. Krupiński, M., Wawrzaszek, A., Drzewiecki, W., Jenerowicz, M., Aleksandrowicz, S. (2020), "What Can Multifractal Analysis Tell Us about Hyperspectral Imagery?", Remote Sensing 12(24):4077, doi:10.3390/rs12244077.
8. Belcore E., Wawrzaszek A., Woźniak E., Grasso N., Piras M. (2020), "Individual Tree Detection from UAV Imagery Using Hölder Exponent", Remote Sensing Remote Sensing 12(15): 2407, doi:10.3390/rs12152407.

Night sky over Warsaw significantly polluted by light – photometric survey reveals

Light pollution can be defined as a situation "when organisms are exposed to light in the wrong place, at the wrong time or at the wrong intensity", "an unintended result of electric lighting", or "an excessive or obtrusive artificial light caused by bad lighting design". It has been recognized as one of the most widely-distributed forms of anthropogenic pollution, and threatens both biodiversity and human health.

One of the most popular indicators is known as night sky brightness (NSB), measured with photometric techniques. A dedicated photometric station for NSB have been installed in Warsaw, at the CBK PAN, based on a sky quality meter (SQM) device. In 2019 results of the very first, long-term photometric survey of NSB over Warsaw have been analyzed and published by CBK PAN. The study covered 636 nights between 2014 and 2016, including 475 astronomical nights.

Data were collected for all-weather conditions, hence the analyses accounted for clouds (fraction, base height, layer height), vertical visibility, and solar and lunar illumination. Furthermore, and also for the very first time, two cloud data sources were investigated simultaneously – surface-based

observations collected at a meteorological station (SYNOP), and satellite-based observations collected by the Meteosat cloud imager.

The results of the study showed that average NSB over Warsaw, at the darkest moment of cloudless, moonless astronomical night was 18.65±0.06 $mag_{SQM}/arcsec^2$, i.e. 15 times higher than unpolluted sky. This value agrees well with model estimations published in 'The new world atlas of artificial night sky brightness'. The average night in Warsaw was so bright that the phase of the Moon had no effect at zenith.

Sun elevation above the horizon was the most important factor influencing NSB, but become irrelevant when the Sun was 12° below the horizon. Clouds became the dominant factor for NSB when the Sun was ~5° below the horizon. The study suggests that the critical solar elevation angle (i.e. when the elevation of the Sun becomes an irrelevant factor, or when clouds become the dominant factor) can be used as a quantitative measure of light pollution intensity.

During astronomical night, clouds amplified NSB by a factor of 7; NSB increased with increasing cloud base height, and cloud fraction (~0.2 $mag_{SQM}/arcsec^2$ per every 10% of cloud fraction). Our study suggests that analyses based on low cloud and low cloud fraction conditions should not use SYNOP-like data as the mismatch between the SQM's and observer's fields of view introduces ambiguities into the data interpretation.

Eventually, we proved that satellite data can be used as an alternative to traditional, visual, surface-based observations. When used to derive average NSB, satellite-based cloud estimates result in statistics that are almost to those based on SYNOP information.

For details see: Kotarba, A.Z., Chacewicz, S., Żmudzka, E. (2019). *Night sky photometry over Warsaw (Poland) evaluated simultaneously with surface-based and satellite-based cloud observations*. Journal of Quantitative Spectroscopy and Radiative Transfer, 235, 95-107,

doi:10.1016/j.jqsrt.2019.06.024.

Fig. 2.6. Nighttime imagery of Warsaw taken by the astronaut onboard the International Space Station. Photo: CBK PAN / NASA

Andrzej Z. Kotarba

More reliable global cloud amounts from MODIS based on CALIOP cloud profiles

Clouds play a key role in distributing solar energy in the Earth's atmosphere. Depending on their frequency and physical properties, clouds can both heat (greenhouse effect: +30 Wm^{-2}) and cool (albedo effect: –48 Wm^{-2}) the atmosphere. Cloud net radiative effect on the planetary energy budget is negative, meaning the Earth would be warmer if all cloud disappeared. Our knowledge of clouds relies largely on remote sensing. Satellite cloud climatology starts with a cloud mask: decision whether cloud is present in a sensor's instantaneous field of view (IFOV), or the IFOV is cloud free.

The Moderate Resolution Imaging Spectroradiometer (MODIS) cloud detection procedure classifies IFOVs as either 'confident clear', 'probably clear', 'probably cloudy', or 'confident cloudy'. The cloud amount calculation requires quantitative cloud fractions to be assigned to these classes. The operational procedure used by the MODIS Science Team assumes that 'confident clear' and 'probably clear' IFOV are cloud-free (cloud fraction 0%), while the remaining categories are completely filled with clouds (cloud fraction 100%). Research at the CBK PAN demonstrated that this 'best guess' approach is unreliable, especially on a regional/ local scale.

We use data from the Cloud-Aerosol Lidar with Orthogonal Polarization (CALIOP) instrument flown on the Cloud-Aerosol Lidar and Infrared Pathfinder Satellite Observation (CALIPSO) mission, collocated with MODIS/ Aqua IFOV. Based on 33,793,648 paired observations acquired in January and July 2015, we concluded that the actual fractions are 21.5%, 27.7%, 66.6%, and 94.7%, rather than the MODIS Science Team-assumed values of 0%, 0%, 100%, and 100% for 'confident clear', 'probably clear', 'probably cloudy', and 'confident cloudy' categories, respectively. Spatial variability of CALIOP-based fractions

was significant, even within a single MODIS algorithm path.

In case a global cloud amount value is required (day and night, for all latitudes), the standard approach can be considered reliable. We found that, in this situation, it was more accurate than other 'best guess' approaches – namely only 'confident clear' is 'clear' (other classes are 'cloudy'), and 'confident cloudy' is 'cloudy' (other classes are 'clear'). However, on a regional scale the standard approach fails. Whenever MODIS cloud amount is estimated regionally or locally it is necessary to assess whether a particular location might be affected by an error of up to ±30%. The largest uncertainties were up to −30% of cloud amount in the polar regions at night, and up to +30% of cloud amount in selected locations over the northern hemisphere, more frequently during the day. It strongly suggests that for a local/ regional applications, local fractions should be used instead of global assumptions.

Methodology developed an applied in our study improved MODIS cloud amount estimates. The polar regions benefit most from the new method. Cloud fractions derived for MODIS/ Aqua may be also adopted for MODIS/ Terra, since the two sensors are expected to produce comparable and homogenous records. Moreover, the occasional collocation of the CALIPSO satellite with AVHRR and VIIRS instruments makes it possible to calculate similar cloud fractions for these missions, and produce more reliable cloud climatologies.

For details see: Kotarba A.Z., 2020. *Calibration of global MODIS cloud amount using CALIOP cloud profiles*. Atmospheric Measurement Techniques, 13, 4995-5012, doi:10.5194/amt-13-4995-2020.

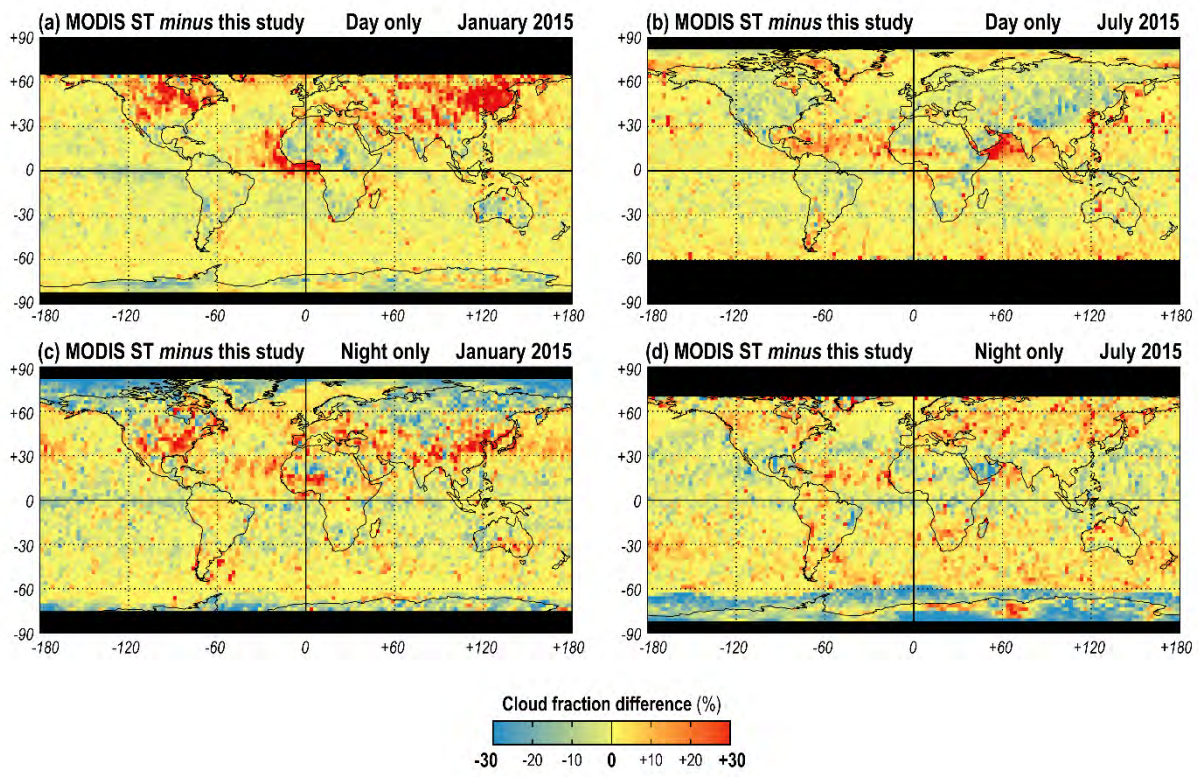

Fig. 2.7. Difference between the MODIS Science Team (MODIS ST) amount product, and cloud amount calculated with the cloud fractions found in CBK PAN study. Positive values indicate that the MODIS operational product overestimates cloud amount (with respect to CALIOP), while negative values indicate a MODIS underestimate. Image: CBK PAN

Andrzej Z. Kotarba

Land cover change detection and change classification on very high resolution satellite images

Automatic change detection is one of the main topics in the field of remote sensing. The workflow (Fig.) for analysis of bi-temporal images acquired in two points in time has been proposed. The method allows for accurate detection of changes and unsupervised changes classification. In the first stage, both images are a subject to pre-processing that aims at eliminating the false positive errors due to radiometric changes caused by differences between image data collection. The essential role in this part plays the atmospheric correction process. Conversion of units from digital numbers to

reflectance values enable initial classification of pixels into spectral categories that are later used for change classification. In the next stage, images are a subject to Multivariate Alteration Detection (MAD) analysis. As a result the MAD layers and change probability layer χ2 are obtained. The MAD layers together with pre-processed image data are then analysed using object-based methods. After segmentation of the images the resulting objects are classified into "change" or "no-change" classes based on χ^2 layer. The "Change" objects are then classified into sub-classes using predefined rules. In the last stage the false positives caused by plant phonological changes on agricultural fields are removed. The proposed method is accurate and assure a high level of automation. Processing of an image pair do not require setting of parameters or thresholds. It also does not require usage of training samples. The change classification rules can be further extended what has been shown on test data. The change detection and classification algorithm has been developed on a pair of WorldView-2 and GeoEye-1 images from the area of Niepołomice county. The testing of the algorithm was done on two pairs of WorldView-2 images from the area of Warsaw. Obtained results show high accuracy of change detection (up to 89% overall accuracy) and of change classification (up to 84% overall accuracy).

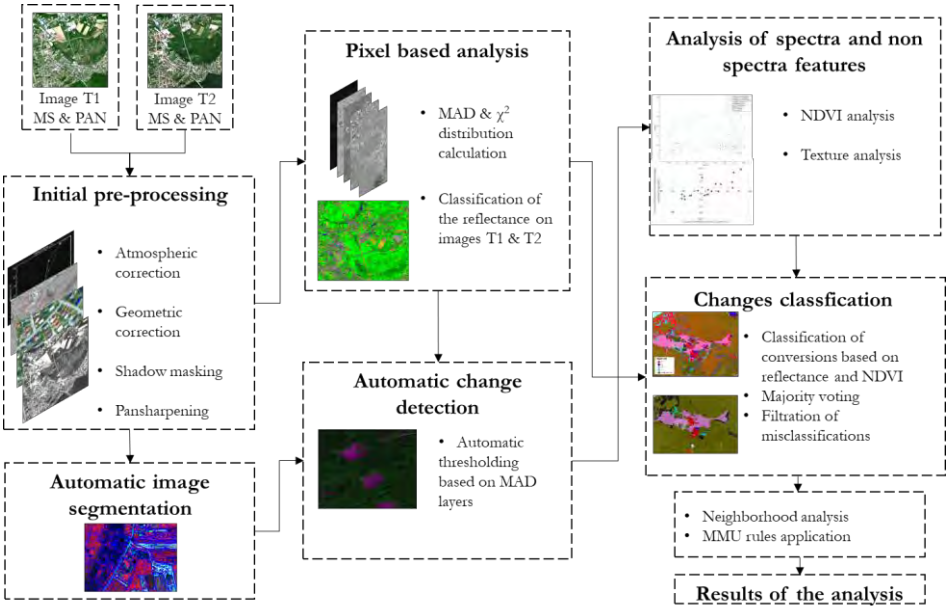

Fig. 2.8 Proposed workflow of change detection and change classification

S. Aleksandrowicz

Remote Sensing Analysis of Landforms in Isidis Planitia, Mars

Duration: 1 January 2018 – 31 December 2019

In 2018, the goal and the scope of the studies have been determined. The goal: to develop the semi-automatic algorithm to analyse the characteristic landforms in Isidis Planitia, Mars.

The scope: The developed the semi-automatic algorithm will enable preliminary processing of imaged data and analysis of structures of interest, i.e. the detection of arcuate ridges, the detection of aligned cones and the classification of detected landforms in relation to their spatial features.

The preliminary activities consists of the selection of input dataset. For the analysis purpose the set of high resolution optical data (of spatial resolution 2m) acquired by a stereoscopic camera of ESA Mars Express mission (The High/Super Resolution Stereo Colour Imager - HRSC) has been selected.

The further steps of proposed methodology are as follows: characterisation of structures of interest on limited set of data, semi-automatic extraction of structures of interest with an use of mathematical morphology operators, and finally, creating libraries of spatial parameters for extracted structures.

These studies will help us to understand the origins of these characteristic cones on Isidis. Showing their spatial distribution will allow to determine the pattern to their arrangement. A characteristic feature is their linearity and arcuateity which is a geological scientific problem.

This studies are carried out in cooperation with the Dynamics of the Solar System and Planetology Department (Zakład Dynamiki Układu Słonecznego i Planetologii, CBK PAN) under the *Ministry* of *Science* and Higher Education's grant for the development of young researchers and doctoral programme participants, financed by way of internal competition.

M. Jenerowicz, N. Andrzejewska

Publications

1. Szulkin, M., Garroway, C.J., Corsini, M., Kotarba, A.Z., Dominoni, D. (2020). How to quantify urbanisation when testing for urban evolution. [w:] Urban Evolutionary Biology, [red:] Szulkin, M., Munshi-South, J., Charmantier, A. Oxford University Press, doi:10.1093/oso/9780198836841.003.0002
2. Woźniak E., Gabryszewski R., Dziob D. (2020), Remote sensing and electromagnetic wave behaviour to measure vegetation phenology with physics, Physics Education doi:10.1088/1361-6552/ab80ff
3. Belcore E., Wawrzaszek E., Woźniak E., Grasso N., Piras M. (2020), Individual Tree Detection from UAV Imagery Using Hölder Exponent, Remote Sensing doi:10.3390/rs12152407
4. Belcore E., Piras M., Woźniak E. (2020), Specific alpine environment land cover classification methodology: Google Earth Engine processing for Sentinel-2 data doi:10.5194/isprs-archives-XLIII-B3-2020-663-2020

5. Dziob D., Krupiński M., Woźniak E., Gabryszewski R. (2020), Interdisciplinary Teaching Using Satellite Images as a Way to Introduce Remote Sensing in Secondary School doi:10.3390/rs12182868
6. Kotarba A. (2020), Calibration of global MODIS cloud amount using CALIOP cloud profiles doi:10.5194/amt-13-4995-2020
7. Malinowski, R., Lewiński, S., Rybicki, M., Gromny, E., Jenerowicz, M., Krupiński, M., Nowakowski, A., Wojtkowski, C., Krupiński, M., Krätzschmar, E., Schauer, P. (2020), Automated Production of a Land Cover/Use Map of Europe Based on Sentinel-2 Imagery doi:10.3390/rs12213523
8. Krupiński, M., Wawrzaszek, A., Drzewiecki, W.,Jenerowicz, M., Aleksandrowicz, S. (2020), What Can Multifractal Analysis Tell Us about Hyperspectral Imagery? doi:10.3390/rs12244077
9. Gromny, E., Lewiński, S., Rybicki, M., Malinowski, R., Krupiński, M., Nowakowski, A. (2019). *Post-processing tools for land cover classification of Sentinel-2*. Proc. SPIE 11176, Photonics Applications in Astronomy, Communications, Industry, and High-Energy Physics Experiments
10. Jenerowicz, M., Wawrzaszek, A., Krupiński, M., Aleksandrowicz, S., Drzewiecki, W. (2019). *Comparison of mathematical morphology with the local multifractal description applied to the image samples processing*. Proc. SPIE 11176, Photonics Applications in Astronomy, Communications, Industry, and High-Energy Physics Experiments, 1117638,
11. Gromny, E., Lewiński, S., Rybicki, M., Malinowski, R., Krupiński, M., Nowakowski, A., Jerenowicz, M. (2019). *Creation of training dataset for Sentinel-2 land cover classification*. Proc. SPIE 11176, Photonics Applications in Astronomy, Communications, Industry, and High-Energy Physics Experiments, 111763D
12. Krupiński M., S. Lewiński, Malinowski, R. (2019). *One class SVM for building detection on Sentinel-2 images*. Proc. SPIE 11176, Photonics Applications in Astronomy, Communications, Industry, and High-Energy Physics Experiments, 1117635
13. Derek M., Woźniak E., Kulczyk S. (2019). *Clustering nature-based tourists by activity. Social, economic and spatial dimensions*, Tourism Management, 75, 509-521
14. Kotarba, A.Z., Chacewicz, S., Żmudzka, E., (2019). *Night sky photometry over Warsaw (Poland) evaluated simultaneously with surface-based and*

satellite-based cloud observations. Journal of Quantitative Spectroscopy and Radiative Transfer, 235, 95-107
15. Jenerowicz M., Banaszkiewicz M. (2018), Asteroid (21) *Lutetia: Semi-Automatic Impact Craters Detection and Classification*. Int. Arch. Photogramm. Remote Sens.
16. Woźniak E., Kofman W., Lewiński S., Wajer P., Rybicki M., Aleksandrowicz S., Włodarkiewicz A. (2018), *Multi-temporal polarimetry in land-cover classification.* International Journal of Remote Sensing,
17. Kotarba A.Z., Nowakowski A. (2018), *Impact of snow cover on impervious surface detection*. International Journal of Remote Sensing
18. Kotarba A.Z. (2018) *Vertical profile of cloud amount over Poland: variability and uncertainty based on CloudSat-CALIPSO observations*. International Journal of Climatology
19. Kulczyk S., Woźniak, E., Derek, M. (2018) *Landscape, facilities and visitors: An integrated model of recreational ecosystem services*, Ecosystem Services
20. Woźniak E., Kulczyk S., Derek M. (2018) *From intrinsic to service potential: An approach to assess tourism landscape potential*, Landscape and Urban Planning, 170, 209-220,
21. Wajer P., Woźniak E., Kofman W., Rybicki M., Lewiński S. (2018) *Simulation of SAR images of urban areas by using the ray tracing method with measured values of backscatter coefficients*, International Journal of Remote Sensing, 39:9, 2671-2689
22. Jenerowicz M., Wawrzaszek A., Krupiński M., Drzewiecki W., Aleksandrowicz S. (2019a), "*Applicability of Multifractal Features as Descriptors of the Complex Terrain Situation in IDP/Refugee Camps*", IGARSS 2019 – 2019 IEEE International Geoscience and Remote Sensing Symposium, Yokohama, Japan, 2019, pp. 2662-2665, doi: 10.1109/IGARSS.2019.8898588.
23. Jenerowicz M., Wawrzaszek A., W. Drzewiecki, M. Krupiński and S. Aleksandrowicz (2019b), "Multifractality in Humanitarian Applications: A Case Study of Internally Displaced Persons/Refugee Camps", in IEEE Journal of Selected Topics in Applied Earth Observations and Remote Sensing, vol. 12, no. 11, pp. 4438-4445, doi: 10.1109/JSTARS.2019.2950970.
24. Drzewiecki W., Wawrzaszek A., Krupiński M., Aleksandrowicz S. Jenerowicz M., "Multifractal Parameters in Prediction of Land-use Components on Satellite Images", 2019 Signal Processing: Algorithms, Architectures,

Arrangements, and Applications (SPA), Poznan, Poland, 2019, pp. 296-301, doi: 10.23919/SPA.2019.893668.

25. Aleksandrowicz S., Wawrzaszek A., Jenerowicz M., Drzewiecki W. and Krupiński M. (2019), "Local Multifractal Description of Bi-Temporal VHR Images", 2019 10th International Workshop on the Analysis of Multitemporal Remote Sensing Images (MultiTemp), Shanghai, China, 2019, pp. 1-3, doi:10.1109/Multi-Temp.2019.8866963.

26. Krupiński M., Wawrzaszek A., Drzewiecki W., Aleksandrowicz S., Jenerowicz M. (2019), "Multifractal Parameters for Spectral Profile Description", IGARSS 2019 – 2019 IEEE International Geoscience and Remote Sensing Symposium, Yokohama, Japan, 2019, pp. 1256-1259, doi: 10.1109/IGARSS.2019.8900247.

27. Jenerowicz M., Wawrzaszek A., Krupiński M., Aleksandrowicz S., and Drzewiecki W. (2019c), "Comparison of mathematical morphology with the local multifractal description applied to the image samples processing", Proc. SPIE 11176, Photonics Applications in Astronomy, Communications, Industry, and High-Energy Physics Experiments 2019, 1117638, doi:10.1117/12.2536408

2.2 Institute of Geodesy and Cartography (IGiK)

The National Centre for Research and Development – NCBiR

GrasSAT - Tools for information to farmers on grasslands yields under stressed conditions to support management practices

Project duration: 2020 – 2023

Project Leader: Prof. Katarzyna Dąbrowska Zielińska

The main objective of GrasSat project is a fully operational system in form of desktop and mobile application, which provides a complementary tool for managing grassland production, mainly for medium and large farms in Poland and Norway. Combining the effectiveness of the application with the support of external advisors is the key to improve grass production management. Experience of the team of remote sensing and grassland specialists will be the firm foundation of the tools to be prepared within the project.

The methodology for monitoring grass growth conditions and yield forecast will be based on synergistic use of remotely sensed data, process-based grassland models and reference in-situ data, indispensable for elaborating reliable models characterizing plant development. Using remote sensing to etimate the expected yield in a grassland can help farmers to prepare for importing forage and to detect areas with high water stress. In addition, process-based models can help estimate the impact of drought or freezing event on the yield. The project assumes the use of ground data for the calibration of satellite data.

The project objectives were defined as follows:

- delivery of the service in the form of desktop and mobile application to optimize farm management like reducing the need for supplementary forage
- development of the method for grassland damage assessment, caused by drought or winterkill on the basis of multi-source satellite data and their

synergy with meteorological data. Novel approaches will be generally based on innovative use of satellite data in the grassland management to increase yield and monitoring of grassland status.

The National Centre for Research and Development - NCBiR

InCoNaDa - Enhancing the user uptake of Land Cover / Land Use information derived from the integration of Copernicus services and national databases.

Project duration: 1.10.2020 – 30.09.2023

Project Leader: Dr hab. Agata Hościło

Project is funded by the Norway Grants via the National Centre for Research and Development', programme 'Applied Research', the POLNOR 2019 Call.

The main goal of InCoNaDa is to improve the user uptake of land cover and land use information derived from the integration of Copernicus Land Monitoring Services (CLMS) and national databases.
The proposed project will address the request for more detailed information on LCLU and its changes (in respect to spatial, temporal and thematic content), than is currently provided in Corine Land Cover (CLC) databases. Furthermore, the assessment of usefulness of enhanced LCLU database and CLMS products for decision makers, reporting obligations in natural resources monitoring, urban and spatial planning, agricultural management and reporting greenhouse gases emissions and removals from LULUCF in Poland and Norway.

The project consortium includes the Institute of Geodesy and Cartography (Centre of Applied Geomatics) (leader), Institute of Environmental Protection – National Research Institute (National Centre for Emissions Management (KOBiZE), Łódz University of Technology (Institute of Architecture and Urban Planning), Eversis Sp z. o.o. and the Nerwegian Institute of Bioeconomy Research (NIBIO). The project website: www.inconada.eu

The National Centre for Research and Development - NCBiR

South Africa - Polish collaborative crop growth monitoring and yield assessment - SAPOL4Crop

Project duration: 2019 – 2021

Project Leader: Prof. Katarz**yna Dąbrowska Zielińska**

The main goal of the project is to create a crop monitoring system based on the synergy of the latest Copernicus missions, low-resolution satellite data, meteorological data and in-situ observations. The system will provide information on the condition of plants during the growing season, water shortages during the development of crops, yield forecasts and early warning against threats to agriculture (occurrence of extreme conditions).

The project aims to achieve the following goals:

- exchange of technological knowledge and experience between Poland and South Africa,
- involvement of young scientists - doctoral students, in order to increase the level of their doctoral dissertations,
- implementation of the results in educational programs and school and university workshops in both countries.

The National Centre for Research and Development - NCBiR

Satellite-based crop identification and crop growth monitoring for agricultural statistics - SATMIROL

Project duration: 2019 – 2021

Project Leader: Dr Jędrzej Bojanowski/ dr Jan Musiał

The project will be carried out by the Central Statistical Office of Poland in consortium with the Space Research Center of the Polish Academy of Sciences and the Institute of Geodesy and Cartography in the years 2018-2021. The main objective of the project is to improve identification and monitoring of

agricultural crops and methods for assessing the effects of extreme weather phenomena. As a result of the project work, there will be developed a system allowing the use of satellite data, wider use of administrative data, getting more targeted data earlier, developing low-aggregated crop data also in spatial perspective. Additionally, obtaining data on agricultural crops from processed data received from satellite imagery reduces labor-intensive input in the preparation and conduction of surveys. The system for identification and monitoring of arable crops will become one of the mechanisms for the development of innovation in agricultural statistics and will reduce the costs and burden of statistical production. The project derives from the existing possibilities of using new digital technologies which determine the development of innovative power and creativity in the field of agricultural statistics, as well as the cooperation between scientific research institutions and the central Statistical Office within the framework of their activities.

The National Centre for Research and Development - NCBiR

Elaboration of innovative method for monitoring the state of agrocenosis with the use of remote-sensing gyro system in terms of precision farming – GyroScan

Project duration: 2017 – 2020

Project Leader: Prof. Katarzyna Dąbrowska Zielińska

The aim of the project was development of the Decision Support System based on the remote sensing method for precision farming (for determination of needs for agricultural practices). This method is also applied for assessment of the degree of degradation of meadows (the method will refer to biodiversity of examined meadows) and for the carbon dioxide balance between the soil – vegetation and the atmosphere.

The analysis were performed for most important crop: wheat and maize, in 2 regions. Meadows were be examined for the Wieprz river valley. The advantages:

- substantial limitation of data derivation costs,
- air-borne data are more representative and more costand time-efficient than soil and plant analyses and give spatial data what is more precise for precision farming than insitu point measurements,
- ensuring all benefits of precision farming, which results in substantial reduction of cost and environmental benefits,
- development of remote sensing method for evaluation of CO2 exchange will ensure faster, cheaper, and easier derivation of data required for greenhouse gas balance. The project implemented the stages of research and development of the remote sensing monitoring system, ground and air-born investigations, and design of a decision support system for precision farming.

The National Centre for Research and Development - NCBiR

Remote sensing based assessment of woody biomass and carbon storage in forests - RemBioFor

Project duration: 2015 – 2018

Project Leader: Dr Agata Hościło

The aim of the project is to develop a complex methodology determining the forest stand descriptions and developing the state-of-the-art aboveground biomass and carbon content retrieval methods based on remote sensed and in situ data. The results of the project will be used to for the purposes of forest management planning. The project encompasses the forest ground inventories, terrestrial and airborne laser scanning and satellite based data. The project is led by the Forest Research Institute. Read more information: http://rembiofor.pl/en/. The role of the Remote Sensing Center of IGIK is to investigate and develop methods for forest above ground biomass retrieval based on various satellite radar data i.e. ALOS-2 (L-band), Sentinel-1 (C-band), TerraSAR-X (X-band) that will be suitable for forest habitats and types present in

Poland. The forest inventory data collected during the RemBioFor project will be used as the reference data.

National Agricultural Support Center – KOWR - **Krajowy Ośrodek Wsparcia** Rolnictwa (National Center for Agriculture Support)

The use of satellite remote sensing data to monitor crop growth conditions, including the identification of agricultural drought, as well as to estimate the reduction of crop yields as a result of unfavourable growth conditions in 2020

Project Leader: Prof. Katarzyna Dąbrowska Zielińska

The main objective of the project was to identify agricultural drought in the country by monitoring the growing conditions of crops during the growing season and to estimate the reduction in yields as a result of unfavourable conditions.

The implementation of the project contributed to the solution of problems due to use of the methodology of identifying plant growth conditions using the DISS satellite drought indicator.

European Space Agency - ESA

Agriculture Poland: Services for Earth Observation-based statistical information for agriculture - EOStat

Project duration: 2018 – 2020

Project Leader: Dr Jędrzej Bojanowski

The ultimate goal of the project was to develop and implement in Statistics Poland and Agency for Restructuring and Modernisation of Agriculture toolboxes for operational and automatic processing of satellite data and production of above-mentioned products.

The EOStat project was carried out by the consortium of IGiK (crop growth monitoring, yield forecasting, early warning, crop classification, agricultural activities detection) and CBK PAN (crop type classification, crop diversification, EFA).

European Space Agency – ESA

Exploitation of Sentinel-1 for Surface Soil Moisture Retrieval at High Resolution

Project duration: 2016 – 2020

Project Leader: Prof. Katarzyna Dąbrowska Zielińska /dr Jan Musiał

The C-band Sentinel-1 (S-1) European Radar Observatory, with its two satellites (S-1A & B), is the only operating SAR mission with monitoring capabilities, frequent revisit and large geographical coverage that will guarantee data continuity over the next decades. S-1 with its advanced observational capabilities opens new perspectives to SAR derived near surface soil moisture (SSM) products as, for the first time ever, they may attract a real interest in a wide user community and stimulate a synergistic interaction with SSM products at low resolution.

The scope of the two-year Exploit-S-1 project is to demonstrate the capabilities of the S-1 mission to support systematic SSM product generation at high resolution (e.g. 500m-1000m) and at regional/continental scale. A suite of SSM retrieval methods will be developed, implemented and validated using S-1 data. The methods will be based on previous research into C-band soil moisture retrieval and will be selected from the great wealth of approaches proposed in the literature and tailored to S-1 data. The emphasis will be on implementing and comparing algorithms presenting the most promising trade-off among robustness, retrieval accuracy and potential matching with the requirements of different applications (e.g. Numerical Weather Prediction, hydrological forecasting, drought events ...) in terms of accuracy, resolution and product frequency. In addition, the suitability of the algorithms to fully exploit the S-1 observational assets (e.g., dual polarization, spatial/temporal resolution, radiometric accuracy) in order to deliver a large scale mapping will be considered.

A key component of Exploit-S-1 will be the validation activity that will include local and regional scale sites (e.g. the Mediterranean basin) in order

to better assess the potential for pre-operational and operational soil moisture products and services.

A further pivotal element of Exploit-S-1 will be the assessment of the optimal pre-processing of S-1 time series for SSM retrieval. This will also have the outreaching effect of consolidating standards for the generation of S-1 multi-temporal products that are well suited for other S-1 retrieval studies.

European Space Agency - ESA

Irrigation Factor 4 potato growth using Sentinel-1 and Sentinel-2 data - IRRSAT

Project duration: 2017 – 2019

Project Leader: Prof. Katarzyna Dąbrowska Zielińska

The main objective of the project was to create pre demonstration System for Irrigation of crop (potato) fields based on Earth Observation (EO) and in-situ data. In order to fulfil the overall Project objective, the following specific objectives of the Project need to be achieved:

- to develop and calibrate a model of soil moisture assessment based on S1 and S2 data using in situ results;
- to validate the SM model using an independent set of measurements, and assess its accuracy, applicability and limitations;
- to develop the model of irrigation factor value calculation throughout the growth period;
- to establish a soil moisture and irrigation factor as pre-demonstrator product and present it for validation (with the SM sensors) and provide dissemination between users from agriculture market.

European Space Agency - ESA

Service 4 Drought Monitoring applying Satellite Data

Project duration: 2017 – 2019

Project Leader: Prof. Katarzyna Dąbrowska Zielińska

The main objective of the project was to create multi-level information System for Drought Monitoring based on Earth Observation (EO) and in-situ data, delivering its services in an operational way for water demanding industry, such as: energy sector, agriculture, environment as surface waters, forest.

The Project is designed to develop the System of drought monitoring and assessment based on the fusion of in-situ (meteorological and hydrological) measurements and satellite derived data. The model based on meteorological, hydrological and satellite data was analysed applying Weather Research and Forecasting Model – WRF with satellite derived model, in order to establish the thresholds indicating the start and extent of drought conditions. The drought effect is monitored through the project delivery and for the years of historical drought in 2006 and 2015 in order to calibrate the WRF and satellite data based drought assessment model.

European Space Agency - ESA

SAT4EST - Earth observation based service supporting local administration in non-state forest management - ESA Project

Project duration: 2017 – 2021

Project Leader: Dr Agata Hościło

The goal of the SAT4EST was to design and build non-state forest focused service dedicated to the local government administration in Poland. This EO based service provides a simple, intuitive and low-cost tool in a form of a web-based SAT4EST application easy to use and expand for another dataset. The application provides the visualisation tool and EO based products dedicated to forest management i.e. forest and woodland extent, forest changes, forest type, canopy coverage, forest health condition. The EO products are generated automatically based on a multi temporal Sentinel-2 datasets. The application provides tools for comparison of the satellite products with the

simplified forest management plans and cadastral data. The SAT4EST application was developed in the consortium of the Institute of Geodesy and Cartography and TaxusIT Sp. z o.o. Demonstration of the SAT4EST application took place in December 2020 and was funded by the Polish Space Agency. The project website: www.sat4est.pl.

The project consortium includes the Institute of Geodesy and Cartography (Centre of Applied Geomatics as a leader).

European Space Agency - ESA

GEO4IRBM – Geoinformational Support for Integrated River Basins Management

Project duration: 2018 – 2019

Project Leader: Dr Dariusz Ziółkowski

The Geo4IRBM project was carried out in a consortium of three institutions: GEOSYSTEMS Polska Sp. z o.o., (leader), Topologic Consulting, Institute of Geodesy and Cartography (Remote Sensing Centre) and financed by European Space Agency (ESA) under the Polish Industry Incentive Scheme. The aim of the project was rapid elaboration and provision of certain informational products and services which will be further used for the needs of support of selected river basins management. The region of the project implementation was provisionally defined as selected rivers' watersheds in the western part of Java island, Indonesia.

The project goals were defined in cooperation with the Jakarta office of the Asia Development Bank and reflects both requirements of the end-user organisation and the project consortium assessment of feasibility in the frame of short service provision time.

The objectives of the Geo4IRBM project cover four research areas areas:

- Land use and crop maps elaboration
- Surface water monitoring
- Surface derformation monitoring
- Environmental impact assessment

European Space Agency - ESA

LPVP - Land Products Validation and Characterisation in support to Proba-V, S-2 and S-3 missions Project duration: 2016 – 2018

Project Leader: Prof. Katarzyna Dąbrowska Zielińska

The Project Land Products Validation and Characterization in support to Proba-V, S-2 and S-3 missions (LPVP) was launched with the main objective to support activities aimed at characterisation and validation of land products generated from Proba-V, Sentinel-2 and Sentinel-3 optical data. In order to perform these activities, thorough analysis of state-of-the-art in the field of deriving land products from new-generation satellite data were done. The analysis were preceded by a short description of new-generation ESA satellite sensors; it was divided into 4 chapters:

- Methods of pre-processing of Proba-V, Sentinel-2 and Sentinel-3 data;
- Methods of deriving land products from Proba-V, Sentinel-2 and Sentinel-3 images;
- Approaches for generating maps characterizing vegetation status based on multi-temporal data;
- Methods of validating EO based land products with the use of ground collected information.

The objectives of the project were:

- O.1. Develop and test a methodology for deriving biophysical variables from the synergetic exploitation of current and future ESA optical sensor missions (Proba-V, Sentinel-2 and Sentinel-3) additional EO and ancillary data;
- O.2. Contribute to the definition of the land products validation approach for the current and future ESA optical missions;
- O.3. Plan and carry out field campaigns measurements of: vegetation cover LAI, fAPAR, carbon balance, biomass wet and dry, soil moisture, vegetation phenology, vegetation hazards, crop yield, biomass growth.

These measurements will be taken at wetland and agriculture areas in Poland and used for validation of derived EO remote sensing data;

- O.4. Contribute to the assessment of products quality and calibration performances for the relevant ESA optical missions;
- O.5. Support Proba-V, Sentinel-2 and Sentinel-3 Cal/Val activities support activity of ESA's Sensor Performances, Products and Algorithm (SPPA) section, which is responsible for mission end-to-end performances assessment, algorithm evolution and Cal-Val activities;
- O.6. Support the exploitation of the derived products for various land applications as wetlands and agriculture monitoring.

European Space Agency - ESA

Exploitation of Sentinel-1 Interferometric Coherence for Land Cover and Vegetation Mapping – SinCohMap

Project duration: 2017 – 2019

Project Leader: Dr Dariusz Ziółkowski

The project evaluated the performance of using the interferometric coherence of S-1 time series for land cover and vegetation mapping. One of the main objectives of the project was to quantify the impact in using S-1 InSAR (Interferometric Synthetic Aperture Radar) data relative to traditional land cover and vegetation mapping using optical data (especially Sentinel-2, hereafter named S-2) or SAR-based (Synthetic Aperture Radar) approaches.

The results of this study indicate that the interferometric coherence provided in multi-temporal matrices is a formidable source of information for land cover mapping, as it has been proven by the fact that three different methodologies, developed by three different research groups, produced an overall accuracy of above 75% for all three study areas, the pixel-based eigenvalue decomposition with a random forest classifier, the KTH-SEG approach performing object based classification using the support vector machine and

the SPKnnLab approach, creating super pixels that are labelled using kNN. It should be highlighted that in all study areas, more than ten different classes are present, covering almost every class from the Corine classification scheme.

European Space Agency - ESA

Advanced Sustainable Agricultural Production - ASAP

Project duration: 2018 – 2020

Project Leader: Mgr Martyna Gatkowska

Building a Service that provides a wide range of products for the agricultural sector based on satellite data. This solution allows to significantly save time and cost of product development compared to traditional methods, and also allows to obtain results in a map format which supports supports farmers. The ASAP service has been built to be a fully comprehensive tool, providing products and professional support in the field of plant production, from sowing to harvest.

European Commission

EO4GEO

Project duration: 2018-2020

Project Leader: dr Marek Baranowski/ dr Agata Hościło

EO4GEO is an Erasmus+ Sector Skills Alliance gathering 26 partners from 13 EU countries, most of which are part of the Copernicus Academy Network. Be they from academia, public or private sector, they are all active in the education and training fields of the space / geospatial sectors.

Technological progress and globalisation offer tremendous opportunities for innovation, job creation and growth. This also requires people to acquire new skills in order to drive and support change.

But which skills are they, and how can we build and shape the workforce of the future? This is where EO4GEO steps in.

EO4GEO aims to bridge the skills gap between the supply and demand of education and training in the space/geospatial sectors, fostering the uptake and integration of space/geospatial data and services in a broad range of application domains.

EO4GEO will work in a multi and interdisciplinary way and apply innovative solutions for its education and training actions: case-based and collaborative learning scenarios; learning-while-doing in a living lab environment; on-the-job training and co-creation of knowledge, skills and competencies.

European Commission

Speeding up Copernicus Innovation for the BSR Environment and Security - BalticSatApps

Project duration: 2017-2019

Project Leader: Prof. Katarzyna Dąbrowska Zielińska

The aim of the project is to overcome information gaps and lead to a more complete exploitation market potential of the Copernicus program across the European Union. Space data connection with digital technologies and other data sources open up many business opportunities for all Member States. Stronger links with the downstream commercial sector are essential to develop tailor-made applications, acquiring new users and connect different sectors.

The BalticSatApps project aims was to accelerate the market introduction of services based on the access and processing of satellite data provided under the Copernicus Program. Project partners come from the countries of the Baltic Sea Region, and it is in these countries that promotional and demonstration activities aimed at a wide audience will be located.

The discussed project has brought many direct benefits for Poland and Polish entities:

- It will allow to create a comprehensive map of users interested in using the data Earth observation;
- It will enable the analysis of entities with the potential to apply Earth Observation data in their activities, which are equated with the opportunity to increase the potential of these institutions and their innovation, and to expand the scope of activities
- It will allow the development of programs and the conduct of training and information meetings regarding Copernicus Program, to be widely used also by institutions outside the project consortium
- It will allow for the establishment of activities supporting the creation of new business entities, using innovations offered by the Copernicus Program.

European Commission

Caroline Herschel Framework Partnership Agreement on Copernicus User Uptake

Developing support for monitoring and reporting of GHG emissions and removals from land use, land use change and forestry – DGCLIMA (FMI, IGiK, SYKE, SRTI-BAS, CUNI, SRC PAS, Castra, IHCantabria, MU)

Project duration: 2020 – 2021

Project Leader: Prof. Katarzyna Dąbrowska Zielińska

Support of monitoring and reporting greenhouse gas emissions and removals from land use, land use change and forestry (LULUCF) in selected Member States (MS). The legal basis is the new EU Regulation on (EU) 2018/841 on greenhouse gas emissions and removals from land use, land use change and forestry (LULUCF) which requires MS to improve their systems for reporting. Article 18 (4) of this regulation and Annex V (Part 3) of Regulation (EU) 2018/1999 require EU Member States to employ methodologies for monitoring of land use conversion according to IPCC Approach 3 (geospatially-explicit) and at least

tier 2 (nationally relevant emission calculations) for key categories of emissions and removals. Thus, the objectives of the action are:

1. to support the MS in monitoring and reporting of GHG emissions and removals from land use, land use change and forestry (LULUCF) taking into account relevant regulation systems and existing reporting systems in the MS
2. to develop a test-version of pan-European system using Copernicus data and services to deliver improved estimates of changes in carbon stocks and resulting GHG emissions and removals from land use, land use change and forestry;
3. to carry out a pilot study on the emerging methods for developing these estimates, building largely on Copernicus data and services such as CLC+ components and Sentinel imagery, with the aim of capitalizing LULUCF monitoring with existing pan-EU data sets;
4. to evaluate these integrated national estimates at selected test regions using long-term time series of maps derived from satellite data.
5. to analyse the role of Copernicus data and benefit they could contribute;

Tasks of the Institute of Geodesy and Cartography which were performed in the scope of the project:

1. One voivodeship (NUTS2) was selected - Podlaskie voivodeship.
2. The LU changes maps were done applying to Sentinel2 satellite data. The High Resolution Layers data (HRL) were applied for detection of changes LULUCF and demonstration of trends.
3. Addittionaly the unsupervised classification has been done to map the forest cover and detection the LU changes.
4. The maps of land use changes between 2012 and 2015 and 2018 were done;

Standardised pan-European approach in support of MS and EU LULUCF reporting. Elaboration of:

- Copernicus –High Resolution Layers
- LPCCLand use categories
- Adjustmentof High Resolution Layers
- Integration of HRLs into Land Use map
- For NUTs Podlaskie - HRL'sLand Use changes2012-2015-2018

Thematic maps for atmosphere pollution and NO2 and SO2 concentration in different climate seasons. The measurement of CO2 has been done for Biebrza for the reference of chamber methodology:

- maps of NO2 content in the troposphere for the province Podlaskie
- maps of monthly averages from July 2018 to November 2020
- the annual average for 2018 (measured from July, due to data availability) and 2019

In October 2020 a two-day international online workshop was organized - Developing support for monitoring and reporting of GHG emissions and removals from land use, land use change and forestry. The project members presented their work and in the end of the each session the panel discussion were performed.

European Commission

Caroline Herschel Framework Partnership Agreement on Copernicus User Uptake

Success stories Poland

Project duration: 2019 – 2020

Project Leader: Prof. Katarzyna Dąbrowska Zielińska

This action aims at raising awareness and knowledge of private business from various sectors. The users has been chosen through a questionnaire.

As we knew from various meetings the following sectors would be interested:

- Insurance companies (risk assessment, calculation of the damage/lost),
- Energy Sector (traceability of energy biomass source/assessment of the energy production potential in regions, alternative energy),
- Potential investors in the renewably energy sector (wind farms),
- Spatial planning (updated information on land use and its changes),
- Transportation company etc.

The outputs will be composed of: communication materials demonstrating the applicability of the Copernicus data and services for various sectors of economy, complex solution-to-problem concepts as well as Seminars' presentations and Users assessment of the quality and utility of the delivered concept notes. In cooperation with the Polish Partner, University of Gdansk (abbreviated to UG) designed a questionnaire for potential users uptake (https://docs.google.com/forms/d/e/1FAIpQLScp014c_8lL6lyhL3dmZOyiSp0TrUmtpqEbkrRz5DpZAuXUbA/viewform?usp=sf_link).

A list of potential users (private companies, services, enterprises etc.) was established and interests in training and workshops related to Copernicus data usage were obtained. In cooperation with UG the experts from IGiK has been working on the website related to the action in Polish (www.fpcup.pl) and established the extent of contents proposed for the target training programmes. There the users can find the link to competition due to aim of the project https://fpcup.pl/konkurs/.

European Commission

Caroline Herschel Framework Partnership Agreement on Copernicus User Uptake

Application of Copernicus products and value-added services for management of environment and forecasting agricultural production (IGiK & UG, PL)

Project duration: 2019 – 2020

Project Leader: Prof. Katarzyna Dąbrowska Zielińska

The Action is principally focused on capacity building and raising awareness of the various stakeholders, responsible in Poland as National Action looking internationally for monitoring and management of the environment, on the scope of applications of the Earth Observation data and services developed in the frame of Copernicus products.

There are five main users groups to whom the designed activities will be targeted:

- agriculture and forestry - Ministry of Agriculture, The Agency for Restructuring and Modernization of Agriculture (ARMA), Agricultural Market Agency (ARR), Agricultural Advisory Offices, State Forest, Regional Directorates of State Forests, Communes and Marshall Offices managing the non-state forests, Main Directorate of Environmental Protection, Regional Directorates of Environmental Protection
- environment and protected areas - Ministry of Environment, Main Directorate of Environmental Protection, Regional Directorates of Environmental Protection, National Parks authorities
- marine environment - Ministry of Maritime Economy and Inland Waterways, Ministry of Environment, Ministry of National Defense, Main Directorate of Environmental Protection, Regional Directorates of Environmental Protection, Spatial planning institution on national and regional level, Maritime Offices

- land use and change detection - Spatial planning institution on national and regional level, Ministry of Infrastructure, National Parks
- atmosphere and climate change - General Directorate of Environment, Ministry of Environment,

  Institute of Meteorology and Water Management National Research Institute, Water Management Boards, institutions on regional level,

A plan was to organize a number of lectures and practical workshops and exercises, together with the specific training materials in order to present a potential of the EO data and services and to collect feedback from participants during the structured discussion. A dedicated website, within the IGiK's website, was developed in the in order to provide access to training materials presented during seminars as well as to provide most important updates on Copernicus Programme and open services available for users, https://fpcup.pl/szkolenia/.

A training plan had been developed and agreed with the responsible institutions, advisory agencies and commercial companies working for environment and for the agriculture sector as well as Central Statistical Office and regional offices. Series of workshops and webinars are still executed online for an agreed number of public sector employees. These is conducted in Polish. The training materials are developed in Polish and English to easily use these materials by consortium partners and adjust them to their national needs
The content of the presentation on the Copernicus program was agreed with the Polish Partner – University of Gdańsk.

National Science Centre – NCN OPUS
Modelling of carbon balance at wetlands applying the newest ESA satellite missions Sentinel-1/2/3
Project duration: 2017-2020
Project Leader: Prof. Katarzyna Dąbrowska Zielińska

The project objective is elaboration of the methodology for carbon balance modelling based on satellite Sentinel-1/2/3 data and insitu measurements of CO2 by chamber method, Leaf Area Index (LAI) by LI-COR 2200, soil moisture by TDR method (TRIME-FM), PAR (AccuPAR), biomass wet and dry (in the laboratory) surface temperature (IR radiometer, EXOTECH), soil temperature, for Biebrza wetlands under changing moisture, biomass and meteorological conditions.

The results will show how the moisture and biomass changes and meteorological conditions influence the carbon balance. It will give the indications for proper renaturalization of the wetland areas. The project is expected to have an important impact on scientific research into the link between remote sensing, plant physiology, agriculture and hydrology. The results will give strong input to the climate models and will give the answer how the biophysical parameters obtained from the newest satellite data has impact on carbon balance. The project will introduce the COPERNICUS climate service on national scale and in the future will integrate the scientific groups playing the role in climate change observations.

National Science Centre

Copernicus Land Monitoring - CORINE Land Cover 2018

Project duration: 2017 - 2019

Project Leader: dr Agata Hościło

The Institute of Geodesy and Cartography, where one of the National Reference Centres of the European Environment Information and Observation Network (EIONET) for land cover is located, was responsible for the development of the Corine Land Cover bases, verification of high-resolution layers HRL2012 and HRL2015, verification of local products Urban Atlas , Riparian Zones and Natura 2000, and refine the Urban Atlas2012 product by adding land use information. In addition, the Institute of Geodesy and Cartography was

obliged to disseminate HRL2015 high-resolution layers and local products with a national range.

National Science Centre – NCN POLONEZ

Variability and change of cloudiness diurnal cycle over the past 30 years: a global analysis based on polar orbiting satellites

Project duration: 2017-2018

Project Leader: dr Jędrzej Bojanowski

The primary goal of this study was to fulfil these requirements, and thus render the satellite-derived dataset suitable for climate analysis. We aimed to:

- develop and validate a method for statistical reconstruction of cloud cover diurnal cycle,
- create a 30-year global cloud fraction climatology (1°×1°) suitable for trend analysis by correcting the satellite orbital drift issue,
- quantify global changes in cloud cover distribution and in diurnal cycle of cloud formation over the last 30 years.

The first outcome of the project is the impact assessment of satellite orbital drift of NOAA and MetOp platforms on quality of cloud fractional cover (CFC) climate data records and on spurious trends observed therein. We revealed that the longest available (almost 4-decades-long) AVHRR-based climate data record called CM SAF cLouds, Albedo and Radiation dataset from AVHRR data (CLARA-A2) is not suitable for climate analysis, i.e. it does not comply with the temporal stability requirements defined by the Global Climate Observing System (GCOS), due to satellite orbital drift and varying sampling frequency.

The unique achievement of the project is the unprecedent analysis of the climatological trends in the cloudiness diurnal cycle over the Meteosat disc, i.e. an area observed by the geostationary satellite positioned at approximately 0° N/S, 0° E/W. The trend analysis was preceded by the following subtasks: (1) an assessment of the overall performance of the CM SAF ClOud Fractional Cover

dataset from METeosat First and Second Generation dataset (COMET) and verification whether the COMET dataset provided in 30-minute resolution can accurately resolve the cloudiness diurnal cycle, and development of the reference dataset composed of frequent (10-minute) ground-based cloud fractional cover estimates derived from the pyrgeometer measurements of incoming longwave radiation.

The National Centre for Science - NCN

Combining GRACE-type mission and GNSS CORS network data for the determination of temporal mass variations in the Earth system on a regional/local scale

Project duration: 2018-05-17 – 2020-11-16

Project Leader: Dr. Walyeldeen Godah

The Gravity Recovery and Climate Experiment (GRACE) was operating within the period from March 2002 to October 2017, while the GRACE Follow-On (GRACE-FO) is a continuation of the GRACE satellite mission launched in May 2018. In order to bridge the gap between GRACE and GRACE-FO, the suitability of data from non-dedicated gravity satellite missions (N-DGSMs) for the determination of temporal variations of geoid heights was assessed. The main findings reveal that Global Geopotential Models (GGMs) developed on the basis of some N-DGSMs data seem useful for the determination of temporal variations of geoid heights in areas characterized with strong mass transport, e.g. the Amazon basin. For areas with a weak mass transport signal, e.g. Poland, NDGSMs-based GGMs investigated seem unsuitable for that purpose. The use of national GNSS (Global Navigation Satellite System) CORS (Continuously Operating Reference Stations) networks for determining temporal mass variations within the Earth's system and for improving GRACE/GRACE-FO solutions has been investigated within the course of this project. Firstly, daily vertical deformations of the Earth's surface for the period

2008-2018 were determined at the location of 96 sites of the ASG-EUOPS (Active Geodetic Network of the European Position Determination System) GNSS CORS network using daily GNSS observations data. Secondly, monthly vertical deformations of the Earth's surface were determined by averaging the daily vertical deformations. Thirdly, monthly vertical deformations of the Earth's surface were inverted into monthly variations of equivalent water thickness using Green's function method.

Monthly vertical deformations of the Earth's surface and monthly variations of equivalent water thickness were independently determined from GRACE-based GGMs using the IGiK-TVGMF software developed within the course of the EPOS-PL (European Plate Observing System Operational - Poland) project. Further, combined models of monthly variations of equivalent water thickness were developed by combining the corresponding monthly variations of equivalent water thickness from GNSS and GRACE satellite mission data. The results obtained indicate that national GNSS CORS networks developed for precise positioning related applications, evidently provide a valuable information for the determination of temporal mass variations (e.g. temporal variations of equivalent water thickness) within the Earth's system complementary to the one obtained from GRACE/GRACE-FO satellite missions data. In Poland, GNSS data from the ASG-EUPOS CORS network improve models of temporal mass variations within the Earth's system obtained from GRACE/GRACE-FO satellite missions' data. The use of other national GNSS CORS networks operated worldwide for determining temporal mass variations within the Earth's system as well as for improving GRACE/GRACE-FO satellite missions' solutions is a subject of further investigation.

Temporal variations of hydrological masses are considered as one of the main sources for temporal variations of orthometric/normal heights. They generate the time-varying gravitational potential and thereby temporal variations of the geoid/quasigeoid surface. They also induce mass loadings

that deform the Earth's surface in both horizontal and vertical directions. The results obtained within this project clearly prove significance of GRACE/GRACE-FO satellite missions' data for determining temporal variations of orthometric/normal heights induced by temporal variations of hydrological masses. For example, they revealed that temporal variations of orthometric/normal heights reach 8 cm over the Amazon river basin and 2.5 cm over Turkey. Such temporal variations are needed for precise determination of orthometric/normal heights to monitor, interpret, analyse and model changes in those heights used in scientific (e.g., crustal motion, subsidence and isostatic readjustment) and engineering (e.g., the deformation of bridges, dams and large constructions) works, especially for areas characterized with significant temporal mass variations within the Earth's system such as hydrological masses in large river basins.

Overall, the results obtained within this project are essential to understand the mechanisms of temporal mass variations within the Earth's system on a regional/local scale and model them using GRACE/GRACE-FO missions' data and GNSS data. They are essentially needed for understanding, monitoring and predicting many issues related to the Earth's system, e.g. (1) crustal deformations due to mass loading – needed for dealing with natural hazard, (2) water mass variations – needed for dealing with climate change, flood, drought, groundwater depletion, (3) temporal variations of orthometric/normal heights – needed for modernization of vertical heights datums/systems. The results obtained within this project will positively contribute to the development of Earth's science-related disciplines, in particular, the geodesy and geodynamics fields.

National Science Centre – NCN OPUS

Determination of the seismic structure of the Earth's mantle from measurements of tidal gravimeters

Project duration: 2018-2021

Project Leader: dr hab. Monika Wilde-**Piórko**

The aim of the project is to determine the seismic structure of the Earth's mantle from the analysis of surface waveforms generated by earthquakes and recorded by gravimeters used commonly to study the tides of the Earth. During the project, the records of earthquakes obtained by the gravimeter-seismometer pairs will be analysed. Group and phase dispersion curves of surface wave will be used to determine velocity distributions of seismic waves with depth by inversion methods: linearized inversion and Monte Carlo inversion. The inversions will be preceded by detailed parameter selection tests and final analysis of error estimation. The models of the Earth's mantle obtained from the analysis of the tidal record will be compared with the models obtained from the seismometer analysis and with previously published regional and global models. The models of the Earth's mantle obtained as a result of the project will be unique because they will be developed on the basis of records from which the absolute values of the velocity of seismic waves in the Earth's mantle could be determined.

Cooperation with The Institute for Sustainable Development (ISD) – Project Life ADAPTCITY - Preparation of a strategy for adaptation to climate change of the city of Warsaw with the use of city climate mapping and with public participation 2019

Project Leader: Prof. Katarzyna Dąbrowska Zielińska

The aim of the project, conducted under the contract between the Institute for Sustainable Development and the Institute of Geodesy and Cartography, was to determine the state of the ecosystem of the Capital City

of Warsaw in the period from the beginning of 2002 to the end of 2018. The analyses were performed for the needs of the final study in the field of monitoring the environmental problem within LIFE_ADAPTCITY_PL project.

The scope of the performed works covered determination of the changes of the following parameters characterizing the area of the capital city of Warsaw:

- biologically active surface,
- impervious and non-impervious surfaces,
- density of built-up land,
- albedo of the active surface,
- surface temperature,
- Normalized Difference Vegetation Index - NDVI.

The performed analyses were based on optical satellite data - Landsat 8 OLI / TIRS and Sentinel-2A / B MSI. Strategy for adaptation to climate change for Warsaw until 2030 with a perspective until 2050, adopted by the City Council of Warsaw, is the result of the project. The album entitled "Warsaw from Space", which includes series of maps and analyses carried out on the basis of satellite images, has been also published.

Statutory project

Monitoring wetlands in the trans-boundary Biosphere Reserve West Podlasie

Project duration: 2017-2018

Project Leader: dr Agata Hościło

The main aim was to exchange experience and knowledge in the use of remote sensed satellite data and technology for monitoring of wetlands located in the transboundary region of Belarus and Poland.

Project objectives:

- to examine the use of the latest European satellites of a series of Sentinel satellites and constellation of the Belarusian-Russian satellites (BKA - Canopus) with a spatial resolution of 2.1m (panchromatic) and 10.5m

(multispectral) for assessment of the current state and condition of wetlands in the Biosphere Reserve;

- to analysis land cover / use and land cover changes and to calculate the seasonal changes in soil moisture using radar Sentinel-1AB;
- to exchange knowledge and experience in data processing, analysis of satellite images and collecting field data using the state-of-the-art portable instruments;
- to organize two workshops integrated with the field visits at the wetland area in Poland and Belarus.

JECAM POLAND STUDY SITE - GEO -GEOGLAM since 2018

JECAM - Joint Experiment of Crop Assessment and Monitoring

Project Leader: Prof. Katarzyna Dąbrowska Zielińska

In 2017 Remote Sensing Centre joined the JECAM initiative - Joint Experiment of Crop Assessment and Monitoring. The goal of JECAM is to reach a convergence of approaches, develop monitoring and reporting protocols and best practices for a variety of global agricultural systems. JECAM will enable the global agricultural monitoring community to compare results based on disparate sources of data, using various methods, over a variety of global cropping systems. It is intended that the JECAM experiments will facilitate international standards for data products and reporting, eventually supporting the development of a global system of systems for agricultural crop assessment and monitoring Agriculture and Agri-Food Canada (AAFC) has taken on the secretariat role of the JECAM project on behalf the GEO Agricultural Monitoring Community of Practice. (Credits: www.jecam.org)

Project Overview:

Crop identification and acreage estimation: Remote Sensing Centre at IGiK conducts researches aimed to develop remote sensing methods for annual land use and crop types mapping and yield assessment at the regional

level.

Soil moisture: Information is required in near-real time (within hours) for watershed and field level estimates of absolute volumetric surface soil moisture and changes in soil moisture. Regional estimates are needed to define risk due to moisture anomalies. These regional estimates are to be provided on a twice/three times a month.

Crop biophysical variables (LAI): Information is needed frequently throughout the growing season (twice/three times a month). LAI estimates are to be assimilated into locally calibrated yield models, and to provide a more quantitative evaluation (relative to NDVI) of crop condition.

The mapping resolution is at 10 m from ESA satellites (Sentinel-1, Sentinel-2) and < 100 m from Canadian RADARSAT-2.

The State Forests National Forest Holding

Identification of forests on the post-agricultural land based on available satellite data.

Project duration:: 29.11.2018 – 29.11.2020

Project Leader: dr Agata Hościło

The aim of the project was to perform the study on the identification of forests on former farmland based on available satellite datasets over the period 1960-2018. The forest cover in the 1960s was developed by the expert manual interpretation based on the satellite images of the U.S. Air Force CORONA program. In case of mapping forests extent in later periods, a modern classification method with the use of machine learning algorithms was applied, using not only static classifiers, but also deep learning. The forest classifications were carried out on the basis of a series of satellite data from the Landsat MSS (1980), Landsat 5, 7 (1990 and 2000) and Sentinel-2 (2018) missions. The project

covered forests of all forms of ownership located in two Regional Directorate of State Forests including the national parks.

The project consortium includes the Institute of Geodesy and Cartography Centre of Applied Geomatics as a leader.

Articles 2018-2020

2018

- Baranowski M., Gotlib D., Olszewski R., 2018, Próba zdefiniowania domeny współczesnej kartografii, Roczniki Geomatyki, Vol. 4 (16), pp. 269-281.
- Bjerke J.W., Elverland E., Jaakola L., Lund L., Zagajewski B., Bochenek Z., Kłos A., Tømmervik H., 2018, High tolerance of a high-arctic willow and graminoid to simulated ice encasement, Boreal Environment Research, Vol. 23, pp. 329-338.
- Bochenek Z., Ziolkowski D., Bartold M., Orlowska K., Ochtyra A., 2018, Monitoring forest biodiversity and the impact of climate on forest environment using high-resolution satellite images, European Journal of Remote Sensing, Vol. 51 (1), pp. 166-181. doi:10.1080/22797254.2017.1414573
- Bojanowski J.S., Stöckli R., Duguay-Tetzlaff A., Finkensieper S., Hollmann R., 2018, Performance Assessment of the COMET Cloud Fractional Cover Climatology across Meteosat Generations, Remote Sensing 2018, Vol. 10 (5), 804. doi:10.3390/rs10050804
- Dabrowska-Zielinska K., Musial J., Malinska A., Budzynska M., Gurdak R., Kiryla W., Bartold M., Grzybowski P., 2018, Soil Moisture in the Biebrza Wetlands Retrieved from Sentinel-1 Imagery, Remote Sensing 2018, Vol. 10 (12), 1979. doi:10.3390/rs10121979
- Dabrowska-Zielinska K., Bartold M., Gurdak R., Gatkowska M., Kiryla W., Bochenek Z., Malinska A., 2018, Crop Yield Modelling Applying Leaf Area Index Estimated from Sentinel-2 and Proba-V Data at JECAM site in Poland, Proceedings of 2018 IEEE International Geoscience & Remote Sensing Symposium (IGARSS), 22 - 27 July 2018, Valencia, Spain. doi:10.1109/IGARSS.2018.8519120
- Gatkowska M., Wróbel K., 2018, Satelite Based (Pre-)System for Assessment of Lost in Agricultural Production Due to Negative Overwintering Pilot Study for Insurance Sector in Poland, Proceedings of

2018 IEEE International Geoscience & Remote Sensing Symposium (IGARSS), 22 - 27 July 2018, Valencia, Spain. doi:10.1109/IGARSS.2018.8518279

- Grad, M., Puziewicz, J., Majorowicz, J., Chrapkiewicz, K., Lepore, S., Polkowski, M., Wilde-Piórko, M., 2018. The geophysical characteristic of the lower lithosphere and asthenosphere in the marginal zone of the East European Craton. International Journal of Earth Sciences, vol. 107, issue 8, pp. 2711-2726, https://doi.org/10.1007/s00531-018-1621-y
- Grzybowski P., Gurdak R., 2018, Changes in the built-up areas at the aeration wedges of City of Warsaw, Geoinformation Issues, Vol. 10, No. 1 (10), pp. 37-51.
- Gurdak R., Grzybowski P., 2018, Feasibility study of vegetation indices derived from Sentinel-2 and PlanetScope satellite images for validating the LAI biophysical parameter to monitoring development stages of winter wheat, Geoinformation Issues, Vol. 10, No. 1 (10), pp. 27-35.
- Hoscilo A., Lewandowska, A., Konieczny A., Mroczek, K., Kulik S., 2018, EO based service for forest management [in:] The Ever Growing Use of Copernicus across Europe's Regions. A selection of 99 user stories by local and regional authorities, European Comission, European Space Agency and NEREUS - the Network of European Regions Using Space Technologies, pp. 88-89.
- Hoscilo A., Lewandowska A., Kaluski M., 2019, SAT4EST – Sentinel-based service supporting local administration in forest management, Living Planet Symposium, 13-17 May 2019, Milan, Italy.
- Hościło A., Lewandowska A., 2019, Mapping Forest Type and Tree Species on a Regional Scale Using Multi-Temporal Sentinel-2 Data, Remote Sensing, Vol. 11 (8), 929. doi:10.3390/rs11080929
- Hościło A., Lewandowska A., Konieczny A., Mroczek K., Kulik S., 2018, Satelitarne wsparcie dla starostów zarządzających lasami niepaństwowymi, Las Polski, 17/2018.
- Hościło A., Lewandowska A., 2018, Zastosowanie danych z satelity Sentinel–2 do szacowania rozmiaru szkód spowodowanych w lasach huraganowym wiatrem w sierpniu 2017 roku, Sylwan, Vol. 162 (8), pp. 619-627.
- Hoscilo A., Lewandowska A., Ziółkowski D., Stereńczak K., Lisańczuk M., Schmullius C., Pathe C., 2018, Forest Aboveground Biomass Estimation Using a Combination of Sentinel-1 and Sentinel-2 Data, Proceedings of 2018 IEEE International Geoscience & Remote Sensing Symposium

(IGARSS), 22 - 27 July 2018, Valencia, Spain. doi:10.1109/IGARSS.2018.8517965

- Kałuski M., Hościło A., Gurdak R., 2018, Accuracy assessment of the Copernicus Building Heights 2012 layer based on the city of Warsaw, Geoinformation Issues, Vol. 10, No. 1 (10), pp. 53-64.
- Kałuski M., Chmiel J., Fijałkowska A., 2018, Wykorzystanie analiz sieciowych przy projektowaniu objazdów imprez masowych, Roczniki Geomatyki, Vol. 4 (16), pp. 347-359.
- Kłos A., Ziembik Z., Rajfur M., Dołhańczuk-Śródka A., Bochenek Z., Bjerke J.W., Tømmervik H., Zagajewski B., Ziółkowski D., Jerz D., 2018, Using moss and lichens in biomonitoring of heavy-metal contamination of forest areas in southern and north-eastern Poland, Science of The Total Environment, Vol. 627, pp. 438-449. doi:10.1016/j.scitotenv.2018.01.211
- Łaszewski M., Kiryła W., 2018, Wpływ zadrzewienia stref nadbrzeżnych na warunki termiczne niewielkich cieków nizinnych w okresie letnim, Leśne Prace Badawcze, Vol. 79 (3), pp. 237-243. doi:10.2478/frp-2018-0023
- Manakos I., Tomaszewska M., Gkinis I., Brovkina O., Filchev L., Genc L., Gitas I.Z., Halabuk A. Inalpulat M., Irimescu A., Jelev G., Karantzalos K., Katagis T., Kupková L., Lavreniuk M., Mesaroš M., Mihailescu D., Nita M., Rusnak T., Stych P., Zemek F., Albrechtová J., Campbell P., 2018, Comparison of Global and Continental Land Cover Products for Selected Study Areas in South Central and Eastern European Region, Remote Sensing 2018, Vol. 10 (12), 1967. doi:10.3390/rs10121967
- Pfeifroth U., Bojanowski J.S., Clerbaux N., Manara V., Sanchez-Lorenzo A., Trentmann J., Walawender J.P., Hollmann R., Satellite-based trends of solar radiation and cloud parameters in Europe, Advances in Science and Research, Vol. 15, pp. 31-37. doi:10.5194/asr-15-31-2018
- Tuszyńska J., Gatkowska M., Wróbel K., Jagiełło K., 2018, A pilot study on determining approximate date of crop harvest on the basis of Sentinel-2 satellite imagery, Geoinformation Issues, Vol. 10, No. 1 (10), pp. 65-77.
- Vicente-Guijalba F., Jacob A., Lopez-Sanchez J.M., Loper-Martinez C., Duro J., Notarnicola C., Ziolkowski D., Mestre-Quereda A., Pottier E., Mallorqui J.J., Lavalle M., Engdahl M., 2018, Sincohmap: Land-Cover and Vegetation Mapping Using Multi-Temporal Sentinel-1 Interferometric Coherence.Proceedings of 2018 IEEE International Geoscience & Remote Sensing Symposium (IGARSS), 22 - 27 July 2018, Valencia, Spain. doi:10.1109/IGARSS.2018.8517926

- Zagajewski B., Kycko M., Tømmervik H., Bochenek Z., Wojtuń B., Bjerke J.W., Kłos A., 2018, Feasibility of hyperspectral vegetation indices for the detection of chlorophyll concentration in three High Arctic plants: Salix polaris, Bistorta vivipara, and Dryas octopetala, Acta Societatis Botanicorum Poloniae: Polar terrestrial ecosystems: ecology, evolution, and biogeography, Vol. 87 (4), 3604. doi:10.5586/asbp.3604

2019

- Baranowski M., Musiał E., 2019, Półwiecze działalności Polskiego Towarzystwa Informacji Przestrzennej pod przywództwem Profesora Jerzego Gaździckiego, Roczniki Geomatyki, Vol. 17, Nr 1 (84), pp. 7-25.
- Bartold M., Bochenek Z., 2019, Wpływ warunków meteorologicznych na początek okresu wegetacyjnego lasów liściastych północno-wschodniej Polski, Sylwan, Vol. 163 (12), pp. 997-1005. doi:10.26202/sylwan.2019044
- Godah W., Szelachowska M., Krynski J., 2019, On the recovery of temporal variations ofgeoid heights determined with the use of GGMs based on SST-hl data from nondedicated gravity satellite missions, Boletim de Ciências Geodésicas, Vol. 25, No. 3. doi.org/10.1590/s1982-21702019000300017
- Hościło A., Lewandowska A., 2019, Mapping Forest Type and Tree Species on a Regional Scale Using Multi-Temporal Sentinel-2 Data, Remote Sensing, Vol. 11 (8), 929. doi:10.3390/rs11080929
- Kossacki K.J., Misiura K., Czechowski L., 2019, Sublimation of buried cometary ice, Icarus, Vol. 329, pp. 72-78. doi:10.1016/j.icarus.2019.03.019
- Kulik M., Warda M., Bochniak A., Stamirowska-Krzaczek E., Turos P., Dąbrowska-Zielińska K., Bzoska-Bakalarz M., Bieganowski A., Trendak M., 2019, The Species Diversity of Grasslands in the Middle Wieprz Valley (PLH060005) Depending on Meadow Type and Mowing Frequency, Rocznik Ochrony Środowiska, Vol. 21 (1), pp. 543-555.
- Mandal D., Hosseini M., McNairn H., Kumar V., Bhattacharya A., Rao Y.S., Mitchell S., Dingle Robertson L., Davidson A., Dabrowska-Zielinska K., 2019, An investigation of inversion methodologies to retrieve the leaf area index of corn from C-band SAR data, International Journal of Applied Earth Observation and Geoinformation, Vol. 82, 101893. doi:10.1016/j.jag.2019.06.003
- Ray J.D., Vijayan M.S.M., Godah W., Kumar A., 2019, Investigation of background noise in the GNSS position time series using spectral analysis – A case study of Nepal Himalaya, Geodesy and Cartography, Warsaw, Poland, Vol. 68, No. 2. doi.org/10.24425/gac.2019.128468

- Rodríguez-Veiga P., Quegan S., Carreiras J., Persson H.J., Fransson J.E.S., Hoscilo A., Ziolkowski D., Sterenczak K., Lohberger S., Stängel M., Berninger A., Siegert F., Avitabile V., Herold M., Mermoz S., Bouvet A., Le Toan T., Carvalhais N., Santoro M., Cartus O., Rauste Y., Mathieu R., Asner G.P., Thiel C., Pathe C., Schmullius C., Seifert F.M., Tansey K., Balzter H., 2019, Forest biomass retrieval approaches from earth observation in different biomes, International Journal of Applied Earth Observation and Geoinformation, Vol. 77, pp. 53-68. doi:10.1016/j.jag.2018.12.008
- Šimanauskienė R., Linkevičienė R., Bartold M., Dąbrowska-Zielińska K., Slavinskienė G., Veteikis D., Taminskas J., 2019, Peatland degradation: the relationship between raised bog hydrology and NDVI, Ecohydrology 2019, e2159. doi:10.1002/eco.2159
- Stöckli R., Bojanowski J.S., John V.O., Duguay-Tetzlaff A., Bourgeois Q., Schulz J., Hollmann R., 2019, Cloud Detection with Historical Geostationary Satellite Sensors for Climate Applications. Remote Sensing, Vol. 11 (9), 1052. doi:10.3390/rs11091052

2020

- Bieganowski A., Dammer K.-H., Siedliska A., Bzowska-Bakalarz M., Kereś P.K., Dąbrowska-Zielińska K., Pflanz M., Schirrmann M., Garz A., 2020, Sensor-based outdoor monitoring of insects in arable crops for their precise control, Pest Management Science. doi:10.1002/ps.6098
- Bojanowski J.S., Musiał J.P., 2020, Dissecting effects of orbital drift of polar-orbiting satellites on accuracy and trends of climate data records of cloud fractional cover, Atmos. Meas. Tech., 13, 6771–6788. doi:10.5194/amt-13-6771-2020
- Chrapkiewicz, K., Wilde-Piórko, M., Polkowski, M., Grad, M., 2020. Reliable workflow for inversion of seismic receiver function and surface wave dispersion data: a "13 BB Star" case study. Journal of Seismology, vol. 24, 101-120, DOI: 10.1007/s10950-019-09888-1, Published: FEB 2020
- Dabrowska-Zielinska K., Malinska A., Bochenek Z., Bartold M., Gurdak R., Paradowski K., Lagiewska M., 2020, Drought Model DISS Based on the Fusion of Satellite and Meteorological Data under Variable Climatic Conditions, Remote Sensing, Vol. 12 (18), 2944. doi:10.3390/rs12182944
- Godah W., Szelachowska M., Ray J.D. ,Krynski J., 2020, Comparison of vertical deformations of the Earth's surface obtained using GRACE-based GGMs and GNSS data – A case study of South-Eastern Poland, Acta Geodynamica et Geomaterialia, Vol. 17, No. 2, DOI: 10.13168/AGG.2020.0012

- Godah W., Szelachowska M., Krynski J., Ray J.D., 2020, Assessment of Temporal Variations of Orthometric/Normal Heights Induced by Hydrological Mass Variations over Large River Basins Using GRACE Mission Data, Remote Sensing, 12(18). doi.org/10.3390/rs12183070
- Godah W., Ray J.D., Szelachowska M., Krynski J., 2020, The Use of National CORS Networks for Determining Temporal Mass Variations within the Earth's System and for Improving GRACE/GRACE-FO Solutions, Remote Sensing, 12(20). doi.org/10.3390/rs12203359
- Gurdak R., Bartold M., 2020, Remote sensing techniques to assess chlorophyll fluorescence in support of crop monitoring in Poland, Miscellanea Geographica, Vol.25, No.3. doi:10.2478/mgrsd-2020-0029
- Gurdak R., 2020, "BALTICSATAPPS" – przyspiesza tworzenie innowacji, Rzecz o Innowacjach, 2020-10-13.
- Gurdak R., Dąbrowska-Zielińska K., 2020, Ocena dokładności modeli szacowania wielkości powierzchni projekcyjnej liści (LAI) na podstawie danych satelitarnych, [W:] Młynarczyk A. (red.): Środowisko przyrodnicze jako obszar badań, Bogucki Wyd. Nauk., Poznań 2020. ISBN 978-837686-302-0
- Jacob A., Vicente-Guijalba F., Lopez-Martinez C., Lopez-Sanchez J.M., Litzinger M., Kristen H., Mestre-Quereda A., Ziółkowski D., Lavalle M., Notarnicola C., Suresh G., Antropov O., Ge S., Praks J., Ban Y., Pottier E., Mallorquí Franquet J.J., Duro J., Engdahl M.E., 2020, Sentinel-1 InSAR Coherence for Land Cover Mapping: A Comparison of Multiple Feature-Based Classifiers, IEEE Journal of Selected Topics in Applied Earth Observations and Remote Sensing, Vol. 13, pp.535-552. doi:10.1109/JSTARS.2019.2958847
- Peng J., Albergel C., Balenzano A., Brocca L., Cartus O., Cosh M.H., Crow W.T., Dabrowska-Zielinska K., Dadson S., Davidson M.W.J., de Rosnay P., Dorigo W., Gruber A., Hagemann S., Hirschi M., Kerr Y.H., Lovergine F., Mahecha M.D., Marzahn P., Mattia F., Musial J.P., Preuschmann S., Reichle R.H., Satalino G., Silgram M., van Bodegom P.M., Verhoest N.E.C., Wagner W., Walker J.P., Wegmüller U., Loew A., 2020, A roadmap for high-resolution satellite soil moisture applications – confronting product characteristics with user requirements, Remote Sensing of Environment, Vol. 252, 112162. doi:10.1016/j.rse.2020.112162
- Zeray-Öztürk E., Godah W., Abbak R.A., 2020, Estimation of Physical Height Changes from GRACE Satellite Mission Data over Turkey, Acta Geodaetica et Geophysica, 55(2). doi.org/10.1007/s40328-020-00294-5

2.3 Department of GIS, Cartography and Remote Sensing, Institute of Geography and Spatial Management, Jagiellonian University

Research and educational activities of the Department of GIS, Cartography and Remote Sensing, Institute of Geography and Spatial Management, Jagiellonian University. Address: 30-387 Kraków, Gronostajowa 7. Contact person: Jacek Kozak, jacek.kozak@uj.edu.pl

Regional Scale Mapping of Grassland Mowing Frequency with Sentinel-2 Time Series

This study aimed to evaluate the potential of a time series of Sentinel-2 data for mapping of mowing frequency in the region of Canton Aargau, Switzerland. Two cloud masking processes and three spatial mapping units (pixels, parcel polygons and shrunken parcel polygons) were tested, and the influence of missing data on the ability to accurately detect and map grassland mowing was investigated. We found that more than 40% of the study area was mown before 15 June, while the remaining part was either mown later, or was not mown at all. The highest accuracy for detection of mowing events was achieved using additional clouds masking and size reduction of parcels, which allowed correct detection of 77% of mowing events. Moreover, we found that using only standard cloud masking leads to significant overestimation of mowing events, and that the detection based on sparse time series does not fully correspond to key events in the grass growth season.

- Kolecka, N., Ginzler, C., Pazur, R., Price, B., Verburg, P.H., 2018. Regional scale mapping of grassland mowing frequency with Sentinel-2 time series. Remote Sens. 10, 1221. doi:10.3390/rs10081221

Contact person: Natalia Kolecka, natalia.kolecka@uj.edu.pl

Field parcel and crop types mapping

The overall goal of this project was to develop methods providing the necessary data for ALMaSS Model (Animal, Landscape and Man Simulation System (Topping et al. 2003)), in particular: field parcel maps and information on crop types. The primary data were satellite Sentinel-1 (S1) and Sentinel-2 (S2) imagery. The S1 and S2 data were accessed and processed via Google Earth Engine (GEE, https://earthengine.google.com/), a planetary-scale platform for Earth science data and analysis, by means of JavaScript API and Google computing power. To derive field boundaries and determine crop types, dense seasonal time series (TS) of S2 and S1 data were used. To delineate field boundaries, spatial segmentation was performed in eCognition software. For crops classification, the supervised classification based on the NDVI TS were used. Additionally, to mask areas of non-agricultural use, Copernicus High Resolution Layers (HRL) were used. The Pan-European High Resolution Layers (HRL) provide information on specific land cover characteristics, and are complementary to land cover / land use mapping such as in the CORINE land cover (CLC) datasets.

- Internal report – EcoStack Project, https://www.ecostack-h2020.eu/

Contact person: Natalia Kolecka, natalia.kolecka@uj.edu.pl

Agricultural land greening vs. land abandonment mapping

The main aim of this study was to investigate the relation between long-term greening and land change dynamics, such as ALA, over varied landscapes in Poland. The 1986 to 2019 Landsat-derived Normalized Difference Vegetation Index (NDVI) time series were spatially-temporally segmented to detect periods of long-term greening, and to assess its relation to actual information on land abandonment. The results showed widespread long-term greening in Poland (up to 60% of its territory), which was independent of former and current land

uses, and affected both transitional and stable land uses.

- Paper in review: Kolecka, N., Greening trends and their relationship with agricultural land abandonment across Poland. Remote Sens. of Environment.

Contact person: Natalia Kolecka, natalia.kolecka@uj.edu.pl

Assessing the suitability of urban-oriented land cover products for mapping rural settlements: the case of the Carpathian ecoregion

In recent years, new settlement mapping products have become available at the global and/or continental scale. Although accuracy assessments have indicated the high quality of these products, they were performed mainly for urban areas. However, there is also a need to monitor rural settlement development, as it is very often located in proximity to biodiversity hotspots, influencing nature conservation measures. In this project, we verified the ability of three urban-oriented, freely available settlement mapping products (the Global Urban Footprint, the European Settlement Map and the Open Street Map) to detect rural settlements, using the Carpathian ecoregion as an example. Two independent accuracy assessment procedures indicated that the Global Urban Footprint captures rural settlements most effectively in the study area (overall accuracy (OA) – 65.4% and 92.5% depending on the procedure). At the same time, the European Settlement Mask overestimated settlement areas (OA – 49.5% and 90.8%), while the Open Street Map (OA – 61.2% and 90.2%) was the most inconsistent source of settlement data. A regional comparison indicated some deviations from these accuracies (e.g., a very good performance of the Open Street Map in the Polish part of the Carpathian ecoregion), reflecting the variability of settlement structures within the study area. This study highlights that although the Global Urban Footprint is the most effective in mapping rural settlements across the Carpathian

ecoregion as a whole, local rural settlement structure has to be taken into account when deciding which settlement product is the most appropriate for analysis at the regional level.

- Paper in review: Kaim D., Ziółkowska E., Grădinaru S.R., Pazur R., Assessing the suitability of urban-oriented land cover products for mapping rural settlements: the case of the Carpathian ecoregion.

Contact person: Dominik Kaim, dominik.kaim@uj.edu.pl

Forest height estimation using passive and active remote sensing data

Recent studies demonstrate a significant increase in a number of forest biomass estimation studies (above-ground biomass, AGB), mainly in relation to carbon sequestration and energy production from biomass. Although several methods to estimate forest biomass exist, there is still a strong need to reduce their uncertainty. One of the most crucial parameters of forest biomass estimation is vegetation (forest) height. National forest inventories (NFIs) provide accurate tree height measurements, however due to cost and time constraints they do not cover the entire forest area. Access to passive and active remote sensing data allows to estimate forest height, but to increase the accuracy, integration with reference data and other datasets is needed. The study focuses on the usage of openly available Sentinel-1 & Sentinel-2 data together with LiDAR, stereo aerial imagery, NFI data and Unmanned Aerial Vehicle imagery to elaborate methods of forest height estimation, for areas with various stand structures. The combination of different models will help to validate the sensitivity of remote sensing sensors and determine crucial limitations of remotely sensed data in terms of forest height estimation, improving the understanding of forest management impact on carbon sequestration and biodiversity.

- research carried out within the PhD dissertation in the Institute of Geography and Spatial Management, Jagiellonian University

Contact person: monika.dobosz@gmail.com

Innovation on Remote Sensing Education and Learning (IRSEL)

Innovation on Remote Sensing Education and Learning (IRSEL, project id: 586037-EPP-1-2017-1-HU-EPPKA2-CBHE-JP) project was carried out in the framework of the Erasmus+ Capacity Building in Higher Education, Key Action 2. It developed an innovative learning platform dedicated to remote sensing, for Asian countries (China and Thailand). The content of the proposed learning platform was designed to meet MSc standards of related disciplines. The learning platforms at the partner universities in China and Thailand (Fujian Normal University and Yunnan Normal University, China; Asian Institute of Technology and Khon Kaen University, Thailand) host currently 20 newly developed modules on remote sensing on Moodle-based platforms, to be applied in the curricula of participating universities, improving the quality of higher education, delivering a background for studying the practical use of the remote sensing techniques and enhancing the practical use of remote sensing on a wide range of applications serving the labour market and society. Modules were developed within the partnership of four European universities (Obuda University, Hungary – the project leader; University of Natural Resources and Life Sciences (BOKU), Austria; Jagiellonian University, Poland; University of Twente, Netherlands). IRSEL project was concluded in October 2020.

- IRSEL webpage: http://irsel.eu/

Contact person: Jacek Kozak, jacek.kozak@uj.edu.pl

Other publications

• Dobosz M., Kozak J., Kolecka N., 2019, Integrating contemporary spatial forest cover data in the polish Carpathians: does abundance of data increase knowledge or uncertainty? Geoinformatica Polonica 18, 31-43, DOI 10.4467/21995923GP.19.002.10886

• Kolecka N., Kozak J., 2019, Wall-to-Wall Parcel-Level Mapping of Agricultural Land Abandonment in the Polish Carpathians. Land 2019, 8, 129; doi:10.3390/land8090129

• Kozak J., 2018, Możliwości wykorzystania źródłowych i przetworzonych zobrazowań satelitarnych pozyskiwanych w ramach programów Unii Europejskiej, [w:] Geoinformacja zmienia nasz świat. Główny Urząd Geodezji i Kartografii, Centrum UNEP/GRID-Warszawa, s. 140-147

• Kozak J., Ziółkowska E., Vogt P., Dobosz M., Kaim D., Kolecka N., Ostafin K., 2018, Forest-Cover Increase Does Not Trigger Forest-Fragmentation Decrease: Case Study from the Polish Carpathians. Sustainability 10, 1472, doi:10.3390/su10051472

• Szwagrzyk M., Kaim D., Price B., Wypych A., Grabska E., Kozak J., 2018, Impact of forecasted land use changes on flood risk in the Polish Carpathians, Natural Hazards 94, 1, 227–240

2.4 Institute of Urban Geography, Tourism and Geoinformation, Faculty of Geographical Sciences University of Lodz

ul. Kopcińskiego 31, 91- 142 Lodz, Poland
https://www.geo.uni.lodz.pl

Research in the field of remote sensing carried out at the Institute of Urban Geography, Tourism and Geoinformation concerned the following issues:

- Monitoring sessile oak phenology with low altitude remote sensing (UAV)
- Quantitative and qualitative assessment of urban greenery using remote sensing techniques
- Modelling solar radiation in the forest using remote sensing data
- Modelling spatial horizontal and vertical structure of forests using LiDAR data
- Studies on land use / land cover changes
- Monitoring of an artificial water reservoir located in a lowland area

The research was carried out as part of the statutory activity of the University of Lodz and following projects:

- MONSUL project in the area PL 03 "Improvement of Environmental Control and Monitoring" in the program of the Norwegian foundation EEA (EEA Funds 2009–2014);
- LIFE+ ForBioSensing PL "Comprehensive monitoring of stand dynamics in the Białowieża Forest as supported by remote sensing techniques", co-funded by Life+ (contract number LIFE13 ENV/ PL/000048) and Poland's National Fund for Environmental Protection and Water Management (contract number 485/2014/WN10/OP-NMLF/D).
- RPLD.01.02.02-10-0131/19 PRO-MIS Program Rekultywacji Obszarowej – Monitoring i Strategia – modelowe rozwiązanie dla zbiorników wodnych na

podstawie przeprowadzonych prac B+R dotyczących Zbiornika Sulejowskiego 2020-2023 [PRO-MIS Area Reclamation Program – Monitoring and Strategy – a model solution for water reservoirs based on R&D works carried out on the Sulejów Reservoir 2020-2023].

Publications

1. Adamiak M., Biczkowski M., Lesniewska-Napierala K., Nalej M., Napierala T., 2020: Impairing Land Registry: Social, Demographic, and Economic Determinants of Forest Classification Errors. Remote Sensing 12 (2628). DOI: 10.3390/rs12162628
2. Będkowski K., 2020: Taxonomic analysis of airborne laser scanning data for the recognition of stand vertical structure and its spatial variability. Sylwan 164 (10): 805-819. DOI: https://doi.org/10.26202/sylwan.2020087
3. Będkowski K., Jaskulski M., Bielecki A., 2018: 23rd Conference on Photointerpretation and Remote Sensing. Acta Universitatis Lodziensis Folia Geographica Socio-Oeconomica 34: 115-117. DOI: 10.18778/1508-1117.34.08
4. Bielecki A., 2018: Comparison of LiDAR data processing software in the field of DTM and DSM generation. Teledetekcja Środowiska T. 58: 5-11. https://teledetekcja.pw.edu.pl/archiwum/tom-58/
5. Bielecki A., Będkowski K., 2020: Ekspertyza dla Urzędu Miasta Łodzi „Określenie metodami zdalnymi stanu zieleni miejskiej" [Expertise for the City of Lodz Municipality „Determining the state of urban greenery with remote methods"].
6. Jaskulski M., 2018: Contemporary remote sensing in geographical environment research – 23rd Conference on Photointerpretation and Remote Sensing – Lodz, 24–25 September 2018. Teledetekcja Środowiska 59 (2018/2): 51-57. https://teledetekcja.pw.edu.pl/archiwum/tom-59/
7. Jaskulski M., Szmidt A., Zbiciński I., Ziemińska-Stolarska A., Adamiec J., 2018: Construction of a bathymetric map (1:25 000) of an artificial water reservoir located in a lowland area: the example of the Sulejów Reservoir, Poland. Teledetekcja Środowiska T. 59: 5-12. https://teledetekcja.pw.edu.pl/archiwum/tom-59/
8. Kałużna U., Będkowski K., 2020: Klasyfikacja pokrycia terenu z wykorzystaniem obrazów Sentinel-2A przetworzonych za pomocą metody głównych składowych (PCA) [Land cover classification using Sentinel-2A images

processed by the principal components method (PCA)]. Teledetekcja Środowiska T. 61: 19-37. https://teledetekcja.pw.edu.pl/archiwum/tom-61/
9. Lechowski Ł., 2019: Przekształcenia funkcjonalno-przestrzenne terenów położonych wzdłuż autostrad A1 i A2 w gminach powiatu zgierskiego [Functional and spatial transformations of areas along the A1 and A2 highways in the communes of the Zgierz district]. Wydawnictwo Uniwersytetu Łódzkiego, Łódź.
10. Lesniewska-Napierala K., Nalej M., Napierala T., 2019: The Impact of EU Grants Absorption on Land Cover Changes - the Case of Poland. Remote Sensing 11(20), 2359. DOI: 10.3390/rs11202359
11. Matuszewska M., Będkowski K., 2019: Analysis of the development of the city Sieradz based on the interpretation of aerial imagery and alorisation of the space using elements of fuzzy sets theory. Acta Scientiarum Polonorum Administratio Locorum 18(4), 381–395. DOI: 10.31648/aspal.3688
12. Nalej M., 2018: Changes of land cover in the western part of the Zduńska Wola city in the years 1933–2015. Teledetekcja Środowiska T. 58: 13-23. https://teledetekcja.pw.edu.pl/archiwum/tom-58/
13. Nalej M., 2019: Pokrycie terenu województwa łódzkiego w latach 2000–2018 w świetle danych Corine Land Cover. Acta Geographica Lodziensia 109: 75-89. DOI: 10.26485/AGL/2019/109/5
14. Olpenda A.S., Stereńczak K.S., Będkowski K., 2018: Modeling Solar Radiation in the Forest Using Remote Sensing Data: A Review of Approaches and Opportunities. Remote Sensing 2018 Vol. 10, 5: 1-22. DOI: 10.3390/rs10050694
15. Olpenda A.S., Stereńczak K., Będkowski K., (2019): Modeling Solar Radiation in the Forest Using Remote Sensing Data: A Review of Approaches and Opportunities. [in:] Kaskaoutis D., Polo J. (eds), Solar Radiation, Modelling and Remote Sensing. MDPI Basel, Beijing, Wuhan, Barcelona, Belgrade, ISBN 978-3-03921-004-6, pp. 130-151.
16. Olpenda A.S., Stereńczak K.S., Będkowski K., 2019: Estimation of Sub-canopy Solar Radiation from LiDAR Discrete Returns in Mixed Temporal Forest of Bialowieza, Poland. International Journal of Applied Earth Observations and Geoinformation 79, July, pp. 116-132. https://doi.org/10.1016/j.jag.2019.03.005
17. Worm A., Będkowski K., Bielecki A., 2018: The use of surface and volume indicators from high resolution remote sensing data to assess the vegetation filling of urban quarters in Łódź city centre, Poland. Teledetekcja Środowiska T. 60: 5-20. https://teledetekcja.pw.edu.pl/a

2.5 KP LABS

Bojkowska 37, Gliwice, 44-100

Deep learning-powered analysis of hyperspectral images

Jakub Nalepa (KP Labs, Silesian University of Technology)

2.5.1 About company

KP Labs is a 50 people company based in Poland, Gliwice which focuses on delivering AI computers and software for space missions. KP Labs is focusing on designing and implementing a battery of machine learning-powered techniques for hyperspectral image analysis and super-resolution reconstruction (both single- and multiple-image). It tackles the problems of hyperspectral data reduction, classification, segmentation, and unmixing. Also, is developing and thoroughly validating techniques that allow us to deploy such algorithms, especially utilizing deep learning, in the target hardware-constrained execution environments. KP Labs develops Intuition-1 satellite that will be equipped with a hyperspectral sensor, alongside on-board deep learning capabilities, planned to be launched in Q4 2022. KP labs actively disseminating their results, their techniques have been published in prestigious journals and conferences, including IEEE GRSL, IEEE IGARSS, Phi Week, and IAC. Company was awarded the Interactive Session Prize Paper Award at the GRSS Symposium (IGARSS 2020) – its paper was selected out of approx. 1500 posters.

2.5.2 Foreword

Hyperspectral imaging has become a mature technology which brings exciting possibilities in various Earth observation applications in a plethora of fields, including precision agriculture, forestry, event detection and tracking, and more. KP Labs address the most important challenges toward effective hyperspectral image analysis and at developing techniques and tools which

will help extract value from such highly dimensional image data. Since the approaches are generic, they can be easily deployed in a range of real-life applications, therefore enable easier adoption of this revolutionizing technology. The work reported below has been performed within the ESA-commissioned projects (HYPERNET and BEETLES), alongside the project co-financed by The National Centre for Research and Development within our Intuition-1 hyperspectral mission.

2.5.3 Supervised classification and segmentation of hyperspectral images

Although the number of manually annotated ground-truth hyperspectral sets is still limited, supervised classification techniques are being actively developed in the literature. Here, the deep learning-powered algorithms have established the current state of the art in the field. KP Labs have implemented both state-of-the-art deep networks for hyperspectral image and proposed numerous new techniques, including attention-based convolutional neural networks (which allow to determine the most informative bands during the training process), and various spectral models [Nalepa2019Validation].

Papers:

[Nalepa2019Validation] Jakub Nalepa, Michal Myller, Michal Kawulok: Validating Hyperspectral Image Segmentation. IEEE Geoscience and Remote Sensing Letters 16(8): 1264-1268 (2019).
https://ieeexplore.ieee.org/document/8642388

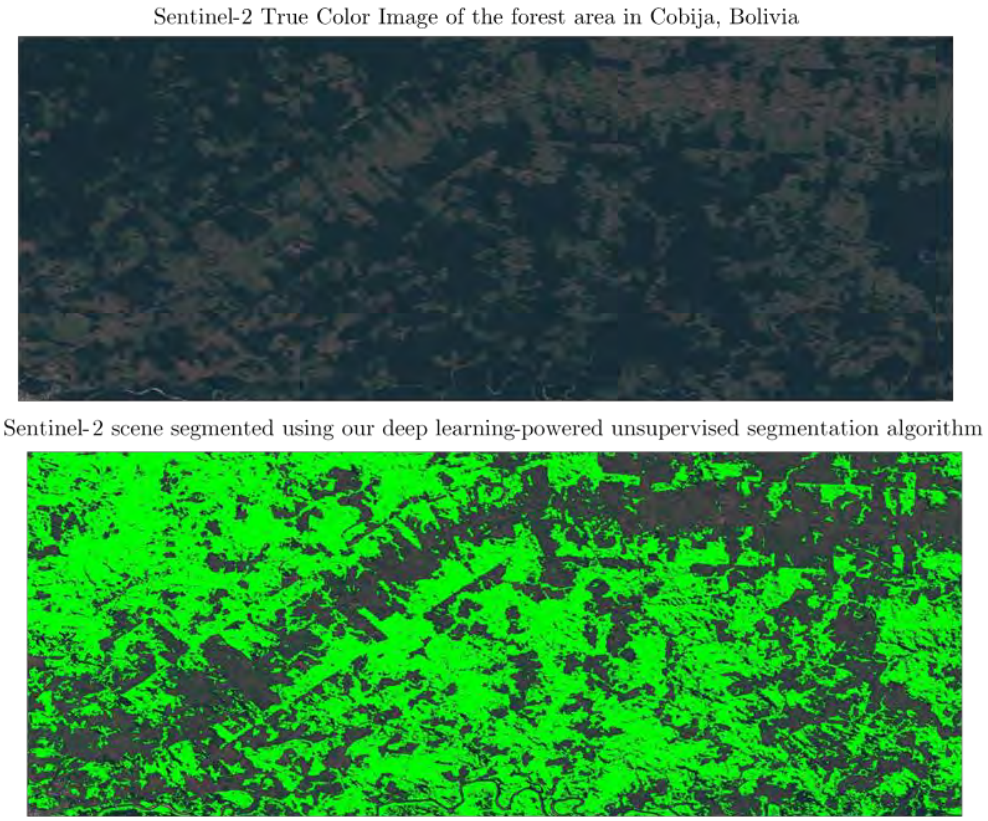

Fig. 2.9. Classification and segmentation of multi/hyperspectral images have wide practical applications – automated segmentation of multi/hyperspectral imagery can help quantify the forest area in a fully reproducible way. Hence, it can be used to detect illegal logging.

2.5.4 Unsupervised segmentation of hyperspectral images

Although deep learning has established the state-of-the-art in the field, it remains challenging to train well-generalizing models due to the lack of ground-truth data. KP Labs tackled this problem and introduced several end-to-end approaches to segment hyperspectral images in a fully unsupervised way. Such techniques include 3-D convolutional autoencoders (3D-CAE) with clustering and showed that it can be used to process any hyperspectral data without any prior class labels available [Nalepa2020CAE].

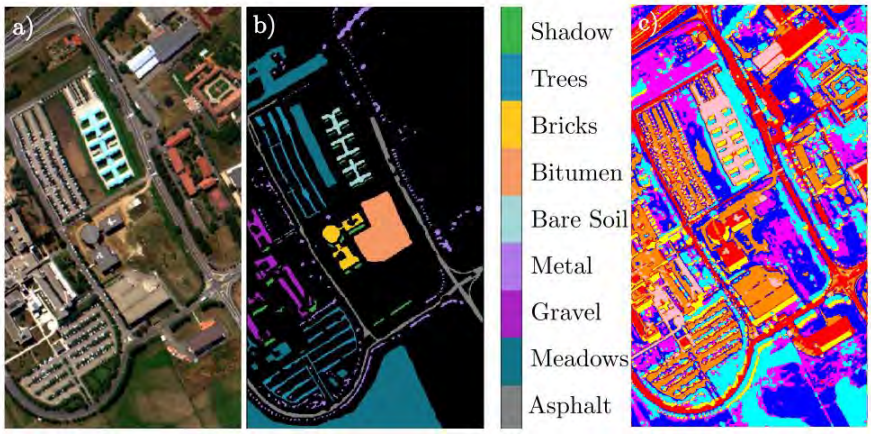

Fig. 2.10. Unsupervised segmentation offers new possibilities of unrevealing information captured within newly acquired hyperspectral images and existent benchmarks. This example shows: 1) the Pavia University scene, 2) its ground truth (black color is "unknown class"), and 2) our full 3D-CAE segmentation which is not only very detailed but also sheds new light on those "unknown" objects. This figure comes from [Nalepa2020CAE].

Papers:

[Nalepa2020CAE] Jakub Nalepa, et al.: Unsupervised Segmentation of Hyperspectral Images Using 3-D Convolutional Autoencoders. IEEE Geoscience and Remote Sensing Letters 2020: 1-5 (2020), in press. https://ieeexplore.ieee.org/document/8948005

2.5.5 Transfer learning for hyperspectral image classification

KP Labs showed how to effectively deal with a limited number and size of available hyperspectral ground-truth sets and apply transfer learning for building deep feature extractors in the supervised setting [Nalepa2020Transfer]. Also, KP Labs exploit spectral dimensionality reduction (by simulating wider spectral bands) to make the technique applicable over hyperspectral data acquired using different sensors.

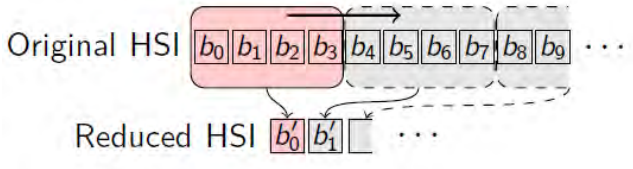

Fig. 2.11. Simulating wider bands from the hyperspectral imagery. This figure comes from [Marcinkiewicz2019MSI].

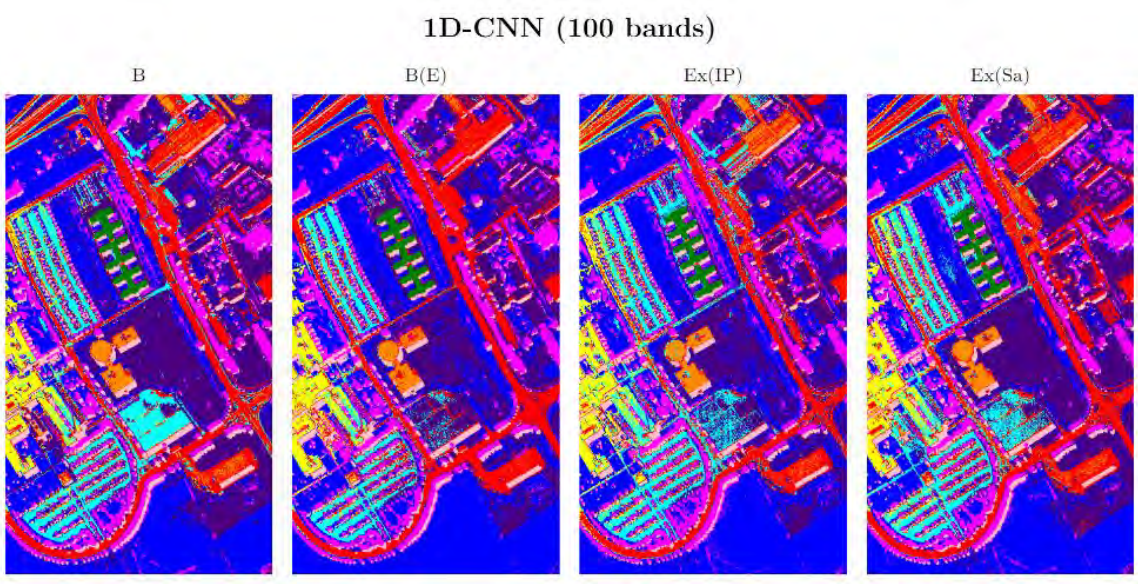

Fig. 2.12. Example visualizations of the segmentations obtained using our spectral convolutional neural network over spectrally reduced data (100 simulated bands) trained in various ways: using the balanced training set (B), reduced balanced data B(E), and with transfer learning, where feature extractors were trained over different source data – Ex(IP) and Ex(Sa) (for details, see [Nalepa2020Transfer]). This figure comes from [Nalepa2020Transfer].

Papers:

[Nalepa2020Transfer] Jakub Nalepa, Michal Myller, Michal Kawulok: Transfer Learning for Segmenting Dimensionally Reduced Hyperspectral Images. IEEE Geoscience and Remote Sensing Letters 2020: 1-5 (2020), in press. https://ieeexplore.ieee.org/document/8864017

[Marcinkiewicz2019MSI] Michal Marcinkiewicz, Michal Kawulok, Jakub Nalepa: Segmentation of Multispectral Data Simulated from Hyperspectral Imagery. IGARSS 2019: 3336-3339 https://ieeexplore.ieee.org/document/8900502/

2.5.6 Training- and test-time augmentation of hyperspectral data

Data augmentation helps improve generalization capabilities of deep networks when only limited ground-truth training data are available. KP Labs proposed test-time augmentation of hyperspectral data, which is executed during the inference rather than before the training of deep networks [Nalepa2020Augmentation]. The experiments revealed that the augmentations boost generalization of deep models and work in real time, and

the test-time approach can be combined with training-time techniques to enhance the classification accuracy.

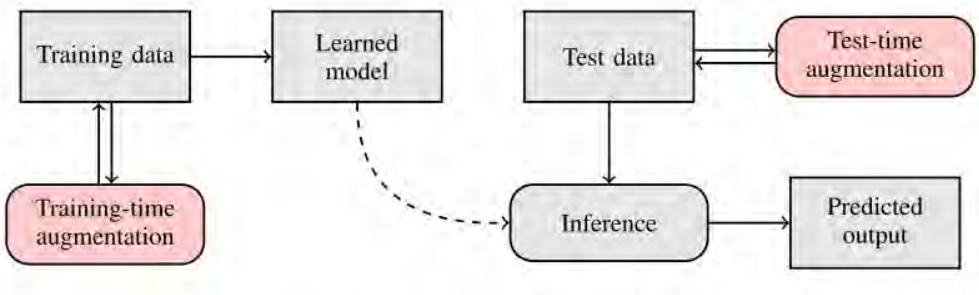

Fig. 2.13. Training-time augmentation increases the size and representativeness of a training set, whereas the test-time augmentation creates synthesized examples based on the incoming one to form a voting classification ensemble. This figure comes from [Nalepa2020Augmentation].

Papers:

[Nalepa2020Augmentation] Jakub Nalepa, Michal Myller, Michal Kawulok: Training- and Test-Time Data Augmentation for Hyperspectral Image Segmentation. IEEE Geoscience Remote Sensing Letters 17(2): 292-296 (2020) https://ieeexplore.ieee.org/document/8746168

2.5.7 Validating hyperspectral image classification and segmentation

Validating hyperspectral image segmentation algorithms is a challenging task due to the limited number of manually annotated ground-truth sets. Practically all segmentation techniques have been tested using up to three benchmarks, with Salinas Valley, Pavia University and Indian Pines constituting the mainstream. A common approach is to extract training and test pixels from the *very same* hyperspectral scene, and almost all algorithms are being validated in the Monte-Carlo cross-validation setting. Such random selection of training and test sets may, however, lead to overoptimistic results (as the training-test information leak can occur), especially for spectral-spatial algorithms. To address this issue, KP Labs have developed a tool for elaborating patch-based training-validation-test splits which help quantify the classification performance of emerging hyperspectral classification algorithms without any information leakages.

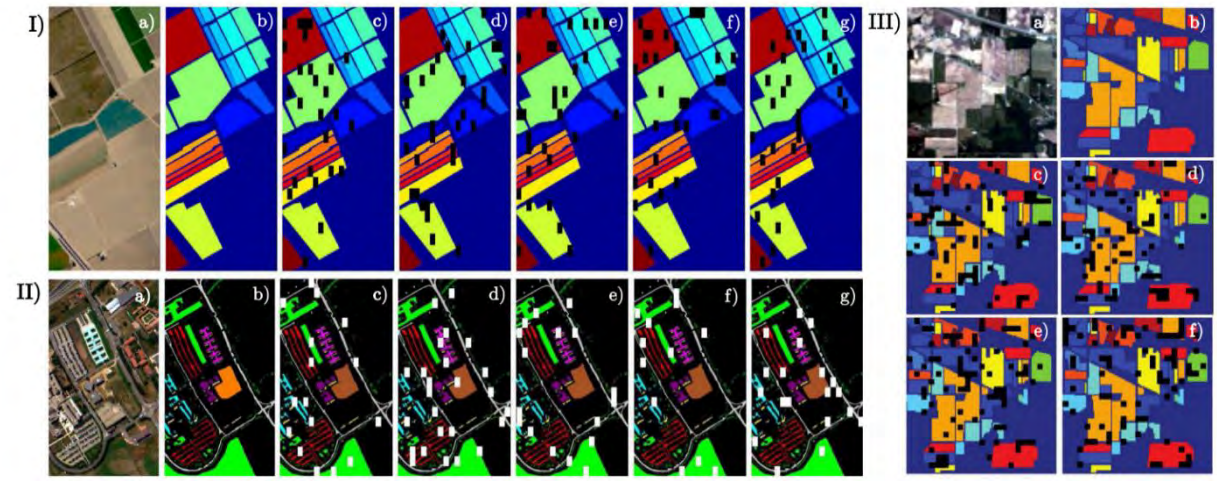

Fig. 2.14. The benchmark data generated over the (I) Salinas Valley (five non-overlapping folds), (II) Pavia University (five folds), and (III) Indian Pines (four folds). (a) True-color composite, (b) ground-truth segmentation, (c)-(g) visualization of all folds for Salinas and Pavia, (c)-(f) visualization of all folds for Indian Pines. Black patches (white for Pavia University) indicate the training pixels, whereas the other pixels are used for testing. This figure comes from [Nalepa2019Validation].

Papers:

[Nalepa2019Validation] Jakub Nalepa, Michal Myller, Michal Kawulok: Validating Hyperspectral Image Segmentation. IEEE Geoscience and Remote Sensing Letters 16(8): 1264-1268 (2019). https://ieeexplore.ieee.org/document/8642388

2.5.8 Attention-based convolutional neural networks for hyperspectral band selection

To reduce the time (and ultimately cost) of transferring hyperspectral data from a satellite back to Earth, various band selection algorithms have been proposed. They are built upon the observation that for a vast number of applications only a subset of all bands convey the important information about the underlying material, hence we can safely decrease the data dimensionality without deteriorating the performance of hyperspectral classification and segmentation techniques. KP Labs introduced a novel algorithm for hyperspectral band selection that couples new attention-based convolutional neural networks used to weight the bands according to their

importance with an anomaly detection technique which is exploited for selecting the most important bands. The proposed attention-based approach is data-driven, re-uses convolutional activations at different depths of a deep architecture, identifying the most informative regions of the spectrum [Ribalta2020Attention].

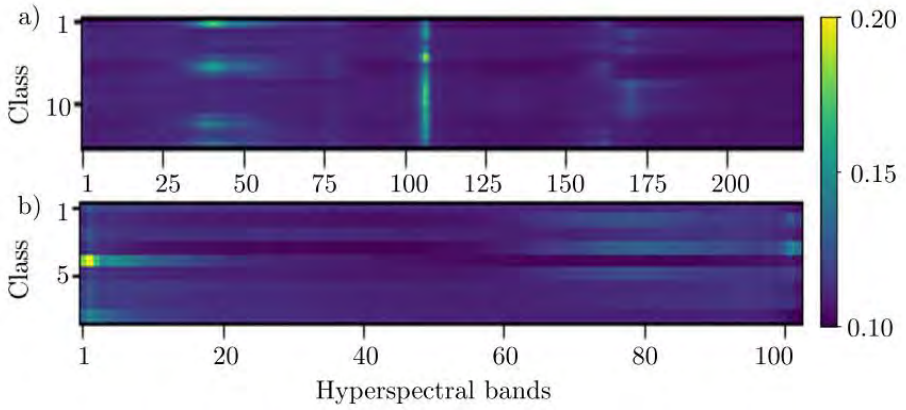

Fig. 2.15. Example average attention-score heatmaps for a) Salinas Valley and b) Pavia University show that certain bands convey more information than the others (the brighter the regions are, the higher attention scores were obtained, hence these bands are more "important"). This figure comes from [Ribalta2020Attention].

Papers:

[Ribalta2020Attention] Pablo Ribalta Lorenzo, Lukasz Tulczyjew, Michal Marcinkiewicz, Jakub Nalepa: Hyperspectral Band Selection Using Attention-Based Convolutional Neural Networks. IEEE Access 8: 42384-42403 (2020) https://ieeexplore.ieee.org/document/9019632

2.5.9 Quantizing deep neural networks for efficient and resource-frugal hyperspectral classification and segmentation

Large-capacity learners, e.g., deep neural networks, are characterized by significant memory footprints. This is a serious obstacle in employing them on board a satellite for Earth observation. To tackle this issue, KP Labs introduced resource-frugal quantized convolutional neural networks, and greatly reduced their size without adversely affecting the classification capability [Nalepa2020Quantization].

Papers:

[Nalepa2020Quantization] Jakub Nalepa, Marek Antoniak, Michal Myller, Pablo Ribalta Lorenzo, Michal Marcinkiewicz: Towards resource-frugal deep convolutional neural networks for hyperspectral image segmentation. Microprocess. Microsystems 73: 102994 (2020) https://www.sciencedirect.com/science/article/pii/S0141933119302844

2.5.10 Full publication list

a) HYPERSPECTRAL DATA

Hyperspectral Image Classification Using Spectral-Spatial Convolutional Neural Networks. Jakub Nalepa, Lukasz Tulczyjew, Michal Myller, Michal Kawulok

International Geoscience And Remote Sensing Symposium, IEEE IGARSS 2020

In this paper, we introduced a spectral-spatial convolutional neural network for hyperspectral image classification.

Segmenting Hyperspectral Images Using Convolutional Neural Networks in the Presence of Noise. Jakub Nalepa, Marek Stanek

International Geoscience And Remote Sensing Symposium, IEEE IGARSS 2020

In this paper, we experimentally investigated the impact of noise of various distributions on the performance of deep learning-powered hyperspectral classification techniques.

Leopard: A new chapter in on-board deep learning-powered analysis of hyperspectral imagery Jakub Nalepa, Piotr Kuligowski, Michał Gumiela, Marcin Drobik, Maciej Nowak

Proc. 71st International Astronautical Congress (IAC) – The CyberSpace Edition, pp. 1 – 4, 12-14 October 2020.

In this presentation, we discuss our approach toward on-board hyperspectral image processing using deep learning deployed over hardware-constrained execution environments, and presented Leopard, our DPU for such tasks.

Toward automated collision avoidance: Predicting the risk of satellite collisions using machine learning-powered techniques Łukasz Tulczyjew, Michał Myller, Michał Kawulok, Daniel Kostrzewa, Jakub Nalepa

Proc. 71st International Astronautical Congress (IAC) – The CyberSpace Edition, pp. 1 – 4, 12-14 October 2020.

In this presentation, we discuss our machine learning techniques for predicting the risk of satellite collisions.

The size matters: On-board hyperspectral data reduction using deep learning Jakub Nalepa, Łukasz Tulczyjew, Michał Myller, Michał Kawulok

Proc. 7th International Workshop on On-Board Payload Data Compression, September 21-23, pp. 1 – 8, European Space Agency Conference, 2020.

In this talk, we discussed our techniques for hyperspectral data reduction that may be deployed on-board imaging satellites.

Look Ma, No Ground Truth! Extracting value from multi- and hyperspectral images using unsupervised learning

Jakub Nalepa, Łukasz Tulczyjew, Michał Myller, Michał Kawulok

European Space Agency Earth Observation Φ-Week, Φ-Week 2020, Online Conference.

In this talk, we discussed our approaches toward dealing with limited (or non-existing) ground-truth datasets in the context of hyperspectral image classification and segmentation.

Unsupervised Feature Learning Using Recurrent Neural Nets for Segmenting Hyperspectral Images

IEEE Geoscience and Remote Sensing Letters, pp. 1-5, 2020 (in press)

Łukasz Tulczyjew, Michał Kawulok, Jakub Nalepa

Full paper available at: https://ieeexplore.ieee.org/document/9165097

In this paper, we presented our unsupervised technique for segmenting hyperspectral imagery that utilizes recurrent neural networks to capture latent

data characteristics. Such techniques may be exploited to accurately segment hyperspectral images without any ground truth. Also, we demonstrated that our approaches can be easily used for segmenting multispectral imagery.

Hyperspectral Band Selection Using Attention-Based Convolutional Neural Networks.

IEEE Access, vol. 8, pp 42384-42403, IEEE, 2020.

Pablo Ribalta Lorenzo, Lukasz Tulczyjew, Michal Marcinkiewicz, Jakub Nalepa

Full paper available at: https://ieeexplore.ieee.org/document/9019632

In this paper, we showed how attention-based convolutional neural networks coupled with anomaly detection can be used for selecting the most informative hyperspectral bands – our attention-based CNNs can not only extract such bands, but are also fully-functional classification models.

Towards resource-frugal deep convolutional neural networks for hyperspectral image segmentation.

Microprocessors and Microsystems, 102994, pp 1-44, Elsevier, 2020.

Jakub Nalepa, Marek Antoniak, Michal Myller, Pablo Ribalta Lorenzo, Michal Marcinkiewicz

Full paper available at:

https://www.sciencedirect.com/science/article/pii/S0141933119302844

In this paper, we tackled the problem of CNN quantisation for making such models memory-efficient and ready to be deployed on-board a satellite. We used training-aware quantization and analyzed its impact on the overall performance of the models.

Unsupervised Segmentation of Hyperspectral Images Using 3-D Convolutional Autoencoders.

IEEE Geoscience and Remote Sensing Letters, pp 1-5, 2019, DOI: 10.1109/LGRS.2019.2960945.

Jakub Nalepa, Michal Myller, Yasuteru Imai, Ken-Ichi Honda, Tomomi Takeda, Marek Antoniak

Full paper available at: https://ieeexplore.ieee.org/document/8948005

Preprint available at: https://arxiv.org/abs/1907.08870

In this paper, we proposed a new deep learning-powered feature extractor (3D convolutional autoencoders) which is followed by a clustering layer in a deep network to perform unsupervised segmentation of a multi/hyperspectral image.

Transfer Learning for Segmenting Dimensionally Reduced Hyperspectral Images.

IEEE Geoscience and Remote Sensing Letters, pp 1-5, 2019, DOI: 10.1109/LGRS.2019.2942832.

Jakub Nalepa, Michal Myller, Michal Kawulok

Full paper available at: https://ieeexplore.ieee.org/document/8864017

Preprint available at: https://arxiv.org/abs/1906.09631

In this paper, we showed how to employ transfer learning to train deep models that generalize well over unseen hyperspectral data. Also, we showed that it is possible to apply transfer learning to the source and target hyperspectral data of different characteristics (i.e., different numbers of bands) if an appropriate hyperspectral data reduction is used.

Training- and Test-Time Data Augmentation for Hyperspectral Image Segmentation.

IEEE Geoscience and Remote Sensing Letters, 17(2): 292-296, 2020, DOI: 10.1109/LGRS.2019.2921011.

Jakub Nalepa, Michal Myller, Michal Kawulok

Full paper available at: https://ieeexplore.ieee.org/document/8746168

Preprint available at: https://arxiv.org/pdf/1903.05580

In this paper, we introduced a data augmentation pipeline that allows for performing both training- and test-time data augmentation. Also, we proposed new augmentation techniques for hyperspectral data that outperform other methods, including generative adversarial networks.

Validating hyperspectral image segmentation.

IEEE Geoscience and Remote Sensing Letters, 16(8): 1264-1268, 2019, DOI: 10.1109/LGRS.2019.2895697.

Jakub Nalepa, Michal Myller, Michal Kawulok

Full paper available at:

https://ieeexplore.ieee.org/iel7/8859/4357975/08642388.pdf

Preprint available at: https://arxiv.org/abs/1811.03707

In this paper, we showed that the Monte-Carlo cross-validation can lead to overoptimistic conclusions on the performance of spectral-spatial deep models for hyperspectral image segmentation, and proposed the algorithm to extract training-test data splits that enable us to thoroughly validate and compare hyperspectral segmentation algorithms. Also, we made our training-test data splits publicly available for the most popular hyperspectral benchmarks.

On data augmentation for segmenting hyperspectral images.

Paper 10996-8, pp 1-8, Proc. SPIE Defense+Commercial Sensing 2019, Baltimore, USA, 2019.

Jakub Nalepa, Michal Myller, Michal Kawulok, Bogdan Smolka

Full paper available at: https://www.spiedigitallibrary.org/conference-proceedings-of-spie/10996/1099609/On-data-augmentation-for-segmenting-hyperspectral-images/10.1117/12.2519517.short

In this paper, we presented our initial findings on the hyperspectral data augmentation and its impact on the overall performance of hyperspectral classification deep models.

Segmentation of multispectral data simulated from hyperspectral imagery.
pp 1-4, Proc. IEEE IGARSS 2019, Yokohama, Japan, 2019.
Michal Marcinkiewicz, Michal Kawulok, Jakub Nalepa
Full paper available at: https://ieeexplore.ieee.org/document/8900502
In this paper, we introduced a technique of "simulating" wider ("multispectral") bands from hyperspectral imagery. Also, we showed that various aggregation algorithms that enable us to simulate wider bands do not adversely affect the classification accuracy of classical machine learning-powered approaches.

Segmentation of reduced hyperspectral image data, European Workshop on on-board data processing.
OBDP 2019, ESA, ESTEC, Noordwijk, The Netherlands, 2019.
Jakub Nalepa, Lukasz Tulczyjew, Michal Myller, Michal Kawulok, Marek Antoniak, Michal Marcinkiewicz, Krzysztof Czyz
In this talk, we investigated the impact of hyperspectral data reduction on the performance of hyperspectral image classification and segmentation algorithms operating on either full or reduced hyperspectral data.

Accurate segmentation of hyperspectral images using deep neural networks – Are we there yet?
PhiWeek 2018, Frascati, Italy, 2018, Video time: 1:09.
Jakub Nalepa, Michal Marcinkiewicz, Pablo Ribalta Lorenzo, Krzysztof Czyz, Michal Kawulok
Presentation available at:
http://phiweek2018.esa.int/agenda/files/presentation235.pdf
In this talk, we reviewed the most important challenges that need to be faced to make hyperspectral image analysis applicable in the wild.

b) SUPER-RESOLUTION RECONSTRUCTION

Deep learning for super-resolution reconstruction of Sentinel-2.
Michal Kawulok, Jakub Nalepa, Pawel Benecki, Daniel Kostrzewa
European Space Agency Earth Observation Φ-Week, Φ-Week 2020, Online Conference.

Evaluating super-resolution of satellite images: A Proba-V case study.
International Geoscience And Remote Sensing Symposium, IEEE IGARSS 2020
Michal Kawulok, Pawel Benecki, Jakub Nalepa, Daniel Kostrzewa

Deep Learning for Multiple-Image Super-Resolution.
IEEE Geoscience and Remote Sensing Letters, 17(6): 1062-1066, 2020, DOI: 10.1109/LGRS.2019.2940483.
Michal Kawulok, Pawel Benecki, Szymon Piechaczek, Krzysztof Hrynczenko, Daniel Kostrzewa, Jakub Nalepa
Full paper (preprint) available at: https://arxiv.org/abs/1903.00440
In this paper, we introduced one of the first deep networks for multiple-image super-resolution reconstruction.

Super-resolution reconstruction using deep learning: should we go deeper?
Communication in Computer and Information Science, Springer 2019.
Kostrzewa D., Piechaczek S., Hrynczenko K., Benecki P., Nalepa J., Kawulok M.
Full paper available at: https://link.springer.com/chapter/10.1007/978-3-030-19093-4_16
In this paper, we compared several state-of-the-art deep learning-powered techniques (using the same experimental setup) for super-resolution reconstruction.

Deep Learning for Fast Super-Resolution Reconstruction from Multiple Images. Defence+Commercial Sensing Conference 2019, Baltimore, US 2019.
Kawulok M., Benecki P., Hrynczenko K., Kostrzewa D., Piechaczek S., Nalepa J., Smolka B.
Full paper available at: https://www.spiedigitallibrary.org/conference-proceedings-of-spie/10996/109960B/Deep-learning-for-fast-super-resolution-reconstruction-from-multiple-images/10.1117/12.2519579.short?SSO=1
In this paper, we analyzed multiple-image super-resolution reconstruction algorithms in the context of their efficient execution.

B4MultiSR: A Benchmark for Multiple-Image Super-Resolution Reconstruction. Proc. International Conference: Beyond Databases, Architectures and Structures, BDAS 2018: Beyond Databases, Architectures and Structures. Facing the Challenges of Data Proliferation and Growing Variety, Communications in Computer and Information Science, Springer 2018, s. 361-375.
Kostrzewa D., Skonieczny L., Benecki P., Kawulok M.
Full paper available at: https://link.springer.com/chapter/10.1007/978-3-319-99987-6_28
In this paper, we introduce a new multi-layer benchmark dataset for systematic evaluation of multiple-image SRR techniques with special emphasis put on satellite imaging.

Evaluating super-resolution reconstruction of satellite images. Acta Astronautica, Vol. 153, Elsevier 2018, s 15-25.
Kawulok M., Kostrzewa D., Benecki P., Skonieczny L.
Full paper available at:
https://www.sciencedirect.com/science/article/abs/pii/S0094576518300109
In this paper, we present our validation framework based on real satellite images acquired at different native resolutions, and we elaborate on

measuring the reconstruction quality. We argue that this is critical to developing new and tuning the existing SRR methods to adapt them to real-world conditions. We investigate several well-established measures and introduce our new metrics that allow for robust evaluation of the SRR outcome given a reference image of higher resolution. In addition to the quantitative tests, we also report qualitative results in which the reconstruction quality measures are used as an objective function in our evolutionary algorithms applied to adapt the SRR methods to a specific imaging model. Overall, the reported study proposes a new way to evaluate the SRR methods, which is an important step towards deploying them in practice.

Evolving imaging model for super-resolution reconstruction.
Proceedings of the Genetic and Evolutionary Computation Conference, GECCO 2018, Kyoto, Japan 2018, s. 284-285.
Kawulok M., Benecki P., Kostrzewa D., Skonieczny L.
Full paper available at: https://dl.acm.org/doi/10.1145/3205651.3205676
In this paper, we introduce a genetic algorithm to optimize the super-resolution reconstruction hyper-parameters and to discover the actual imaging model what was hypothetically used for extracting low-quality image data from its high-resolution counterpart by evolving the kernels exploited in the IM.

Towards Evolutionary Super-Resolution.
Proc. International Conference on the Applications of Evolutionary Computation, EvoApplications 2018: Applications of Evolutionary Computation, Lecture Notes in Computer Science, Vol. 10784, Springer 2018, s. 480-496.
Kawulok M., Benecki P., Kostrzewa D., Skonieczny L.
Full paper available at: https://link.springer.com/chapter/10.1007%2F978-3-319-77538-8_33

In this paper, we demonstrate that the reconstruction process is sensitive to the actual relation between low-resolution and high-resolution images, and we argue that this is a substantial obstacle in deploying super-resolution reconstruction in practice. We propose to search the hyper-parameter space using a genetic algorithm, thus adapting to the actual relation between low- and high-resolution images, which has not been reported in the literature so far.

Towards Robust Evaluation of Super-Resolution Satellite Image Reconstruction. Proc. Asian Conference on Intelligent Information and Database Systems, ACIIDS 2018, Lecture Notes in Computer Science, Vol. 10751, Springer 2018, s. 476-486.
Kawulok M., Benecki P., Nalepa J., Kostrzewa D., Skonieczny L.
Full paper available at RG:
https://www.researchgate.net/publication/323153975_Towards_Robust_Evaluation_of_Super-Resolution_Satellite_Image_Reconstruction
In this paper, we briefly review the state of the art on SRR algorithms and we argue that commonly adopted strategies for their evaluation do not reflect the operational conditions. Also, we report our study on assessing the SRR outcome, relying on new quantitative measures.

Optimizing Super-resolution Reconstruction using a Genetic Algorithm. Proc. 10th International Conference on Agents and Artificial Intelligence, Vol. 2, ScitePress 2018, s. 599-605.
Kawulok M., Kostrzewa D., Benecki P., Skonieczny L.
Full paper available at:
https://www.scitepress.org/papers/2018/66543/66543.pdf
In this paper, we propose to optimize the super-resolution reconstruction hyperparameters using a genetic algorithm, which has not been reported in

the literature so far. We argue that this may substantially improve the capacities of learning the relation between low- and high-resolution images.

On training deep networks for satellite image super-resolution

IEEE International Geoscience and Remote Sensing Symposium - IGARSS 2019 - Yokohama, Japan - 28 July - 2 August 2019

Michal Kawulok, Szymon Piechaczek, Krzysztof Hrynczenko, Pawel Benecki, Daniel Kostrzewa, Jakub Nalepa

Full paper (pre-print) available at: https://arxiv.org/abs/1906.06697

In this paper, we investigate how the SRR performance is influenced by the way such low-resolution training data are obtained, which has not been explored up to date. Our extensive experimental study indicates that the training data characteristics have a large impact on the reconstruction accuracy, and the widely adopted approach is not the most effective for dealing with satellite images.

2.6 Department of Photogrammetry, Remote Sensing and Spatial Information Systems, Warsaw University of Technology

Projects (2018-2020)

1. The innovative approach supporting monitoring of non-forest Natura 2000 habitats, using remote sensing methods – HabitARS, 2016-2019.

   The project was realized as part of the BIOSTRATEG strategic program for research and development work „ Natural environment, agriculture and forestry" funded by The National Centre for Research and Development in Poland. Conortium: MGGP Aero Ltd. (leader), Institute of Technology and Life Sciences, University of Lodz, University of Warsaw, University of Silesia in Katowice, Warsaw University of Life Sciences, Warsaw University of Technology.

   The project develops an innovative approach supporting non-forest Natura 2000 habitats monitoring using remote sensing methods. The existing methods of habitats monitoring are based on subjective assessments of experts made on location. Information is extrapolated from points to the whole area.

   The main aim of the HabitARS project was to develop an objective and repeatable method of identification of non-forest habitats and threats to those habitats, such as desiccation, succession and encroachment of invasive alien and expansive domestic plant species, using remote sensing methods and field botanical reference measurements. The project was carried out in 37 locations across Poland, from the Biebrza Marshes and Drawa Wilderness in the North to Bieszczady and Karkonosze mountains in the South.

2. Advanced technologies in the prevention of flood hazard – SAFEDAM, 2015-2020.

   The project is financed by National Centre for Research and Development in Defense, Security Programme. It is carried out by the consortium of Warsaw University of Technology Faculty of Geodesy and Cartography, Institute of Meteorology and Water Management, MSP Marcin Szender, Astri Polska Sp. o.o., Central School of the State Fire Service in Częstochowa.

   The aim of the SAFEDAM project is the creation of system for levees monitoring using a non-invasive, unmanned aerial platform, which scans from low-altitude, and optical, radar satellite and aerial imagery. For this purpose innovative, photogrammetry and remote sensing technologies will be used. Endangered areas, detected preliminarily by images will be measured by non-invasive, flying measuring platform with centimeter accuracy using 3D measurement technique. The methodology of system application, training program and proposals of procedures related to the management of flood risk will be also prepared.

   A comprehensive system will enable the collection, automatic data analysis and 3D visualization for hydrological services and crisis management professionals. The system will also allow society for geoparticipation in monitoring the levees. Its implementation will ensure effective management of flood risk. System will complement the already implemented projects of flood protection.

List of publication (2018-2020)

1. Araszkiewicz Andrzej, Kiliszek Damian, Podkowa Anna: Height variation depending on the source of antenna Phase Centre Corresctions: LEIAR25.R3 case study, w: Sensors, Multidisciplinary Digital Publishing Institute, nr 19, 2019, ss. 1-12, DOI:10.3390/s19184010, IF(3,031),
2. Bakuła Krzysztof, Mills J. P., Remondino F.: A Review of Benchmarking in Photogrammetry and Remote Sensing, in: The International Archives of the

Photogrammetry, Remote Sensing and Spatial Information Sciences, International Society for Photogrammetry and Remote Sensing, vol. XLII-1/W2 , 2019, ss. 1-8, DOI:10.5194/isprs-archives-XLII-1-W2-1-2019,
3. Bakuła Krzysztof, Ostrowski Wojciech, Pilarska Magdalena, Szender Marcin, Kurczyński Zdzisław: Evaluation and calibration of fixed-wing multisensor UAV mobile mapping system: improved results, in: The International Archives of the Photogrammetry, Remote Sensing and Spatial Information Sciences, International Society for Photogrammetry and Remote Sensing, vol. XLII-2/W13, 2019, ss. 189-195, DOI:10.5194/isprs-archives-XLII-2-W13-189-2019,
4. Bakuła Krzysztof, Ostrowski Wojciech, Pilarska Magdalena, Szender Marcin, Kurczyński Zdzisław: Evaluation and calibration of fixed-wing UAV mobile mapping system equipped with lidar and optical sensors, in: The International Archives of the Photogrammetry, Remote Sensing and Spatial Information Sciences, International Society for Photogrammetry and Remote Sensing, vol. XLII-1, 2018, ss. 25-32, DOI:10.5194/isprs-archives-XLII-1-25-2018,
5. Bakuła Krzysztof, Zelaya Wziątek Dagmara, Weintrit Beata, Jędryka Marcin, Ryfa Tomasz, Pilarska Magdalena, Kurczyński Zdzisław: Multi-sourced, remote sensing data in levees monitoring: case study of SAFEDAM project, in: The International Archives of the Photogrammetry, Remote Sensing and Spatial Information Sciences, International Society for Photogrammetry and Remote Sensing, vol. XLII-3/W4, 2018, ss. 101-108, DOI:10.5194/isprs-archives-XLII-3-W4-101-2018,
6. Bałazy Radomir, Hycza Tomasz, Kamińska Agnieszka, Osińska-Skotak Katarzyna: Factors Affecting the Health Condition of Spruce Forests in Central European Mountains-Study Based on MultitemporalRapidEye Satellite Images, in: Forests, nr 10, 2019, ss. 1-18, DOI:10.3390/f10110943, IF(2,116),
7. Bocheńska Agnieszka, Markiewicz Jakub, Łapiński Sławomir: The combination of the image and range-based 3D acquisition in archaeological and architectural research in the Royal Castle in Warsaw, in: The International Archives of the Photogrammetry, Remote Sensing and Spatial Information Sciences, International Society for Photogrammetry and Remote Sensing, nr XLII-2/W15, 2019, ss. 177-184, DOI:10.5194/sprs-archives-XLII-2-W15-177-2019,
8. Choromański K., Łobodecki J., Puchała K., Ostrowski Wojciech: Development of Virtual Reality Application for Cultural Heritage

Visualization from Multi-Source 3D Data , in: The International Archives of the Photogrammetry, Remote Sensing and Spatial Information Sciences, International Society for Photogrammetry and Remote Sensing, vol. XLII 2019 , nr 2/W9, 2019, ss. 261-267, DOI:10.5194/isprs-archives-XLII-2-W9-261-2019,
9. Jełowicki Łukasz, Ostrowski Wojciech, Osińska-Skotak Katarzyna, Bakuła Krzysztof: Evaluation of Rapeseed Winter Crop Damage Using UAV-Based Multispectral Imagery, in: Remote Sensing, vol. 12, nr 16, 2020, ss. 1-21, DOI:10.3390/rs12162618, IF(4,118),
10. Kamola Aleksander, Różycki Sebastian, Bylina Paweł [i in.] : Forgotten Nazi Forced Labour Camps: Arbeitslager Riese (Lower Silesia, SE Poland) and the Use of Archival Aerial Photography and Contemporary LiDAR and Ground Truth Data to Identify and Delineate Camp Areas, w: Remote Sensing, vol. 12, nr 11, 2020, ss. 1-21, DOI:10.3390/rs12111802
11. Kogut Tomasz, Weistock Milena, Bakuła Krzysztof: Classification of Data from Airborne Lidar Bathymetry with Random Forest Algorithm Based on Different Feature Vectors, in: The International Archives of the Photogrammetry, Remote Sensing and Spatial Information Sciences, International Society for Photogrammetry and Remote Sensing, vol. XLII-2/W16, 2019, ss. 143-148, DOI:10.5194/isprs-archives-XLII-2-W16-143-2019,
12. Kogut Tomasz, Bakuła Krzysztof: Improvement of Full Waveform Airborne Laser Bathymetry Data Processing based on Waves of Neighborhood Points, in: Remote Sensing, vol. 11, nr 10, 2019, ss. 1-13, DOI:10.3390/rs11101255, IF(4,118),
13. Kot P., Markiewicz Jakub, Muradov M. [i in.] : COMBINATION OF THE PHOTOGRAMMETRIC AND MICROWAVE REMOTE SENSING FOR CULTURAL HERITAGE DOCUMENTATION AND PRESERVATION – PRELIMINARY RESULTS, w: The International Archives of the Photogrammetry, Remote Sensing and Spatial Information Sciences, vol. XLIII-B2-2020, 2020, ss. 1409-1413, DOI:10.5194/isprs-archives-XLIII-B2-2020-1409-2020
14. Kupidura Przemysław: The Comparison of Different Methods of Texture Analysis for Their Effcacy for Land Use Classification in Satellite Imagery, in: Remote Sensing, vol. 11 , nr 10, 2019, ss. 1-20, DOI:10.3390/rs11101233, IF(4,118),
15. Kupidura Przemysław, Osińska-Skotak Katarzyna, Lesisz Katarzyna, Podkowa Anna: The Efficacy Analysis of Determining the Wooded and Shrubbed Area Based on Archival Aerial Imagery Using Texture Analysis, in:

ISPRS International Journal of Geo-Information, vol. 8, nr 10, 2019, ss. 1-26, DOI:10.3390/ijgi8100450, IF(1,84),
16. Łoś Helena, Osińska-Skotak Katarzyna, Pluto-Kossakowska Joanna, Bernier Monique, Gauthier Yves, Pawłowski Bogusław: Performance evaluation of quad-pol data compare to dual-pol SAR data for river ice classification, in: European Journal of Remote Sensing, vol. published online, 2018, ss. 1-17, DOI:10.1080/22797254.2018.1540914, IF(1,904),
17. Markiewicz Jakub, Abratkiewicz Karol, Gromek Artur, Ostrowski Wojciech, Samczyński Piotr Jerzy, Gromek Damian: Geometrical Matching of SAR and Optical Images Utilizing ASIFT Features for SAR-based Navigation Aided Systems, in: Sensors, Multidisciplinary Digital Publishing Institute, vol. 19, nr 24, 2019, ss. 1-33, DOI:10.3390/s19245500, IF(3,031),
18. Osińska-Skotak Katarzyna, Jełowicki Łukasz, Bakuła Krzysztof, Michalska-Hejduk D., Wylazłowska J., Kopeć D.: Analysis of Using Dense Image Matching Techniques to Study the Process of Secondary Succession in Non-Forest Natura 2000 Habitats , in: Remote Sensing, vol. 11, nr 8, 2019, ss. 1-28, DOI:10.3390/rs11080893, IF(4,118),
19. Osińska-Skotak Katarzyna, Radecka Aleksandra, Piórkowski Hubert, Michalska-Hejduk Dorota, Kopeć Dominik, Tokarska-Guzik Barbara, Ostrowski Wojciech, Kania Adam, Niedzielko Jan: Mapping Succession in Non-Forest Habitats by Means of Remote Sensing: Is the Data Acquisition Time Critical for Species Discrimination?, in: Remote Sensing, vol. 11 (22), 2019, ss. 1-36, DOI:10.3390/rs11222629, IF(4,118),
20. Osińska-Skotak Katarzyna, Bakuła Krzysztof, Jełowicki Łukasz, Podkowa Anna: Using Canopy Height Model Obtained with Dense Image Matching of Archival Photogrammetric Datasets in Area Analysis of Secondary Succession, in: Remote Sensing, vol. 11 (18), 2019, ss. 1-28, DOI:10.3390/rs11182182, IF(4,118),
21. Ostrowski Wojciech, Pilarska Magdalena, Charyton Jakub, Bakuła Krzysztof: Analysis of 3D building models accuracy based on the airborne laser scanning point clouds, in: The International Archives of the Photogrammetry, Remote Sensing and Spatial Information Sciences, International Society for Photogrammetry and Remote Sensing, vol. XLII-2, 2018, ss. 797-804, DOI:10.5194/isprs-archives-XLII-2-797-2018,
22. Ostrowski Wojciech, Miszk Ł., Winiarska W.: Three-dimensional stratygraphy reconstruction and GIS – postprocessing issues in archaeological field 3D documentation, in: Studies in Ancient Art and

Civilization, vol. 22, 2018, ss. 219-240, DOI:10.12797/SAAC.22.2018.22.10, 13 punktów
23. Pilarska Magdalena: Classification of dual-wavelength airbornelaser scanning point cloud based on the radiometric properties of the objects, in: The International Archives of the Photogrammetry, Remote Sensing and Spatial Information Sciences, International Society for Photogrammetry and Remote Sensing, vol. XLII-2, 2018, ss. 901-907, DOI:10.5194/isprs-archives-XLII-2-901-2018,
24. Pilarska Magdalena, Ostrowski Wojciech: Evaluating the Possibility of Tree Species Classification with Dual-Wavelength ALS Data, in: The International Archives of the Photogrammetry, Remote Sensing and Spatial Information Sciences, International Society for Photogrammetry and Remote Sensing, vol. XLII-2/W13, 2019, ss. 1097-1103, DOI:10.5194/isprs-archives-XLII-2-W13-1097-2019,
25. Pluto-Kossakowska Joanna: Automatic detection of grey infrastructure based on VHR image, w: The International Archives of the Photogrammetry, Remote Sensing and Spatial Information Sciences, vol. XLIII-B3, 2020, ss. 181-187, DOI:10.5194/isprs-archives-XLIII-B3-2020-181-2020
26. Radecka Aleksandra, Michalska-Hejduk Dorota, Osińska-Skotak Katarzyna, Kania Adam, Górski Konrad, Ostrowski Wojciech: Mapping secondary succession species in agricultural landscape with the use of hyperspectral and airborne laser scanning data, in: Journal of Applied Remote Sensing, vol. 13 (3), 2019, ss. 1-22, DOI:10.1117/1.JRS.13.034502, IF(1,344),
27. Salach Adam, Bakuła Krzysztof, Pilarska Magdalena, Ostrowski Wojciech, Górski Konrad, Kurczyński Zdzisław: Accuracy Assessment of Point Clouds from LiDAR and Dense Image Matching Acquired Using the UAV Platform for DTM Creation, in: ISPRS International Journal of Geo-Information, nr 7, 2018, ss. 1-16, DOI:10.3390/ijgi7090342, IF(1,84),
28. Różycki Sebastian, Zapłata Rafał, Karczewski Jerzy [i in.] : Integrated Archaeological Research: Archival Resources, Surveys, Geophysical Prospection and Excavation Approach at an Execution and Burial Site: The German Nazi Labour Camp in Treblinka, w: Geosciences, vol. 10(9), 2020, ss. 1-26, DOI:10.3390/geosciences10090336
29. Terefenko Paweł, Zelaya Wziątek Dagmara, Dalyot Sagi, Boski Tomasz, Lima-Filho Fransisco Pinheiro: A High-Precision LiDAR-Based Method for Surveying and Classifying Coastal Notches, in: ISPRS International Journal of

Geo-Information, nr 7(8), 295, 2018, ss. 1-16, DOI:10.3390/ijgi7080295, IF(0,371),
30. Weintrit Beata, Bakuła Krzysztof, Jędryka Marcin, Bijak Wojciech, Ostrowski Wojciech, Zelaya Wziątek Dagmara, Ankowski Artur, Kurczyński Zdzisław: Emergency rescue management supported by UAV remote sensing data, in: The International Archives of the Photogrammetry, Remote Sensing and Spatial Information Sciences, International Society for Photogrammetry and Remote Sensing, nr 42 (3W4), 2018, ss. 563-567, DOI:10.5194/isprs-archives-XLII-3-W4-563-2018,
31. Weintrit Beata, Osińska-Skotak Katarzyna, Pilarska Magdalena: Feasibility study of flood risk monitoring based on optical satellite data, in: Miscellanea Geographica, vol. 22, nr 3, 2018, ss. 1-9, DOI:10.2478/mgrsd-2018-0011,
32. Zawieska Dorota, Markiewicz Jakub, Kopiasz J.: Development of true orthophotomaps of the fortified settlement at Biskupin, Site 4, based on archival data, in: Archaeological Prospection, vol. online, 2019, ss. 1-28, DOI:10.1002/arp.1748, IF(1,5).

3

SPACE PHYSICS

3. SPACE PHYSICS

Compiled by **Roman Schreiber and Małgorzata Michalska**

3.1 Wrocław Solar Physics Division CBK PAN

DIOGENESS B. Sylwester, J. Sylwester

Diogeness (DIOG) soft X-ray spectrometer operated aboard the Russian *CORONAS-F* satellite in 2001. The instrument collected hundreds of high resolution spectra from a period high solar activity, including X5.3 on 25 August 2001.This flare (see Fig. 3.1) was also observed by *GOES* X-ray monitor and *Yohkoh* JAXA/NASA satellite.

A complete re-analysis of DIOG spectra has been continued resulting in *The Astrophysical Journal* publication (Phillips et al., 2018).

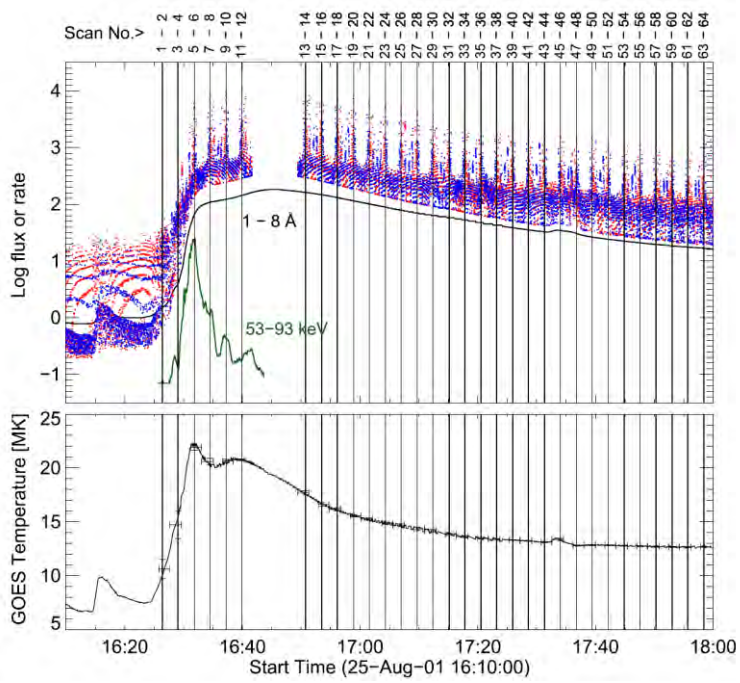

Fig. 3.1. Upper panel: logarithmic plots of the GOES light curve in the 1–8 Å channel, DIOGENESS channel 1 (red dots), and channel 4 (blue dots), with Yohkoh Hard X-ray Telescope (53–93 keV; green curve) photon count rates during the 2001 August 25 X5 flare shown. The DIOGENESS points show peaks due to the Ca XIX line group as the crystals repeatedly scanned over their ranges. The data gap between 16:42 UT and 16:49 UT is due to telemetry loss. Lower panel: temperature derived from the intensity ratio of the two GOES channels (horizontal error bars are periods over which averages were obtained; vertical error bars are standard deviations in temperature estimates).

In the spectra averaged over selected *GOES* temperatures (see Fig. 3.2), we identified tens of lines, many of them for the first time in astrophysical plasma.

Identified lines belong to He & Li- like ions of Ca and to a number of higher transitions in H- and He- like Ar. The theoretical calculations of line intensities have been performed with the use of Cowan Hartree–Fock atomic code for hundreds of transitions falling in the observed spectral range. These new calculations describe exceptionally well the relative line intensities formed in various Ca lines. Absolute Ar and Ca line intensities can be explained by taking the Ar/Ca abundance ratio fixed at 0.33. The fit to longer wavelength satellite lines (~3.23 Å) required modification in the Ca ion equilibrium.

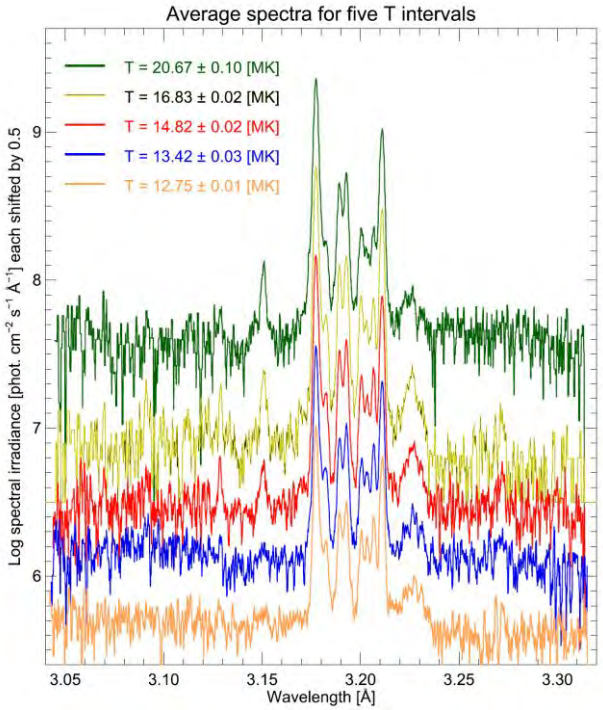

Fig. 3.2. DIOGENESS spectra plotted on a logarithmic scale during the 2001 August 25 flare averaged over five time intervals defined by T_{GOES}, as indicated in the figure legend. The vertical scale units are shown, valid for the T_{GOES}=12.8 MK spectrum, with successive higher-temperature spectra increased by 0.5 in the logarithm for clarity.

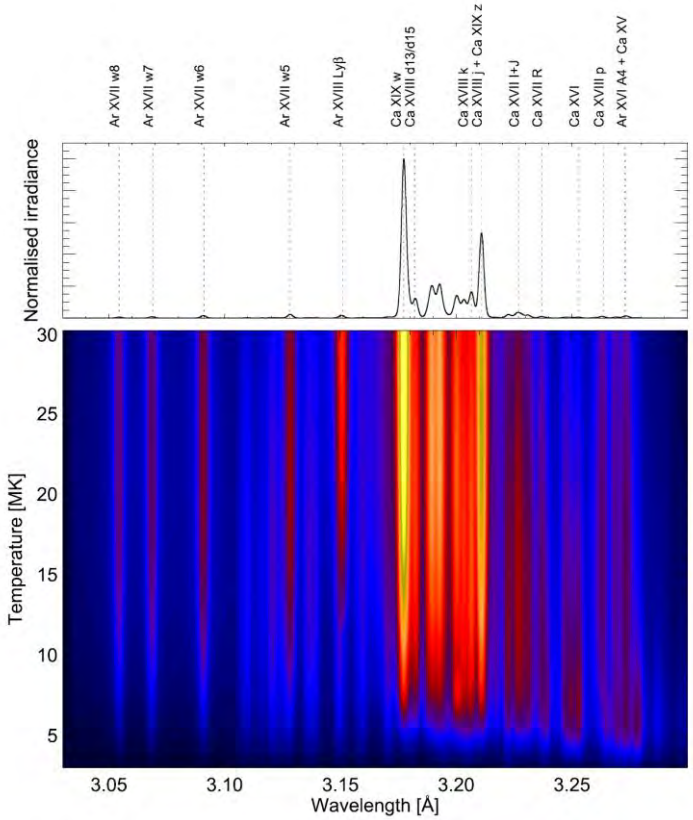

Fig. 3.3. Synthetic spectra in the range 3.00–3.30 Å for temperatures in the range 4 MK (bottom) to 30 MK (top), color-coded with blue, orange, red, yellow indicating increasing intensities. The chief lines are identified at the top of the figure with a theoretical spectrum with temperature equal to 13.8 MK.

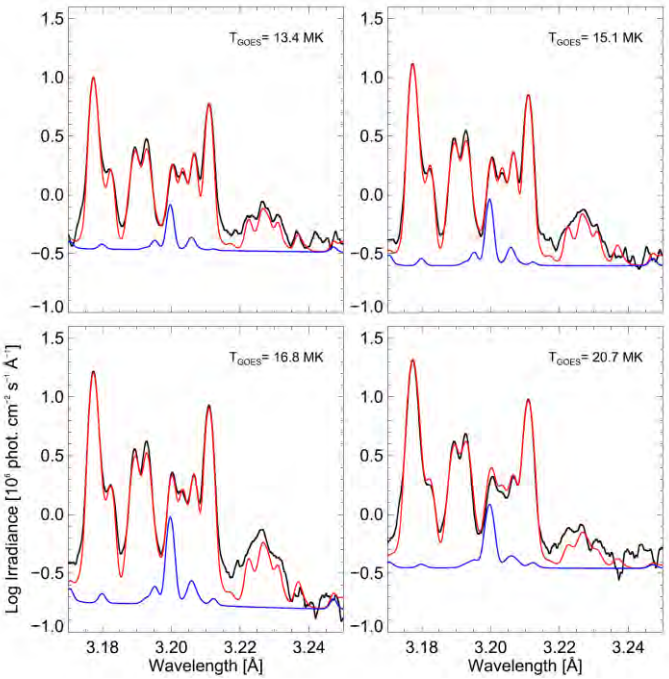

Fig. 3.4. DIOGENESS spectra (3.17–3.25 Å) for T_{GOES}=13.4 MK, 14.8 MK, 16.8 MK, and 20.7 MK with the best-fit theoretical spectra (red continuous line), with an argon spectrum (blue line) for a wavelength range that includes only the region around the Ca XIX lines and Ca XVIII and Ca XVII satellites. The Ca+16 and Ca+17 ion fractions were multiplied by 1.3 and 2.0, respectively. The values of reduced χ2 for these fits are 2.41, 3.23, 5.84, and 9.86.

Present updated line formation theory has been successfully applied to explain earlier flaring plasma spectra observed by NRL SOLFLEX experiment aboard *P78-1* as well as laboratory ALCATOR C-ModTokamak spectra. We found the flaring plasma temperatures determined spectroscopically (fit to entire spectrum) to agree well with the temperatures T_{GOES} determined in the isothermal approach from flux ratios of *GOES* 0.5-4 Å to 1-8 Å broad-band X-ray The analysis of DIOG spectra in channels 2 & 3 has been performed also. We removed all spectral data disturbed by telemetry & detector problems and averaged the spectrum over entire flare duration for which ~30 scans were available.

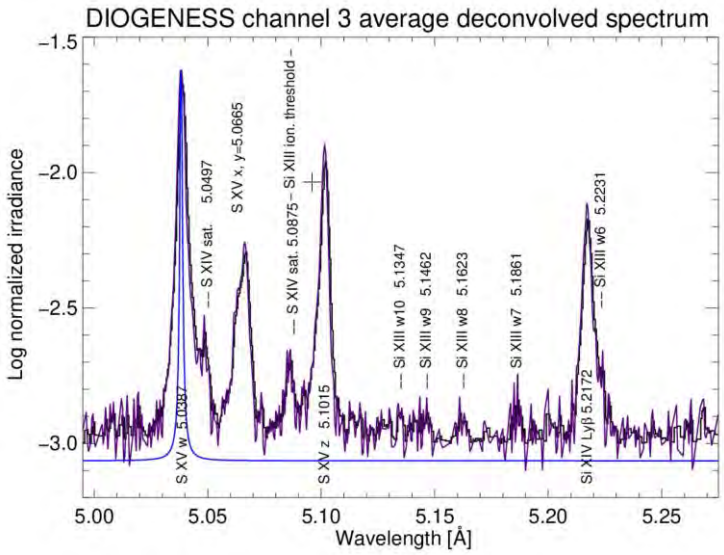

Fig. 3.5. Logarithmic plot of the average spectrum in DIOGENESS channel 3 (black) together with spectrum (violet) after deconvolving the instrumental profile (rocking curve of the ADP crystal). The Lorentzian rocking curve profile is shown (in blue) under the resonance line (w) of He-like ion of S XV.

Example average spectrum for DIOGENESS Channel #3 is presented in Fig. 3.5. In order to decrease the influence of statistical noise, we deconvolved (remove) the instrumental profile due to finite width of the ADP rocking curve. The flat ADP monocrystal has been used as dispersive element in this respect. Deconvolution has been performed using the Withbroe-Sylwester (WS) Bayesian maximum likelihood algorithm. Except the stronger lines already identified, there are a number of weak lines clearly seen in the average spectrum, belonging to the higher transitions in He-like Si XIII ion. These weaker lines are observed and identified for the first time in the astrophysical plasmas. In a similar way, we performed the reduction of spectra obtained in DIOGENESS Channel #2. In this case monocrystal of Beryl (a piece from the spare SMM XRP mantle) was used as dispersive elements for Bragg reflections. The average spectrum in the spectral range 6.3 – 6.8 Å is shown in Fig. 3.6.

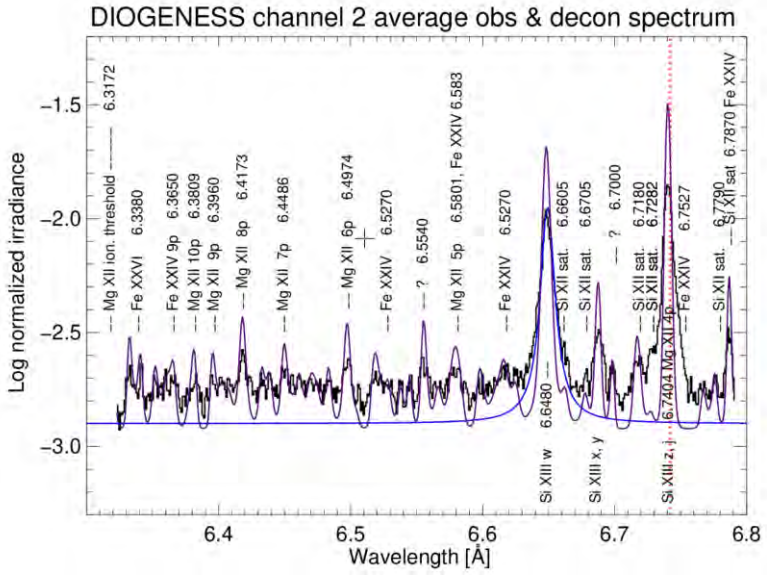

Fig. 3.6. Logarithmic plot of the average spectrum in DIOGENESS channel 2 (black) together with spectrum (violet) after deconvolving the instrumental profile (rocking curve of the ADP crystal). The Lorentzian rocking curve profile is shown (in blue) under the resonance line (w) of He-like ion of Si XIII. The dotted vertical line represents the position of Si absorption jump.

Also here, the violet line represents the spectrum after removing the instrument profile (in blue). Except the strongest, already known, lines of He-like Si XIII, there are tens of weaker lines present in this spectral range. All of these lines are observed for the first time and identified by us using atomic data from CHIANTI and Kelly (ISBN 0883185504, 9780883185506) spectral line tables. These weaker lines belong to the H-like Mg XII ion (up to 1s 2S1/2 - p 2P3/2,1/2) and represent spin doublet transitions. Possibly a few lines of highly ionized Fe show-up in the spectral range of this Channel. The paper describing respective spectra reduction, deconvolution and line identification is in the final stage of preparation for submission to the ApJ.

SphinX B. Sylwester, J. Sylwester

We have extended, revised and deepened the scope of the analysis of spectra from Polish spectrophotometer SphinX as recorded during the minimum activity periods of its operation. We have used much improved

instrumental data than was used previously. In accordance with we have subtracted an average background spectrum as obtained by summing a total of ~34 hours of spacecraft night-time observations, taken from regions that avoided SC passages through the SAA, polar auroral regions and times outside the magnetic substorms. This background (essentially at energies ≤ 2 keV) includes electronic noise, particle emission and fluorescence from aluminium which makes the bulk of the instrument structure. It was subtracted from every analysed spectrum selected as for the background but for day-time observations during periods of at least 5 min. when D1 detector count rate was less than 140 s^{-1}. We have selected 576 such intervals (non-active, NA) marked in red in Fig. 3.7. Additionally we selected 40 small brightenings (B, in green) and 16 micro-flares (F, blue vertical lines).

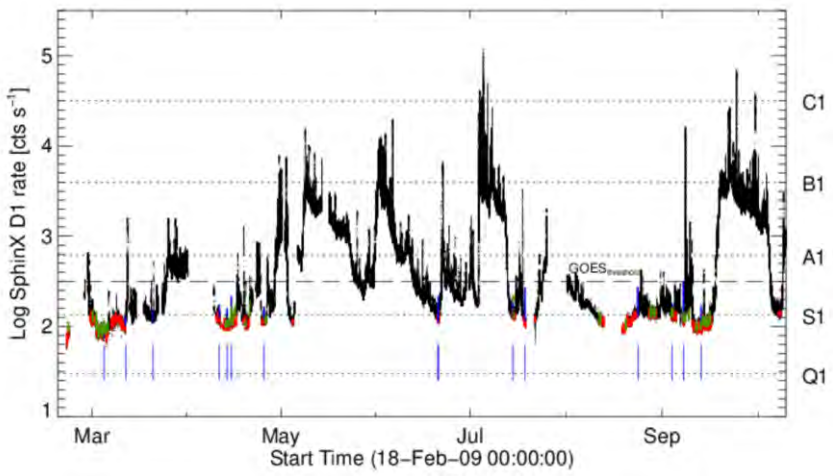

Fig. 3.7. The X-ray emission as recorded by the SphinX D1 detector (photon counts s^{-1}), plotted logarithmically over the period 20 Feb. to 9 Oct. 2009 (at later times solar activity increased and data were excluded for this study). Red points indicate the times of the 576 non-active (NA) intervals when the count rate was < 140 s^{-1} and green portions times of 40 brightenings (B). Times of the 16 micro-flares (F) are indicated by thin vertical blue lines beneath the light curve. The GOES 1-8 Å lover threshold is indicated by the horizontal dashed line, and the GOES A1,B1, C1 levels and the S1 and Q1 levels (introduced based on SphinX data analysis) are indicated by horizontal dotted lines.

The spectra for all 576 intervals together with the average spectrum (black histogram) are shown in Fig. 3.8. The spectra in those intervals have been

analysed adopting an isothermal approximation and the corona average temperature T and the emission measure EM have been determined. The temperature has been obtained by fitting the observed spectrum to the theoretical one in the statistically important range (1.2 keV< E < 2.7 keV). The emission measure has been estimated based on the total number of photons detected above 1 keV. The best fit isothermal spectrum to the average one is shown in blue in Fig. 3.2.

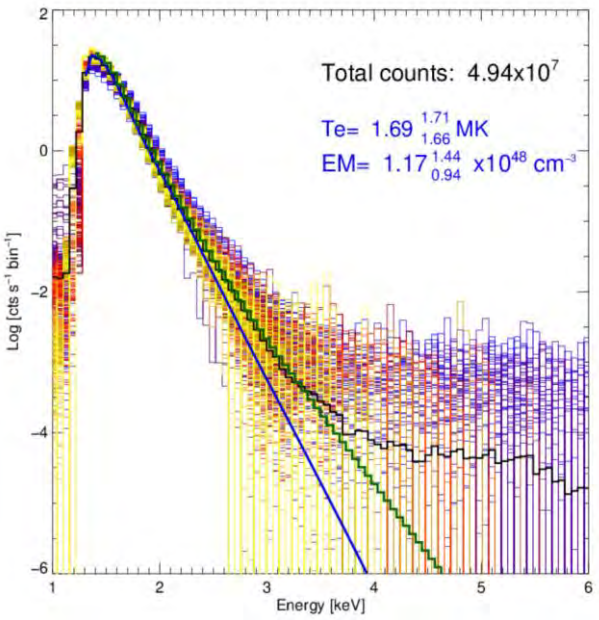

Fig. 3.8. SphinX NA spectra in the 1-6 keV range (thin-line histograms) for 576 time intervals when there was no discernible solar activity and their average (thick black histogram). A rough distinction in the times of the spectra is indicated by the colours of the histogram (blue = early in the mission, red = middle, yellow = late in the mission). For all shown spectra the background spectrum has been subtracted which is the novel of the present analysis. The best fit isothermal spectrum is shown by the thick blue curve (the corresponding temperature and emission measure values shown in the figure) and the thick green-line histogram shows the fit by folding the DEM solution.

It is seen that an agreement is not good above 2.5 keV and a high temperature component is needed to account for emission above this energy. So in the next step we analysed the spectra in 576 intervals assuming that the plasma is multi-temperature (the differential emission measure DEM distributions have been calculated adopting the Withbroe-Sylwester algorithm). The results

are presented in Fig. 3.9 together with the DEM as calculated for an average spectrum (red thick histogram). The spectrum calculated for this average DEM distribution is shown in green in Fig. 8. It is seen that the agreement is much better as compared with the isothermal approach.

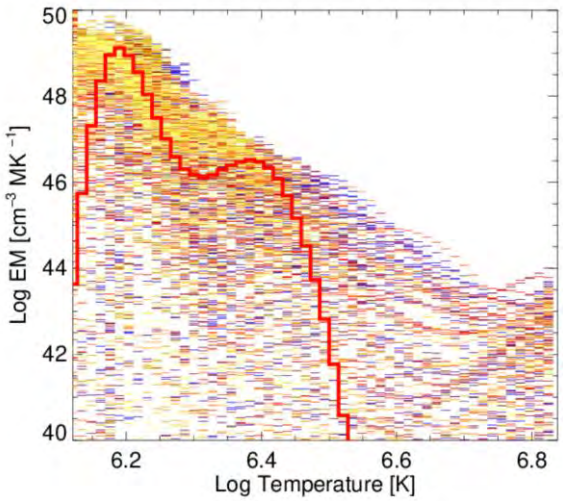

Fig. 3.9. The differential emission measures DEM (cm^{-3} MK^{-1}) plotted against the logarithm of temperature (in K) derived for each of the 576 individual non-active NA (shown in various colours), together with the DEM calculated for the average of the 576 spectra (thick red histogram).

Shapes of DEMs calculated indicate that in addition to the existence of cooler component with temperatures around 1.6 MK, a bulk amount of plasma present for all spectra, a hotter component of plasma around 2.4 MK is present. This component has an emission measure almost 3 orders of magnitude smaller than the cooler one. The similar analysis have been made for the brightenings and sub-flares. Presence of a cooler component is evident. The hotter one is also seen but the temperature in this case is around 3.2 MK. This is illustrated in Fig. 3.10.

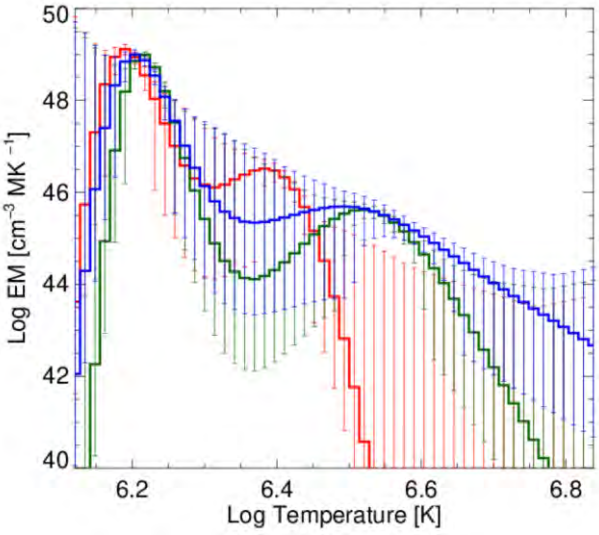

Fig. 3.10. DEM distributions for the average spectra for the NA (red), brightenings B (green) and sub-flares F (blue) intervals. The uncertainties in the DEM solutions are indicated by the error bars in appropriate colours.

The paper describing in detail the results of this study was published in Solar Physics, (Sylwester et al., 2019).

SMM BCS B. Sylwester, J. Sylwester

The Bent Crystal Spectrometer on the NASA Solar Maximum Mission spacecraft observed the X-ray spectra of numerous solar events during the periods February to November, 1980 and 1984 - 1989 in spectral regions around the highly ionized resonance lines of He-like Ca (Ca XIX) and Fe (Fe XXV), allowing the plasmas to be diagnosed for temperature, plasma turbulence, mass motions etc. Since to date there has not been a comparable spectrometer equaling the spectral resolution of the BCS over such a long observing period, there is continued interest in BCS data analysis. A re-assessment of the BCS calibration and its operational history was recently made by Rapley, Sylwester, and Phillips (Solar Physics, 2017, 292:50).

Over the years 2019 &2020, we (JS, BS and prof. prof. Ken Phillips and Chris Rapley from London) performed precise analysis of spectra obtained during a spacecraft scan in November 1980 that highlight anomalies in the crystal curvature of the important channel 1 (viewing lines of He-like Ca, Ca XIX) and

associated Ca XVIII dielectronic satellites), helping to explain a long-standing anomaly in the intensity ratio of the Ca XIX intercombination lines x and y. Also, we made an in-flight estimation of the BCS collimator extent which gives a better estimate for the absolute intensity of BCS spectra. Finally, an important implication of this work is that the result of an earlier analysis of BCS Ca XIX spectra implying a time-variable flare abundance of Ca is confirmed.

In Fig. 3.11 we present the path scheme of X-rays being Bragg reflected from the Ge BCS Channel #1 crystal. The SMM spacecraft performed raster-like scans over active region AR2779 while the M3.5 flare (SOL1980-11-06T22:27) was occurring enabling line shifts in BCS spectra to be precisely related to the spatial shifts. The spacecraft scanning motion causes the line positions to "drift" in a wavy motion as illustrated in Fig. 3.12. Each normalized spectrum in this bin range (3rd panel) was cross-compared with a normalized reference

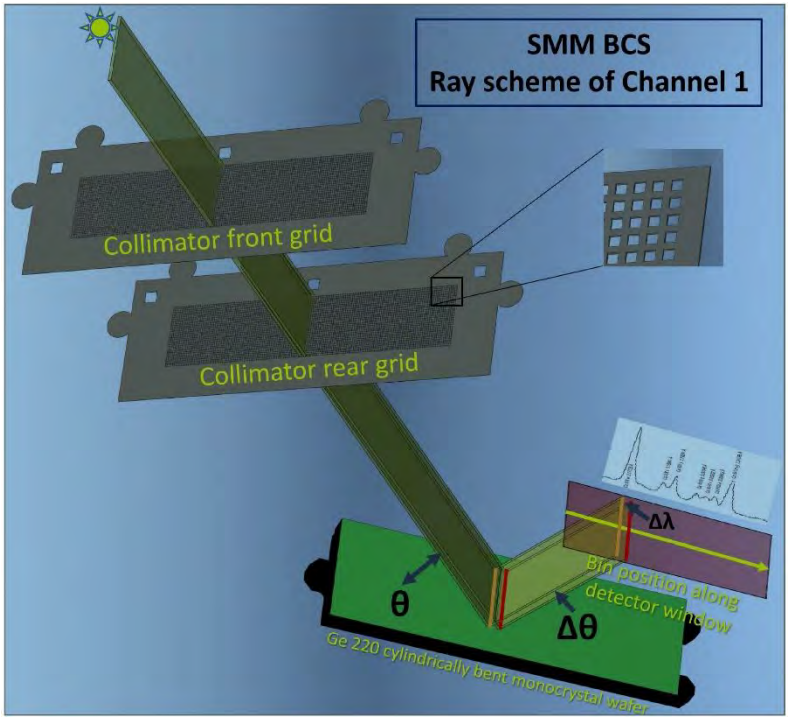

Fig. 3.11. Ray path scheme for BCS channel 1 (CaXIX) generated by CAD (Computer Aided Design, courtesy of Jarosław Bąkała). X-rays from the Sun (upper left) are incident through the 6 x 6 arcmin (FWHM) square multi-grid collimator (front and rear grids indicated) and a thermal filter on to the Ge 220 cylindrically bent crystal wafer. The diffracted rays, incident on the bent crystal at angle θ, have slightly different wavelengths according to their position along the crystal, so the radiation received by the position-sensitive detector over a data-gathering interval forms a complete spectrum over a limited wavelength range (3.165 - 3.231 Å for an on-axis flare in BCS channel 1).

average spectrum to determine an optimum shift in BCS bins. Two criteria were applied: firstly, a multiplicative approach (black points) in which the shift corresponding to a maximum in the product of the analyzed and reference spectra was obtained; secondly (red points), the shift corresponding to the traditionally defined $\chi 2$ difference attained a minimum value. For all phases except C (when no BCS spectra were observed), the red points coincide with the black points to within 0.05 bin.

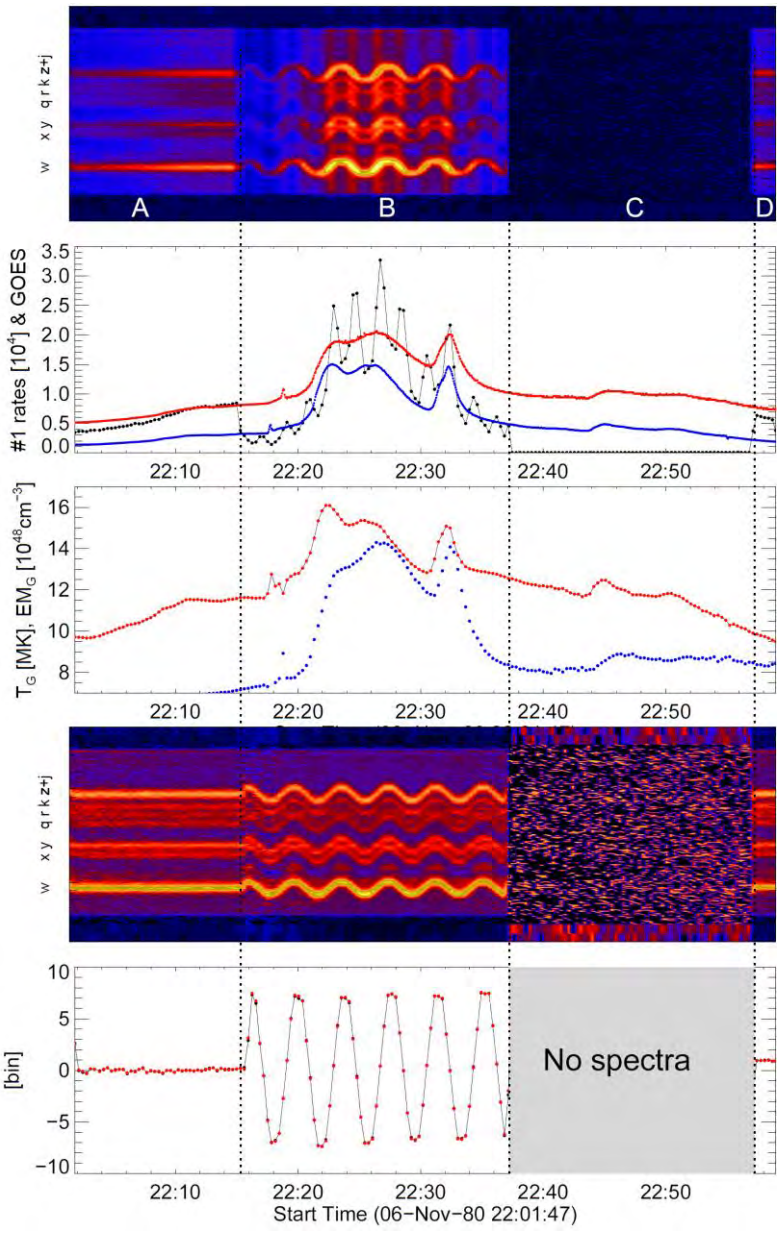

Fig. 3.12. Time history of GOES, BCS Channel 1 (Ca XIX) spectra, and spectral line shifts over the period of the 06 November, 1980 flare (22:02 - 22:59 UT). Top panel: Channel 1 spectra plotted on a red temperature intensity scale (yellow for high intensities, blue low) with wavelengths in the channel 1 range (3.165 - 3.231 Å) on the vertical scale increasing upwards. Second panel: BCS channel 1 photon count rates in the bin range 33 - 220 (wavelength range 3.174 - 3.227 Å for an on-axis flare) in units of 10^4 s^{-1} with GOES 0.5-4 Å (blue, multiplied by 2 x 10^5) and 1- 8 Å (red, multiplied by 6x 10^4) light curves. Third panel: temperature (MK, red) and emission measure (multiplied by 1.2, units of 10^{48} cm^{-3}, blue) derived from the emission ratio of the two GOES channels. Fourth panel: Channel 1 spectra (like those in the top panel but normalized to the BCS total count rate in the 3.167 - 3.224 Å range). Bottom panel: wavelength shifts of spectra, expressed as relative bin number, determined from two different approaches.

The analysis of the line positions (offsets) during spacecraft scans allowed to determine the respective correction to be applied to convert spectral bins to wavelengths as well as to correct for the intensity distortions caused by the non-ideally-cylindrical surface of the Ge monocrystal wafer used to Bragg-reflect the X-rays illuminating it through the triangular profile (6 x 6 arcmin collimator). In Fig. 3.5 we illustrate determined bin-wavelength and offset-intensity correction matrixes to be used in the future to reduce many (~ 100 000) archive BCS spectra not-yet properly reduced.

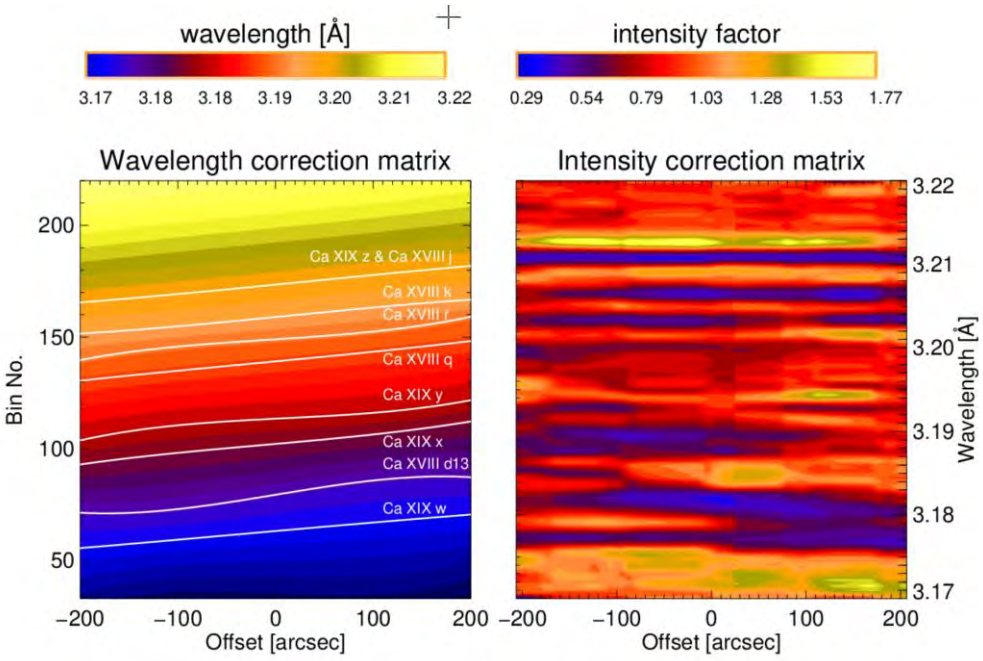

Fig. 3.13. Correction matrixes for wavelength and intensity to be used when reducing the BCS bin-spectra observed in Channel #1 to linear units. Provided the curvature of the Ge 220 monocrystal wafer had ideal cylindrical shapes, the white lines in the left panel should be straight, as well as corresponding background colour pattern. In such case the right panel should be of the uniform red colour equal to 1.00. The patterns determined and shown indicate for substantial non-cylindrical profile of the Bragg-reflecting crystal surfaces.

After introducing the recommended (cf. Fig. 3.13) corrections the spectra have been averaged over Phases A, B & D and fitted with the modern atomic theory. This is illustrated in Fig. 3.14.

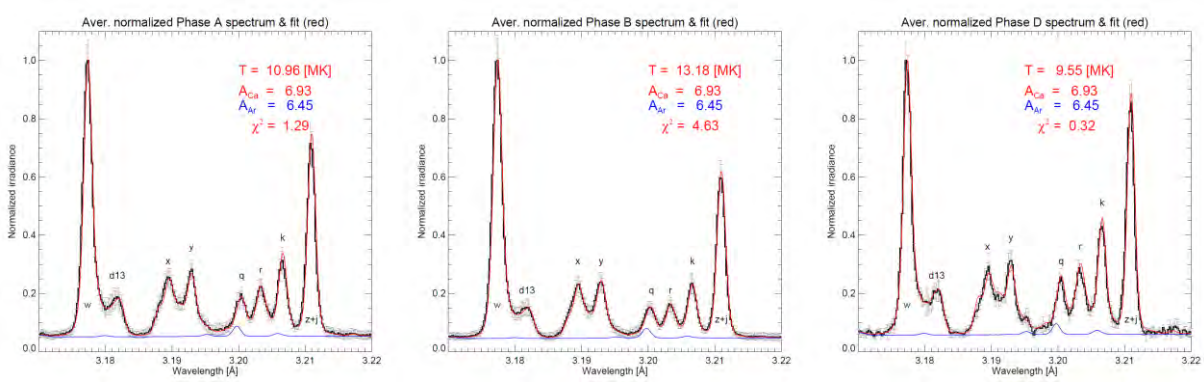

Fig. 3.14. Spectra (in black) averaged over Phase A, Phase B, and Phase D after introducing neccessary corrections. Reduced average spectra have been best fitted with the most recent atomic theory counterparts (in red) containing not only the contribution of lines formed in Ca ions but also in Ar (blue) falling to the spectral range of SMM BCS Channel #1. Nearly perfect agreement is observed.

Based on the ratios of total signal measured in BCS Channel #1 and these observed by GOES in its 0.5-4 Å and 1-8 Å ranges a detailed pattern of spacecraft scans can be revealed showing location of the flaring compact source within the FOV of the collimator. This pattern is presented in Fig. 3.15.

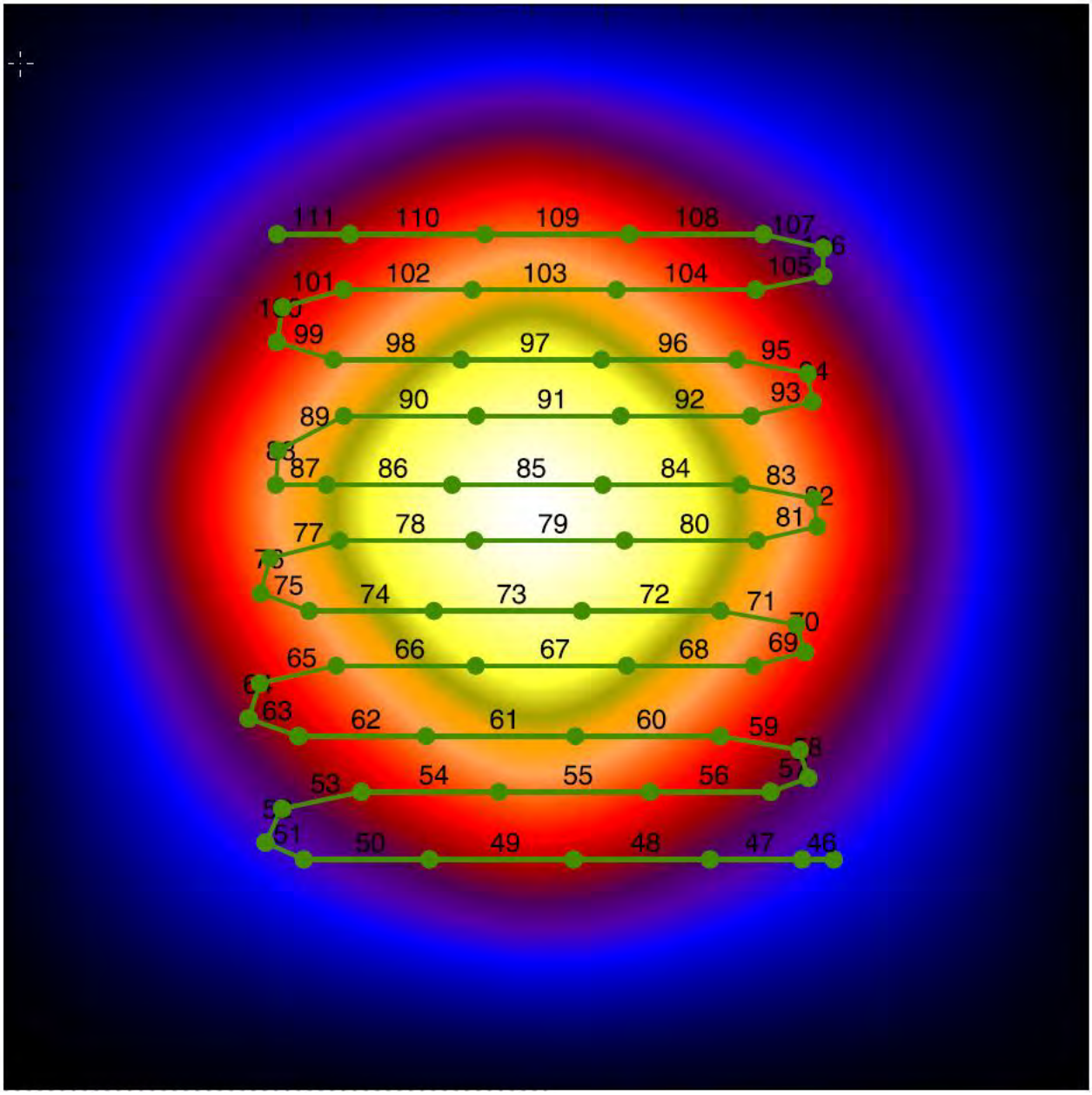

Fig. 3.15. Pattern showing location of the source (green) for 67 consecutive time points representing start & stop times of spectra collections in Phase B, when the spacecraft performed scanning in both along E-W and N-S tracks. In the background the transmission profile is represented by regular pattern, triangular along E-W and N-S lines directions

The paper describing the results obtained has been published in The Astrophysical Journal, 894:137 (11pp), (2020 May 10), https://doi.org/10.3847/1538-4357/ab86ba.

This paper received *welcome and positive* attention of Susanna Kohler, the Editorial Manager for the AAS (https://aasnova.org/2020/07/15/bent-crystals-and-solar-flares/) who wrote: "*Now, in a new study led by Janusz Sylwester (Space Research Center, Polish Academy of Sciences), a team of scientists has conducted a valuable recalibration of BCS spectra.(...)*

By examining data produced during the scan of a solar flare in November 1980, Sylwester and collaborators are able to identify and quantify the effect of small deformations in the crystal curvature of one of the channels. Accounting for these deformations resolves a long-standing mystery of certain anomalies in the ratios of emission lines in BCS data. The authors additionally improve other calibration aspects, ultimately producing high-resolution line spectra that they suggest could now be used as templates for the analysis and interpretation of future observed X-ray spectra — in particular, spectra gathered from other active, flaring stars in our galaxy.

With revitalization efforts like this, observations from BCS thus continue to be valuable many years after the mission end — well justifying the daring in-orbit rescue of SolarMax.".

STIX T. Mrozek

The Spectrometer Telescope for Imaging X-rays (STIX) is an X-ray imaging spectrometer operating in the 4-150 keV range installed on board the Solar Orbiter mission. It is equipped with 30 pairs of grids and pixelized Caliste-SO detectors which allow for measuring the Fourier components of solar flare HXR emission distribution. Using them we are able to reconstruct images with the angular resolution of the order of 7 arc sec. Taking into account that the perihelion distance for the Solar Orbiter will be 0.3 au the HXR images will achieve an unprecedented spatial resolution of 1000 km (on the Sun).

The STIX imaging concept is based on pairs of grids which were previously used in several instruments (Fourier imagers). The main characteristic of Fourier

imagers is that the image is not obtained directly. Rather, the imager consists of pairs of grids with various pitches and orientations. Each pair of grids modulates the incoming radiation depending on source size and location. Having sets of intensities measured with dozens of grid pairs, we can reconstruct the spatial distribution of X-ray emission. In previous experiments the front and rear grids were shifted in phase while slats were parallel. In STIX, the front and rear grids are slightly tilted, producing a characteristic Moiré pattern in the detector plane.

We aimed to develop the image reconstruction algorithm without any analytical simplifications and restrictions. In our method we abandon Fourier's approach to image reconstruction, and instead use the number of counts recorded in each detector pixel, and then reconstruct each image using a classical Richardson-Lucy (R-L) algorithm. Knowing the instrument geometry we are able to calculate the detector response for point sources. We assume a point source of a 1x1 arc sec pixel on the Sun. Having calculated the point source response for a grid covering entire the solar disc, we can iteratively combine point source responses with varying weights until the best match between reconstructed and observed detector responses is achieved.

We performed tests on various emission sources configurations, and compared results with CLEAN-Vis. The testing configurations were:

- Two Gaussians, dynamic range 3 : 5;
- Two Gaussians, higher dynamic range 1 : 5;
- Two Gaussians, low signal - the total number of counts recorded by all 30 detectors was less than 1000;
- Faint structure, small sources located close to each other, each source is smaller than instrument angular resolution;
- Typical flaring geometry: two foot points, loop-top source, above the loop-top source.

Figure 3.16 presents simulated configurations (first column), images

reconstructed with CLEAN-Vis algorithm (middle column), and results of reconstruction made with R-L algorithm (right column). The images reconstructed with both algorithms show the same number of sources. The exception is a fine structure, but in that case size of model sources were below the STIX angular resolution.

The developed algorithm is the most straightforwad approach to the image reconstruction problem. Despite its simplicity, it is very well constrained for detailed photometry of solar HXR sources. Preliminary tests revealed that the developed algorithm reproduces high quality images. The main conclusions about the algorithm performance are as follow:

- The algorithm gave stable results with small tendency for over-resolution which may be easily avoided by using the stopping parameter related to the rate of χ^2 change.
- The algorithm is slow, but the result comparable to Clean-Vis is obtained within 20-50 iteration steps only which takes less than 2 seconds on typical portable computer configuration.
- Sources are reconstructed very well. The location, size and intensity are very close to simulated ones. Therefore the algorithm is very well suited for the detailed photometry of the solar HXR sources.

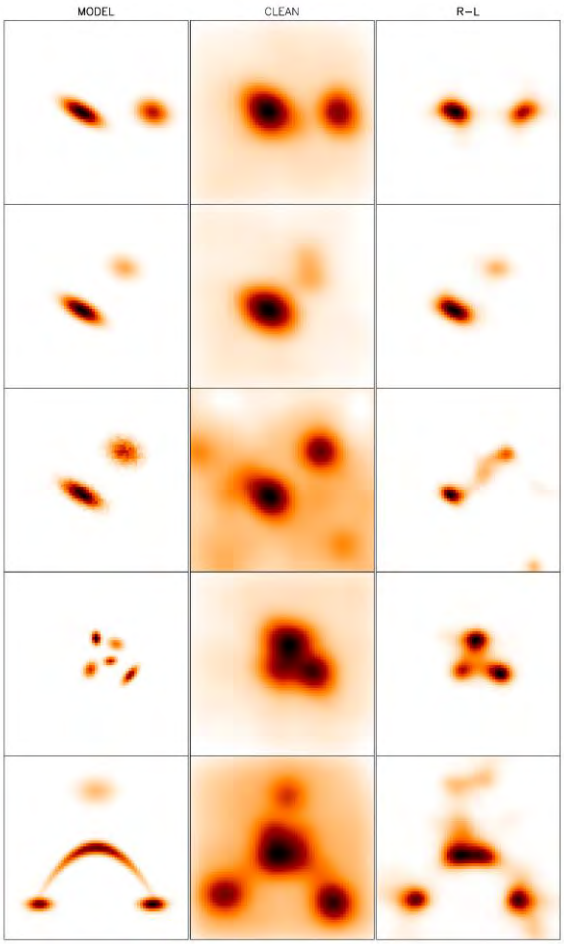

Fig. 3.16. Simulated emission sources configurations (left column), and images reconstructed with the CLEAN-Vis (middle column), and RL (right column) algorithms.

Tomasz Mrozek

3.2 Heliospheric Physics

Laboratory for Solar System Physics and Astrophysics (LSSPA) CBK PAN

Heliospheric physics M. Bzowski

The hypersonic, ionized solar wind carves out a cavity in the interstellar matter, called the heliosphere. The size of the heliosphere is determined by a balance between the pressures of the solar wind and the interstellar gas, both of which are magnetized. The heliosphere is bounded by a contact

discontinuity layer called the heliopause, which separates the solar wind and interstellar plasmas. While the interstellar plasma is deflected and flows past the heliopause, the neutral component of interstellar matter, mainly hydrogen and helium, penetrates freely into the heliosphere, where it can be directly observed. An artist's impression of the heliosphere is shown in Figure 3.17.

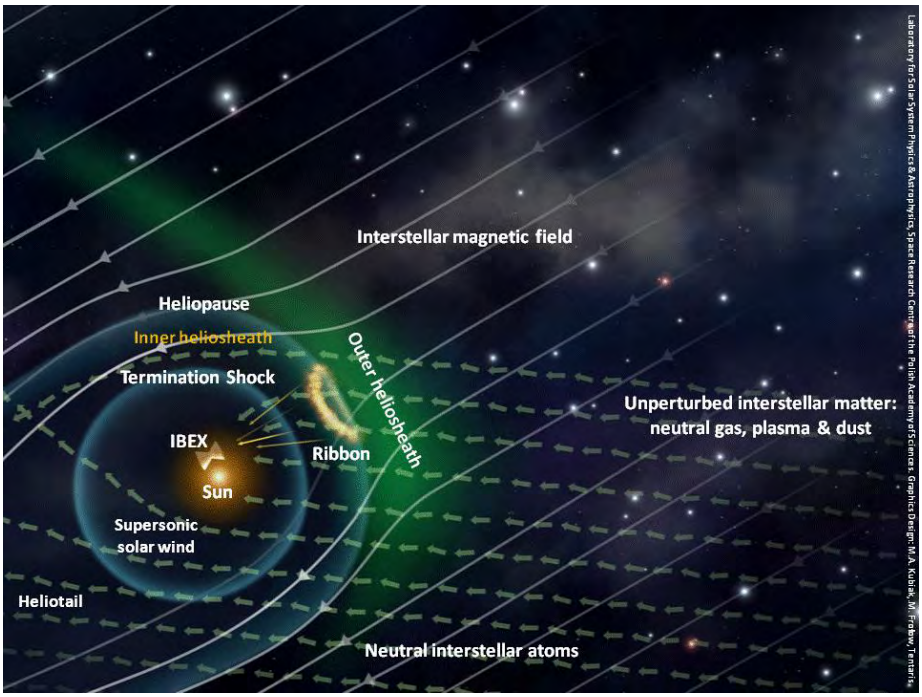

Fig. 3.17. Artist's impression of the heliosphere and its nearest Galactic neighborhood as it emerges based on the analysis of recent IBEX observations and several years of research carried out in the Laboratory for Solar System Physics and Astrophysics.

The figure shows the Sun embedded in the local cloud of interstellar matter composed of ionized and neutral atoms and dust grains of various sizes. This cloud is one of many similar clouds within the Local Interstellar Medium—an astrophysical object spanning approximately 200 pc across that is a remnant of a series of Supernova explosions that happened a few million years ago. The Sun moves through the Local Interstellar Cloud from right to left in Figure 3.17, emitting the *solar wind*—an ever-evolving, omnidirectional, latitudinally-structured, hypersonic outflow of solar plasma. Subjected to the ram pressure of the ambient interstellar matter, the solar wind slows down

through a shock wave—the solar wind termination shock—and eventually flows downstream, forming a contact discontinuity surface called the *heliopause*, which separates the solar and interstellar plasmas, and an elongated *heliotail* (bottom-left corner of Figure 3.17). The heliopause, impenetrable for charged particles except for cosmic rays, is transparent for neutral atoms, which thus freely enter the heliosphere. Inside the heliosphere, the interstellar atoms become the seed population for energetic neutral atoms (ENAs). ENAs are formed everywhere in the heliosphere due to the charge exchange reaction between the ions from local plasma and the neutral interstellar atoms. Once created, they travel without being ionized or absorbed at large distances, comparable to the size of the heliosphere.

The charge exchange process operates both in the supersonic solar wind and in the *inner heliosheath* (centre-left in Figure 3.17), i.e., in the region between the termination shock and the heliopause. Some of the ENAs created in these regions freely escape from the heliosphere and, due to eventual collisions, slightly modify the inflowing interstellar gas. Others run in the opposite direction and reach detectors located in the Earth's orbit (in Figure 3.17, schematically drawn close to the Sun).

Neutral atoms from the interstellar matter (whose streamlines are marked by the short arrows in Figure 3.17) typically have energies of between a few dozen and about 150 eV. Due to interaction between the heliosphere and the interstellar medium, a disturbed region called the *outer heliosheath* (the green haze in the figure) is formed in front of the heliosphere. In this region, the flows of interstellar plasma and interstellar neutral gas decouple from each other. This leads to the formation of another population of neutral atoms through charge exchange reactions between ions from the perturbed plasma flow past the heliopause and the hardly perturbed interstellar neutral atoms. Some of the atoms being products of this reaction also enter the heliosphere and are detected as the so-called *secondary population of neutral interstellar gas*.

Together with all the other populations of neutral atoms, they provide an important means for analysis of the physical state of the distant regions that they originated from.

During recent years, a very important insight into the heliosphere, Local Interstellar Medium, and processes responsible for the coupling of these astrophysical objects was obtained based on observations by the NASA space probe Interstellar Boundary Explorer (IBEX). This mission was developed and is being led by the Southwest Research Institute in San Antonio, Texas under the NASA Small Explorers program. It is managed by the Goddard Space Flight Center for the NASA Science Mission Directorate in Washington, DC. The research facilitated by IBEX is carried out by the IBEX Science Team of researchers from the United States, Poland, Switzerland, Germany, and Russia. CBK PAN has participated in the IBEX effort since the planning phase, at the Co-Investigator level.

During 2018, scientists from Laboratory for Solar System Physics and Astrophysics (LSSPA) carried out studies of various aspects of the heliosphere and the surrounding interstellar medium. All research results obtained in 2018 by LSSPA scientists were published in sixteen scientific papers in international, peer-reviewed scientific journals. Some of these results are presented below.

The heliosphere is not round!

The solar wind expansion stops at a certain distance to the Sun. This happens in the locations where the solar wind pressure becomes equal to the pressure of the interstellar matter. The solar wind matter cannot accumulate infinitely inside the heliosphere and must find an exit path to the interstellar space. But where exactly is this path located? And is there just one evacuation path or more? These questions cannot be answered directly because up to now there have been just two active space probes – Voyager 1 and 2 – to reach the boundary regions of the heliosphere, and this happened in the

regions least suspect of being anywhere close to the solar wind evacuation path. Therefore, the question of solar wind exhaust location can only be answered by means of remote-sensing measurements and theoretical modelling.

The laws of physics suggest that the shape of the heliosphere depends on the speed of the Sun's motion through the interstellar gas, the density of this cloud, the intensity and direction of the interstellar magnetic field, as well as the spatial distribution of the total pressure of the solar wind. The key factor is the pressure balance between the solar wind and interstellar matter. The interstellar magnetic field exerts a certain stress force on the heliosphere, which can be conveniently represented as an additional pressure term known as the magnetic pressure. The magnitude of this pressure is proportional to the square of the strength of the component of the magnetic field vector perpendicular to the heliopause. The ram pressure of the ionized component of interstellar matter is proportional to the total density of the interstellar plasma and to the square of Sun's speed relative to the surrounding interstellar plasma. If the interstellar magnetic field is so strong that the magnetic pressure is much larger than the ram pressure of the interstellar plasma, then the heliosphere is expected to be approximately spherical in shape, and the solar wind is evacuated via two channels parallel to the direction of the local interstellar magnetic field. If, however, the ram pressure is much larger than the magnetic pressure, then the heliosphere will take an elongated, comet-like shape (somewhat distorted from axial symmetry by the magnetic pressure), and the solar wind will be evacuated via one channel directed 'backwards', i.e., along a long tail pointing approximately opposite to the Sun's motion. An extensive study on the shape of the heliosphere for various combinations of the ram and magnetic pressures was published in 2017 by two scientists from LSSPA: Dr. Andrzej Czechowski and Jolanta Grygorczuk MSc.

Based on available extensive insights from experimental and modelling

studies using various measurement techniques, it had been concluded that most likely, the interstellar dynamic pressure is much larger than the magnetic pressure, and consequently the heliosphere has a comet-like form. However, in 2017, a team of US scientists published a hypothesis that the heliosphere is round in shape (in *Nature Astronomy*). They considered measurements of the flux of energetic neutral atoms (ENAs) with energies of several dozen keV (an order of magnitude larger than typical energies of solar wind protons), performed by the INCA instrument onboard the Cassini space probe. They found that: (1) variations in time of the flux are unexpectedly rapid; (2) they are strongly correlated with each other, with the phase of the 11-year cycle of solar activity, and with time variations of *in situ* point measurements of energetic ions in the outer heliosheath (the parent population for ENAs observed by INCA); and (3) the fluxes of these ENAs from the upwind and downwind sides of the heliosphere have similar magnitudes, and their variations are correlated in time. On this basis, the team of US researchers concluded that the distances to, and the dimensions of, the source region of these ENAs must be very similar for all directions. Consequently, the heliosphere must be approximately round and, if so, then it must be shaped by a strong interstellar magnetic field.

This hypothesis is at odds with previous views on the shape of the heliosphere because the strength of the interstellar magnetic field, the plasma density, and the speed of Sun's motion through the Local Interstellar Medium have been measured with a sufficiently good accuracy and suggest that interstellar magnetic pressure is lower than the plasma ram pressure. However, the INCA observations used by the aforementioned team of scientists are an enigma that must not be ignored. Dr. Nathan Schwadron from the University of New Hampshire and Dr. Maciej Bzowski from the LSSPA suggested that the INCA observations can be understood based on the conventional, comet-like paradigm of the heliosphere. In a paper published in *The Astrophysical Journal* (Schwadron & Bzowski, 2018) they suggested some reasons for the correlation

between observed fluctuations of INCA ENAs, fluctuations of the charged particles observed by Voyager, and the phase of solar activity.

Schwadron and Bzowski pointed out that the ENA fluctuations are related to the ENA production rate, which is strongly dependent on fluctuations in the temperature and density of the solar wind plasma penetrating the solar wind termination shock. This is a quasi-stationary shock wave structure that separates the hypersonic and subsonic regimes of the solar wind outflow. When a portion of plasma with an increased density and speed crosses the termination shock, the plasma just downstream of the termination shock is heated and, before cooling, for some time propagates with the plasma flow in the inner heliosheath. The temperature of such plasma flow is much larger than that of the shock-processed 'regular' solar wind plasma. Therefore, the charge exchange rate between protons in the heated plasma and the ambient interstellar neutral H atoms increases rapidly and, consequently, an enhanced flux of ENAs is produced for a certain time before the heat dissipates. Since the occurrence of fast and dense gusts of the solar wind increases during high solar activity and, on the one hand, these gusts have a global range and, on the other hand, the difference in arrival times between various locations along the shock is relatively small (a few months) a strong spatial correlation eventually appears between time fluctuations of the ENA flux from various regions of the termination shock, and a time correlation between the charged energetic particles processed by the termination shock, measured by the Voyagers, and the ENA fluxes from the heliosheath, measured (with a well-understood time delay) by INCA.

Consequently, the seemingly strange observations reported by the team of US researchers can be explained on the basis of the conventional heliospheric paradigm and the heliosphere, which, as the title of Schwadron and Bzowski's paper claims, is not round!

Conclusions from ENA observations from the HSTOF: The heliosphere has a tail

and is asymmetrical A. Czechowski, M. Bzowski

Since the speed and direction of motion of heliospheric ENAs reflect the speed and direction of motion of their parent ions, ENA observations offer a good insight into the energy distribution of cosmic plasma located far away from the observation site.

The High energy Suprathermal Time Of Flight sensor (HSTOF) instrument onboard the Solar and Heliospheric Observatory (SOHO) space probe has been carrying out ENA observations since 1996. The instrument is sensitive to ENAs with energies from 55 to 88 kiloelectronvolts (keV), i.e., to atoms traveling at 3250 to 4100 km/s. Other instruments observing ENAs (in different energy bands) include INCA, onboard the Cassini Saturn probe (observations between 2005–2013), the ASPERA instruments onboard the planetary probes Mars Express and Venus Express (also presently inactive), and the IBEX satellite (carrying out observations from 2009 until present).

The implications of HSTOF observations carried out from 1996 to 2010 were studied by a team of scientists from LSSPA: Andrzej Czechowski, Maciej Bzowski, and Stanisław Grzędzielski, Justyna M. Sokół and Jolanta Grygorczuk., in collaboration with Professor K.C. Hsieh from the University of Alabama, who formulated the concept of the HSTOF experiment and Dr. M. Hilchenbach from the Max-Planck-Institut für Sonnensystemforschung in Göttingen, Germany, who processed the data. The researchers found a clear downward trend in observed ENA intensities, which seems to be correlated with the secular systematic decrease in the solar wind flux observed *in situ* at the Earth's orbit, but not with periodic variation in the solar wind related to the solar activity cycle. A similar downward trend in ENA observations was found by INCA and IBEX. The correlation of the ENA flux with the solar wind flux supports the hypothesis that observed ENAs originate from the aforementioned charge exchange reactions between protons from the shocked solar wind plasma and interstellar hydrogen atoms in the boundary regions of the heliosphere.

Furthermore, these observations corroborate the hypothesis that the heliosphere's axial symmetry is distorted due to the action of the interstellar magnetic field. This is because the observed ENA flux in the "starboard flank" (ecliptic longitudes from 120° to 210°) is larger than the flux from the "portside flank" (ecliptic longitudes from 300° to 30°). The observed asymmetry is in agreement with recent estimates of the direction of interstellar magnetic field. Finally, HSTOF observations lend strong support to the existence of the heliospheric tail: the flux observed from the upwind region of the heliosphere, i.e., from the direction of Sun's motion through the local interstellar matter, is much lower than the flux from the opposite direction. This behavior is expected if the heliosphere has a long tail. The upwind to downwind ratio of the ENA fluxes observed by HSTOF differs from the ratios observed by INCA and IBEX. Researchers from the CBK PAN demonstrated that this difference is a natural consequence of the larger energies observed by IBEX: 55 to 88 keV in comparison with 5 to 55 keV observed by INCA and 0.7 to 4.3 keV observed by IBEX, and the resultant difference in reaction cross sections. This result is another confirmation that "The heliosphere is not round!".

In addition to the data from the HSTOF, the research team used results of earlier determinations of the densities of interstellar hydrogen and helium at the termination shock of the solar wind, based on data from the Voyager and Ulysses spacecraft, with an important contribution from scientists from LSSPA as well as the Warsaw Test Particle Model of the density distribution of interstellar H and He in the heliosphere developed in LSSPA, and the Warsaw MHD model of the heliosphere.

The results and conclusions were presented by the team led by Dr. Andrzej Czechowski in a paper published in *Astronomy & Astrophysics* (Czechowski et al., 2018a).

Structure of the heliosphere revealed by the spectrum of energetic neutral

atoms A. Czechowski, M. Bzowski

Energetic Neutral Atoms (ENAs) are an important tool for investigating the structure of the heliosphere and for diagnosing the enigmatic processes of acceleration of charged particles in the heliospheric boundary region. Observations of ENAs with energies below ~50 keV by the Cassini space probe, performed at the Saturn orbit, showed that ENA fluxes from the upwind and downwind regions of the heliosphere are similar in strength. This led the authors of these observations to hypothesise that the heliosphere is bubble-like rather than comet-like (i.e., it has no extended tail). An international team of scientists, led by A. Czechowski from the LSSPA investigated the hypothesis that these ENAs are created by charge exchange of solar wind pickup ions that have been accelerated at the solar wind termination shock, and subsequently advected with the plasma flow beyond the termination shock.

The research team simulated a directional distribution of ENAs within a wide energy range, from 3 to 88 keV, i.e., almost the entire energy range covered by available observations from IBEX, Cassini, and SOHO space probes (IBEX-Hi, INCA, and HSTOF instruments, respectively). The calculation of ENA fluxes was performed using a multi-tier simulation scheme. The global structure of the plasma flow inside and outside the termination shock was obtained using MS-FLUKSS – one of the most sophisticated global heliosphere models currently available. The PUI flux at the termination shock was calculated using the Warsaw Test Particle Model (WTPM) to simulate the spatial distribution of ISN H filling the space between the Sun and the termination shock, forming the seed population for PUIs. The PUI flux at the termination shock was calculated based on this density distribution and the most recent version of the LSSPA model of ionisation factors in the heliosphere (developed by the LSSPA during the past decade, see below).

An essential element of the simulation was a model of the acceleration

of pickup ions at the termination shock. The research team applied a theory of acceleration developed several years ago by one of the team members (Gary Zank from the University of Alabama, Huntsville, USA) and his collaborators. In this theory, a fraction of the pickup ion population with energies below the electric potential threshold at the shock cannot penetrate this threshold and is reflected upstream of the solar wind. These ions are picked up and accelerated by the inflowing solar wind plasma, thus gaining energy. The reflection/ energisation cycle repeats until an ion has a sufficient energy to penetrate the potential threshold and enter the inner heliosheath. The energised ions are subsequently carried by the solar wind plasma in the inner heliosheath. While the kinetic energy of individual ions is large, the mean flow speed of their population is close to that of the bulk plasma, which leaves them enough time to exchange charge with ambient H atoms and produce a sufficiently large amount of ENAs.

The sequence of models used in the simulation drew upon the most-credible, currently-available values for relevant parameters obtained from observations. Equally important was adopting a proton spectrum just downstream of the termination shock, which on the one hand was in agreement with solar wind measurements and the Zank PUI acceleration theory, and on the other hand agreed with the Voyager LECP *in situ* measurements of the ion spectrum and of the termination shock strength (Fig. 3.18).

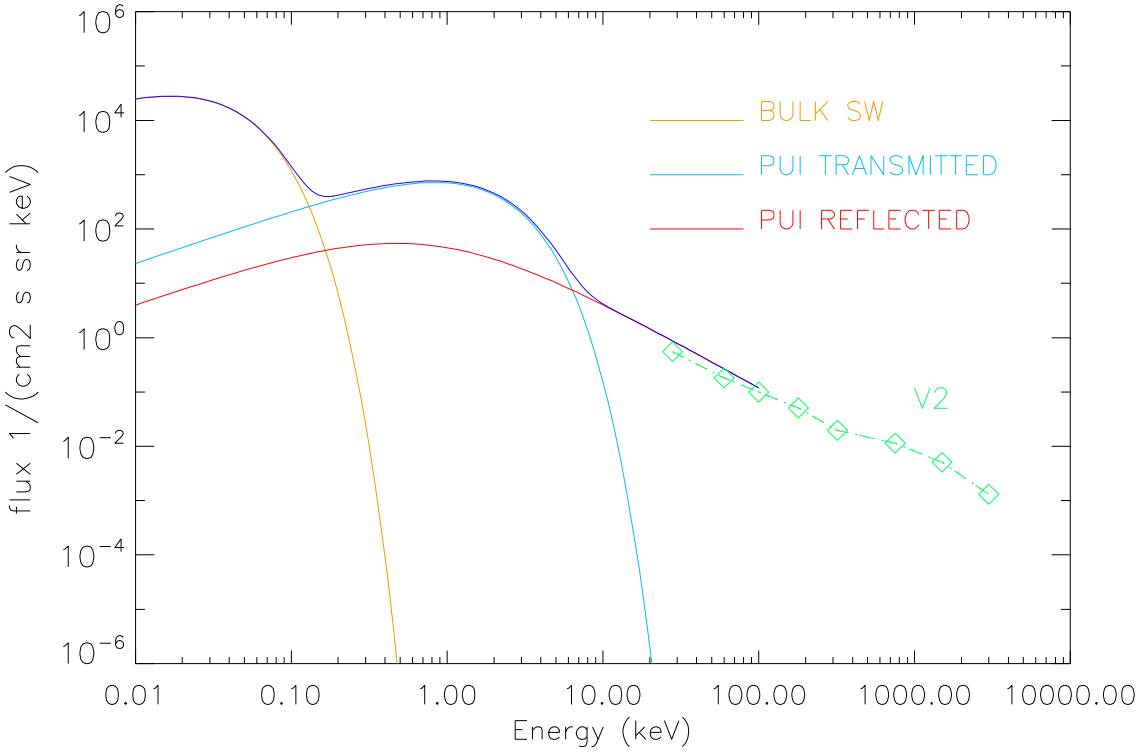

Fig. 3.18. A model spectrum of ions used to simulate the observed ENA flux. The model has three components: bulk solar wind (orange), pickup ions reflected off the termination shock (red), and pickup ions transmitted across the shock (blue). The three components add up to make the total spectrum (purple). This spectrum agrees very well with the spectrum of suprathermal ions measured by the Voyager 2 spacecraft in the corresponding energy ranges. Note that the energy of the reflected component is shown after energisation of these ions and their resulting penetration of the termination shock. Source: Czechowski et al., Ap. J. 888:1, 2020.

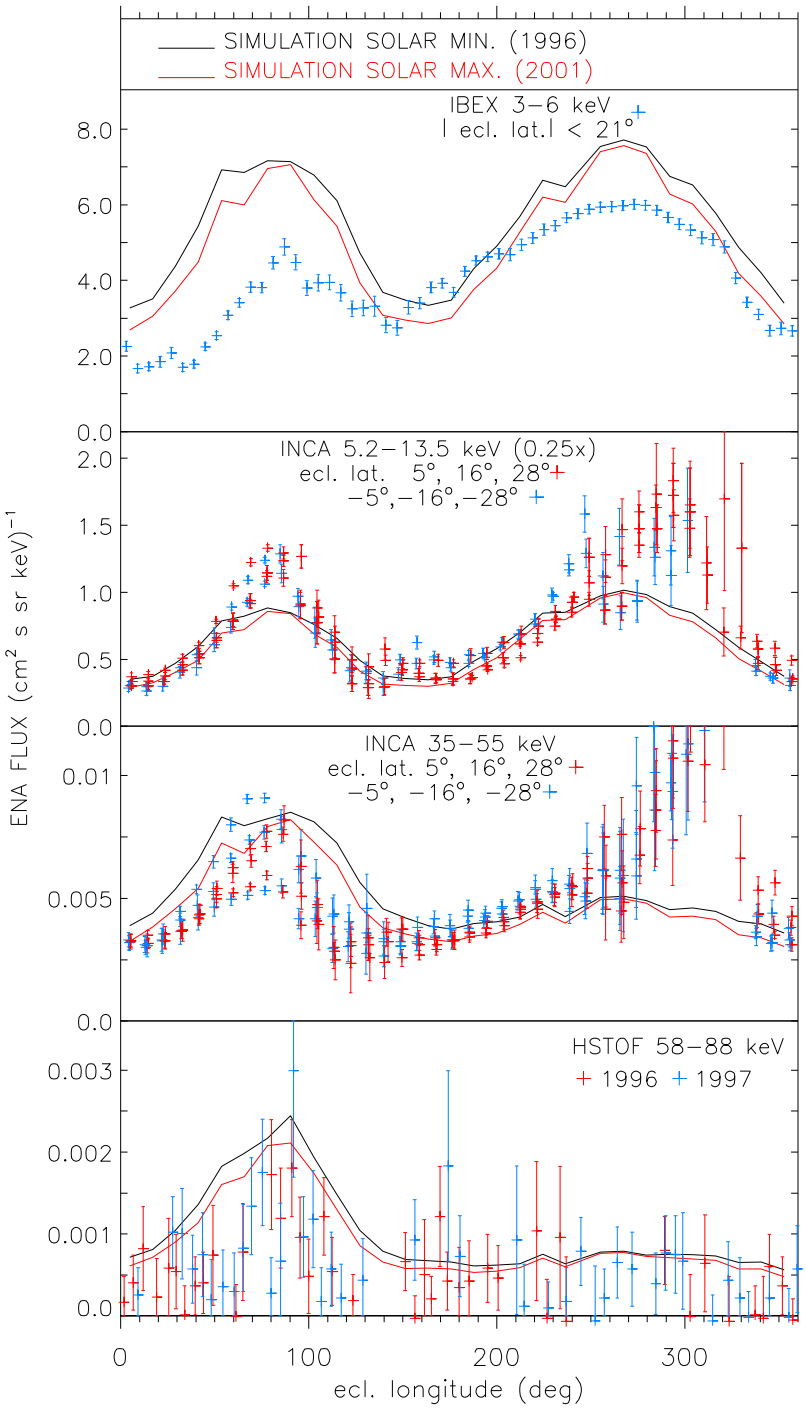

Fig. 3.19. Model of ENA flux (solid lines) for four energy bands (top–bottom panels), compared with actual observations from IBEX-Hi (first), INCA (second and third), and HSTOF (fourth). The data are presented by dots, and measurement uncertainties by error bars. There is relatively little difference between simulations performed separately for a maximum and a minimum of solar activity (red and black lines, respectively). Source: Czechowski et al., Ap. J. 888:1, 2020.

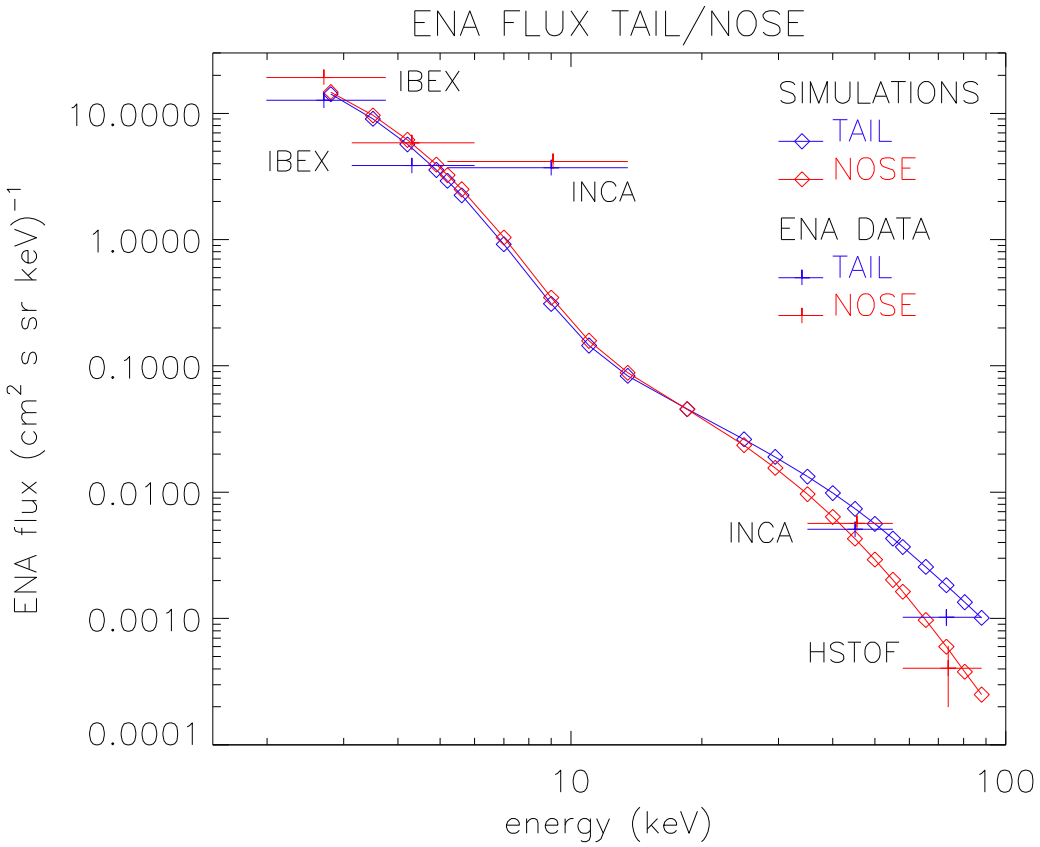

Fig. 3.20. Spectra of ENAs for the upwind (red) and downwind (blue) regions of the heliosphere, obtained from observations (points with bars) compared with the corresponding spectra obtained from simulations (diamonds). Horizontal bars mark the energy bands of the respective energy channels. Vertical bars represent uncertainties in observations. Source: Czechowski et al., Ap. J. 888:1, 2020.

This successful reproduction of the observed flux distribution and spectrum by a simulation using a model of the heliosphere with a long tail strongly suggests that there is no need to deviate from the classical paradigm of the heliosphere. In other words, the heliosphere is not round!

The results of this work by the team led by Dr. A. Czechowski from LSSPA, including Dr. M. Bzowski, Dr. J.M. Sokół, Ms. M.A. Kubiak, and Ms. J. Grygorczuk from the LSSPA, and researchers from Princeton University, the University of Alabama in Huntsville, the University of New Hampshire, and the Max Planck Institute for Solar System Research were published in *The Astrophysical Journal* 888:1, 2020, in a paper by Czechowski et al. (https://doi.org/10.3847/1538-4357/ab5b14).

Interstellar neutral helium atoms observed in three IBEX-Lo energy channels
P. Swaczyna, M. Bzowski

Interstellar neutral atoms of helium from the Local Interstellar Medium are observed by the Interstellar Boundary Explorer (IBEX) spacecraft in the Earth orbit. Researchers from LSSPA, Dr. Paweł Swaczyna, Dr. M. Bzowski, Ms. Marzena A. Kubiak MSc, Dr. Justyna M. Sokół, and their international collaborators analysed these observations to determine the Sun's motion with respect to the Local Interstellar Medium and the temperature of this medium. From a broader perspective, the results of these analyses provide an important insight into how the heliosphere interacts with its surroundings. In a paper published in The Astrophysical Journal (Swaczyna et al., 2018), they analysed data from two energy channels of the IBEX-Lo detector previously not used, in addition to the data from the channel previously used, and obtained a better assessment of these quantities.

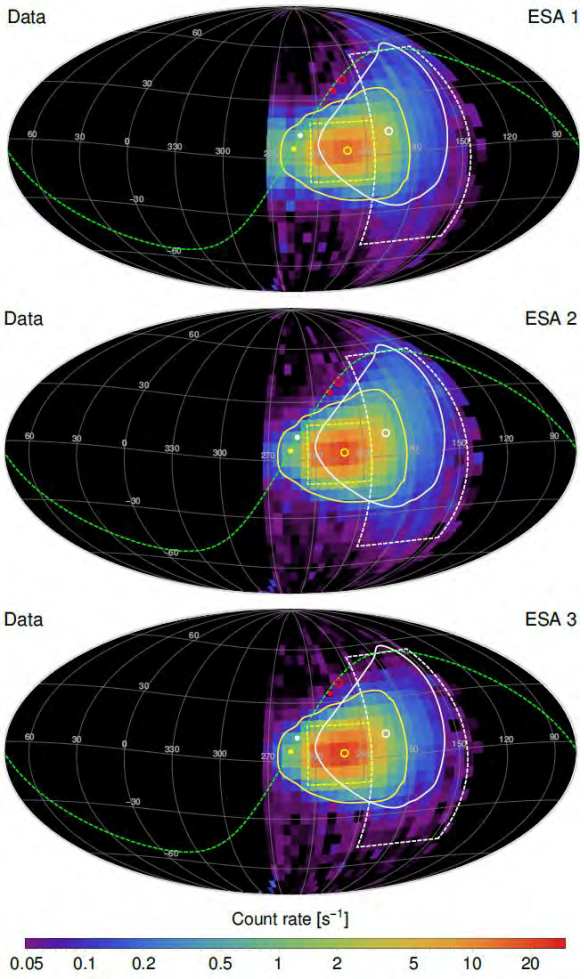

Fig. 3.21. Sky maps of counting rates of interstellar neutral atoms observed by IBEX in the analysed energy channels. The maps are centered at the direction of the Sun's motion with respect to the interstellar medium. Atoms are deflected by the Sun's gravity and thus observed predominantly away from this direction. Differences between observed counting rates in these energy channels are caused by the contribution of hydrogen atoms (not considered in this analysis) and the different energy-dependent sensitivities of the IBEX-Lo detector in these channels.

The structure of the interstellar medium at scales of tens and hundreds of parsecs around the Sun is not homogeneous. The Sun is within a system of multiple, partially-ionized, warm (5000–8000 K) and dense (~0.2 cm^{-3}) clouds, embedded in a very hot (~10^6 K), completely ionized and rarefied (~0.005 cm^{-3}) region. Telescopic observations of the absorption lines towards the closest stars show that the Sun is located either in one of two clouds known as the Local Interstellar Cloud and G Cloud, or – more likely – in a boundary region between

them. However, the ultimate determination is not possible from telescopic observations. The results of the IBEX mission may make it possible to resolve this enigma and answer the question of how conditions in the interstellar medium along the Sun's path will change during forthcoming millennia.

Previously, only data from one of the energy channels of the IBEX-Lo detector had been used in the analysis of the local interstellar gas. This was due to limited knowledge of the sensitivity of the detector to incoming atoms with various velocities (i.e., with various kinetic energies). As a first approximation, the energy channel that had been used in previous analyses was assumed to have a sensitivity independent of the atom energy. In this study, scientists from LSSPA analysed observations from the three energy channels of the IBEX-Lo detector in which interstellar neutral helium is visible, and abandoned the assumption of uniform energy sensitivity. The analysis aimed to determine the temperature and velocity vector of interstellar neutral helium simultaneously with the determination of the velocity-dependent sensitivity. Researchers found that the previously-obtained parameters of the interstellar medium did not need revision. This is important because this analysis lends more credence to earlier analyses of interstellar neutral gas and its secondary component, the so-called Warm Breeze, and to conclusions stemming from these analyses concerning the orientation of the interstellar magnetic field.

Density of interstellar He^+ ions and the ionization state of the Very Local Interstellar Medium M. Bzowski

The physical state of the interstellar medium surrounding the Sun is the subject of extensive research. The Sun is penetrating a cloud of warm, partly ionized gas, but the ionization state, temperature, and other physical parameters of this cloud are believed to be controlled to a large extent by ambient EUV radiation emitted by several relatively nearby stars that are very bright in this spectral region. Differential absorption, and the resulting ionization

of various ions of interstellar species and heating of interstellar matter by radiation from these stars make it challenging to determine the physical state of interstellar matter near the Sun. The ionization state and mean density of interstellar neutral and ionized components can be approximately determined by averaging over lines of sight to nearby stars, i.e., on spatial scales exceeding the size of the heliosphere by many orders of magnitude. However, to understand the interaction of the solar wind with the interstellar medium, an understanding of the local interstellar conditions, within several thousand au from the Sun is necessary. This insight was discovered in 2019 by an international team of researchers led by Dr. M. Bzowski from the LSSPA.

The heliosphere is created as a result of a pressure balance between the magnetized solar wind and the magnetized interstellar plasma. Interstellar neutral atoms mediate the interaction via charge exchange. The interstellar plasma is composed mostly of protons and He^+ ions. While the number abundance of He^+ ions in the plasma is on the order of 10%, its contribution to the plasma ram pressure acting on the heliosphere is fourfold bigger, because He^+ ions are fourfold heavier than protons. Therefore, determining the absolute density of He^+ ions in the unperturbed interstellar medium is important for heliospheric studies. However, up to now it has proved challenging because of the lack of available observables.

The flow of neutral interstellar helium through the perturbed interstellar plasma in the outer heliosheath (OHS) results in the creation of a secondary population of interstellar He atoms, the so-called Warm Breeze, which is due to charge exchange with perturbed He^+ ions. This secondary population brings an imprint of the OHS conditions to the IBEX-Lo instrument, and was discovered in 2010 by a research team led by CBK scientists M. Bzowski and M.A. Kubiak.

In 2019, an international team of researchers led by Dr. M. Bzowski, including Ms. M.A. Kubiak, Dr. J.M. Sokół, Dr. A. Czechowski and Ms. J. Grygorczuk from the LSSPA determined the number density of the interstellar

He^+ population in the unperturbed interstellar medium in front of the Sun. This finding was based on IBEX-Lo observations (for the years 2010–2014) of neutral He atoms fitted using a global simulation of the heliosphere, and a detailed kinetic simulation of the filtration of He in the OHS. This density was found to be $(8.98\pm0.12) \times 10^{-3}$ cm^{-3}. From this, they obtained the absolute density of interstellar H^+ as 5.4×10^{-2} cm^{-3} and that of electrons as 6.3×10^{-2} cm^{-3}. Consequently, the ionization degree of H was found to be equal to 0.26 and that of He to 0.37. These conclusions agree with estimates of the parameters of the Very Local Interstellar Matter obtained from fitting observed spectra of diffuse interstellar EUV and the soft X-ray background.

These results were published in *The Astrophysical Journal*, in a paper by Bzowski et al. (Ap. J. 882:60, 2019, https://doi.org/ 10.3847/1538-4357/ab3462).

Density of interstellar H measured by means of pickup ions observed in the outer heliosphere

M. Bzowski

The density of interstellar neutral H which is the dominant component of the interstellar matter in the Sun's vicinity, had been established in 2008 using several complementary observation data sets and analysis methods. One of the was observation of pickup ion flux observed by the Ulysses spacecraft on its circumsolar polar orbit, another was measuring the slowdown of the solar wind due to the "friction" of the solar wind plasma against the inflowing interstellar H atoms. This "friction" is a complex process involving exchanging charge and momentum between the interacting components, involving as a by-product creation of pickup ions. It seems, then, that pickup ion observations are the key to the density of interstellar H.

An international team of scientists led by Dr. Paweł Swaczyna from the Princeton University analyzed observations of pickup ion spectra obtained from the SWAPI experiment on-board the NASA New Horizons mission to Pluto.

Observations were collected during the cruise in the solar wind before and after the close encounter with Pluto. Analysis of the ion spectra resulted in determination of the density of pickup ions along the trajectory of the New Horizons spectra on one hand, and of the density of the solar wind protons on the other hand. Combined with the knowledge of other ionization processes responsible for the production of pickup ions, mostly photoionization by the solar EUV radiation, and models of the density distribution of interstellar H along the New Horizons trajectory enabled determining the density of interstellar H at the termination shock of the solar wind, which turned out to be 40% larger than thought before. Consequently, the density of neutral H in the unperturbed interstellar gas is likely to be larger by this factor.

Since this change is large and potentially has important consequences for the views on the interaction of the heliosphere with the interstellar gas, the team led by Paweł Swaczyna re-analyzed the original observations, reported back in 2008 and 2009. They found that the measurement of the solar wind slowdown observed by the Voyager spacecraft is compatible with the present result when a more accurate formula for the velocity-dependent cross section for charge exchange is used in the analysis. For the Ulysses pickup ion measurement, repeating the analysis using an updated radiation pressure (Kowalska-Leszczyńska et al. 2018b, 2020a) and ionization rate models (Sokół et al. 2019a, 2020) resulted in an increase of the density obtained from this experiment by 10%. While the agreement with the result obtained from New Horizons is not perfect, the two determinations agree now within the uncertainty ratio.

The research team included Dr. M. Bzowski, Dr. I. Kowalska-Leszczynska and Ms. M.A. Kubiak from LSSPA, CBK PAN. The results were published in a paper Swaczyna et al., ApJ 903:48, 2020.

Interstellar neutral gas species and their pickup ions inside the heliospheric termination shock

J.M. Sokół, M. Bzowski

The expected distribution of interstellar neutral (ISN) gas and PUI density of H, He, Ne, and O inside the heliosphere has been revised. Dr. Justyna M. Sokół and Dr. Maciej Bzowski from the LSSPA, together with Dr. Munetoshi Tokumaru (ISEE, Nagoya, Japan) and Dr. David McComas from the Princeton University overviewed the current state of knowledge about solar ionization rates for heliospheric atoms inside the termination shock. They compiled a list of ionization processes relevant for the ISN H, O, Ne, and He inside the heliosphere. The team focused on modulations with heliocentric distance, heliolatitude and time over the last three solar cycles. Three reactions: charge exchange with solar wind particles (protons and alpha particles), photoionization, and electron impact ionization were considered. Similarities and differences between ionization processes for the given species, as well as a comparison of the total ionization rates between the four species in the ecliptic plane and in the polar regions were presented. The ionization rates were considered within a consistent and homogeneous system of calculation, based on multi-source data from direct and indirect measurements of the solar wind and the solar EUV flux.

The study showed that ionization at 1 au is the strongest for H and O and, thus, the resulting modulation of the H and O fluxes of heliospheric particles is expected to be strongest. Modulation due to solar factors is weakest for He – it is almost an order of magnitude smaller than that for H and O at 1 au in the ecliptic plane. For He and Ne, the main source of ionization losses is photoionization. Consequently, modulation for these species is well correlated with variation in the solar activity. ISN H atoms are prone to solar wind variations both in time and in latitude. In the case of ISN O, both charge exchange and photoionization losses can be a dominant ionization source, depending on the

phase of solar activity and long-term changes in the solar wind. Total ionization rates are highest outside the ecliptic plane for O. Solar ionizing factors act differently on different heliospheric particles, which results in different modulation of these particles throughout the heliosphere. Total ionization rates for He and Ne vary in time with solar activity, whereas the rates for H and O follow variation in the cyclic solar wind outside the ecliptic plane, and aperiodic variations within it. This has important consequences for the study of heliospheric particles such as ISN gas, PUIs and ENAs, as well as physical processes in the inner and outer heliosphere.

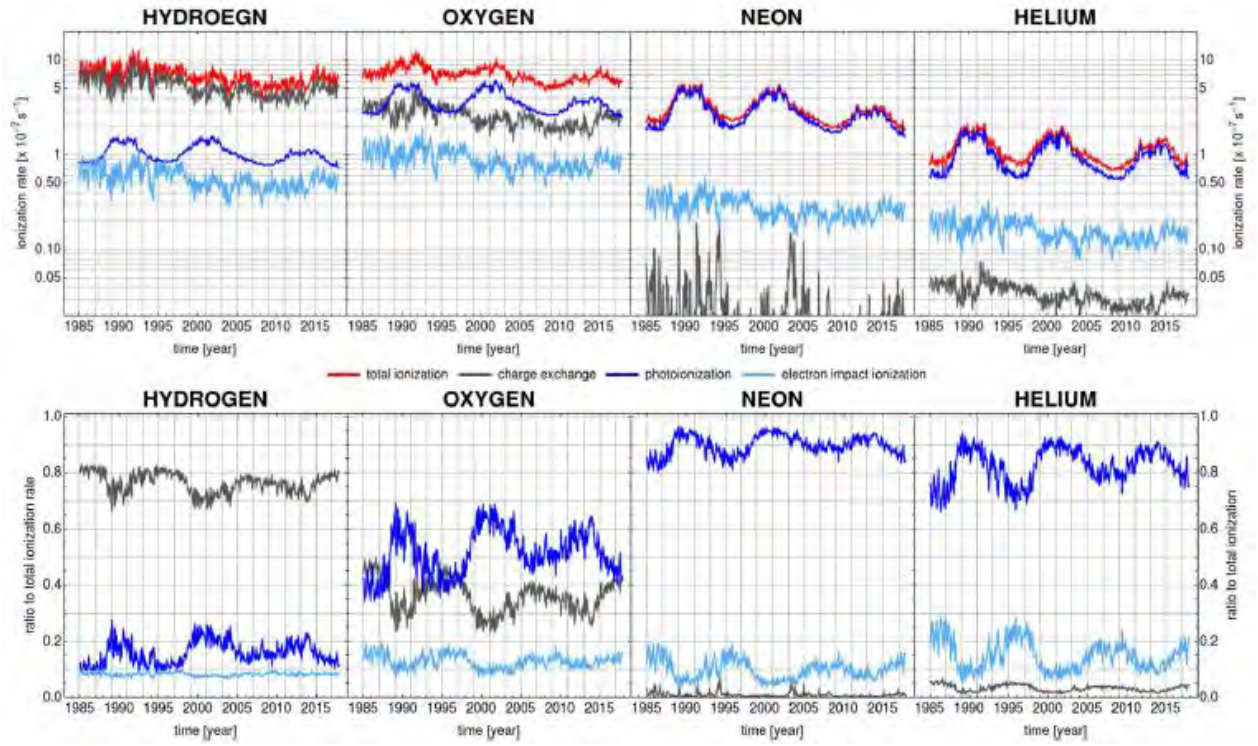

Fig. 3.22. Time series of ionization rates of neutral hydrogen, oxygen, neon and helium at 1 au in the ecliptic plane, presented for the time interval 1985–2019, with a time resolution corresponding to the solar rotation period (upper row). Red corresponds to the total ionization rate, which is a sum of the rates of charge exchange (grey), photoionization (dark blue), and electron impact ionization (pale blue). The lower row presents the percentage contribution of the three reaction rates to total rates for the four species, and its variation with time. Source: Sokół et al., Ap. J. 872:57, 2019.

These results were presented in papers by J.M. Sokół, M. Bzowski, M. Tokumaru, and D. McComas published in *The Astrophysical Journal* 872:57, 2019 and 897:179, 2020.

These revised solar ionization rates were used by scientists from the LSSPA (Dr. J.M. Sokół, Dr. M. Bzowski, and Ms. M.A. Kubiak) to study the spatial distribution of ISN gas density for H, He, Ne, and O and the PUI density for H^+, He^+, Ne^+, and O^+ in the region between 1 au and the termination shock of the solar wind, both in and out of the ecliptic plane, during minimum and maximum solar activity. The study focused on similarities and differences in the large-scale structures of ISN gas and PUI densities between various species that formed in the heliosphere.

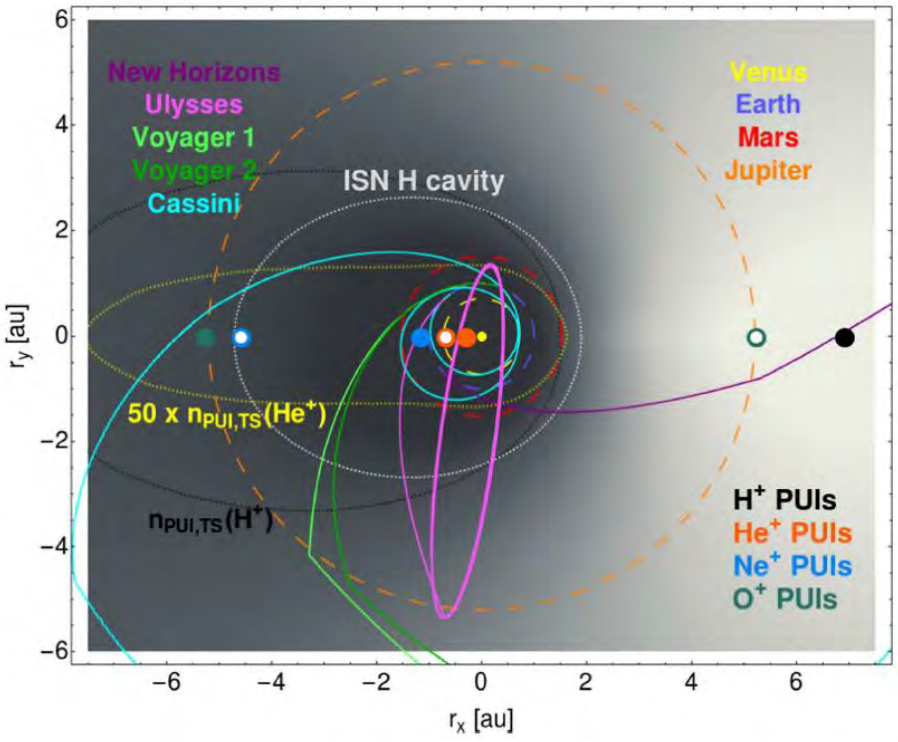

Fig. 3.23. The density distribution of H^+ pickup ions in the ecliptic plane is shown as a background for the locations of the maximum pickup ion densities of H^+ (black), He^+ (orange), Ne^+ (blue), and O^+ (green) in 1996 (full circles) and 2001 (empty circles). The upwind direction is shown on the right-hand side. For comparison, orbits of Venus, Earth, Mars, and Jupiter are shown as broken lines. Also shown are portions of the trajectories of selected spacecraft: Ulysses, Voyagers 1 and 2, New Horizons, and Cassini. The boundary of the cavity in the density distribution of ISN H in 1996 is marked by the grey dotted line. The yellow dotted line marks a region where the He^+ PUI density exceeds by a factor of 50 the upwind density of He^+ at the termination shock. Source: Sokół et al., Ap. J. 879:24, 2019.

These results show that different species have different ISN and PUI density structures. This is due to differences in modulation by solar ionizing factors, even though the inflow direction, speed and temperature of these species are identical (except for H). The latitudinal anisotropy of the ionization rates causes anisotropy in ISN gas and PUI densities measured along the ecliptic plane. Because this anisotropy is different for different species, relative abundance ratios of ISN and PUI densities vary non-uniformly in space and time. The study, performed for the first time for a homogeneous system of ionization rates for the species in question, showed that while the ISN density maxima are expected outside 1 au, the PUI density maxima are expected to be found closer to the Sun. The PUI densities, throughout the heliosphere, are expected to be highest for He^+ PUIs, then H^+ PUIs, Ne^+, and O^+ PUIs. The optimal location for the detection of He^+ PUIs is downwind, within 1 au. For Ne^+ PUIs, during the solar minimum detection is optimal at 1 au, while during the solar maximum the peak is shifted almost to Jupiter's orbit, with a density reduction of over 50%. Although O^+ PUIs can be searched for in both upwind and downwind regions (as intensities are expected to be similar), acceptable locations are found at distances starting from the Jupiter orbit, up to a few tens of au. The upwind hemisphere is confirmed as the best location to detect H^+ PUIs.

The research team identified the location of the cavity in ISN gas density for the four species, and variation of the size and shape of the cavity with time. The greatest cavity is expected for ISN H, while the smallest cavity is expected for ISN He. The study also discussed relative abundance ratios of Ne/O, H/He, Ne/He, and O/He for ISN gas and PUIs densities, together with their variation with location in the heliosphere, and their modulation along the TS. For relative abundance ratios of ISN gas densities of the species in question, the distribution at the TS is uniform up to about 40° off the downwind direction, where an increase in the ab solute density is expected. For PUIs, the variation at the TS is

not uniform in time and is a function of the angle off the upwind-downwind axis and heliolatitude; it also varies with the phase of solar activity.

These results were presented in a paper by Sokół et al. published in *The Astrophysical Journal* 879:20, 2019.

A "forgotten" population of neutral gas inside the heliosphere M. Bzowski

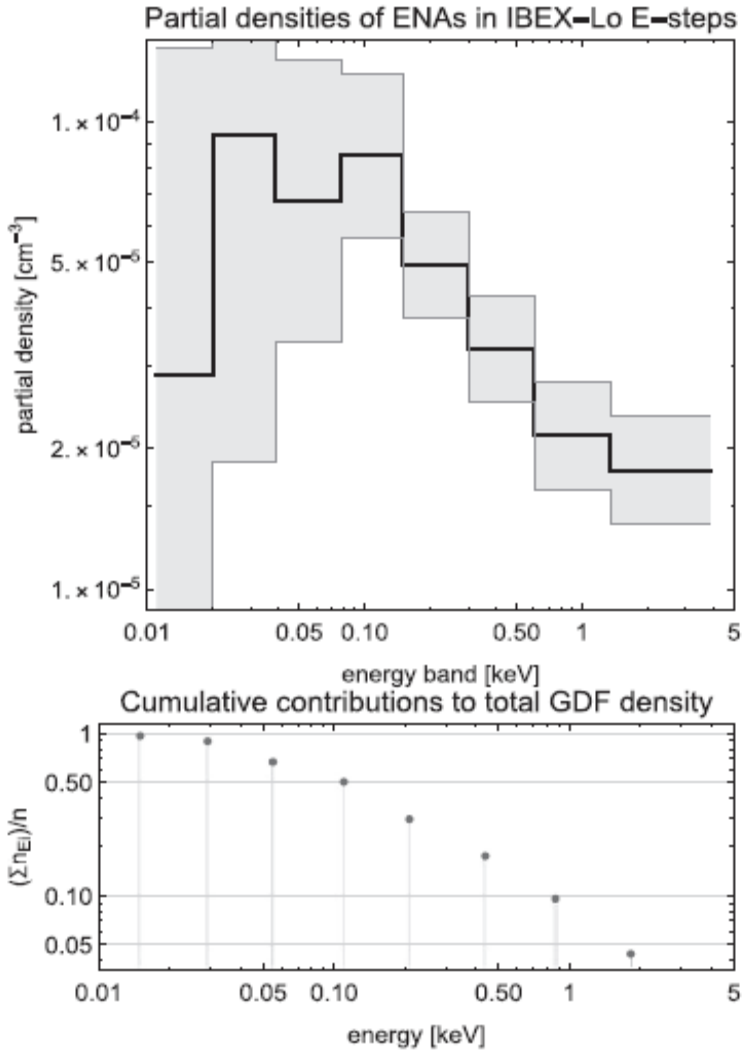

Fig 3.24. Partial densities of H ENAs observed by IBEX-Lo in its eight energy steps (upper panel) and a plot of cumulative density of the H ENA population from highest to lowest energies (lower panel). Densities are marked with a black line, and their uncertainties by grey shading. Most of the atoms forming the ENA population at 1 au from the Sun have energies less than 0.1 keV. Consequently, their speeds relative to the Sun are sufficiently low to locate their Doppler shifts inside the spectral range of the solar Lyman-α line. Hence, these atoms are illuminated by solar Lyman-α radiation, which they re-emit by the fluorescence mechanism. This ENA glow is one of the components of the Lyman-α helioglow observed from Earth-orbiting spacecraft. Source: Bzowski & Galli, Ap. J. 870:58, 2019.

Interstellar neutral H penetrates the heliopause and continues its flow towards the Sun. On the way, it is strongly depleted inside the termination shock. Nevertheless, fractions of both primary and secondary populations of this gas reach the Earth's orbit. In these regions of the heliosphere, ISN H is the source population for interstellar pickup ions and the heliospheric backscatter glow.

The globally distributed flux (GDF) of ENAs, created by charge exchange in the inner heliosheath, has been sampled directly by the Interstellar Boundary Explorer for almost a full cycle of the solar activity. Usually, these ENAs are treated as test particles bringing information on remote regions of the heliosphere. However, in fact, these atoms form a separate non-thermal population of neutral H atoms deep inside the heliosphere.

The energy spectrum of ENAs measured by IBEX is approximately described by a power law function, i.e., partial densities of atoms with energies corresponding to increasing energy channels of IBEX detectors rapidly decrease. Therefore, to assess the total density of ENAs at the Earth orbit, it is sufficient to analyze observations from the low-energy part of the spectrum, observed by the IBEX-Lo detector.

Based on available measurements from IBEX-Lo, Dr. M. Bzowski from the LSSPA and Dr. A. Galli from Bern University, Switzerland, calculated the number density of the GDF ENA population at the Earth's orbit. They found that this density is between 10^{-4} and 10^{-3} cm^{-3}, i.e., comparable in magnitude to the density of ISN H in the downwind portion of the Earth's orbit. Half of this atom population has energies less than ~80 eV. Consequently, this GDF population of neutral hydrogen is likely to provide a significant contribution to the intensity of heliospheric glow in the downwind hemisphere. It may also be the seed population for the ambiguous inner source of hydrogen pickup ions, and may be responsible for the excess production of pickup ions found in the analysis of magnetic wave events induced by the proton pickup process in the downwind

region 1 au from the Sun, which was discovered in 2018 by a research team that included scientists from the LSSPA.

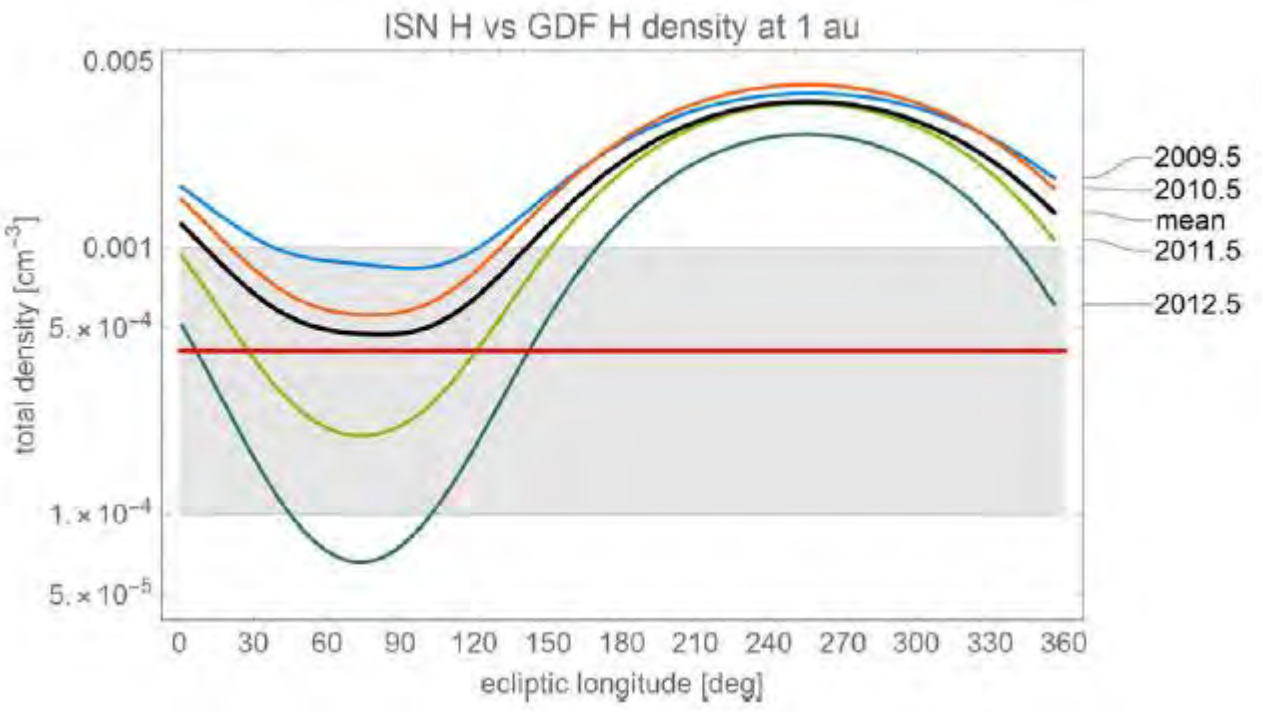

Fig. 3.25. Comparison of mean ENA density at 1 au (the thick orange line) with the density distribution of ISN H along the Earth orbit, simulated using the WTPM model for four dates in the solar activity cycle. While in the upwind portion of the Earth orbit (ecliptic longitudes 165–345°) the ENA density is lower than the ISN density by almost an order of magnitude during all phases of the solar cycle, in the downwind hemisphere they become comparable and, in certain years, ENA density may exceed that of ISN H gas. Source: Bzowski & Galli, Ap. J. 870:58, 2019.

The uncertainty of this density is high, and the spatial distribution of GDF ENAs density remains to be established. However, the analysis performed by Bzowski and Galli clearly suggests that GDF ENAs, treated as a gas population, deserve further analysis. These results were published in *The Astrophysical Journal* in a paper by Bzowski & Galli (870:58, 2019).

Uncertainty of the cross section for charge exchange in the outer heliosheath
M. Bzowski

Models play an important role in our understanding of the global structure of the solar wind and its interaction with the interstellar medium. A critical ingredient in many types of models is the charge-exchange collisions between ions and neutrals. Some ambiguity exists in the charge-exchange cross-section for protons and hydrogen atoms, depending on which experimental data is used. The differences are greatest at low energies and, for the plasma-neutral interaction in the outer heliosheath, may exceed 50% (Fig. 3.26).

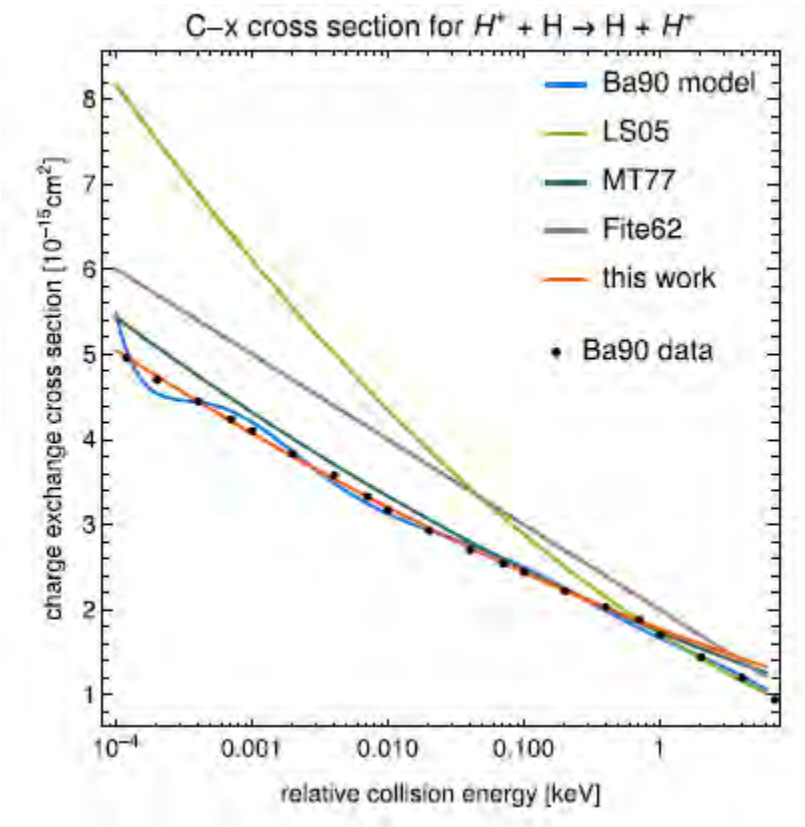

Fig. 3.26. Measurements of the charge-exchange cross-section between protons and H atoms shown as a function of the kinetic energy of particle collision (black dots), compared with various model formulae. The selected measurement data were chosen based on a review of the literature. Three models are in a very good agreement with the selected dataset, while two others are not. Model LS05 agrees with a different subset of experimental data (not shown) and has been widely used in the modelling of the heliosphere, becoming a de facto standard. It seems, however, that it is not appropriate in the context of the outer heliosheath. Source: Bzowski & Heerikhuisen, Ap. J. 888:24, 2020.

The charge-exchange cross-section is important because it directly affects the intensity of coupling between neutral gas and plasma in the outer heliosheath. A larger cross-section implies stronger heating and a slowdown of the plasma, on the one hand, and more intense production of the secondary H component and attenuation of the primary component, on the other hand. A smaller cross-section implies weaker mass-loading of the plasma, less intense production of the secondary component, and a different ratio between thermal and ram pressures in the plasma.

Dr. M. Bzowski from the LSSPA and Dr. J. Heerikhuisen from the University of Waikato, New Zealand, assessed a number of existing datasets and formulae for proton–hydrogen charge-exchange. They used a global simulation of the heliosphere to quantify differences between the currently-favored cross-section (the green line in Figure 3.26) and suggested a formula for the charge-exchange cross-section that most closely matches the majority of available data.

The two researchers also sought to identify uncertainty in the model of the heliosphere stemming from different cross-section models. To do this, they performed simulations of the heliosphere that only differed with respect to the adopted cross-section. They used the same model of the heliosphere that was used in the determination of the density of interstellar He^+, presented in this report. They found that in order to make the resulting two model heliospheres the same size, interstellar proton and hydrogen densities needed to be adjusted by 10%–15% (Figure 3.27). This observation provides a way to link uncertainty in the cross-section to uncertainty in the parameters of the pristine interstellar plasma.

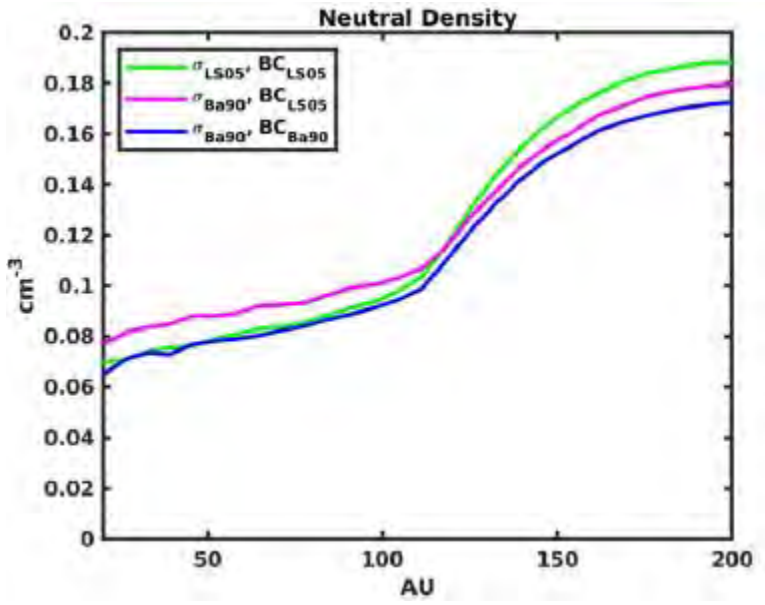

Fig. 3. 27. Comparison of density profiles of neutral H in model heliospheres, simulated assuming two alternative cross-sections for charge exchange (LS05 vs Ba90), and different densities of interstellar plasma. Simulations based on identical plasma densities and different cross-sections are shown by green and blue lines. The purple line corresponds to the case where the preferred cross-section (Ba90) was used, and the density of interstellar plasma was adjusted. This figure illustrates the level of uncertainty in the model's results (or, in other words, the model's sensitivity) to the magnitude of the adopted charge-exchange cross-section. Source: Bzowski & Heerikhuisen, Ap. J. 888:24, 2020.

This study was reported in a paper by Bzowski & Heerikhuisen published in *The Astrophysical Journal* (888:24, https:// doi.org/10.3847/1538-4357/ab595a).

Distribution function of neutral helium in the heliospheric boundary region
M. Bzowski

Interactions between the solar wind and interstellar matter involve, among other processes, charge exchange between interstellar neutral atoms and plasma, which results in the creation of a secondary population of interstellar neutral (ISN) atoms. These secondary atoms are former interstellar ions from the perturbed plasma, flowing around the heliosphere. They inherit the kinematic parameters of their parent ions and move freely across large distances as they are no longer tied to the plasma by electromagnetic forces.

The secondary population of interstellar helium was detected by IBEX. However, the interpretation of these measurements was mostly based on an approximation which assumed that in the outer heliosheath, the primary interstellar neutral atoms and the secondary atoms form two non-interacting homogeneous Maxwell–Boltzmann populations. Although this approximation is incorrect from the fundamental viewpoint, it was able to explain observations with surprising fidelity. LSSPA scientists M.A. Kubiak, M. Bzowski and J.M. Sokół investigated this apparent contradiction and sought to understand the distribution function of interstellar neutral helium in the boundary region of the heliosphere, based on information about the physical state of interstellar matter in this region.

The researchers adopted the global model of the heliosphere used in the study of He^+ density in the VLISM, and simulated the distribution function in the outer heliosheath and inside the heliopause using the method of characteristics. The statistical weights used in this method were obtained from solutions of the production and loss equations for secondary atoms due to charge-exchange collisions in the outer heliosheath. This simulation method was developed by the LSSPA in 2017, and has been successfully used in the determination of He^+ density in the very local interstellar medium (these results are presented in this report).

Results of the simulation, performed using the aforementioned secondary population synthesis method, are shown in Figure 3.28. The intensity of the secondary population increases when going from the outside to the inside of the outer heliosheath. A left-right asymmetry of the secondary population appears approximately 300 au from the Sun and attains maximum magnitude between 200 and 115 au, where production of the secondary population is most intense. Moving closer to the Sun, inside the heliopause, the distribution function narrows but maintains a certain level of asymmetry, which is a signature of the presence of the secondary population in the sample. At 1

au, the only remaining asymmetry is at the fringe of the distribution function, in qualitative agreement with IBEX observations.

These results were compared with those obtained using the approximation of two Maxwell–Boltzmann populations. The researchers found that the two-Maxwellian approximation for the distribution function of neutral He is poor within the outer heliosheath, but reasonable inside the termination shock. This is due to a strong selection effect: He atoms able to penetrate the termination shock are a small, peculiar subset of the entire secondary He population. Nevertheless, the two-Maxwellian approximation is a good reproduction of the density distribution of ISN He inside the termination shock, and provides a realistic reproduction of the orientation of the plane defined by the Sun's velocity vector through the local interstellar matter and the vector of the unperturbed interstellar magnetic field. Its temperature and velocity parameters, however, are not representative of those of the secondary population in the region where it is produced, or for the plasma in this region.

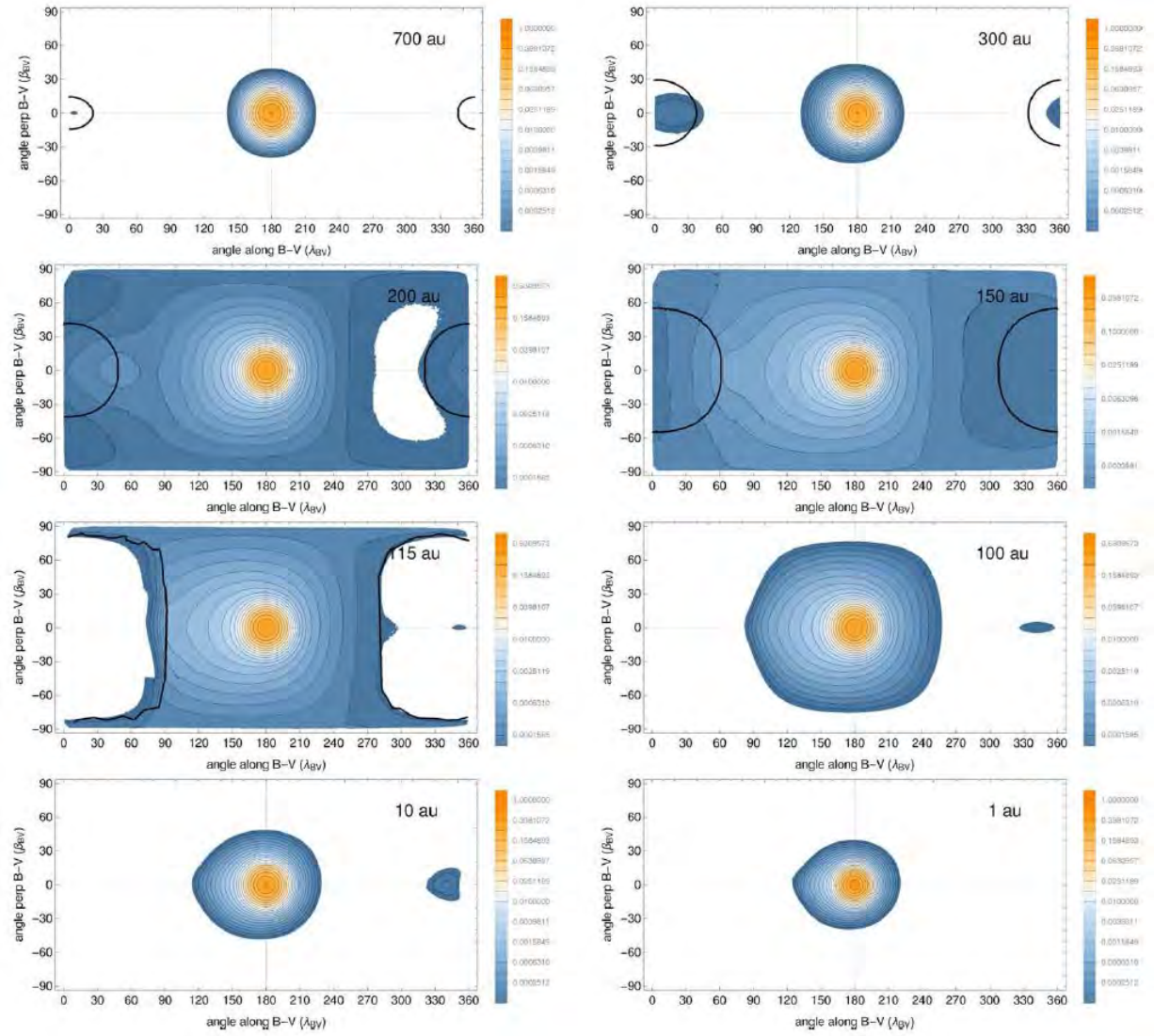

Fig. 3.28. Maps of the full distribution function of neutral He obtained from simulations for locations distributed along the direction of the Sun's motion through the interstellar medium (i.e., along the so-called upwind line). It starts from 700 au and 300 au, where the He population consists almost solely of primary interstellar atoms, runs through 200, 150 and 115 au, where the production of secondary atoms is most intense, ending at 100, 10 and 1 au from the Sun, where there is no secondary atom production and an increasing effect of ballistic selection is visible. The reference frame is based on the so-called B-V frame. The horizontal axis is the angle off the upwind direction along the plane defined by the upwind direction and the direction of the vector of the unperturbed interstellar magnetic field (the B-V plane). The vertical axis is the elevation angle with respect to this plane. This figure shows full distribution functions of neutral He, integrated over atom speeds and normalized to the peak value at 1000 au. Unperturbed interstellar atoms flow in from the centers of the panels and are represented by yellow disks. Secondary atoms are represented in blue and white. Source: Kubiak et al., Ap. J. 882:114, 2019.

These conclusions were published by Kubiak et al. in ApJ 882:114, 2019.

What epoch do we probe when observing interstellar neutral He atoms? M. Bzowski

In situ measurements of the heliospheric particle populations by the Voyager spacecraft can only be put in an appropriate context with remote-sensing observations of energetic and interstellar neutral atoms (ENAs and ISN, respectively) at 1 au when the time delay between the production and the observation times is taken into account. ENA times of flight from the production regions in the heliosheath are relatively easy to estimate because these atoms follow almost constant speed, force-free trajectories. For the ISN populations, dynamical and ballistic selection effects are important, and times of flight are much longer. But how long are they?

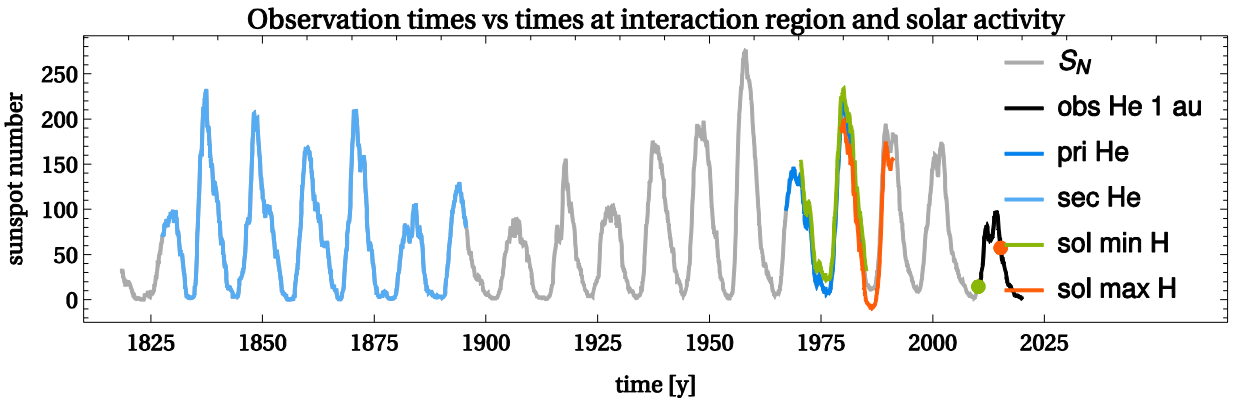

Fig. 3.29. Sunspot number is shown for a time interval from the early 19-th century until present to illustrate variations in the solar activity level (gray line). Color lines illustrate the time intervals when various populations of interstellar atoms observed nowadays by IBEX were traversing the outer heliosheath, where the charge exchange interaction responsible for the creation of the secondary interstellar atoms operates. The figure illustrates that the presently observed atoms belonging to the primary and the secondary populations originate from epochs separated in time by several solar cycle. Therefore, the conditions in the outer heliosheath at the times of their creation differed from each other and from those being probed nowadays by the Voyager spacecraft.

Dr. M. Bzowski and Ms. M.A. Kubiak, MSc, estimated these times for ISN He and H atoms observed by IBEX and in the future by IMAP using the WTPM model with synthesis method. This model calculates individual trajectories of

interstellar atoms and estimates the production an d loss rates of the secondary atoms, that are created due to charge exchange between interstellar ions and interstellar atoms in the perturbed region in front of the heliopause. The researchers showed that for the primary population atoms, the times of flight are on the order of three solar cycle periods, with a spread equivalent to one solar cycle. For the secondary populations, the times of flight are on the order of ten solar cycle periods, and during the past ten years of observations, IBEX has been collecting secondary He atoms produced in the outer heliosheath during almost the entire 19th century. ISN atoms penetrating the heliopause at the time of Voyager crossing will become gradually visible about 2027, during the planned IMAP observations. Hypothetical variations in the ISN flow in the Local Interstellar Medium are currently not detectable. Nevertheless, it is expected that steady-state heliosphere models used with appropriately averaged solar wind parameters are suitable for understanding the ISN observations.

These findings were published by M. Bzowski and M.A. Kubiak in ApJ 901:12, 2020.

Science opportunities from observations of interstellar neutral gas with an adjustable detector boresight direction M. Bzowski

The interstellar neutral (ISN) gas that has entered the heliosphere can be detected at a few au from the Sun, as demonstrated by Ulysses and the Interstellar Boundary Explorer (IBEX) space probes. Ulysses observed the ISN gas from a set of vantage points distributed along its solar polar orbit from 1994 to 2007, while IBEX has been observing from the Earth's orbit in an almost fixed direction relative to the Sun since 2009. A follow-on mission for IBEX will be NASA's Interstellar Mapping and Acceleration Probe (IMAP), which will be launched in 2024. Researchers from the LSSPA are involved in the preparation of this mission. In particular, Dr. M. Bzowski, Dr. J.M. Sokół, and Ms. M.A. Kubiak

are Co-Investigators in the IMAP Science Team. During 2019, LSSPA scientists were deeply involved in the science development of the IMAP-Lo instrument, which draws its heritage from the IBEX-Lo detector. One of the significant improvements in this new instrument will be an ability to vary the angle of the boresight relative to the Sun. This capability will enable IMAP-Lo to track ISN flux in the sky during almost the entire year and, consequently, significantly lengthen the observation time.

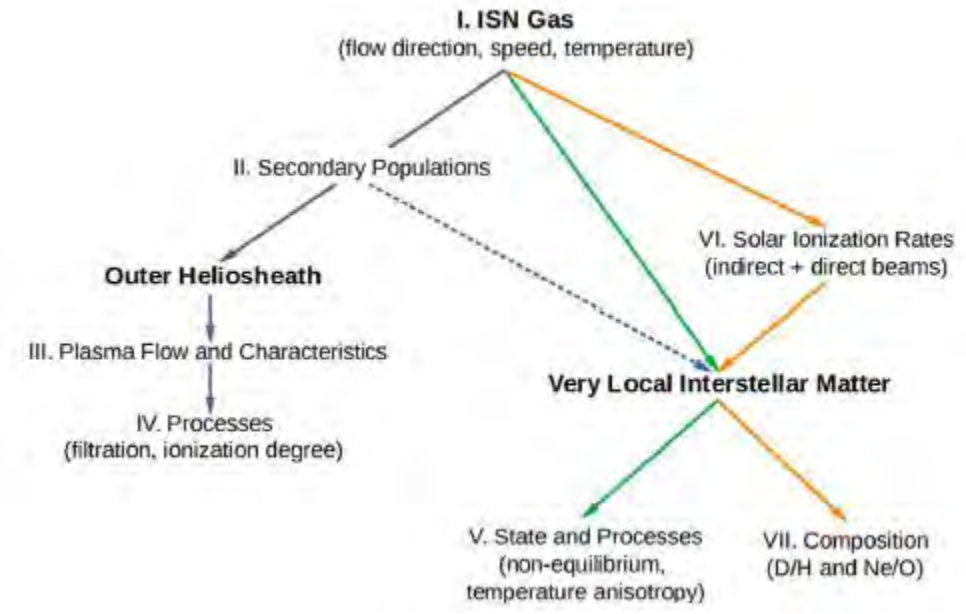

Fig. 3.30. Graphic representation of science opportunities for a study of the local interstellar medium by direct sampling of interstellar neural H, He, Ne, O, and D using a scanning instrument located at the Earth's orbit that is able to vary the angle between the Sun and the instrument boresight. This configuration is similar to that planned for the IMAP-Lo experiment. Source: Sokół et al., Ap. J. S. 245:26, 2019.

A team of LSSPA scientists (J.M. Sokół, M.A. Kubiak, M. Bzowski) in collaboration with the IMAP-Lo Lead Professor N. Schwadron and Professor E. Möbius from the University of New Hampshire studied the science opportunities afforded by this new capability. This study identified alternative advantageous ISN gas observation geometries for the detector moving along the Earth orbit

over the course of a year, and suggested a multi-choice, annual ISN observation scheme. Science opportunities provided by these alternative schemes were identified as a function of time of year and phase of solar activity. Observation geometries and seasons were determined separately for various ISN species and populations.

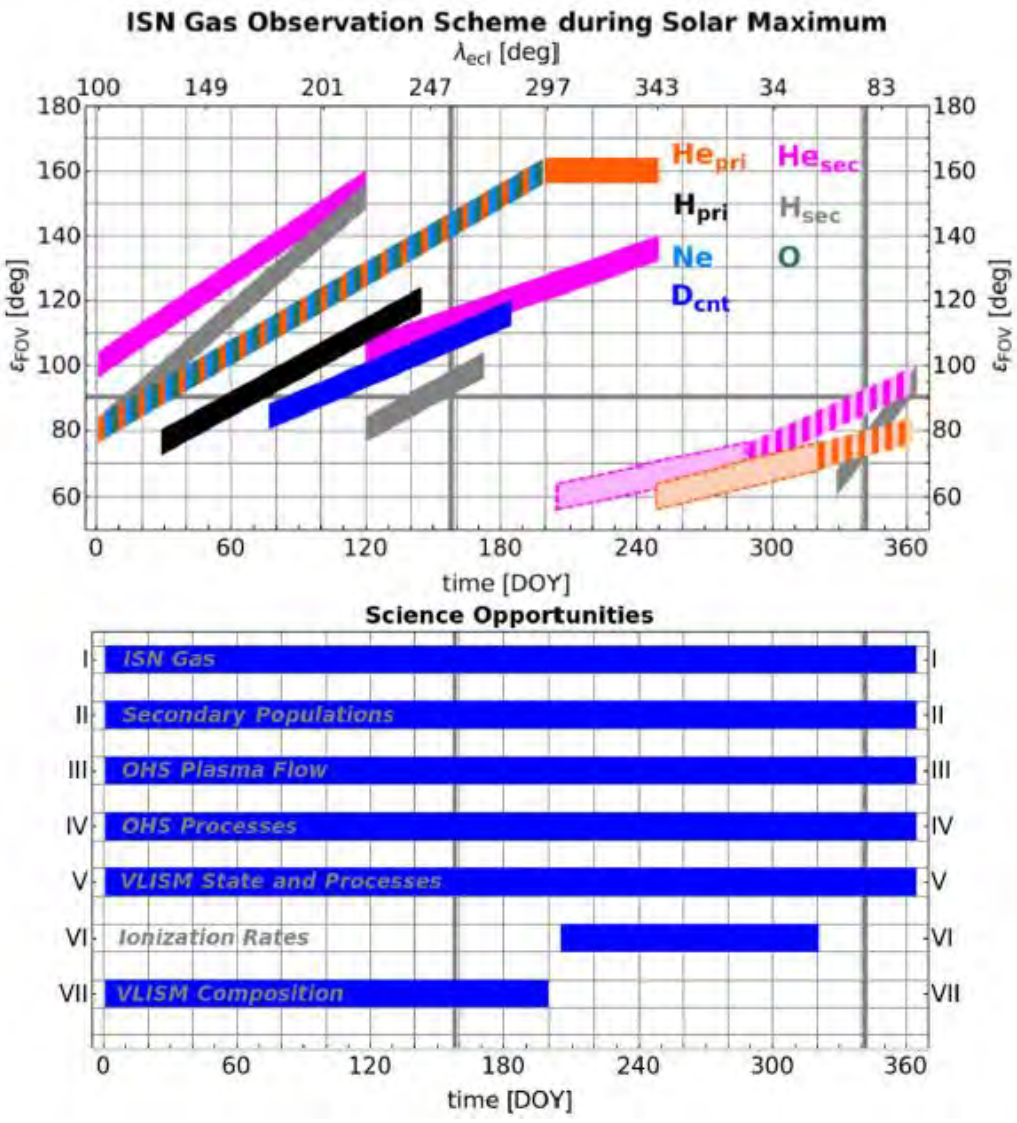

Fig. 3.31. Timeline for science opportunities stemming from the ability to adjust the boresight in the planned IMAP-Lo experiment (lower panel). Alternative schedules are presented in the upper panel. The ϵ_{FOV} angle is the angle between the spacecraft's rotation axis, directed towards the Sun, and the boresight of the mounted instrument. Source: Sokół et al., Ap.J.S. 245:26, 2019.

The researchers found that using an adjustable viewing direction allows to perform sampling ISN gas in the upwind hemisphere, where the signal is not distorted by gravitational focusing. However, ISN species can be sampled almost throughout the year, which enables improving the observation statistics. They demonstrated that with appropriately-adjusted observation geometries, primary and secondary populations can be fully separated. Additionally, they showed that atoms of ISN gas on indirect trajectories can be detected, and pointed out the impact of this capability on the study of ionization rates of ISN species.

The results of this study, which may be regarded as a yearly observation plan for such an experiment, were published in a paper by Sokół et al. in ApJS 245:26, 2019.

Evolution of the solar Lyman-**α** profile line and radiation pressure for interstellar hydrogen

M. Bzowski

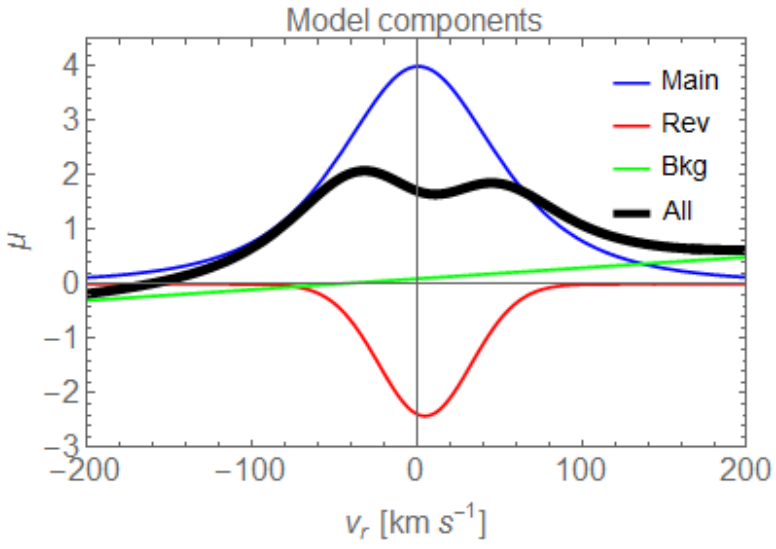

Fig. 3.32. Schematic illustration of building-blocks of the model of the profile of the solar Lyman-α spectral line.

The blue line represents the main Gaussian-like shape, the red line the central self-reversal, and the green line the spectral background of the line. The actual profile is a superposition of these building-blocks; it is represented by the black line. The Lyman-α line is one of the most prominent features in the UV part of the solar spectrum. It is responsible for the resonance radiation pressure acting on hydrogen atoms in the heliosphere, i.e., for an effective anti-solar force that is exerted on these atoms by photons from the Sun. Next to the solar gravity force, radiation pressure is the main factor that determines the trajectories of neutral hydrogen and deuterium atoms inside the heliosphere. Accurate knowledge of the dynamics of these atoms is necessary to calculate the density of interstellar neutral hydrogen inside the heliosphere and, consequently, to investigate derivative populations of H atoms important for heliospheric physics, including pickup ions and energetic neutral atoms. To that end, one needs a model of the spectral shape of the solar Lyman-α line and its evolution during the cycle of solar activity.

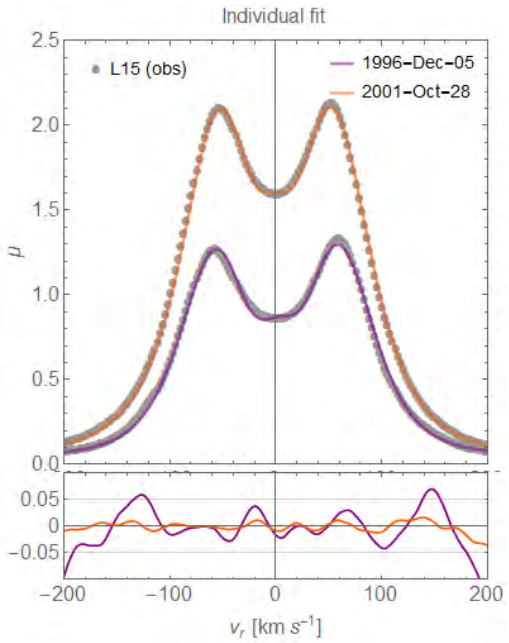

Fig. 3.33. Example solar Lyman-α line profiles obtained from the newly-developed model for the solar maximum (orange) and solar minimum epochs (purple). The bottom panel presents relative differences between model predictions and actually-measured profiles.

Previous models of the Lyman-α line profile were based on just a few observations, and therefore they were not able to reproduce the evolution related to variations in solar activity with sufficient accuracy. A team of scientists from LSSPA: Dr. Izabela Kowalska-Leszczyńska, Dr. Maciej Bzowski, Ms. Marzena A. Kubiak MSc, and Dr. Justyna M. Sokół developed a new model of the evolution of the solar Lyman-α line profile based on new observations from the SOHO satellite that have been available since 2015. Based on these observations, the researchers proposed an analytical formula composed of three parts. Each describes a different feature of the line profile, shown in Figure 3.32 (the main line – blue line, the self-reversal in the center – red line, and a slight slope of the whole line with respect to the vertical axis – green line). It turned out that by using the proposed formula, the team could reproduce solar line profile observations collected over several years (covering almost a full cycle of solar activity) with very good accuracy. An example is shown in Figure 3.33, where two observed profiles (dots) are compared with fitted functions (lines). Furthermore, the team of researchers found that the parameters of the proposed function (e.g., the widths of component functions, the depth of the self-reversal, and the shifts of the profile component relative to each other) can be expressed as linear functions of total solar irradiance in the Lyman-α line. The evolution of the latter quantity is closely related to the level of solar activity. The results of this analysis were presented in a paper published in *The Astrophysical Journal* (Kowalska-Leszczyńska et al., 2018a).

Subsequently, the team from LSSPA examined how the new radiation pressure model affects the interstellar neutral hydrogen distribution in the heliosphere, and distributions of its derivative populations of particles. The analysis started with a comparison of the densities of interstellar hydrogen inside the heliosphere predicted by the old and new models. It turned out that during periods of low solar activity the new model predicts more hydrogen close to Earth's orbit than the old one, but during high solar activity, the new model

predicts less gas. The largest differences between the two considered models are in a region located opposite to the direction of inflow of the interstellar gas to the heliosphere, i.e., in the downwind region.

Another aspect considered by the research team was the value of the density of interstellar neutral hydrogen at the termination shock. In 2008, scientists from the CBK PAN carried out estimates using the old model of radiation pressure and the flux of pickup ions observed by the Ulysses mission. The new value of hydrogen density calculated using the new model of radiation pressure turned out to be statistically consistent with the old one due to the large measurement uncertainty, which was 25% of the measured value. Another question was the influence of the new radiation pressure model on the hydrogen atom flux seen by the IBEX-Lo detector. Several years ago, scientists from the USA and Russia discovered that the ratios of fluxes of hydrogen atoms observed by IBEX-Lo in different energy channels are inconsistent with models. They had suggested that the reason for this may be an insufficient understanding of the radiation pressure acting on hydrogen atoms in the heliosphere. Simulations performed by scientists from LSSPA showed that indeed, expected fluxes of hydrogen atoms are very sensitive to details in the radiation pressure model, but even using the newly-developed model does not remove the observed discrepancy.

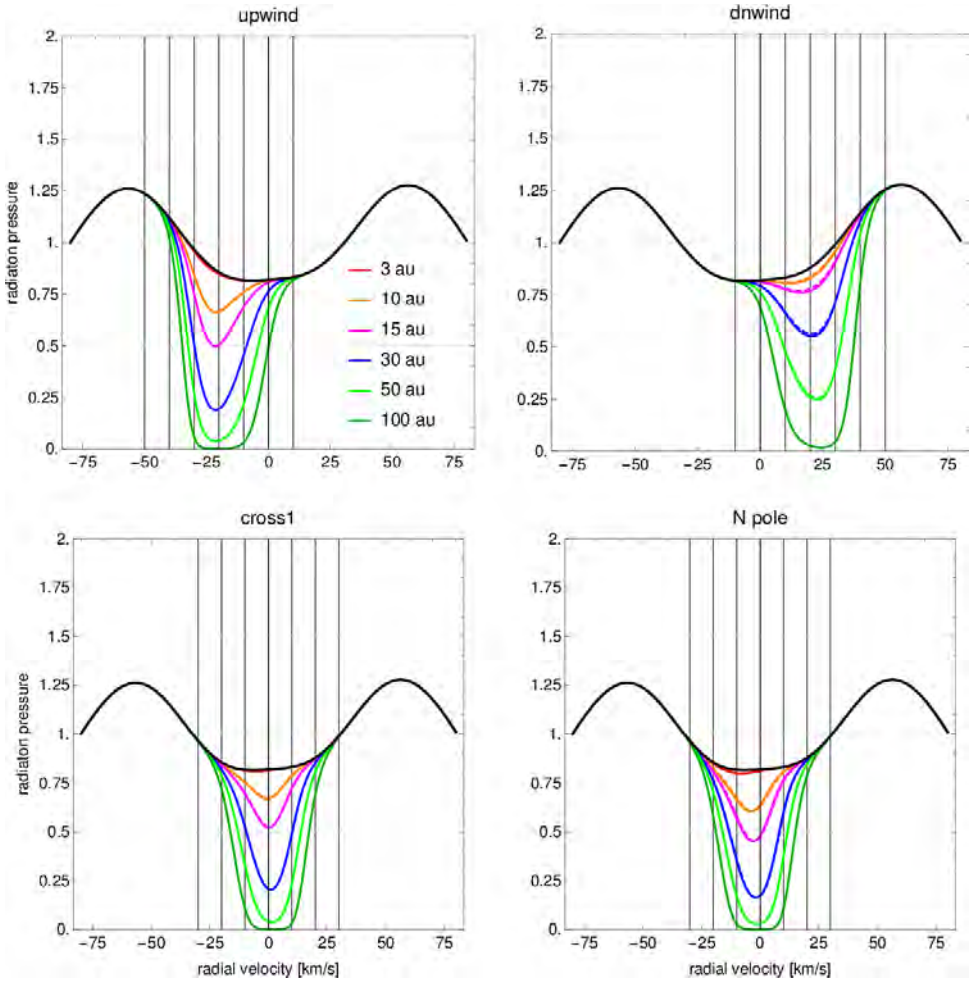

Fig. 3.34. Evolution of effective radiation pressure (expressed in units of solar gravity force) acting on hydrogen atoms in the heliosphere with distance from the Sun. Absorption of solar photons that are responsible for radiation pressure results in a gradual decrease of the effective spectral flux from the Sun in the frequency range corresponding (due to the Doppler effect) to radial velocities of interstellar neutral atoms in the heliosphere. As a result, the magnitude of radiation pressure effective for interstellar hydrogen atoms is closely related to the column density of interstellar hydrogen between a given location in space and the Sun. Hence, the approximation in which radiation pressure is just a factor that is scaled with the square of the distance to the Sun (represented by black profiles) is unlikely to be valid. The four panels present the evolution of spectral profiles of the solar Lyman-α line along upwind, downwind, crosswind and north-pole lines in the heliosphere at selected distances from the Sun.

Therefore, researchers from LSSPA challenged the existing paradigm regarding how the radiation pressure in the heliosphere actually works. It had been assumed that if the flux of photons from the Sun decreases with the square of solar distance, then the force due to the radiation pressure should behave in the same way. This is because the gravity force also decreases with

the square of solar distance. Consequently, the ratio of the gravity and radiation pressure forces acting on hydrogen atoms should be constant, regardless of where it is measured. But is that assumption true, if some of the solar photons are scattered by hydrogen atoms? Scientists from LSSPA calculated how many of the original photons emitted by the Sun are scattered from the beam of hydrogen atoms located between the Sun and a given location in the heliosphere. They found that even at relatively small distances (within approximately 10 astronomical units – around Saturn's orbit) scattering losses can reach 30% of the original Lyman-α photons emitted by the Sun within the spectral sensitivity band of hydrogen. Thus, the force caused by radiation pressure decreases much faster with distance than previously thought.

The modification of the radiation pressure force due to the absorption effect is larger than the differences between the two radiation pressure models. Therefore, a new radiation pressure model in the heliosphere is needed, which should take absorption processes into account. However, this new model must also include the distribution of interstellar neutral hydrogen in the heliosphere as the two phenomena are closely related to each other.
The results of this analysis were presented by the team lead by Dr. Izabela Kowalska-Leszczyńska in Kowalska-Leszczyńska et al., ApJS 2018a,b, 2020).

Magnetic waves excited by newborn interstellar pickup ions measured by the **Voyager spacecraft up to Pluto's orbit** M. Bzowski

New ions in the solar wind are created by ionization of interstellar atoms that penetrate inside the heliosphere. They are called pickup ions because immediately after creation they are "picked up" by the Lorentz force from the magnetic field "frozen" in the solar wind and advected with the solar wind into the interplanetary space. Pickup ions gyrate in the magnetic field, producing characteristic magnetic waves. These waves can be detected via careful analysis of time series of the intensity and direction of the magnetic field,

observed by the interplanetary probes.

Magnetic waves produced by ion pickup have characteristic signatures in observed time series of interplanetary magnetic field, and are different for each of the pickup ion species. However, these signatures can be detected only when the growth rate of the wave is greater than the turbulence level of the solar wind. Searching for wave-growth events is challenging, but very important, because it enables models of the distribution of neutral gas in the heliosphere, and the pickup ion creation processes in the solar wind magnetic field to be verified. The growth rate of magnetic waves depends, among other things, on the production rate of pickup ions. This rate is directly proportional to the density of the interstellar neutral gas in the interplanetary space, and ionization rates, which vary both temporally and spatially with heliographic latitude. The spatial distribution of interstellar neutral hydrogen and helium densities, and the rates of their ionization are totally different and, consequently, the resulting pickup ion production rates are significantly different. For solar distances smaller than three astronomical units, the production rate for helium pickup ions is much greater than that for hydrogen ions. Consequently, we can expect to find more magnetic wave events characteristic of the creation of helium than hydrogen pickup ions. Beyond 3 au, more hydrogen pickup ions are produced.

Magnetic waves excited by newborn interstellar pickup ions are observed within the supersonic solar wind from a few tenths to several dozens of astronomical units from the Sun. They were detected by instruments on the ACE (at 1 au) and Ulysses missions (from 1 to 5 au). Very important data were gathered by the Voyager spacecraft between 1 and 45 au. A team of researchers from the University of New Hampshire studied magnetic field data from Voyager 1 and Voyager 2 missions collected in the period from 1997 to 1990, and identified more than 600 events associated with magnetic waves excited by newly-born interstellar pickup ions, both helium and hydrogen.

Scientists from LSSPA (Dr. Justyna M. Sokół, Dr. Maciej Bzowski, and Ms. Marzena A. Kubiak MSc) studied pickup ion production rates for interstellar hydrogen and helium using the Warsaw Test Particle Model simulation code, models of the solar wind evolution in time and heliographic latitude, and solar wind extreme ultraviolet ionizing radiation. These research tools, developed by the team from LSSPA, were employed to calculate the distribution of interstellar neutral hydrogen and helium gas inside the heliosphere and production rates for pickup ions along Voyager 1 & 2 trajectories. The results of these studies were applied by the team at the University of New Hampshire in their research on magnetic wave creation. The study showed that magnetic waves due to pickup ions can be excited as far from the Sun as Pluto's orbit and beyond, i.e., up to 45 au from the Sun. Both teams of researchers found good agreement between the model's predictions and observed rates of magnetic waves due to pickup ion creation.

The results of the study were published in a series of three articles by Hollick et al. in ApJ and ApJS (Hollick et al., 2018a,b,c).

A corridor to the Sun for select nanodust particles A. Czechowski

The smallest dust grains in the circumsolar dust cloud are nanodust particles, i.e., dust grains with sizes of a few, to a few ten millionth parts of a millimeter. They are so small they only include a few dozens of thousands of atoms. Like all dust grains in the Solar System, they are electrically charged, and their high charge to mass ratio makes the Lorentz force from the magnetic field in the solar wind similar in strength to the solar gravity force, or even larger. Therefore, the motion of nanodust grains significantly differs from the motion of typical dust grains, which resembles the motion of asteroids.

Nanodust is predominantly produced by collisional fragmentation of larger dust particles. Initial velocities of particles produced by this mechanism are close to the orbital velocities of their parent dust grains. The newly-created

dust grains quickly become electrically charged, are picked up by the solar magnetic field, frozen in the solar wind, accelerated to velocities comparable to that of solar wind, and move away from the Sun. However, particles that are created sufficiently close to the Sun become "trapped" in bound orbits around it, due to an interplay between solar gravity and magnetic forces. Therefore, it is likely that a population of trapped nanodust particles is present in the vicinity of the Sun.

Another hypothetical source of nanodust is comets and, in particular, sungrazing comets. Such comets have perihelia deep inside Mercury's orbit and aphelia somewhere between the orbits of Mars and Jupiter. The initial velocities of nanodust particles released by these comets shortly before perihelion are much larger than those of collisional nanodust particles. If the release of a nanodust particle occurs inside the Mercury orbit, its speed may be comparable to that of the solar wind, but in the opposite direction. Therefore, it is expected that the orbital dynamics of these nanodust particles are different to those of collisional nanodust grains. This topic was investigated by Dr. Andrzej Czechowski from LSSPA and Dr. Ingrid Mann from the Arctic University of Norway in Tromosoe, Norway, who created a particle motion model.

Based on numerical simulations of the forces acting on nanodust particles, Czechowski and Mann concluded that unlike "regular" nanodust particles, particles from sungrazing comets cannot be trapped close to the Sun, even those released very close to the Sun. Therefore, sungrazing comets are unlikely to be an additional source of the trapped nanodust population. However, the two researchers identified an interesting phenomenon that they called a "corridor to the Sun".

Some nanodust grains, released in the inbound leg of the comet orbit, can enter peculiar trajectories leading them deep into the solar corona, i.e., the upper, hot part of the solar atmosphere, visible from Earth during solar

eclipses. Due to electromagnetic forces, these grains approach the Sun at a distance much closer than the perihelion of the parent comet, which may lead to destruction of nanodust grains by sublimation or collisions with ions. Most nanodust grains are, however, picked up by the solar wind and ultimately escape the Sun.

The results of this study were presented in a paper in *Astronomy & Astrophysics* (Czechowski & Mann, 2018).

A novel method of establishing the unresolved background in the EUV surveys of the sky

M. Bzowski

In observations of diffuse emissions like, e.g., the Lyman-α heliospheric glow, contributions to the observed signal from point sources (e.g., stars) are considered to be a contamination. There are relatively few bright point sources that are usually properly resolved and can be subtracted or masked. Others are unresolved partly due to the helioglow foreground, and partly due to resolution and sensitivity limitations of the detector. Nevertheless, the radiation from these sources is registered by the instruments and must be subtracted from the signal. Up to now, however, a suitable method to establish this contribution was lacking.

A team of scientists from LSSPA CBK PAN led by Dr. M. Strumik proposed such a method and applied it to observations of the helioglow performed by the Solar Wind Anisotropies (SWAN) experiment onboard the SOHO spacecraft. To estimate the unresolved EUV background, the team used spectroscopic observations of several thousand astrophysical objects available from databased of observations from International Ultraviolet Explorer (IUE).

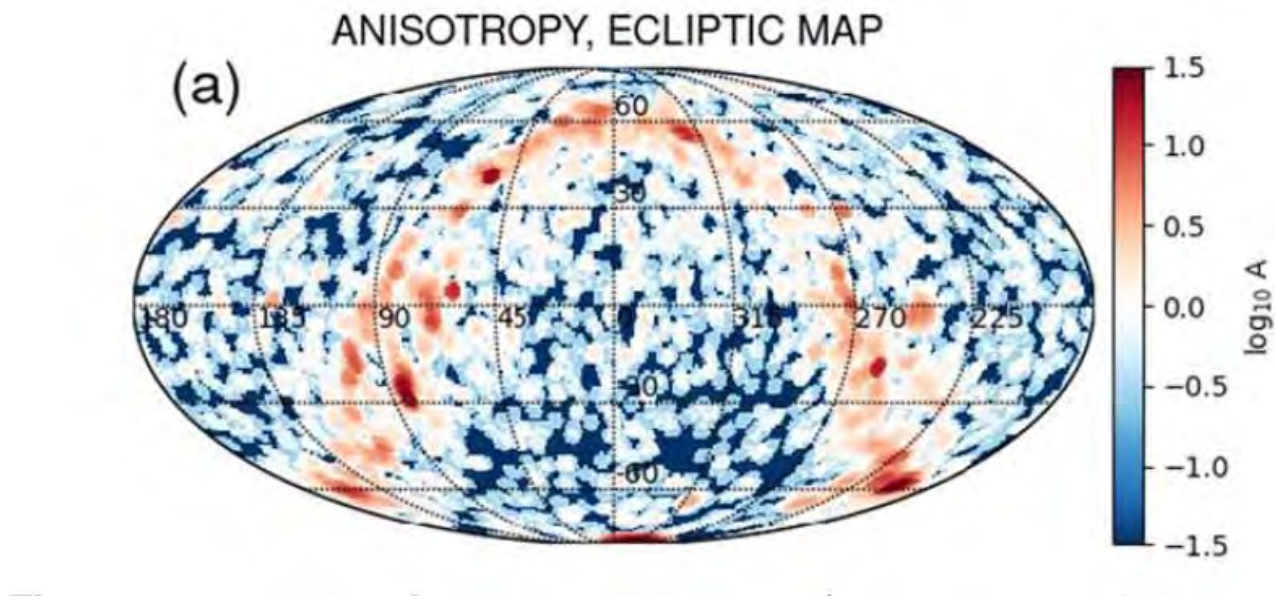

Fig. 3.35. The distribution in the sky of the unresolved EUV background for the sky survey by SOHO/SWAN, obtained by scientists from CBK PAN. The magnitude of the spatial fluctuations of the EUV radiation from spatially unresolved stars is presented in the logarithmic scale. Source: Strumik et al., ApJ 899:48, 2020

The estimated distribution suggests that the number of these sources increases with decreasing intensity. Below a certain threshold, these sources cannot be resolved against the diffuse signal from the backscatter glow, that results in a certain physical background from unresolved point sources. Detection, understanding, and subtraction of the point-source background has implications for proper characterization of diffuse emissions and accurate comparison with models. Stars are also often used as standard candles for in-flight calibration of satellite UV observations, thus proper understanding of signal contributions from the point sources is important for the calibration process. The team proposed a general approach to quantify the background radiation level from unresolved point sources in UV sky survey maps. In the proposed method, a distribution of point sources as a function of their intensity is properly integrated to compute the background signal level. These general considerations were applied to estimate the unresolved-point-source background in the SOHO/SWAN observations that on average amounts to

28.9 R. The team found that, unsurprisingly, the distribution in the sky of the unresolved background is patchy.

These results were published by Strumik et al. in ApJ 899:38, 2020. The research team included Dr. M. Strumik, Dr. M. Bzowski, Dr. I. Kowalska-Leszczyńska, and Ms. M.A. Kubiak.

Studies of the intermittent nature of the turbulence in magnetospheric plasma and solar wind out of the ecliptic plane A. Wawrzaszek

The solar wind is considered as a natural plasma laboratory to study turbulence and its intermittent nature. One approach uses the multifractal formalism, which is a generalization of the fractal description and allows us to classify processes and data with a high level of heterogeneity.

Dr. Anna Wawrzaszek from the LSSPA, in cooperation with scientists from Belgium and Italy conducted a multifractal analysis of magnetic field measurements obtained by the Ulysses space probe during two solar minima (1997–1998, 2007–2008) and one solar maximum (1999–2001), separately within the fast and slow solar wind regimes. These studies were based on a much larger number of cases than previous research, and showed that outside the ecliptic plane, the degree of multifractality/ intermittency slowly decreases with distance from the Sun (regardless of the component or reference system). The researchers concluded that this radial dependence may be explained by the slower evolution of turbulence outside the ecliptic plane, and the decreased efficiency of intermittency drivers with distance from the Sun. Additionally, the analysis showed that the greatest differences between magnetic field components are found close to the Sun, where intermittency is the strongest. Moreover, it was observed that the slow solar wind during the maximum of solar cycle 23 has a lower level of multifractality (intermittency) than the fast solar wind, which can be related to the idea of the existence of a new type of Alfvénic slow solar wind.

These results were published in *The Astrophysical Journal* in a paper by Wawrzaszek et al. (876:153, 2019, https://doi.org//10.3847/1538-4357/ab1750).

To better understand the process of hydromagnetic convection in space plasma, Dr. Anna Wawrzaszek and a PhD student, Ms Agata Krasińska, performed systematic studies of the dynamics of a four-dimensional generalized Lorenz system. This model, which was proposed in 2010 by other scientists from the LSSPA (W. Macek and M. Strumik), was supplemented by a fourth variable that described the profile of the magnetic field induced in a convected magnetized fluid. Analytical and numerical analyses of this system were performed in 2019. They revealed several types of dynamical states, including nondegenerate and subcritical Hopf bifurcation, and forward and backward bifurcation structures (tangent, pitchfork, period-doubling). Moreover, they determined an analytic formula for control parameters at which Hopf bifurcation exists. This advance makes it possible to control the linear stability of the considered system. In particular, the two researchers found that magnetic field control parameters significantly influence the linear stability regime of the generalized Lorenz model. Moreover, the study showed the existence of several windows of nonchaotic variation (windows of order). In particular, period-3 windows were observed, at the edge of which the researchers identified new cases of type I intermittency.

These results were published in a paper in the *International Journal of Bifurcation and Chaos* (29 No 14, 1920042, 2019, https://doi.org/10.1142/S0218127419300428).

Trajectories of dust particles around stars A. Czechowski

The motivation for this work was observations of excessive infrared emission in the vicinity of some stars. One proposed explanation is that the emission comes from small dust grains trapped by the stellar magnetic field. In

the case of the Sun, trapped small dust particles (ranging from a few to a few ten nm) was theoretically predicted by A. Czechowski from the LSSPA and I. Mann.

In 2019, this hypothesis was tested. An international team of researchers, including A. Czechowski, applied the theory to the cases of Vega and Fomalhaut. Vega and Fomalhaut are young, hot stars of the A spectral type, with high rotation rates (20–40 times faster than that of the Sun). Theoretical arguments put forward by Czechowski and Mann imply that trapping of nanodust grains around these stars is unlikely, for two reasons. First, for a hot star, the high radiation pressure acting on dust grains overcomes the gravity force. Consequently, the attractive force, which is necessary for trapping, is absent and dust grains cannot be trapped. Second, for a rapidly rotating star, the outer limit of the trapping region contracts, consequently, the hypothetical trapped dust would have to survive the extreme conditions inside the stellar corona. These theoretical suggestions were confirmed by numerical calculations performed using simplified models of the stellar wind and the magnetic field for Vega and Fomalhaut. These conclusions were published in a paper by Stamm et al. in *Astronomy & Astrophysics* (626, A107, 2019, https://doi.org/ 10.1051/0004-6361/201834727).

An additional chapter in this paper discusses the effect of corotation of the coronal plasma (not included in earlier models developed by Czechowski and Mann) on the process of nanodust trapping. The conclusion is that including plasma corotation in dust trajectory simulations does not affect trapping, provided that the magnetic field and the plasma flow satisfy freezing-in equations. This observation lends credence to earlier conclusions.

Exact solutions and singularities of an X-point collapse in Hall magnetohydrodynamics A. Janda

Magnetic reconnection is a topological rearrangement of the global magnetic field. It is believed to be responsible for fast conversions of magnetic field energy into other energy forms, like kinetic energy of the plasma flow, as well as thermal and radiation energies. Despite multiple, decades-long attempts to fully understand how some basic concepts can explain the overall picture of plasma dynamics in various environments, like the solar corona, the Earth's magnetosphere, relativistic astrophysical plasmas, or tokamak physics, the most fundamental questions have remained poorly understood, and magnetic reconnection continues to be one of the most challenging problems in plasma physics.

One of the many challenging aspects of magnetic reconnection is the question of its onset. Long ago, Dungey argued that neutral X-points in the magnetic field are unstable and collapse into thin, elongated regions of significantly-increased resistivity, called current sheets. In principle, the formation of current sheets requires a kinetic description of the process. Nonetheless, an acceptable understanding has been obtained using an appropriate magnetohydrodynamical approach. Various plasma fluid approximations have facilitated our understanding of the specific physical phenomena involved in the formation of current sheets. One of them is Hall magnetohydrodynamics (MHD), which is a monofluid approximation of a two-fluid description of plasmas that is much more detailed than more frequently-exploited ideal or resistive magnetohydrodynamics. In Hall magnetohydrodynamics, unlike classical magnetohydrodynamics, resistivity is non-zero; the magnetic field becomes frozen in the electron fluid, rather than the bulk plasma flow, and dispersive whistler waves appear due to the Hall effect. Such a theory is useful in the solar corona as well as in the Earth's magnetosphere.

To reduce the complexity of the global dynamics of magnetic collapse, Artur Janda MSc from LSSPA hypothesised a specific, self-similar structure for the magnetic field and incompressible plasma flow. Having reduced the Hall MHD equations for the case of an X-point collapse, and using an appropriate ansatz, he obtained a definition of a dynamic system that could be solved in terms of elliptic functions. He found that there are two possible classes of solutions. One consists of periodic regular solutions, and the other includes singular solutions. Surprisingly, it turned out that singular solutions are more physically relevant, because regular ones exhibit a superalfvenic plasma flow. An exact formula, based on initial conditions at the time when singularities form, was found. These results were published in the *Journal of Mathematical Physics* (Janda, 2018).

Exact solutions within Hall MHD are very rare. The solution obtained by Artur Janda seems to be the only one in the literature that is singular. It is very important to identify its physical meaning. Although self-similarity has to break down at a certain point, shock waves accompanying the current sheet are expected to appear. Moreover, intuitively, from the physical point of view, the emerging resistivity is unlikely to be homogeneous, and it can be expected that the reconnection rate will explosively increase. This picture seems to be complementary to the well-known secondary tearing instability of elongated current sheets, the so-called plasmoid instability that leads to the acceleration of magnetic reconnection.

The exact solutions found by Artur Janda are a convenient tool to derive appropriate initial conditions, leading generically to the formation of singularities, which in general is a challenging mathematical task. Another interesting task would be to extend this class of solutions to nonlinear magnetosonic waves forming singularities. Such solutions would clarify the outstanding problem of the heating of the solar corona.

The IMAP GLOWS Experiment M. Bzowski, P. Orleański, R. Wawrzaszek

The CBK PAN participates in the NASA space mission, Interstellar Mapping and Acceleration Probe (IMAP). The selection of the winning proposal, submitted in response to the Announcement of Opportunity released in 2017, was announced in Washington DC on 1 June, 2018 (https://www.nasa.gov/press-release/nasa-selects-mission-to-study-solar-wind-boundary-of-outer-solar-system). The CBK PAN will supply a Lyman-α photometer called GLOWS (GLObal solar Wind Structure). The objective of the IMAP mission is to investigate the interaction of the solar wind with the Sun's galactic environment and cosmic ray acceleration processes, as presented in a paper by McComas et al. published in *Space Science Reviews* (https://link.springer.com/article/10.1007%2Fs11214-018-0550-1).

A scheme of the GLOWS instrument and the geometry of the planned observations are presented in Fig. 3.36.

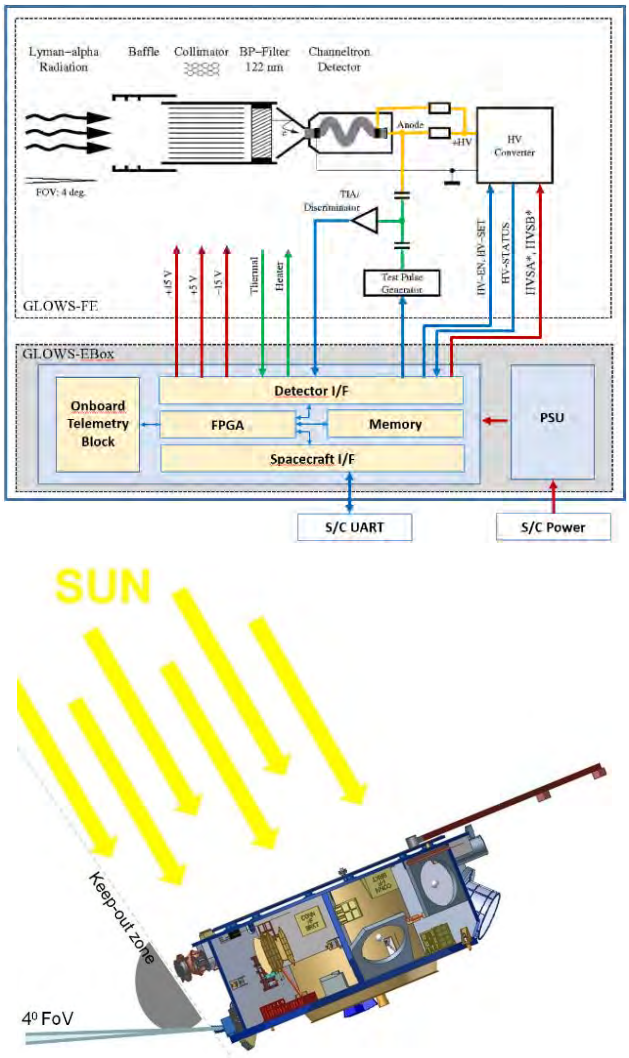

Fig. 3.36. Block scheme of the GLOWS instrument (left panel) and the planned geometry of observations, with the location of the instrument at the IMAP spacecraft (right panel).

The IMAP mission is being developed and will be carried out by an international science team led by Principal Investigator Dr. David J. McComas from Princeton University. The project is managed by the Applied Physics Laboratory of Johns Hopkins University. IMAP will have ten science instruments, including GLOWS, and will operate near the libration point L1 between the Earth and the Sun, about 1.5 million km from the Earth.

A team of scientists and engineers from the CBK PAN, led by Dr. Maciej Bzowski from the LSSPA as the Principal Investigator, proposed an instrument to perform observations of the heliospheric resonant backscatter glows in the

hydrogen Lyman-α spectral line (121.6 nm). The team will use these remote-sensing observations to investigate variation of the solar wind flux with heliolatitude and its evolution during the cycle of solar activity. The observations will provide daily lightcurves of the helioglow, collected from a Sun-centered circle with a radius of 75°. By the end of 2020, GLOWS has completed Phases A and B in the experiment development schedule.

A second element of the CBK PAN involvement in the IMAP mission is the IMAP-Lo experiment, led by Dr. Nathan Schwadron and Dr. Eberhard Moebius from the University of New Hampshire. Here, LSSPA scientists in collaboration with their US partners will investigate the neutral gas that enters the heliosphere from the solar galactic environment. The results of these studies will improve our understanding of the physical state of interstellar matter near the Sun and its interaction with the solar wind.

Involvement in the IMAP project is very important for the CBK PAN. The IMAP program will be one of its most important research activities during the coming decade. The GLOWS experiment will result in a better understanding of the three-dimensional structure of the solar wind and its evolution during the cycle of solar activity as well as the latitudinal anisotropy of the solar EUV radiation. Equally important are studies of the interstellar matter surrounding the Sun.

The IMAP mission is a continuation of a multi-year program of researching the heliosphere and its galactic environment, in the context of the existing NASA mission Interstellar Boundary Explorer (IBEX), as well as other projects. GLOWS represents a quantum leap for the Centre's research activities as it will be the first heliospheric experiment to be conceived, developed, and operated by its scientists. The Centre's role in the GLOWS instrument is a natural continuation of work carried out by its FPGA Laboratory of Satellite Applications. It draws upon experience gained in the past from the many highly-successful space missions the Laboratory's engineers have been

involved in, including Integral, MEX, Chandrayaan, Herschel, CaSSIS, ASIM, Solar Orbiter, and presently OpSat, PROBA3 and JUICE. The high level of technical readiness of the proposal, supported by a vast heritage of space-proven solutions, was an important factor in the selection of the GLOWS instrument, which is a great opportunity for the Centre's engineering team to develop another specialization. A very important aspect, in this respect, is close collaboration between engineering and scientific teams during the development of the experiment and its planned operation in space.

Studies of the heliosphere and its cosmic environment are a very important part of the Centre's science mission. The development and implementation of the GLOWS experiment is a natural continuation of a long-standing collaboration between the Centre's scientists and US colleagues: Dr. David McComas from Princeton University, and Dr. Eberhard Moebius and Dr. Nathan Schwadron from the University of New Hampshire. Furthermore, the Centre's engineers have a long record of successful collaboration with international partners from Europe (the ESA), Russia, China, and India. GLOWS is the start of a technical collaboration with NASA.

The IMAP mission is carried out by an international science team led by Principal Investigator Dr. David J. McComas from the Princeton University. The IMAP project is managed by the Applied Physics Laboratory of the Johns Hopkins University. Dr. Maciej Bzowski and Ms. Marzena A. Kubiak MSc from the LSSPA are Co-Investigators on the IMAP Science Team. The GLOWS science team includes Dr. Maciej Bzowski (lead), Ms. Marzena Kubiak, Dr. Marek Strumik, and Dr. Izabela Kowalska-Leszczyńska from LSSPA. The GLOWS engineering team, led by Dr. Piotr Orleański (GLOWS Project Manager) and Dr. Roman Wawrzaszek (GLOWS Systems Engineer) includes Mr. Kamil Ber, Dr. Mirosław Rataj, Mr. Przemysław Kaźmierczak, Mr. Tomasz Kowalski, Mr. Jędrzej Baran, Mr. Marek Winkler, Mr. Waldek Bujwan, and Mr. Maciej Daukszo, and Mr. Jakub Mądry.

3.3 Ionospheric and Magnetospheric Physics

Progress on the LOFAR for Space Weather project H. Rothkaehl

The LOFAR for Space Weather (LOFAR4SW) proposal is part of the Horizon 2020 Work Programme, and addresses the INFRADEV-1-2017 Call – 'Design Studies'. The aim of the project is to prepare facility which produces unique research data that will have a key impact on advanced predictions of space weather events that affect crucial technological infrastructures of today's society. LOFAR4SW will design a significant upgrade to current hardware, software and algorithms, and will maximally leverage the current technology and infrastructure of the LOw Frequency ARray (LOFAR) already the world's foremost telescope for radio astronomy research in the low-frequency 10–240 MHz observing window. A key aspect of LOFAR4SW is the preparation of a large-scale, high-end research facility in which simultaneous, independent observing modes and signal paths are made available to two research communities: radio astronomy and space weather.

The LOFAR4SW project officially started in December 2017 and, since then, rapid progress has been made regarding its conceptual and technical design. In the course of the project specific directions for further development have been defined, so-called 'Science Use Cases'. Their main goal is to establish both, the scientific and technical requirements that should be taken into account in the preparation of LOFAR infrastructure for space weather

purposes. There are a total of 51 Use Cases, which have been grouped into Solar, Planetary, Heliospheric and Ionospheric. Each has been described in terms of its scientific motivation and expected contribution to the state-of-the-art, and a detailed technical description has been prepared regarding required hardware and software upgrades. An example Use Case for each topic is shown below.

1) Solar Use Case 1 - Monitoring Solar Radio Activity for Space Weather Operations.

Aim: To make regular observations of solar radio emissions in order to identify eruption times and locations, source positions, radio source drift rates and velocities, fluxes/brightness temperatures, and coronal hole positions.

2) Planetary Use Case 1 - Spectro-imaging monitoring of Jovian for outer Solar System Space Weather

Aim: Provide monitoring observations of radiation belts (metre and decimetre wavelengths) with imaging capabilities. Observe auroral Jovian radio emissions (decametre wavelengths) spectrograms (flux and polarization) triggered by solar event (coupled with propagation model covering up to 5 AU).

3) Heliosphere Use Case 1 - Multi-station Interplanetary Scintillation (IPS) data for space weather measurements

Aim: Make daily observations of IPS to investigate solar wind structure and do basic scientific research both on individual interesting events (whether earthbound or not) and on the general climatology of the solar wind.

4) Ionosphere Use Case 2 - Monitoring ionospheric S4 index to track scintillation above LOFAR

Aim: Establish scintillation index measures equivalent to the S4 indices calculated from GNSS data and provide these along with power-spectrum

indices in near real time as measures of ionospheric scintillation conditions across Europe.

Operations at the Polish LOFAR station in Borówiec B. Matyjasiak, H. Rothkaehl, M. Pożoga, M. Grzesiak, K. Budzińska, R. Wronowski, D. Przepiórka, Ł. Tomasik, B. Atamaniuk, A. Pełech

The LOFAR station (PL610) at Borówiec has been operating since 2015. For most of the time, the station works in interferometric mode as part of the International LOFAR Telescope (ILT). The LOFAR interferometer is an international infrastructure designed by the Dutch institute ASTRON consisting of 50 stations acrossin Europe. Centrum Badań Kosmicznych PAN as station owner, has a guaranteed amount of about 10% of annual observing time per year when the station is switched to local mode and operates as a single instrument. During this time, the station performs observations that are mainly focused on monitoring ionospheric conditions, Sun and Jupiter observations and, on request, observations for selected projects.

Routine PL610 observations are managed by dedicated for this purpose software developed by the CBK PAN researchers. This enables semi-automatic scheduling of observations in local mode. Target observations can be manually selected for a specific time, for example, this takes place for the international project where every two months observations of the pulsar B1508+55 are performed. For the remaining time slots, a scheduler searches for available

visible radio sources (e.g. Cas A, Cyg A, Tau A, Vir A, the Sun, Jupiter) and fits them into four possible beams. Sample observations made at station PL610 are presented below.

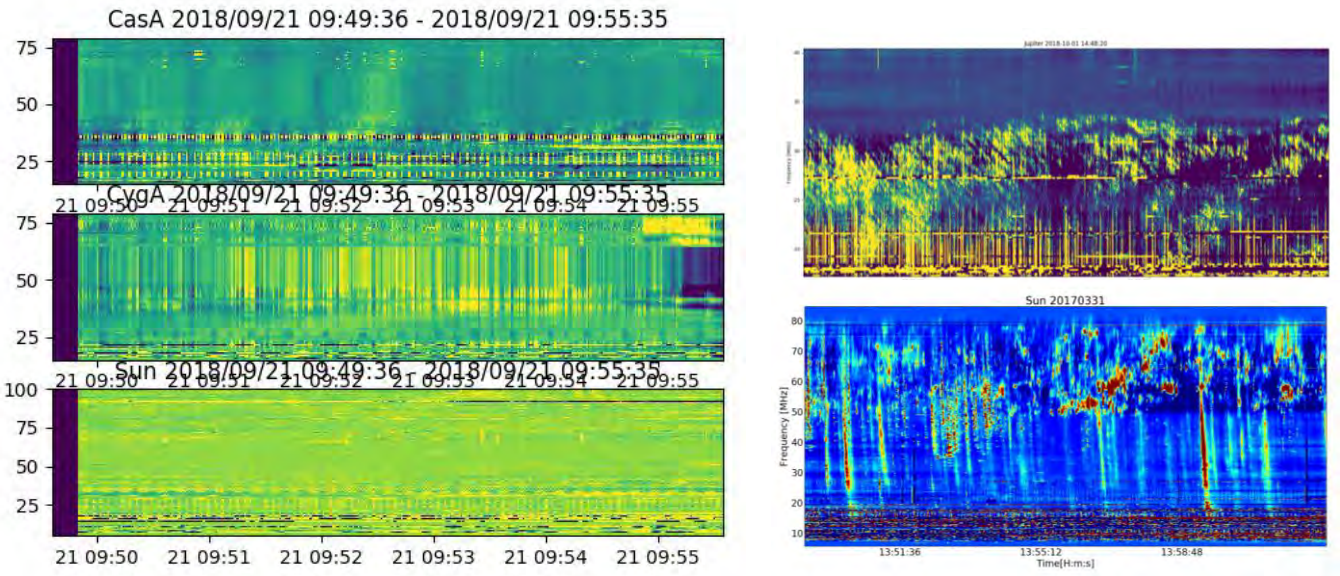

Fig. 3.37. Left: simultaneous observations of three radio sources (Cas A, Cyg A, the Sun). Top-right: Jupiter DAM emissions. Bottom-right: a Solar type III radio burst.

Lofar scintillation measurements M. Grzesiak, M. Pożoga, B. Matyjasiak

As a part of the Low Frequency Array (LOFAR) network, the Polish station PL610 in Borówiec provides observational data useful for studying distant radio sources in the frequency range 10–270 MHz. These data can also be used to investigate weak scintillation regimes commonly found in the mid-latitude ionosphere. Strong radio sources (such as Cassiopea A and Cygnus A) and bright quasars have been observed in the local mode of the station to study ionospheric and interplanetary scintillations. As an electromagnetic wave propagates through a medium where electron density fluctuations are present, variations in the refractive index occur. Since observations carried out in low frequency range are more sensitive to ionospheric disturbances than those recorded in higher frequency ranges, they can provide information on the irregular structure of this layer, which influences, for example, low frequency

radioastronomy and radio communication.

Data used in this research come from the sixth cycle of LOFAR core observations the 6th observing cycle. Data presents measured amplitudes in resolution of about 10Hz in a 100 frequency subbands between 75.97 and 21.87 MHz, 38 stations (core and remote station) has been considered. We used three datasets: L547449, L547785 and L552177 (respectively quiet, disturbed and stormy conditions). In each case, the source of observations was CasA, as it has the best cross-correlation function. We have transform the spatial coordinates so that all the stations (antennas) are placed on the same surface. Further we have selected subband 70 (out of 100). For this data cross-correlation function has been calculated.

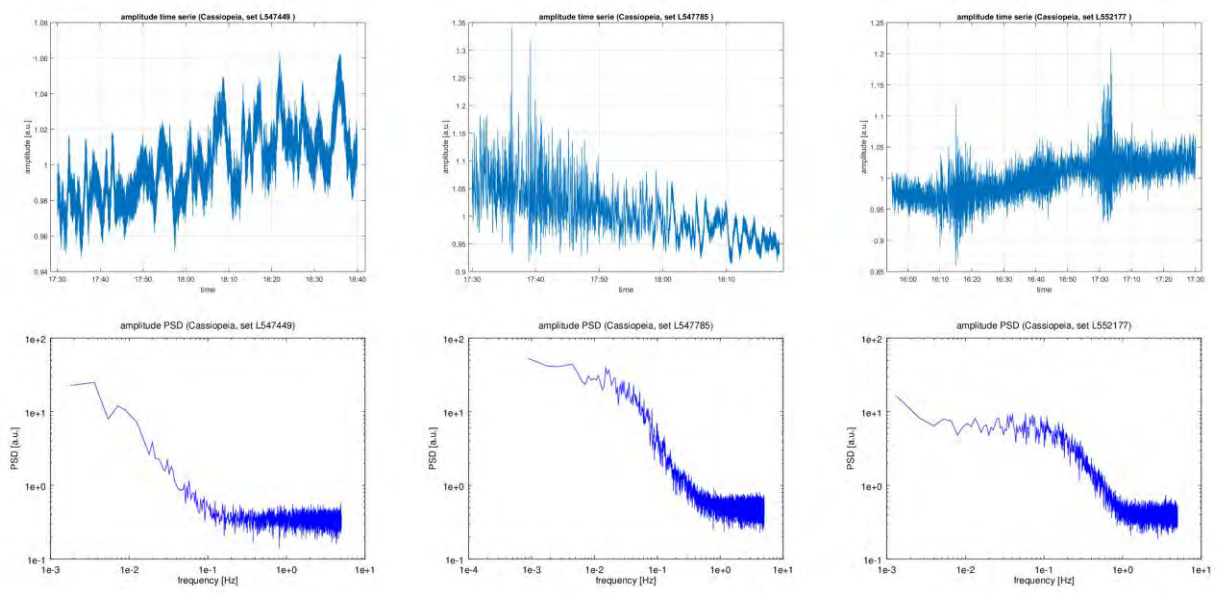

Fig. 3.38. Top row: amplitude time series; Bottom row: amplitude power spectrum density. Left column: quiet conditions (set L547449); Centre column: disturbed conditions (set L547785); Right column: stormy conditions (set L552177) Special thanks to Richard Fallows for providing LOFAR core data.

Each column of Fig. 3.38 shows in upper panel amplitude time series and on bottom panel its power spectral density (PSD) for three considered cases. One can see that with increasing disturbance level amplitude scintillates stronger and PSD broadens. Having established by correlation analysis that the

studied amplitude of LOFAR interferometry agrees well with the picture of ionosphere modifying interstellar radioemission we can try to estimate drift velocity of diffraction pattern observed on the ground. We used the method of relating characteristic features on auto- and cross-correlation function described in variety of papers.

$$\tau_{max} = \frac{\zeta^T Q v}{v^T Q v} \quad (1)$$

Above formula gives time lag for maximum of temporal correlation between two stations separated by vector ξ. The quantity Q is the matrix of quadratic form which describes anisotropy of the random field and v is the drift velocity. One can see that the τ max is linear function of separation and depends both on drift velocity and geometry of irregularities.

In Figure 3.39 (similarly to Figure 3.38) correlation function evaluated at available positions for null time lag in top panel and in bottom panel time lag for the maximum correlation evaluated at available positions (as above) is shown for each dataset. For weak and moderate scintillation (sets L547449 and L547785) the correlation function is anisotropic while for stormy conditions (set L552177) it tends to isotropy. On the other hand, time lag for the maximum correlation behaves accordingly to Equation 1 linearly what confirms hypothesis on the drifting irregularities.

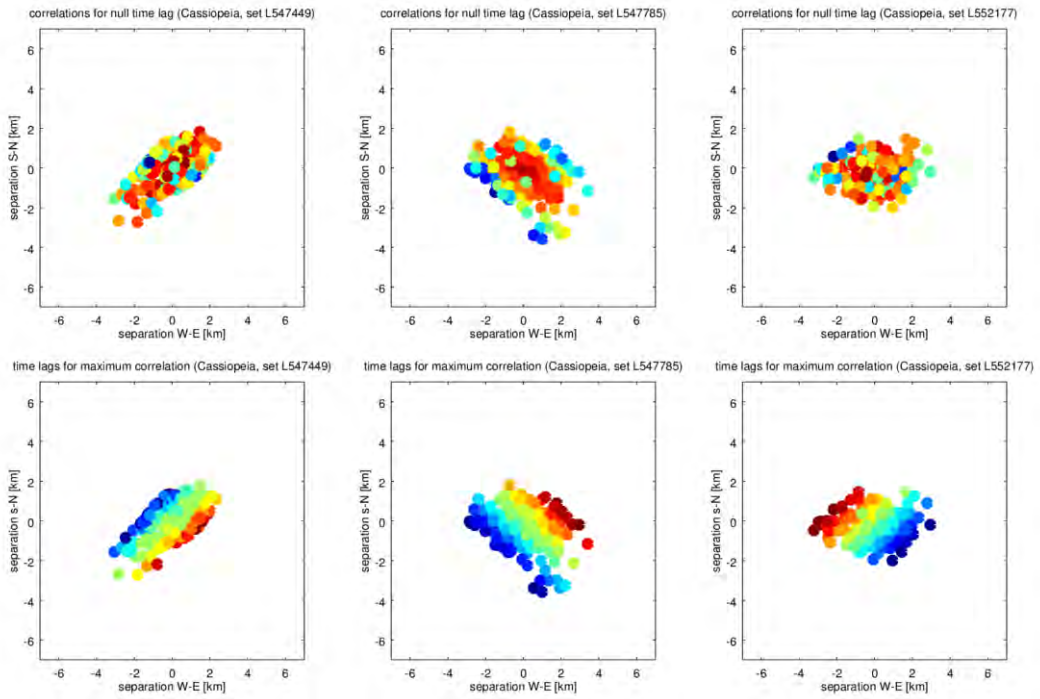

Fig. 3.39. Left: top - correlation function evaluated at available positions for null time lag, bottom - time lag for the maximum correlation evaluated at available positions (as above) for quiet conditions (set L547449); center: correlation function evaluated at available positions for null time lag, bottom - time lag for the maximum correlation evaluated at available positions (as above) for disturbed conditions (set L547785); left: correlation function evaluated at available positions for null time lag, bottom - time lag for the maximum correlation evaluated at available positions (as above) for stormy conditions (set L552177).

COMET INTERCEPTOR H. Rothkaehl PI of DFP instrument, J. Baran Project Manager of DFP Instrument, M. Morawski Lead electronic engineer, T. Barcinski lead mechanical engineer.

Comet Interceptor is new mission F1(fast) to a Dynamically New Solar System Object selected by ESA in July 2019. The mission will be launched in 2028 on the same rocket as M4 mission Ariel.

The main goal of this mission is to explore a comet very likely entering the inner Solar System for the first time, or, possibly, to encounter an interstellar object originating at another star. Based on both the catalogue of historic LPCs and simulations of a large synthetic set of LPC orbits, Comet Interceptor will have to wait only 2-3 years for a target it can reach. The satellites will be

launched the launch to a stable halo orbit around the Sun-Earth L2 point and wait for the discovery of a suitable comet that it can reach.

The Comet Interceptor mission will involve 3 separate spacecraft working together to obtain multi-point measurements and get the 3D information provided on the target and its jets/coma. Similarly, in situ observations of the cometary environment can be also obtain from multiple sampling paths. The multiple elements can sample gas composition and density, dust flux, and plasma and solar wind interactions, to build up a 3D 'snapshot' of the region around the target. One spacecraft will make remote and upstream in situ observations of the target from afar, to protect it from the dust environment of an active comet, and act as the primary communications hub with Earth for all other mission elements. Two other spacecraft will be deployed to venture closer to the target, carrying complementary instrument payloads, to build up a 3D picture of the comet.

Space Plasma department is involved in construction one of the primary instruments DFP, Dust Field, Plasma for the main spacecraft and one smaller one, daughter satellite, provides five sensors and central electronics that will provide multi-point, in situ measurements of the dust, electric and magnetic field and the charged and neutral particles in the cometary environment. CBK PAN is response for management and prof H. Rothkaehl is PI of DFP instrument. CBK PAN responsibilities in the instrument implementation are: PSU supply redundancy system and instrument. The scientific involvement includes data analysis and science interpretation of registered data and also preparing the details of scientific program for mission. In 2019 the overall the design for each subunits of DFP instrument was prepared and the appropriate documents were completed, Instrument Design Report IDR, Instrument Management Plan IMP, Instrument Development Plan IDP, Instrument Interface Development Plan IIDD. Also the first phase of the project was successfully finished.

Scientist from CBK have participated in the development of the new service for the International Civil Aviation Organisation (ICAO) in frame of the Pan-European Consortium for Aviation Space WeAther User Services (PECASUS) The CBK PAN provides products related to the high frequency communication changes and serve advisory support for users. In frames of PECASUS activity the techniques for building the foF2 global nowcast maps.

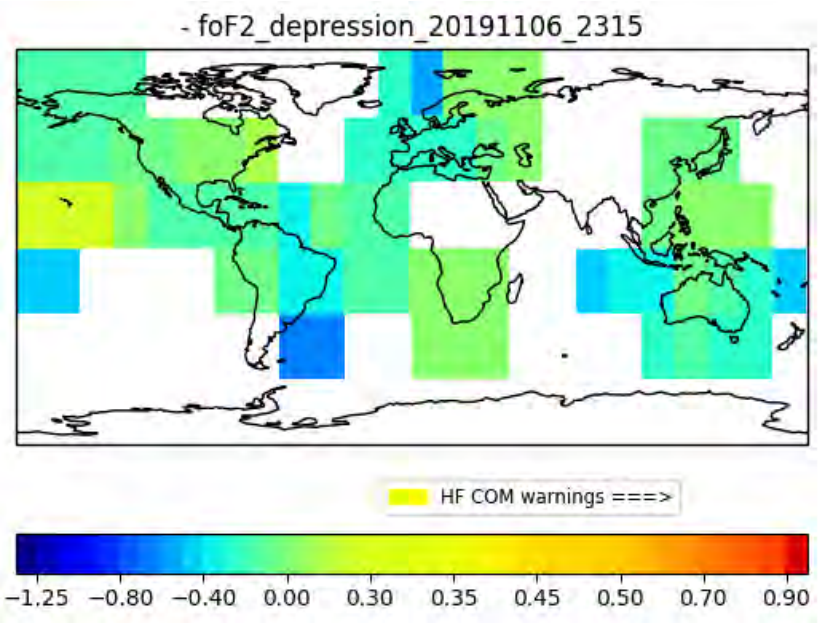

Fig. 4.40. Near real time foF2 depression map.

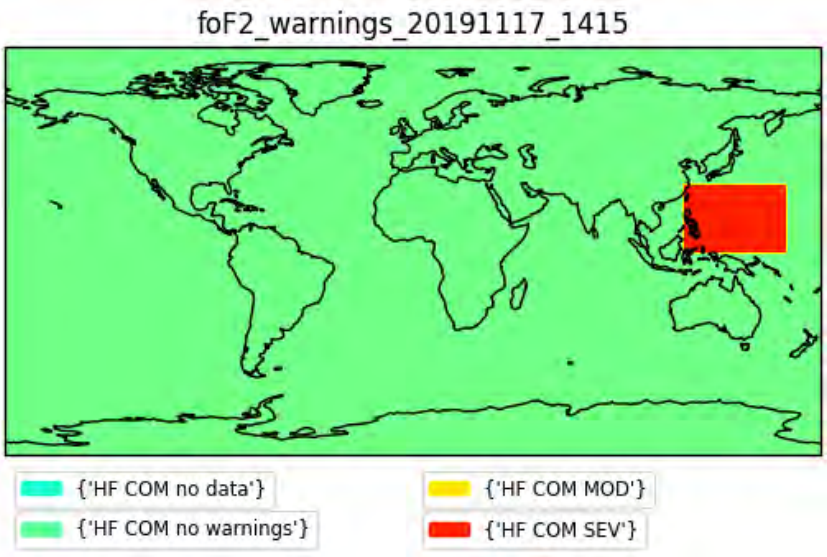

Fig. 3.41. Communication interference warnings map for civilian aviation.

SRC PAS SRC SGIArv and SRC RIO services B. Dziak-Jankowska, Ł. Tomasik, M. Pożoga

The SRC PAS provides support in as one of designed Ionospheric Weather Expert Service Centre to the European Space Agency's Space Situational Awareness Space Weather Segment (SSA SWE) network, notably in the form of the observation, monitoring, interpretation, modeling and forecasting of ionospheric and upper atmosphere weather conditions. Within the framework of the Agency's 'Ionospheric Weather' project, the HPS Centre host two services SRC SGIArv and SRC RIO. The current version is being updated according to user needs.

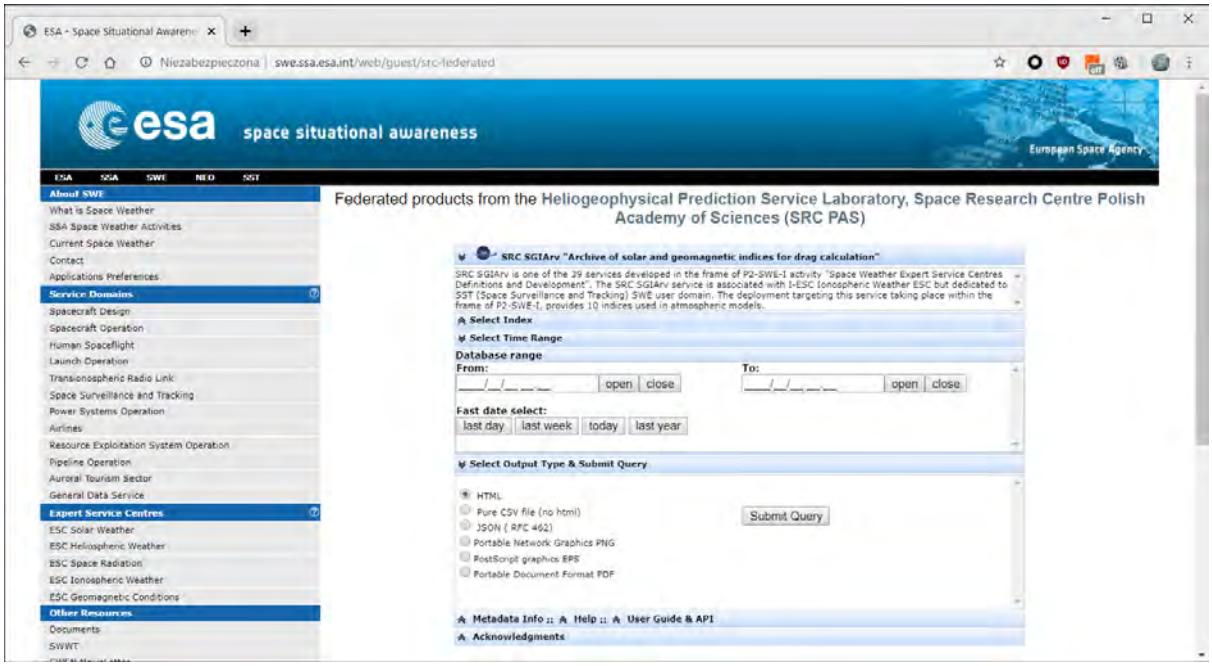

Fig. 3.42. Screenshot of SRC SGIArv service in ESA framework

Other projects and activities Ł. Tomasik, M. Pożoga

Within the framework of the EUROPLANET RI H2020 project, RWC Warszawa started the warning by implementing VOEvent technology. The historical databases of RWC Alerts is available by the VESPA service.

In Galileo Monitoring project the HPSC produces the quarterly reports of Galileo single frequency ionospheric model performance compared to Warsaw ionosonde data and H2PT TEC output.

The HPSC provides specific products and expertise and experts knowledge for National Radio Frequency Agency Poland, power grid operators and other polish government institutions in various effects related to the impact of the Space Weather effects on technical infrastructure.

Analysis of Auroral Kilometric Radiation bursts M. Marek, R. Schreiber

In the years 2018-2019, working in the frame of a SOC concept, we concluded analysis of the Auroral Kilometric Radiation (AKR) bursts occurrence as a function of their intensity. We used data collected by the Polish POLRAD

and the French MEMO (F. Lefeuvre, M. Parrot) experiments, in the framework of the Interball-2 mission. Our preliminary results were reported in our paper *"Is The AKR Cyclotron Maser Instability A Self–Organized Criticality System?*" and presented at the 8th International Workshop on Planetary, Solar and Heliospheric Radio Emissions in Graz, Austria and has been published in the Proceedings of the conference. Self-organized criticality is a rather general concept and we initially decided to fit the AKR bursts data to a simple analytical model, the logistic–growth model. We used AKR waveform data from the MEMO experiment. We determined both shapes and durations of single AKR bursts filtered within a 4 kHz bandwidth. MEMO data are very scarce, but we were still able to show, that the characteristics of single AKR bursts determined from the logistic growth model agree well with the Electron Cyclotron Maser mechanism producing AKR, in particular, with expected growth rates for the AKR bursts. Our result is a strong argument in favor of the AKR as a SOC system.

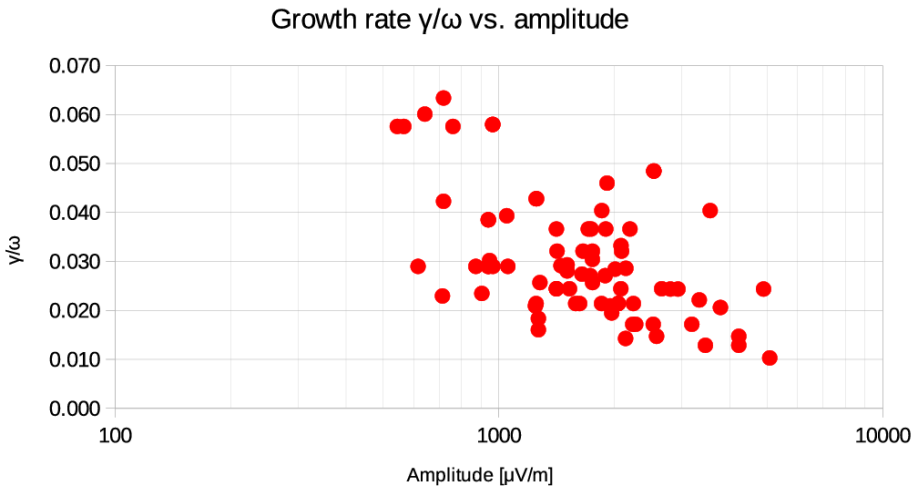

Fig. 3.43. – Normalized single AKR bursts growth rates estimated via the self-organized criticality (SOC) logistic growth model from the MEMO AKR waveforms.

Analysis of variations in plasma density and the intensity of field aligned currents (FACs) during the geomagnetic storm of September 2017 A. Chuchra and B. Matyjasiak

The analyzed geomagnetic storm covers the period of 6–10 September 2017 during which the Active Region AR12673 on the Sun emitted twenty-seven M-class and four X-class flares and released several strong Coronal Mass Ejections (CMEs). Two X-flares occurred on September 6th - the confined X2.2 flare at 08:57 UT and the eruptive flare X9.3 at 11:53 UT - the strongest flare of Solar Cycle 24. The next intense flare X1.3 occurred at 14:20 UT on September 7. The material of CME produced by the X9.3 solar flare on 6th of September 2017 reached Earth at 23:04 UTC on 7th of September 2017, after which began severe geomagnetic storm (G4) on 07-08.09.2017 with Ap = 106. It was a complex geomagnetic event that resulted in dynamic changes in Earth's auroral region.

In reference to the above-mentioned phenomena on the Sun and B_z component of interplanetary magnetic field (IMF) changes in field-aligned currents were analyzed. Changes in FACs intensity and variations in electron density were also examined in response to the variations of Dst index . The interaction and correlation of the mentioned parameters were studied in the context of different phases of this geomagnetic event. There is observed a clear response in strength of field-aligned currents to September 2017's geomagnetic storm. The energisation of the storm developed strong R1 and R2 FACs. The main conclusions and plots are presented below.

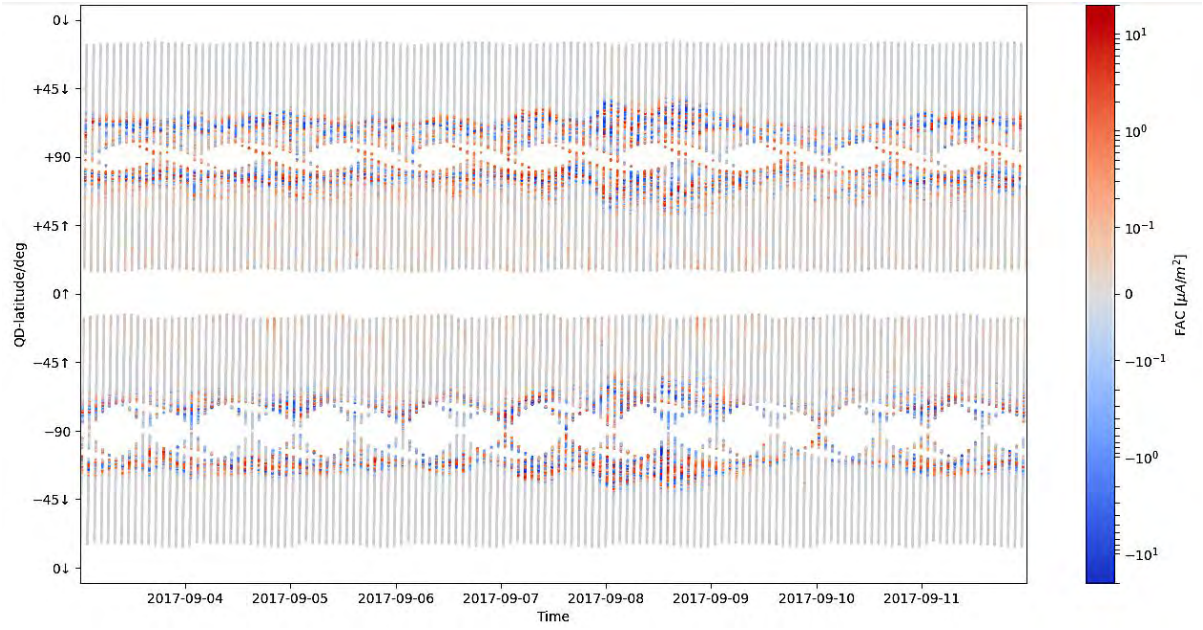

Fig. 3.44. Intensity of field-aligned currents for 4-11 September 2017 from Swarm data.

In this plot (Fig. 3.44) positive values of FACs (red) indicate upward currents (away from the ionosphere), and negative values (blue) indicate downward currents (toward the ionosphere). There can be observed clear intensification of FACs after the main phase of the storm. Field-aligned currents in the Northern Hemisphere are stronger than in the Southern Hemisphere. Before the beginning of the storm (4-6 September) the currents seem to be withdrawn towards the poles, and on 7-8 September shifts of FACs to lower latitudes (< 50°) can be observed. On 9-10 September FACs withdrew to higher latitudes again and their intensity has decreased significantly to return to the typical values on September 11.

Changes in the intensity of FACs before (Sep. 6) and after (Sep. 7 around 23:35-23:38 UTC) sudden commencement are presented in Fig. 3.45. In the period before the onset of the geomagnetic storm, intensity of FACs is approx. 5-10 μA/m^2, over time increasing to mean values in the range 10-15 μA/m^2 and several times up to 20-25 μA/m^2. After sudden commencement the field-aligned currents intensified and their density reached values above 25 μA/m^2

but after 23:38 decreased again. It can be noticed that usually downward currents are stronger. Second peak of the geomagnetic activity on 8 September (Fig. 3.46) caused the FACs to intensify again, even to 50 μA/m².

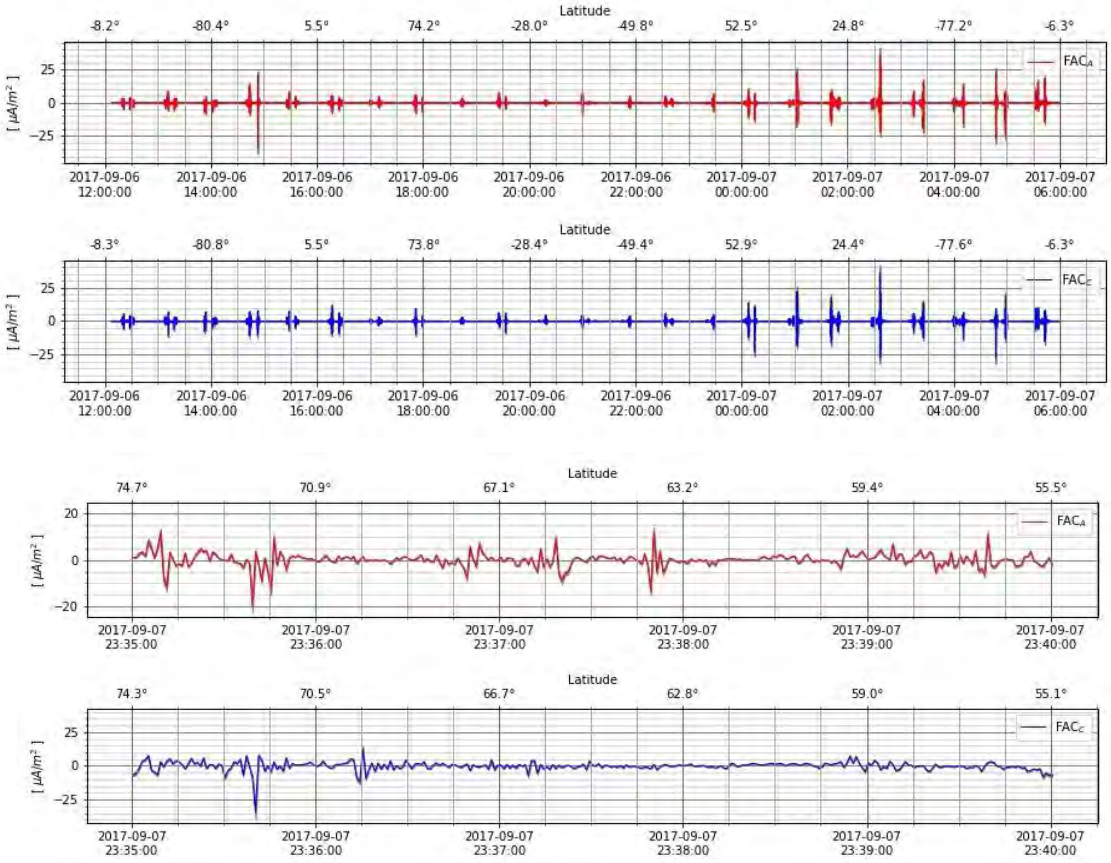

Fig. 3.45. Intensity of field-aligned currents before the onset of the geomagnetic storm (upper plot) and in time after sudden commencement (lower plot).

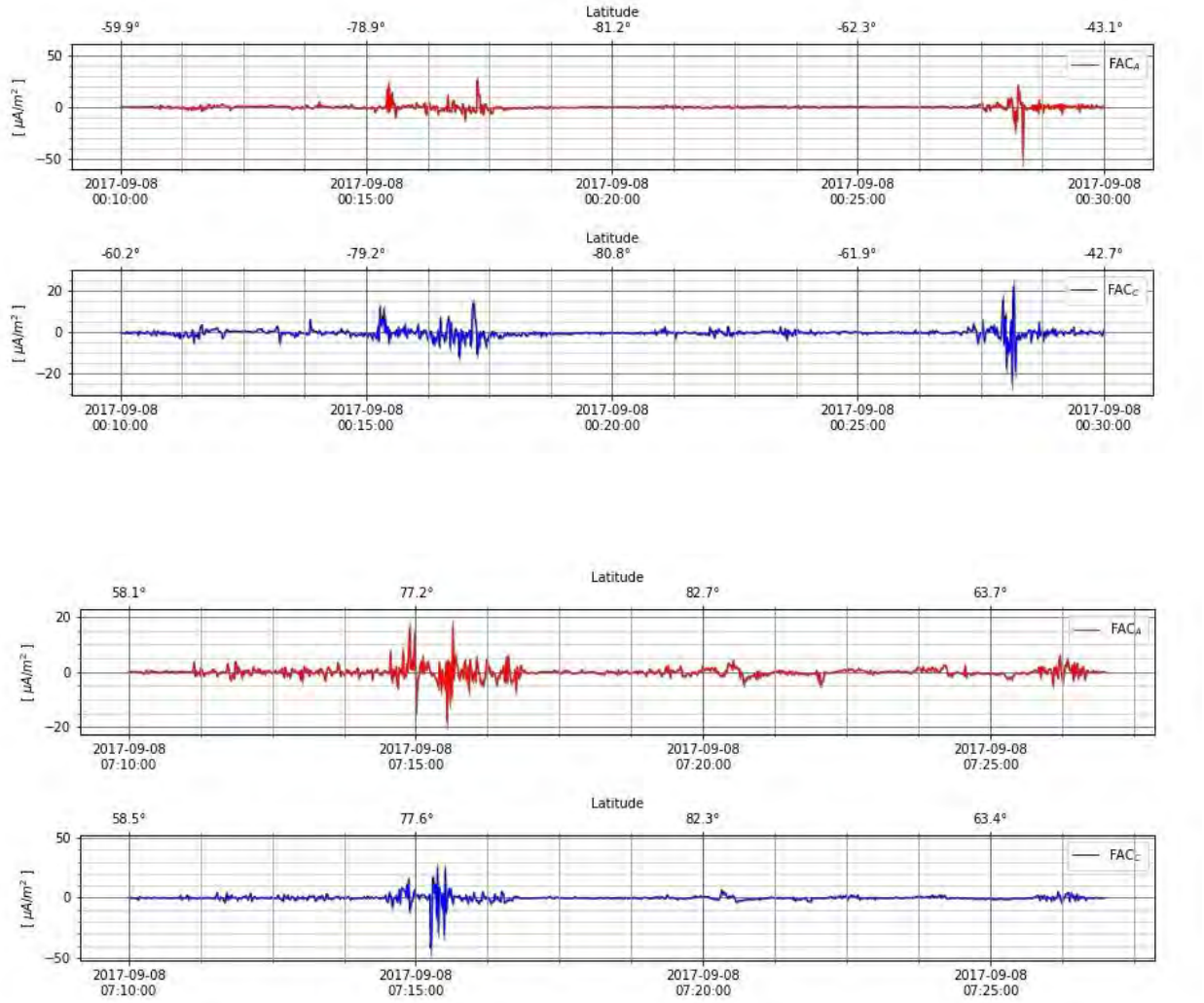

Fig. 3.46. Intensity of field-aligned currents on 8 September during geomagnetic storm.

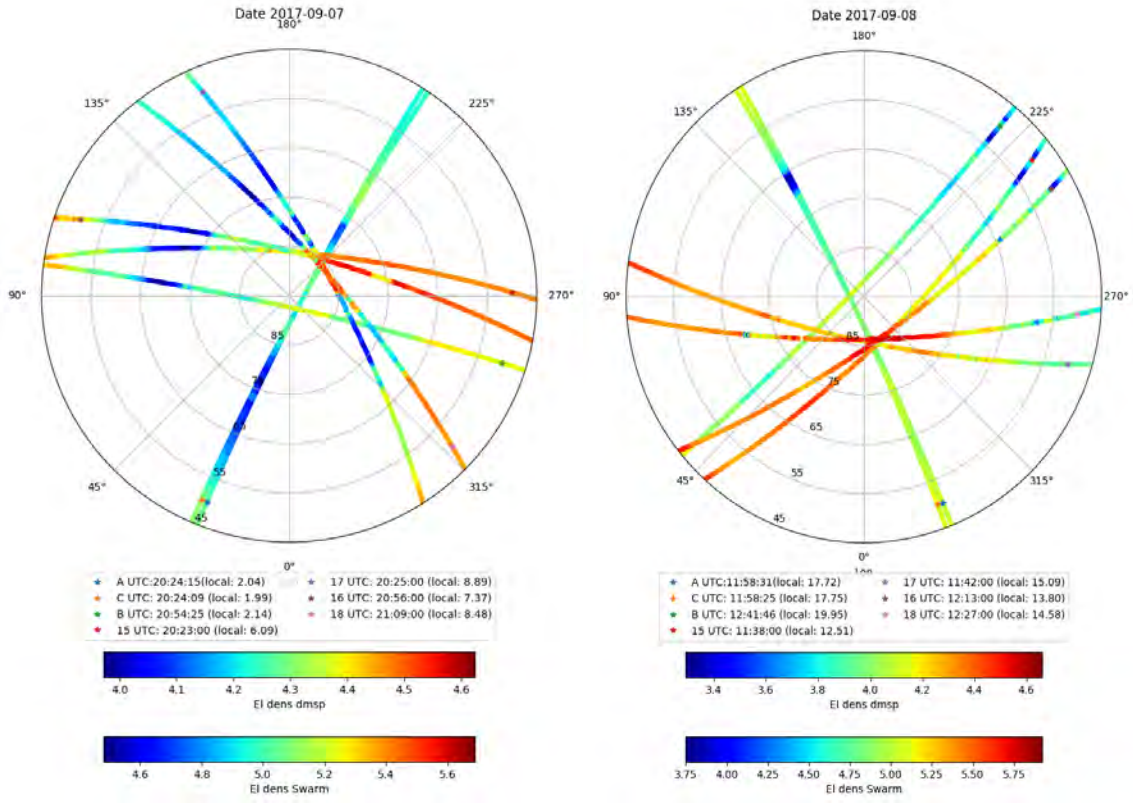

Fig. 3.47. Polar view of electron density data from Swarm and DMSP satellites around 20 UTC on 7 (left) and 8 (right) September 2017.

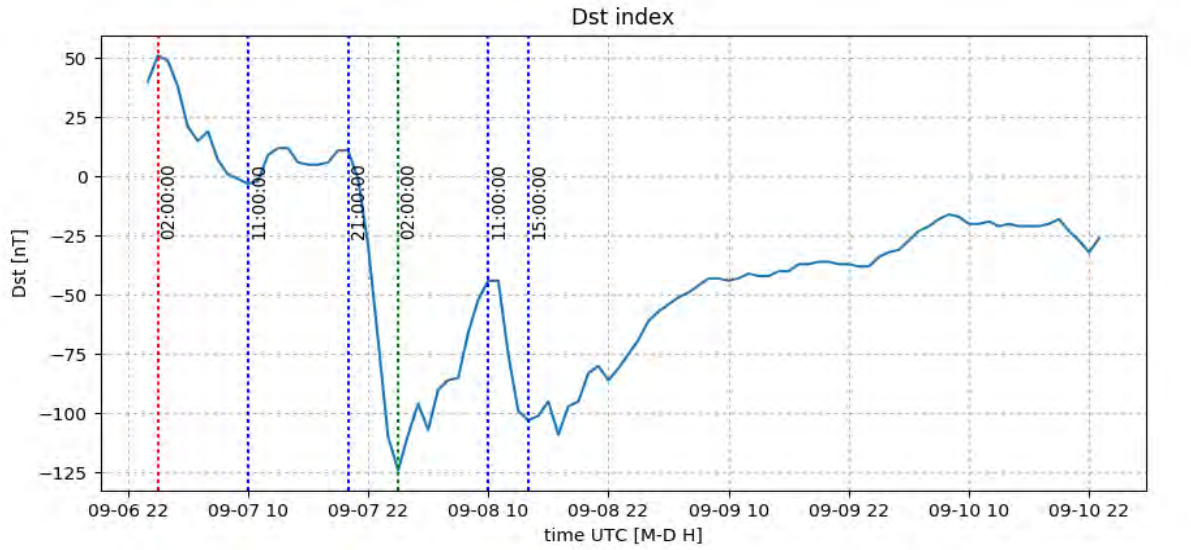

Fig. 3.48. Dst-index for 6-8 September 2017 with two minimum values on 8 Sep.: -124 nT at 02:00 UT and -109 nT at 18:00 UT.

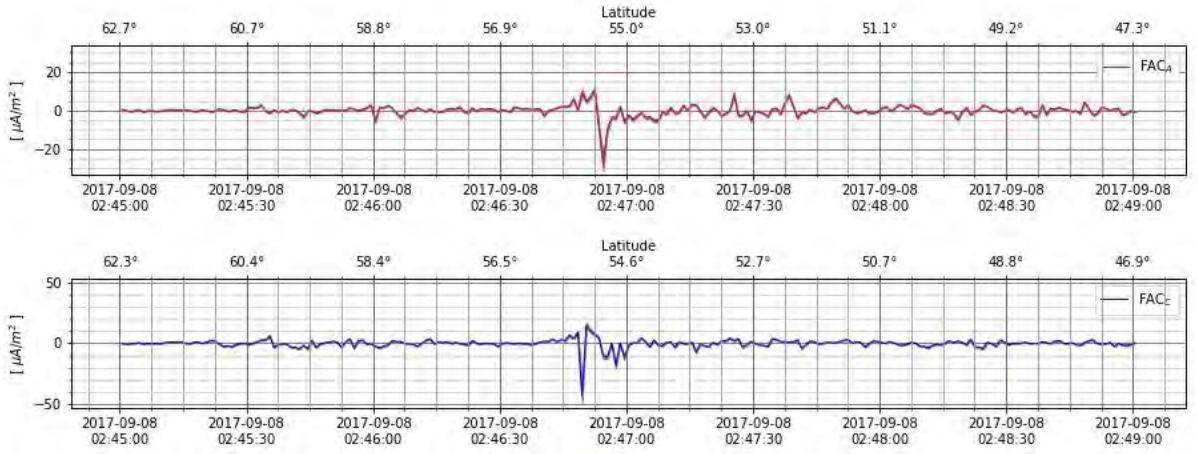

Fig. 3.49. Intensity of field-aligned currents on 8 September in response to first Dst-index minimum.

On 8 September there is observed an increase in electron density compared to electron densities on September 7 (Fig. 3.47) resulting from increased energetic particles precipitation during the main phase of this geomagnetic storm. An intensification of FACs' intensity is observed in response to the minima of Dst-index on 8th September, even to the values around 50μA/m² (Fig. 3.48 and 3.49).

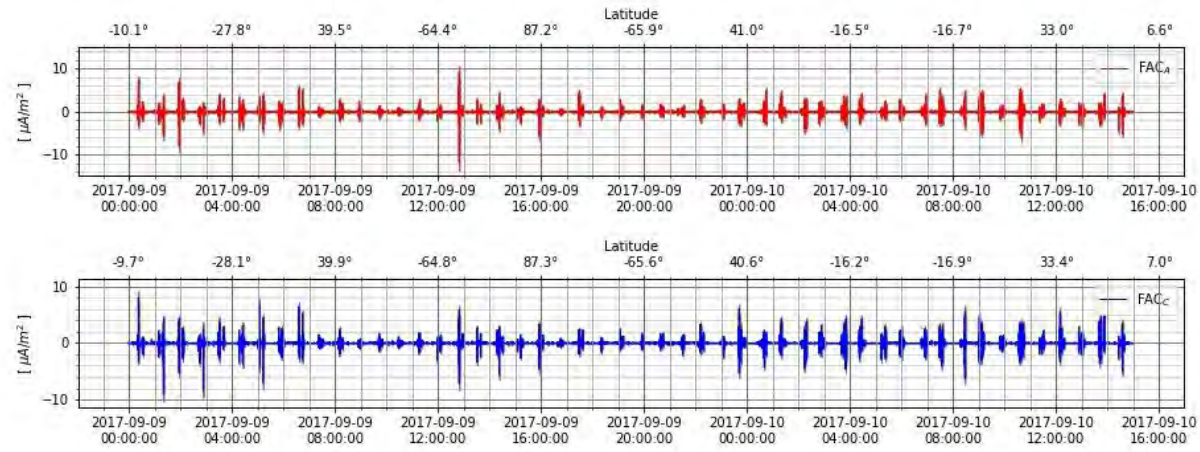

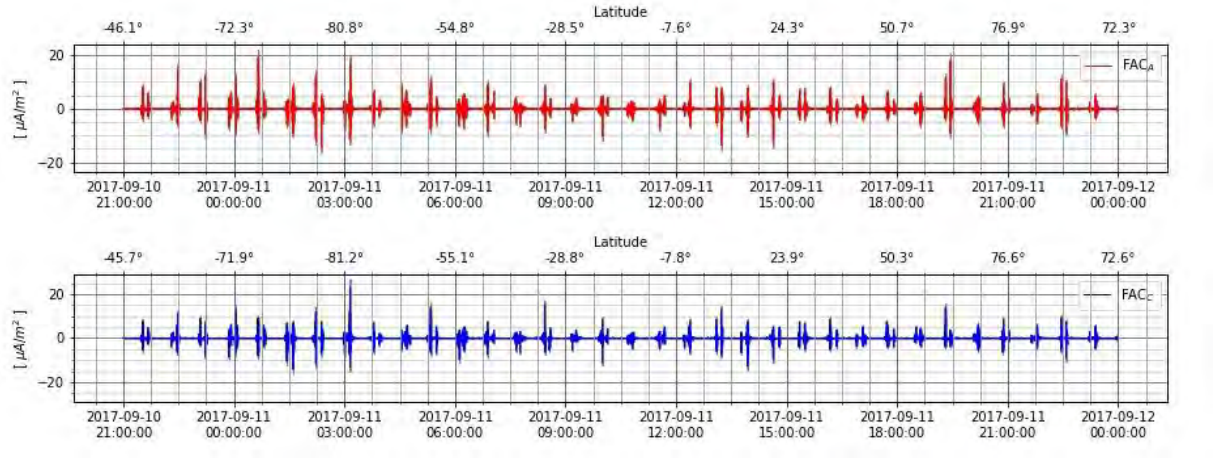

Fig. 3.50. Intensity of field-aligned currents for 9-12 September 2017.

On 9 and 10 September (Fig. 3.50) intensity of FACs doesn't exceed 10 μA/m² (on average it is around 5 μA/m²). In the recovery phase (11 Sep.) values of the intensity of field-aligned currents usually are equal or higher than 10 μA/m2, and several times reach 20 μA/m².

Analysis of small and medium scale ionospheric irregularities based on LOFAR radiotelescope diagnostics K. Budzińska

The aim of this work is development of the method to determine the time evolution of geometric characteristics of the ionosphere based on LOFAR calibration data.

In order to obtain spectral and temporal information, wavelet transform is applied. In an early version of the method Ricker wavelet transform was used, and coefficients were then transformed with Hilbert transform- this has been combined into one step by applying complex second order gaussian wavelet. Amplitude envelope and instantaneous phase/frequency are then calculated. This is done because even in the simplest situation of one wave-like type of irregularities existing within the LOFAR field, interferometer detects difference between the stations, which results in modulated amplitude of such original wave while instantaneous frequency would have constant value.

These calculations are done for LOFAR dTEC, as well as magnetic dB/dt time series; examples for one of the observations are shown in Fig. 3.51and 3.52.

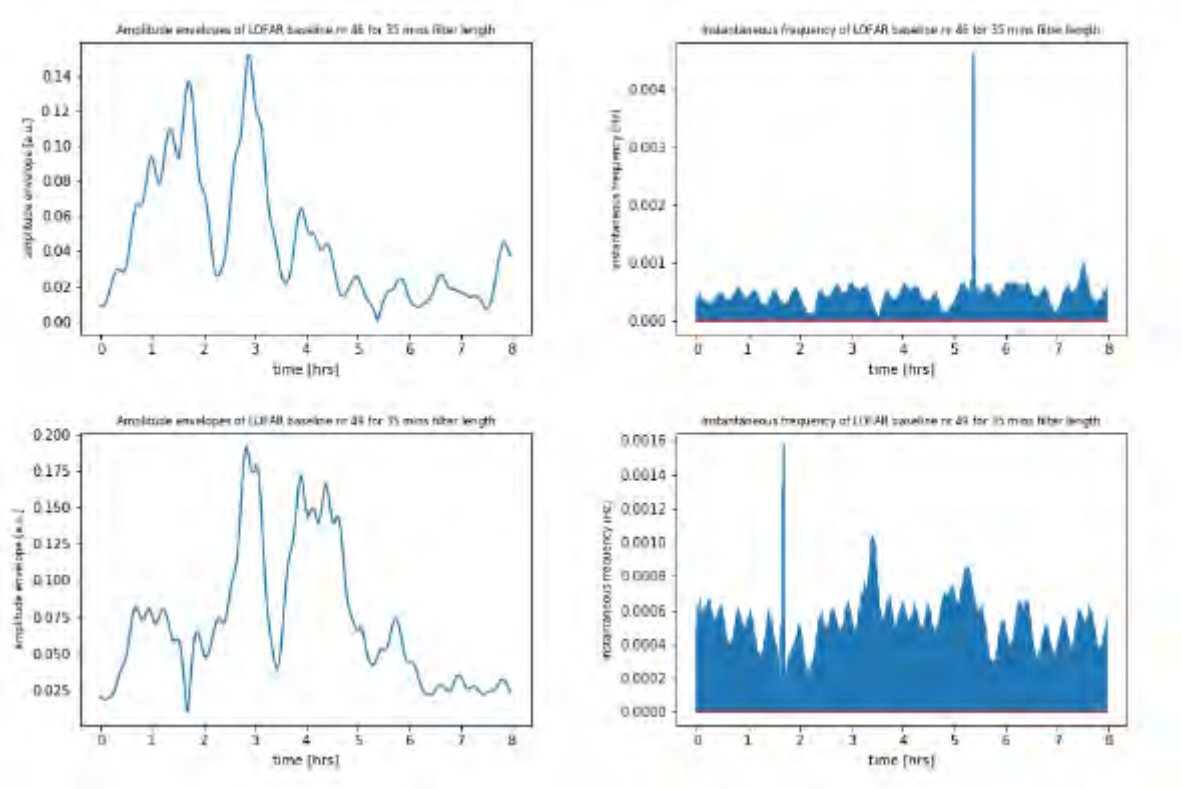

Fig. 3.51. Example of amplitude envelopes and instantaneous frequency plots for two of LOFAR stations, almost perpendicular to each other

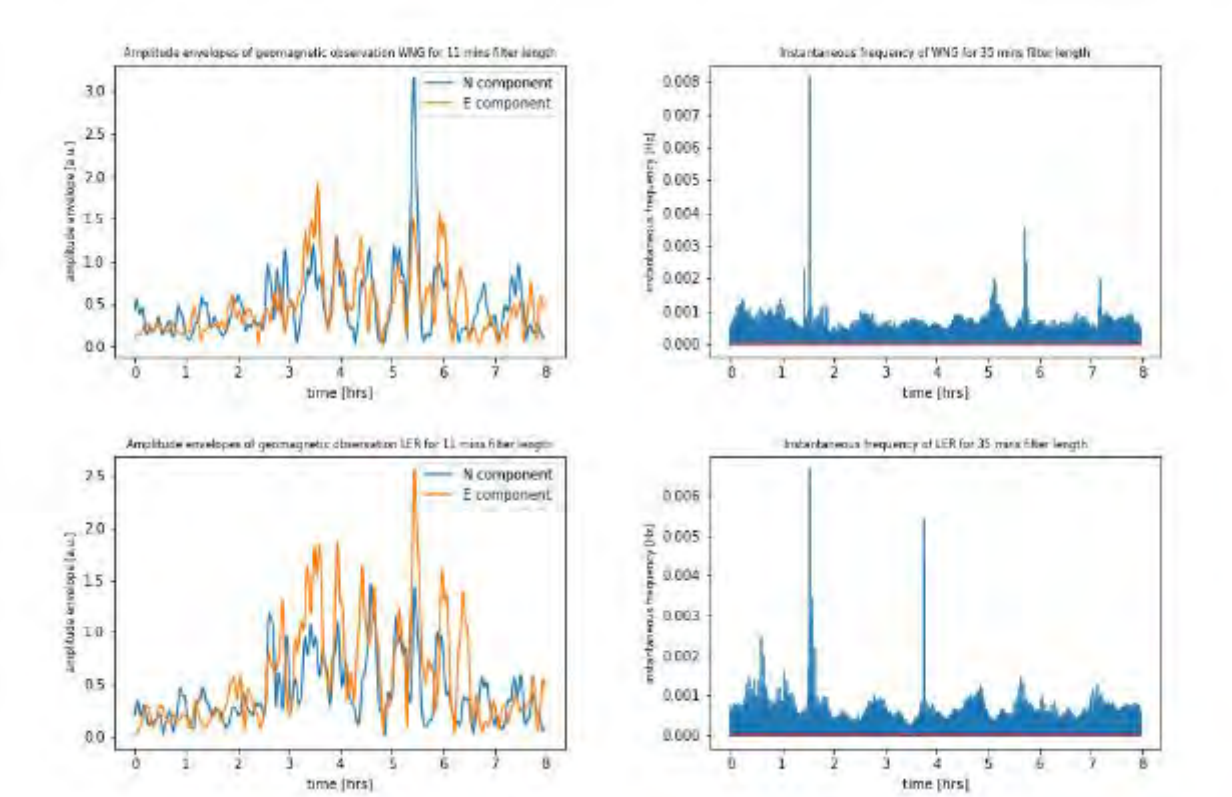

Fig. 3.52. Amplitude envelopes and instantaneous frequency plots for two magnetometers, WNG and LER

To compare results from LOFAR and magnetometers, time lag of thebest correlation was calculated. Fig. 3.53 shows good agreement between the directions of the biggest changes, which indicates that the signal is not an artifact.

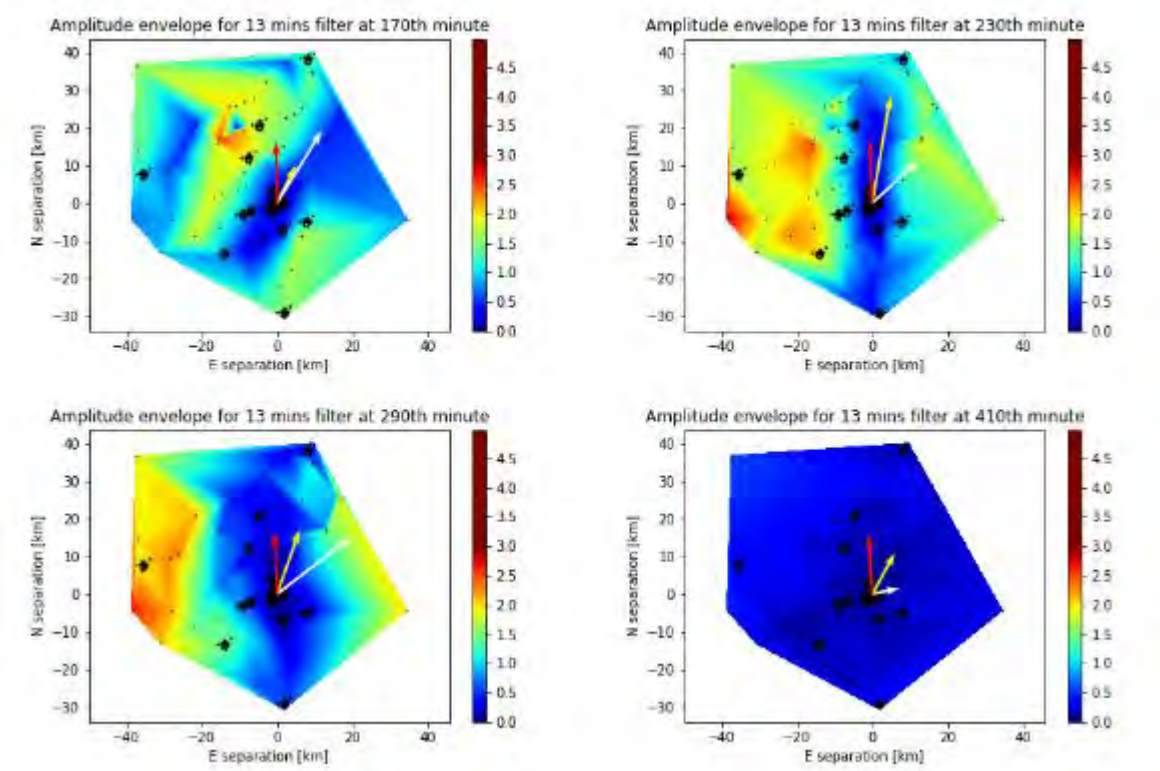

Fig. 3.53. Comparison of LOFAR field and the rate of change of geomagnetic field vector. Red arrow- main geomagnetic field model coordinates for LOFAR center of the field view at 800 km height; yellow arrow- direction of disturbance dB/dt from WNG magnetometer and filter length 13 mins; white arrow- same as yellow but for 1 hour filter length.

Presented method gives a tool to obtain information on the time evolution of the ionospheric irregularities of different scales, based on very sensitive LOFAR calibration data. Not only dominant structure sizes can be detected as is done with up-to-date statistical approaches, but time of their occurrence can be assessed, and better links with geomagnetic field changes can be established. However, more study is needed to extend this type of analysis into method for determination of other characteristics, like drift velocities.

Beamforming of LOFAR Radio Telescope for Passive Radiolocation Purposes

A. Droszcz, K. Jędrzejewski, J. Kłos, K. Kulpa, M. Pożoga

The paper presents the results of investigations on beamforming of a low frequency radio-telescope LOFAR which can be used as a receiver in passive coherent location (PCL) radar for aerial and space object detection and tracking. Especially, the use of LOFAR radio-telescope for space object passive tracking can be a highly cost-effective solution due to the fact that most of the necessary equipment needed for passive radiolocation already exists in the form of LOFAR station. The capability of radiolocation of planes by a single LOFAR station in Borówiec is considered as the proof of concept of the future research focused on localization of space objects. Beam patterns of single sets of LOFAR antennas (known as tiles) as well as for the entire LOFAR station are presented and thoroughly discussed in the paper. Issues related to grating lobes in LOFAR beam patterns are also highlighted. A beamforming algorithm used for passive radiolocation purposes, exploiting data collected by LOFAR station, is also discussed. The results of preliminary experiments carried out with real signals collected by the LOFAR station in Borówiec, Poland confirm that the appropriate beamforming can increase significantly the radar's detection range and detection's certainty

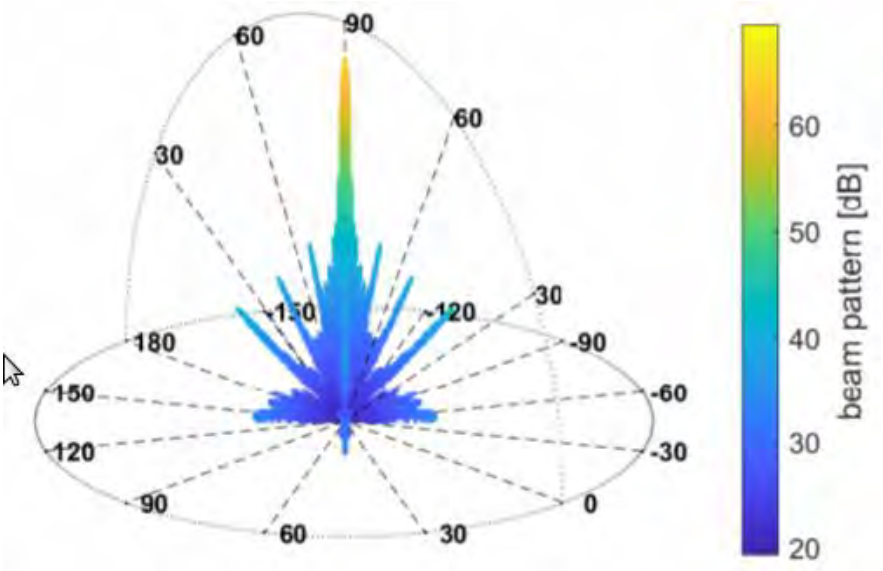

Fig. 3.54. The beam pattern of an unsteered LOFAR station, fc = 223.936 MHz

Experimental Verification of the Concept of UsingLOFAR Radio Telescopes as Receivers in Passive Radiolocation Systems J. Kłos, K. Jędrzejewski, A. Droszcz, K. Kulpa, M. Pożoga, J. Misiurewicz

The paper presents a new idea of using a low frequency radio telescope belonging to the LOFAR network as a receiver in passive radar system. The structure of a LOFAR radio telescope station is described in the context of applying this radio telescope for detection of aerial (airplanes) and space (satellite) targets. The theoretical considerations and description of the proposed signal processing schema for the passive radar based on LOFAR radio telescope are outlined in the paper. The results of initial experiments verifying the concept of a LOFAR station use as a receiver and a commercial digital radio broadcasting (DAB) transmitters as illuminators of opportunity for aerial object detection are presented.

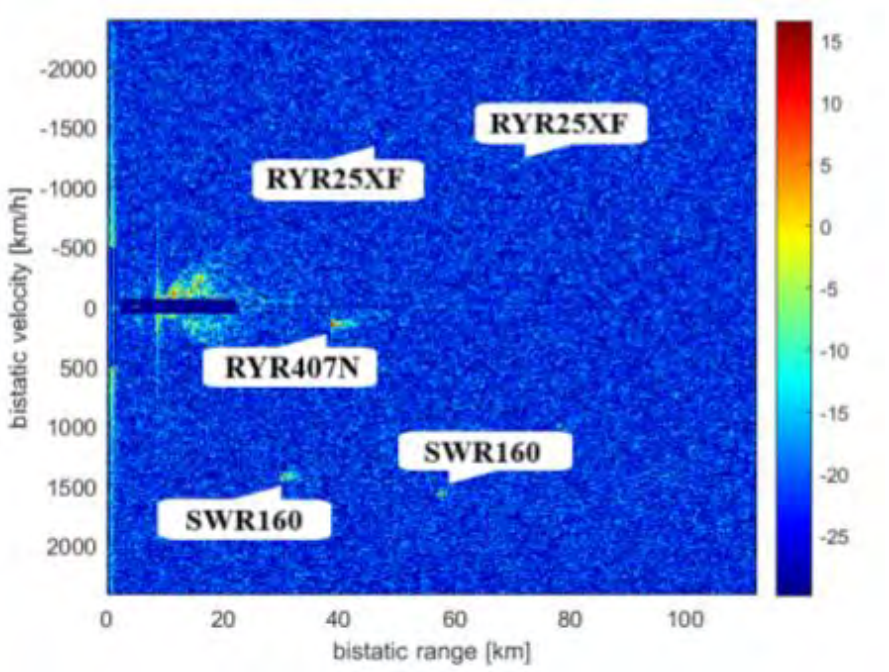

Fig. 3.55. The beam pattern of an unsteered LOFAR station, fc = 223.936 MHz

Heliogeophysical Prediction Service Centre H. Rothkaehl

The Heliogeophysical Prediction Service Centre (HPSC) is part of the global International Space Environment Service (ISES). It is responsible for measurements and predictions of solar activity and related Earth phenomena. The ISES is an international organization that coordinates the rapid exchange of parameters concerning the Sun, the Earth and the Earth's environment between participating observatories. The Warsaw centre has a special status as a Regional Warning Centre (RWC). The Centrum Badań Kosmicznych PAN exchanges data with other Warning Centres, and receives large amounts of data from national observatories in different countries. Data from Polish observatories are also collected. Together with the Geophysical Institute of the Polish Academy of Sciences, the Warsaw Centre provides data from the polar region (provided by the Polish Polar Station in Hornsund). Ionosonde data is

completed by riometers and scintillation measurements. A special daily bulletin (URSIGRAM Warsaw) is published and broadcast to ISES members.

The Ionospheric Dispatch Centre provided by , which is part of the European web service, provides online access to a database of critical frequency F2 ionospheric layer forecasts for all sites. Continuous nowcasting of regional ionospheric conditions over Europe, East Asia and Australia is also available. The HPS Centre provides the W-index over Europe based on European Geostationary Navigation Overlay Service ionospheric maps obtained from global navigation satellite system (GNSS) measurements. The same analysis can be obtained using data from the Russian System for Differential Corrections and Monitoring messages via GNSS observations. This will make it possible to show plasma flow from the eastern region, which can be used as a fast warning for Polish GNSS users.

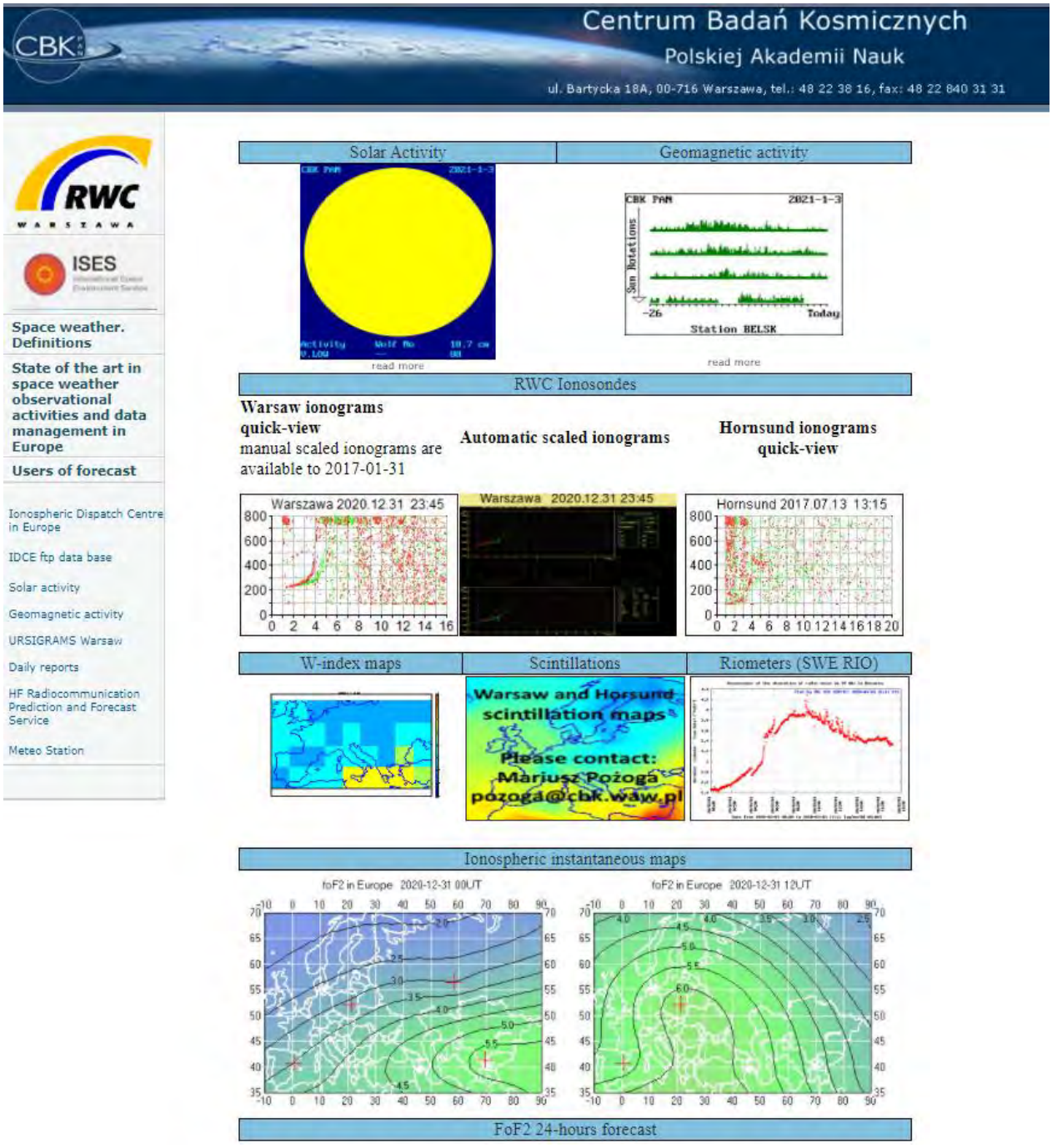

Fig. 3.56. RWC Warsaw Website

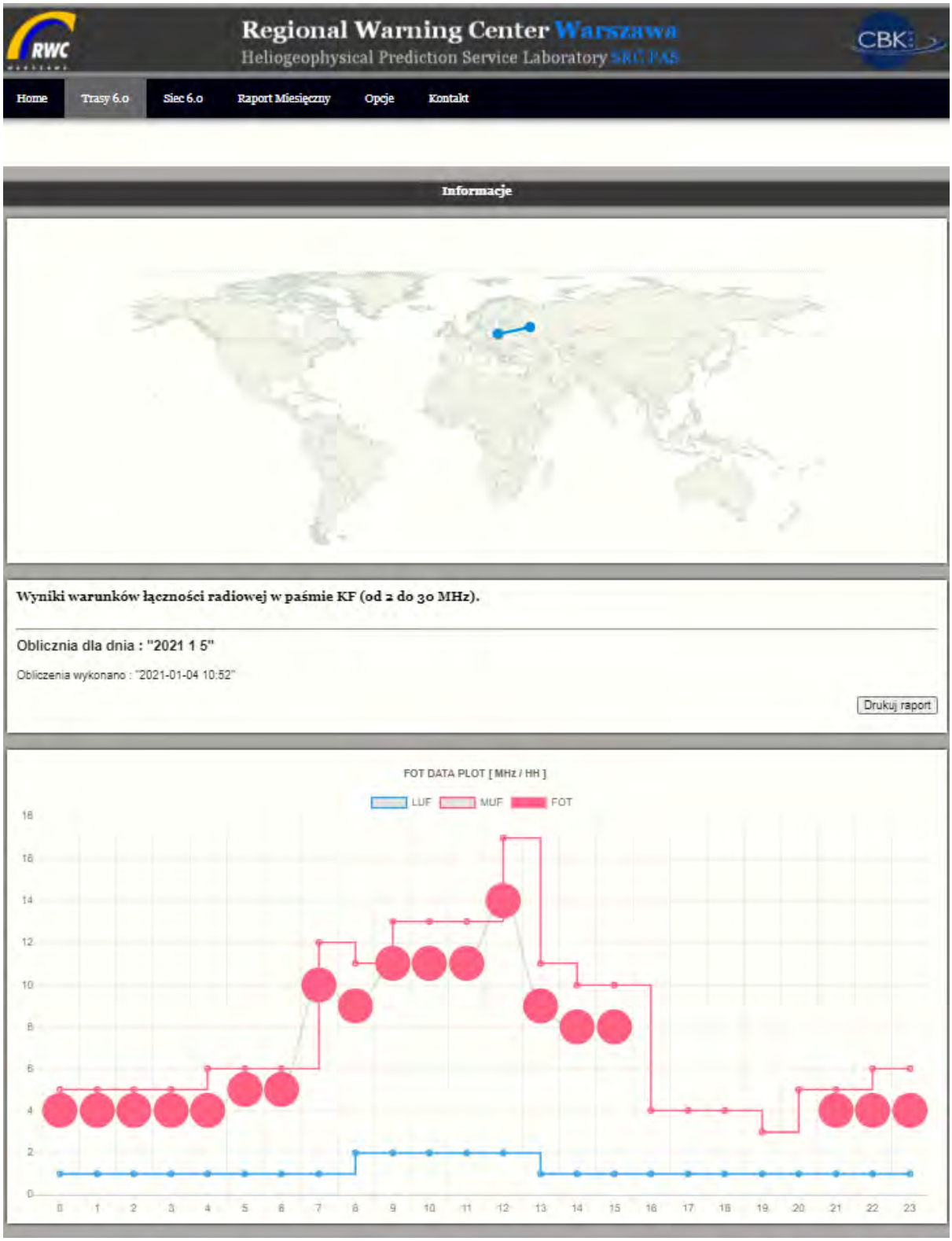

Fig. 3.57. Example of Trasy 6.0 HF parameters computation output.

The CBK PAN's Ionosphere model Ł. Tomasik, M. Pożoga

In 2018, the CBK PAN's assimilated ionosphere model Helgeo2PT (H2PT) became operational, and has been used as source of total electron count (TEC) maps for GALILEO monitoring. The model includes global navigation satellite system observations, bottom vertical and, if possible, oblique sounding. The H2PT is an empirical model, which means that TEC maps are restricted by data availability and mapping function efficiency. In 2019 and 2020 the stability and performance of the model have been increased.

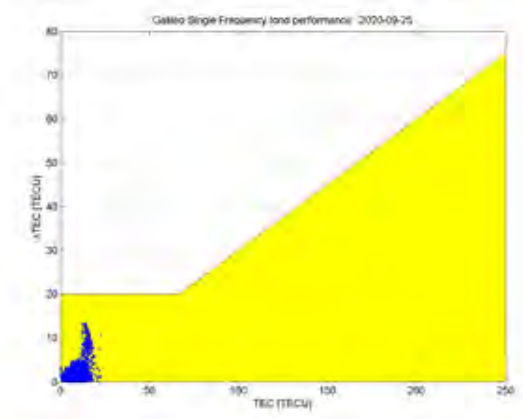

Spatial data availability plot for H2PT model (time period from 2020-07-01 to 2020-09-30)

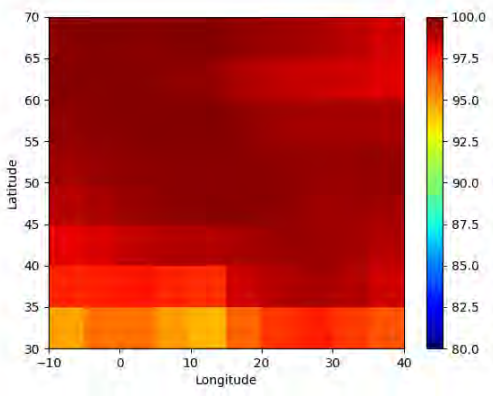

Spatial data availability plot for H2PT model (time period from 2020-07-01 to 2020-09-30)

The developed model is used in GALILEO monitoring service (GRC MC)

Comparison of the Disturbances in the Ionosphere Registered by DEMETER and Swarm Satellites during Geomagnetic and Thunderstorms **(Błęcki et al.**, 2019)

J. Błęcki, J. Słomiński, R. Wronowski, E. Słomińska, R. Iwański, M. Parrot, R. Haagmans

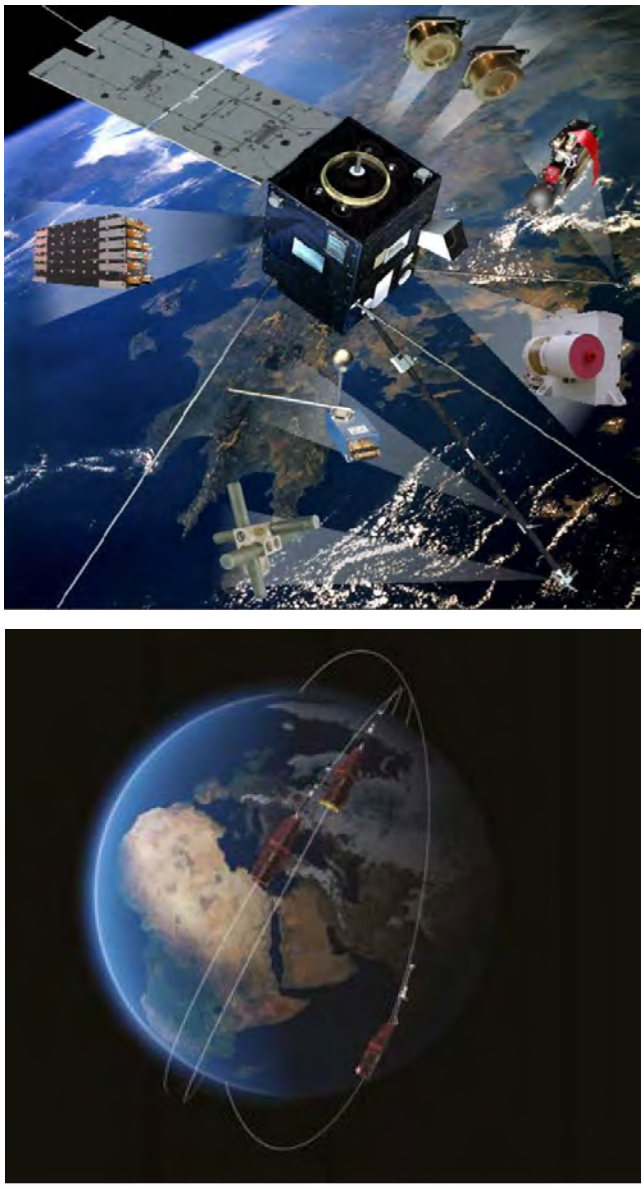

Fig. 3.58. Configuration of DEMETER satellite and 3 satellites creating Swarm mission. (courtesy of ESA)

Lightnings and particularly TLEs (sprites, jets, elves, halos) are associated with the electromagnetic connections and interactions between atmosphere, ionosphere and magnetosphere and with strong thunderstorm activity. The geomagnetic storms are known as a source of strong disturbances in the ionosphere. Analysis of the data from DEMETER and Swarm shown some similarities and diferencies between effects of both types of events.

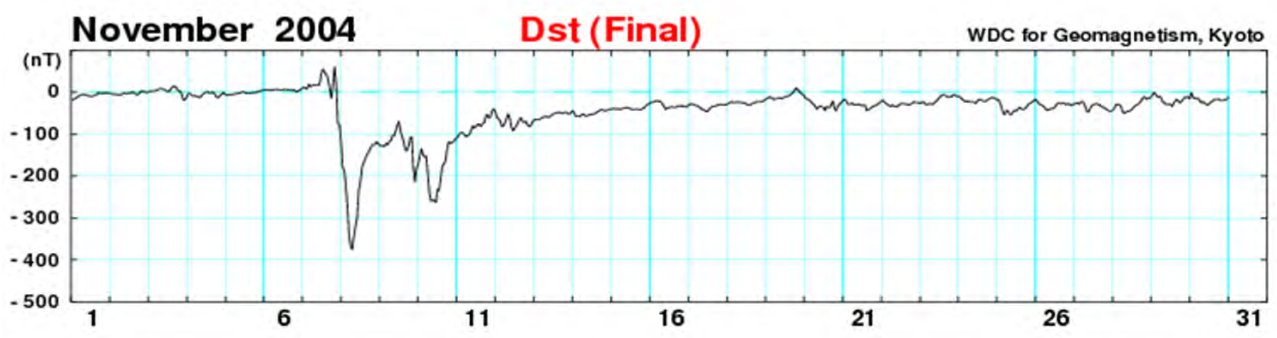

Fig. 3.59. Magnetic storm November 2004

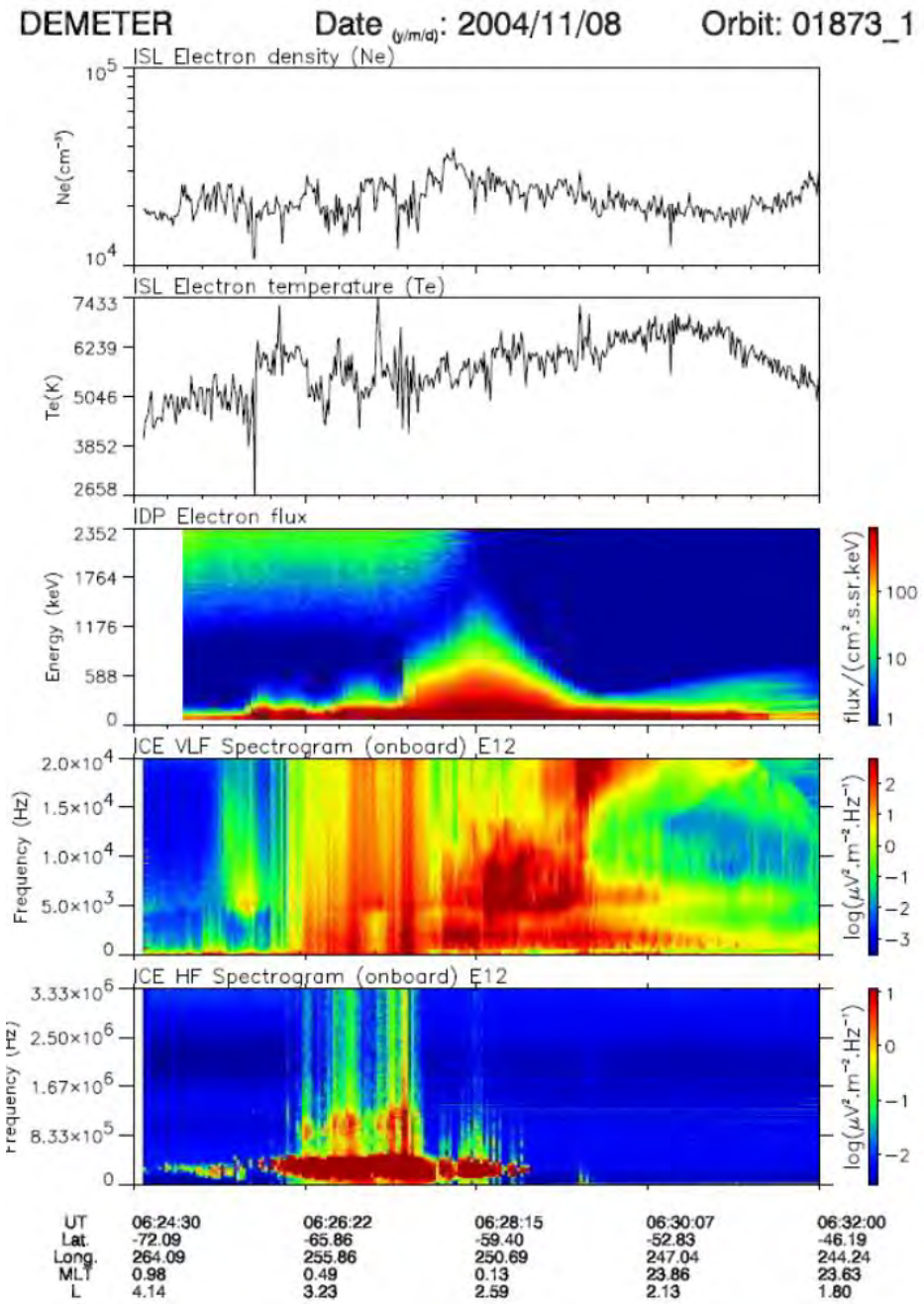

Fig. 3.60. Disturbances in the ionosphere registered by DEMETER during main phase of geomagnetic storm.

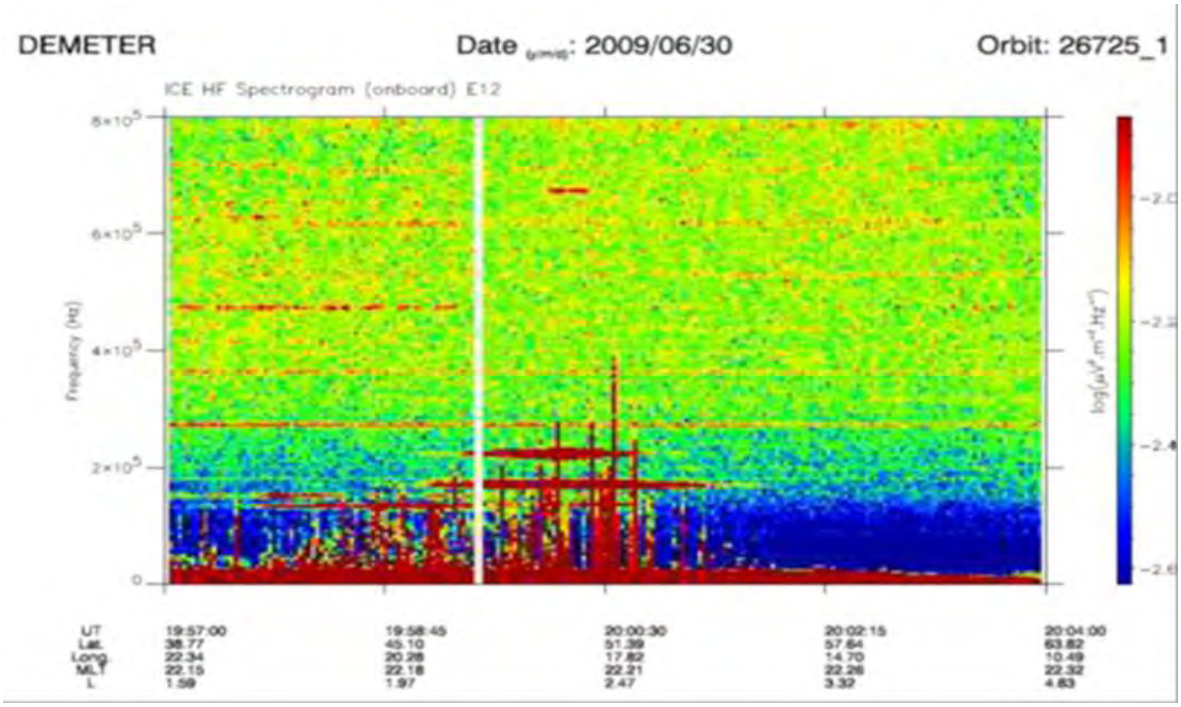

Fig. 3.61. Registrations of the HF emissions associated with fluxes of energetic electrons in the ionosphere during thunderstorm

Fig. 3.63 shows dynamical spectra of the magnetic field and electron density variations on March 26 2016 registered during flight over African center of the thunderstorm. The diamonds in Fig. 3.62 indicate time of strong strokes registered by WWLM system.

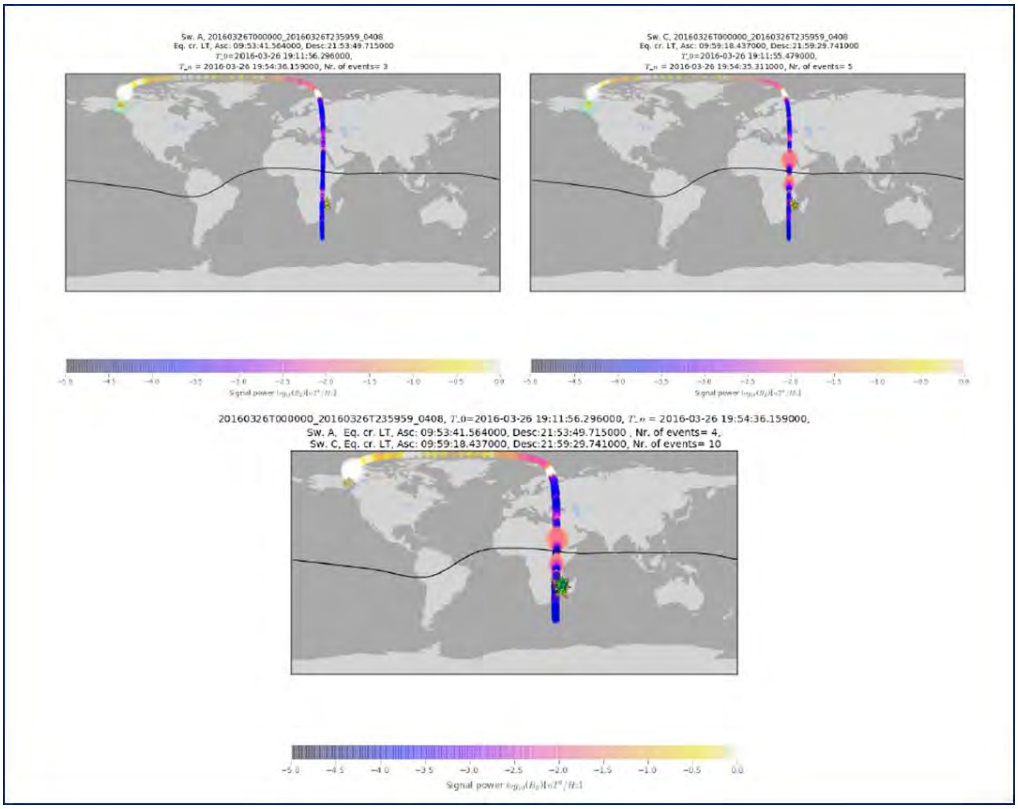

Fig. 3.62. Location of tracks and lightnings for a thunderstorm in Africa on March 26, 2016

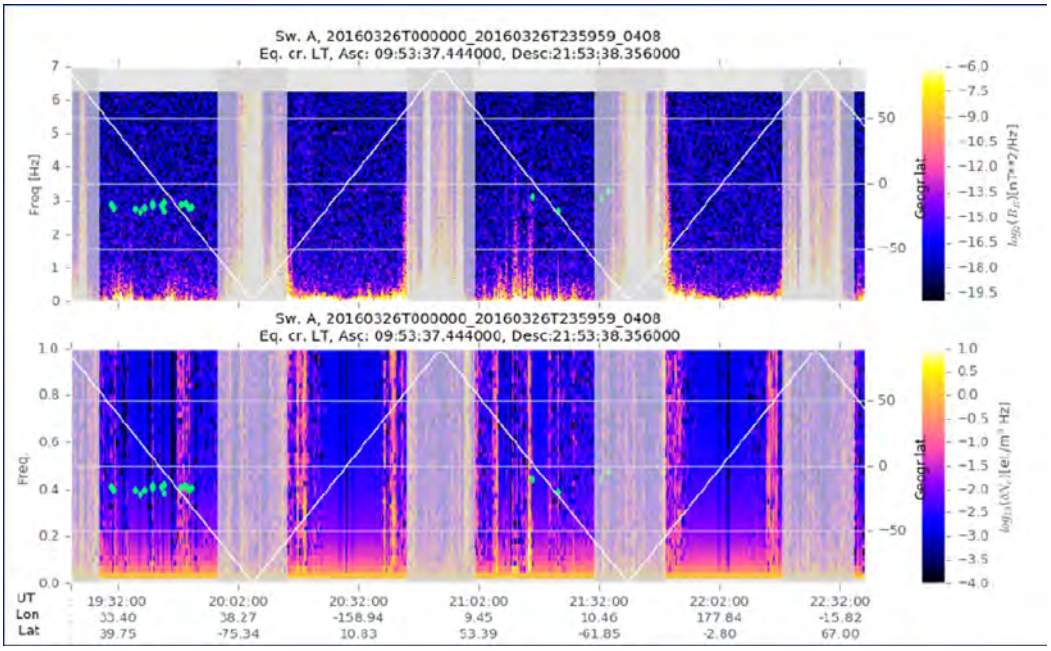

Fig. 3.63. Dynamical spectrograms (δB - top panel, δNe – bottom panel) for selected passes of Swarm A over active African thunderstorm center.

Similarities: Presence of energetic electrons

Strong variations of the electron density and temperature, Turbulence seen in the electric and magnetic fields as well as in plasma parameters.

Differences: Globality vs. Locality.

Satellite Detection of Ionospheric ULF Magnetic Field Fluctuations Caused by Lightnings (Strumik et al. 2021) M. Strumik, J. Slominski, E. Slominska, J. Mlynarczyk, J. Blecki, R.Haagmans, A. Ku-lak, K. Martynski, R. Wronowski.

One can expect that electromagnetic fluctuations caused by lightnings can propagate from the lower atmosphere higher into the ionosphere, which is an ionized and electrically conducting medium. This process however requires conversion of the electromagnetic perturbation propagating in the neutral atmosphere into an ionospheric plasma wave, which for so called ultra low frequency (ULF) regime can attenuate strongly the wave amplitude. The attenuations are considered to be so significant that one could argue that it is virtually not possible to observe ionospheric magnetic field perturbations caused by lightnings using currently available satellite magnetometers.

There are many remote observations of lightnings and direct satellite measurements of ionospheric magnetic field fluctuations, that can be analyzed searching for a possible link between the two phenomena. Using two types of lightning observations and Swarm satellite measurements, we provide an evidence that lightnings can generate electromagnetic perturbations that propagate into the ionosphere and can be measured with magnetometers onboard low-Earth-orbit satellites, e.g., by the Swarm constellation. We reveal links between lightnings and ionospheric wave properties, that suggest a real causality relationship between the two phenomena. To our knowledge this is the first direct experimental confirmation of such a relation in the ULF range.

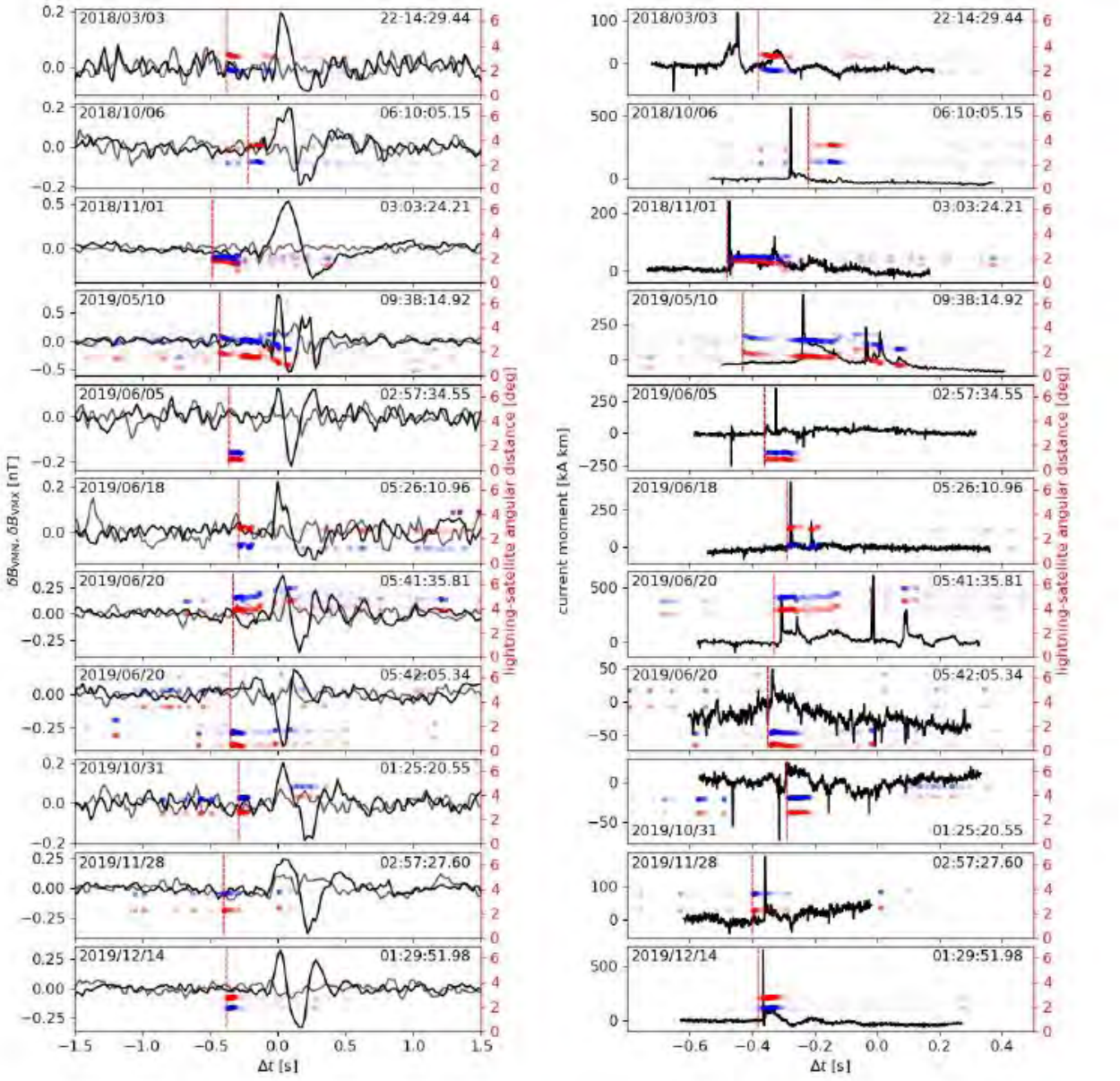

Fig. 3.64. A juxtaposition of Swarm-GLM (left column) and GLM-WERA observations (right column).

Connections between electromagnetic signals generated by Mesoscale Convective Systems, observed by an ELF ground station and DEMETER satellite **(Martyński et al., 2021)**. J. Błęcki, K. Martyński, A. Kułak, J. Młynarczyk, R. Wronowski, R. Iwański.

In recent days intensified thunderstorm activity in Europe is observed, both for the number of appearances and intensity. It is especially visible in summer time, when there is an advection of warm maritime air from west. The advection of air masses is enriched by water vapour, which source can be found over the Mediterranean Sea. In propitious atmospheric conditions, thus mentioned above thermal conditions and significant convection, atmospheric instability or strong vertical thermal gradient lead to the development of strong thunderstorm systems. In this paper, Mesoscale Convective Systems (MCS)(Bonner 1968, Banta i in. 2002, Houze 2014), cases are discussed it is believed that they belong to the strongest storm phenomena that have been ever registered on Earth. Their genesis can be found in strong developed Cumulonimbus clouds, which may cover up an area above 100 000 km2. MCSs are able to generate strong atmospheric discharges or significant precipitation of rain and/or hail. (Chomicz, 1951) and significant wind blows, often exceeding 150 km/h. Identification of the MCS is a complex process, due to many variables, which have to be taken into account. These parameters are responsible for positive verification of this phenomenon. CAPPI belongs to this parameters - cloud reflectivity. This product is based on satellite data in IR spectrum (Maddox, 1980), atmospheric soundings or measurements from PERUN system based on detectors in VHF range (Very High Frequencies 113.5 – 114.5 Hz). Mentioned tools allowed to identify two MCSs, that had happened in Poland in 23th of July 2009 and 24th of May 2010. We would like to emphasise, that selection of these cases is not random. Both of them were designated due to correlation between DEMETER flybys and measurements from the ELF

(Extremely Low Frequencies) Hylaty station, placed in Bieszczady mountains (Kulak et al., 2014).

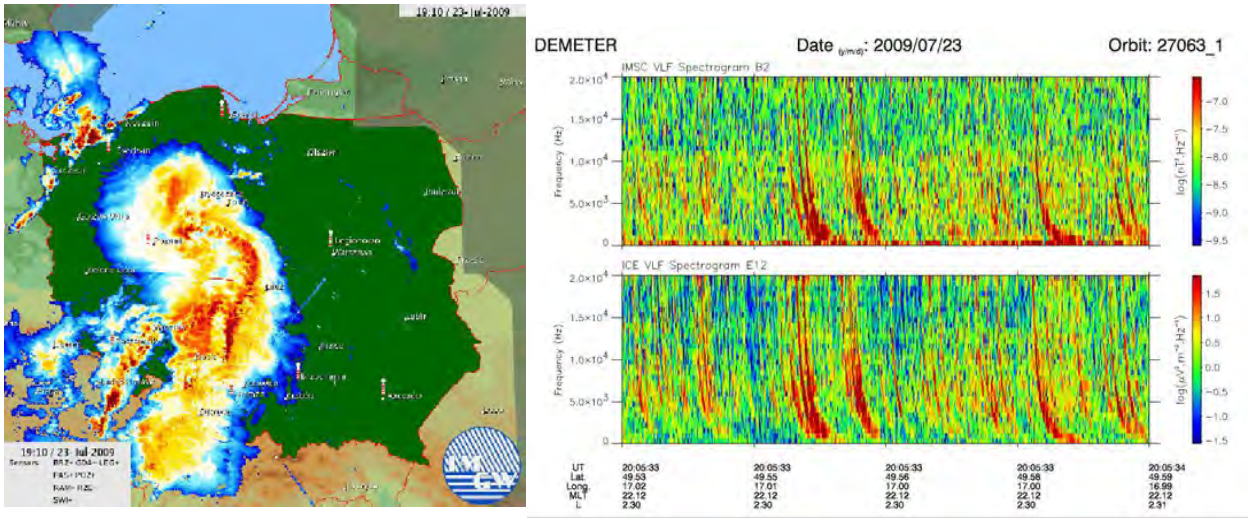

Fig. 3.65.

Comparative study of the energetic electrons registered together with the broad band emissions in different regions of the ionosp**here (Błęcki et al. 2020)**
J. Błęcki, R. Wronowski, J. Słomiński, S. Savin, R. Iwański, R. Haagmans.

The main reservoirs of energetic particles in the Earth's environment are radiation belts (Van Allen belts) within the magnetosphere. Nevertheless, fluxes of electrons and ions with high energy are registered in many other places of the space surrounding the Earth, even in the atmosphere. The origin of these fluxes is different and, some originate from a distant astronomical object even outside our Galaxy. These are galactic cosmic rays. Some of them originate from the Sun and are solar cosmic rays. In this paper, we will present observations of energetic particles together with ELF/VLF/HF plasma waves as a result of the plasma processes going on in the vicinity of Earth. The plasma waves are the most general feature of the plasma environment. These play an important role leading to anomalous processes like diffusion, resistivity, energy redistribution and particle acceleration in collision free space plasma. Different

types of waves are present in different regions of space. These are one of the characteristics of these regions with different particle populations. One of the most interesting regions is the polar cusp. Plasma particles from the magnetosheath directly enter there. The primary types of wave emissions observed in the polar cusp region are: broadband ULF-ELF magnetic noise, whistler mode bursts, broadband electrostatic noise, electron cyclotron harmonics waves, auroral hiss, and auroral kilometric radiation. Earlier observations of waves in the polar cusp originate from Hawkeye - in the outer cusp, from Viking in the middle cusp, and from Freya and DE-1 in the lower cusp. These indicate the presence of Alfven, lower hybrid, electron and ion cyclotron waves as the most typical modes in this region of the magnetosphere Later, the Polar, Interball and Cluster satellites enabled the discovery of the presence of high energetic particles (electrons and ions) in the polar cusps. Strong wave activity is associated with this population of plasma particles. Further analysis of the plasma waves and energetic particles by DEMETER satellite in the ionosphere at the altitude 660 km shows the presence of the fluxes of energetic electrons together with plasma waves in other areas as the ionospheric trough and over thunderstorms areas. The analysis of data from Swarm satellites gave the additional information about ULF/ELF waves together with plasma parameters- electron density and temperature in mentioned regions of the ionosphere.

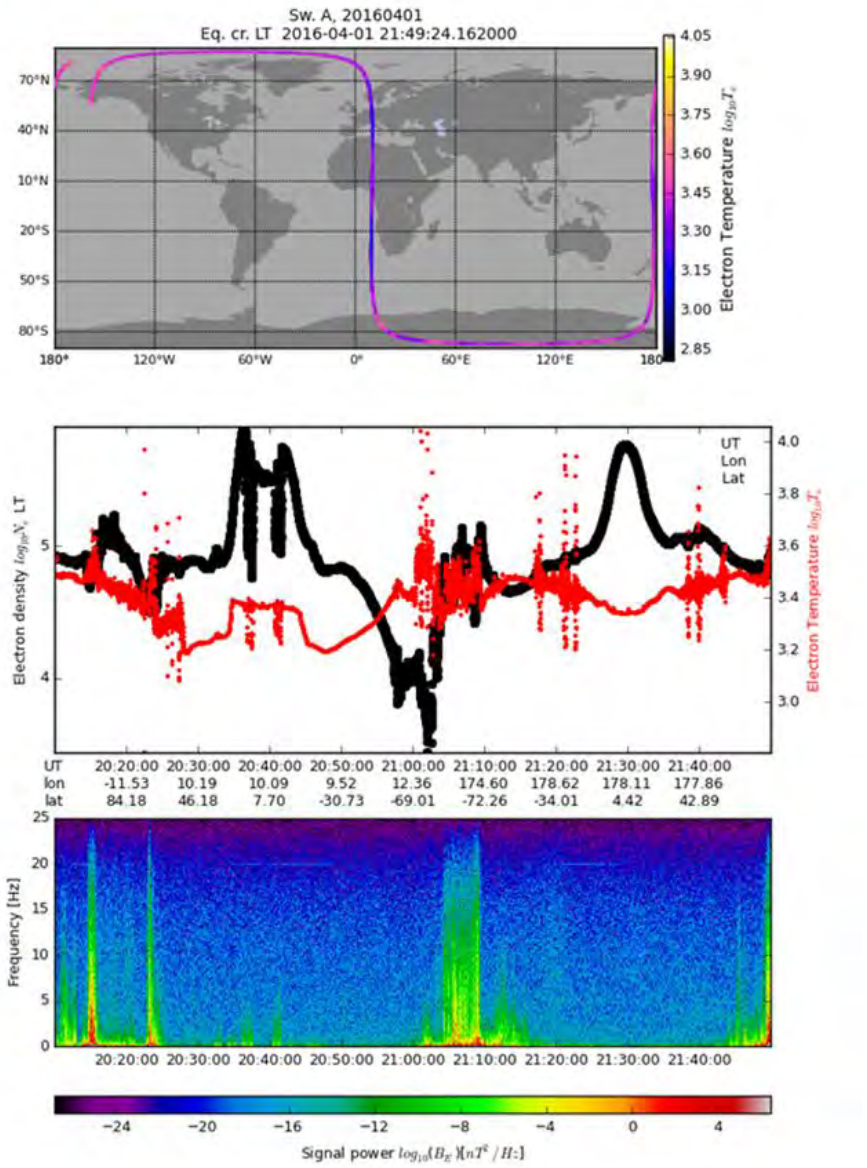

Fig. 3.66. A plot of electron temperature along a complete Swarm A satellite orbit (upper panel) on April 1 2016. The values of the temperature measured along the orbit are shown by dots with different colors. Measurements of the electron temperature (red line) and concentration (black line) are presented in the middle panel. The bottom panel shows the dynamic spectrogram of the magnetic field variations.

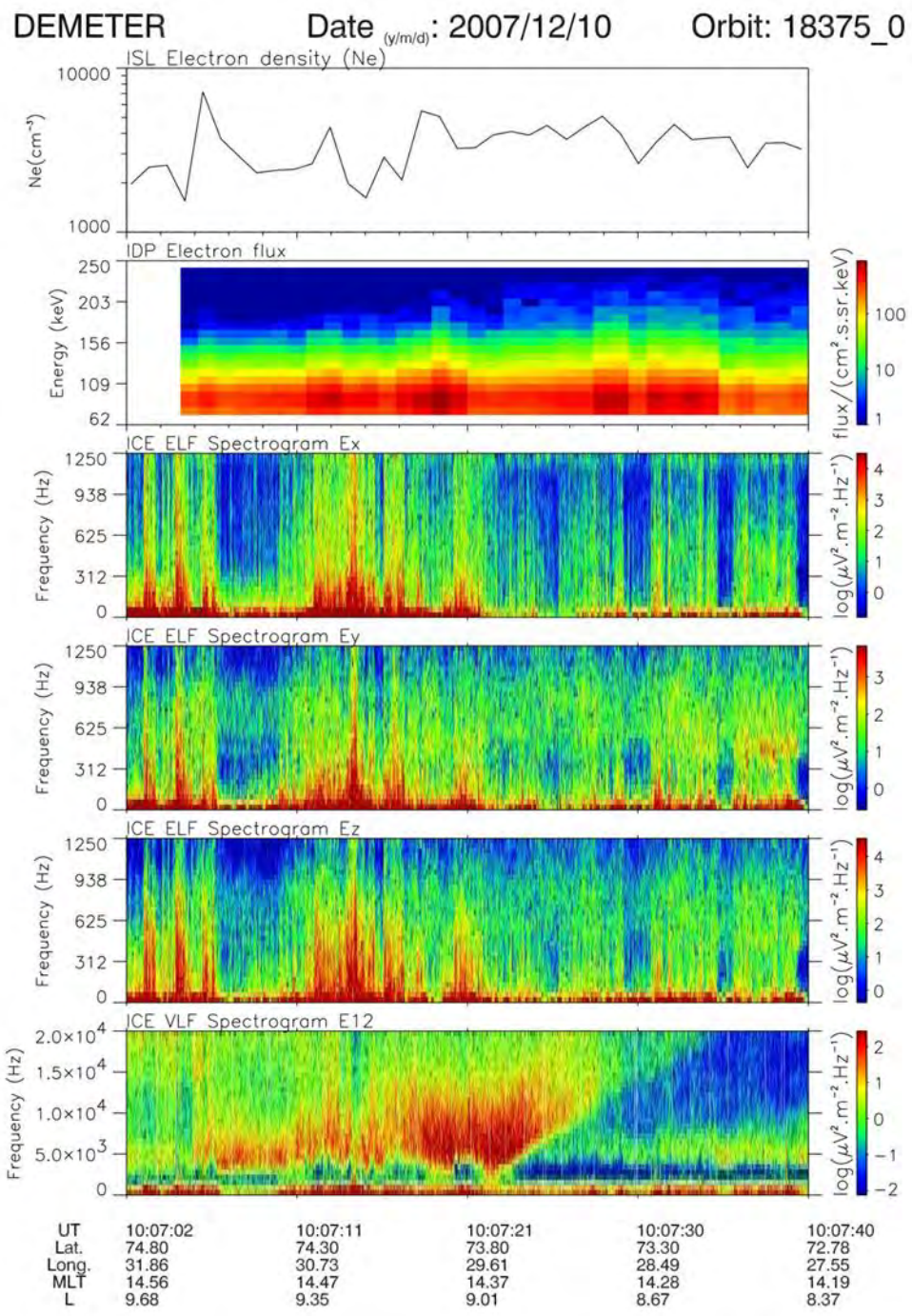

Fig. 3.67. Electron density (upper panel), spectrogram of electron energy (second panel) and wave spectra of three components of the electric field in the ELF range and one component in the VLF range (4 bottom panels) observed by DEMETER in the polar cusp at ionospheric altitude.

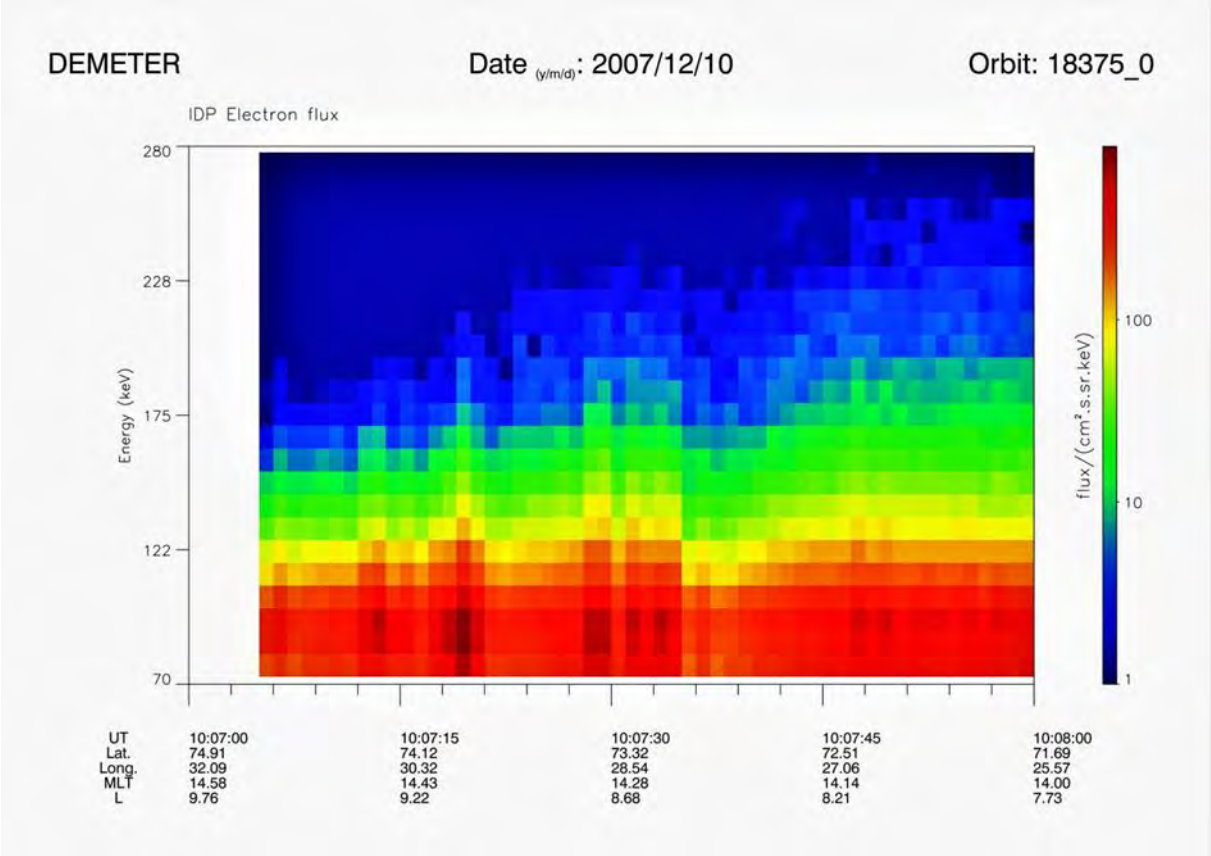

Fig. 3.68. Spectrogram of electron energy from DEMETER in the polar cusp. Fluxes of electronselectrons with energy up to 230 keV are seen at 10:07:16, 10:07:30 and 10:07:45 until 10:08:00 UT The beams of electrons can be distinguished at 10:07:13, 10:07:18, 10:07:29, 10:07:33 UT around energy 80-–90keV.

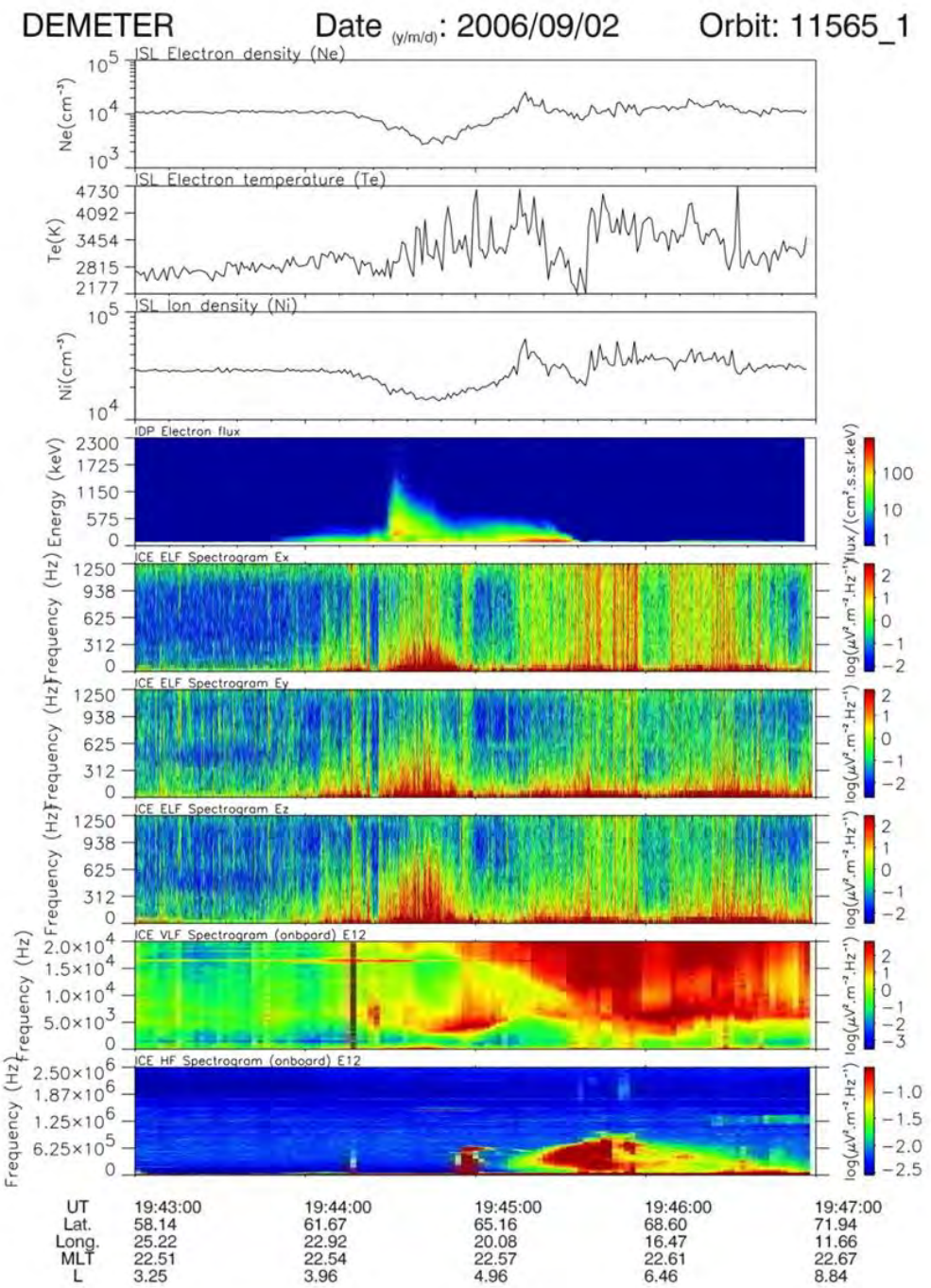

Fig. 3.69. The measurements (from top to bottom) of the electron density, electron temperature, ion density, spectrogram of the electron energy, spectrograms of the electric field variations – three components in ELF, one component in VLF and one in HF frequency range. The entry of DEMETER satellite in the ionospheric trough was around 19:44:00 and exit around 19:45:00 UT.

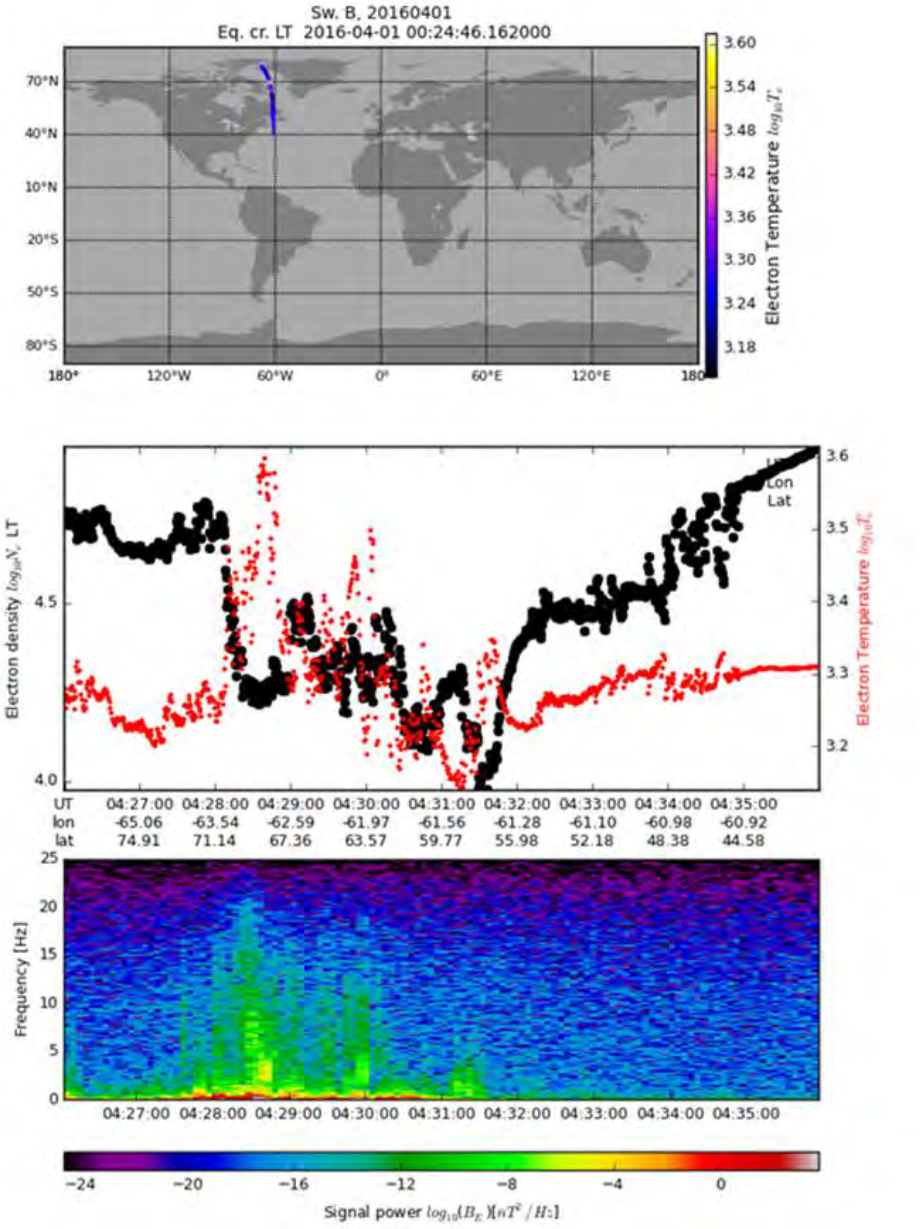

Fig. 3.70. The trough crossing by the Swarm B satellite. The upper panel shows the part of orbit related to measurements presented in the middle and bottom panels. The colors of dots along the orbit correspond to the value of the electron temperature. The plots in the middle panel represent the electron concentration (black line) and temperature (red line). The bottom panel gives the spectrogram of the magnetic field variations.

Collisionless Plasma Processes at Magnetospheric Boundaries: Role of Strong Nonlinear Wave Interactions (Savin et al. 2019) S. Savin, J. Błęcki et al.

Interaction of the variable solar wind (SW) plasma flow with the Earth's magnetosphere leads to the formation of the bow shock, turbulent magnetosheath downstream and magnetopause. The resulting turbulence often becomes non-equilibrium one, non-steady and intermittent, accompanied by plasma jets with the dynamic pressure higher than that of the unshocked Solar wind . The low frequency eigen modes in the region bounded by the bow shock and magnetopause range from surface and cavity/waveguide modes (0.2–10mHz) to ion cyclotron fluctuations (0.05–0.5Hz).

An analysis of the registrations done by INTERBALL-1, CLUSTER-4 and DOUBLE STAR TC1 shown the presence of the sunward Poynting flux throughout magnetosheath and foreshock and its correlation and bi-correlation with the dynamic pressure of the solar plasma flow. It demonstrates, for the first time, that perturbations, caused by the resonances in the magnetospheric boundary layers, propagate upstream towards the bow shock as the short impulses of the sunward Poynting flux, which excite the strongest 3-wave resonances.

They are initiated in the foreshock and regulate the bow shock surface oscillations. Another interaction zone near the magnetopause assists plasma flow extra deflection and acceleration around the magnetopause. At the outer boundary of stagnant cusp the turbulent barrier can separate the flowing and stagnant plasmas namely by the 3-wave cascades. So, both experiment and MHD modeling demonstrate the leading role of the discovered waves and nonlinear processes in the collisionless interaction of the plasma flow and magnetic barrier.

Recent studies have analyzed the waves and resonances at about 0.8–10mHz and their propagation toward ionosphere. Impacts of interplanetary shocks with the magnetosphere can produce dynamic pressure pulses and waves, propagating upstream from MP to BS. The excitation of the resonances from MP to BS has been identified as triggered by the short wave impulses with the sunward

Poynting flux. First time it was detected near MP by INTERBALL-1 and CLUSTER. It was proposed that (with the 3-wave interactions) these impulses can trigger strong jets in MSH flowing around MP, which reduces the normal to MP flow in its vicinity down to the Alfven speed, thus creating, e.g., conditions for sunward motion of the MP . The sunward Poynting flux bursts could trigger surface waves at BS, which in turn modulate the jet production at the BS, deformed by the surface waves. The sunward – propagating electric field impulses can also decelerate the MSH plasma in the vicinity of MP in the Sun-Earth direction by the ion finite-gyroradius effects and inertial drift.

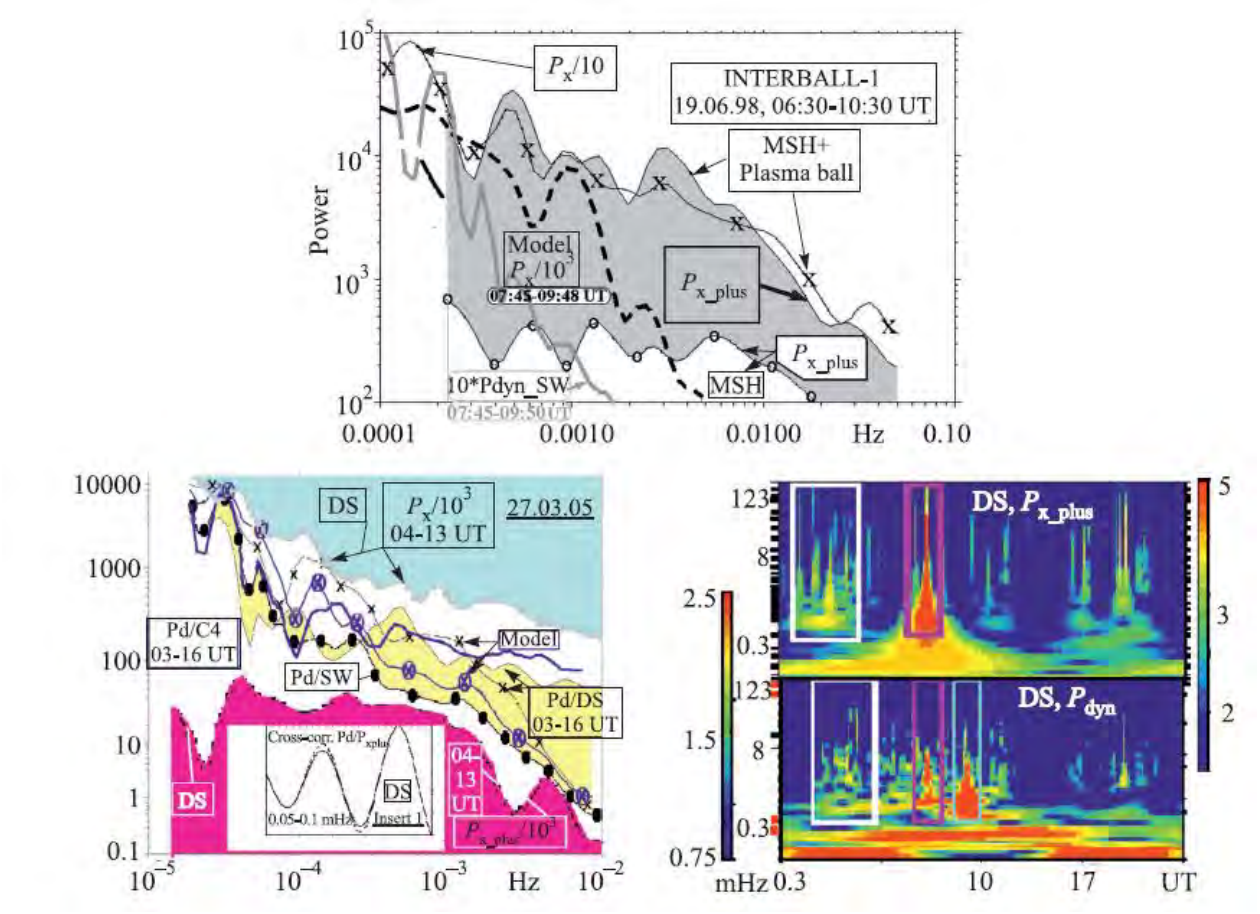

Fig. 3.71. Analysis of the data gathered in the vicinity of bow shock.

GALACTIC COSMIC RAYS A. Gil-Świderska

In galactic cosmic rays (GCR), measured by the neutron monitors (NMs) (e.g., Simpson, 2000) around the whole Globe (www.nmdb.eu), there was detected a new type of the GCR changes, i.e. anisotropic cosmic-ray enhancement, ACRE (Gil et al., 2018). It was apparent as a small enhancement (≤ 5%) in the polar NMs count rates during 12 - 19 UT on 07 June 2015 (Fig. 3.72). The increase was immensely anisotropic, as was observed only by NMs with asymptotic directions in the southwest quadrant in geocentric solar ecliptic (GSE) coordinates. The heliospheric conditions were moderately disturbed, as

the heliospheric magnetic field strength progressively increased during the event, followed by a growth of the solar wind speed after the event. It was proposed that the ACRE event was linked to a crossing of the boundary layer between two regions with different heliospheric parameters, with a strong gradient of low-energy particles.

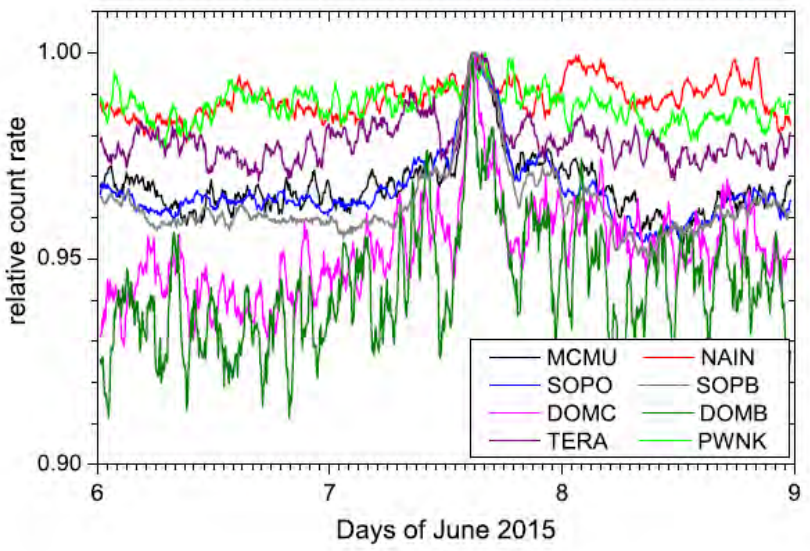

Fig. 3.72. Normalized smoothed NMs count rates smoothed by the 45-minute running average and normalized to unity on 15:00 UT 7 June 2015 (from Gil et al., 2018).

An adjustment of a method of assessment of GCR variability over different timescales, using energy-integrating NM and cosmogenic isotopes ^{10}Be and ^{14}C stored in natural archives, was performed. A redefinition of an effective energy of a detector was proposed (Asvestari et al., 2017; Gil et al. at COSPAR 2018, EGU 2018). A revision of Ground Level Enhacement, GLE, data base was accomplished (Usoskin et al., 2020). An update of neutron monitor yield function was computed and extended to different atmospheric depths (Mishev et al., 2020).

The nature of the solar rotation recurrence of GCR during various epochs of solar activity was discussed (Gil and Mursula, 2018) based on the

comparison of two exceptional intervals: August 2014 - March 2015 and September 2007 - June 2008. During the first interval (near solar maximum) the GCR intensity measured by NMs presented a very strong changeability with a rather long solar rotation period of 28.9 days (Fig. 3.73a). It was shown that the enhanced solar rotation GCR variability was linked to the large and longitudinally asymmetric, covering a wide range of latitudes the southern polar coronal hole. In the case of the second interval (near solar minimum) the GCR variation period was shorter: ~27.5 days (Fig. 3.73b). During that time a low-latitude coronal hole caused the exceptional recurrence. It was presented that the physical mechanisms of coronal holes affecting cosmic rays are somewhat different in the two studied cases: convection in 2014–2015, and convection as well heliospheric current sheet structure in 2007–2008. Moreover, the polarity and rigidity dependence of the 27-day variations of GCR detected in the data from space missions: PAMELA and ARINA (Modzelewska, et al., 2020a), ACE/CRIS, STEREO, SOHO/EPHIN (Modzelewska and Gil, 2021) was examined.

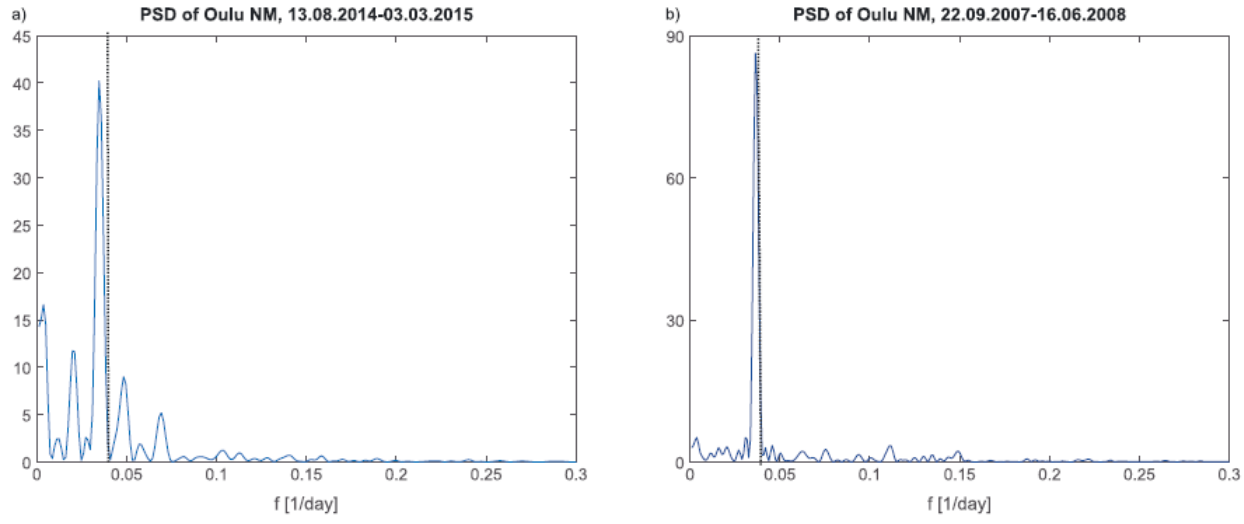

Fig. 3.73. Power spectrum density of Oulu NM count rates during 13 August 2014-3 March 2015 (a) and 22 September 2007 - 16 June 2008, where at x axis is frequency in unit of 1/day with dotted vertical line marking the frequency corresponding to the period of exactly 27 days (from Gil and Mursula, 2018)

An existence of a stable long-living active heliolongitudes was confirmed by the behavior of the 27-day variation of the 3-dimenssional anisotropy of GCR (Modzelewska and Alania, 2018). There was distinguished a tendency of the 22-year changes in the amplitudes of the 27-day variation of the 2D anisotropy (connected with the solar magnetic cycle) and the 11-year (solar cycle) in the amplitudes of the 27-day variation of the north-south component of the anisotropy.

Properties of the GCR variations and related heliospheric modulation parameters for solar cycle 24 and solar minima 23/24 and 24/25 were derived from neutron monitors data (Modzelewska, et al., 2019) and muon telescopes observations (Ahluwalia and Modzelewska, 2020). The role of the drift effect in the temporal changes of the GCR anisotropy and the influence of the sector structure of the heliospheric magnetic field on it was analyzed (Modzelewska et al., 2019). It was shown that in the solar minimum 23/24, in 2007 - 2009 (qA<0), the drift effect wasn't clearly observable in the changes of the radial component, i.e. diffusion dominated model of GCR transport was more suitable. Around the solar minimum 24/25, in 2017 - 2018 (qA>0), the drift effect was evidently manifested.

There was presented the stochastic simulation of GCR particles heliospheric transport based on the solution of the Parker transport equation (Parker, 1965). Both approaches: the forward- and backward-in-time (Fig. 3.74) were applied showing their full comparison in various dimensions for the first time (Wawrzynczak et al., 2018, and at COSPAR 2018).

It was proposed that the quasi-biennial oscillations of GCR (QBO) originates from solar differential rotation. As countless intermediate heliolatitudes rotate with different tempo from 25-27 at the equator to 35-37 days at pools, the effects created on the Sun, being carried by various field lines, might interfere with each other producing oscillations varying from 0.30 to 3.65 years (Gil and Alania 2018, and at COSPAR 2018, ICRC 2019).

Based on heliospheric parameters analysis and PAMELA (a Payload for Antimatter Matter Exploration and Light-nuclei Astrophysics) observations of cosmic rays it was established that in the rising phase of the solar cycle 24 in all analyzed parameters appeared some wave packages, periodically enhanced, averagely each 1.5-2 years, suggesting the occurrence of the quasi-biannual oscillations (Modzelewska et al., 2019).

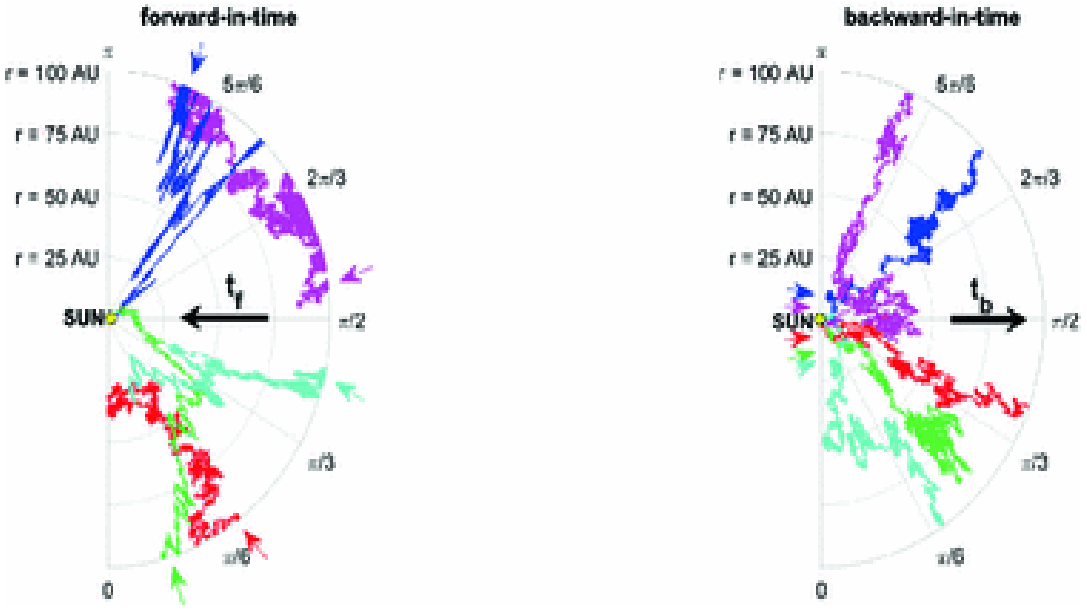

Fig. 3.74. Pseudoparticles trajectories projected on a two-dimensional plane in the forward- and backward-in-time approach with marked initial position of pseudoparticle by an arrow in color corresponding to trajectory's color and the black arrow signalized how time passes from the 'pseudoparticle perspective'. In the backward scenario, all pseudoparticles start from the same point (from Wawrzynczak et al., 2018)

There was shown the existence of varying delay times between the changes of GCR intensity and the parameters characterizing solar activity, such as sunspot number and tilt angle, especially different delay times in epochs with different global solar magnetic field polarities were recognized (Iskra et al., 2019; Siluszyk, et al. 2020). The existence of a varying delay time in Solar Cycles 21 and 23 was proved theoretically.

Temporal changes of the resonant frequency, f_{res}, of GCR protons in the heliospheric magnetic field turbulence in relation to solar activity are mainly caused by variations of the induction of *B* components from year to year, while the contribution of the solar wind speed remains insignificant (Siluszyk et al. 2018).

All of the above described studies show various aspects of solar behavior mirrored in cosmic rays flux (Fig. 3.75).

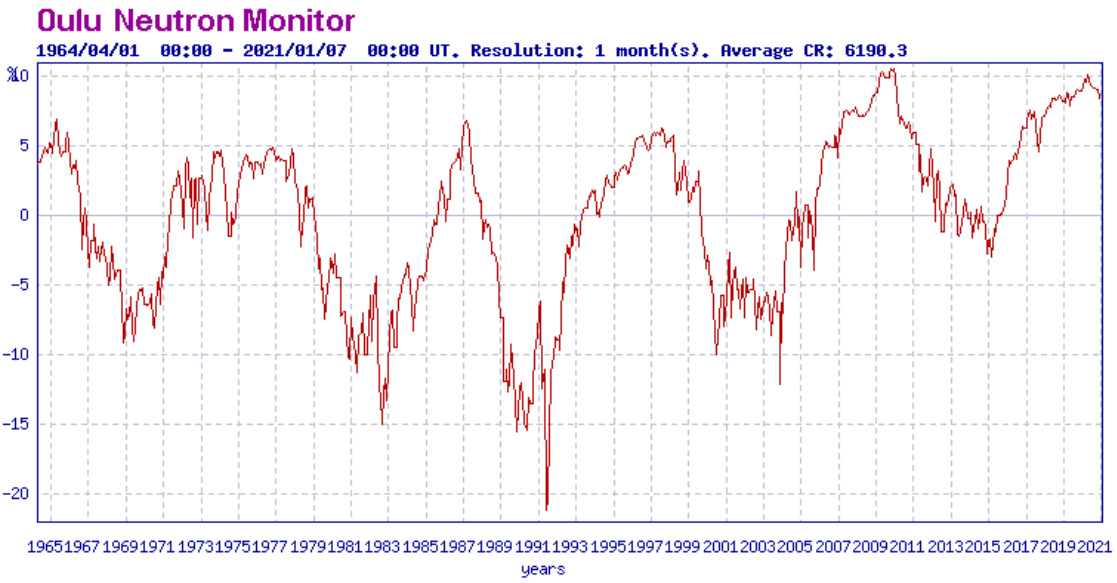

Fig. 3.75. Cosmic rays measured by Oulu neutron monitor from 04.1964 to 01.2021 with clearly visible anticorrelation with solar activity (cosmicrays.oulu.fi)

The analysis of the time variations of the near-surface air temperature in Poland and in Tbilisi for period of 1881–2016 (Modzelewska, et al., 2020b) showed that the centenary changes of temperature (global warming effect) generally is related with the changes of solar activity. It is a confirmation that Poland and Tbilisi data show the same relation with solar activity as already existed in literature.

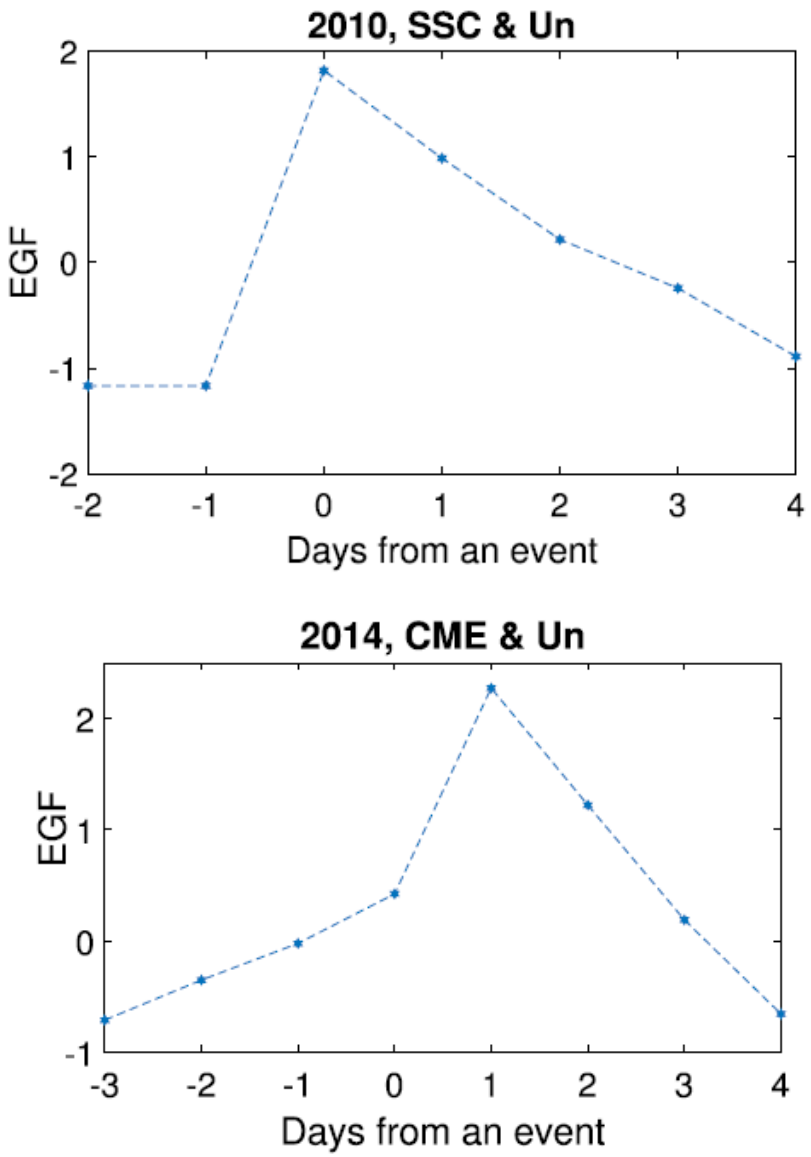

Fig. 3.76. The superposed averaged numbers for electrical grids failures (EGFs) having unidentified reasons (Un) with a key time connected to sudden storm commencement (a) and fast halo coronal mass ejecta occurrence (b) in 2010 (a) and in 2014 (b) (from Gil et al., 2019b)

Studies presented below were performed in the frame of the project founded by the Polish National Science Centre (grant no. 2016/22/E/HS5/00406) are devoted to the direct impacts of space weather effects. The impact of space weather events on energy infrastructure via

geomagnetically induced currents (GICs) is very well known and widely studied since, at least, Quebec blackout on 13rd of 15 March 1989 (e.g. Bolduc, 2002). Those effects were not very extensively studied in relation to Polish energy infrastructure. Pulkkinen et al. (2005), describing the Halloween Storm's aftermath mentioned an episode on SwePol Link cable connecting, under the Baltic Sea, Polish and Swedish energy infrastructure. Comparison of the total number of electrical grids failures which might be of solar origin in southern Poland, near the solar minimum (2010) and around the solar maximum (2014), showed that the number of failures was twice greater in 2014 than in 2010 (Gil et al., 2020a). It might be an indicator of solar cycle phase dependence (Gil et al., 2019b, and at COSPAR 2018, EGU 2018). The growth of the superposed averaged number of transmission lines failures appeared around one day after the fast halo coronal mass ejecta occurrence, as well as on the day of sudden storm commencement (Gil et al., 2019ab) (Fig. 3.76). Analysis of the geomagnetic storm that happened on 15 July 2012 during the 602nd anniversary of the Polish Battle of Grunwald (the proposed name: "Battle of Grunwald Day Storm") showed a significant growth in the failures of the Polish electric transmission lines, which might have a solar origin (Gil et al., 2020b). Using various mathematical and statistical methods, among them neural net clustering, it was demonstrated that there exist links between groups of the parameters characterizing the state of Earth vicinity during strong magnetic storms (Siluszyk et al., 2019).

3.4 Planetology and Solar System Dynamics

Comet 67P/Churyumov-Gerasimenko from Rosetta mission

VIRTIS – Rosetta measurements of 67P/C-G. VIRTIS-Rosetta Team including M. I. Błęcka

The simulations of spectrometric measurements of the comet 67P/C-G were restarted. Analysis of new geometric calibrations were performed and presented on EPSC 2019 by Kappel et al. entitled "*Geometric preprocessing for Rosetta/VIRTIS-M measuremens of comet 67P/C-G*".

Post-rendezvous radar properties of comet 67P/CG from the Rosetta Mission: understanding future Earth-based radar observations and the dynamical evolution of comets. E. Heggy et al. (including W. Kofman)

Radar observations provide crucial insights into the formation and dynamical evolution of comets. This ability is constrained by our knowledge of the dielectric and textural properties of these small-bodies. Using several observations by Rosetta as well as results from the Earth-based Arecibo radio telescope, we provide an updated and comprehensive dielectric and roughness description of Comet 67P/CG, which can provide new constraints on the radar properties of other nuclei. Furthermore, contrary to previous assumptions of cometary surfaces being dielectrically homogeneous and smooth, we find that cometary surfaces are dielectrically heterogeneous ($\varepsilon_r' \approx 1.6–3.2$), and are rough at *X*- and *S*-band frequencies, which are widely used in characterization of small-bodies. We also investigate the lack of signal broadening in CONSERT observations through the comet head. Our results suggest that primordial building blocks in the subsurface are either absent, smaller than the radar wavelength, or have a weak dielectric contrast ($\Delta \varepsilon_r'$). To constrain this ambiguity, we use optical albedo measurements by the OSIRIS

camera of the freshly exposed subsurface after the Aswan cliff collapse. We find that the hypothetical subsurface blocks should have $|\Delta \varepsilon_r'| \gtrsim 0.15$, setting an upper limit of ~1 m on the size of 67P/CG's primordial building blocks if they exist. Our analysis is consistent with a purely thermal origin for the ~3 m surface bumps on pit walls and cliff-faces, hypothesized to be high-centred polygons formed from fracturing of the sintered shallow ice-bearing subsurface due to seasonal thermal expansion and contraction. Potential changes in 67P/CG's radar reflectivity at these at *X*- and *S*-bands can be associated with large-scale structural changes of the nucleus rather than small-scale textural ones. Monitoring changes in 67P/CG's radar properties during repeated close-approaches via Earth-based observations can constrain the dynamical evolution of its cometary nucleus. This paper was published in October 2019 in *Monthly Notices of the Royal Astronomical Society.*

Homogeneity of 67P/Churyumov-Gerasimenko as seen by CONSERT: implication on composition and formation A. Hérique et al. (including W. Kofman)

Context. After the landing of Philae, CONSERT probed the nucleus of 67P/Churyumov-Gerasimenko (67P) and observed no heterogeneities at metric scale within the probed part of the small lobe of 67P. Further studies have then quantified the observed homogeneity in terms of maximum permittivity contrast versus the typical size of heterogeneities.

Aims. The aim of this article is to interpret the sensitivity limits of CONSERT measurements in terms of composition, and to provide constraints on the maximum variability in composition, porosity, and local dust-to-ice ratio.

Methods. The sensitivity of CONSERT measurements to local variations in density, dust-to-ice ratio, and composition was analyzed using permittivity modeling of mixtures.

Results. We interpret the maximum detectable heterogeneity size and

contrast in terms of composition and porosity of the nucleus. The sensitivity to porosity is ±10 percent points for heterogeneities with a characteristic length scale of a few meters; the sensitivity to local variations in the composition is limited. The results of our research were published in *Astronomy & Astrophysics* (October 2019)

Revisiting CONSERT results taking into account the exact lander position on the comet. W. Kofman, S. Zine and A. Hérique

CONSERT experiment measured the signals that propagated trough the small lobe of 67P/C-G comet between the lander and ROSETTA spacecraft (Kofman et al, SSR, 2007). The main observed parameters are the propagation time and amplitude of the signal at given orbital positions of the Rosetta spacecraft. The exact position of Philae lander was not known until September 2016 and before its finding we knew only the area (Herique et al, PSS, 2015) where Philae landed. Due to this we were only able, minimizing the error between the measured and simulated propagation time of the signals, to determine the average dielectric properties of the interior (Kofman et al, Science, 2015). In this work using 3D modeling of propagation (Kofman et al, Science, 2015; Herique et al, MNRAS, 2017), we determine exactly rays propagating through the comet, which propagation time have the best matches with those of the measured signals. The matching is obtained by adjusting the dielectric properties of the cometary interior, the position of the lander being fixe and exact. Based on this we determined rays, their travel, their lengths and depth of propagation, as a closest distance to the surface, and places from which signals left comet and propagated to the spacecraft. In our presentation we discuss the dielectric properties obtained for each rays some of them propagated deep inside the comet and some propagated close to the surface. The main result of present analysis is the observed variability of the dielectric properties with the depth of the cometary interior. We conclude that

close to the surface, on average within 15 m depth, the permittivities are between 1.5 to 1.86 then, below, the permittivity is lower between 1.27 and 1.4. This is the indication that the materials vary from higher density, which means or denser dust or higher dust to ice ratio close to the surface, to more ices inside (i.e. a average density that decreases inward.). There is also the possibility that the porosity increases inside the comet with depth but this is difficult to conclude only based on CONSERT measurements and probably this is less plausible while an increase in ice/dust ratio with depth is certainly possible. We discuss these results as function of possible materials composition as well as their influence on the model of the cometary interior. The results were presented at AGU general assembly, San Francisco 2019.

The interior of Comet 67P/C–G; revisiting CONSERT results with the exact position of the Philae lander. W. Kofman , S. Zine , A. Herique , Y. Rogez, L. Jorda and A-C Levasseur-Regourd

CONSERT, a bistatic radar onboard the Rosetta spacecraft and its Philae lander, was designed to probe the nucleus of comet 67P/Churyumov–Gerasimenko with radio waves at 90 MHz frequency. In 2016 September, the exact position of Philae was retrieved, within the region previously identified by CONSERT. This allowed us to revisit the measurements and improve our analysis of the properties of the interior, the results of which we present here. The relative permittivity of the materials is found to range from about 1.7 to 1.95 in the shallow subsurface (<25 m) and about 1.2 to 1.32 in the interior. These differences indicate different average densities between the shallow subsurface and the interior of comet. They can be explained by various physical phenomena such as different porosities, the possible compaction of surface materials, or even perhaps different proportions of the same materials. This strongly suggests that the less dense interior has kept its pristine nature.

ESA/Rosetta/Philae/CONSERT

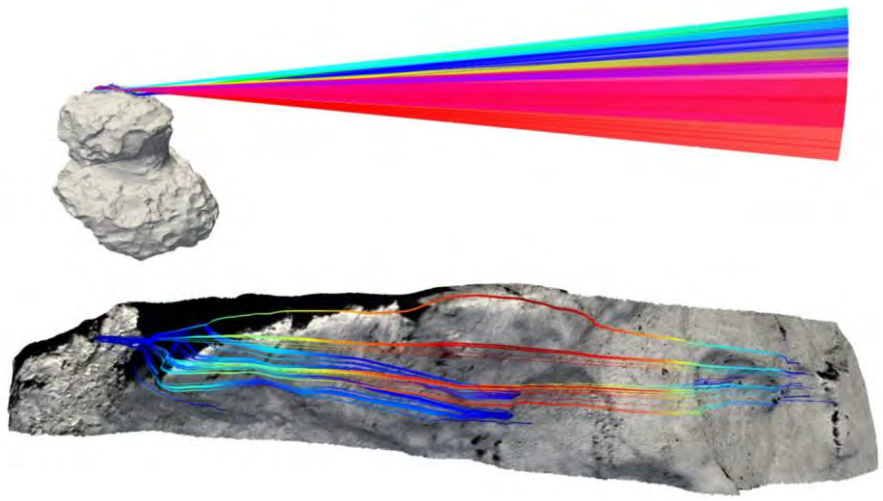

Fig. 3.77. The graphic shows the signal connecting the CONSERT instrument on Philae, on the surface of the comet, to the one on the Rosetta orbiter. The fan like appearance is a result of the motion of Rosetta along its orbit, with the colours marking the separate signal paths as the orbit evolves. The image below shows the signals in more detail, propagating inside the comet from Philae to the points from where they leave the comet to the orbiter. The curving is a result of the projection of its paths on the bumpy surface of the comet. The bluer colour indicates more shallow paths (just a few centimetres), while the redder tones show where the signals penetrated below 100 m in depth.

Paper described this research was published in the September 2020 volume of the *Monthly Notices of the Royal Astronomical Society.* This article was also disseminated through press releases on the CBK and ESA websites, on the latter website in three languages: English, Polish and French; at the end of 2020: approximately 9300 visits, see for example: http://www.esa.int/ESA_Multimedia/Images/2020/09/,

3.5 Long-period and interstellar comets – their activity, dynamics and statistics

Discovery statistics and the 1/a-distribution of long-period comets over the 1801- 2017 period. M. Królikowska and P. A. Dybczyński

The past two decades have seen a huge increase in discoveries of long-period comets (LPCs), especially those with large perihelion distances. To find out more, we collected a full dataset of LPCs discovered in the period 1801–2017, including their osculating orbits, discovery moments (to study discovery distances), and original semi-major axes (to study the ratio of large-perihelion to small-perihelion LPCs as a function of 1/a-original, and to construct the precise distribution of an 1/a-original). To minimize the influence of parabolic comets on these distributions, we determined definitive orbits (which included eccentricities) for more than 20 LPCs previously classified as parabolic comets. We found that the percentage of large-perihelion comets is significantly higher within Oort spike comets than in a group of LPCs with a<10 000 AU, and that the ratio of large-perihelion to small-perihelion comets for both groups has grown systematically since 1970 (see Fig. 3.78).

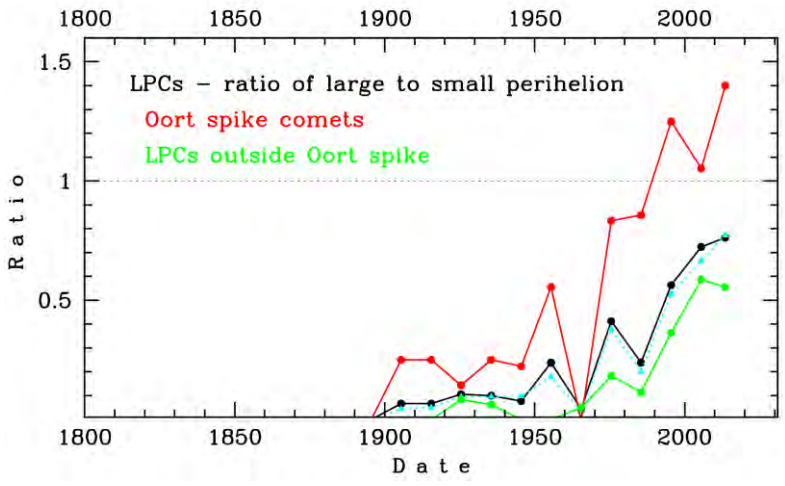

Fig. 3.78. Ratio of large-perihelion (q>3.1 AU) to small-perihelion comets (q<3.1 AU) as a function of the discovery period. The red curve shows statistics for Oort spike comets, while the green curve describes LPCs outside the Oort spike. The overall ratio for the whole sample of LPCs is plotted in black (parabolic comets not included) and cyan (including parabolic comets). These ratios were calculated for 10 year bins, except for the last bin which covers a 7-year period (from 2011 to 2017).

Different shape of the Oort spike for small-perihelion and large-perihelion LPCs is also discussed. Additionally, we observed a spectacular decrease in the ratio of large-perihelion to small-perihelion LPCs as the semimajor axis shortens to within a range of 5000–100 AU. Analysing discovery circumstances, we found that in statistical terms, Oort spike comets are discovered at larger geocentric and heliocentric distances than other LPCs. This difference in the percentage of large-perihelion comets in both groups of LPCs is probably a direct consequence of a well-known comet fading process that is due to ageing of their surface during consecutive perihelion passages and/ or reflects different actual q-distributions. A paper was published in February 2019 in *Monthly Notices of the Royal Astronomical Society.*

First stars that could significantly perturb comet motion are finally found.

R. Wysoczańska, P. A. Dybczyński , and M. Królikowska

Since 1950 when Oort published his paper on the structure of the cloud of comets it is believed that stars passing near this hypothetical cometary reservoir (named Oort Cloud) play an important role in the dynamical evolution of long period comets and injecting them into the observability region of the Solar System. The aim of our work was to discuss two cases in which the data obtained from observations were used and stellar perturbations (of different intensity, strong case of C/2002 A3 LINEAR and weaker case of C/2013 F3 PANSTARRS) on cometary motion were detected. Using the best available data from the *Gaia* DR2 catalogue and some other sources, we searched for close stellar passages near the Sun. Our study took into account that some of the stars are parts of multiple systems. Over 600 stars or systems that approached or will approach the Sun closer than 4.0 pc were found. Having the list of perturbers completed, we studied their influence on a sample of 277 Oort spike comets that were observed since 1901. We discovered that two comets might

have their orbits fundamentally changed due to a close stellar encounter. Our results show how much different the dynamical evolution of comets would have looked when their motion was considered only in the Galactic potential. Uncertainties both in stellar and cometary data were carefully taken into account. Our analysis indicates that the occurrence of stellar perturbations on cometary motions is very rare and the uncertainties of these effects are hard to estimate. The results of our work were already published in *Monthly Notices of the Royal Astronomical Society* in the January 2020 volume.

Kruger 60 as a home system for 2I/Borisov – a case study. P. A. Dybczyński , M. Królikowska, and R. Wysoczańska

At the end of August the second interstellar comet, 2I/Borisov, was discovered when it was 2.99 au from the Sun, and 3.72 au from the Earth. We searched for a candidate for its home system a month later, using orbital solution based on 548 positional measurements span over about one month. We will never be sure which star or stellar system does this comet come from but obtaining a very small relative velocity and a promisingly small miss-distance, when tracing the motion of 2I/Borisov back in time in its movement through the space, makes an encountered body a good candidate for a source of this comet. In our long-standing project on studying Oort spike comets dynamics, we recently updated a list of potential stellar perturbers of cometary motion (using *Gaia* DR2 catalogue). This list was checked against a past, close and slow encounter with 2I/Borisov. Only one object from among 647 stars or stellar systems in our list, a double star Kruger 60, appeared as a potential candidate for the origin of this comet. Later, some prediscovery positions of 2I/Borisov was found in astronomical data archives, so we repeated our calculations using more data of 2I/Borisov (1711 observations from the period 2018 Dec.13 – 2019 Nov. 2) and the results were very similar. However, a detailed analysis of radial velocity uncertainty of Kruger 60 showed, that the

probability that this binary star is a home system of 2I/Borisov is small. Finally, the usage of a new, unpublished radial velocity of Kruger 60 system practically ruled out this possibility. Two stages of our research were published in *arXiv.org* (in September and November 2019).

Non-gravitational effects change the original 1/a-distribution of real near-parabolic comets. M. Królikowska in collaboration with P. A. Dybczyński

Seven decades ago, Oort (1950) postulated the existence of a huge cloud built from billions of kilometer-sized bodies or larger. His hypothesis was based on a very small number of near-parabolic comets that visit the inner part of the Solar System. Since then, the number of such detected comets has increased tenfold, but we still know very little about the number and distribution of the objects that constitute the Oort Cloud. Our knowledge of the Oort Cloud is poor, largely because so few parameters can be derived from the observational data. The only relatively reliable information we have is a distribution of the original 1/a for the near-parabolic comets discovered so far. Moreover, to interpret this distribution realistically, we need to be able to dynamically separate new comets (that visit the inner Solar System for the first time) from the dynamically old comets because the latter have distorted orbits as a result of the earlier passages through the planet zone, in which planetary perturbations changed their semi-major axes.

This work is a part of long-standing research on origin of Oort Cloud comets. In one of our previous paper (Królikowska & Dybczyński, 2017, KD17), we investigated the dynamical evolution of Oort spike comets (original semimajor axes greater than 10,000 au) with perihelion distances exceeding 3.1 au. This selection minimized the potential effects of nongravitational (NG) forces on the comet motion. In the sample of 100 such objects, only 16% of the comets showed some deviation from the purely gravitational (GR) motion within the observed arc.

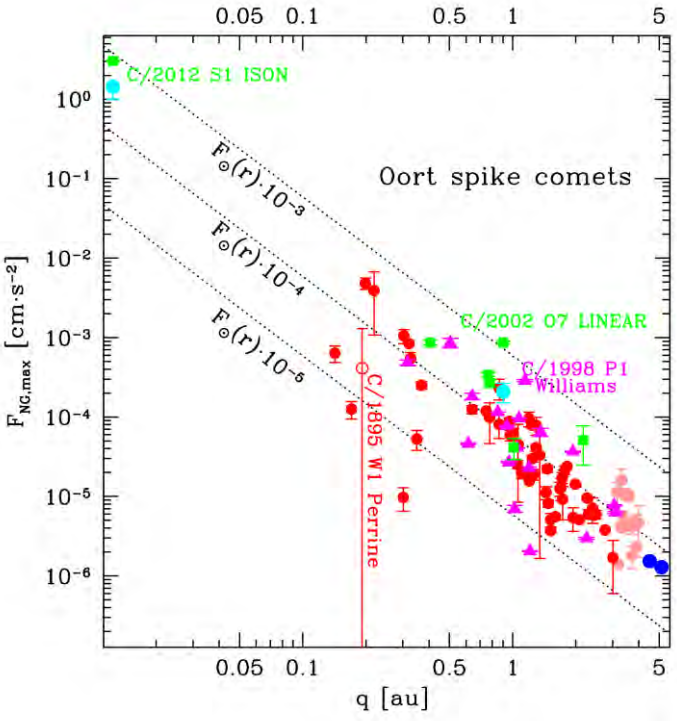

Fig. 3.79. Strength of NG acceleration acting on cometary nuclei at perihelion for the sample of Oort spike comets. Solutions obtained in KD17 are shown by light red (NG orbit based on the standard g(r)-function) and blue dots (g(r)-like function adequate for CO-sublimation). The solutions presented here are shown by green squares, magenta triangles, and red dots, all of which represent preferred solutions based on the standard g(r)-function. The two solutions marked as cyan dots represent models for comets C/2012 S1 and C/2002 O7 based on the CO-driven formula.

Here, I consider a sample of 122 long-period comets (LPCs) with small perihelion distances ($q < 3.1$ au) with original $1/a_{ori} < 0.000100$ au^{-1} for purely GR orbits. They form an almost complete sample of such objects discovered in the period 1885–2012. In this sample the NG effects play an important role. I determined NG orbits for the majority of this small-perihelion comets (78 comets). As a result, I present here a statistical analysis of the magnitudes of the NG acceleration for about 100 Oort spike comets (Fig. 3.79)

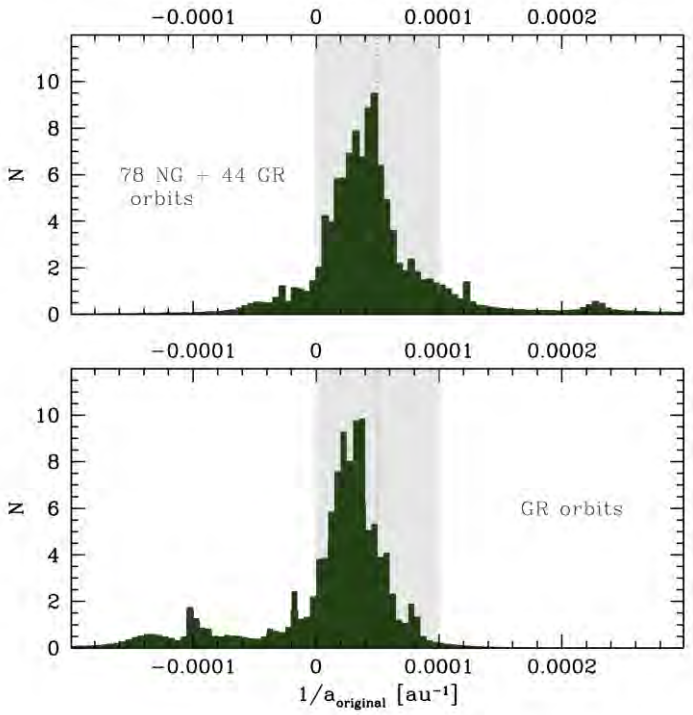

Fig. 3.80. Upper panel: Distribution of original 1/a based on preferred orbits for the whole sample of small-perihelion LPCs, where 64% are NG orbits. For comparison, the lower panel shows the origina 1/a-distribution for purely GR orbits.

By obtaining a sufficiently large sample of NG orbits for small-perihelion LPCs, it was possible to construct a distribution of $1/a_{ori}$ for an almost complete sample of these comets, 64% of which were based on NG orbits. The resulting distribution is shifted by about 10^{-5} au^{-1} to higher values of $1/a_{ori}$ compared with the distribution that is obtained when the NG effects on comet motion are ignored (Fig. 3.80). Additionally, I show the differences in the $1/a_{ori}$-distributions between LPCs with $q < 3.1$ au and those with $q > 3.1$ au. These findings indicate the important role of NG acceleration in the motion and origin of long-period comets and in the formation of the Oort Cloud. The results of this work have been published in *Astronomy & Astrophysics,* 2020.

In 2020, I continued orbital studies on Oort Cloud comets with small perihelion distances, but I was focused on those discovered in the last decade (over 20 comets from 2012-2018). In this sample of contemporary comets it was possible to determine the non-gravitational (NG) orbit for about 75% of investigated Oort Cloud comets. It is notable larger percentage of comets with determinable NG effects using positional data than for the samples of small-perihelion Oort Cloud comets discovered in 20th century. In studied sample, it was possible to distinguish many comets with extremely interesting and clearly visible NG effects in the orbital motion, the most prominent examples are: C/2013 A1 Siding Spring, C/2013 US_{10} Catalina, C/2015 G2 MASTER, C/2015 V2 Johnson, C/2017 T1 Heinze, and C/2017 T2 PANSTARRS (see Fig. 3.81). I have applied some dedicated approaches to orbit determination from available positional data for all above comets and some others with particularly pronounced or variable NG effects.

First stage of this study was finished, and the dynamical evolution of these comets over several millions of years backward and forward in time will be next studied. The project is still ongoing and at least one more publication on this topic is expected in the next years.

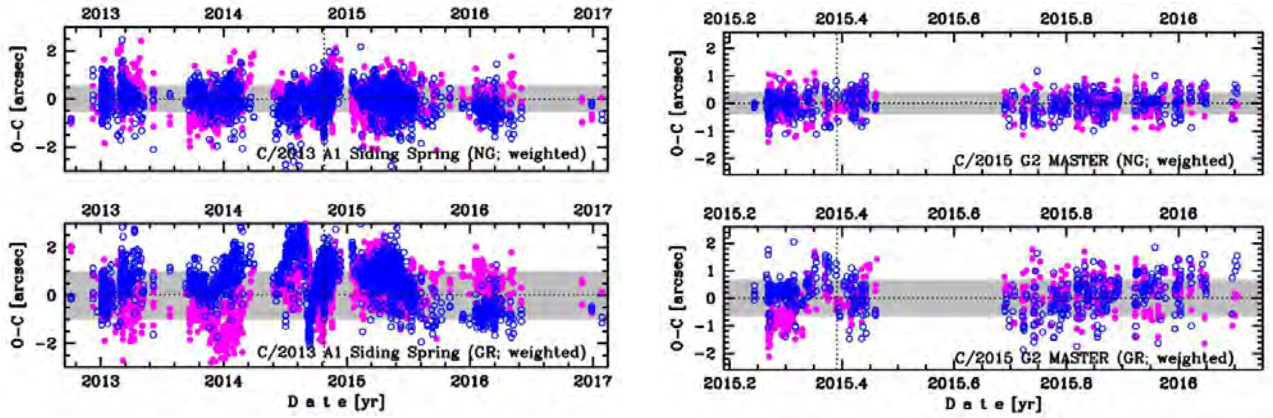

Fig. 3.81. O-C (Observed – Calculated) diagram for two investigated comets with notable NG effects in residuals, where residuals in right ascension are shown using magenta dots and in declination by blue open circles; vertical doted lines represent moment of perihelion passage. Upper panels represent NG solutions, lower panels – pure gravitational (GR) solutions. One can see large decrease of RMS (root-mean-square), between NG and GR solutions in both cases (magnitude of RMS is represented by grey horizontal bands around zero in O-C); however, still some trends in NG residuals in the case of C/2013 A1 (left-hand panel) are clearly visible, thus dedicated approach was next applied for this comet.

Catalogue of Cometary Orbits and their Dynamical Evolution (CODE catalogue). M. Królikowska and P. A. Dybczyński

One of the useful outcomes of the long-standing orbital study of Oort Cloud comets is a unique catalogue of the orbits of such comets discovered over the past 130 years. It was created thanks to the cooperation with Piotr Dybczyński from OAUM. CODE catalogue currently provides information about orbits of almost 300 near-parabolic comets with original gravitational semimajor axes greater than 10,000 au and discovered between the years 1885–2017.

This is the first catalogue showing orbital evolution of long-period comets during the three consecutive perihelion passages: previous – observed – next, and covering their dynamical evolution over a period of typically 1–10 million years. This is implemented in the form of five snapshots representing o*sculating orbit* (snapshot '1' at the epoch close to the moment of perihelion passage during observed cometary passage within the planetary zone), *original orbit* (snapshot '2' at 250 au from the Sun, that is before entering the

planetary zone), f*uture orbit* (snapshot '3' at 250 au from the Sun, that is after leaving the planetary zone), and p*revious* and *next orbits* (snapshot '4' and '*5*', at the previous or next perihelion passage or at the distance limit of 120,000 au from the Sun if semimajor axis is larger than this limit, respectively) (see Fig. 3.82) .

The positions of these five snapshots on a cometary trajectory are shown on the example of C/2012 T7 LINEAR orbit in the figure given below.

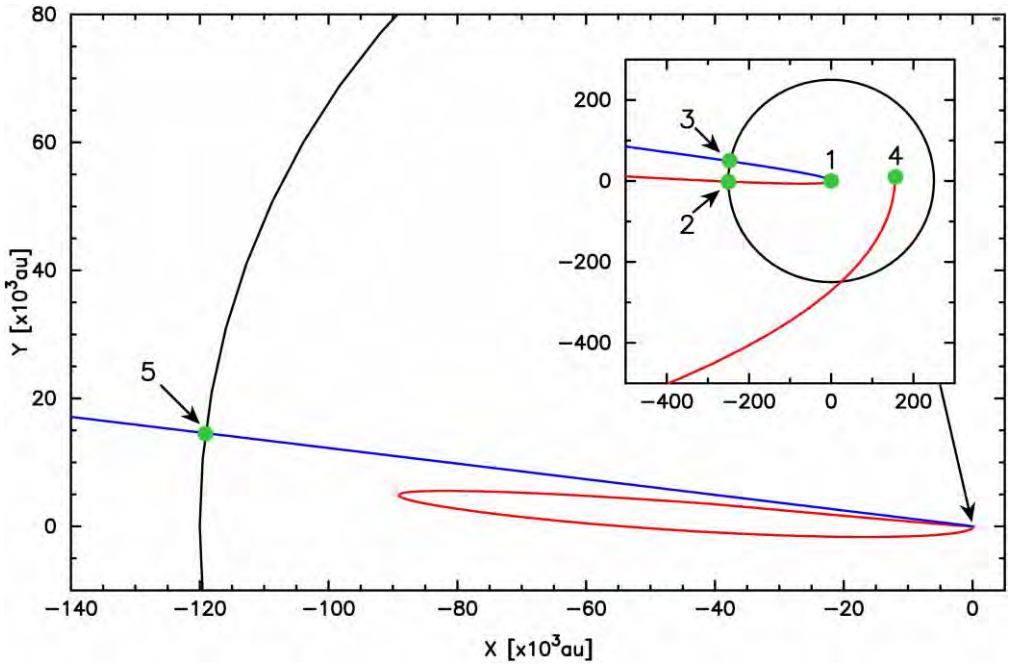

Fig. 3.82. An example of a comet dynamical evolution described in CODE catalogue. This particular plot describes orbital changes of C/2002 T7 projected on its original orbit plane. Red line depicts the past motion of this comet while the blue one depicts its future evolution. Marked are five epochs (snapshots) when orbital elements are recorded: 1 — osculating heliocentric orbit near the center of the observational interval (typically near the perihelion), 2 — original barycentric orbit recorded in past at 250 au from the Sun, 3 — future barycentric orbit recorded in future at 250 au from the Sun, 4 — previous orbit, recorded at the previous perihelion, 5 — next orbit, in this case recorded at the escape border taken at 120,000 au from the Sun, but for many other comets recorded in the next perihelion.

The second novelty is that for many of presented comets, the CODE Catalogue includes different orbital solutions, based on alternative force models or various subsets of positional data. The preferred orbit is always clearly indicated (see Fig. 3.82). Moreover, for about 100 of these long-period comets, their non-gravitational orbits are given as well as orbits obtained while neglecting the existence of non-gravitational acceleration, given for comparison.

At the moment, the CODE catalogue offers orbital solutions for almost the complete sample of comets discovered in the period 1885–2017 with an original semimajor axis greater than 10,000 au for a purely gravitational orbit. We call these objects Oort spike comets in the CODE Catalogue. Paper described CODE Catalogue was published in August 2020 in *Astronomy & Astrophysics*. Since mid-2020 on-line catalogue is publicly available on the Websites: https://pad2.astro.amu.edu.pl/comets and https://code.cbk.waw.pl/ .

Less than about twenty Oort spike comets with q<3.1 au discovered in a period 2013–2017 are still missing in CODE catalogue; however, they will be added in 2021 (see also previous research description). Then, this catalogue will soon contain the complete set of Oort spike comets discovered in the period from 1885 to 2017.

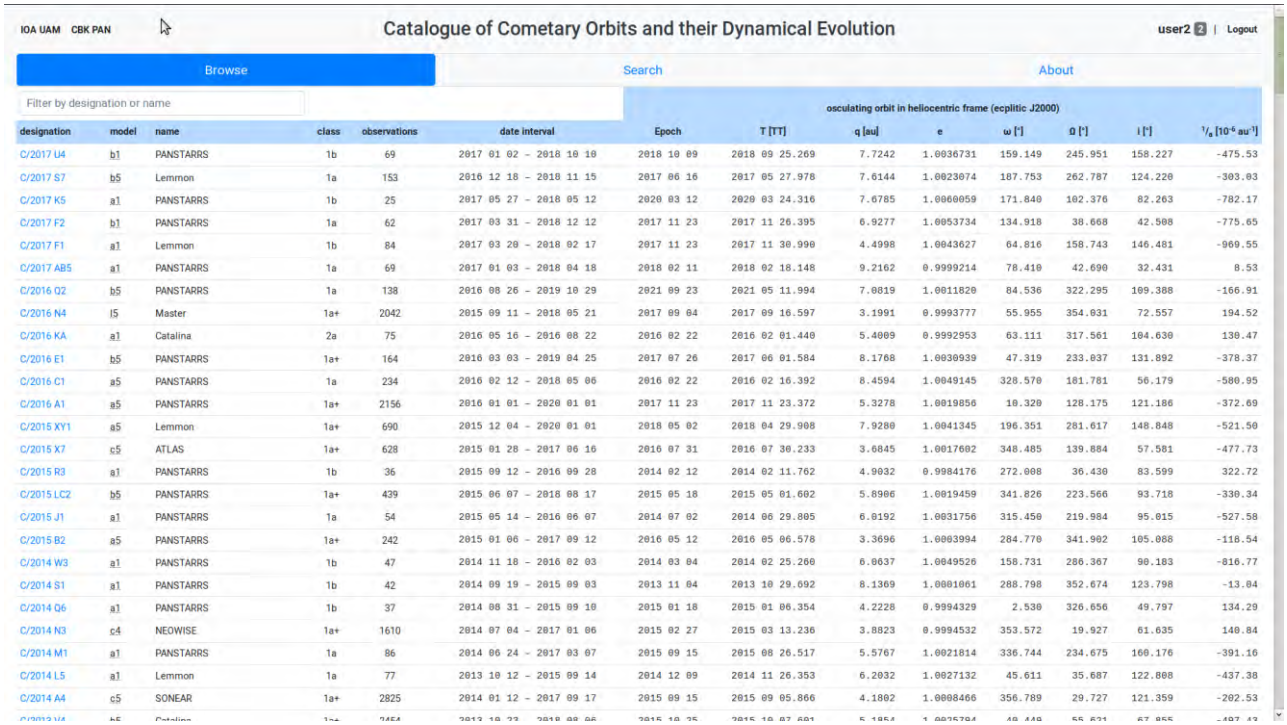

Fig. 3.83. A default view of the CODE database is Bowse mode presented in this picture.

Use of production rate curves and non-gravitation acceleration model for long-period comets. S. Szutowicz

I selected the sample of long-period comets for which photometric data and production rates measurements as well as the astrometric data were good enough to determine both the outgassing profile and the nongravitational effects. The detected production rates of volatile components (mostly H_2O and CO) of cometary nucleus provide information about outgassing as a function of heliocentric distance, *r*. The production rate detections can be completed by much more numerous the brightness measurements at the different orbital positions. However, these measurements must first be converted into the gas production rate. I derived the empirical correlations between visual magnitudes and gas production rates for each comet separately. Magnitudes measured by different observers with different instruments can differ by several units of magnitude. Thus, a special effort was

made to construct the high quality cometary light curves with a slight dispersion.

In the standard formalism the orbital calculation of the nongravitational effects is based on a special function, $g(r)$, that simulates the water production rate. However, the shapes of the cometary production rate curves differ from $g(r)$ function. Thus, the proposed non-gravitational force model relies on the observed production rates (g-like function). The non-gravitational perturbations in orbital motion of the comets are investigated based on positional observations and the modified g-like functions. Additionally, the derived non-gravitational acceleration and gas production rates are used to estimate the masses of studied comets.

Some preliminary results were presented at the conference ACM 2012 by S. Szutowicz and reported in 2012. This research is ongoing.

Self-consistent approach to light-curves of long-period comets. S. Szutowicz

The cometary activity is a strong function of heliocentric distance. When a comet approaches the Sun, the volatile species near the subsurface sublimate, dragging with them nonvolatile dust grains embedded in the ices. Thus cometary coma shines due to the presence of dust and gas surrounding the nucleus. To process the brightness measurements of comets, I have written more than 20 Fortran programs that select and reduce both visual and CCD observations. The software package allows for the uniform development of numerous photometric data of bright long-period comets. Important steps in the iterative process of observations reduction are those that lead to determination of the magnitude corrections for the instruments used by observers. In general, the comet will look fainter in a telescope of large aperture than in one of small aperture. This aperture effect varies both from comet to comet and among different instruments used by different observers.

The improved light-curve of the comet is characterized by a low scattering of observations, in contrast to the original set of brightness measurements. In the next step the reduced magnitudes are converted into water production rate using the appropriate empirical correlations. Finally, the water production curve together with the non-gravitational perturbations in orbital motion of the comet are used to estimate the mass of the studied comet. This research is ongoing and strongly related to the previous studies described immediately above.

Jan Walery Jędrzejewicz (1835-1887) and his observations of comets. M. Królikowska and A. M. Sołtan

This study was devoted to historical research on the quality of cometary observations made by Jan Walery Jędrzejewicz, a medical doctor with active practice in Płońsk and an astronomer by passion. In fact, astronomy was a second profession for `Dr. Jedrzejewicz', as he signed his astronomical publications. He built his own observatory in Płońsk, which he equipped with professional instruments. Thanks to that, he could perform precise astronomical observations. In the astronomical community, he was known and esteemed for his precise measurements of double stars. However, he also measured the position of many comets discovered at that times, including long-period ones. This study is devoted to the analysis of precision of Jędrzejewicz measurements on the examples of three long-period comets (Oort Cloud comets), today known as C/1885 X1 Fabry, C/1885 X2 Barnard, and C/1886 T1 Barnard-Hartwig. Paper on this research was submitted in 2020 to *Journal for the History of Astronomy*.

3.6 Outer solar system dynamics in a stellar cluster H. Rickman, T. Wiśniowski, P. Wajer, J. Baran, A. Morbidelli, D. Nesvorný

Hans Rickman led a research project aiming to clarify the role of the Sun's birth cluster in shaping the most remote small body populations of the solar system – generally referred to as the Oort cloud and the Inner Oort cloud. The team also includes Drs. Paweł Wajer and Tomasz Wiśniowski. In addition, PhD student Jędrzej Baran from Space Mechatronics and Robotics Laboratory was invited to participate in a related study of cluster dynamics, and two new PhD students at CBK, Błażej Kowalski and Robert Przyłuski, were accepted for studies and thesis work within our group.

Simulations of cluster evolution have been carried out using the NBODY6++GPU code, concerning a grid of four cluster models with 1,000 initial member stars assuming a 30% binary fraction. These models differ with regard to the degree of concentration assumed for the Plummer density function and the timing of the blowoff of the residual gas from the cluster. We represent each basic model by three random realizations of the initial conditions. The simulations cover 10 Myr, and in accordance with observations of embedded clusters, the large majority of our clusters are rapidly dispersed.

For each of the 12 cluster variants, we identified six randomly chosen stars as solar templates, based only on having masses very close to one solar mass. We considered eight additional cluster variants with different numbers of stars and virial ratios and for each we selected three solar template stars. We equipped each of the 96 stars with two planets, representing Jupiter and Saturn, and 4,000 planetesimals with initial orbits in the Jupiter-Saturn region.

Using the RA15 code, we simulate the orbital evolution of these objects under the influence of planetary perturbations and the dynamical effects of the cluster. Our attention is focussed on the extraction of perihelia beyond the limits of the planetary system to identify objects that might contribute to the present Oort cloud or Inner Oort cloud populations.

Our representation of the cluster effects is based on the standard procedure, whereby the gravitational potential of the cluster is separated into a smooth background field and a fluctuating component in the vicinity of each separate star. We find the smooth field by fitting a generalized Plummer density function to a time sequence of outputs from our cluster simulator. We simulate the fluctuating component by identifying the closest and strongest stellar encounters and treating the relevant stars as temporary intruders in the RA15 integrations. Most of the work performed has been devoted to developing and verifying these procedures.

Jędrzej Baran has worked on an application of our results on cluster evolution to the understanding of the so-called infant mortality of stellar clusters, *i.e.*, the evidence that a large majority of clusters do not survive the first 10 Myr. Concerning Błażej Kowalski's work, we have initialized collaboration with David Nesvorný and Alessandro Morbidelli, aiming to study Oort cloud formation in a more long-lived cluster. We will assume that the Nice Model instability and subsequent formation of the scattered disk occurred within such a cluster, and we will investigate what this would mean for the origin of the Oort cloud. Błażej will actively contribute to this project.

For Robert Przyłuski's thesis, the plan is to perform a general study of how dynamical cluster effects may influence and potentially destabilize the planetary systems of member stars. This should help to provide a background to interpret the observations of exoplanet systems and thus assist in the analysis of the forthcoming results of the ARIEL mission.

At the end of 2020, three papers are in preparation as a result of above studies:

On the Formation of the Inner Oort Cloud in an Embedded Cluster. H. Rickman, T. Wiśniowski, P. Wajer

This is intended for *Icarus* and will present our results on how the efficiency of Inner Oort Cloud production during the embedded cluster stage is affected

by accounting for the growth time of the giant planets and the possibility of very early gas expulsion. We will also point out the wide scatter of this efficiency between different solar template stars of the same cluster – something that has not been properly recognized in previous work.

Formation of Sednoid and Primitive Oort Cloud Populations in a Long-Lived Stellar Cluster. H. Rickman, T. Wiśniowski, P. Wajer

This is intended for *Icarus* and will explore the possibility that the solar birth cluster was relatively long-lived and provided a dense stellar environment at the time of the Nice Model planet instability and subsequent scattering of trans-planetary planetesimal populations. Possibly, this paper will provide a new paradigm for Oort Cloud formation.

Infant Mortality of Embedded Clusters Amplified by GMC Tide. J. Baran, T. Wiśniowski, H. Rickman

This is intended for *Monthly Notices of the Royal Astronomical Society* and will report on how the observed high mortality rate of young clusters upon gas expulsion may be explained by the curtailing action of the tidal field in a typical Giant Molecular Cloud (GMC) environment.

3.7 Long-term evolution of the Main Belt Active Asteroids

Long term evolution of the Main Belt Active Asteroids. R. Gabryszewski and P. Wajer

Solar System small bodies are conventionally named as comets or asteroids depending on their distinct observational and dynamical properties. Objects with unbound atmospheres and the dynamical parameter measured with a respect to Jupiter's orbit, the Tisserand parameter lower than 3 are known as comets, while objects without the atmosphere and having the

dynamical parameter larger than 3 are called asteroids. This standard classification is difficult to consider as complete since we can observe bodies on cometary orbits with no activity and objects on asteroidal orbits which exhibit cometary activity. The last ones are called active asteroids. These bodies have semi-major axes lower than 5 AU, Tisserand parameter larger than 3 and show the evidence of mass loss (having a comae or a tail).

Most of currently known active asteroids are located in the Main Belt, where their dynamics is driven by mean motion resonances (MMRs) with Jupiter and Saturn and υ_6 secular resonance. Yarkovsky and YORP effects are another important factors impacting small bodies dynamics in this region. Unfortunately, both the factors strongly depend on physical parameters (i.e. surface and bulk thermal conductivity, surface heat capacity, surface density, spin, shape of a body etc) which are hard to determine. Recent papers indicated detections of non-gravitational acceleration for most of active asteroids.

We want to study the dynamics of active asteroids in 2 distinct models of non-gravitational forces - first one using Yarkovsky effects, the second using the standard model of non-gravitational cometary type activity - and compare their influence on long term evolution of investigated small bodies. The research should allow us to conclude on ejection mechanisms in different parts of Main Belt, the influence of the models on the observed structure of NEO population. In 2020, numerical code has undergone a series of modifications. The first massive tests were performed. Eleven objects which show activity were chosen and non-gravitational accelerations were applied to the equations of motion to better understand their dynamical evolution. Over 450 numerical processes were performed and several dozens of charts were made for the analysis of the results. These massive tests allowed to reshape the research idea but also indicated some inconsistencies in the results which have to be explained. This research is ongoing.

The role of non-gravitational forces in orbital evolution of Encke-type comets.

M. Królikowska

Encke-type comets (ETCs) are comets moving on orbits with semimajor axes less than the semimajor axis of Jupiter's orbit ($a<a_{Jupiter}$) and Jupiter Tisserand invariant, $T_{jupiter}>3$ (all other cometary populations have $T_{jupiter}<3$). Today, more than 50 such comets are known and the current orbit of the prototype of this group, 2P/Encke, is mysteriously unique (see light red dots in Fig. 3.84). This is a very interesting area of orbital parameters, where there are a wealth of resonance possibilities and perturbations from Jupiter may still operate although they relatively weaken the further to the left of the $Q=q_{Jupiter}$ curve the studied object is. Therefore, the dynamical evolution of ETCs is still unclear in many details.

The present research aims to look at some aspects of these obscure puzzles of dynamical evolution in detail, in particular the role of non-gravitational effects (NG) in comets entry onto this evolutionary path is in focus. Four objects with very similar orbital elements were selected as a preliminary sample for this study, two of them today belong to the Encke type comets (87P/Bus and 94P/Russell 4), and the other two are classified as comets from the Jupiter family comets (JFCs: 172P /Yeung and 347P/PANSTARRS), all of them currently have $T_{jupiter}$ between 2.9 and 3.1. The value of $T_{jupiter}$ may undergo slight changes during dynamical evolution, this changes may cause the formal transition of analyzed comet from the ETCs to JFCs and vice versa. Detailed orbital evolution studies have now been carried out in the period of about 100,000 yr forward in time; for each of comet various models of motion (purely gravitational motion and non-gravitational one with various magnitude of non-gravitational forces) are applied.

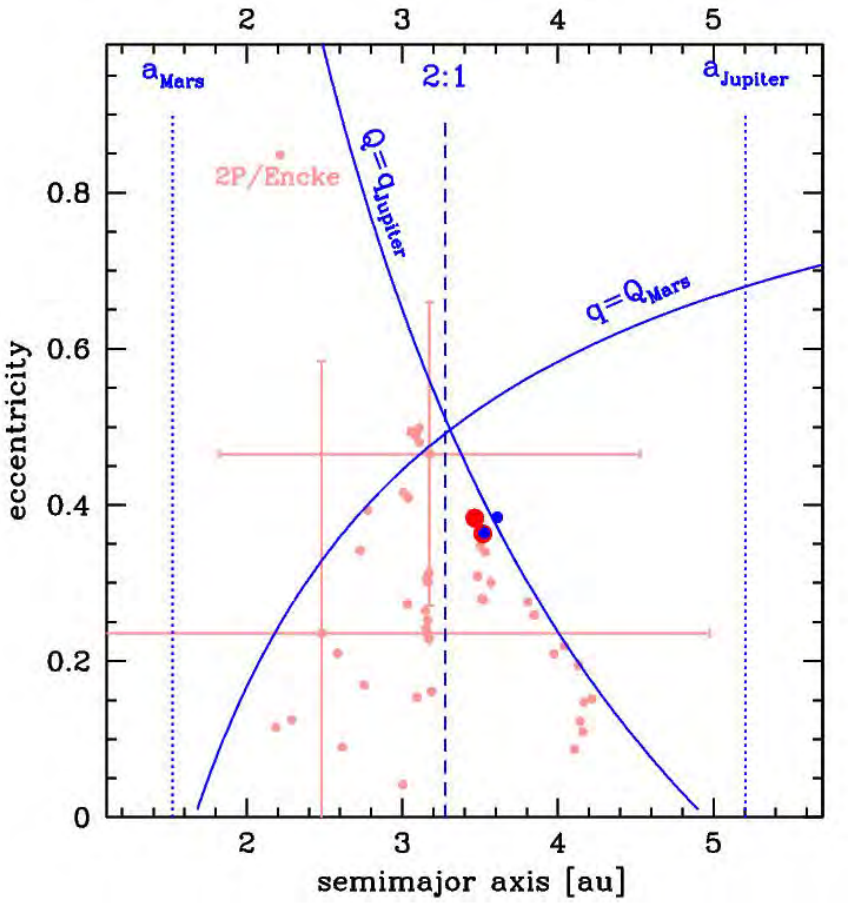

Fig. 3.84. Encke-type comets (light-red dots) occupy orbital area of parameters on the left of $Q=q_{Jupiter}$ curve, where Q is aphelion distance and $q_{Jupiter}$ is about 5.2 au; one can see that only for two comets the uncertainties of determined orbital parameters are uncertain, all remaining orbits are precisely determined (uncertainties are inside dots). Current orbital parameters for analyzed ETCs and JFCs are given by large red dots and blue dots, respectively.

Currently, the results are analyzed to quantify the evolution of these objects into several basic dynamical types (JFCs, ETCs, Chiron-type comets, Centaurs, interstellar comets) in a function of time. Depending on the results obtained, it may turn out to be also instructive to explore another narrow sub-area occupied by today's ETCs. The project started this year and is ongoing.

3.8 Estimations of Lapunov exponents for small bodies in the Solar System

A comparison between different methods to compute estimations of Lapunov exponents for a selected sample of small objects in the Solar System is undertaken. P. Wajer, J. Suchecki and M. Królikowska

Lapunov characteristic exponents are widely used tools for identification of chaotic motion of objects in the Solar System. Additionally, Lapunov exponents can help to localize chaotic regions in the Solar System and associated with the mean motion resonances or three body resonances (for example asteroid-Jupiter-Saturn resonance). The purpose of this study is to identify the advantages and disadvantages of the two most popular methods of estimating this parameter. The first method bases on solutions obtained by direct numerical calculation of variational equations together with the solutions of the N-body problem. Alternatively, one can estimate Lapunov exponent by measurement of distance between nominal body and another test particle kept in a relative close surrounding of the first (see Fig. 3.85).

As a part of this research, Jakub Suchecki received (August 2020) bachelor's degree in astronomy at Warsaw University under supervisions of Paweł Wajer and Marcin Kiraga (Warsaw University).

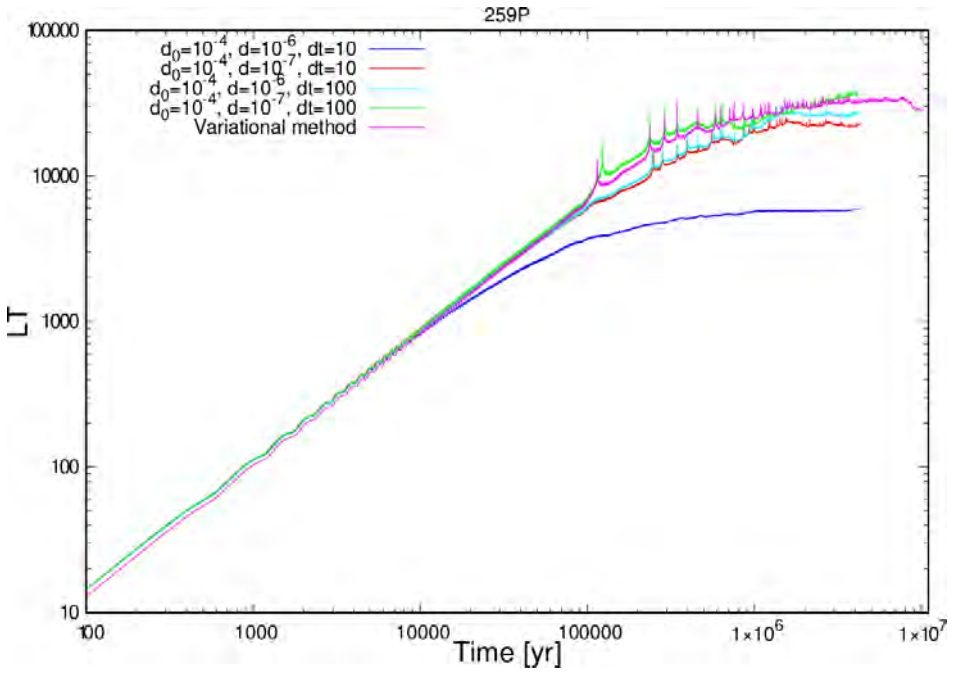

Fig. 3.85. Preliminary results of estimation of the Lapunov maximum exponent for the comet 259P/Garradd using the renormalisation method (for 4 different parameters connected with this method) and the variational method. In the calculations we used the REBOUND integration package.

This work is ongoing.

3.9 Missions to solar system objects

GALAGO: Highland terrain hopper – cutting edge planetary locomotion system.

J. Gurgurewicz, D. Mège and A. Nicolau-Kukliński

This project, carried out in cooperation with Astronika, aims to develop GALAGO, the light and robust jumping locomotion system designed to be dropped anywhere on the surface of celestial bodies with reduced gravity in comparison to Earth. After analyzing quickly the surroundings, it will hop, leap, or crawl to wherever investigators want it to work, within a maximum single jump distance of several meters (depending on the gravity) vertically and horizontally. Its low mass makes it possible to launch simultaneously several

hoppers to work as a fractionated explorer at a very competitive cost. After reviewing payload that may be placed on board hoppers, we illustrated the scientific capabilities of hopper and hopper networks in performing basic geologic observations at distinct study sites in a variety of geological environments, obtaining data along steep geological cross sections, surveying geophysical anomalies in the subsurface, prospecting resources, monitoring microenvironments, or characterizing dust activity on the Moon. Finally, we selected the payload and proposed experiment scenarios to be executed during test campaign.

Design of the Martian far-IR ORE Spectrometer MIRORES. J. Ciążela, J. Bąkała, J. Barylak, M. Ciążela, M. Kowalinski, S. Płocieniak, J. Gurgurewicz, D. Mège, B. Pieterek, Ż. Szaforz, P.-A. Tesson, M. Giuranna, F. Pirajno

Sulfide ores are a major source of noble metals (Au, Ag, Pt) and base metals (Cu, Pb, Zn, Sn, Co, Ni, etc.), and therefore will be vital to self-sustainment of future Mars colonies. Martian meteorites are rich in sulfides, which reflects in recent findings from Martian rovers. Yet the only high-resolution (18 m/px) infrared spectrometer orbiting Mars, CRISM (Compact Reconnaissance Imaging Spectrometer for Mars) on board Mars Reconnaissance Orbiter (MRO), struggles to detect sulfides on the martian surface. Spectral interferences with silicates impede sulfide detection in the 0.4-3.9 μm CRISM range. In contrast, at least four common sulfides on Earth and Mars (pyrite, chalcopyrite, marcasite, pyrrhotite) possess prominent absorption peaks in a narrow far-infrared (FIR) wavelength range of 23-28 μm. Providing global distribution and chemical composition of sulfide ores would help to choose useful targets for future Mars exploration missions. Therefore, we are starting to design a relatively cheap and simple pyroelectric detector-based Martian far-IR ORE Spectrometer (MIRORES) measuring three wide spectral bands limited with filters, including the main band of 23-28 μm and two

reference bands at 18-21 μm and 35-40 μm. Focusing on sulfides only will allow reducing instrument dimensions to the microsatellite size. The largest challenge related to this design is the small field of view conditioned by high resolution required for this study (10-20 m/px), which in limited space can be only achieved by the use of the Cassegrain optical system. The probe might be launched as a piggyback mission with a larger satellite (for example Japanese Martian Moons Exploration) during the 2024 or 2026 Mars launch window. Preliminary results have been presented at the COSPAR conference in Herzliya, Israel.

A Low Frequency Radar to Fathom Asteroids from Juventas Cubesat on HERA
A. Herique et.al (including W. Kofman)

After several asteroid-orbiting missions, an asteroid's internal structure has never been observed directly, even though this question is crucial for science, planetary defense and exploration. With the HERA mission, the LFR on the Juventas Cubesat will fathom Didymos's moonlet in 2026. This paper presents the scientific rationale, the mission and the radar planned for exploring the interior.

HERA mission has been accepted by the Ministerial Conference in November 2019. Presented at EPSC Vol. 13, EPSC-DPS2019-807-2, 2019

The works on real data from Mars (HiRISE) and Mercury (Messenger) - M.I. Błęcka and A. Wawrzaszek - were also continued in 2020. The aim of the work was to improve the quality and highlight additional details in the considered images. The local multifractal analysis developed by Anna Wawrzaszek was used. It seems that the method will be applicable to a more detailed study of dark areas of Mercury that are so far poorly understood. Currently, the method is tested and compared with the standard approaches to the image content description (e.g. statistical parameters, filtration process).

SIMBIO-SYS: Scientific Cameras and Spectrometer for the BepiColombo Mission. G. Cremonese, F.Capaccioni, M.T. Capria, A. Doressoundiram, P. Palumbo, M. Vincendon, M. Massironi, S. Debei, ... G. Arold,..., M. Blecka, D. Borrelli, J.R. Brucato, C. Carli, et al.

The SIMBIO-SYS (Spectrometer and Imaging for MPO BepiColombo Integrated Observatory SYStem) is a complex instrument suite part of the scientific payload of the Mercury Planetary Orbiter for the BepiColombo mission, the last of the cornerstone missions of the European Space Agency (ESA) Horizon + science program.

The SIMBIO-SYS instrument will provide all the science imaging capability of the BepiColombo MPO spacecraft. It consists of three channels: the STereo imaging Channel (STC), with a broad spectral band in the 400-950 nm range and medium spatial resolution (at best 58 m/px), that will provide Digital Terrain Model of the entire surface of the planet with an accuracy better than 80 m; the High Resolution Imaging Channel (HRIC), with broad spectral bands in the 400-900 nm range and high spatial resolution (at best 6 m/px), that will provide high-resolution images of about 20% of the surface, and the Visible and near-Infrared Hyperspectral Imaging channel (VIHI), with high spectral resolution (6 nm at finest) in the 400-2000 nm range and spatial resolution reaching 120 m/px, it will provide global coverage at 480 m/px with the spectral information, assuming the first orbit around Mercury with periherm at 480 km from the surface.

The article providing both technical information about the instruments and the research objectives appeared in June 2020 in *Space Science Review*. This work describes also the results of the Near-Earth Commissioning Phase performed few weeks after the Launch (20 October 2018). According to the calibration results and the first commissioning the three channels are working very well.

Asteroids Inside Out: Radar Tomography. Community White Paper for the Planetary Decadal Survey US, 2023-2032. M. Haynes, A. Virkki, F. Venditti, D. Hickson, N. Pinilla-Alonso, J. Brisset, L. Benner, C. Raymond, J. Lazio, A. Freeman, J. Castillo-Rogez, E. Asphaug, P. Taylor, A. Herique, W. Kofman, P. Sava, M. Pajola, A. Lucchetti, M. Nascimento De Pra, E. G. Rivera-Valentín

The interior structures of small bodies, also known as primitive bodies in the 2003-2013 Planetary Science Decadal Survey, provide key constraints on their formation and the origin of planets. Interior structure is also of vital importance for developing mitigation strategies for potentially hazardous near-Earth asteroids (NEAs), should they be needed for planetary defense, and for successful landed operations. NEAs, in turn, are representative and accessible samples of Main Belt and other solar-system populations [1]. Yet to date there is only limited knowledge of asteroid interiors from a few determinations of gravitational potentials and magnetic fields. We know next to nothing about typical asteroid structure, or the variability amongst populations. Long-wavelength radar, that penetrates the interiors, can deliver 3D characterizations of small asteroid structure, and, in particular, it has the potential to provide information about composition by mapping the dielectric properties throughout the interior. Radar tomography involves monostatic or multistatic observations that sample the interior propagation and scattering from different orientations relative to a target body. Radar reflections are then processed to improve image resolution or invert for the dielectric properties. Radar can propagate through kilometers of cometary materials, as demonstrated by the Rosetta mission at Comet 67P/C-G. Asteroids are likely to be more conductive, but propagation through hundreds of meters is expected. There is also potential synergy between ground-based radar telescopes that can be combined with low-cost asteroid orbiters or precise flybys that could change our understanding of small bodies in the coming decades.

This white paper summarizes the science opportunities, state of the art, and outstanding knowledge gaps, with a particular emphasis on the 99942 Apophis encounter when it flies by within six Earth radii (near the outer geostationary satellite belt) on April 13, 2029 (White Paper by Binzel et al. 2020).

Towards Asteroid Tomography: Modellings and Measurements Using an Analogue Model. C. Eyraud, L.-I. Sorsa, A. Herique, J. -M. Geffrin, S. Pursiainen, W. Kofman

The interior structures of the comets and asteroids, still poorly known, might hold a unique key to understand the early Solar System. Considering the interaction of an illuminated electromagnetic wave with this kind of targets, these "objects" are very large compared to the applicable wavelength. Consequently, tomographic imaging of such targets, i.e., reconstructing their interior structure via multiple measurements, constitutes a challenging inverse problem. To reach this objective and to develop and test inverse algorithms, we need to investigate electromagnetic fields that have interacted with structures analogous to real asteroids and comets. In this study, we focus on the acquisition of these fields considering three methods: calculated fields obtained with (1) time and (2) frequency domain methods and (3) microwave measurements performed for an analogue model, i.e., a small-scale asteroid model.

This issue was presented in March 2020 at 14th European Conference on Antennas and Propagation (EuCAP), Copenhagen, DENMARK, and published in Book Series: Proceedings of the European Conference on Antennas and Propagation.

3.10 Mars

MoMo: a new empirical model of the Mars ionospheric total electron content based on Mars Express MARSIS data. N. Bergeot et.al (including W. Kofman)

Aims: Several scientific landers and rovers have reached the Martian surface since the 1970s. Communication between the asset (i.e., lander or rover) and Mars orbiters or Earth antennas uses radio signals in UHF to X-band frequencies passing through the Mars' ionosphere. It is consequently necessary to take into account electron density variation in the Mars' ionosphere to correct the refraction of the signal transmitted.

Methods: We developed a new empirical model of the Mars' ionosphere called MoMo. It is based on the large database of Total Electron Content (TEC) derived from the subsurface mode of the Mars Express MARSIS radar. The model provides vertical TEC as a function of solar zenith angle, solar activity, solar longitude and location. For validation, the model is compared with Mars Express radio occultation data as well as with the numerical model IPIM (IRAP Plasmasphere-Ionosphere Model).

Results: We discussed the output of the model in terms of climatology behaviour of the Mars' ionosphere. The output of MoMo is then uses to quantify the impact of the Martian ionosphere for radio-science experiments. From our results, the effect is of the order of 10^{-3} mm s^{-1} in Doppler observables especially around sunrise and sunset. Consequently, this new model could be used to support the data analysis of any radio-science experiment and especially for present InSight RISE and future ExoMars LARA instruments aiming at better understand the deep-interior of Mars. This research was published in *Journal of Space Weather Space Climate* (October 2019)

A new method for determining the total electron content in Mars' ionosphere based on Mars Express MARSIS data. P. Conroy et. al (including W. Kofman)

We present a new method for determining the total electron content (TEC) in the Martian ionosphere based on the time delay of received radar pulses of the Mars Advanced Radar for Subsurface and Ionospheric Sounding (MARSIS) on board the Mars Express spacecraft. Previous studies of the same dataset have produced differing results for the day-side ionosphere, so it is useful to have an alternative way to compute the TEC in this region. This method iterates a model ionosphere in order to simultaneously match the ionospheric delays of the signals received by the radar's two channels by finding the model which minimizes the root mean square error (RMSE) between the measured and simulated delays. Topographical information is obtained from data from the Mars Orbiter Laser Altimeter (MOLA) instrument. The model parameters are held constant for a given orbit, and a very good agreement between the simulated and measured delays is obtained. The TEC can then be inverted from the ionospheric model. Matching the delays of both channels simultaneously applies an additional constraint to the model which has not been made in previous studies. The model is additionally validated by matching the simulated pulses with the raw range-compressed measurements for one orbit. Finally, typical model parameters are compared to those obtained by previous studies, which are also simulated. The method is applied to orbits during moderate solar activity, and results show very good agreement with previous studies. The results of these studies were published in the March 2020 volume of the *Planetary and Space Science.*

The Colour and Stereo Surface Imaging System (CaSSIS) for the ExoMars Trace Gas Orbiter. An international team led by N. Thomas, including M. Banaszkiewicz, W. Kofman, P. Orleański, P.-A. Tesson, P. Wajer and P. P. Witek

CaSSIS camera onboard ExoMars TGO was designed to acquire colour and stereoscopic images of the martian surface and provide geological context to potential trace gas sources. Since the beginning of the Science Phase of TGO in April 2018, members of the ZDUSiP (especially EXOMHYDR team) proposed potential targets in several are as of interest using the CaSSIS Suggestion Targeting (CaST) web tool. CaSSIS images are planned weeks in advance based on the predicted spacecraft trajectory provided by ESA. From that, images are planned based on the previously made suggestions and the potential targets which TGO is flying over during a specific orbit.

In March 25-29 2019, P.-A. Tesson and in April-May 2019 P. P. Witek planned observations based on suggestions made by people, potential targets and technical constraints.

Images planned by P.-A. Tesson were acquired by CaSSIS in May 2019 and were made available by the people in Bern to the Science Team. In such planning sessions, several areas of interest for the EXOMHYDR project could be imaged according to the image suggestion priority list, in stereo and/or colour, such as Tharsis volcanoes summit calderas and tectonic features on Valles Marineris floor.

Imaged planned by P. P. Witek were acquired by CaSSIS in July 2019. The acquisitions were severely limited by the lack of stereo and targeting capability. Because of that he has chosen mainly the targets with rich stratigraphy and varied composition, such as layered deposits of different colors and deposits of sulfates and chlorides.

Another CaSSIS data acquisition planning session was made in December 2019 by P.-A. Tesson for images to be taken in March 2020.

An overview of the first 9 months of imaging with CaSSIS was presented at *50th the Lunar and Planetary Science Conference* as well as at the *9th International Conference on Mars*.

Trace gases on Mars. M. I. Błęcka

Continuation of the works connected with the measurements of the stereoscopic camera CASSiS (The Colour and Stereo Surface Imaging System) and NOMAD spectrometer a parts of payload of *ExoMars Trace Gas Orbiter* (TGO) of the ESA mission.

The CASSiS camera give the opportunity of analysis the structure and locations on the surface of Mars possible sources of trace gases e.g. methane. Identification and monitoring minor species in the atmosphere are performed from orbiter by spectrometric instruments (e.g. NOMAD, ACS).

There are various types of features on Martian surface that could be associated with trace gases release e.g. methane. In various locations the processes making possible emission of methane were probably created in different ways among others the production from serpentinized rocks.

The common influence of optical spectral features of the surface and atmosphere contains trace gases on radiance spectra were analysed. The elaborated models provide estimates of the spectral reflectance/emittance and total radiance from Martian surface and atmosphere in the Mid-infrared spectral range. The various kinds of surfaces were spectrally described by presumable reflectance or emissivity of minerals and rocs (e.g. the serpentinized rocks) appropriate for selected locations. Spectral reflectance or emissivity of the modelled regions were calculated from optical constants (n,k) with Mie and Hapke theories. The physical properties of the atmosphere were characterized by its thermodynamical parameters and absorbing or scattering properties. The performed analysis of Mid-infrared spectral signatures of the surface and the atmospheric trace gases in various physical conditions on total radiance were shown.

The results of numerical modelling were discussed during the meetings of Martian group at CBK and presented on IUGG General Assembly 2019 in Montreal ("Study of the influence the composition and textures of Martian surface on detection the atmospheric methane – the numerical simulations"); see also Fig. 3.86.

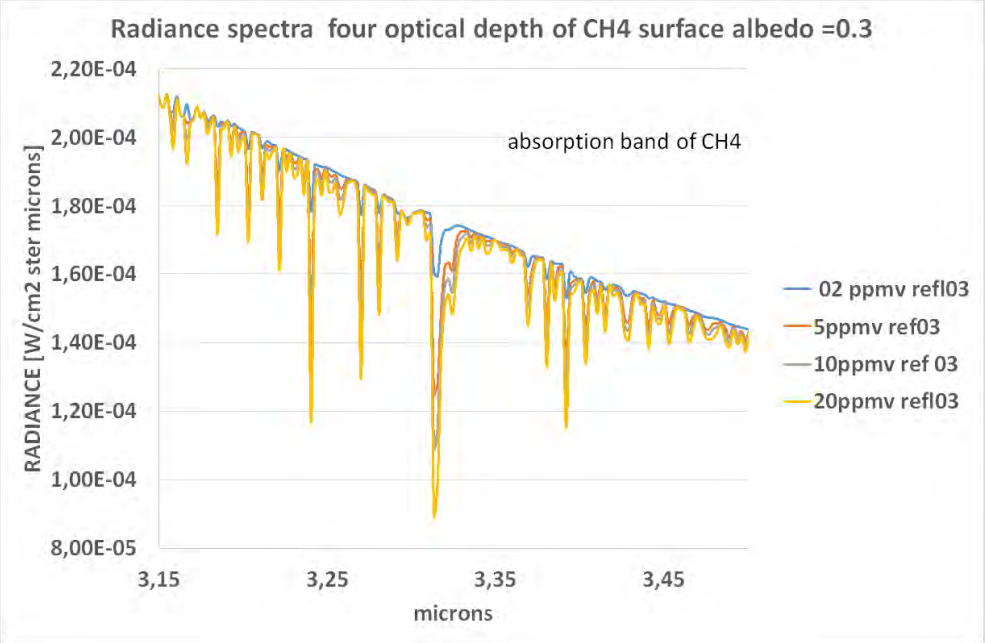

Fig. 3.86. The results of numerical simulations. The nadir measurement of the surface and atmosphere of Mars. The radiance at the top of the atmosphere in the spectral region of strong absorption of methane. The calculations include: the constant reflectance of the surface equal 0.3 and four concentrations of CH_4 in the atmosphere.

The preliminary conclusions related visibility of spectral features of trace gases (methane) in radiance spectra were discussed in the first draft of the paper (2020). Our analysis shows that in the spectral region around 3.32 micrometers where is the strong absorption band of methane, it is possible to detect this gas by the nadir spectrometric measurements over hypothetical purely serpentine regions on the Martian surface. So it seems that observing the atmosphere over serpentine zones should result in methane detection. But serpentine rather does not exist in its pure form on Mars. Based on our recent

calculations, we suppose that additional ground components (e.g. water ice) can make methane detection difficult.

The article is being prepared for publication and it will be supplemented with the results of these new calculations.

Modelling the transport of trace gases in the Martian atmosphere. P. Wajer, P. P. Witek, W. Kofman and M. Banaszkiewicz

The European-Russian ExoMars Trace Gas Orbiter (TGO) is since 2018 on its scientific orbit. The data returned by the probe, especially by the NOMAD (Nadir and Occultation for MArs Discovery) and CaSSIS (Colour and Stereo Surface Imaging System) instruments will help to understand the origin and evolution of trace gases, especially methane (CH_4), in the Martian atmosphere. The orbiter furnishes data on abundance of trace gases as well as colour and stereo images of the surface, that are useful in characterizing the sources and sinks of some atmospheric trace gases. One of the most interesting subjects of investigation is appearance and disappearance of methane (CH_4) on Mars on short timescales. The study of the possible methane sources and its transport in the atmosphere is one of the objectives of this research. This leads to develop the Martian atmosphere model, with the production and the transport of major as minor species of the atmosphere.

We develop a single-column model of the Martian atmosphere to compute its steady-state chemical composition. All constituents of the atmosphere are subjected to solar radiation and react with each other, in presence of the atmospheric aerosols. Starting there, we will study the release, propagation and loss of trace gases such as methane and other hydrocarbons, and sulphur and species. Then we will compare our simulations with data acquired by the probe.

This model will help us to better understand the origin and evolution of trace gases, especially CH_4. We also plan to use the simulations of gases transport from subsurface to the surface and compare the data obtained from the spacecraft instruments to describe the lower boundary conditions (at the surface) that we need for our atmospheric photochemical model.

In 2019 the chemical and photochemical part of this model was we developed and tested. In 2020 we were working on a separate numerical code to solve diffusion part of the model(the molecular and turbulent diffusion is included). We performed many tests with different boundary conditions, for example when at lower and upper boundary initial densities (or fluxes) of molecules are know; however we do not solved all interesting cases of these conditions. This work will be continued in the next year and we plan to finish merging the two parts of the model: chemical/photochemical with diffusion. This research is ongoing.

Investigation of friction weakening of terrestrial and martian landslides using discrete element models. T. Borykov, D. Mège, A. Mangeney, P. Richard, J. Gurgurewicz and A. Lucas

Understanding what controls the travelling distance of large landslides has been the topic of considerable debate. We show that the normalized runout distance starts to depend on the volume involved only above a critical slope angle > 16–19°, as observed experimentally. The empirical friction coefficient, calibrated to reproduce the observed runout of terrestrial and Martian landslides, is shown to decrease with increasing landslide volume (or velocity), going down to values as low as 0.1-0.2. No distinguishable difference is observed between the behaviour of terrestrial and martian landslides. The paper was published in the *Landslides* (March 2019).

Evidence for thermal-stress-induced rockfalls on Mars impact crater slopes. P.-A. Tesson, S.J. Conway, N. Mangold, J. Ciążela, S.R. Lewis, and D. Mège

Recent rockfalls (<100 ka) in relatively fresh impact crater slopes on Mars display a slope aspect and latitudinal trends (equator-facing rockfalls are more numerous than pole-facing ones between −50° and + 40°). Rockfall events triggered by phase changes (as on Earth) seem to occur where water ice can condense and/or be preserved from previous ice ages (i.e. on pole-facing slopes at mid to high-latitudes and not at the equator). This suggests that H_2O or CO_2 phase changes do not play a role in present-day rockfall activity. Instead, our results show that it is more likely to be related to insolation. Numerical simulation of solar flux on Martian slopes (~45°) at equatorial and mid-latitudes indicates a correlation between high rockfall activity and high energy received on the surface. This finding highlights the role of solar-induced thermoelastic stress in the weathering of Martian rocks. The paper describing results was published online in *Icarus* (October 2019).

Deep Learning-Driven Detection and Mapping of Rockfalls on Mars. V.T. Bickel, S.J. Conway, P.-A. Tesson, A. Manconi, S. Loew, U. Mall

Several gravitational mass movements occur on the surface of Mars today. Among these, metric-scale rockfalls (i.e. clasts detaching from a hanging cliff and rolling downslope) are visible on HiRISE images (25-50 cm/pixel) as they leave a track the surface while they bounce/roll downhill. Studying rockfall activity can provide insights on the weathering mechanisms occurring on the surface of Mars today or potential trigger mechanisms in the form of marsquakes. Quantifying this activity requires a large-scale mapping of rockfalls in order to highlight any trend. However, manual mapping of rockfalls is extremely time consuming. Over the recent years, progress in Convolution Neural Networks (CNN) and Deep-Learning techniques in image analysis as allowed us to develop automatic method to detect surface features on

remote sensing data. We developed and trained a CNN to automatically scan HiRISE images and detect rockfall tracks with their associated clast (Fig. 3.87). We managed to achieve a maximum recall of up to 0.78 and a maximum precision of up to 1.0, with a mean average precision of 0.71. The average time of detection was ~30 sec for one HiRISE image vs ~30 min for an experienced human.

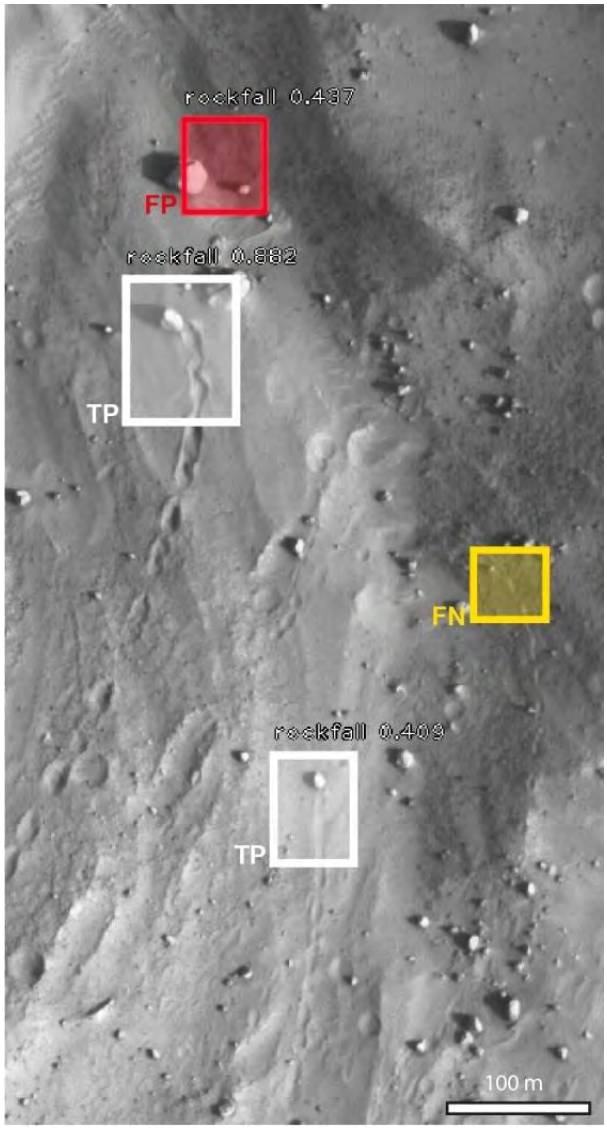

Fig. 3.87. Example of rockfalls after scanning of the HiRISE image by the CNN. TP boxes represents True Positive (i.e. actual rockfalls correctly detected), FN = False Negative, and FP = False Positive. The number above each box represents the percentage of confidence give by the detector.

Further work will consist on implementing a pipeline to scan the whole HiRISE dataset and run global and regional studies on current rockfall activity on Mars.

Construction, training and performance of the neural network were published in 2020 in *IEEE Journal of Selected Topics in Applied Earth Observations and Remote Sensing* under the title: *Deep Learning-Driven Detection and Mapping of Rockfalls on Mars.*

Deep-seated gravitational slope deformation scaling on Mars and Earth: same fate for different initial conditions and structural evolutions. O. Kromuszczyńska, D. Mège, K. Dębniak, J. Gurgurewicz, M. Makowska and A. Lucas

The topography of selected paraglacial deep-seated gravitational slope deformation scarps on Mars and in the Tatra Mountains is investigated. Some of the most spectacular instances of deep-seated gravitational slope deformation (DSGSD) are found in the Valles Marineris region on Mars. They provide an excellent opportunity to study DSGSD phenomenology using a scaling approach. The topography of selected DSGSD scarps in Valles Marineris and in the Tatra Mountains in Eastern Europe is investigated after their likely similar postglacial origin is established. Deformed Martian ridges are larger than their terrestrial equivalents by one to two orders, although their height-to-width ratio is similar (~0.24). Measured finite strain of the Valles Marineris ridges is three times higher than in the Tatra Mountains, suggesting that although initial conditions were different, with steeper slopes in Valles Marineris, the final ridge geometry is now similar. As DSGSD is now thought to be inactive in both regions, their comparison suggests that whatever the initial ridge morphology, DSGSD proceeds until a mature profile is attained. On both planets, strain is distributed over the same number (~5) of major scarps; fault displacements are therefore much larger on Mars. The large offsets suggest the reactivation of DSGSD fault scarps in Valles Marineris, while a single seismic event would have been enough

in the Tatra Mountains. The longer period of activity of Martian faults may be correlated with a long succession of climate cycles generated by the unstable Mars obliquity. In sum, despite current similarities in their global geometry, the studied ridges on Mars and Earth affected by DSGSD did not start from similar initial conditions and did not follow the same structural evolution. The paper was published in the *Earth Surface Dynamics* (April 2019).

Dynamic accretion beneath a slow-spreading ridge segment: IODP Hole 1473A and the Atlantis Bank Oceanic Core Complex. H. Dick et al. (incl. J. Ciazela) and the Expedition 360 Scientists

809-m-deep IODP Hole U1473A at Atlantis Bank, SWIR, is 2.2 km from 1,508-m Hole 735B and 1.4 from 158-m Hole 1105A. With mapping, it provides the first 3-D view of the upper levels of a 660-km^2 lower crustal batholith. It is laterally and vertically zoned, representing a complex interplay of cyclic intrusion, and ongoing deformation, with kilometer-scale upward and lateral migration of interstial melt. Transform wall dives over the gabbro-peridotite contact found only evolved gabbro intruded directly into the mantle near the transform. There was no high-level melt lens, rather the gabbros crystallized at depth, and then emplaced into the zone of diking by diapiric rise of a crystal mush followed by crystal-plastic deformation and faulting. The residues to mass balance the crust to a parent melt composition lie at depth below the center of the massif-likely near the crust-mantle boundary. Thus, basalts erupted to the seafloor from >1,550 mbsf. By contrast, the Mid-Atlantic Ridge lower crust drilled at 23°N and at Atlantis Massif experienced little high temperature deformation and limited late-stage melt transport. They contain primitive cumulates and represent direct intrusion, storage, and crystallization of parental MORB in thinner crust below the dike-gabbro transition. The strong asymmetric spreading of the SWIR to the south was due to fault capture, with the northern rift valley wall faults cutoff by a detachment fault that extended across most of the zone of

intrusion. This caused rapid migration of the plate boundary to the north, while the large majority of the lower crust to spread south unroofing Atlantis Bank and uplifting it into the rift mountains. This research was mainly conducted in the previous year and in 2019 the paper has been published in *Journal of Geophysical Research: Solid Earth*.

Calcium isotopic compositions of oceanic crusts at various spreading rates. C. Chen, J. Ciazela, W. Li, W. Dai, Z. Wang, S. F. Foley, M. Li, Z. Hu, Y. Liu

The oceanic crust consists mainly of a lower layer of cumulate gabbroic rocks and an upper layer of differentiated basalts. The thicknesses and proportions of the gabbroic and basaltic layers in different oceans are largely controlled by spreading rate, magma supply, and magmatic differentiation processes. Evaluating the effects of complex magmatic differentiation as a function of spreading rate on Ca isotope composition is critical to understanding whether the Ca isotope compositions of oceanic crust from different oceans are homogeneous and thus whether the observed considerable variation of $\delta^{44/40}$Ca in basalts (up to 0.4‰) results from magmatic differentiation or mantle source heterogeneity. To address the question, we present $\delta^{44/40}$Ca measurements of a series of gabbroic rocks (n = 38) and mineral separates from the 810-m-long U1473A hole drilled into the gabbroic lower crust at the ultraslow-spreading Southwest Indian Ridge (SWIR), along with 12 mid-ocean ridge basalts (MORBs) from the slow-spreading South Mid-Atlantic Ridge (SMAR) and the fast-spreading East Pacific Rise (EPR). Although the gabbroic rocks of the SWIR reflect several events of magma supply and strong magmatic differentiation (bulk rock Mg# of 64–79 for each event), their δ44/40Ca values (0.85 ± 0.09‰, 2sd, n = 37) are uniform. The results are consistent with limited inter-mineral Ca isotope fractionation between plagioclase (Pl) and co-existing clinopyroxene (Cpx) in the accumulated gabbros (average $\Delta^{44/40}Ca_{Pl\text{-}Cpx} = -0.10$‰, n = 5). This indicates that no

measurable Ca isotope fractionation occurs during formation of ultraslow-spreading oceanic crust. The MORBs from the SMAR and EPR show consistent $\delta^{44/40}$Ca values (0.82 ± 0.08‰ (2sd, n = 4) and 0.86 ± 0.09‰ (2sd, n = 8), respectively), regardless of the degree of fractional crystallization. On the whole, the ultraslow-, slow- and fast-spreading gabbroic cumulates and MORBs display indistinguishable $\delta^{44/40}$Ca within analytical uncertainty, suggesting a homogenous Ca isotope composition for the global igneous oceanic crust ($\delta^{44/40}$Ca = 0.85 ± 0.09‰, 2sd, n = 49) even if they experience complex magmatic differentiation. Comparison with values for fertile mantle rocks ($\delta^{44/40}$Ca = 0.94 ± 0.10‰) reveals that partial melting triggers only slight Ca isotope fractionation (0.09 ± 0.02‰, 2se). In this light, the considerable variation of previously reported $\delta^{44/40}$Ca values for basalts may result from their different mantle sources, and is probably attributable to the recycling of crustal materials. This research was mainly conducted in the previous year, and in 2019 the paper has been published in *Geochimica et Cosmochimica Acta*.

Shear tectonics in Valles Marineris. D. Mège, J. Gurgurewicz, S. Douté, F. Schmidt and R.A. Schultz

The presence of a dense swarm of dikes several tens of meters thick on the floor of Ophir Chasma, which do not cut the surrounding Interior Layered Deposits, indicates that kilometers of bedrock must have been eroded or are missing in this part of Valles Marineris. We report on the existence of brittle-plastic, NE-SW oriented dextral shear zones similarly exposed in the deepest parts of Ophir Chasma (Fig. 3.88), as well as Hebes Chasma. We discuss their identification, kinematics, age, the nature and mineralogical composition of the deformed rock, and their role in the tectonic, erosional, and geomorphological evolution of Valles Marineris. Preliminary results were published in *LPSC Abstracts* (March 2019).

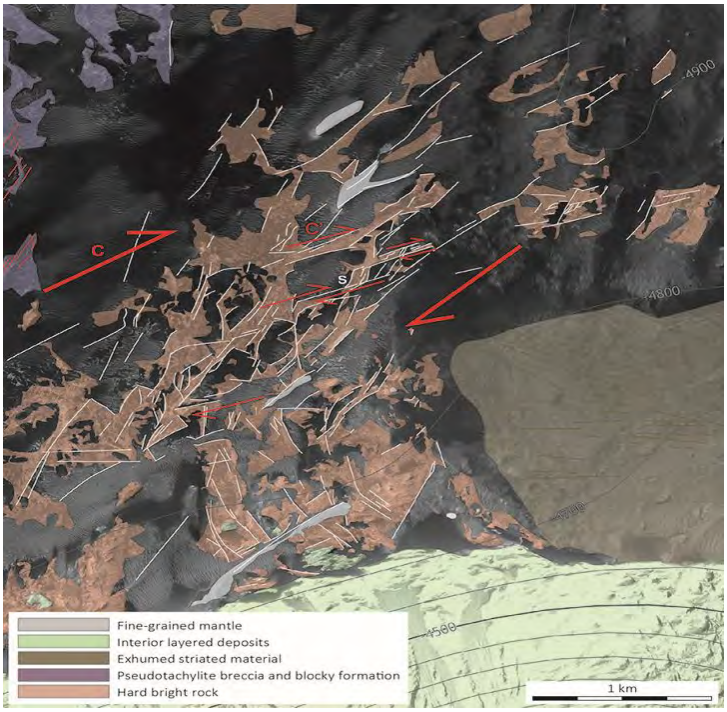

Fig. 3.88: Tectonic map of the main shear zone exposure in Ophir Chasma in Valles Marineris, Mars.

Dielectric properties of the Valles Marineris canyons and surrounding areas.

D. Mège, W. Kofman, L. Castaldo, G. Alberti, J. Gurgurewicz

This work is part of the activities related to the ExoMars TGO mission and the earlier missions to Mars. It investigates the existence of equatorial water ice and other low permittivity material (dust, porous rock) in the Valles Marineris canyons. Global climate models claim that water ice is not stable at the surface in the equatorial region of Mars, including in Valles Marineris, in the current environmental conditions. However, the landforms and sediment composition in Valles Marineris point to major ice activity in the past. Celestial dynamics models suggest indeed that many climate cycles succeeded under which water ice was alternatively stable/instable at the surface in Valles Marineris, and geophysical models that include such cycles predict net ice accumulation in the canyons today. Furthermore, the ExoMars/TGO FREND neutron counts suggest that a fair amount of subsurface hydrogen is nowadays

escaping to the atmosphere. Combining geology from ExoMars TGO/CaSSIS and previous imaging instruments with Mars Express/SHARAD ground-penetrating radar data, and comparing the whole with the hydrogen escape data from the FREND instrument, we may discriminate the nature of the shallow subsurface in Valles Marineris, and identify areas where low permittivity is due to ice, dust or porous rocks. During the whole 2020, we proceeded to, and evaluated the results of, SHARAD data calibration tests. This research is ongoing.

Mineralogy of the shear zone host rock in Valles Marineris, Mars. J. Gurgurewicz, D. Mège, F. Schmidt

The deep, ~1 380km wide, brittle-plastic shear zones have been found in the deepest parts of the Valles Marineris trough system. The shear zone host rock is massive and shows fracture patterns reminiscent of plutonic bodies. The massive structure is sometimes seen to change to pseudotachylite. Nonlinear spectral unmixing of CRISM data revealed that the deformed rock is a mafic crustal basement through which hydrothermal fluids have circulated. It contains olivine, pyroxenes, and plagioclases, associated with various sulfates of likely alteration origin. Such tectonic style and rock composition open a window for ore deposits investigations at the surface of Mars that were thought to be accessible on Earth only. Arguing that plate tectonics has been absent on Mars, some researchers predicted an obstacle in finding some types of metalliferous mineralizations (Au, Cu, W, Bi, As, Mo…) in the Martian crust which are thought to be plate tectonic dependent. Our findings allow to argue that whatever the underlying driving mechanism of Martian tectonics, conditions are actually met to mine such ore deposits, providing new opportunities for in situ resource utilization.

This research is in preparation for publication.

ExoMars TGO/CaSSIS colour imaging of late lava flows and hydrothermal alteration in Ladon Basin, Mars. D. Mège and J. Gurgurewicz

The CaSSIS colour stereo camera of ExoMars/TGO views the surface of Mars with 4 filters in the range 0.4-1.2 μm and pixel size 4.6 m. Its colour capabilities for geological interpretations are explored in the Ladon impact basin, where it reveals a surprising diversity of terrains, that CRISM, CTX, and HiRISE data help interpret further. Most likely, the surface is capped by a rather fresh thin mafic or ultramafic flow, dated middle Amazonian, underlain by a serpentinised flow of similar composition. These results indicate that a long time after formation, the Ladon basin had undergoing volcanic and hydrothermal activity, and reveals the exceptional potential of CaSSIS for geologic mapping. Preliminary results published in *Geophysical Research Abstracts* (April 2019) and *EPSC Abstracts* (September 2019).

Isidis Planitia: its regional and local characteristics. N. Zalewska, L. Czechowski, J. Ciążela, M. Jenerowicz

In the years 2018-2020, we studied the area of Isidis Planitia. This region for years, i.e. since Martian probes began sending images of this area, aroused a lot of controversy and was a kind of morphological imponderable. We began by identifying the types of chains that form little cones. As part of this research, Małgorzata Jenerowicz created a mathematical algorithm that reflected the morphological structure of Isidis Planitia. The algorithm is gradually being refined. Our research covers the morphology and geological structure of this area.

The cones have diameters of 300–500 m and heights of ~30 m. Many cones form subparallel chains several kilometers in length. Their origin is discussed in many papers; however, the mechanism of their formation is not explained, nor the reason for their arrangement in subparallel chains.

The cones may be: rootless cones, cinder cones, tuff cones, pingos, mud volcanoes etc. Some of chains have a characteristic furrow suggesting possibility of fissure volcanism.

The prevalence of these chains indicates that large-scale processes are responsible for their formation. Proper their classification can be helpful in identifying their origin as well as explaining other large-scale processes on Isidis Planitia. There are a few works about statistics of cones on these region. However, we approached the problem in a different way.

Our analysis of chains of cones indicates that they can be grouped in larger systems. In this way we divided Isidis Planitia into several characteristic regions described in the Fig. 3.89. This division is based on well-distinguished morphological structures, i.e., cones, cone chains and their orientations.

Our current Isidis Planitia division includes 36 regions. We distinguished 11 regions with the predominant arrangement of arcs in the directions between ENE and ESE (see Fig. 3.91 for notation of directions), 5 regions with the directions between WNW and WSW, 2 regions with the directions between NNE and NNW and 15 areas with the directions between SSE and SSW, 3 areas where the arcs of the cones form circles. In the rest of our regions there are no chains of cones.

In Fig. 3.89, we marked also sinuous ridges, cracks and serial depressions, occurring near craters, fields with polygonally cracked surface and quasi-circular depressions – ghost craters.

Conclusions: Our division is made according to consistent characteristic morphological features. The next stage of the work will be to explain the mechanism of the formation of these forms, based on known geological phenomena but in relation to Mars. We want to clarify whether the designated areas were created in the same geological processes, or whether a different mechanism is responsible for the differences in these forms.

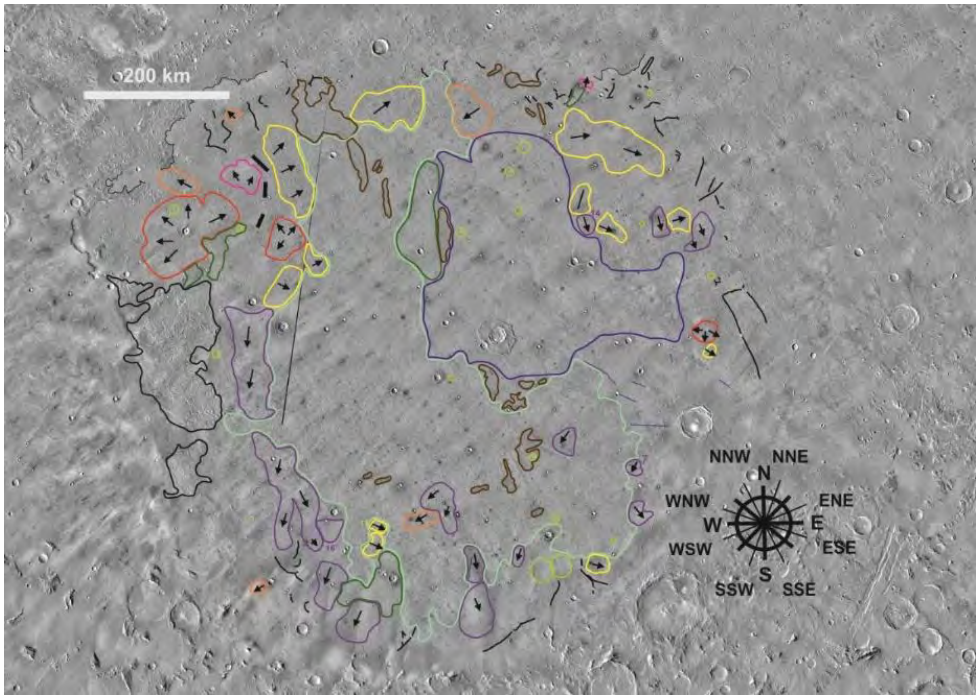

Fig. 3.89. THEMIS mosaic - a division into areas characterized by certain features: the predominant direction of cones arches was taken into account (yellow, red, pink and orange and purple fields), sinuous ridges (black, winding lines), areas with a large number of small craters (brown areas), areas with few or no cones (green areas), quasi-circular depressions sQCDs -ghost crater (light green circles), cracks and serial depressions (blue lines), areas with polygonally cracked surface (black fields), the direction of the parallel and serial cones are shown by thick black lines .The black arrows indicate the direction of the parallel chains of cones. Two big areas: area without parallel arcs with chaotic chains (cyan field) and area with groups of cones creating fields, not forming chains, with varying degrees of form (navy blue field).

The formation of some cone chains in Chryse Planitia on Mars. L. Czechowski, N. Zalewska, A. Zambrowska, M. Ciążela, P. Witek, J. Kotlarz

In 2020, we continued work that began in 2018 on determining the genesis of the arrangement arched forms of small cones on their surface, on the border of Acidalia and Chryse areas. We analyzed the region on Chryse Planitia/Acidalia centered in ~38°13' N and ~40°35'W, see Fig. 3.90, where several chains of cones are observed. The main subject of our research is a hill ~15x11 km. The hill is separated from other hills by a valleys (with the chains of cones labeled by 7 and 8, Fig. 3.90).

We investigate: (1) the processes responsible for the formation of the cones, (2) energy required for cones formation, and (3) why the cones form subparallel chains. We focus on the hypothesis connecting the formation of cones with the loss of water from the regolith due its instability.

We consider three mechanisms of cone formation: (i) a grains' ejection, (ii) from mud or fluidized sand and (iii) explosive formation. The (iii) and (ii) are possible when an additional heat source (e.g., hot magma) has increased the temperature. Of course, the cones may be formed by several processes.

We present the numerical calculation of the interaction of a magma intrusion and an aquifer using 3D, time dependent model based on equation of thermal conduction developed and published earlier by Czechowski. The model takes into account highly nonlinear terms resulting from phase transitions.

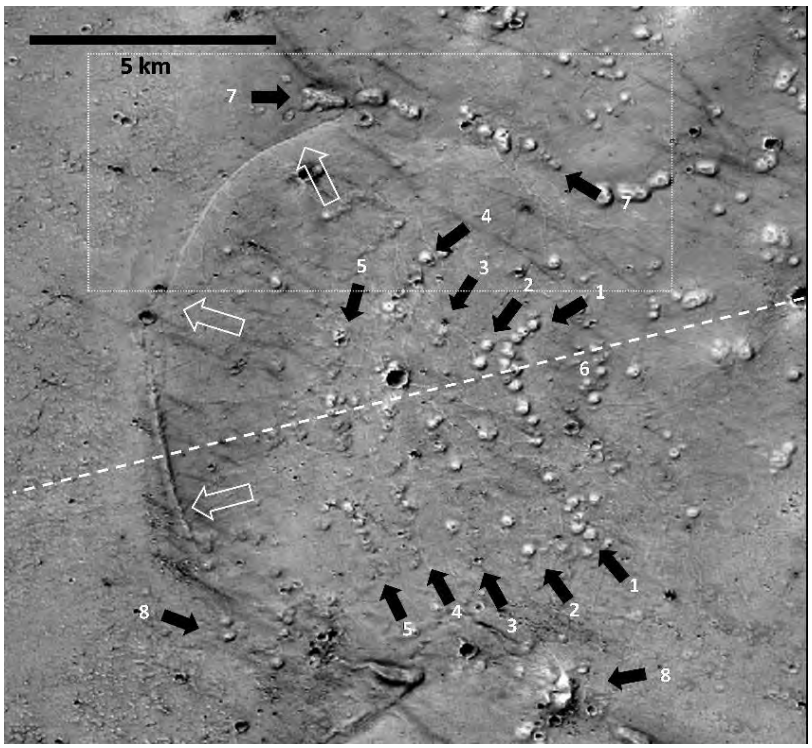

Fig. 3.90. The region considered in the paper. The subparallel chains of cones are indicated by black arrows and labeled by 1, 2, 3, 4, 5. According to our hypotheses, some of these chains were formed along the outcrops of sediments with high content of volatiles. The chains 7 and 8 may be rootless cones formed at the bottom of the valleys. NASA, P22_009485_2187_XN_38N040W.

We suggest some role of clathrates as volatile and heat transport by advection. In conclusions we obtained:

1) Considered cones could be a result of outgassing of regolith due to pressure drop. Additional heating can lead to total outgassing and explosive formation of cones. 2) Subparallel chains of cones may be formed along the outcrops of volatile-rich sediments. This mechanism seems to be most probable for subparallel chains. Non-subparallel chains are probable chains of rootless cones. 3) Numerical modeling indicates that magma intrusions may not be enough for completely degassing some aquifers.

In 2020, an article entitled: *Formation of cone chains in Chryse Planitia region of Mars and thermodynamics of this process* was submitted to the *Icarus* journal.

A cones system on the border of the Acidalia and Chryse. N. Zalewska, L. Czechowski, M. Ciążela, J. Kotlarz, P. Witek

Work is underway as a continuation of 2018 on determining the genesis of the arrangement of tongue forms with the concentric forms of small cones on their surface on the border of the Acidalia and Chryse areas. Last year, we suggested a type of volcanism rootless cones but there are some inaccuracies that exclude this type of volcanism. In the photos from THEMIS V55617012 and CTX P22_009485_2187_XN_38N040W (Fig. 3.91), a number of individual volcanoes have been noticed along the tongue borders. We suggest that these are, however, volcanic deposits and not lava tongues, although we do not exclude the origin of groundwater, which would be responsible for mud volcanism. First of all, the slope of the terrain with characteristic tongues runs from west to east which excludes lava flow in the opposite direction and thus rootles cones. An unusual type of volcanism, unheard of on Earth, shows something like flat lava domes flowing out of semicircular furrows, along which

and at a distance from them form parallel small volcanic cones with a base of 50 m. An article is being prepared for submission under the working title: Some remarks about the origin of chains of cones in Chryse Planitia.

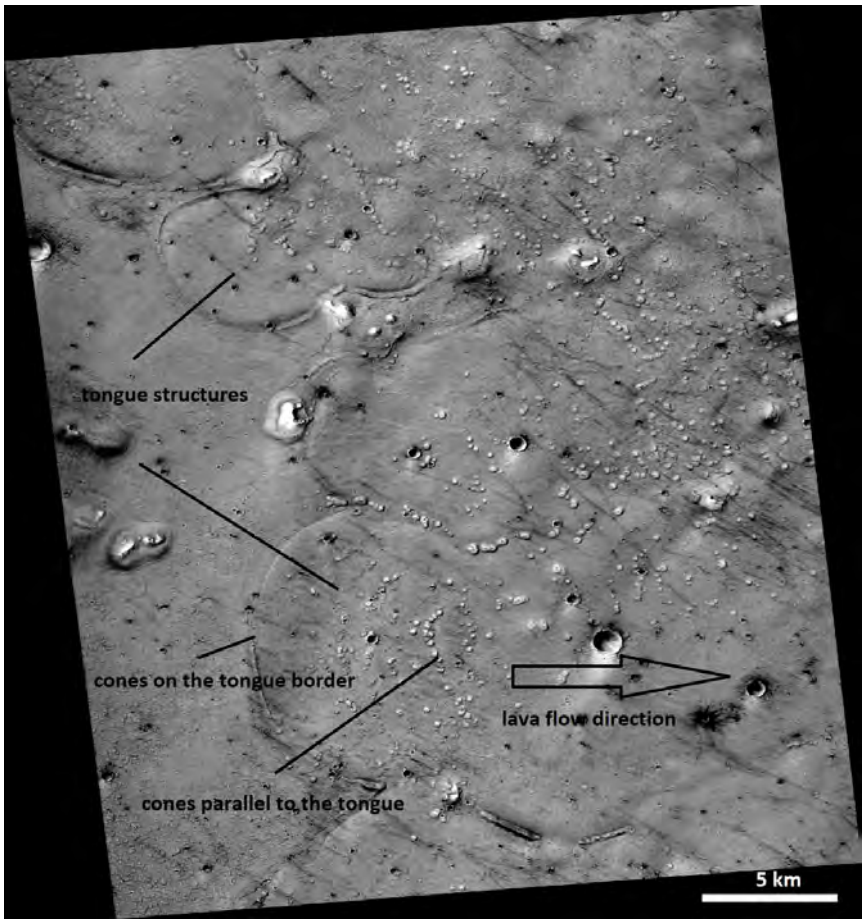

Fig. 3.91. CTX P22_009485_2187_XN_38N040W. Acidalia/Chryse- Marking of cones on tongue structures and lava flow direction.

Surface temperature from PFS/MEX dataset to track ice distribution on Mars.

M. Ciążela, J. Ciążela, D. Mège, M. Giuranna, P. Podgórski, B. Pieterek, J. Gurgurewicz, P.-A. Tesson, and P. Wolkenberg

Tracking surface temperature distribution on Mars can provide unique

information on thermophysical surface properties that complement information from images in the visible range. At first, we generated night-time temperature maps of Mars for 12 time intervals (months) to investigate thermal distribution changes over time. We then calculated thermal inertia maps for Martian summer (Ls=90°–150°) and winter (Ls=270° – 330°) using the apparent thermal inertia (ATI) approach: ATI=(1-A)/ΔT, where A is albedo and ΔT is temperature difference. We used the PFS night-time and daytime temperatures database along with the global NIR 1-micrometer albedo map of Mars from the same mission. Albedo map is based on reflectance data acquired by the OMEGA spectrometer from January 2004 to August 2010. The presence of ice may indirectly indicate also hydrothermal sites on Mars. These method is especially efficient at identifying seasonal surface ice showing highly enhanced thermal inertia (>1000 J m^{-2} $K^{-1}s^{-1/2}$ units) compared to martian soils (<600) due to higher thermal conductivity and heat capacity of ice. We are using PFS/MEX dataset consisting of 1,424,366 surface temperature retrievals collected over 18438 Mars Express orbits, encompassing 9 successive Mars years (Ls=331° of MY26 to Ls=21° of MY34). This research is ongoing.

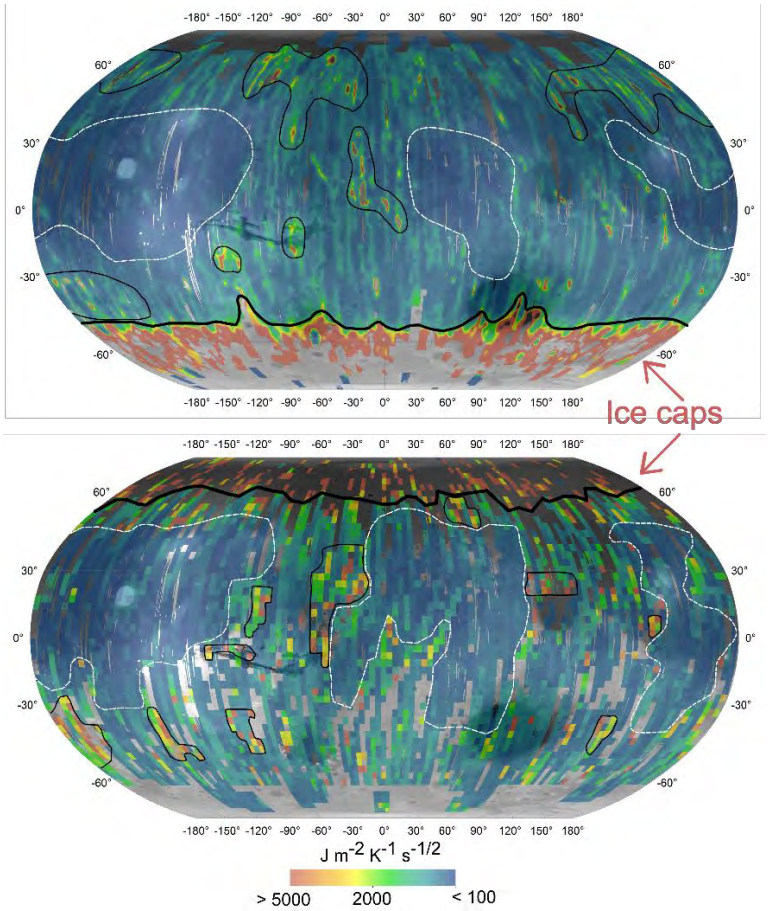

Fig. 3.92. Thermal inertia maps for Ls=90°–150° (on top) and Ls=270°–330° (at the bottom) following ATI approach. The black lines indicate the the global boundary (along ~ 1000 J m^{-2} K^{-1}s$^{-1/2}$) between the high thermal inertia values interpreted as polar ice (the red domains) and the lower thermal inertia values marked with white dashed lines representing martian soils (the blue domains)

Active magma chambers on Mars. J. Ciążela, D. Mege, B. Pieterek, M. Ciążela, J. Gurgurewicz, A. Lagain, P.-A. Tesson

In the absence of volcanic activity captured by the Mars exploration spacecrafts or associated effects such as enhanced surface thermal signatures, volcanism on Mars may appear to be extinct. Yet martian volcanic terrains are dated from Late Amazonian (2.4 Ma) to Noachian (>3.7 Ga), and atmospheric CO2 isotopic signatures indicate recent volcanic degassing. Volcanism on Mars could thus be dormant rather than extinct. We modelled magma fluxes in the two largest Martian igneous provinces, Tharsis and Elysium,

and found that the largest volcanoes of Tharsis should have erupted on average ~150 km^3/Myr in the last 10 Ma. We predict the largest active magma reservoirs to feed Olympus Mons and the Tharsis Montes. Active magma chamber under Olympus Mons would explain 2.4 Ma young lava flows found on its western flanks. In 2019, the paper was submitted to Icarus.

Hydrae Cavus: a tectonic basin in the Valles Marineris region. P.-A. Tesson, D. Mège, J. Gurgurewicz, M. Ciążela, and J. Ciążela

Previous work revealed dextral brittle-plastic NE-SW shear zones that affect the deepest parts of Hebes Chasma and Ophir Chasma, (Mège, D. and Gurgurewicz, J., 2018). Results suggested that the northern part of Valles Marineris is probably composed of large sheared tectonic blocks that moved relative to each other while Valles Marineris was being stretched perpendicular to its main, ESE trend (Schultz, 1995; Mège and Masson, 1996). Following this work, we have sought for other tectonic features linked to this shearing episode in the vicinity of Valles Marineris. Hydrae Cavus is a 20 by 60 km, 1600m deep, steep-sided depression located 130km east from Candor Chasma. Previous morphological mapping (Marra et al., 2015) suggests a tectonic origin for the opening of the basin. Using available dataset (CTX imagery and HRSC Digital Elevation Models), we have mapped the tectonic features bounding the basin and around, as well as the different terrains (early Hesperian lava flows). Preliminary results were presented during *First National Martian Seminar* and *Second Planetary Mapping and Virtual Observatory Workshop.*

Recent volcanic activity at Arsia Mons. P.-A. Tesson, D. Mège, A. Lagain, J. Gurgurewicz

Arsia Mons is the southernmost shield volcano of the Tharsis Montes. Previous study found ash-deposits north of the caldera indicating episodes of explosive activity. Effusive episodes in the form of lava flows located within the

caldera and in the southern lava apron, show transition away from explosive activity at 200 Ma. We investigated a set of fresh-looking lava flows located SE of Arsia Mons in order to constrain its late Amazonian chronology. Using available imagery (CTX, HiRISE, CaSSIS), we performed geological mapping of the individual lava flows. In order to indicate the relative stratigraphy within the geological map, we used an innovative symbology. In order to assess the absolute chronology, we use impact crater retention age derivation. The impact crater database was automatically generated from CTX mosaic by a collaborating team from Curtin University (Perth Australia) using Deep-Learning. The obtained ages range from 200 Ma to 50 Ma, with an apparent peak at 150 Ma. These ages corelates with the ones found within the caldera. Morphology of lava flows indicate magma of mafic composition. Our results confirm that after effusive volcanism resumed, activity at Arsia Mons was not restricted to the caldera or the main flanks. Future work will focus on studying the relationship between these lava flows, the ash deposits and older underlying lava fields.

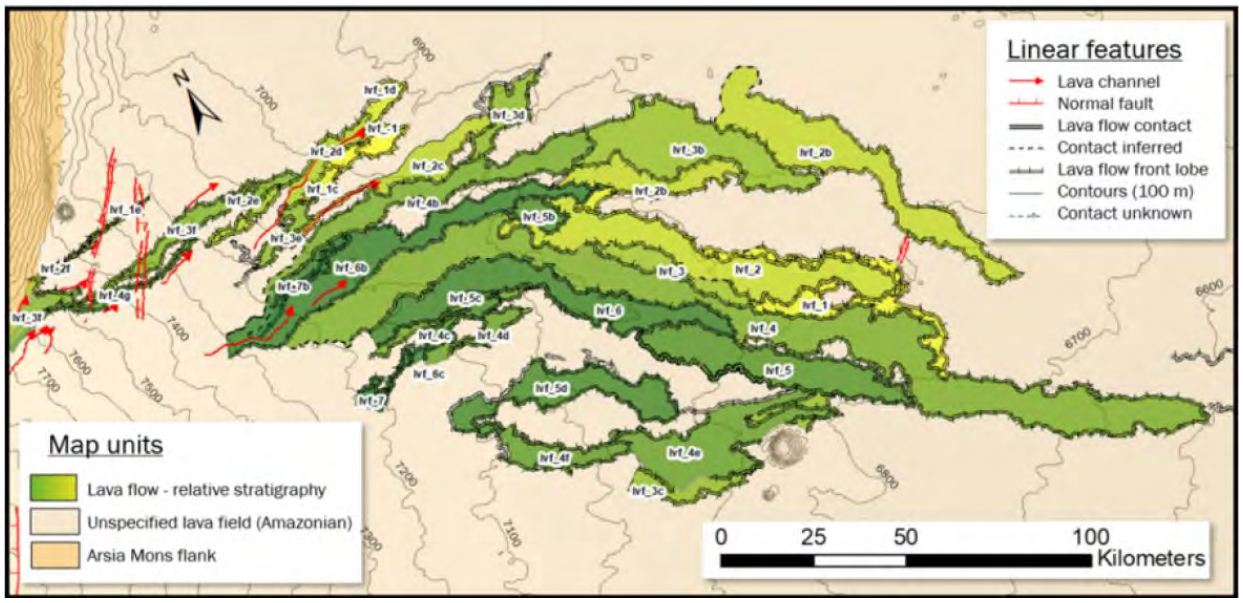

Fig. 3.93. Geological map of individual lava flows SE of Arsia Mons. Color from yellow (old) to green (young) represents the relative stratigraphy.

This work was presented during the EPSC 2020 conference as well as the Second National Mars Seminar in Cracow, Poland.

Investigation of the spectral range of the methane Q-branch in PFS spectra to detect hydrothermal activity on Mars. J. Ciążela, D. Mège, M. Giuranna

Seventeen years of Planetary Fourier Spectrometer (PFS) data has revealed absorptions in the spectral range of one of the main absorption bands of methane over the Tharsis region of Mars in 2014. Specifically, these atmosphere absorptions are observed above a site where recent (<25 Ma) small volcanic cones were built. Methane is one of the products released in small quantities among volcanic and hydrothermal gases, and the Tharsis region probably has ongoing hydrothermal activity. However, similar absorptions may be due to ozone and carbon dioxide. In this work the origin of the detected absorptions is studied.

The Global search for liquid water on Mars from orbit: current and future perspectives. R. Orosei, C. Ding, W. Fa, A. Giannopoulos, A. Hérique, W. Kofman, S. E. Lauro, C. Li, E. Pettinelli, Y. Su, S. Xing and Y. Xu

Due to its significance in astrobiology, assessing the amount and state of liquid water present on Mars today has become one of the drivers of its exploration. Subglacial water was identified by the Mars Advanced Radar for Subsurface and Ionosphere Sounding (MARSIS) aboard the European Space Agency spacecraft Mars Express through the analysis of echoes, coming from a depth of about 1.5 km, which were stronger than surface echoes. The cause of this anomalous characteristic is the high relative permittivity of water-bearing materials, resulting in a high reflection coefficient. A hdetermining factor in the occurrence of such strong echoes is the low attenuation of the MARSIS radar pulse in cold water ice, the main constituent of the Martian polar caps. The present analysis clarifies that the conditions causing exceptionally strong

subsurface echoes occur solely in the Martian polar caps, and that the detection of subsurface water under a predominantly rocky surface layer using radar sounding will require thorough electromagnetic modeling, complicated by the lack of knowledge of many subsurface physical parameters. Higher-frequency radar sounders such as SHARAD cannot penetrate deep enough to detect basal echoes over the thickest part of the polar caps. Alternative methods such as rover-borne Ground Penetrating Radar and time-domain electromagnetic sounding are not capable of providing global coverage. MARSIS observations over the Martian polar caps have been limited by the need to downlink data before on-board processing, but their number will increase in coming years. The Chinese mission to Mars that is to be launched in 2020, Tianwen-1, will carry a subsurface sounding radar operating at frequencies that are close to those of MARSIS, and the expected signal-to-noise ratio of subsurface detection will likely be sufficient for identifying anomalously bright subsurface reflectors. The search for subsurface water through radar sounding is thus far from being concluded. This review paper was published in July issue of *Life* 2020.

3.11 Comparative planetology

Nanotopographic characterization of microfractures in rocks by Atomic Force Microscopy. J. Gurgurewicz, D. Mège, M. Skiścim and J. Pers

The study of microfractures is one of the keys to understanding a variety of geological issues including: microcrack initiation and propagation; process zone characterisation and the evolution toward large-scale fracturing; the characterisation of reservoirs of geological fluids; and the identification of microhabitats outside Earth.

Atomic Force Microscopy (AFM) records nanoscale digital terrain models (nDTM), making it possible to carry out quantitative, nanoscale structural

analyses of rocks (illustrated here with two basalt samples). AFM coupled with techniques able to provide some mineralogical information, such as Scanning Electron Microscopy (SEM), has huge potential in this field, with the possibility to put fracture nanotopography into context. Not only can micro- or nanofractures be described with a resolution of ~1 nm, and be compared to ~1 µm resolution obtained using other methods, but also AFM can correct misleading SEM observations. The paper was published in *Journal of Structural Geology* (April 2019).

SOlar SYstem analogues database POLand (SOSYPOL). J. Gurgurewicz and D. Mège

The database content was described in Annual Report 2018. This year, new elements of the database infrastructure were added, allowing to create DOI of SSHADE databases and their experiments. Three experiments with NIR and MIR reflectance spectra of tholins were released to the public. The SOSYPOL database currently includes 18 experiments with over 250 spectra. Available online at *https://www.sshade.eu/db/sosypol* (December 2019).

Very high-resolution ground magnetics characterisation of hydrothermal processes in the Danakil depression. D. Mège, H. Choe, J. Dyment, H. Tsegaye, B. Ayele, B. Tadesse, H. Hansen

Understanding hydrothermal processes in salts has applications on Mars, where thick salt (sulfate) sequences are common and past or present hydrothermal systems probably widespread. Due to dissolution, hydrothermal circulation alters rock magnetization. High-resolution magnetic surveying is therefore able to distinguish between areas of strong and weak hydrothermal activity, as well as associated structural discontinuities. Preliminary results from very high-resolution magnetic surveying at unprecedented resolution were

obtained in Lake Asale, Danakil depression, near Dallol. Hydrothermal circulation patterns are correlated with geologic evidence at surface such as open fissures, hydrothermal pools, noise generated by subsurface bubbling, and moist ground. Preliminary results published in *EPSC Abstracts* (September 2019).

The 2004 tectonic and hydrothermal crisis in the Danakil depression: documenting the last continental step prior to oceanic spreading. D. Mège, D. Hauber, P. Allemand, H. Moors, M. De Craen, H. Choe, J. Dyment

This work has been conducted as a terrestrial analogue study, as well as a hazard monitoring study. The Danakil depression in Ethiopia, at the end of the southern Red Sea, has been the locus of volcanic crises in 2004-10, with emplacement of 15 dykes: one, non-emergent, in Lake Asale next to Black Mountain and south of the Dallol dome during fall 2004, the others in the Dabbahu-Manda Hararo rift segment between September 2005 and May 2010. We report on a hydrothermal crisis that opened a 4.5 km long fissure in the ground, at the same time the Black Mountain dyke was intruding the crust 2 km away and parallel to it. The fissure, located north and south of Yellow Lake (Gaet'ale) and trending NNW-SSE, is still active. Its morphology is remarkably diversified, but surface evidence of the structural deformation has been lost over the years. Its formation is coeval with the intrusion of the Black Mountain dyke intrusion. It is suggested that after its documented propagation, the Black Mountain dyke propagated aseismically eastward as a sill, disrupting the stress equilibrium in the long-living Yellow Lake hydrothermal environment. The stress field was brought to rupture by the increased deviatoric stress, triggering the nucleation of a tensile fracture that propagated to the surface and released the far-field stress already released at depth by the emplacement of the dyke. This study documents the delicate intermingling of magmatic, tectonic, and hydrothermal processes at the ultimate step of continental rifting prior to the

earliest stage of oceanic spreading. Submitted to *Geophysics, Geochemistry, Geosystems* (December 2020).

3.12 EXOMHYDR project web site. D. Mège and the EXOMHYDR team

The web site, updated monthly, introduces the objectives, activity, people, and latest news of the FNP/TEAM funded project *EXOMHYDR – Magmatic plumbing systems and tectonic control of hydrothermal activity on Mars revealed by ExoMars/TGO: constraints for life and resources*.

Available online at *http://exomhydr.eu* (December 2020).

3.13 Interdisciplinary teaching

Remote sensing and electromagnetic wave behaviour to measure vegetation phenology with physics. E. Woźniak, R. Gabryszewski, D. Dziob

Interdisciplinary models of teaching have been present in education systems for at least 30 years. The idea of the interdisciplinarity is to show students the contextualisation of subject knowledge, its relation to real-life problems and to build skills across traditional disciplinary boundaries. This is essential to future competitiveness since innovations frequently occur at the interface of disciplines when people are able to collaborate. Schools try to respond to the need to prepare students for an interdisciplinary and collaborative job market by modifying the curricula and training teachers. But one of the most primary and difficult problems is preparing a truly interdisciplinary lesson or a project. It seems that all complex issues could be good examples for this purpose. One of these complex issues is the study of climate change, which requires the collaboration of different specialists and a comprehensive understanding of the problem in different scientific fields: physical, geographical, biological, social, engineering, etc. The paper presents an interdisciplinary project which links knowledge within a few different science areas around the real-life

problem important for students. The work shows the developed and tested interdisciplinary educational project 'Panta Rhei' which integrates physics and other STEM subjects to present the biological and social consequences of changes in vegetation periods for different climate zones. It shows how Earth observation research can be utilised in schools for teaching physics and other science subjects. The project was validated on a group of Polish teachers. In the paper we present the whole project together with teachers' opinions. The article was published in May 2020 in *Physics Education*.

Interdisciplinary Teaching Using Satellite Images as a Way to Introduce Remote Sensing in Secondary School. D. Dziob, M. Krupiński, E. Woźniak, R. Gabryszewski

This article aims to meet two needs: (i) the need for skilled workers and students in the area of remote sensing and (ii) the need to make school science interesting for students. This article addresses both needs by proposing a project for high school students entitled "The colors of Earth". The main aim for students was to distinguish between different types of land cover via the creation of various false color band compositions from the satellite Sentinel-2. Achieving this goal requires knowledge from various subjects and enables their practical application via work performed using real data. The project was presented to 39 high-school teachers and 184 high-school students (K-9 and K-10) in the summer semester of the 2019/2020 school year, and their opinions about the project were collected. Overall, both students and teachers judged the project to be interesting, worth introducing to the school, and capable of influencing student opinions of science. In addition, introducing remote sensing elements during pre-university education can help meet the demands for students and workers to study Earth observation. The article was published in September 2020 in *Remote Sensing*.

The FUTURE SPACE PROJECT

The EU-funded FUTURE SPACE project is focused on astronomy and space exploration. It aims to be a catalyst for change in understanding and teaching STEM subjects in European education. The two main deliverables are the Space Schools Programme and the Space Programme for science centres and other informal education organizations.

In 2020 the consortium prepared the first deliverables to be evaluated at schools and science centres. The following SRC PAS employees were involved in creation of deliverables: Ryszard Gabryszewski, Aleksandra Grzegorczyk, Michał Krupiński, Joanna Pietrzak, Małgorzata Michalska, Paweł Wajer, Gordon Wasilewski, Edyta Woźniak and Natalia Zalewska.

The consortium consists of 5 partners: Computer Assisted Education and Information Technology Centre (OEliZK), Warszawa, Poland; NEMO Science Museum, Amsterdam, the Netherlands; NOESIS Science Centre and Technology Museum at Thessaloniki, Greece; Polish Space Agency in Gdańsk, Poland and Space Research Centre Polish Academy of Sciences.

PUBLICATIONS

1. Ahluwalia, H. S., MODZELEWSKA, R., *Galactic Cosmic Ray Transport in the Heliosphere: Study with Muon data,* Advances in Space Research, vol. 66, 2, 462-467, (2020) https://doi.org/10.1016/j.asr.2020.03.042
2. Baranets, N., Ruzhin, Yu., Dokukin, V., Ciobanu, M., ROTHKAEHL, H., KIRAGA, A., Vojta, J., Šmilauer, J., Kudela, K., *Injection of 40-kHz-modulated electron beam from the satellite: II. Excitation of electrostatic and whistler waves*, Advances in Space Research Volume 65, Issue 1, 1 January 2020, Pages 30-49, https://doi.org/10.1016/j.asr.2019.08.027
3. BARYLAK, J., Dudnik, O.V., Wozniczak, T, Adamenko, V.O., Antypenko, R.V., Yezerskyi, N.V., KOWALINSKI, M., Lazarev, I.Y., ZIELINSKA, A., SYLWESTER, J., BAKALA, J., PODGÓRSKI, P., *Simulation of CubeSat caliber particle detector "MiRA_ep" response to energetic electrons and protons using GEANT4 package*, Proceedings of the SPIE, 11176, id. 111763C (2019), doi: 10.1117/12.2536748
4. Bergeot, N., Witasse, O., Le Maistre, S., Blelly P.-L., KOFMAN W., Peter K., Dehant V., Chevalier, J.-M., *MoMo: a new empirical model of the Mars ionospheric total electron content based on Mars Express MARSIS data*, Journal of Space Weather and Space Climate, Volume 9, A36 (2019a), doi: 10.1051/swsc/2019035
5. Bergeot, N., Witasse, O., Le Maistre, S., Blelly P.-L., KOFMAN W., Peter K., Dehant V., Chevalier, J.-M., *A new empirical model for Mars Ionospheric to correct radio signal experiments*, EPSC Abstracts, 13, EPSC-DPS2019-642 (2019b)
6. Bickel, V. T., S. J. Conway, P. -A. TESSON, A. Manconi, S. Loew and U. Mall., *Deep Learning-Driven Detection and Mapping of Rockfalls on Mars*, IEEE Journal of Selected Topics in Applied Earth Observations and Remote Sensing, vol. 13, pp. 2831-2841, 2020; DOI: 10.1109/JSTARS.2020.2991588.
7. Borykov, T., MÈGE D., Mangeney A., Richard P., GURGUREWICZ J., Lucas A., *Empirical investigation of friction weakening of terrestrial and Martian landslides using discrete element models*., Landslides 16, 1121–1140 (2019), doi: 10.1007/s10346-019-01140-8
8. BŁĘCKI, J., SŁOMIŃSKI, J., WRONOWSKI, R., SŁOMIŃSKA, E., IWAŃSKI, R., Parrot, M., Haagmans, R., *Comparison of the Plasma Disturbances in the Ionosphere Registered by DEMETER and Swarm Satellites during Geomagnetic and Thunderstorms*, 16-th European Space Weather Week, 18-22 November 2019, Liège, Belgium, (2019)

9. BŁĘCKI JAN, WRONOWSKI ROMAN, SŁOMIŃSKI JAN, Sergey Savin, IWAŃSKI RAFAŁ, Roger Haagmans, *COMPARATIVE STUDY OF THE ENERGETIC ELECTRONS REGISTERED TOGETHER WITH THE BROAD BAND EMISSIONS IN DIFFERENT REGIONS OF THE IONOSPHERE*, 2020, Art. Sat. vol.55, No 4,, DOI: 10.2478/arsa-2020-0010
10. BZOWSKI, M., CZECHOWSKI, A., Frisch, P.C., Fuselier, S.A., Galli, A., GRYGORCZUK, J., Heerikhuisen, J., KUBIAK, M.A., Kucharek, H., McComas, D.J., Möbius, E., Schwadron, N.A., Slavin, J., SOKÓŁ, J.M., Swaczyna, P., Wurz, P., Zirnstein, E.J. – 2019, *Interstellar neutral helium in the heliosphere from IBEX observations. VI. The He+ density and the ionization state in the Very Local Interstellar Matter,* Astrophysical Journal 882:60, 10.3847/1538-4357/ab3462
11. BZOWSKI, M., GALLI, A. – 2019, *Energetic neutral atoms from the heliosheath as an additional population of neutral hydrogen in the inner heliosphere*, Astrophysical Journal 870:58, 10.3847/1538-4357/aaf1b2
12. BZOWSKI, M., Heerikhuisen, J. – 2020, *On the sensitivity of heliosphere models to the uncertainty of the low-energy charge exchange cross section*, Astrophysical Journal 888:24, 10.3847/1538-4357/ab595a
13. BZOWSKI, M., KUBIAK, M.A. – 2020, *Time delay between outer heliosheath crossing and observation of interstellar neutral atoms*, Astrophysical Journal 901:12, 10.3847/1538-4357/abada2
14. Carley, E. P., Baldovin, C., Benthem, P., Bisi, M. M., Fallows, R. A., Gallagher, P. T., Olberg, M., ROTHKAEHL, H., Vermeulen, R., Vilmer, N., Barnes, D., and the LOFAR4SW Consortium, *Radio observatories and instrumentation used in space weather science and operations,* J. Space Weather Space Clim., 2020, 10, 7, https://doi.org/10.1051/swsc/2020007
15. Chen, C., CIĄŻELA, J., Li, W., Dai, W., Wang, Z., Jin, Z., Foley, S.F., Ming, L., Hu, Z., and Liu, Y. *Calcium isotopic compositions of oceanic crusts at various spreading rates*, Geochimica et Cosmochimica Acta. Published online: July 2019, (2019a), doi: 10.1016/j.gca.2019.07.008
16. CIĄŻELA, M., CIĄŻELA J., MÈGE D., Giuranna M., PODGÓRSKI P., PIETEREK B., GURGUREWICZ J., TESSON P-A, WOLKENBERG P., *First thermal inertia maps from PFS/MEX dataset to track ice distribution on Mars*. EPSC Abstracts, 13, EPSC-DPS2019-1523 (2019a)
17. CIĄŻELA, J., MÈGE D., PIETEREK B., CIĄŻELA M., GURGUREWICZ J., Lagain A., TESSON P.-A., *Largest Tharsis Volcanoes keep growing and mark >4-Ga-lasting martian hot spots*, 50th LPSC, Abstract 1364, (2019b)

18. CIĄŻELA, J., PIETEREK B., Boulanger M., Dick H., France L., Koepke J., Kuhn T., MUSZYŃSKI A., Strauss H., and WĘGORZEWSKI A., *Sulfide differentiation at the lower oceanic crust with high magma supply fractional crystallization and melt-rock reaction* (IODP Hole U1473A, Atlantis Bank)., Geophysical Research Abstracts 21, EGU2019-1516-1, (2019c)
19. Conroy, P., Quinsac, G., Floury, N., Witasse, O., Cartacci, M., Orosei, R., KOFMAN, W., Sánchez-Cano, B., (2020). *A new method for determining the total electron content in Mars' ionosphere based on Mars Express MARSIS data*. Planetary and Space Science, 182, article id. 104812, doi: 10.1016/j.pss.2019.104812.
20. Cremonese, G.; Capaccioni, F.; Capria, M. T.; Doressoundiram, A.; Palumbo, P.; Vincendon, M.; Massironi, M.; Debei, S.; Zusi, M.; Altieri, F.; Amoroso, M.; Aroldi, G.; Baroni, M.; Barucci, A.; Bellucci, G.; Benkhoff, J.; Besse, S.; Bettanini, C.; BLECKA, M.; Borrelli, D. Brucato, J. R.; Carlo, C.; Carlier, V.; Cerroni, P.; Cicchetti, A.; Colangeli, L.; Dami, M.; Da Deppo, V.; Della Corte, V.; De Sanctis, M. C.; Erard, S.; Esposito, F.; Fantinel, D.; Ferranti, L.; Ferri, F.; FicaiÂ Veltroni, I.; Filacchione, G.; Flamini, E.; Forlani, G.; Fornasier, S.; Forni, O.; Fulchignoni, M.; Galluzzi, V.; Gwinner, K.; Ip, W.; Jorda, L.; Langevin, Y.; Lara, L.; Leblanc, F.; Leyrat, C.; Li, Y.; Marchi, S.; Marinangeli, L.; Marzari, F.; MazzottaÂ Epifani, E.; Mendillo, M.; Mennella, V.; Mugnuolo, R.; Muinonen, K.; Naletto, G.; Noschese, R.; Palomba, E.; Paolinetti, R.; Perna, D.; Piccioni, G.; Politi, R.; Poulet, F.; Ragazzoni, R.; Re, C.; Rossi, M.; Rotundi, A.; Salemi, G.; Sgavetti, M.; Simioni, E.; Thomas, N.; Tommasi, L.; Turella, A.; Van Hoolst, T.; Wilson, L.; Zambon, F.; Aboudan, A.; Barraud, O.; Bott, N.; Borin, P.; Colombatti, G.; ElÂ Yazidi, M.; Ferrari, S.; Flahaut, J.; Giacomini, L.; Guzzetta, L.; Lucchetti, A.; Martellato, E.; Pajola, M.; Slemer, A.; Tognon, G.; Turrini, D., *SIMBIO-SYS: Scientific Cameras and Spectrometer for the BepiColombo Mission*, Space Science Reviews, 2020, Volume 216, Issue 5, article id.75. DOI: 10.1007/s11214-020-00704-8
21. CZECHOWSKI, A., BZOWSKI, M., SOKÓŁ, J.M., KUBIAK, M.A., Heerikhuisen, J., Zirnstein, E.J., Pogorleov, N.V., Schwadron, N.A., Hilchenbach, M., Grygorczuk, J., Zank, G.P. – 2020, *Heliospheric structure as revealed by the 3 – 88 keV H ENA spectra*, Ap.J. 888:1, 10.3847/1538-4357/ab5b14
22. CZECHOWSKI, A.,, M. Hilchenbach, K. C. Hsieh, M. BZOWSKI, S. GRZEDZIELSKI, J. M. SOKÓŁ, J. GRYGORCZUK, *Structure of the heliosheath from HSTOF energetic neutral atoms measurements*, Astronomy & Astrophysics, 618, A26, (2018a), doi: 10.1051/0004-6361/201732432

23. CZECHOWSKI, A., I. Mann, *Dynamics of nanodust particles emitted from elongated initial orbits*, Astronomy & Astrophysics, 617, A43, (2018b), doi: 10.1051/0004-6361/201832922
24. CZECHOWSKI L., ZALEWSKA N., CIĄŻELA J., *Isidis Planitia: its regional and local characteristics*, European Planetary Science Congress Abstracts, Vol.14, EPSC2020-795, 2020
25. CZECHOWSKI L., ZALEWSKA N., ZAMBROWSKA A., CIĄŻELA M., WITEK P., KOTLARZ J., *Mechanism of Origin of Chains of Cones in Chryse Planitia*, European Planetary Science Congress Abstracts. Vol.14, EPSC2020-895, 2020.
26. CZECHOWSKI L., ZALEWSKA N., WITEK P., KOTLARZ J., *Origin of chains of cones in Chryse Planitia*, 51st Lunar and Planetary Science Conference. 2982, 2020
27. Dick, H.J.B., MacLeod, C.J., Blum, P., Abe, N., Blackman, D.K., Bowles, J.A., Cheadle, M.J., Cho, K., CIĄŻELA, J., Deans, J.R., Edgcomb, V.P., Ferrando, C., France, L., Ghosh, B., Ildefonse, B.M., Kendrick, M.A., Koepke, J.H., Leong, J.A.M., Liu, C., Ma, Q., Morishita, T., Morris, A., Natland, J.H., Nozaka, T., Pluemper, O., Sanfilippo, A., Sylvan, J.B., Tivey, M.A., Tribuzio, R., and Viegas, G., *Dynamic accretion beneath a slow-spreading ridge segment: IODP Hole 1473A and the Atlantis Bank Oceanic Core Complex*, Journal of Geophysical Research: Solid Earth, published online in November 2019, (2019d), doi: 10.1029/2018JB016858
28. Dudnik, O.V., SYLWESTER, J., KOWALINSKI, M., BARYLAK, J., *Utilization of design features of the particle telescope STEP-F and solar x-ray spectrophotometer SphinX for exploration of the Earth's radiation belt properties*, Proceedings of the SPIE, Volume 11176, id. 111763L (2019), doi: 10.1117/12.2537296
29. DYBCZYŃSKI, P.A., KRÓLIKOWSKA, M., WYSOCZAŃSKA, R., *Kruger 60 as a home system for 2I/Borisov – a case study*, arXiv e-print : arXiv:1911.01735 (2019)
30. DZIOB D., KRUPIŃSKI M., WOŹNIAK E., GABRYSZEWSKI R. (2020), *Interdisciplinary Teaching Using Satellite Images as a Way to Introduce Remote Sensing in Secondary School,* Remote Sens. 2020, 12(18), 2868. doi:10.3390/rs12182868
31. Dzurilla, K., Chevrier V., Nna-Mvondo D., MÈGE D., Farnsworth K., *Detection and reactivity of Titan tholin in liquid hydrocarbon*, 50th LPSC, Abstract 3234, (2019a)

32. Dzurilla, K., Nna-Mvondo D., MÈGE D., Chevrier, V., *Detection and reactivity of Titan tholin in liquid hydrocarbons*, EPSC Abstracts, 13, EPSC-DPS2019-1855, (2019b)
33. Dzurilla, K., Nna Mvondo, D., MÈGE, D., Chevrier, V.F., 2020, *Detection and reactivity of Titan tholins in liquid hydrocarbons containing polar compounds,* 51st Lunar and Planetary Science Conference 2020, Abstract 2624c.
34. Eyraud, C., Sorsa L.-I., Hérique A., Pursiainen S., KOFMAN W., *Imaging the interior of small solar bodies: towards a quantitative approach*, 2019 International Conference on Electromagnetics in Advanced Applications (ICEAA) Pages 0695-0695, (2019)
35. Eyraud, C., Sorsa, L. -I., Herique, A., Geffrin, J. -M., Pursiainen, S., KOFMAN, W., *Towards Asteroid Tomography: Modellings and Measurements Using an analogue model*,
Proceedings of the European Conference on Antennas and Propagation, 14th European Conference on Antennas and Propagation (EuCAP), Copenhagen, Denmark, Mar 15-20, 2020.
36. Fallows, R. A. and 58 co-authors including H. ROTHKAEHL and B. MATYJASIAK from CBK PAN, *A LOFAR Observation of Ionospheric Scintillation from Two Simultaneous Travelling Ionospheric Disturbances*, J. Space Weather Space Clim., Volume 10, 2020, Topical Issue - Scientific Advances from the European Commission H2020 projects on Space Weather, https://doi.org/10.1051/swsc/2020010
37. GABRYSZEWSKI, R., and GRZEGORCZYK, A., *The FUTURE SPACE Project Progress Meeting May 2020*, oral communication, FUTURE SPACE transnational virtual project meeting, Centrum Badań Kosmicznych PAN, May 27th, 2020.
38. GABRYSZEWSKI, R., and GRZEGORCZYK, A., *The FUTURE SPACE Project Progress Meeting October 2020 – COVID Amendment*, oral communication, FUTURE SPACE second transnational virtual project meeting, Centrum Badań Kosmicznych PAN, Oct 21st, 2020.
39. GIL, A. and ALANIA, M.: *α-ω effect and recurrent changes of galactic cosmic rays intensity*, Proceedings of Science (35th International Cosmic Ray Conference), Vol. 301, (2018), https://pos.sissa.it/cgi-bin/reader/conf.cgi?confid=301, id.30
40. GIL, A.; Kovaltsov, G. A.; Mikhailov, Vladimir V.; Mishev, Alexander; Poluianov, Stepan; Usoskin, I. G. *An Anisotropic Cosmic-Ray Enhancement Event on 07-June-2015: A Possible Origin*, Solar Physics,

Volume 293, Issue 11, id. 154, 10 pp., (2018), doi: 10.1007/s11207-018-1375-5
41. GIL, A.; Mursula, K.: *Comparing Two Intervals of Exceptionally Strong Solar Rotation Recurrence of Galactic Cosmic Rays*, Journal of Geophysical Research: Space Physics, Volume 123, Issue 8, pp. 6148-6160, (2018), doi: 10.1029/2018JA025523
42. GIL, A., MODZELEWSKA, R., MOSKWA, S., SILUSZYK, A., SILUSZYK, M., WAWRZYNCZAK, A., ZAKRZEWSKA, S., *Does time series analysis confirms the relationship between space weather effects and the failures of electrical grids in South Poland?*, Journal of mathematics in industry, 9, 7, (2019b), doi: 10.1186/s13362-019-0064-9
43. GIL, A.; Asvestari, E.; Kovaltsov, G.; Usoskin, I., *Effective Energy of Neutron Monitors and Cosmogenic Isotopes* (p.10485), 20th EGU General Assembly, EGU2018, 4-13 April, 2018, Vienna, Austria, (2018)
44. GIL, A., R. MODZELEWSKA, SZ. MOSKWA, A. SILUSZYK, M. SILUSZYK, A. WAWRZYNCZAK, S. ZAKRZEWSKA: *Electrical grids' failures in southern Poland in 2010 and 2014 in association to space weather effects*, 15 European Space Weather Week, 5-9 November 2018, Leuven, Belgium, (2018)
45. GIL, A..; MODZELEWSKA, R.; SILUSZYK, M.; WAWRZYNCZAK-SZABAN, A.; MOSKWA, SZ.: F*ailures in electrical grids in southern Poland in 2010 and 2014 in relation to space weather effects*, (C1.3-38-18), 42nd COSPAR Scientific Assembly, 14-22 July 2018, Pasadena, California, USA, (2018)
46. GIL, A., and M. ALANIA, *How Sun produces quasi-biennial oscillations of cosmic rays*, (D1.3-41-18), 42nd COSPAR Scientific Assembly, 14-22 July 2018, Pasadena, California, USA, (2018)
47. GIL, A.; Usoskin, I.; Kovaltsov, G. A.; Asvestari, E.: *The effective energy for neutron monitors and cosmogenic isotopes-redefined concept*, (D2.4-34-18), 42nd COSPAR Scientific Assembly, 14-22 July 2018, Pasadena, California, USA, (2018)
48. GIL, A.; Mursula, K., *Comparing the recurrence of cosmic ray intensity at solar rotation period in solar cycles 23 and 24*, (D1.3-21-18), 42nd COSPAR Scientific Assembly, 14-22 July 2018, Pasadena, California, USA, (2018)
49. GIL, A.; MODZELEWSKA, R.; WAWRZYNCZAK, A., *Does space weather effect energy infrastructure in Poland?* (10541), 20th EGU General Assembly, EGU2018, 4-13 April, 2018, Vienna, Austria, (2018)
50. GIL, A., R. MODZELEWSKA, S. MOSKWA, A. SILUSZYK, M. SILUSZYK AND A. WAWRZYNCZAK, *Indicators of Space Weather Events in Cosmic Rays Flux*

During the Solar Cycle 24, 36 International Cosmic Ray Conference (ICRC), Madison, Wisconsin, USA, 24 July - 1 August, 2019, (2019a)

51. GIL, A., G. Kovaltsov, V. Mikhailov, A. Mishev, S. Poluianov and I. Usoskin, *Anisotropic Cosmic-ray Enhancement (ACRE): Case Studies of 07-Jun-2015 and 26-Aug-2018*, 36 International Cosmic Ray Conference (ICRC), Madison, Wisconsin, USA, 24 July - 1 August, 2019, (2019)
52. GIL, A., and M. ALANIA, *Differential Rotation of the Sun as a Source of Galactic Cosmic Rays Quasi-biennial Oscillations*, 36 International Cosmic Ray Conference (ICRC), Madison, Wisconsin, USA, 24 July - 1 August, 2019, (2019)
53. GIL, A.; MODZELEWSKA, R.; MOSKWA, SZ.; SILUSZYK, A.; SILUSZYK, M.; WAWRZYNCZAK, A.: *Relationship between space weather effects and failures of electrical grids in South Poland* (id.16259), 21st EGU General Assembly, 7-12 April, 2019, Vienna, Austria, (2019)
54. GIL, A., R. MODZELEWSKA, SZ. MOSKWA, M. POZOGA, A. SILUSZYK, M. SILUSZYK, L. TOMASIK, A. WAWRZYNCZAK: *Space weather effects on the energy infrastructure in Poland*, International Workshop on GNSS Ionosphere (IWGI2019)-Theory, Algorithms, Modelling and Applications, Neustrelitz, Germany, September 23-25, 2019, (2019)
55. GIL, A., R.MODZELEWSKA, SZ. MOSKWA, A. SILUSZYK, M. SILUSZYK, A. WAWRZYNCZAK: *Electrical grids failures in Poland related to space weather effects*, Space Climate 7 Symposium, 8-11 July 2019 in Orford, Canada, (2019)
56. GIL, A., R. MODZELEWSKA, SZ. MOSKWA, A. SILUSZYK, M. SILUSZYK, A. WAWRZYNCZAK: *Geomagnetically induced currents and electrical grid failures in Poland during solar cycle 24*, 16 European Space Weather Week, 18-22 November 2019, Liège, Belgium, (2019)
57. GIL, A., MODZELEWSKA, R., MOSKWA, S., SILUSZYK, A., SILUSZYK, M., WAWRZYŃCZAK, A., POZOGA, M., DOMIJANSKI, S., *Transmission Lines in Poland and Space Weather Effects*, Energies, 13, 9, (2020a), doi: 10.3390/en13092359
58. GIL, A., MODZELEWSKA, R., MOSKWA, S., SILUSZYK, A., SILUSZYK, M., WAWRZYŃCZAK, A., POZOGA, M., TOMASIK, L., *The Solar Event of 14–15 July 2012 and Its Geoeffectiveness, Solar Physics*, 295, 135, (2020b), doi: 10.1007/s11207-020-01703-2
59. GRZEGORCZYK, A., and GABRYSZEWSKI, R., *Projekt FUTURE SPACE*, webinarium PAK / ESERO Polska „Edukacja kosmiczna w szkole i nie tylko", Sep 17th, 2020.

60. GRZEGORCZYK, A., and GABRYSZEWSKI, R., *The FUTURE SPACE Project Progress Meeting October 2020*, oral communication, FUTURE SPACE second transnational virtual project meeting, Centrum Badań Kosmicznych PAN, Oct 21st, 2020.
61. GURGUREWICZ J., MÈGE D., Skiścim M., Pers J., *Nanotopographic characterization of microfractures in rocks by Atomic Force Microscopy*, Journal of Structural Geology 124, 70-80 (2019), doi: 10.1016/j.jsg.2019.04.010é
62. Heggy E., Palmer E.M., Hérique A., KOFMAN W., El-Maarry M. R., *Post-rendezvous radar properties of comet 67P/CG from Rosetta Mission: understanding future Earth-based radar observations and the dynamical evolution of comets*, Monthly Notices of the Royal Astronomical Society, 489, p. 1667-1683 (2019), doi: 10.1093/mnras/stz2174
63. Herique A., KOFMAN W., Zine S., Blum J., Vincent J. -B., Ciarletti V., *Homogeneity of 67P/Churyumov-Gerasimenko as seen by CONSERT: implication on composition and formation*, Astronomy and Astrophysics 630, A6 (2019), doi: 10.1051/0004-6361/201834865
64. Hérique A., KOFMAN W., Zine S., Blum J., Vincent J.-B., Ciarletti V., *Composition Homogeneity of 67P as seen by CONSERT*, EPSC Abstracts, 13, EPSC-DPS2019-1483,(2019)
65. Hérique, A., Plettemeier D., KOFMAN W., Rogez Y., Buck C., Goldberg H., *A Low Frequency Radar to Fathom Asteroids from Juventas Cubedat on HERA*, EPSC Abstracts, 13, EPSC-DPS2019-807, (2019)
66. Hollick Sophia, J., Charles W. Smith, Zackary B. Pine, Matthew R. Argall, Colin J. Joyce, Philip A. Isenberg, Bernard J. Vasquez, Nathan A. Schwadron, JUSTYNA M. SOKÓŁ, MACIEJ BZOWSKI, and MARZENA A. KUBIAK, *Magnetic Waves Excited by Newborn Interstellar Pickup Ions Measured by the Voyager Spacecraft from 1 to 45 au. I. Wave Properties*, The Astrophysical Journal, 863, (2018a), doi: 10.3847/1538-4357/aac83b
67. Hollick Sophia, J., Charles W. Smith, Zackary B. Pine, Matthew R. Argall, Colin J. Joyce, Philip A. Isenberg, Bernard J. Vasquez, Nathan A. Schwadron, JUSTYNA M. SOKÓŁ, MACIEJ BZOWSKI, and MARZENA A. KUBIAK, *Magnetic Waves Excited by Newborn Interstellar Pickup Ions Measured by the Voyager Spacecraft from 1 to 45 au. {II}. Instability and Turbulence Analyses*, The Astrophysical Journal, 863, (2018b), doi: 10.3847/1538-4357/aac839
68. Hollick Sophia, J., Charles W. Smith, Zackary B. Pine, Matthew R. Argall, Colin J. Joyce, Philip A. Isenberg, Bernard J. Vasquez, Nathan A.

Schwadron, JUSTYNA M. SOKÓŁ, MACIEJ BZOWSKI, MARZENA A. KUBIAK, *Magnetic Waves Excited by Newborn Interstellar Pickup Ions Measured by the Voyager Spacecraft from 1 to 45 au. {III}. Observation Times*, The Astrophysical Journal Supplement Series, 237, (2018c), doi: 10.3847/1538-4365/aac83a

69. ISKRA, K.; SILUSZYK, M.; ALANIA, M.; WOZNIAK, W.: *Experimental Investigation of the Delay Time in Galactic Cosmic Ray Flux in Different Epochs of Solar Magnetic Cycles, 1959 - 2014,* Solar Physics, Volume 294, Issue 9, article id. 115, 14 pp., (2019), doi: 10.1007/s11207-019-1509-4
70. JANDA, A. Z., *Exact solutions and singularities of an X-point collapse in Hall magnetohydrodynamics*, Journal of Mathematical Physics, American Institute of Physics, 59, 061509, (2018), doi: 10.1063/1.5026876
71. Kappel, D., Arnold G., Moroz, L., Raponi A., Ciarniello M., Tosi F., Erard S., Leyrat C., BŁĘCKA M.I., Filacchione G., Capaccioni F., *Geometric preprocessing for Rosetta/VIRTIS-M measurements of comet 67P/C-G*, EPSC Abstracts, 13, EPSC-DPS2019-456, (2019)
72. KEPA, A., SYLWESTER, B., SYLWESTER, J., GRYCIUK, M., SIARKOWSKI, M., *Analysis of the differential emission measure distributions for solar flares observed by RESIK*, Journal of Atmospheric and Solar-Terrestrial Physics, Volume 179, (2018), doi: 10.1016/j.jastp.2018.09.004
73. KEPA, A., SYLWESTER, B., SYLWESTER, J.,MROZEK, T., SIARKOWSKI, M.,A *Multiwavelength Analysis of the Long-duration Flare Observed on 15 April 2002*, Solar Physics, Volume 295, id.22 (2020), doi: 10.1007/s11207-020-1581-9
74. KOFMAN W., Zine S., Hérique A.,, Rogez Y., Jorda L., *Revisiting CONSERT results taking into account the exact lander position on the comet,* AGU Fall Meeting 2019, P31B-3438 https://agu.confex.com/agu/fm19/meetingapp.cgi/Paper/514517, (2019)
75. KOFMAN W., Zine S., Herique A., Rogez Y., Jorda L., Levasseur-Regourd A.Ch. (2020). *The interior of Comet 67P/C–G; revisiting CONSERT results with the exact position of the Philae lander*. Astronomy & Astrophysics, 497, 2616–2622 doi: 10.1093/mnras/staa2001.
76. KOFMAN, W., and Herique, A., (Invited paper) *Ionospheric measurements using the subsurface sounding radars: MARSIS, SHARAD, RIME and REASON*, URSI GASS 2020, Rome, Italy, 29 August - 5 September 2020 (shifted to 2021)

77. KOWALSKA-LESZCZYNSKA, IZABELA ,MACIEJ BZOWSKI, JUSTYNA M. SOKÓŁ, and MARZENA A. KUBIAK, *Evolution of the Solar Lyα Line Profile during the Solar Cycle*, The Astrophysical Journal, 852, (2018a), doi: 10.3847/1538-4357/aa9f2a
78. KOWALSKA-LESZCZYNSKA, IZABELA, MACIEJ BZOWSKI, JUSTYNA M. SOKÓŁ, and MARZENA A. KUBIAK, *Evolution of the Solar Lyα Line Profile during the Solar Cycle. II. How Accurate Is the Present Radiation Pressure Paradigm for Interstellar Neutral H in the Heliosphere?*, The Astrophysical Journal, 868, (2018b), doi: 10.3847/1538-4357/aae70b
79. KOWALSKA-LESZCZYŃSKA, I., BZOWSKI, M., KUBIAK, M.A., SOKÓŁ, J.M. – 2020, *Update of the solar Lyman-alpha profile line model*, Ap.J.S. 247:62, 10.3847/1538-4365/ab7b77
80. KOTLARZ J., ZIELENKIEWICZ U., ZALEWSKA N., KUBIAK K., *Microbial Component Detection in Enceladus Snowing Phenomenon*, Astrophysical Bulletin, volume 75, pages 166-175. DOI: 10.1134/s199034132002008x, 2020.
81. KROMUSZCZYŃSKA O., MÈGE D., DĘBNIAK K., GURGUREWICZ J., MAKOWSKA M., Lucas A., *Deep-seated gravitational slope deformation scaling on Mars and Earth: same fate for different initial conditions and structural evolutions*, Earth Surface Dynamics 7, 361–376, (2019), doi: 10.5194/esurf-7-361-201
82. KRÓLIKOWSKA M., DYBCZYŃSKI P.A., *Discovery statistics and the 1/a-distribution of long-period comets detected over the 1801--2017 period*, Monthly Notices of the Royal Astronomical Society, 484, p. 3463-3475, (2019), doi: 10.1093/mnras/stz025
83. KRÓLIKOWSKA M. and DYBCZYŃSKI P. A. *The catalogue of cometary orbits and their dynamical evolution,* Astronomy and Astrophysics 2020, Volume 640, id: A97. doi: 10.1051/0004-6361/202038451.
84. KRÓLIKOWSKA, M., (2020). *Non-gravitational effects change the original 1/a-distribution of near-parabolic comets,* Astronomy & Astrophysics, 633, id. A80, doi: 10.1051/0004-6361/201936316.
85. Krucker, S., Hurford, G.J., Grimm, O., Kögl, S., Gröbelbauer, H.-P., Etesi, L., Casadei, D., Csillaghy, A., Benz, A.O., Arnold, N.G., Molendini, F., ORLEANSKI, P., Schori, D., Xiao, H., Kuhar, M., Hochmuth, N., Felix, S., Schramka, F., Marcin, S., Kobler, S., Iseli, L., Dreier, M., Wiehl, H.J., Kleint, L., Battaglia, M., Lastufka, E., Sathiapal, H., Lapadula, K., Bednarzik, M., Birrer, G., Stutz, St., Wild, Ch., Marone, F., SKUP, K.R., CICHOCKI, A., BER, K., RUTKOWSKI, K., BUJWAN, W., JUCHNIKOWSKI, G., WINKLER, M.,

DARMETKO, M., MICHALSKA, M., SEWERYN, K., BIALEK, A., OSICA, P., SYLWESTER, J., KOWALINSKI, M., SCISLOWSKI, D., SIARKOWSKI, M., STESLICKI, M., MROZEK, T., PODGÓRSKI, P., Meuris, A., Limousin, O., Gevin, O., Le Mer, I., Brun, S., Strugarek, A., Vilmer, N., Musset, S., Maksimovic, M., Fárník, F., Kozácek, Z., Kašparová, J., Mann, G., Önel, H., Warmuth, A., Rendtel, J., Anderson, J., Bauer, S., Dionies, F., Paschke, J., Plüschke, D., Woche, M., Schuller, F., Veronig, A. M., Dickson, E. C. M., Gallagher, P.T., Maloney, S.A., Bloomfield, D.S., Piana, M., Massone, A.M., Benvenuto, F., Massa, P., Schwartz, R.A., Dennis, B.R., van Beek, H.F., Rodríguez-Pacheco, J., Lin, R.P., *The Spectrometer/Telescope for Imaging X-rays (STIX)*, Astronomy & Astrophysics, id.A15, (2020), doi: 10.1051/0004-6361/201937362)

86. KUBIAK, M.A., BZOWSKI, M., SOKÓŁ, J.M. – 2019, *Distribution function of neutral helium outside and inside the heliopause*, Astrophysical Journal 882:114, 10.3847/1538-4357/ab3404
87. Kuzin, S.V., Kirichenko, A.S., STESLICKI, M., SYLWESTER, J., SIARKOWSKI, M., SZAFORZ, Z., PLOCIENIAK, S., BAKALA, J., BARYLAK, J., PODGÓRSKI, P., SCISLOWSKI, D., KOWALINSKI, M., Bogachev, S.A., Pertsov, A.A., *SOLPEX Complex for Studies of Solar Radiation in the Soft X-Ray Range*, Technical Physics, 64 (2020), doi: 10.1134/S1063784219120132
88. Lai I.L., and 45 co-authors including H.RICKMAN, *Seasonal variations in source regions of the dust jets on comet 67P/Churyumov-Gerasimenko*, Astronomy and Astrophysics, 630, A17, (2019), doi: 10.1051/0004-6361/201732094
89. MARTYNSKI, KAROL & KULAK, ANDRZEJ & MLYNARCZYK, JANUSZ & BLECKI, J. & WRONOWSKI, ROMAN & IWANSKI, RAFAŁ, *Connections between electromagnetic signals generated by Mesoscale Convective Systems, observed by an ELF ground station and DEMETER satellite*. Publications of the Institute of Geophysics, Polish Academy of Sciences; Geophysical Data Bases, Processing and Instrumentation. 425. 85-88, (2019), doi: 10.25171/InstGeoph_PAS_Publs-2019-016
90. MARTYNSKI KAROL, BLECKI JAN, WRONOWSKI ROMAN, KULAK ANDRZEJ, MLYNARCZYK JANUSZ, IWANSKI RAFAL, *Mesoscale Convective Systems as a source of electromagnetic signals registered by ground-based system and DEMETER satellite*, Annales Geophysicae, 2021, accepted
91. Massironi M., De Toffoli B., Pozzobon R., MÈGE D., Marinangelli L., GURGUREWICZ J., Pompilio L., Rossi A.P., Sauro F., Pajola M., Lucchetti A., Tornabene L., Cremonese G., Thomas, N., *Late lava flows and*

hydrothermal alteration in Ladon basin, Mars, Geophysical Research Abstracts 21, EGU2019-19135, (2019)
92. Matonti and 47 co-authors including H.RICKMAN, *Bilobate comet morphology and internal structure controlled by shear deformation*, Nature Geoscience, 12, pp 157-162, (2019), doi: 10.1038/s41561-019-0307-9
93. MÈGE D., *Report and interview on field investigations in the Danakil depression,* Ethiopia, in a popular science journal: "Dallol, laboratoire extraterrestre", Ciel & Espace 564, 34–42, by Emilie Martin (journalist), March/April 2019, (2019)
94. MÈGE D., Choe H., Dyment J., Tsegaye H., Ayele B., Tadesse B., Hansen H., *Very high-resolution ground magnetics characterisation of hydrothermal processes in the Danakil depression*, EPSC Abstracts, 13, EPSC-DPS2019-804, (2019)
95. MÈGE D., GURGUREWICZ J., Douté S., Schmidt F., Schultz R.A., *Brittle-plastic shear zones on Valles Marineris floor: identification and implications*. 50th LPSC, Abstract 2064, (2019)
96. MÈGE D., Massironi M., De Toffoli B., GURGUREWICZ J., Marinangeli L., Pompilio L., Pozzobon R., Davis J., Douté S., Hauber E., KOFMAN W., Pajola M., Perry J., Pommerol A., Seelos F., Tornabene L., Lucchetti A., McEwen A., Cremonese G., Thomas N., *CaSSIS colour imaging of late lava flows and hydrothermal alteration in Ladon Basin, Mars*., EPSC Abstracts, 13, EPSC-DPS2019-504, (2019)
97. MÈGE, D., GURGUREWICZ, J., TESSON, P.-A., 2020. *Structural remapping and recent findings in Valles Marineris, Mars*. 51st Lunar and Planetary Science Conference 2020, Abstract 1541.
98. MÈGE, D., 2020. *Planetary geology activities on the Wroclaw side of the Space Research Centre*. Second National Martian Seminar, Kraków, 16 October 2020.
99. Mishev, A.L., Koldobskiy, S.A., Kovaltsov, G.A., GIL, A., Usoskin, I.G., *Updated Neutron-Monitor Yield Function: Bridging Between In Situ and Ground-Based Cosmic Ray Measurements*, Journal of Geophysical Research: Space Physics, 125, 2, article id. e27433, (2020), doi: 10.1029/2019JA027433
100. MODZELEWSKA, R.; ISKRA, K.; WOZNIAK, W.; SILUSZYK, M.; ALANIA, M. V.: *Features of the Galactic Cosmic Ray Anisotropy in Solar Cycle 24 and Solar Minima 23/24 and 24/25*, Solar Physics, Volume 294, Issue 10, article id. 148, 16 pp., (2019), doi: 10.1007/s11207-019-1540-5

101. MODZELEWSKA R., A Mayorov, R Munini on behalf of PAMELA collaboration: *27-day variation of galactic cosmic ray intensity by PAMELA experiment. Relationship with heliospheric parameters*, Journal of Physics: Conf. Series 1181, 2019, 012015, (2019), doi:10.1088/1742-6596/1181/1/0120151
102. MODZELEWSKA, R.; ALANIA, M. V.: *Quasi-periodic changes in the 3D solar anisotropy of Galactic cosmic rays for 1965-2014*, Astronomy & Astrophysics, Volume 609, id.A32, 7 pp., (2018), doi: 10.1051/0004-6361/201731697
103. MODZELEWSKA, R., G. A. Bazilevskaya, M. Boezio, S. V. Koldashov, M. B. Krainev, N. Marcelli, A. G. Mayorov, M.A. Mayorova, R. Munini, I. K. Troitskaya, R. F. Yulbarisov, X. Luo, M. S. Potgieter, And O. P. M. Aslam, *Study of the 27 Day Variations in GCR Fluxes during 2007–2008 Based on PAMELA and ARINA Observations*, ApJ, vol. 904 3, (2020a) https://doi.org/10.3847/1538-4357/abbdac
104. MODZELEWSKA, R., ALANIA, M. V.,Kapanadze, N. I., and Khelaia, E. I., *Temporal changes of near-surface air temperature in Poland for 1781–2016 and in Tbilisi (Georgia) for 1881–2016*. Earth and Space Science, vol. 7, e2020EA001174, (2020b) https://doi.org/10.1029/2020EA001174
105. MODZELEWSKA, R., GIL, A., *Recurrence of galactic cosmic-ray intensity and anisotropy in solar minima 23/24 and 24/25 observed by ACE/CRIS, STEREO, SOHO/EPHIN and neutron monitors. Fourier and wavelet analysis*, Astron. Astrophys, Forthcoming article, (2021) https://doi.org/10.1051/0004-6361/202039651
106. Molotkov I. A., ATAMANIUK B., I*nteraction of interplanetary shock wave with the solar wind*., Journal of Atmospheric and Solar-Terrestrial Physics, Volume 207, 1 October 2020, 105340, https://doi.org/10.1016/j.jastp.2020.105340
107. MROZEK, T., GBUREK, S., SIARKOWSKI, M.,SYLWESTER, B., SYLWESTER, J., KEPA, A., GRYCIUK, M., *Solar Microflares Observed by SphinX and RHESSI*, Solar Physics, 293, id. 101, (2018), doi: 10.1007/s11207-018-1319-0
108. Patko L., CIĄŻELA J., Aradi L.E., Liptai N., PIETEREK B., Kovacs I.J., Holtz F., and Szabo C., *Fe and Cu isotope and trace element contents of sulfide blebs from peridotite xenoliths beneath the Nógrád-Gömör Volcanic Field (Northern Pannonian Basin)*, Geophysical Research Abstracts 21, EGU2019-1655-1, (2019)
109. Phillips, K.J.H., SYLWESTER, J., SYLWESTER, B., KOWALIŃSKI, M., SIARKOWSKI, M., TRZEBIŃSKI, W., PŁOCIENIAK, S., and KORDYLEWSKI, Z.,

Highly Ionized Calcium and Argon X-Ray Spectra from a Large Solar Flare, The Astrophysical Journal, 863, (2018), doi: 10.3847/1538-4357/aace5b

110. PIETEREK B., CIĄŻELA J., MÈGE D., TESSON P.-A., CIĄŻELA M., GURGUREWICZ J., Lagain A., MUSZYŃSKI A., *Parasitic cones in the Tharsis volcanic province on Mars: Implications for its recent magmatic plumbing system*, 50th LPSC, Abstract 1369, (2019a)
111. PIETEREK B., CIAZELA J., MÈGE D., Lagain A., TESSON P., CIĄŻELA M., GURGUREWICZ J., and MUSZYŃSKI A., *Link between parasitic cones and giant Tharsis volcanoes: New insights into the Tharsis magmatic plumbing system*, Geophysical Research Abstracts 21, EGU2019-12535, (2019b)
112. PRZYLIBSKI T. A., KACZOROWSKI M., FIJAŁKOWSKA-LICHWA L., KASZA D., ZDUNEK R., WRONOWSKI R., *Testing of 222Rn application for recognizing tectonic events observed on water-tube tiltmeters in underground Geodynamic Laboratory of Space Research Centre at Książ (the Sudetes, SW Poland)*, Applied Radiation and Isotopes, Volume 163, September 2020, 108967, https://doi.org/10.1016/j.apradiso.2019.108967
113. RICKMAN H., BŁĘCKA M., GURGUREWICZ J., Jørgensen U.G., SŁABY E., SZUTOWICZ S., ZALEWSKA N., *Water in the History of Mars: An Assessment*, Planetary and Space Science, 166, pp. 70-89, (2019a), doi: 10.1016/j.pss.2018.08.003
114. RICKMAN H., *The IAU and the Impact Hazard, Under One Sky*: The IAU Centenary Symposium. Proceedings of the International Astronomical Union, Volume 349, pp. 71-74, (2019b)
115. RICKMAN, H., *Planetary systems in stellar clusters – A lesson from Planet Nine?* (oral presentation), ARIEL Science, Mission and Community Conference, ESTEC 14-16 January 2020.
116. RICKMAN, H., *New Directions in Comet Research*, on-line invited talk at the Erglis workshop of the Latvian Astronomical Society, 15 August 2020.
117. Savin S., Amata E., Zelenyi L., Wang C., Li H., Tang B., Pallocchi G., Safrankova J., Nemecek Z., Sharma A. S., Marcucci F., Kozak L., Rauch J.-L., Budaev V., BLECKI J., Legen L., Nozdrachev M., *Collisionless Plasma Processes at Magnetospheric Boundaries: Role of Strong Nonlinear Wave Interactions*, 2019, JETP Letters, DOI: 10.1134/S0021364019170028
118. Савин С. П., Ляхов В. В., Нещадим В. М., Зеленый Л. М., Немечек З., Шафранкова Я., Климов С. И., Скальский С. А., Рязанцева М. О.,. Рахманова Л. С, Ванг Ч., Ли Х., БЛЕНЦКИ Я., Рош Ж.-Л., Козак Л., Суворова А., Лежен Л. А., *СОБСТВЕННЫЕ КОЛЕБАНИЯ ГРАНИЦЫ*

МАГНИТНОГО БАРЬЕРА, ОБТЕКАЕМОГО ПЛАЗМОЙ: МЕМБРАННАЯ МОДЕЛЬ ГРАНИЦЫ, ЛИНЕЙНЫЕ И НЕЛИНЕЙНЫЕ РЕЗОНАНСЫ И СВЯЗИ С ВНУТРЕННИМИ МОДАМИ, ЖЭТФ, 2021, том 159, вып. 2, стр. 1–11, DOI: 10.31857/S0044451021020000

119. Schwadron, N. A. and BZOWSKI, M., *The Heliosphere Is Not Round*, The Astrophysical Journal, 862, (2018), doi: 10.3847/1538-4357/aacbcf
120. SIARKOWSKI, M., MROZEK, T., SYLWESTER, J., LITWICKA, M., Dabek, M., *The non-Fourier image reconstruction method for the STIX instrument*, Open Astronomy, 29, (2020), doi: 10.1515/astro-2020-0022
121. SILUSZYK M., ISKRA K., ALANIA M.V., MIERNICKI S., *Interplanetary Magnetic Field Turbulence and Rigidity Spectrum of the Galactic Cosmic Rays Intensity Variation (1968-2012),* Journal of Geophysical Research – Space Physics, vol. 123, (2018), DOI: 10.1002/2017JA023994
122. SILUSZYK, A.; GIL, A.; MODZELEWSKA, R.; MOSKWA, SZ; SILUSZYK, M.; WAWRZYNCZAK, A.: *Neural net clustering in the study of electrical grids failures in relation to geomagnetic storms*, 8th International Conference on Mathematical Modeling in Physical Science, (2019), 26 - 29 August 2019, Bratislava, Slovakia
123. SILUSZYK, A.; GIL, A.; MODZELEWSKA, R.; MOSKWA, SZ; SILUSZYK, M.; WAWRZYNCZAK, A.: *Neural net clustering in the study of electrical grids failures in relation to geomagnetic storms*, Journal of Physics: Conference Series, Volume 1391, Issue 1, id. 012107, (2019), doi: 10.1088/1742-6596/1391/1/012107
124. SILUSZYK M., ISKRA K., *Modeling the Time Delay Problem of Galactic Cosmic Ray Flux in Solar Cycles 21 and 23,* Solar Physics 295, 68, (2020), DOI: 10.1007/s11207-020-01628-w
125. SLOMINSKA EWA, STRUMIK MAREK, SLOMINSKI JAN, Haagmans Roger, Floberghagen Rune, *Analysis of the impact of long-term changes in the geomagnetic field on the spatial pattern of the Weddell Sea Anomaly*, Journal of Geophysical Research: Space Physics, 2020/5, e2019JA027528
126. SOKÓŁ, J.M., BZOWSKI, M., Tokumaru, M. – 2019, *Interstellar neutral gas species and their pickup ions inside the heliospheric termination shock. Ionization rates for H, O, Ne, and He*, Astrophysical Journal 872:57, 10.3847/1538-4357/aafdaf
127. SOKÓŁ, J.M, KUBIAK, M.A., BZOWSKI, M. – 2019, *Interstellar neutral gas species and their pickup ions inside the heliospheric termination shock. The large-scale structures*, Astrophysical Journal 879:24, 10.3847/1538-4357/ab21c4

128. SOKÓŁ, J.M, KUBIAK, M.A., BZOWSKI, M., Möbius, E., Schwadron, N.A. – 2019, *Science opportunities from observations of the interstellar neutral gas with an adjustable boresight direction*, Astrophysical Journal Supplement Series 245:28, 10.3847/1538-4365/ab50bc
129. Sokół, J.M., McComas, D.J., BZOWSKI, M., Tokumaru, M. – 2020, *Sun-Heliosphere Observation-based Ionization Rates Model*, Astrophysical Journal 897:179, 10.3847/1538-4357/ab99a4
130. Stamm, J., CZECHOWSKI, A., Mann, I., Baumann, C., Myrvang, M. – 2019, *Dust trajectory simulations around the Sun, Vega and Fomalhaut*, Astronomy & Astrophysics 626, A107, 10.1051/0004-6361/201834727
131. STRUMIK, M., BZOWSKI, M., KOWALSKA-LESZCZYNSKA, I., KUBIAK, M.A. – 2020, *Inferring contributions from unresolved point sources to diffuse emissions measured in UV sky surveys: General method and SOHO/SWAN case study*, Astrophysical Journal 899:48, 10.3847/1538-4357/ab9e6f
132. STRUMIK, M., SLOMINSKI J., SLOMINSKA E., MLYNARCZYK J., BLECKI J., Haagmans R., KULAK A., MARTYNSKI K., WRONOWSKI R., *Satellite Detection of Ionospheric ULF Magnetic Field Fluctuations Caused by Lightnings*, 2021, GRL, accepted
133. SWACZYNA, PAWEŁ, MACIEJ BZOWSKI, MARZENA A. KUBIAK, JUSTYNA M. SOKÓŁ, Stephen A. Fuselier, Andre Galli, David Heirtzler, Harald Kucharek, David J. McComas, Eberhard Möbius, Nathan A. Schwadron, and P. Wurz, I*nterstellar Neutral Helium in the Heliosphere from IBEX Observations. V. Observations in IBEX-Lo ESA Steps 1, 2, and 3*, The Astrophysical Journal, 854, (2018), doi: 10.3847/1538-4357/aaabbf
134. Swaczyna, P., McComas, D.J., Zirnstein, E.J., Sokół, J.M., Elliott, H.A., BZOWSKI, M., KUBIAK, M.A., Richardson, J.D., KOWALSKA-LESZCZYNSKA, I., Stern, A.S., Weaver, H.A., Olkn, C.B., Singer, K.N., Spencer, J.R. – 2020, *Density of neutral hydrogen in the Sun's neighborhood*, Astrophysical Journal 903:48, 10.3847/1538-4357/abb80a
135. SYLWESTER, B., SYLWESTER, J., SIARKOWSKI, M., Phillips, K.J.H., PODGORSKI, P., and GRYCIUK , M., *Analysis of Quiescent Corona X-ray Spectra from SphinX During the 2009 Solar Minimum*, (2019), Solar Physics, 294, id. 176, (2019), doi: 10.1007/s11207-019-1565-9
136. SYLWESTER, J., STESLICKI, M., BAKALA, J., PLOCIENIAK, S., SZAFORZ, Z., KOWALINSKI, M.;, SCISLOWSKI, D., PODGÓRSKI, P., MROZEK, T., BARYLAK, J., MAKOWSKI, A., SIARKOWSKI, M., KORDYLEWSKI, Z., SYLWESTER, B., Kuzin, S., Kirichenko, A., Pertsov, A., Bogachev, S., *The soft X-ray spectrometer*

polarimeter SolpeX, Experimental Astronomy, (2019), doi: 10.1007/s10686-018-09618-4

137. SYLWESTER, J., SYLWESTER, B., Phillips, K.J.H., KEPA, A., Rapley, C.G., *A Unique Resource for Solar Flare Diagnostic Studies: The SMM Bent Crystal Spectrometer*, The Astrophysical Journal, 894, id. 137, (2020), doi: 10.3847/1538-4357/ab86ba
138. SZEWCZAK K, ŁOŚ H, GLUBA Ł, ŁUKOWSKI M, RAFALSKA-PRZYSUCHA A, USOWICZ B, DOROSZEWSKI A, PUDEŁKO R, SŁOMIŃSKI J., *Agricultural Drought Monitoring by MODIS Potential Evapotranspiration Remote Sensing Data Application*, Remote Sensing, 2020 No. 20 Vol. 12, 10.3390/rs12203411, https://www.mdpi.com/2072-4292/12/20/3411/pdf
139. TESSON, P.-A., Conway, S. J., Mangold, N., CIĄŻELA, J., Lewis, S. R., & MÈGE, D., *Evidence for thermal fatigue on Mars from rockfall patterns on impact crater slopes*, 50th LPSC, Abstract 2352, (2019)
140. TESSON, P.-A., Conway, S. J., Mangold, N., CIAZELA, J., Lewis, S. R., MÈGE D. (2020). *Evidence for thermal-stress-induced rockfalls on Mars impact crater slopes*. Icarus, 342, article id. 113503, doi: 10.1016/j.icarus.2019.113503.
141. TESSON, P.-A., Lagain, A., MÈGE, D., CIAZELA, J., CIAZELA, M., GURGUREWICZ, J., *Investigation of distinct Late Amazonian eruptive episodes southeast of Arsia Mons*, 51st Lunar and Planetary Science Conference 2020, Abstract 2506, 2020.
142. TESSON, P.-A., MÈGE, D., Lagain, A., GURGUREWICZ, J., *Late Amazonian lateral lava flows coeval with caldera eruptions at Arsia Mons*, European Planetary Science Congress Abstracts, vol. 14, EPSC2020-710.
143. TESSON, P.-A., MÈGE, D., Lagain, A., GURGUREWICZ, J., *Amazonian Chronology of Arsia Mons and Southeast Tharsis*, 2nd National Mars Science Seminar, Kraków, 16 October 2020.
144. Thomas, N. and 41 co-authors including M. BANASZKIEWICZ, P. ORLEAŃSKI, P.-A. TESSON, P. WAJER and P. P. WITEK from CBK PAN, *CaSSIS: Overview of imaging in the first 9 months of the prime mission*, 50th LPSC, Abstract 1585, (2019a)
145. Thomas, N. and 46 co-authors including M. BANASZKIEWICZ, W. KOFMAN, P. ORLEAŃSKI, P.-A. TESSON, P. WAJER and P. P. WITEK from CBK PAN, *The Effects of Past and Current Geologic Processes Observed by the CaSSIS Imager Onboard ESA's ExoMars Trace Gas Orbiter*, 9th International Conference on Mars, Abstract 6156, (2019b)

146. Usoskin, I., Koldobskiy, I., Kovaltsov, G., GIL, A., Usoskina, I., Willamo, T., Ibragimov, A., *Revised GLE database: Fluences of solar energetic particles as measured by the neutron-monitor network since 1956*, Astronomy & Astrophysics, 640, (2020), doi: 10.1051/0004-6361/202038272
147. WAWRZASZEK, A., KRASIŃSKA, A. – 2019, *Hopi bifurcations, periodic windows and intermittency in generalized Lorenz model*, International Journal of Bifurcation and Chaos, 29 No 14, 1920042, 10.1142/S0218127419300428
148. WAWRZYNCZAK A., MODZELEWSKA R., GIL A., *Algorithms for Forward and Backward Solution of the Fokker-Planck Equation in the Heliospheric Transport of Cosmic Rays*. In: Wyrzykowski R., Dongarra J., Deelman E., Karczewski K. (eds) Parallel Processing and Applied Mathematics. PPAM 2017. Lecture Notes in Computer Science, vol 10777, (2018), Springer
149. WAWRZYNCZAK, A.; MODZELEWSKA, R.; GIL, A., *The stochastic solution of the Parker transport equation. Comparison of the backward-in-time vs. forward-in-time approach in the 1D, 2D, and 3D heliosphere*, (D1.3-42-18), 42nd COSPAR Scientific Assembly, 14-22 July 2018, Pasadena, California, USA, (2018)
150. WOŹNIAK E., GABRYSZEWSKI R., DZIOB D. (2020). *Remote sensing and electromagnetic wave behaviour to measure vegetation phenology with physics*. Physics Education, doi:10.1088/1361-6552/ab80ff.
151. WYSOCZAŃSKA, R., DYBCZYŃSKI P.A., and KRÓLIKOWSKA M., *First stars that could significantly perturb comet motion are finally found*, EPSC Abstracts, 13, EPSC-DPS2019-1532, (2019)
152. WYSOCZAŃSKA, R., DYBCZYŃSKI, P.A., KRÓLIKOWSKA, M., (2020). *First stars that could significantly perturb comet motion are finally found,* Monthly Notices of the Royal Astronomical Society, 491, 2119-21280, doi: 10.1093/mnras/stz3127.
153. ZALEWSKA N., CZECHOWSKI L., CIĄŻELA J., *Geology of Isidis based on study of mascon and chains of cones*, European Planetary Science Congress EGU2020-20648, https://doi.org/10.5194/egusphere-egu2020-20648
154. ZALEWSKA N., CZECHOWSKI L., CIĄŻELA J., *Isidis Planitia: its regional and local characteristics*, Second National Martian Seminar, Kraków, 16 October 2020

4

ASTRONAUTICS AND SPACE TECHNOLOGIES

4. ASTRONAUTICS AND SPACE TECHNOLOGIES

Compiled by **Piotr Orleański**

During the last three years (2018-2020) Poland continued the space activities based on the ESA membership support. The last Polish Industry Incentive Scheme projects have been granted in 2019. It is worth to state that at the same time a serious number of national projects have been given to industry and academia. Such important steps gave the engineering, organizational and financial support for many of Polish entities, especially for industrial ones.

In 2018 – 2019 a few important projects, where Poland was involved in space hardware development, have been finalized with launch campaigns. This includes the missions: ESA BepiColombo and ASIM missions, NASA InSight, Chinese ChangE'4 or DLR DESIS.

The COVID pandemic in 2020 slightly slows down the activities, laboratories are working with reduced staff, the works in the projects are concentrated, in a big part, on remote activities. However even in such difficult time many of real technical achievements can be found in Polish space scene. The most important was the launch (fortunately just before the pandemic) of the Solar Orbiter probe with the STIX instrument on-board, where Polish teams delivered the important part of the science, flight hardware and software. This is also the year of the continuation (practically finalization) of the JUICE FM hardware delivery for RPWI and SWI instruments. In ESA PROBA-3 mission the

Coronograph Control Box and Filter Wheel Assembly are well advanced for FM delivery in 2021. The activities in ESA ATHENA and Ariel missions are on-going. Finally the EagleEye project dedicated for development and launch of the small remote sensing satellite has been formally initiated by National Center for Research and Development and the first activities are currently on-going.

This chapter summarises the most important activities in Polish up-stream space domain.

4.1 Participation at ESA Science missions: BepiColombo, ASIM, Solar Orbiter, JUICE, ATHENA, ExoMars, THESEUS and ARIEL

The BepiColombo project is a joint venture between space agencies European Space Agency (ESA) and Japan (JAXA). It designs Mercury and his closest cosmic surroundings using two independent probes. The first, weighing 1150 kg Mercury Planetary Orbiter, corresponds to ESA. For preparing the second, four times lighter Mercury Magnetospheric Satellite, JAXA responds. Both were launch together, on board the Ariane-5ECA rocket from the European spaceport in French Guiana (South America). The launch of the rocket took place on the 19th of October 2018.

The task of the Mercury Planetary Orbiter is to measure the geophysical properties of the Mercurian globe. The probe will observe the planet with eleven scientific instruments, including the MERTIS spectrometer (MErcury Radiometer and Thermal Infrared Imaging Spectrometer) developed with the participation of Poles. The device will provide information on the mineral composition of rocks and thermal properties of Mercury's surface. On this basis, the scientists will attempt to recreate the geological past of the planet. nThe maps made by MERTIS will be the first of its kind - the instrument records the

range of infrared radiation, which has never been included in the missions of space probes sent to Mercury.

Centrum Badań Kosmicznych PAN (CBK PAN) was involved in the design, production and testing of one of the key subsystems of MERTIS: the module of aiming the optical axis of the instrument (pointing unit). It is from the setting of the mirror, which is part of the modules, what determines the line of sight of MERTIS. Strictly controlled mirror movement allows you to scan the planet's surface (to acquire scientific data), but also to regularly visualize calibration standards (ie to collect engineering data necessary for the correction of scientific data). The CBK PAN engineers worked closely with colleagues from the German Space Agency (DLR), who were responsible for all work on MERTIS.

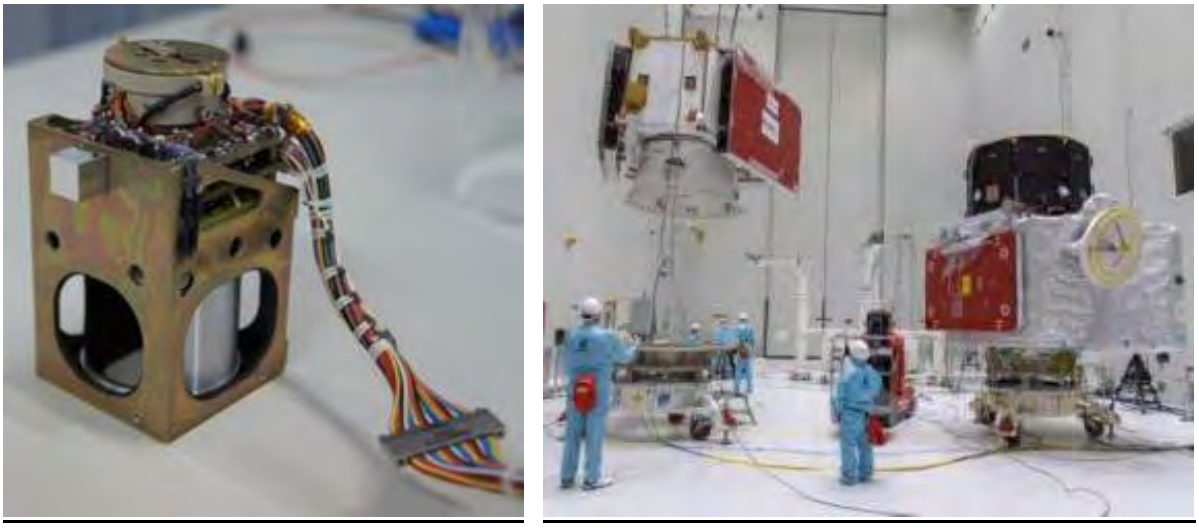

Fig. 4.1. MERTIS Pointing Unit (left photo), © CBK PAN, the engineers prepare the BepiColombo Mercury Transfer Module (left) and the two science orbiters (right) for integration to complete the spacecraft stack. (Credit ESA, right photo).

The aim of the Atmosphere-Space Interactions Monitor (ASIM) onboard the International Space Station is to study high-altitude optical emissions from the stratosphere and mesosphere related to thunderstorms. One of the two main ASIM instruments is the Miniature-X and Gamma-ray Sensor designed by

the University of Bergen and the University of Valencia in cooperation with the CBK PAN. CBK PAN was responsible for the design and manufacturing of the Power Supply Unit and its autonomous (FPGA-based) Housekeeping System. The whole ASIM has been delivered to SPACE-X and launched in 2018. The first, very interesting results from observations have been published, for example, at the beginning of 2020 in Science

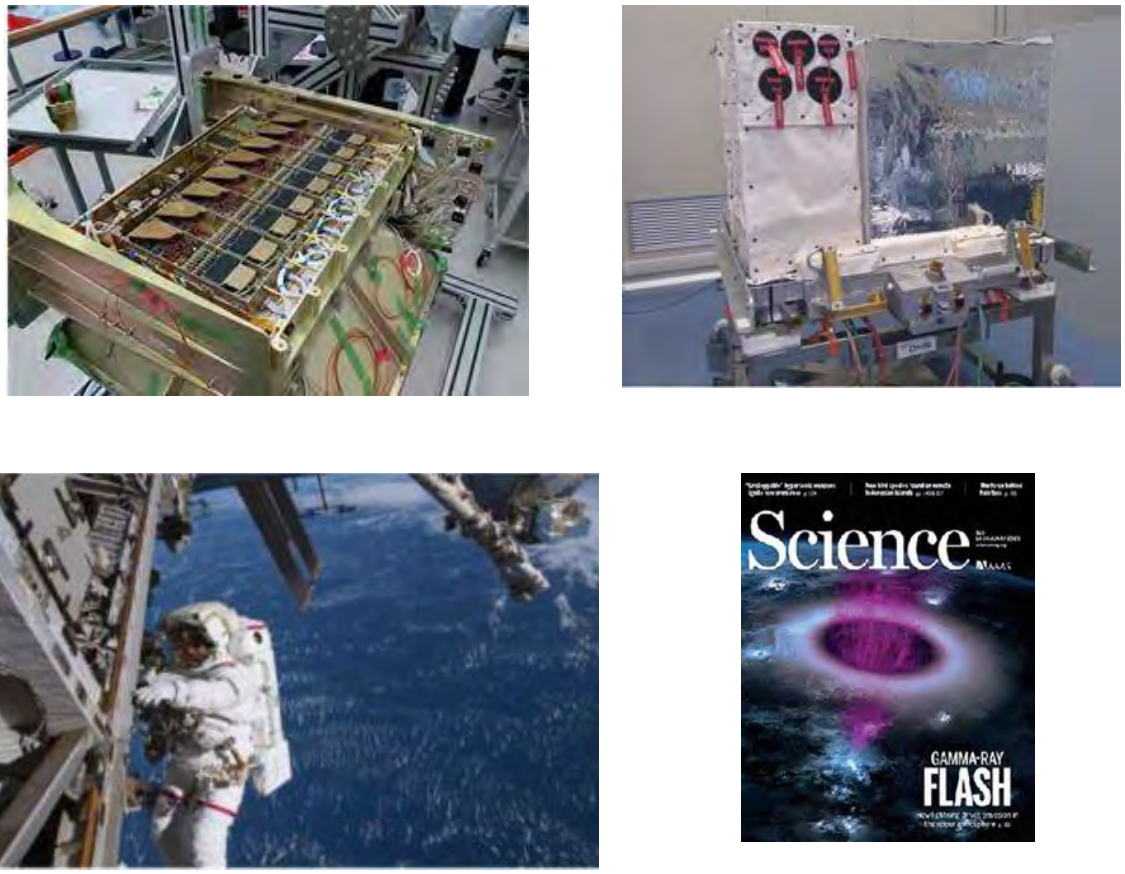

Fig. 4.2. Power Supply Unit for MXGS/ASIM integrated with the rest of MXGS electronics (top left), whole ASIM integrated (top right), both photos © INTA. Bottom left: the photo of US astronaut Ricky Arnold taken outside ISS 14 June 2018. The part of COLUMBUS module with the ASIM experiment mounted on CEPA platform is visible at top right corner. Courtesy of NASA. Bottom right: ASIM paper in Science

The Solar Orbiter (SOLO) ESA mission will perform observations of the Sun, the inner heliosphere and solar wind. SOLO will fly towards the Sun and will approach the star closer than any other previously launched spacecraft. X-ray

Spectrometer/Telescope Instrument (STIX), one of 6 remote sensing instruments on-board SOLO, provides imaging spectroscopy of solar thermal and non-thermal X-ray emission. STIX will provide quantitative information on the timing, location, intensity, and spectra of accelerated electrons as well as of high temperature thermal plasmas, mostly associated with flares and/or microflares. The Polish participation in STIX consists of four work-packages. CBK PAN was responsible for: a) participation in STIX scientific program and in data reduction and archiving, b) Instrument Data Processing Unit (IDPU) including IDPU hardware, low level flight software and mechanical frame, c) thermal modeling of the instrument and its subsystems and d) Instrument EGSE including STIX Detector Simulator. In 2018 and 2019 the whole STIX flight hardware has been integrated in the Switzerland and then delivered to Airbus UK for satellite integration and tests. Satellite has been shipped to Florida, integrated with Atlas V411 launcher and launched in February 2020. The Solar Orbiter satellite and, in particular, the STIX instrument on-board, successfully passed the commissioning phase and now are on the way to the target orbit around the Sun.

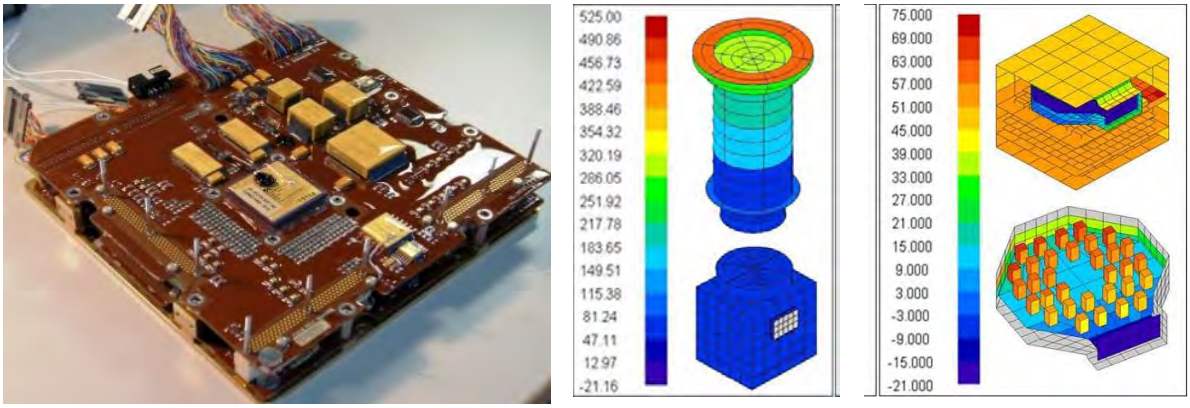

Fig. 4.3. Left: STIX Digital Processin Unit, middle and right: the examples of the thermal modelling of STIX instrument, © CBK

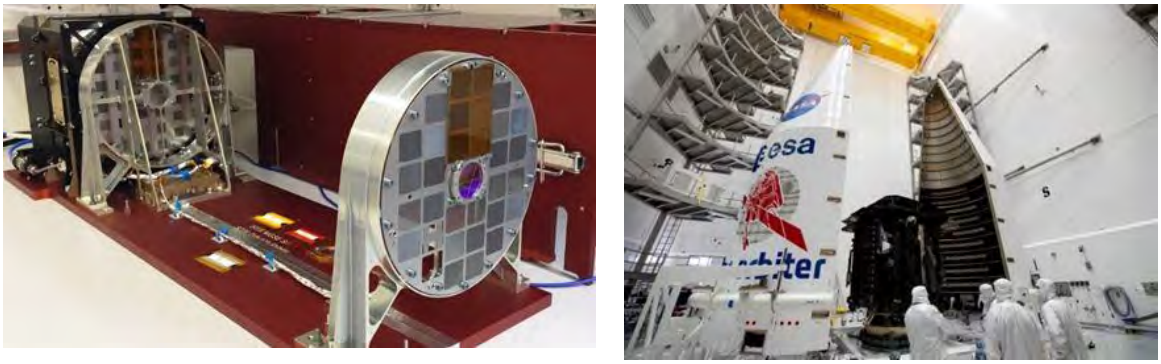

Fig. 4.4. Left: STIX instrument integrated before delivery to Airbus UK, © FHNW, right: ESA's Solar Orbiter spacecraft being encapsulated into the fairing of the US Atlas V 411 rocket at the Astrotech payload processing facility near Kennedy Space Center in Florida, courtesy of ESA

The activities at different levels (requirements, first breadboards, simulations and analysis, engineering models, qualification tests and in some cases the flight hardware deliveries) have been performed in other important ESA science missions: JUICE (RPWI, Radio Plasma Wave Instrument and SWI, Short Wave Instrument), ATHENA (X-IFU and WFI, Wide Field Instrument), PROBA-3 (CCB, Coronograph Control Box and FWA, Filter Wheel Assembly) and finally ARIEL (FGS, Fine Guidance System). CBK PAN, CAMK PAN and the representatives of Polish industry: Astronika, Solaris Optics, SENER PL are involved in this missions.

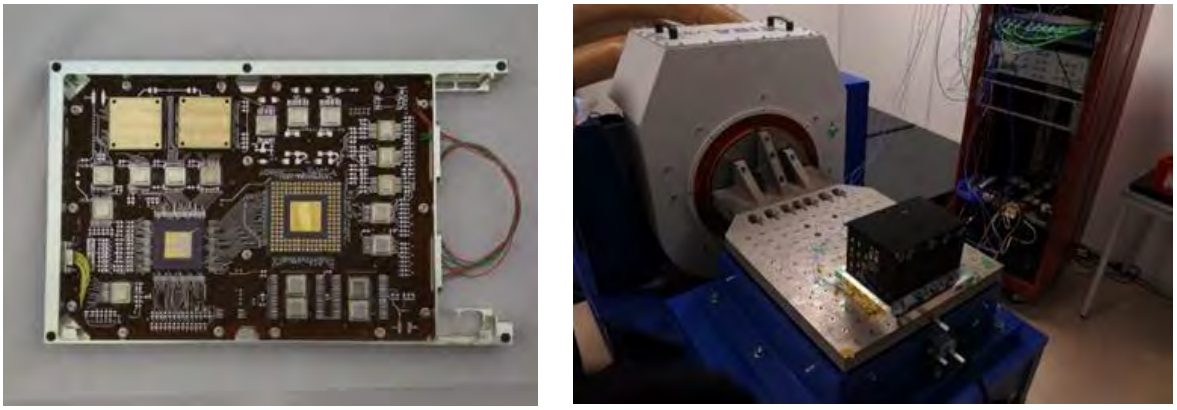

Fig. 4.5. The details of the JUICE RPWI: DPU STM (left), RPWI Electronics Box STM under vibration tests (right), all photos © CBK PAN

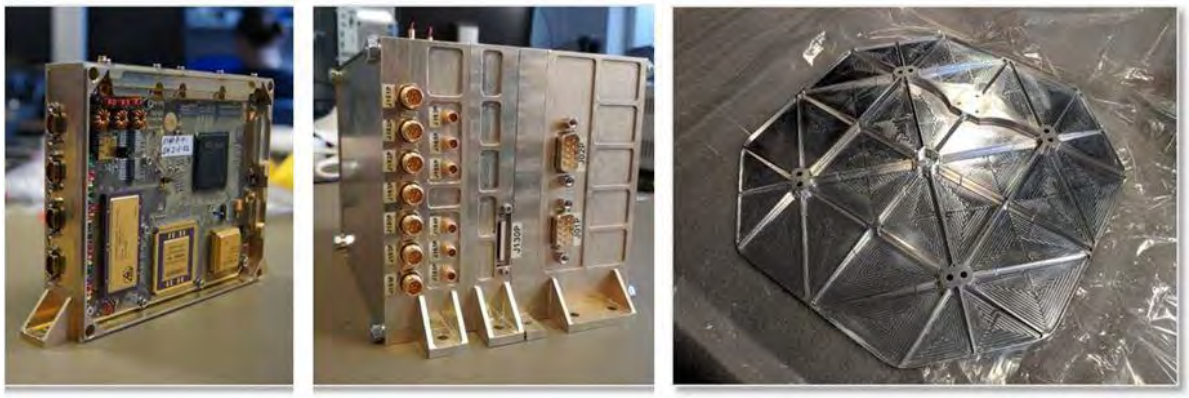

Fig. 4.6. The details of JUICE SWI: DPU EM (left), PSU EM (middle), Radiator STM (right), all photos © CBK PAN

SENER Poland has long track record of projects for mechanisms and MGSE. In 2019 the company raised its client portfolio and started to build up position on the commercial MGSE market procurements. That year was also a time to deliver the Umbilical Release Mechanisms (URM) for ExoMars mission. SENER Poland was responsible for designing, manufacturing, testing of URM for the rover vehicle. Its aim was to provide electrical connection between rover and lander platform during launch, cruise, entry, descent and landing phases of the mission.

Another fundamental SENER PL activity of 2019 was development for the prototype of Athena Instrument Selection Mechanism (ISM) where the company was responsible for the build to spec process from design up to testing campaign. SENER Poland had to overcome many challenges as huge load induced during the launch, damping and shock attenuation during the launch. The main task in this project was to design a very precise positioning system for the mirror with a design goal to minimize the loads transferred to spacecraft and also to design and create comprehensive system to protect the mirror during the flight and allow for precise positioning mechanisms. A 6 degrees of freedom hexapod was selected as a baseline similarly to another unit used in International Berthing and Docking mechanism.

Fig. 4.7. The examples of space mechanisms developed in SENER Polska, © Sener Polska

In 2020 CBK PAN started the activities on power systems dedicated for the instruments for within THESEUS mission. THESEUS consortium prepares the documentation within the ESA M5 competition.

4.2 Participation at NASA Science missions: InSight, IMAP

Astronika has delivered of Hammering Mechanism for HP3 project - an experiment developed by the German Aerospace Center (DLR) for NASA's InSight mission to Mars, launched in 2018. The Hammering Mechanism provides a main drive of the HP3 penetrator ensuring delivery of HP3 heat probe below the surface of Mars to conduct thermal measurements of Martian soil.

Fig. 4.8. Left: one of the assembled mechanisms (HP3 Flight Spare model,©Astronika), right: InSight lander with HP3 Instrument (Credit NASA).

CBK PAN participates in a NASA space mission, Interstellar Mapping and Acceleration Probe (IMAP), scheduled for launch in 2025 to operate near the liberation point L1, about 1.5 million km sunward from the Earth.

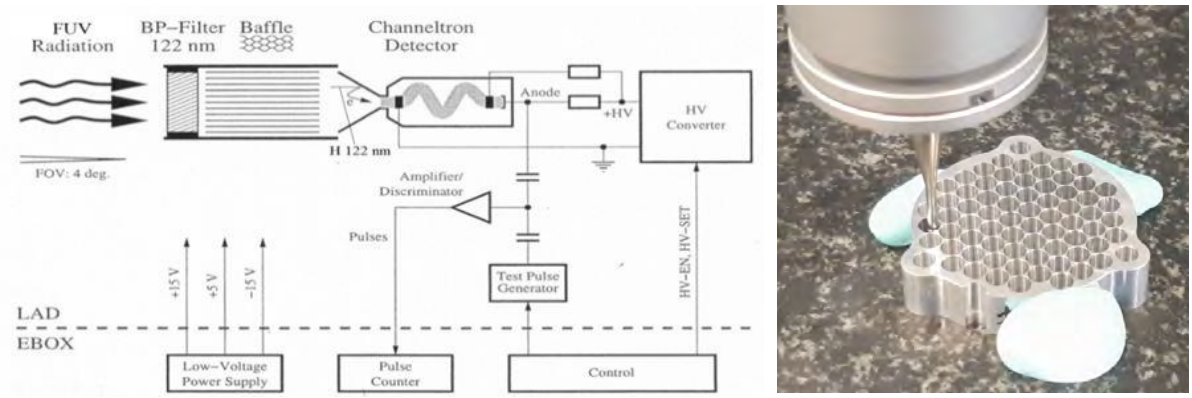

Fig. 4.9. Left: the one-channel UV photometer has been agreed as the baseline for GLOWS instrument, right: the first measurements of the sample of GLOWS Collimator, © CBK PAN

The objective of the IMAP mission is to investigate the interaction of the solar wind with the Sun's galactic environment and cosmic ray acceleration processes CBK will provide a Lyman-α photometer called GLOWS (GLObal solar Wind Structure), one of the ten science instruments on IMAP. GLOWS is the

only one, fully European instrument, all other nine instruments are developed in US. The GLOWS experiment will use remote-sensing photometric observations of the heliospheric backscatter glow to investigate the variation of the solar wind flux with heliolatitude and its evolution during the cycle of solar activity. The observations will provide daily light curves of the helioglow, collected from a Sun-centered circle with a radius of 75°.

In 2019, the IMAP mission completed Phase A. The IMAP project (with GLOWS among the other mission experiments) successfully passed the IRR in December 2019, and a successful evaluation by NASA was officially announced on January 28, 2020, which formally closes Phase A and initiates Phase B of the mission.

The GLOWS hardware activities in 2020 concentrated on the breadboarding of the critical parts of instruments, mostly baffle and collimator. The end of Phase B is scheduled at the beginning of 2021.

4.3 Participation at CNES Science mission: TARANIS

TARANIS is CNES low-altitude microsatellite mission that will provide a set of unprecedented and complementary measurements of physical events associated with TLEs (Transient Luminous Events) and TGFs (Terrestrial Gamma ray Flashes). The MEXIC Power Units (development in CBK PAN) consists of two blocks (MPU1 and MPU2) of electronics and is responsible for the conversion, distribution and management of electrical power for the entire scientific payload on board the TARANIS satellite.

In 2019, MPU modules, integrated with the entire TARANIS satellite were intensively tested by CNES. TARANIS was launched from the Centre Spatial Guyanais on 17 November 2020. However, the rocket failed after launch and the mission was lost.

Fig. 4.10. The TARANIS satellite (Credits: Prodigma Films, "CNES - Taranis - AIT Préparation")

4.4 Participation at Chinese Science missions: Chang'E4 and eXTP

The Chang'E-4 DSL-P (Discovering the Sky at Longest wavelengths) mission is a pathfinder for future higher-resolution, higher-sensitivity ultra-long wavelength radio diagnostic missions. The Chang'E-4 mission was successfully launched from the Xi-chang Satellite Launch Centre in Sichuan Province at 5:28 pm on 21 May, 2018. Two microsatellites, Longjiang-1 and Longjiang-2 (meaning Dragon River) equipped to carry out radio diagnostics in the frequency range 1–30 MHz are part of the mission. Their aim is to collect radio emissions from the solar system, and galactic and extra galactic sources. Unfortunately, maneuvers during the lunar orbit failed, and contact with Longjiang-1 was lost. However, Longjiang-2 did not experience the same problems, and started operations in an elliptical lunar orbit (200–9000 km). The far side of the moon serves as a natural shield against electromagnetic interference from Earth. Both Longjiang-1 and Longjiang-2 were equipped with low-frequency radio spectrometers developed by the National Space Science Centre of the Chinese Academy of Sciences and CBK PAN. In particular, the CBK PAN was responsible for designing and building part of the radio-wave analyzer, and the dipole antenna system.

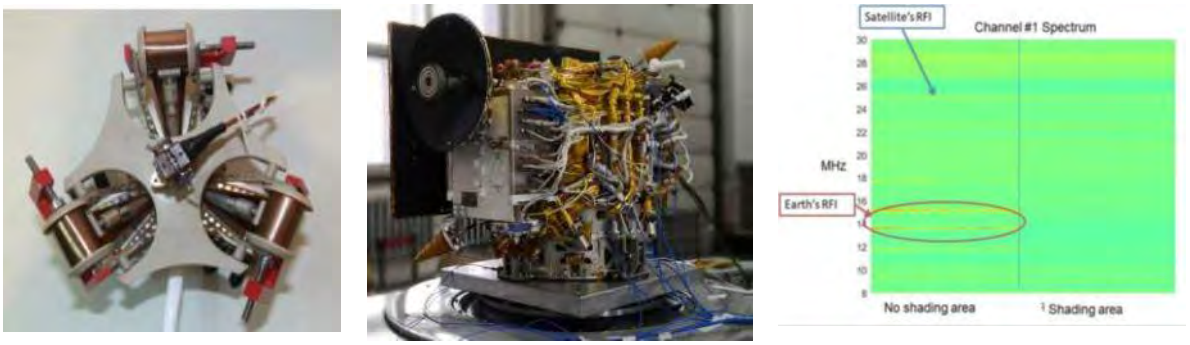

Fig. 4.11. Left: dipole antenna system for Radio-Wave Spectrometer, © CBK PAN, middle: microsatellite Longjiang during the tests, courtesy NSSC CAS, right: the radio spectrum detected on the far side of Lunar orbit, © CBK PAN

The activities on the two instruments, LAD, Large Area Detector, and WFM, Wide Field Monitor, to be developed for Chinese (with, probably, ESA involvement) mission eXTP are ongoing. CBK PAN is responsible for power systems for both instruments and for part of DPU for WFM.

4. 5 Participation at RKA Science mission: JONOSOND

In order to diagnose top-side ionosphere the constellation of JONOSOND satellites was proposed by Russian Space Agency. The four identical satellites will be located at the polar circular orbit at the altitude 600 km and 800 km. In frame of the contract with Russian company Radioexport – Moscow, the four LAERT active ionosondes were designed by CBK PAN. The last two of them have been integrated and tested in CBK PAN in 2019. Each instrument consists of two parts: receiver and transmitter boxes, and an antenna preamplifier.

This active investigation of the near-Earth environment is a unique opportunity to diagnose its complex space plasma. The project is a milestone for future spaceborne services, which will focus on diagnoses of ionospheric perturbations caused by seismic activity. Nonlinear resonance of extraordinary waves has already been examined. This found that plasma conditions are

unconnected with resonance plasma properties, but are determined by the magnitude of the magnetic field and electron concentrations in the transparency band for the considered waves. Special LAERT regimes will be designed to register both first and second wave harmonics using both a trans-ionospheric sounding regime and the satellite itself in sounding and radio-spectrometer modes.

Fig. 4.12. Two sets of Flight Model of LAERT instruments for JONOSONDE mission, © CBK PAN

4. 6 Participation at DLR Science mission: DESIS

The DESIS (DLR Earth Sensing Imaging Spectrometer) is hosted on the Earth Observation Platform, as part of the EXPRESS Logistics Carrier on the International Space Station (ISS). It consists of a hyperspectral imaging spectrometer that covers the visible and near-infrared spectral range, in combination with separate power and instrument control units. The Pointing Unit (CBK PAN responsibility) is the part of the imaging spectrometer that allows the instrument's line of sight (LOS) to be steered under different in-track viewing

angles, and to provide views of the in-flight calibration units. The main part of the unit is the mirror, which is rotated by a stepper motor. DESIS has been installed on ISS in 2018

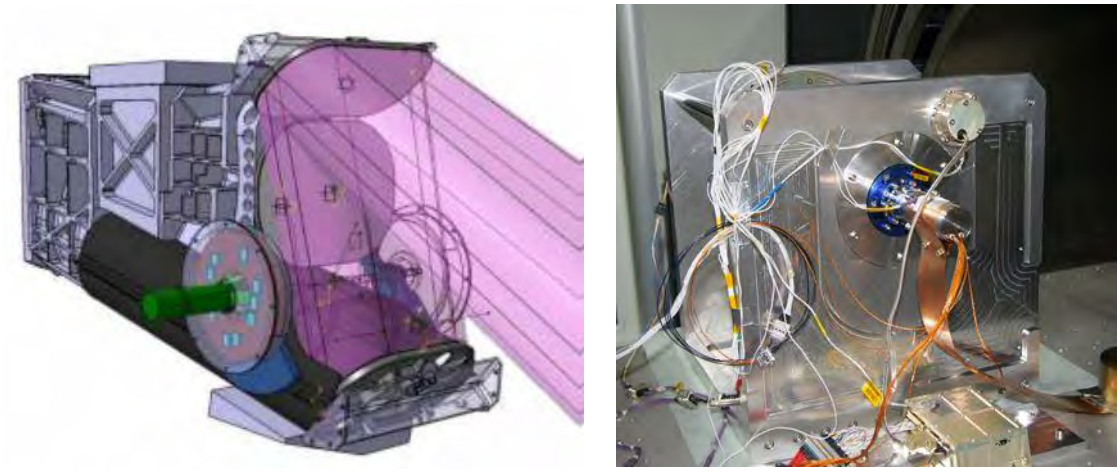

Fig. 4.13. Left: DESIS view from mirror side, credit DLR, right: DESIS Pointing Unit QM, © CBK PAN

4. 7 Participation at ESA technological projects: PROBA3, OP-SAT

PROBA-3 is the 3rd mission of the PROBA (Project for Onboard Autonomy) line. It is an experimental mission devoted to the in-orbit demonstration of formation flying techniques and technologies. The mission will be implemented with a pair of small spacecraft, which together form a coronagraph. One spacecraft will carry the Coronagraph Instrument and auxiliary units while the second spacecraft will carry the occulter disk. Each spacecraft will be able to maneuver itself. The typical separation distance between the spacecraft will be about 150 m. CBK PAN is responsible for delivery of important blocks of Coronograph: Filter Wheel Assembly and Coronograph Control Box.

Filter Wheel Assembly (FWA) optomechanical subsystem is situated in front of the focal plane assembly. Its main task is to sequentially position the different filter/ polarisers in the optical beam of the Coronagraph Instrument. In 2019, the CBK designed and manufactured a complete FWA Qualification Model that performed successfully in the qualification campaign at unit level, and was

delivered to the Centre Spatial de Liège (CSL) for instrument-level testing. The Flight Model has been delivered to the CSL in 2020.

The Coronagraph Control Box(CCB) is the main controller, providing all processing capabilities and supplying power to the rest of the scientific equipment. In particular, it is designed to: interface with the spacecraft's on-board computer, drive the Camera Electronic Box, drive the Filter Wheel Assembly (FWA), drive the Front Door Assembly, drive the Shadow Position Sensor, drive the Coronagraph instrument thermal hardware.

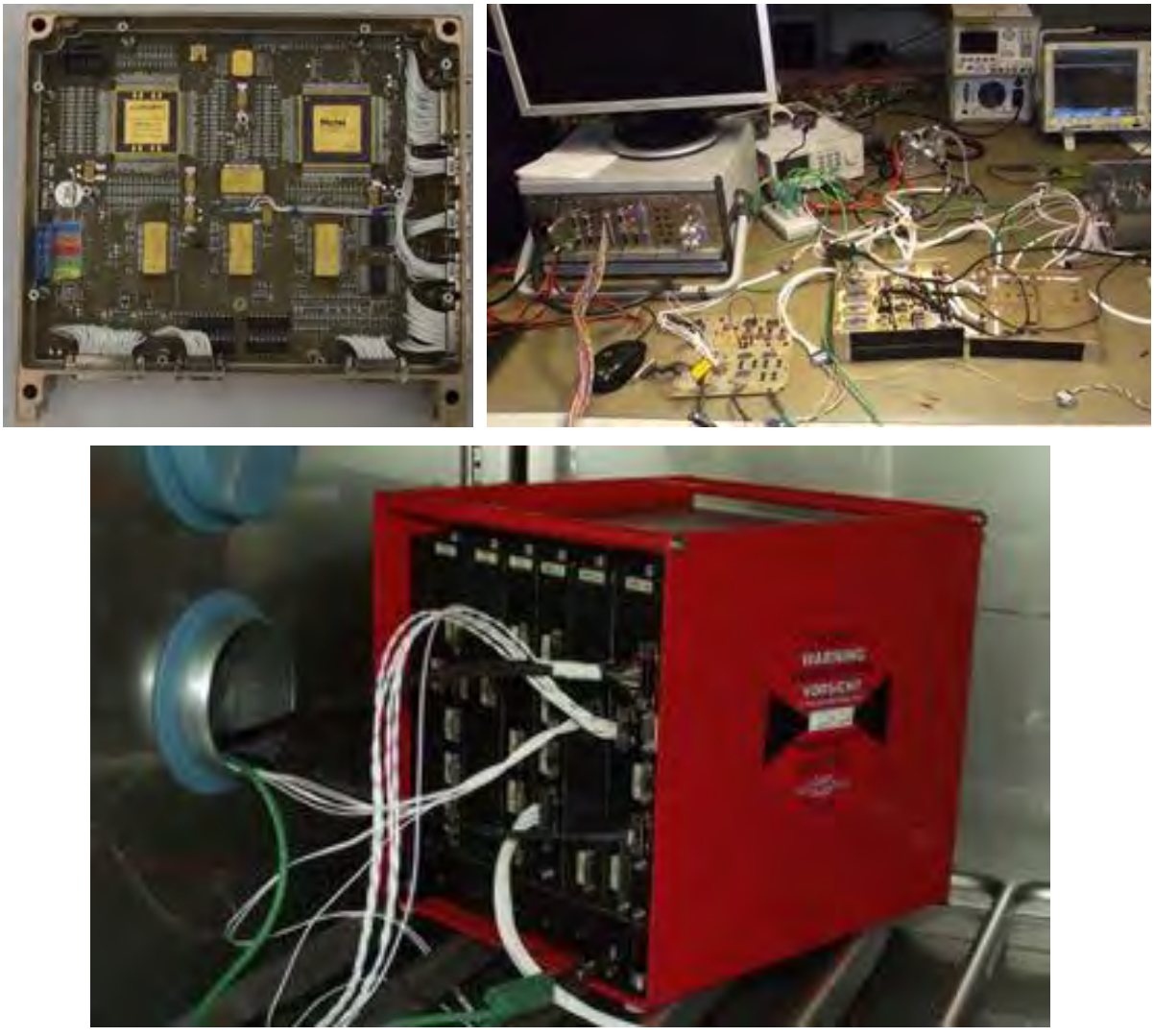

Fig. 4.14. PROBA3 CCB: DPU EQM PCB (top left), the functional tests of CCB modules (top right) and the thermal tests of integrated CCB EQM(bottom), © CBK PAN

The design of the CCB, DPU and PCU, system engineering, housing and harness manufacturing are all managed and executed by CBK PAN, while other manufacturing tasks and some design activities have been outsourced to subcontractors. In particular, N7 Space have been contracted for software development while Creotech Instruments will design the EGSE and the AEU subsystems and will assembly all flight electronics. The main activities in 2018 and 2019 were concentrated on the Engineering Model of CCB. The assembly of flight hardware has been started in 2020.

In 18th of December 2019 ESA has launched OPS-SAT satellite. So far, more than 100 companies and institutions from 17 European countries have volunteered to test their space technologies on board this on-orbit laboratory. Within the OPS-SAT mission, GMV Poland performed critical tasks which included the development of the full on-board software for the mission as well as the design and implementation of a number of systems for the satellite. The latter include, among others, ADCS (Attitude Determination and Control System), one of the most important software elements of each satellite, responsible for the proper communication with the device and for the control of the trajectory of its movement in orbit, as well as FDIR (Failure Detection Identification and Recovery), which makes it possible to monitor the parameters of the satellite's subsystems, and – in case of detecting irregularities – to put it into safe mode. GMV's specialists were also responsible for the integration of the new data compression algorithm, POCKET+, as well as for the preparation and implementation of the MOS (Mission Operation Services) information exchange protocol standard. That was the first time when the so-called flight software designed and manufactured in Poland for ESA's satellite has been put into operation in orbit.

In parallel to GMV activities CBK PAN (hardware development and Creotech Instruments S.A. (FPGA firmware delivery) were contracted by ESA for developing the CCSDS Engine (the satellite's communication protocol converter) for OP-SAT satellite.

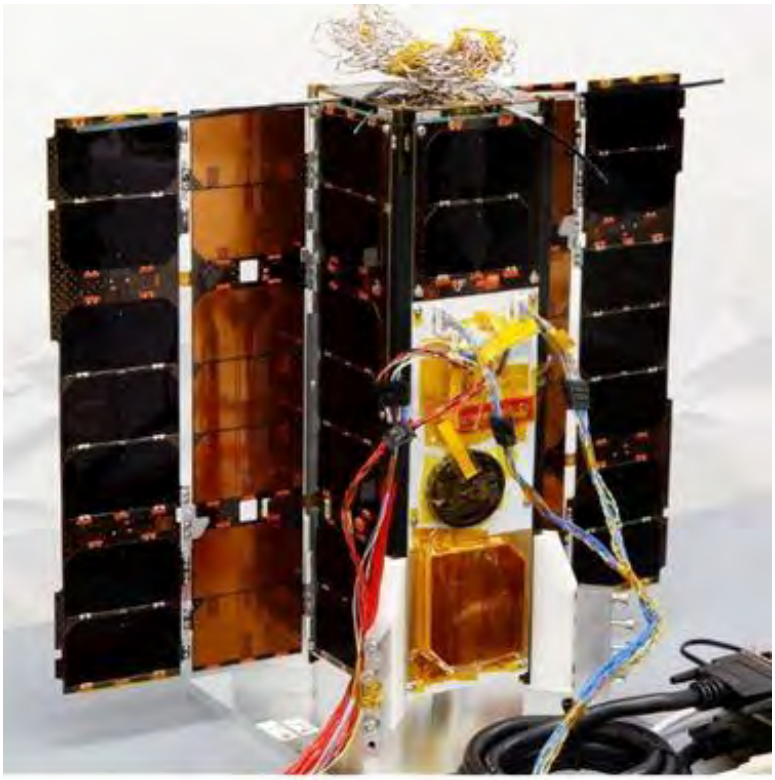

Fig. 4.15. OP-SAT satellite, courtesy of ESA

4. 8 Other projects dedicated for satellite HW/SW development

In 2019 GMV Poland finished its BIBLOS project. Increasing number of EO missions develop performance simulators in early stages (phase A, B1) to assess requirements, evaluate the instrument characteristics, the products, etc. These simulators often evolve into the operational simulators, which are costly. The BIBLOS was built as an answer to this drawback. The main goal of BIBLOS is to provide a library of software units called "Building Blocks", or simply "Blocks", that can be used to build an end-to-end simulator of different EO satellites

instruments. Many Blocks are common across simulators, for example the geometry-related ones. Some Blocks are common for a certain type of instrument, like the Radiative Transfer Model, or parts of the Instrument model. BIBLOS targets the Blocks most frequently used by the engineering and scientific community. The user can access the library through the BIBLOS website https://gmv-biblos.gmv.com/ download the Blocks and use them directly, in combination with their own developments or modify them. All of the Blocks are provided with the source code, and are under ESA Software Community License.

GMV in Poland provides solutions and services not only for European Space Agency. In 2019 GMV in Poland together with its partner Sybilla Technologies, has delivered operational software for the development of the Polish Space Surveillance and Tracking (SST) Operations Centre (SSAC-PL) for the Polish Space Agency. The system is used for collecting, verifying and processing Polish sensor network's data about space objects. The system is also facilitate the exchange of information with the EU SST consortium database. GMV is a prime contractor and is responsible for development, deployment and maintenance of the system. The part of the software delivered to Polish Space Agency by GMV is based on the sstod COTS proprietary solution designed to carry out orbit determination and propagation computations based on measurements obtained by SST sensors for resident space objects. The software provides two separate functions: orbit determination, based on SST measurements (including bias estimation for SST sensors calibration purposes); and orbit propagation, based on a previously computed orbital state.

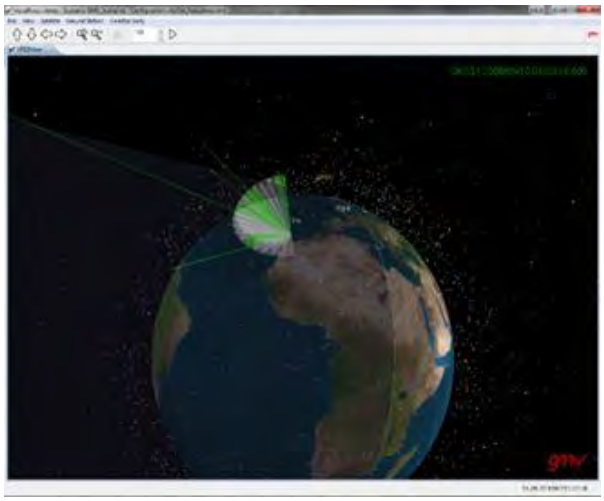

Fig. 4.16. The example of the screen shot from Polish Space Surveillance and Tracking (SST) Operations Centre (SSAC-PL), courtesy of GMV Poland

In 2018 Creotech Instruments S.A. completed its contract on part of EGSE for the Metop 2G mission.

An R&D project on development of modular microsatellite platform HyperSat has been started by Creotech (with CBK PAN as subcontractor responsible for AOCS). The project is financed by the Polish National Centre for R&D. The platform will allow for versatile satellite building of the mass from 10 to 60 kg. In 2019 the HyperSat platform passed PDR with participation of renown experts from Poland and Europe, including former employees of ESA. In 2020 most of the hardware activities went to the final stage making possible to finalyze the project in 2021.

The continuation of the HyperSat has been initiated by National Center for Research and Development in 2020 as the new project with EagleEye Earth Observation microsatellite (Creotech Instr., ScanWay and CBK PAN) to be launched in 2023.

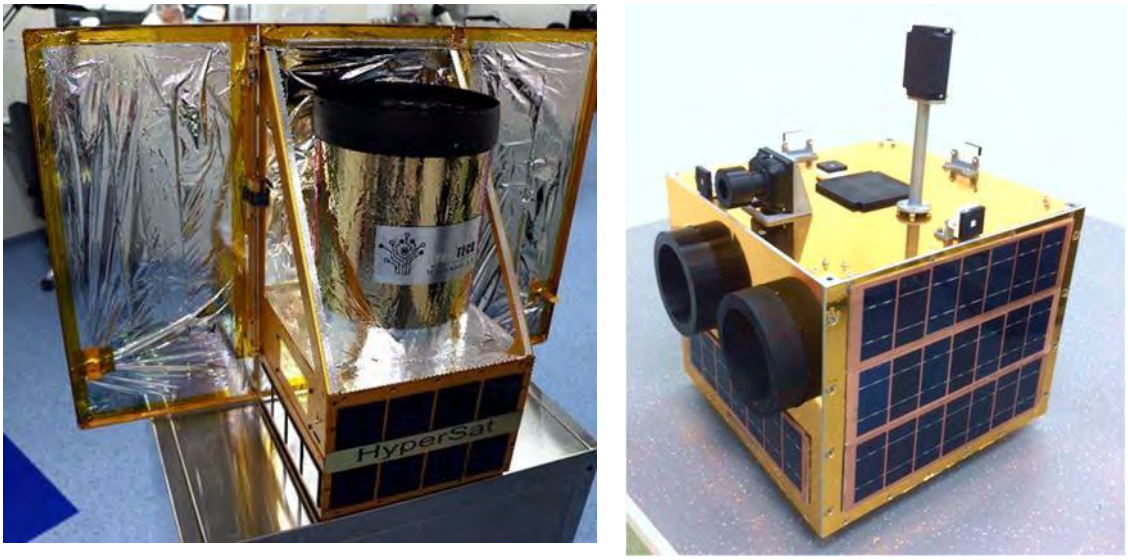

Fig. 4.17. The two different mockups of HyperSat satellite, the generic platform at the left and the platform proposed for UV Satellite at the right, courtesy of Creotech SA

In 2018 the new development of modern on-board computer for small satellites has been initiated in CBK PAN within two projects: ESA, HIPERO and Foundation for Polish Science, TeamTech. The goal is to propose at TRL 3 (HIPERO) and then TRL6 (TeamTech) the computing unit based on the ARM processor and dynamically reprogrammed FPGA designed in accordance to SAVOIR architecture and protected against radiation in space. The first application the above computing platform is planned to be used is EagleEye satellite.

Fig. 4.18. Left: Integration and tests of ScanSAT engineering model at German Orbital Systems, Scanway's partner in the project, right: Current (12.2020) design of the EagleEye telescope, © Scanway

Scanway, Polish SME which specializes in optics, vision systems and optical payloads started developing nanosatellite Earth Observation payload for self-made 6U CubeSat called ScanSAT. Project ended in 2020 with engineering model of payload with definition of short and easy path to the flight model. It consisted of multispectral sensor, RC telescope and athermal structure which is necessary to keep optical parameters within requirements. ScanSAT was designed to observe objects from 500 km SSO with GSD (in VIS) equal to 3,7 m. R&D activities in ScanSAT project included also laser communication.1

Based on ScanSAT, which further development to flight model was suspended because of COVID-19, company started new project – EagleEye – in consortium with leading Polish space entities. Scanway's role in that consortium is to design, build and test optical payload for an EagleEye microsatellite. High resolution optical instrument will nominally operate at 350 km SSO and deliver 1 meter optical resolution with a swath of 4 km at NADIR, 15° (field of regard). Richey-Chrétien telescope with the lens corrector has been applied. Preliminary aperture of the telescope is 200 mm, focal length is 1580 mm. Optical beam is splitted by the beamsplitter into two bands – VIS and NIR. Sensing takes places on four channels (RGB+NIR) within two CMOS imaging sensors. Total dimensions of the instrument are 280 x 280 x 400 mm and total mass will not exceed 10 kg. In EagleEye payload development Scanway also focuses on athermality of the design and on using COTS and ITAR-free components, which will make the future production process fast and independent.

Fig. 4.19. The proposed design of the new DOE optics, © CBK PAN

A lightweight, compact optical system based on DOE and aspherical elements. The main objective of this project conducted in Solaris Optics, CBK and ITME is to design, manufacture and test a compact optical system based on state-of-the-art design, manufacturing and assembly technologies, notably DOE and aspherical surfaces. The proposed design is characterised by parameters that perform better than any of the systems currently available on the market, or described in the scientific/ technical literature. Polish technological expertise in manufacturing and mounting precision lenses that meet the highest global standards will be mobilised. The project is the result of a contract with the European Space Agency.

In 2019, the first laboratory model was produced and tested. A progress report was delivered to the European Space Agency.

Creotech continued work on competence building in space electronics assembly – lead-free solder processes, press-fit connectors and embedded components. Further work on qualification of electronics assembly processes, including an automatic SMT line, for deep space missions has been carried on.

A few contracts for space electronics assembly for the JUICE mission have been started – one on JUICE RPWI, another one for JUICE SWI and then for PROBA-3 CCB and FWA electronics. Creotech works here as a subcontractor to CBK PAN. Electronics assembly for commercial microsatellite integrators has been also started in the company.

4. 9 Recent research on spacecraft propulsion and rocket technologies in Poland

During 2018-2020 significant advances in the field of spacecraft propulsion and rocket technologies have been made in Poland. Over 20 entities declare work and interest in R&D in these fields. Most projects are funded via the European Space Agency, European Commission and National Centre for Research and Development. The largest contributor is the Lukasiewicz Research Network – Institute of Aviation, where over 60 people are devoted to developments in space propulsion and transportation and 20 out of 24 projects of the European Space Agency in this field in Poland are carried out. Other active entities include: Astronika, Lukasiewicz Research Network – Institute of Industrial Organic Chemistry, Jakusz SpaceTech, Creotech Instruments, SpaceForest, Mesko, ZPS Gamrat, Military Institute of Armaments Technology, Bowman Dynamics, PZL Mielec, Military Aviation Works no. 1 and Warsaw University of Technology. A dedicated new workgroup within the Committee for Space and Satellite Research of the Polish Academy of Sciences has been initiated in 2019. It is to focus on the area of space transportation, including suborbital flight, orbital launch vehicles and spacecraft propulsion.

Lukasiewicz Research Network – Institute of Aviation leads the development of propulsion systems for direct deorbitation. The ESA project is being conducted within a fourth consecutive project in this niche for ESA. The

range of potential applications is almost unlimited in terms of spacecraft size. With density specific impulse higher than for classical hydrazine-based propulsion, good storability and direct deorbitation capabilities, it is a promising solution for space debris mitigation. A dedicated non-aluminized propellant with low burn rate and high performance in terms of specific impulse has been pre-qualified at Lukasiewicz Research Network – Institute of Aviation.

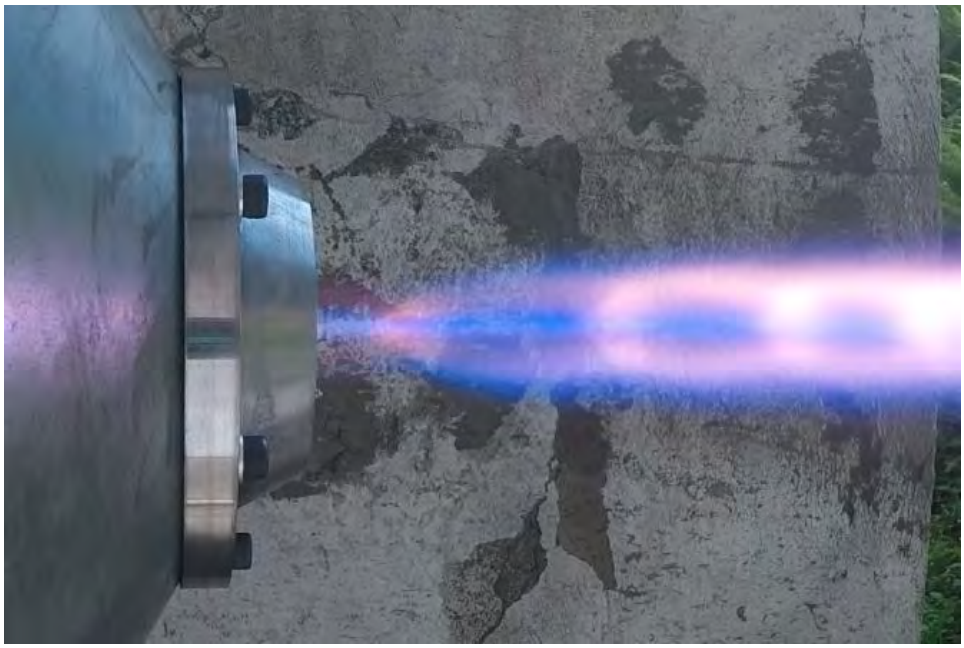

Fig. 4.20. Atmospheric firing of motor using dedicated solid propellant for deorbiting sapcecraft

Another advancement concerns green Liquid Apogee Engines. Successful demonstrations took place at Lukasiewicz Research Network - Institute of Aviation. This technology may be applied either as a spacecraft propulsion subsystem or the main engine of a microlauncher kick stage. The engine operates with the highest-class hydrogen peroxide: 98%+ and a green fuel. High-Test Hydrogen Peroxide is a product developed in-house (EPO Patent). HTP is obtained in the process of vacuum distillation, under strictly controlled conditions and meets the MIL-PRF-16005F standard. Studies on novel green propellants are being continued and the Rocket Propulsion Test Stand of

Lukasiewicz Research Network - Institute of Aviation has undergone further modernization.

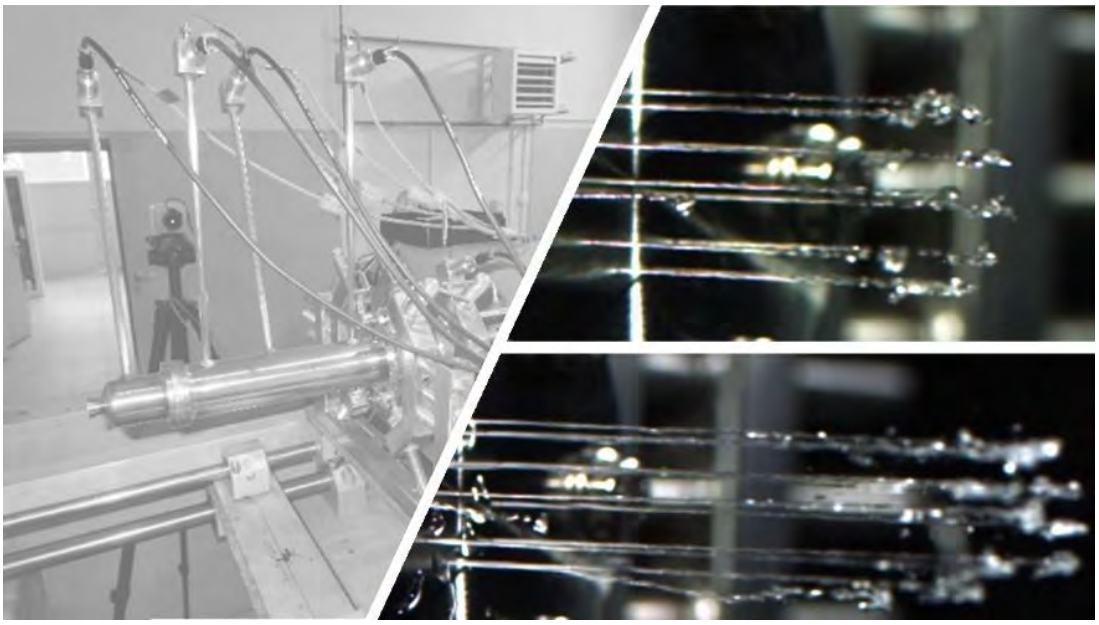

Fig. 4.21. Indoor Rocket and Spacecraft Propulsion Test Facility at Lukasiewicz Research Network – Institute of Aviation

Green high-performance monopropellant thrusters have also been under development by Lukasiewicz Research Network - Institute of Aviation, Jakusz SpaceTech and Warsaw University of Technology. In-house developed catalysts provide high performance and long lifetime. Thrusters are designed for spacecraft propulsion systems to operate within ACS or as main propulsion. Delivery of larger thrusters for rocket ACS is also possible. The possibility of using peroxide with such a high concentration in larger systems has been confirmed during successful launches of the ILR-33 AMBER suborbital rocket.

Work on small resistojet propulsion has been ongoing at the Warsaw University of Technology.

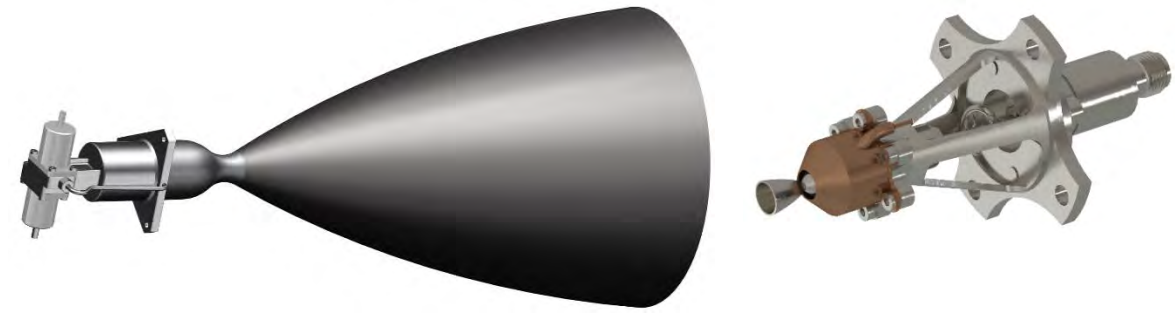

Fig. 4.221. Example designs of green spacecraft thrusters: using bipropellants and H_2O_2 monopropellant

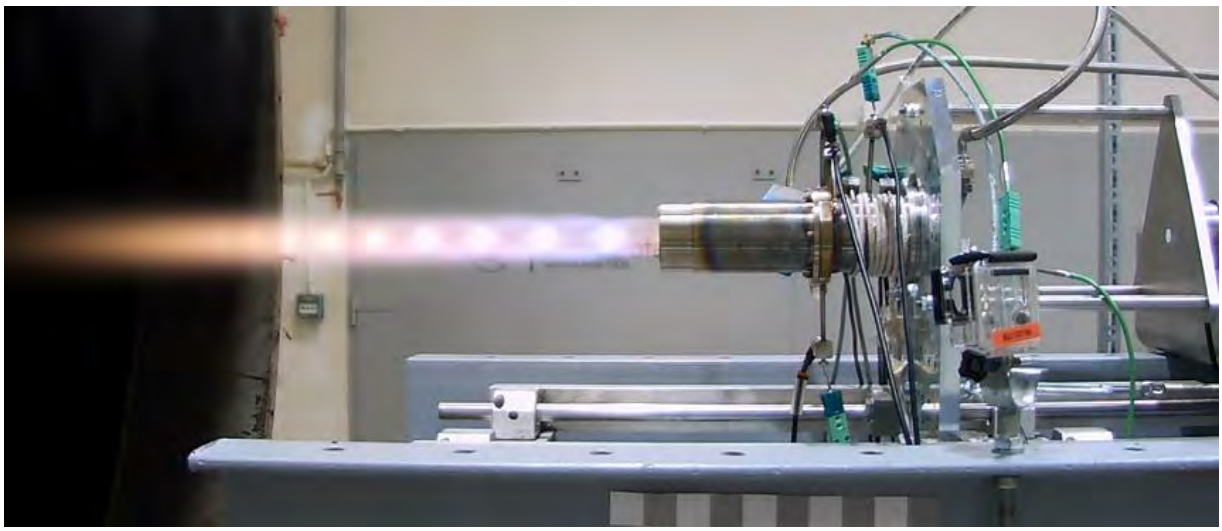

Fig. 4.23. Liquid Apogee Engine ground firing during early ESA test campaign

The ILR-33 AMBER rocket is a suborbital vehicle developed at Lukasiewicz Research Network - Institute of Aviation. It is a cost-effective, scalable and green platform, enabling efficient technology validation, microgravity experimentation and atmosphere sounding, Its most advanced version AMBER 2K can accommodate 10 kg experiments during flights up to 100 km of altitude. Besides use strictly for research purposes it can be also utilized for validation of new avionics systems, attitude control verification, 1U/2U/3U CubeSats qualification, tests of booster separation mechanisms and on-ground infrastructure testing. Sea and land payload recovery is possible, what has

been demonstrated in 2017 and 2019.The ILR-33 AMBER 2K rocket offers quick and dedicated access to microgravity experimentation or to mesosphere and lower thermosphere sounding for small payloads, what is in line with NewSpace trends. Thanks to the hybrid motor and solid boosters, the rocket allows highly flexible mission planning, as opposed to all-solid vehicles. The AMBER vehicle has been successfully validated in flight. Concepts of micro launcher technologies have emerged based on these advances.

Fig. 4.24. Suborbital flight of the ILR-33 AMBER rocket

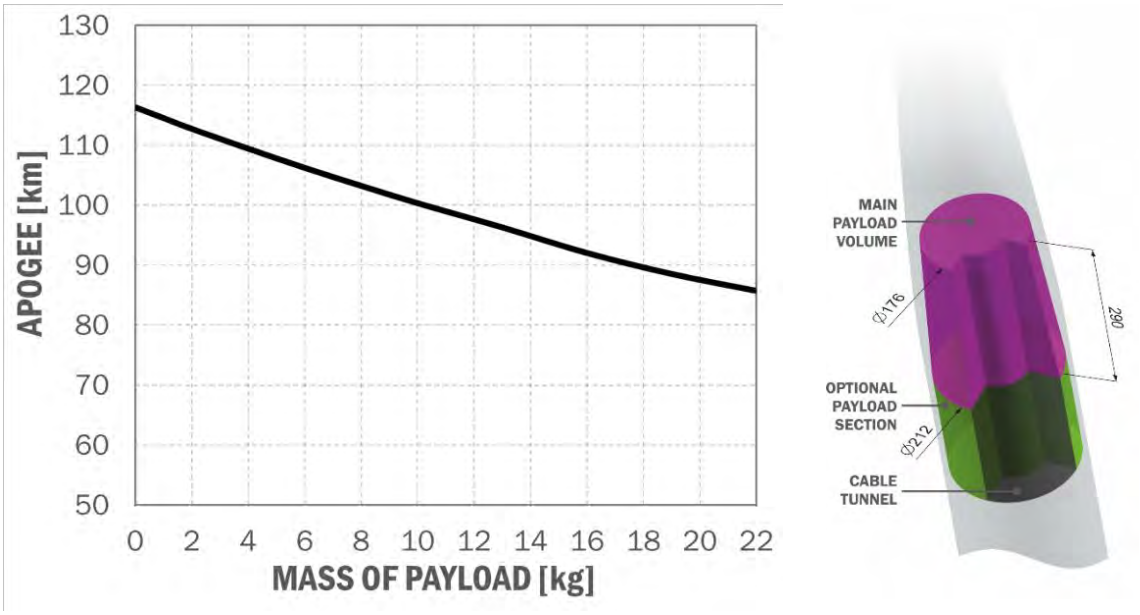

Fig. 4.25. Payload and performance of the ILR-33 AMBER suborbital rocket

Another important application of green propulsion systems concerns work for ESA in the field of throttleable engines. In 2019 Poland initiated two projects, where deep-throttling is to be demonstrated. This technology is to allow development of effective next-generation lunar landers and is also useful for potential European launch vehicle stage recovery. One of these projects is in frame of ESA's Future Launchers Preparatory Programme, where Lukasiewicz Research Network – Institute of Aviation, Astronika and Jakusz SpaceTech are involved.

Lukasiewicz Research Network – Institute of Aviation and Warsaw University of Technology continue international cooperation in the field of detonative propulsion. Rotating Detonation Engines are under development – both In terms of rocket and airbreathing configurations. Green liquid fuels are considered.

Other rocket developments in Poland include work of Bowman Dynamics, which's in-flight test platform called PACMAN enables annual launches of experiments for the Polish ESERO (ESA European Space Education Resource Office). On-going is also the development of the Perun suborbital

rocket of SpaceForest and a three-staged rocket developed at Military Aviation Works no. 1, Military Institute of Armaments Technology and ZPS Gamrat.

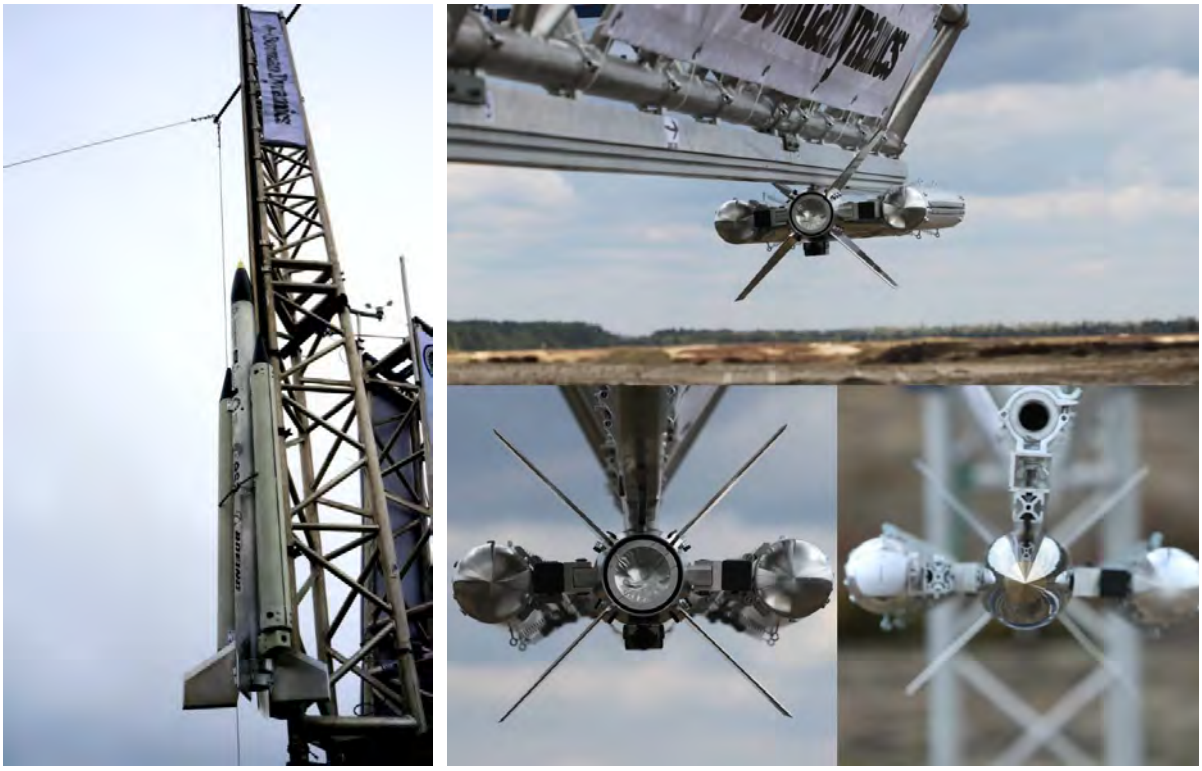

Fig. 4.26. Other rocket technology demonstrations in Poland: PACMAN rocket of Bowman Dynamics

Fig. 4.27. Ongoing development includes the PERUN suborbital rocket of SpaceForest

4.10 Student's activities

PW-Sat2 is a student satellite project started in 2013 at Warsaw University of Technology by the Students Space Association members. Among a few technological experiments and educational purpose for the students, the main technical goal of the project is to test the new deorbit technology in form of a large deorbit sail. In 2018 PW-Sat2 became fully integrated and has been launched by Falcon 9.

PW-Sat2 launches the large square-shaped deorbit sail that, once opened, will dramatically decrease a life-time of the satellite. Satellite passed successfully the commissioning phase on the orbit, then the sail has been deployed, however the surface of the sail was partially destroyed. The experiment, with reduced sail capabilities, is continued.

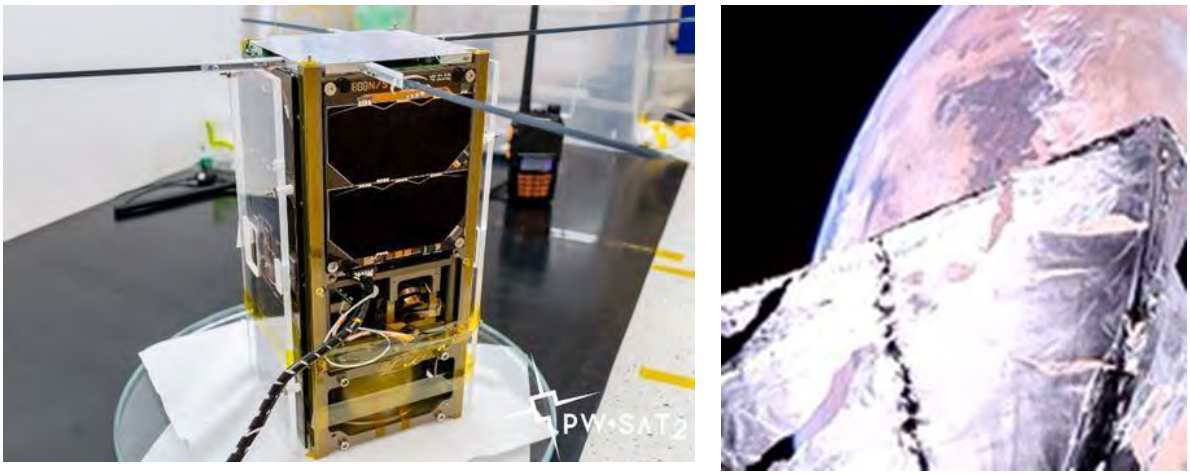

Fig. 4.28. PW-Sat2 integrated (left), sail opened and partially broken, photo taken by PW-Sat2 camera (right), credit: PW-Sat2/Students Space Asso2018

4.11 Publications related to Space Technologies in 2018-2020

1 F. Fuschino et al, "The XGIS instrument on-board THESEUS: the detection plane and on-board electronics", Proceedings of SPIE, Volume 11444, 2020, https://doi.org/10.1117/12.2561002

2 Warmuth A. et al, The STIX Aspect System (SAS): an optical aspect system of the Spectrometer/Telescope for Imaging X-rays (STIX) on Solar Orbiter", Solar Physics 295, Article 9/2020, March 2020, https://doi.org/10.1007/s11207-020-01660-w

3 Zang ShuangNan, et al, "The enhanced X-ray Timing and Polarimetry mission – eXTP", Science China, Physics, Mechanics & Astronomy, 2019, Vol. 62 No. 2:029502, pp. 029502-1 do 029502-21, https://doi.org/10.1007/s11433-018-9309-2

4 Ostgaard N., et al, "The Modular X- and Gamma-Ray Sensor (MXGS) of the ASIM Payload on the International Space Station", 2019, Space Science Reviews 215(2), DOI: 10.1007/s11214-018-0573-7

5 Barret D., et al, "The ATHENA X-ray Integral Field Unit (X-IFU)", Conference: SPIE Astronomical Telescopes + Instrumentation 2018Volume: 10699

6 Ferroci M., et al, "The Large Area Detector onboard the eXTP mission", Conference: Space Telescopes and Instrumentation 2018: Ultraviolet to Gamma Ray, DOI: 10.1117/12.2312466

7 Hernanz M., et al, "The Wide Field Monitor onboard the eXTP mission", 2018, arXiv.org > astro-ph > arXiv:1807.09330

8 Tatischeff V., et al, "The e-ASTROGAM gamma-ray space observatory for the multimessenger astronomy of the 2030s", 2018, arXiv:1805.06435v1 [astro-ph.HE] 16 May 2018

9 Orleanski P., Kosiec J., Sarna M., Wawrzaszek R., "UVSat and other Polish satellite missions", 2018, XXXVIII Polish Astronomical Society Meeting, tom 7 pp. 355-360

10 Gotz D., et al, "The Infra-Red Telescope on board the THESEUS mission", Feb.2018, Memorie della Societa Astronomica Italiana, Vol. 89 N. 2, 2018, pp 148-156arXiv.org > astro-ph > arXiv:1802.01676

11 Brandt S., et al, "The wide field monitor onboard the eXTP mission", Conference: Space Telescopes and Instrumentation 2018: Ultraviolet to Gamma Ray, DOI: 10.1117/12.2313214

12 CICHOCKI, A., K. Pozniak, R. Romaniuk; Modelling of soft fault propagation in sequential circuits by fuzzy-logic simulations; Proceedings of SPIE - The International Society for Optical Engineering Volume 11176, Article number
13 111763B DOI: 10.1117/12.2536693, 2019 7. Dacko, A., T. Kowalski, J. B. BARAN, T. BARCINSKI; Electronic box structural analyses for a space flight; Proceedings of SPIE - The International Society for Optical Engineering,
14 Säm Krucker et al, "The Spectrometer/Telescope for Imaging X-rays (STIX)", ASTRONOMY & ASTROPHYSICS 2019
15 Amati L., et al, "The THESEUS space mission concept: science case, design and expected performances", 2018, Advances in Space Research 62(1), DOI:10.1016/j.asr.2018.03.010
16 Kozłowski, S., K. Kurek, J. Skarzynski, K. Szczygielska, M. DARMETKO; Verifying a concept of adaptive communication with LEO satellites using SDR-based simulations; International Journal of Microwave and Wireless Technologies, DOI: 10.1017/S1759078719000552, 2019
17 ALEKSIEJUK, K., J. BARAN, T. BARCINSKI, J. MUSIAŁ; Planetary penetrator control electronics design concept; Proceedings of SPIE - The International Society for Optical Engineering, Volume 11176, Article number 1117 63X, DOI: 10.1117/12.2538027, 2019,
18 29. PALMA, P., K. SEWERYN; Space robot equipped with compliant linear actuator on end effector: Simulations results; Proceedings of SPIE – The International Society for Optical Engineering, Volume 11176, Article number 111763H, DOI: 10.1117/12.2537207, 2019
19 PALMA, P.; Linear Electromagnetic Actuator with Mechanical Impedance Control for Experimental Investigation of Landing and Transient Contact in Low Gravity; IFToMM World Congress on Mechanism and Machine Science, Volume 73, 2019, Pages 2691-2700, DOI: 10.1007/978-3- 030-20131-9_266, 2019
20 POLAK, S., M. RATAJ, A. BIAŁEK, T. PAŁGAN, P. Hartogh, J. P. Garcia, S. Stämm; Design of the radiator for detection part of the Submillimeter Wave Instrument (SWI) of JUICE mission; Proceedings of SPIE - The International Society for Optical Engineering, Volume 11176, Article number 111763U, DOI: 10.1117/12.2537980, 2019
21 RATAJ, M., R. PIETRZAK, P. WAWER, P.ORLEANSKI; Design of the MERTIS pointing unit for BEPI Colombo mission; Proceedings of SPIE - The International Society for Optical Engineering Volume 11176, Article number 111763F, DOI: 10.1117/12.2536807, 2019

22 RATAJ, M., P. WAWER, K. SKUP, M. SOBIECKI; Design of fine guidance system (FGS) for ARIEL mission; Proceedings of SPIE – The International Society for Optical Engineering, Volume 11176, Article number 111763E, DOI: 10.1117/12.2536800, 2019
23 SEWERYN, K., P. PASKO, G. Visentin; The Prototype of Regolith Sampling Tool Dedicated to Low Gravity Planetary Bodies; IFToMM World Congress on Mechanism and Machine Science, Volume 73, 2019, Pages 2711-2720, DOI: 10.1007/978-3-030-20131-9_268, 2019
24 SKUP, K. R., A. CICHOCKI, K. BER, M. DARMETKO, G. JUCHNIKOWSKI, W.BUJWAN, M. MICHALSKA, M. WINKLER, S. Krucker, S. Koegl, O. Grimm; STIX IDPU: Very efficient and reliable controller for a scientific instrument; Proceedings of SPIE – The International Society for Optical Engineering Volume 11176, Article number 111763J, DOI: 10.1117/12.2537272, 2019
25 Sokal, E., R. WAWRZASZEK,G. JUCHNIKOWSKI, J. ADAMIEC, T. Zawistowski T.; Design and test of magnetorquer in PCB technology for nanosatellites; Proceedings of SPIE – The International Society for Optical Engineering, Volume 11176, Article number 111763R, DOI: 10.1117/12.2537411, 2019
26 WAWRZASZEK, R., M. RATAJ; Optimization of angular rotation control for high accuracy and repeatability mirror positioning system of space hyperspectral spectrometer DESIS; Proceedings of SPIE - The International Society for Optical Engineering, Volume 11176, Article number 1117640, DOI: 10.1117/12.2538030, 2019
27 BARYLAK, J., A. BARYLAK, T. MROZEK, O. Grimm, A. Howard, P. PODGÓRSKI, M.STESLICKI; Simulation of charge sharing in the Caliste-SO detector; Nuclear Instruments and Methods in Physics Research Section A: Accelerators, Spectrometers, Detectors and Associated Equipment, Volume 903, Pages 234-240, DOI: 10.1016/j.nima.2018.05.062, 2018
28 McComas, D.J., et al, 2018, Interstellar Mapping and Acceleration Probe (IMAP): A new NASA mission, Space Science Reviews, 214:116, 54pp, DOI:10.1007/s11 214-018-0550-1, 2018
29 RYBUS, T., K. SEWERYN, J. OLES, F. L. BASMADJI, K. TARENKO, R. MOCZYDŁOWSKI, T. BARCINSKI, J. Kindracki, Ł.Meżyk, P. Paszkiewicz, P. Wolanski; Application of a planar air-bearing microgravity simulator for demonstration of operations required for an orbital capture with a manipulator; Acta Astronautica, Volume 155, Pages 211-229, DOI: 10.1016/j.actaastro. 2018.12.004, 2018
30 Tinetti, G., P. WOLKENBERG, M. RATAJ, W. BUJWAN, M. BŁECKA, M. BANASZKIEWICZ, R. GRACZYK, K. SKUP, P. WAWER, A. WAWRZASZEK, and 230

others authors; A chemical survey of exoplanets with ARIEL; Experimental Astronomy, Volume 46, Issue 1, pp 135–209, DOI: 10. 1007/s10686-018-9598-x, 2018

31 Turrini, D., Y. Miguel, T. Zingales, A. Piccialli, R. Helled, A. Vazan, F. Oliva, G. Sindoni, O.Panic, J. Leconte, M. Min, S. Pirani, F. Selsis, V. Coudé du Foresto, A. Mura, P. WOLKENBERG; The contribution of the ARIEL space mission to the study of planetary formation; Experimental Astronomy, Pages 1-21, DOI: 10.10 07/s10686-017-9570-1, 2018

32 Chmaj, G., K. SEWERYN, T. RYBUS, T.Buratowski, M. Musioł, M. BANASZKIEWICZ; The dynamics aspects of modeling and control of the flying robot with attached two Degree of Freedom manipulator; GeoPlanet: Earth and Planetary Sciences, Aerospace Robotics III, 121-148, 10.1007/978-3-319-94517-0_8, 2018

33 RYBUS, T., K. SEWERYN, J. Z. SASIADEK; Nonlinear Model Predictive Control (NMPC) for free-floating space manipulator; Geo-Planet: Earth and Planetary Sciences, 17-29p, DOI: 10.1007/978-3-319-94517-0_2, 2018

34 WAWRZASZEK, R., M. Waraksa, M. KALARUS, G. JUCHNIKOWSKI, T. Górski; Detection and Decoding of AIS Navigation Messages by a Low Earth Orbit Satellite; GeoPlanet: Earth and Planetary Sciences, 45-62p, DOI: 10.1007/978-3-319-94517-0_4, 2018

35 Wolski, L., W. Matelski, K. SEWERYN, P.PASKO; Supercapacitors based driving system for space fast surface sample acquisition system [Superkondensatorowy układ napedowy gruntowego próbnika kosmicznego]; Przeglad Elektrotechniczny, Volume 94, Issue 5, Pages 153-158; DOI: 10.15199/48.2018.05.27, 2018

36 Barbera, M.et al, ; ATHENA WFI optical blocking filters development status toward the end of the instrument phase-A; Proceedings of SPIE - The International Society for Optical Engineering, Volume 10699, Article number 106991K, DOI: 10.1117/12.2314448, 2018

37 Barret, D. et al., The ATHENA X-ray Integral Field Unit (X-IFU); Proceedings of SPIE - The International Society for Optical Engineering Volume 10699, Article number 106991G, 2018

38 BARYLAK, J., A. BARYLAK, T. MROZEK, M. STESLICKI, P. PODGÓRSKI; Investigation of cosmic ray and solar energetic particle Finebackground of STIX using GEANT4 simulation; Proceedings of SPIE - The International Society for Optical Engineering Volume 10808, Article number 1080848, DOI: 10.1117/12.2501722, 2018

39 Ferroci M. et al, The Large Area Detector onboard the eXTP mission; Proceedings of SPIE – The International Society for Optical Engineering, Volume 10699, Article number 106991C, DOI: 10.1117/12.2312466, 2018
40 Galano, D. et al., Development of ASPIICS: A coronagraph based on Proba-3 formation flying mission; Proceedings of SPIE - The International Society for Optical Engine-ering, Volume 10698, Article number 106982 Y, 2018
41 Hernanz, M et al, The wide field monitor onboard the eXTP mission; Proceedings of SPIE - The International Society for Optical Engineering, Volume 10699, Article number 1069948, DOI:10.1117/12.2313214, 2018
42 Parodi, G., F. D'Anca, U. Lo Cicero, L. Sciortino, M. RATAJ, S. POLAK, A. Pilch, N.Meidinger, K. Dittrich, J. Hartwig, V. Samain, A. Collura, S. F. Bonura, A. Buttacavoli, M.Barbera; Structural modelling and mechanical tests supporting the design of the ATHENA X-IFU thermal filters and WFI optical blocking filter; Proceedings of SPIE - The International Society for Optical Engineering, Volume 10699, Article number 106994C, DOI: 10.1117/12.2314451, 2018
43 Pascale, E. et al, The ARIEL space mission; Proceedings of SPIE - The International Society for Optical Engineering, Volume 10698, Article number 106980H, DOI: 10.1117/12.2311838, 2018
44 SEWERYN, K., T. RYBUS, P. Colmenarejo, L. Mollinedo, G. Novelli, J. OLES, M. Pietras, J. Z. SASIADEK, M. Scheper, K. TARENKO; Validation of the Robot Rendezvous and Grasping Manoeuvre Using Microgravity Simulators; 2018 IEEE International Conference on Robotics and Automation (ICRA), DOI:10. 11 09/ICRA.2018.8460475, 2018
45 SKUP, K., S. POLAK, M. RATAJ, P. Zycki, A. Ró¿anska; Polish contribution to the ATHENA Wide Field Imager; Proceedings of the Polish Astronomical Society, Vol. 7, 349-354, 2018
46 D. Stepanova, M. Podgorski, W. Ballheimer, M. Zieba, J. Kowalewski, C. Jonas, Optical Payload For Small Satellite Laser Communications, Proceedings of the International Astronautical Congress, IAC 2019, IAC-19-B2.1.1
47 Cieśliński, D., Okniński, A., Pakosz, M., Noga, T., Mayer, T., Kaniewski, D., Florczuk, W., Bartkowiak, B., Surmacz, P., Wolański P. ILR-33 „Amber" Rocket - a Platform For Microlauncher System Technology Developmnt, 69th International Astronautical Congress, IAC-18,D2,9-D6.2,11,x45735, Bremen, October 2018.

48 Gamal, H., Magiera, R., Matusiewicz, A., Hubert, D., Kant, P., Szczepinski, P., Chelstowski, T. Development of a Suborbital Inexpensive Rocket for Affordable Space Access, 69th International Astronautical Congress (IAC), Bremen, Germany, 1-5 October 2018.
49 Kindracki, J, Mezyk, L., Paszkiewicz P. Resistojet thruster with supercapacitor power source – design and experimental research, Aerospace Science and Technology, Vol. 92, 2019, pp. 847-857, DOI:10.1016/j.ast.2019.07.010.
50 Kublik, D., Kindracki, J., Wolański P. Evaluation of wall heat loads in the region of detonation propagation of detonative propulsion combustion chambers, Applied Thermal Engineering, 156 (2019) 606–618; DOI:https://doi.org/10.1016/j.applthermaleng.2019.04.08.
51 Marciniak, B., Okniński, A., Bartkowiak, B., Pakosz, M., Sobczak, K., Florczuk, W., Kaniewski, D., Matyszewski, J., Nowakowski, P., Cieśliński, D., Rarata, G., Surmacz, P., Kublik, D., Rysak, D.,Smętek, J., Wolański P. Development of the ILR-33 "Amber" sounding rocket for microgravity experimentation, Aerospace Science and Technology, 2018, Vol. 73, pp. 19-31, doi: 10.1016/j.ast.2017.11.034.
52 Okniński, A., Nowakowski, P. and Kasztankiewicz, A., Survey of Low-Burn-Rate Solid Rocket Propellants. In Innovative Energetic Materials: Properties, Combustion Performance and Application (pp. 313-349). Springer, 2020, Singapore.
53 Okniński, A., Kindracki, J., Wolański P. Multidisciplinary optimisation of bipropellant rocket engines using H2O2 as oxidiser, Aerospace Science and Technology, Vol. 82–83, 2018, pp. 284-293, doi: 10.1016/j.ast.2018.08.036.
54 Okniński A. On use of hybrid rocket propulsion for suborbital vehicles, Acta Astronautica, Vol. 145, 2018, pp. 1-10, doi: 10.1016/j.actaastro.2018.01.027.
55 Okniński, A., Loroch, L., Wolański P. Development of Green Rocket Propulsion in Poland, UNISPACE +50, 61. UN COPUOS, Vienna, 25 June 2018.
56 Nowakowski, P., Okniński, A., Kasztankiewicz, A., Marciniak, B., Rysak, D., Pakosz, M., Noga, T., Majewska, E., Wolański, P. Challenges of Developing a Solid Rocket Motor for Direct Deorbitation, 69th International Astronautical Congress, IAC-18,A6,5,9,x47145, Bremen, October 2018.
57 Pakosz, M., Noga, T., Kaniewski, D., Okninski, A. and Bartkowiak, B., ILR-33 AMBER rocket–quick, low cost and dedicated access to suborbital flights for small experiments. In 24th ESA Symposium on European Rocket and Balloon Programmes and Related Research. 2019, June.
58 Sobczak, K., Surmacz, P., Bartkowiak, B., Okniński, A., Rarata, G., Kublik, D., Mayer, T., Szklarek, R., Wolański, P. Progress In Green Liquid Bi-Propellant

Rocket Engine Using Catalytically Decomposed 98% Hydrogen Peroxide, 11th International Symposium on Special Topics in Chemical Propulsion & Energetic Materials (11-ISICP), Stuttgart, 9-13 September 2018.

59 Surmacz, P., Kostecki, M. , Gut, Z., Olszyna A. Aluminum Oxide–Supported Manganese Oxide Catalyst for a 98% Hydrogen Peroxide Thruster, Journal of Propulsion and Power, 35(3), 2019, pp.614-623.

60 Surmacz, P., Sobczak, K., Bartkowiak, B., Rarata, G., Okniński, A., Mayer, T., Wolański, P., Valencia Bel F. Development Status of 500 N-class HTP/TMPDA Bi-propellant Rocket Engine, 69th International Astronautical Congress, IAC-18,C4,3,12,x43293, Bremen, October 2018.

61 Wolański, P., Kalina, P., Balicki, W., Rowiński, A., Perkowski, W., Kawalec, M., Łukasik, B. Development of gasturbine with detonation chamber, In Detonation Control for Propulsion, (pp. 23-37), 2018, Springer, Cham.

62 Wolański, P., Kawalec M. "Experimental Research of Performance of Combined Cycle Rotating Detonation Rocket-Ramjet Engine." In Proceedings of the 27th International Colloquium on the Dynamics of Explosions and Reactive Systems. 2019.

63 Xie, Q., Wang, B., Wen, H., He, W., Wolanski P. Enhancement of continuously rotating detonation in hydrogen and oxygen-enriched air, Proceedings of the Combustion Institute, 37(3), 2019, pp.3425-3432.

5

ASTROBIOLOGY AND SPACE MEDICINE

5. ASTROBIOLOGY AND SPACE MEDICINE

Compiled by Ewa Szuszkiewicz and Franco Ferrari

Life in the Universe, its origin, evolution and distribution is one of the fundamental subjects of study. It requires a highly interdisciplinary approach and in a natural way stimulates scientific collaboration. Like in many other countries, also in Poland the research activities, education and outreach in Astrobiology are conducted in the framework of a national centre. Moreover, one of the divisions of the Committee on Space and Satellite Research of the Polish Academy of Sciences (PAS) is devoted to astrobiology and space medicine. The name of the Polish national centre is Centre for Advanced Studies in Astrobiology and Related Topics (CASA*), a virtual scientific institution in Poland which started its activity in 2003. Since 2007 CASA* is formally organized as a consortium of five Founding Institutions. Three of them, the Space Research Center (CBK) of the Polish Academy of Sciences (PAS), the Nicolaus Copernicus Astronomical Center (CAMK) of PAS and the Institute of Paleobiology (IP) of PAS are based in Warsaw. The Nicolaus Copernicus University (UMK) and the University of Szczecin (US) are located in Torun and Szczecin respectively. The headquarters of CASA* are at the University of Szczecin. CASA* is coordinated by Ewa Szuszkiewicz (US) and Franco Ferrari (US) and its scientific policy is governed by the Scientific Board.

The main goals of the centre are:

- to stimulate, perform and coordinate interdisciplinary research in astrobiology in Poland;
- to develop advanced technologies, in particular biotechnologies and modern information technologies and to promote their commercial exploitation;
- to promote the collaboration on astrobiological topics of Polish research teams with other countries in Europe
- to train the next generations of astrobiology researchers and to increase the public awareness for science.

At present, CASA* groups together a total of ten research teams whose experience spans over the topics of astronomy, astrophysics, biopolymer physics, statistical physics, cosmic physics, medical genetics, space medicine, microbiology, biogeology, biosedimentology and geomicrobiology.

One of the largest CASA* programme „Through Cosmic Dust to DNA" is organized along five scientific topics, namely:

1. Origins, structure and evolution of planetary systems;
2. Mutagenic effects of cosmic radiation;
3. Effects of ionizing radiation on organic and inorganic molecules;
4. Search for life under extreme conditions;
5. Carbonate and siliceous minerals and sediments as carriers of traces of extant and past microbial life.

The research conducted in the previous three years (2018-2020) led to several interesting findings. Here we present selected results.

5.1 Origins, structure and evolution of planetary systems

5.1.1. The revolutions of planets in the system TRAPPIST-1 tell a story about planet habitability

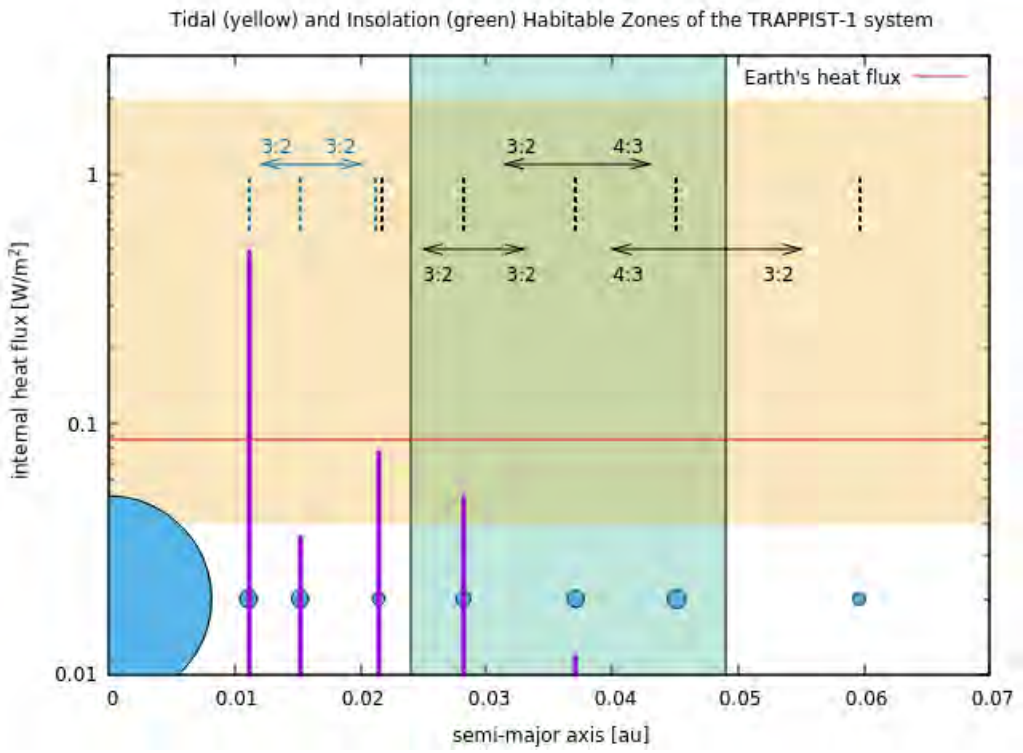

Fig. 5.1. The inner three planets are linked by a Laplace resonance where the commensurabilities indicated such as 3:2 hold exactly in an appropriately rotating frame. A similar situation applies to the outer five planets which are linked by a sequence of three Laplace resonances.

The seven confirmed TRAPPIST-1 planets with masses in the terrestrial mass range orbiting very close to their central star compose a remarkable configuration: The frequencies of their revolutions form a chain of commensurabilities (resonances) – see Figure 5.1.

In the article appeared in the Monthly Notices of the Royal Astronomical Society in 2018, John Papaloizou, Ewa Szuszkiewicz and Caroline Terquem have linked, for the first time, the dynamics of the system to the planet habitability. The dynamical simulations performed by the authors have shown clearly that the current configuration can be understood in a natural way in terms of post formation migration together with tidal interaction with the central star acting over the lifetime of the system. One of the interesting outcomes of these simulations is that the TRAPPIST-1 system most likely consists of two subsystems merged together. The three innermost planets remaining in a Laplace relation (chain of two consecutive commensurabilities) form the first subsystem. The second subsystem includes the five outermost planets joined with each other with a sequence of the Laplace relations. The existence of these commensurabilities is crucial for maintaining the eccentricities of the planetary orbits that enable the tidal heating to work. In turn, the production of tidal heating could lead to tectonic plate activity, which is essential for life as we know it. Taking into account the most fundamental requirements for habitability, the authors have demonstrated that the best conditions for harbouring life can exist on TRAPPIST-1 e. This planet is located in the insolation habitable zone (the stellar flux received is sufficient to enable the existence of liquid water on the planet's surface) as well as in the tidal habitable zone (the internal heat produced by tides can support plate tectonic activity).

Examining the current structure, orbital evolution of planets and tidal dissipation in the TRAPPIST-1 system, the authors have succeeded in putting self-consistent constrains on the formation scenario of this system, the values of the eccentricities of the planetary orbits, the interior structure of the planets, the system age and the internal heat produced by tidal interaction between the star and its planets. All of these has been possible thanks to the elegant resonant configuration of the TRAPPIST-1 system.

5.1.2. New developments in understanding of the radial migration of planets in protoplanetary disks

Motivated by recent progress in the comprehension of the migration of partial gap-opening planets, we have investigated the orbital evolution of planet pairs in a wide range of masses and disk properties with the aim to find out when resonance capture is likely to happen (Kanagawa and Szuszkiewicz, 2020). Using the formula for the migration timescale of a gap-opening planet developed in our previous work (Kanagawa, Tanaka and Szuszkiewicz, 2018), we have derived a simple criterion that allows us to predict when the migration will be convergent (divergent). Further, we have verified the criterion using two-dimensional hydrodynamic simulations. We have found that the resonant pair of planets formed at the early phase of evolution can depart from resonance at later times because the migration speed of the outer planet slows down due to gap formation. Moreover, adopting our formula for the migration timescale, we have also carried out three-body simulations, which confirm the results of hydrodynamic simulations. Finally, we have compared our predictions with observations, selecting a sample of known two-planet systems.

These works have been done in the framework of the project "The formation and evolution of mean motion resonances in planetary systems" funded by Polish National Science Centre DEC-2012/06/A/ST9/00276.

Publications:

• Kanagawa, K. D., Tanaka, H., Szuszkiewicz, E. (2018), Radial Migration of Gap-opening Planets in Protoplanetary Disks. I. The Case of a Single Planet, The Astrophysical Journal 861, 140

• Kanagawa, K. D., Szuszkiewicz, E. (2020), Radial Migration of Gap-opening Planets in Protoplanetary Disks. II. The Case of a Planet Pair, The Astrophysical Journal 894, 59

• Papaloizou, J. C. B., Szuszkiewicz, E., Terquem, C. (2018), The TRAPPIST-1 system: orbital evolution, tidal dissipation, formation and habitability, Monthly Notices of the Royal Astronomical Society 476, p.5032-5056

5.2 Mutagenic effects of cosmic radiation

In the field of mutagenic effects of cosmic radiation the research activity focused on the project "Feasibility study of Standardized Career Dose Limits in **LEO and outlook for BLEO"** carried out by Franco Ferrari under the framework of the Study Group 3.19 of the International Academy of Astronautics led by Susan McKenna-Lawlor. In their work Ferrari and co-workers study the biological response of humans to the impingement of high energy particle radiation.

This research is related to manned space missions on Mars or other objects that require a long travel in the presence of cosmic radiation without the protective shields of the Earth's magnetic field and atmosphere. While space missions with human crews are in plan and both the public and private sectors are developing the next generation technologies that will serve to that purpose, the question of how harmful will be cosmic radiation for humans is still open. Particularly dangerous is the radiation due to heavy, high energetic ions. This kind of radiation could be very dangerous. For example, it has been proved to damage the brain on mice. Also in this case there is a fundamental question which sounds as follows: is the risk of stochastic effects like cancer for astronauts after a mission to Mars comparable to that of an average inhabitant of the Earth? It is very difficult to evaluate such a risk, because there is not enough statistics in order to use the powerful methods of the probability theory.

The traditional experiments in vivo on animals or in vitro using cultures of cells are inadequate. Animal models and cells in culture are far from reproducing the conditions of tumor progression in humans. A possible tool that can be helpful for estimating the threats posed to human crews by ionising radiation in space are human stem cell organoids. Pluripotent stem cells, when put in a favourable environment and feed with suitable grow factors, can differentiate and form structures that mimic those of the real organ. The missing ingredient is the knowledge of the early stages of the onset of cancer. This piece of knowledge is now available thanks to the advances of molecular medicine and precision oncology. Organoids mimicking the brain or the bowel can be grown and irradiated with doses and dose rates that are very near to those of cosmic rays in space. The techniques of molecular medicine will be used to ascertain at different stages of the exposure if the markers of an ongoing oncogenic process have appeared.

5. 3 Martian meteorites

Martian meteorites are the only source of material from Mars, so they are crucial for deciphering the magmatic evolution of the planet and the geochemical effects of fluid activity in deep and surface reservoirs. These meteorites are divided into three main groups, shergottites, nakhlites, and chassignites, often denoted as SNC. They can provide information regarding the Martian mantle and volcanism, the geochemical effects of fluid activity on the Martian surface, atmospheric composition, liquid water, and potential environments for life.

Apatites from Martian nakhlites NWA 10153 and NWA 10645 were used to obtain insight into their crystallization environment and the subsequent postcrystallization evolution path. The research results acquired using multi-tool analyses show distinctive transformation processes that were not fully

completed. The crystallization history of three apatite generations (OH-bearing, Cl-rich fluorapatite as well as OH-poor, F-rich chlorapatite and fluorapatite) were reconstructed using transmission electron microscopy and geochemical analyses. Magmatic OH-bearing, Cl-rich fluorapatite changed its primary composition and evolved toward OH-poor, F-rich chlorapatite because of its interaction with fluids. Degassing of restitic magma causes fluorapatite crystallization, which shows a strong structural affinity for the last episode of system evolution.

Three types of apatite in nakhlites have been classified by McCubbin and collaborators based on their volatile compositions. Type 1 is represented by apatites from the NWA 998 meteorite and consists of OH-bearing, Cl-rich fluorapatite. This type is considered to be of magmatic origin and crystallized from magmas that interacted with Cl- and REE-rich fluids prior to apatite saturation. Type 2 includes OH-poor, F-rich chlorapatite, which is characterized by the large variability in the F:Cl ratio. When the type-2 apatite crystallization occurred, which is represented by the Nakhla, Governador Valadares, and Lafayette meteorites, the magma body had most likely reached chloride saturation due to interactions with exsolved Cl-rich fluids that migrated upward through a partially solidified crystal pile, which caused an upward enrichment in Cl in the interstitial liquid and apatite. Type 3 consists of fluorapatites and apatites from the MIL nakhlites, NWA 817, and NWA 5790. These apatites should be considered products of the crystallization from a residual melt after the exsolution and degassing of Cl-rich fluids. Since the order of volatiles preference in the residual melt is F >> Cl >> OH, during degassing, the apatite compositions evolve toward the F-rich member. Three populations of apatite can also be distinguished in both studied meteorites (NWA 10153 and NWA 10645) based on the volatile composition. The research done of both meteorites clearly indicates the possibility of the appearance of volatile components in magma, their evolution during its differentiation and their

separation in the form of fluids at the last stage of its differentiation. Thus hydrothermal activity is undoubtedly present both in the Martian crust and on its surface and is connected to magmatic / volcanic activity.

Publication:

Łukasz Birski, Ewa Słaby, Elias Chatzitheodoridis, Richard Wirth, Katarzyna Majzner, Gabriela A. Kozub-Budzyń, Jiří Sláma, Katarzyna Liszewska, Izabela Kocjan and Anna Zagórska; 2019 Apatite from NWA 10153 and NWA 10645—The Key to Deciphering Magmatic and Fluid Evolution History in Nakhlites. Minerals, *9*, 695; doi:10.3390/min9110695

5.4 Remote Sensing detection of methanogenic archaea in water plumes

In 2018-2020, at the Center of Space Technologies of the Łukasiewicz Research Network - Institute of Aviation, the investigation on the possibility of detecting methanogenic archaea in the icy satellite water plumes (Enceladus, Europe) using remote sensing instruments was conducted. The following missions were analyzed: Enceladus Orbiter (NASA), Enceladus Life Finder (NASA), The Explorer of Enceladus and Titan (ESA in collaboration with NASA), Testing the Habitability of Enceladus's Ocean (JPL, MissionX). Examples of pigments supporting the survival of microorganisms in the oceans of gas giants (some rhodopsins, carotenoids, tyrosine derivative, siderophore, prodignine, Indole derivative, and luciferin) and model microorganisms were selected. Based on the physical parameters of individual cells, kinetic simulations (method: Particle - In - Cell) of the spread of the microbiological component were created 1) in an ocean with a depth of 10 km and a salinity of 2%, and 2) in water plumes for parameters corresponding to the surface of Enceladus. Based on the technical parameters of the proposed multi-spectral and navigation cameras MAC, TIGER, and DRIPS, a technique for the detection of methanogens for high-phase-angle scientific orbits was proposed. The

methodology was tested in the experiment in a vacuum chamber (Figure 5.2) in simulated water geysers and then described as a patent.

Fig. 5.2. Vacuum chamber experiment with methanogenic archaea and Enceladus' ocean analog.

Collected data of microorganisms, including their spectral signatures and a model of light scattering on spherical particles representing individual species, were published as M2INAVI database at www.ilot.edu.pl/m2inavi (Figure 5.3). At the end of 2019, integration of the optical system with sensors in the 460 - 950 nm range was started to create a prototype of the device performing the detection of methanogens automatically using artificial intelligence in the "Edge Device" architecture.

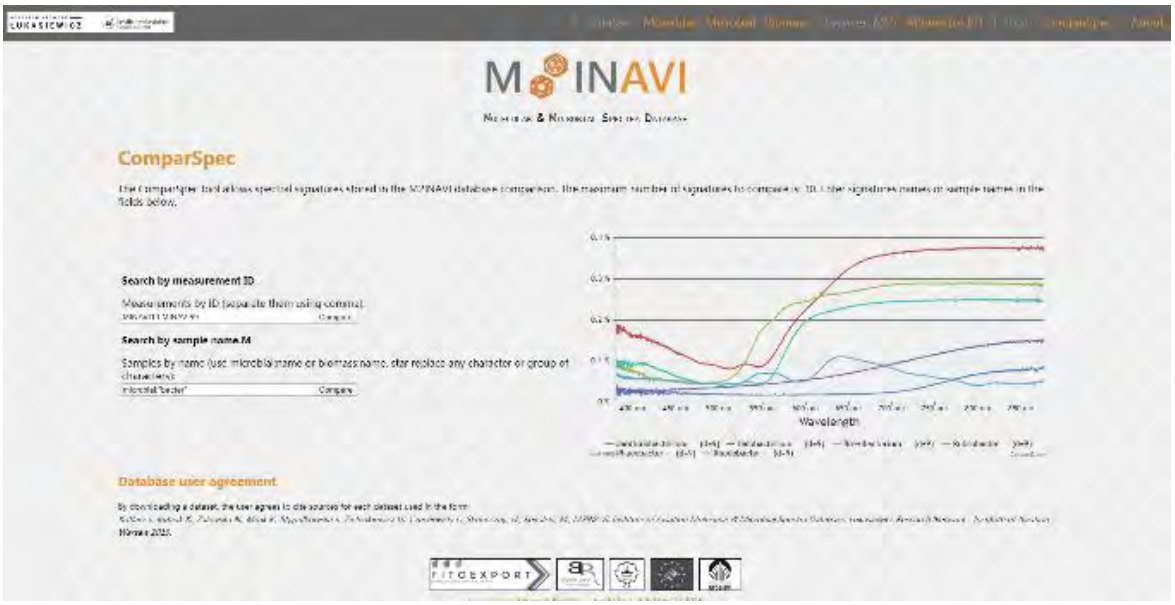

Fig. 5.3. M2INAVI database with extremophiles spectral signatures published for the IoT systems.

5.5 Tardigrade research

Finding life on other worlds is a long-term goal of astrobiology. Presently, over 3500 exoplanets, representing a very wide range of physical and chemical environments, are known. Scientists are not only looking for traces of life outside Earth, but also are trying to find out which of Earth's known organisms would be able to survive on other planets. Tardigrades (water bears) are microscopic invertebrates that inhabit almost all terrestrial, freshwater and marine habitats, from the highest mountains to the deepest oceans. Thanks to their ability to live in a state of cryptobiosis, which is known to be an adaptation to unpredictably fluctuating environmental conditions, these organisms are able to survive when conditions are not suitable for active life; consequently, tardigrades are known as the toughest animals on Earth. In their cryptobiotic state, they can survive extreme conditions, such as temperatures below -250°C and up to 150°C, high doses of ultraviolet and ionising radiation, up to 30 years without liquid water, low and high atmospheric pressure, and exposure to many toxic chemicals. Active tardigrades are also resistant to a wide range of

unfavourable environmental conditions, which makes them an excellent model organism for astrobiological studies.

Publication:

Kashyap J.M., Roszkowska M., Kaczmarek, Ł. 2018. Tardigrade indexing approach on exoplanets, *Life Sciences in Space Research*, 19, 13–16. doi:10.1016/j.lssr.2018.08.001

5.6 Extant and past microbial life

The study of Kremer, Kaźmierczak and Środoń identifies for the first time in the Late Ediacaran terrestrial deposits of Western Ukraine soil crusts enclosing patches of colonial coccoidal cyanobacteria associated with large unicellular microalgae reminiscent of modern chlorococcaleans.

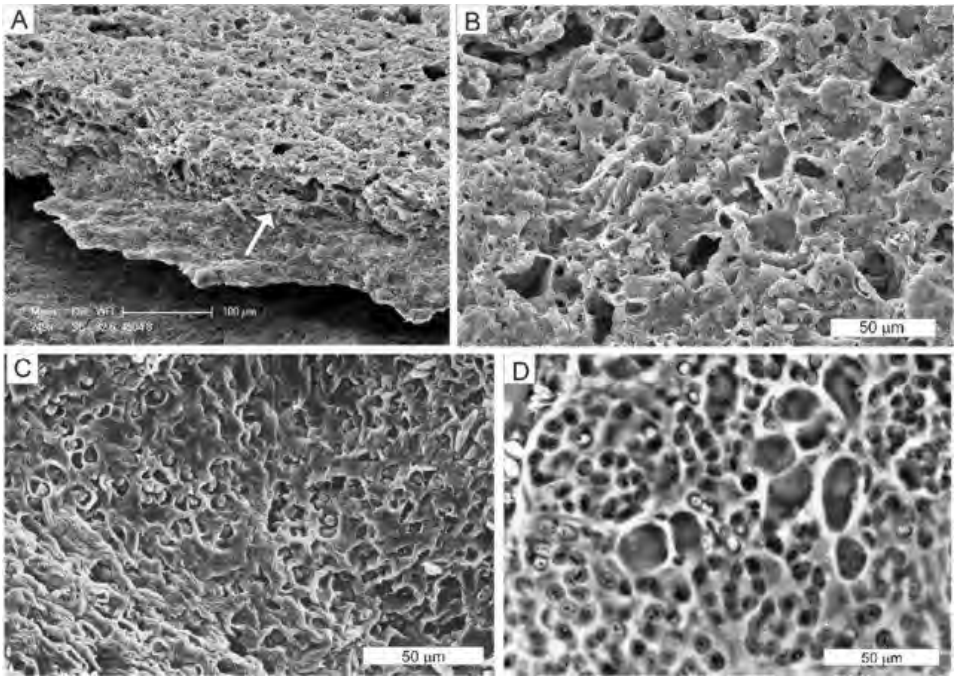

Fig. 5.4. (A) Thin layer of Ediacaran coccoidal cyanobacteria (arrow) in SEM images of HF-etched polished rock platelets. Visible are the remains of common mucilage sheaths grown on mudstone sediment. (B) Magnified portion of the above to show the web-like texture of the mineralized coccoidal mucilage sheaths (glycocalyx). (C) and (D): For comparison sectioned air-dried colonies of modern coccoidal (pleurocapsalean) cyanobacteria in SEM (C) and transmitted light microscope (D) images (both from Lake Van, Turkey). Note the volumetric predominance of the mucilage sheaths comparing with the volume of cells in colonies. Photos A and B from sample 4504-8. From Kremer, Kaźmierczak and Środoń (2018).

Publication:

Kremer, Barbara ; Kaźmierczak, Józef ; Środoń, Jan (2018), Cyanobacterial-algal crusts from Late Ediacaran paleosols of the East European Craton, Precambrian Research, vol. 305, pp. 236-246, doi.org/10.1016/j.precamres.2017.12.018

Scientific collaboration

The highly interdisciplinary character of astrobiological studies requires a joint effort of scientists working in the different fields, having their expertise in applying a variety of different methodologies: observing, making experiments, interpreting data, constructing theoretical models and implementing advanced computational techniques. That is why the international collaboration is so important.

Since 2003, Poland, is a member of the EANA (European Astrobiology Network Association) network of the 19 European nations active in astrobiology: Austria, Belgium, Czech Republic, Denmark, Finland, France, Germany, Greece, Hungary, Italy, Poland, Portugal, Romania, Russia, Spain, Sweden, Switzerland, The Netherlands and United Kingdom. Astrobiology groups in Brazil, China, Japan, Mexico and USA are associated members.

We have participated in the COST Action "Origins and Evolution of Life on Earth and in the Universe" (2014-2018), playing the leading role in the Working Group 1: Understanding the formation and evolution of planetary systems and habitable planets. The achievements of this action have been presented during the 20th EGU General Assembly, EGU2018, on the 5th of April 2018 in Vienna and published in the proceedings of the conference.

Publication:

Muriel Gargaud, Wolf Geppert, John Brucato, Elias Chatzitheorides, David Dunér, Ján Hrušák, Emmanuelle Javaux, Zuzana Kanuchova, Terence Kee, Akos Kereszturi, Purificación López-García, Anna Losiak, Christophe Malatere, Nigel Mason, Riho Motlep, Lena Noack, Olga Prieto-Ballesteros, Ewa

Szuszkiewicz, Inge Loes ten Kate, and Ján Žabka, (2018), The COST Action "Origin and Evolution of Life on Earth and in the Universe": An interdisciplinary research, training and outreach effort, Geophysical Research Abstracts Vol. 20, EGU2018-7133-2.

As it was planned, the end of the COST action „Origin" coincided with the beginning of the European Astrobiology Institute (EAI). The latter is a consortium of European research and higher education institutions and organisations as well as other stakeholders aiming to carry out research, training, outreach and dissemination activities in astrobiology in a comprehensive and coordinated manner and thereby securing a leading role of the European Research Area in the field. The First General Assembly of the EAI took place in May 2019 in Liblice, Czech Republic. At that time, two Polish institution joined EAI, namely the University of Szczecin and the Nicolaus Copernicus University in Toruń. Polish groups are particularly active in the Scientific Working Group: Formation and Evolution of Planetary Systems and Detection of Habitable Worlds. This Working Group is led by Antonello Provenzale, CNR Italy and Ewa Szuszkiewicz, University of Szczecin, Poland, appointed by the General Assembly.

Collaborative research has been carried out also by Polish members of the *PLATO Mission Consortium* (PMC) as well as under the umbrella of the EUROPLANET Society. In 2020 most of the activities have moved to the virtual meetings. They were very well attended and allowed to disseminate high-quality results across the scientific community. It is worth mentioning the following events: European Astronomical Society Annual Meeting EAS 2020 (Special session: European forum of astronomical communities, 2 July 2020), European Astrobiology Network Association Conference EANA 2020 (27-28 August 2020), Europlanet Science Congress 2020 (21 September – 9 October 2020) and PLATO Exoplanet thematic workshop on "Planetary interiors and system architectures" (30 November – 3 December 2020).

6

LAW AND THE SPACE POLITICS

6. LAW AND THE SPACE POLITICS

Compiled by Katarzyna Myszona-Kostrzewa

The Members of the Section of Law and Space Policy of the Committee on Space and Satellite Research affiliated with Presidium of the Polish Academy of Sciences participate in the works of the Polish Center for Space Law of Manfred Lachs (PCSL) which was established under the leadership of the Warsaw University in 2017. Its purpose is to propagate knowledge about space activities, in particular space law. At the moment the PCSL consists of 13 members which are the leading research centers in Poland: the Committee on Space and Satellite Research of the Polish Academy of Sciences, the University of Warsaw, the Cardinal Stefan Wyszyński University, the Warsaw School of Economics, the University of Rzeszow, the University of Gdansk, the University of Wrocław, the Cracow University of Economics, the University of Silesia, the Maria Curie-Sklodowska University in Lublin, the John Paul II Catholic University of Lublin, the University of Szczecin and the Main School of Fire Service of Warsaw.

The PCSL was one of the organizers of the nationwide conference entitled "the Current challenges of space law and international security" which took place at the Warsaw University on November 15, 2019 and had been preceded by the ceremony of handing over the presidency in the PCSL from the Warsaw University to the John Paul II Catholic University of Lublin. It was also connected with the ceremony of the admission of new members to it - the University of Szczecin and the Main School of Fire Service of Warsaw.

The papers presented at the conference were published in 2020.

The PCSL together with the Polish Space Agency organised the Space Mining Conference on the 26th of November 2020.

Table of Contents